Alma Mater Studiorum – Università di Bologna

DOTTORATO DI RICERCA IN

Scienze della Terra

Ciclo XXVI

Settore Concorsuale di afferenza: 02/C1

Settore Scientifico disciplinare: FIS/06

ORIGIN AND VARIABILITY OF PM_{10} AND ATMOSPHERIC RADIOTRACERS AT THE WMO-GAW STATION OF MT. CIMONE (1998-2011) AND IN THE CENTRAL PO VALLEY

Presentata da: **Dott.ssa BRATTICH ERIKA**

Coordinatore Dottorato **Relatore**

Prof. Vincenzo Picotti **Prof.ssa Tositti Laura**

Esame finale anno 2014

Abstract

Particulate matter is one of the main atmospheric pollutants, with a great chemical-environmental relevance. Aerosol deeply affects climate, local weather, visibility, human health, damages environment and cultural heritage. In the last two decades particulate matter has increasingly attracted the interest of the scientific community because, in spite of the ever improving efforts in the abatement technologies, its concentration is locally still very high often exceeding the thresholds. Despite many studies, the knowledge of sources, formation mechanisms and chemical characterization is still limited. Improving knowledge of the sources of particulate matter and of their apportionment is needed to handle and fulfill the legislation regarding this pollutant, to support further development of air policy as well as air pollution management.

Various instruments have been used to understand the sources of particulate matter and atmospheric radiotracers at the site of Mt. Cimone (44.18° N, 10.7° E, 2165 m asl), hosting a global WMO-GAW station. Thanks to its characteristics this location is suitable investigate the regional and long-range transport of polluted air masses on the background Southern-Europe free-troposphere.

In particular, PM_{10} data sampled at the station in the period 1998-2011 were analyzed in the framework of the main meteorological and territorial features: the time series is characterized by a strong seasonal fluctuation with a winter minimum and a summer maximum, attributed to the seasonal fluctuation of the mixed layer height as well as to the intense vertical exchange occurring in the warm season at this latitude. A receptor model based on back trajectories was applied to study the source regions of particulate matter. Highest PM_{10} data at the site can be attributed to three classes of events:

- Saharan dust transports from the northern African deserts;
- Uplift of polluted air masses from the Italian areas north of the Apennines range (i.e., Po Valley), especially during intrusion events from the boundary layer favoured by deep convection;
- Advection of PM_{10} enriched air masses from the European continent North and East of the Italian peninsula.

Simultaneous measurements of atmospheric radionuclides ^{210}Pb and ^{7}Be acquired together with particulate mass load have also been analysed to acquire a better understanding of vertical and horizontal transports able to affect atmospheric composition. Due to their contrasting natural origin, ^{210}Pb and ^{7}Be have often been used as a pair to investigate vertical transport and the scavenging of the aerosols. At Mt. Cimone ^{210}Pb is characterized by a seasonal fluctuation similar to that of PM_{10}, characterized by a summer maximum due to thermal convection and higher mixing height, while

^{7}Be is characterized by two relative maxima, one during the cold season linked to Stratosphere-to-Troposphere transport and one in the warm season, mainly associated to tropospheric subsidence balancing the ascent of air masses from the low troposphere. Seasonal variations of atmospheric radiotracers have been studied both analysing the long-term time series acquired at the measurement site as well as by means of a state-of-the-art global 3-D chemistry and transport model (GMI CTM): in particular, the use of the model enabled a better understanding of the transport and precipitation scavenging processes on the ^{210}Pb and ^{7}Be seasonalities at Mt. Cimone.

Advection patterns characterizing the circulation at the site have been identified by means of clusters of back-trajectories. The analysis revealed that the seasonality of transports is a relevant factor affecting atmospheric composition. In particular, one of the most interesting aspects of this study is the connection between Saharan Dust incursion events and increases not only in ^{210}Pb (and PM_{10}) but also in ^{7}Be, linked to two independent mechanisms occasionally acting together: the desert dust uplift and a strong downward movement from the upper troposphere. The analysis showed also that in general the cold period is mainly affected by long-range transports, while on the contrary short-range transports dominate the warm season. The relationship between NAO (North Atlantic Oscillation) and advection patterns has all-year-long important effects in terms of atmospheric composition at Mt. Cimone.

The study of source regions of the ratio ^{7}Be/^{210}Pb and of high potential vorticity values pointed out once more the usefulness of these tracers in the understanding of vertical transports. Locations highlighted by this kind of analysis are areas frequently affected by mechanisms promoting Stratosphere-to-Troposphere transport (areas interested by lee cyclogenesis, preferred regions for cyclone formation, and areas where the polar jet stream is generally stronger): North America, Northern Atlantic, the Arctic region and the Alps. Analysing the seasonal and trend components of the time series, it was highlighted that, even though some advection patterns and ^{210}Pb and PM_{10} are associated to a decreasing trend, the largest variability of the time series is in general associated with seasonal fluctuations and small time-scale changes.

Finally, the results of a source apportionment study of particulate matter carried on in a midsize town of the Po Valley (actually recognised as one of the most polluted European regions) are reported. Receptor models have identified six sources, interpreted as mineral dust, road dust, traffic, secondary aerosol, biomass burning and a pseudo-marine factor linked to the use of salt as de-icing agent on roads during winter. The source apportionment result was that on the average about 30% of PM_{10} is attributed to the coarse fraction, while the fine fraction contributes to about the 70%.

An approach exploiting different techniques, and in particular different kinds of (mostly, but not only receptor) models, successfully achieved a characterization of the processes/sources of particulate matter at the two sites, and of atmospheric radiotracers at the site of Mt. Cimone.

Riassunto

Il particolato atmosferico è uno degli inquinanti secondari di maggiore rilevanza chimico-ambientale. L'aerosol esercita importanti effetti sul clima, sul tempo atmosferico, sulla visibilità, sulla salute umana, danni all'ambiente ed ai beni culturali. Negli ultimi due decenni il particolato atmosferico ha attratto sempre più l'attenzione della comunità scientifica perché, nonostante le sempre migliori tecnologie di abbattimento, la sua concentrazione è ancora molto alta a livello locale, superando spesso i limiti legislativi. Nonostante il gran numero di studi, la conoscenza delle sorgenti, dei meccanismi di formazione e della caratterizzazione chimica del particolato sono ancora limitate. Una migliore conoscenza delle sorgenti di particolato e del loro apporzionamento sono necessarie anche a fini legislativi, a supporto di ulteriori sviluppi delle politiche in materia di qualità dell'aria e per il contenimento dell'inquinamento atmosferico.

Vari strumenti sono stati utilizzati volti alla comprensione delle sorgenti di particolato atmosferico e radiotraccianti al sito di Monte Cimone (44.18° N, 10.7° E, 2165 m asl), che ospita una stazione globale WMO-GAW e che, grazie alle sue caratteristiche, rappresenta un luogo utile all'investigazione del trasporto regionale ed a lungo raggio di masse d'aria inquinate al di sopra del fondo fornito dalla troposfera libera sud-europea.

In particolare, i dati di PM_{10} raccolti alla stazione nel periodo 1998-2011 sono stati analizzati nel contesto delle principali caratteristiche meteorologiche e territoriali: la serie temporale mostra una forte fluttuazione stagionale con un minimo invernale ed un massimo estivo, attribuito alla fluttuazione stagionale dell'altezza dello strato di rimescolamento ed all'intenso scambio verticale che avviene nella bassa troposfera a questa latititudine. Un modello a recettore basato sull'utilizzo di *back trajectories* è stato utilizzato per studiare le regioni sorgente di particolato atmosferico. Gli aumenti di PM_{10} al sito di misura sono attribuibili a tre classi di eventi:

- Trasporti di sabbia sahariana dai deserti del Nord-Africa;
- Trasporto verso l'alto di masse d'aria inquinate dalle aree italiane a nord dell'arco appenninico (Pianura Padana), specie durante eventi di intrusione dal *boundary layer* favoriti dalla convezione spinta;
- Avvezione di masse d'aria arricchite dal continente europeo a Nord ed a Est della penisola italiana, inclusa l'area balcanica.

Sono state anche analizzate le misure simultanee di radionuclidi atmosferici ^{210}Pb e ^{7}Be raccolti assieme alla massa di materiale particolato per ottenere una migliore comprensione dei trasporti verticali ed orizzontali in grado di influire sulla composizione atmosferica. Infatti, grazie alla loro origine naturale contrapposta, la coppia ^{210}Pb e ^{7}Be è stata spesso usata per studiare il trasporto verticale e lo

scavenging degli aerosols. A Monte Cimone il ^{210}Pb è caratterizzato da una fluttuazione stagionale simile a quella del PM_{10}, caratterizzata da un massimo estivo dovuto alla convezione termica ed alla maggiore altezza di rimescolamento, mentre il ^{7}Be è caratterizzato da due massimi relativi, uno durante la stagione fredda legato al trasporto Stratosfera-Troposfera ed uno nella stagione calda, principalmente associato alla subsidenza troposferica che bilancia l'ascesa di masse d'aria dalla bassa troposfera. Le variazioni stagionali dei radiotraccianti atmosferici sono state studiate sia tramite l'analisi della lunga serie temporale acquisita al sito di misura, sia tramite un modello globale 3-D di chimica e del trasporto (GMI CTM), che ha consentito in particolare una migliore comprensione dell'influenza dei processi di trasporto e dello *scavenging* della precipitazione sulle stagionalità di ^{210}Pb e ^{7}Be a Monte Cimone.

I *patterns* di avvezione che caratterizzano la circolazione al sito sono stati identificati per mezzo dell'analisi dei clusters di *back trajectories*. L'analisi ha rivelato che la stagionalità dei trasporti è un fattore rilevante per la sua influenza sulla composizione atmosferica. In particolare, uno degli aspetti più interessanti risultante da questo studio è la connessione degli eventi di trasporto di sabbia sahariana con aumenti non solo di ^{210}Pb (e PM_{10}) ma anche di ^{7}Be, legata a due meccanismi indipendenti che agiscono talvolta contemporaneamente: la salita di polvere desertica con un forte movimento verso il basso dall'alta troposfera. La ricerca ha mostrato anche che in generale il periodo freddo è interessato in prevalenza da trasporti a lungo raggio, mentre al contrario i trasporti a corto raggio dominano la stagione calda. La relazione tra la NAO (*North Atlantic Oscillation*) e *patterns* di avvezione ha importanti effetti in termini di composizione atmosferica a Monte Cimone, lungo tutto il corso dell'anno.

L'analisi delle regioni sorgente del rapporto ^{7}Be/^{210}Pb e di valori elevati di vorticità potenziale ha messo ancora una volta in rilievo la loro utilità nella comprensione dei trasporti verticali. Le regioni evidenziate da questo tipo di analisi sono aree interessate frequentemente da meccanismi promotori del trasporto stratosfera-troposfera (regioni interessate da ciclogenesi di *lee*, regioni preferite per la formazione di cicloni, ed aree dove si localizza generalmente la corrente a getto polare): il Nord America, l'Atlantico settentrionale, la regione artica e le Alpi. Lo studio delle componenti stagionali e dei *trends* delle serie temporali hanno posto in evidenza come, sebbene per alcuni *patterns* di avvezione e per ^{210}Pb e PM_{10} sia stato rivelato un trend in calo, la maggiore variabilità delle serie temporali è associata alle fluttuazioni stagionali ed alle fluttuazioni a piccola scala temporale.

Da ultimo, vengono riportati i risultati di uno studio di *source apportionment* di particolato atmosferico condotto in una città di medie dimensioni della Pianura Padana, attualmente riconosciuta come una delle regioni più inquinate dell'intera Europe. I modelli a recettore hanno individuato sei sorgenti, interpretate come polvere minerale, polvere stradale, traffico, aerosol secondario, combustione di biomassa ed un fattore pseudo-marino legato all'utilizzo di sale come agente anti-gelo sulle strade durante l'inverno. Il risultato del *source apportionment* è stato che in

media circa il 30% del PM_{10} è attribuibile alla frazione grossolana, mentre la frazione fine contribuisce per il 70% circa.

L'utilizzo di un approccio che ha sfruttato diverse tecniche, ed in particolare diversi modelli (principalmente, ma non solo, a recettore), ha consentito di caratterizzare completamente sorgenti/processi di particolato ai due siti, e quelle dei radiotraccianti atmosferici al sito di Monte Cimone.

INDEX

APPENDIX II – Comparison of Radioactivity Data Measured in PM_{10} Aerosol Samples at two Elevated Stations in Northern Italy during the Fukushima Event

CHAPTER 1 – General Introduction

Premise

Particle pollution (also called particulate matter or PM) is the term indicating a mixture of solid particles and liquid droplets found in the air. Some particles, such as dust, dirt, soot, or smoke, are large or dark enough to be seen with the naked eye. Others are so small that they can only be detected using an electron microscope. These particles come in many sizes and shapes and can be made up of hundreds of different chemicals. Particle pollution includes "inhalable coarse particles", with diameters larger than 2.5 micrometres and smaller than 10 micrometres and "fine particles" with diameters that are 2.5 micrometres and smaller. Particle pollution contains solid or liquid droplets that are so small that they can get deep into the lungs and cause serious health problems (Davidson *et al.*, 2005; Pope and Dockery, 2006; Pope *et al.*, 2009). Particles have also deep effects on climate, cloud formation, and visibility reduction (Finlayson-Pitts and Pitts, 1999; Usher *et al.*, 2003; Seinfeld and Pandis, 2006; Forster *et al.*, 2007; Myhre *et al.*, 2013), and can damage the environment and cultural heritage (Camuffo *et al.*, 2001; Godoi *et al.*, 2006; Nava *et al.*, 2010). At present, fine and coarse particles are regulated in the USA and in Europe. At European level, Directive 2008/50/EC on ambient air quality and cleaner air for Europe requires Member States to limit the exposure of citizens to the airborne particles and sets limit values for PM_{10} and $PM_{2.5}$. Improving knowledge of the sources and apportionment of these sources of airborne particulate matter is useful to handle and fulfil the legislation regarding this pollutant, to support further development of air policy as well as air pollution management.

The main objective of this work is to understand the sources of particulate matter and atmospheric radiotracers ^{7}Be and ^{210}Pb at the global WMO-GAW station of Mt. Cimone (44.18°N, 10.7°E, 2165 m asl, Italy) and in the Po Valley, recognised as one of the most polluted regions in Europe. Aside from being the most elevated peak of the Northern Apennines, lying above the planetary boundary layer during most of the year, Mt. Cimone is also fairly off cities and industrialized areas and has a 360° free horizon. Owing to these characteristics, it represents a suitable location to investigate the regional and long-range transport of polluted air masses on the background Southern Europe-Mediterranean free troposphere (Fischer *et al.*, 2003; Marinoni *et al.*, 2008). It is to note in this framework that Southern Europe and the Mediterranean basin are considered as a hot-spot region both in terms of climate change (e.g., Forster *et al.*, 2007; Hesselbjerg *et al.*, 2013) and air quality (Monks *et al.*, 2009), also representing a major crossroad of different air mass transport processes (Lelieveld *et al.*, 2002; Millàn *et al.*, 2006; Duncan *et al.*, 2008; Tositti *et al.*, 2013). Various approaches are used in this work for the purpose of studying the

sources of particulate matter and atmospheric radiotracers at the site of Mt. Cimone, both in terms of physical processes as well as of long-range and regional transport: the main tool which will be applied in the present work is receptor modelling, especially incorporating the use of back trajectories, but other analyses have been carried out and will be thoroughly described to gain better insights into the processes responsible of PM_{10} and atmospheric radiotracers variabilities.

Because of their contrasting natural origin, atmospheric radiotracers ^{7}Be and ^{210}Pb can be used to understand the atmospheric composition and its variations, and the vertical motions in the atmosphere. In particular, this pair has been often used in the study of Stratosphere-to-Troposphere Exchange (STE) and to determine the contribution of Stratosphere-to-Troposphere Transport (STT) to tropospheric ozone (O_3). As a matter of facts, while ^{7}Be, being a cosmogenic radionuclide mostly produced in the stratosphere and upper troposphere, is considered a tracer of stratospheric influence, ^{210}Pb is considered a tracer of air masses with continental origin, as it is the decay daughter of ^{222}Rn emitted from soils. O_3 is a greenhouse gas and one of the most important gases involved in photochemical reactions (Crutzen *et al.*, 1999; Volz-Thomas *et al.*, 2002), one of the key agents determining the oxidation capacity of the troposphere (Gauss *et al.*, 2003), but most of all is a secondary pollutant in the lower troposphere dangerous to human health (Hoek *et al.*, 1993; Kinney, 1993), ecosystems (Scebba *et al.*, 2006), and agricultural yields (Fuhrer and Booker, 2003), playing also a central role in the radiative budget of the atmosphere (Ramaswamy *et al.*, 2011). Due to anthropogenic emissions, tropospheric O_3 concentrations have increased significantly since pre-industrial ages (Staehelin *et al.*, 1994), leading to an equivalent radiative forcing of about 19% of that from carbon dioxide as from the last IPCC (Intergovernmental Panel on Climate Change) assessment (Myhre *et al.*, 2013). In fact, there are two sources of O_3 in the troposphere: photochemical production from oxidation of carbon monoxide and hydrocarbons in the presence of nitrogen oxides, and transport from the stratosphere (Crutzen, 1973; Jacobson, 2002), often in connection with tropopause folding events (e.g., Holton *et al.*, 1995 and references therein). While the former process is directly affected by anthropogenic emissions of O_3 precursors, the downward branch of the Brewer-Dobson circulation in middle and high latitudes (Haynes *et al.*, 1991) is the process controlling the total amount of O_3 that is exchanged from the stratosphere to the troposphere. It is to note here that besides being very suitable to study tropospheric background conditions (Wotawa *et al.*, 2000; Stohl *et al.*, 2000; Cuevas *et al.*, 2013), mountain peak stations are also appropriate locations to investigate specific aspects of STT (Cristofanelli *et al.*, 2006). Data acquired so far at the station constitute a time series long enough to provide a sort of short-term climatology of the site. Moreover, the data time extension is so long that the application of receptor modeling in order to identify the sources of atmospheric particulate matter is possible. In fact,

receptor modeling tools typically use complex chemical composition dataset to characterize and estimate the contribution of each source type to the observed concentration, but can also be based on the identification of the locations of the sources through the use of ensembles of air parcel back trajectories. Both the methods are used in the present work. In particular, statistical techniques based on a long term series of back trajectories calculated at the Mt. Cimone site is aimed at a thoroughly elucidation of the role of atmospheric transports (most of all, but not only, vertical) affecting variations in atmospheric composition. The use of receptor modeling tools based on complex chemical composition dataset to characterize and estimate the contribution of each source type to the observed concentration was instead applied to gain insights into the sources of particulate matter in Bologna, a mid-size town located in the central Po Valley, and in quantifying their contribution.

This work consists of 8 chapters and is organized as follows. The remainder of **Chapter 1** is used to pose the scientific basis for the understanding of the thesis work: a general introduction to particulate matter, atmospheric radiotracers and receptor modelling tools is given in the following sections of this chapter. **Chapter 2** describes the average behaviour of PM_{10} at the Mt. Cimone site and investigates its variations both in relation to data acquired at the station and on the regional scale as well as with receptor modelling involving back trajectories techniques. A source receptor modelling based on the application of back trajectories is specifically applied to investigate the source regions associated to events of elevated PM_{10} measured at Mt. Cimone. **Chapter 3** presents a basic overview of the ^{7}Be and ^{210}Pb time series collected at the site and discusses the data in terms of seasonal and interannual variations with the purpose of gaining better insights into physical mechanisms responsible of their variabilities. To the same aim in **Chapter 4** simulations of ^{7}Be and ^{210}Pb at Mt. Cimone are conducted with a state of the art global 3-D chemistry and transport model: the use of the model enables to examine how transport and precipitation scavenging affect their concentrations. In **Chapter 5** the main advection patterns at Mt. Cimone are examined by means of back trajectories clustering analysis. The temporal series of air masses back trajectories and of the data acquired at the station are analysed in terms of seasonal fluctuations, trends and association to NAO (north Atlantic Oscillation). The roles of atmospheric transport and NAO in the observed variations of atmospheric composition are also studied. **Chapter 6** uses a different statistical trajectory analysis to investigate the influence of stratospheric air masses on radiotracers and ozone. In particular, the geographical areas associated to events of high ^{7}Be, ^{210}Pb and ozone are identified, and the major mechanisms promoting stratosphere-to-troposphere exchange events are investigated. In **Chapter 7** a more classical source apportionment study applied on a chemical composition dataset is carried on. The study evaluates the source contributions in a midsize town located at the centre of the Po Valley by means of multivariate statistical techniques and receptor

modelling. The impact of a long range transport event due to Saharan Dust outbreaks is also evaluated. Finally, conclusions coming from all of these works are drawn.

During the first year of my PhD, a relevant event occurred on March 11th, 2011: the accident in the Fukushima Dai-ichi nuclear power plant after the devastating tsunami in Japan. This event has been the occasion for me to deal not only with natural but also with artificial radioactivity released in the atmosphere during the nuclear accident. The analysis of radioactivity also served to me as a tool to test atmospheric transport models capabilities in representing this (very) long-range transport event. The work carried on during this event is presented in Appendix II, while Appendix I describes my first studies of natural radiotracers with more rudimental tools, also conducted during the first year of my PhD in occasion of a IAEA (International Atomic Energy Agency) conference held in Monaco.

1.1 Atmospheric particulate matter

1.1.1 Physical characteristics

Atmospheric particulate matter is generally defined as a complex and dynamic mixture of solid and/or liquid particles present in suspension in a gas (air) having organic and inorganic components (vanLoon *et al*., 2000). Particulate matter has extremely variable dimensions, origin and chemical composition and for this reason forms a complex and heterogeneous mixture. Atmospheric PM has a profound effect on our lives, as it affects global climate, local weather, visibility, personal health and conservation of built heritage. Nevertheless, the knowledge of sources, formation mechanisms, fate and properties of PM is still limited, most of all regarding some constituent compounds and some aspects related to formation processes.

Atmospheric PM can be emitted by a wide variety of sources that influence its physical properties (size, surface area, density), chemical composition and size distribution. Particulate matter is produced by lots of sources and processes, both of natural and anthropogenic origin, from crumbling of material by abrasion/erosion to complex photochemical mechanisms in troposphere (Manahan, 2000). In particular, PM may be classified as primary or secondary in accordance with its formation mechanism: **primary** particles are directly emitted into the atmosphere (dust, pollen, smoke) while **secondary** particles are formed after chemical transformation of their gaseous precursors and lead to production in condensed phase. In this case both organic and inorganic particles are involved in oxidative reactions (vanLoon *et al.*, 2000).

Bio-geo-chemical cycle of atmospheric aerosol may be outlined as in Figure 1.1:

1 primary particles and precursor gases of secondary aerosol are emitted by natural and anthropogenic sources;

2 particles may undergo further modifications after chemical-physical processes of different nature;
3 particles may be removed from the atmosphere by either wet (meteorology) or dry deposition;
4 removed particles may rearrange their chemical content to the deposition environment (hydrosphere and pedosphere), interacting with the biosphere in direct or indirect way (Pöschl, 2005).

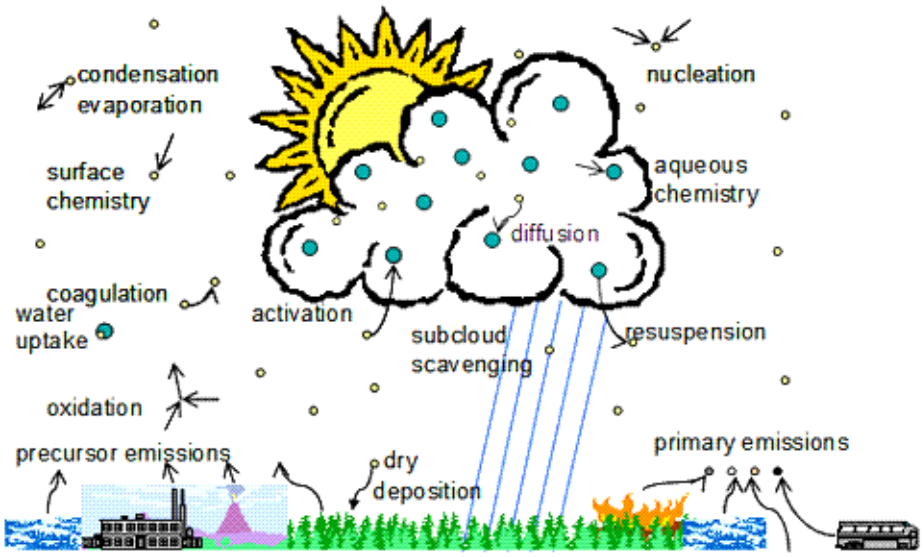

Figure 1.1 *Natural cycle of atmospheric aerosol (Image downloaded from Pacific Northwest National Laboratory,* http://www.pnnl.gov/atmospheric/research/aci/aci_aerosol_indeffects.stm*).*

Atmospheric particles are mainly characterized by their size. It is mainly expressed in terms of equivalent (or effective) radius or diameter, assuming that particles have spherical shape. In reality, atmospheric particles are characterized by various shapes: from the rough edge-shape of a crustal particle, to the long branched chains of small nanoparticles characterizing diesel exhausts emission, to the flat appearance of a skin fragment, to the cubic shape of a sodium chloride crystal. For this reason, the concepts of radius or diameter have a relative value and the concept of equivalent diameter, depending from physical rather than geometric characteristics, is introduced to assign a diameter to any (even irregular) particle. The equivalent diameter is generally defined as the diameter of a sphere or circle having some specific property or behaviour as the particle under consideration. The most used is the **aerodynamic diameter D_a**, that is the diameter of a sphere of unity density (1 kg m^{-3}) with the same settling (sedimentation) velocity as the particle in question (Heyder *et al.*, 1974). The mathematical law that describes D_a is:

$$D_a = D_g k \sqrt{\rho_p / \rho_0} \qquad (1.1)$$

where D_g is geometrical diameter, ρ_p the particle density, ρ_0 the density of the reference spherical particle, k a spatial factor (equal to 1.0 in the case of a spherical particle). The terms PM_{10} and

$PM_{2.5}$ are related to this definition, and define suspended masses of particulate formed by particles less than 10 and 2.5 μm, respectively. In both cases the choice of these upper limits refers to the ability to penetrate into the respiratory system depending on their size (PM_{10} can be inhaled and accumulate in the respiratory system, while $PM_{2.5}$ can lodge deeply into the lungs, and PM_1 can reach alveolar area thereby depositing deep inside respiratory tract).

PM may vary in size from a few nanometres to several tenths of micrometres. Its typical size distribution, shown in Figure 1.2, includes four different modes, differing also in terms of generation processes (John, 2001). Moreover, size controls and determines also environmental fate of the particle. Basically, the number of particles decreases increasing the size of particles. The four modes in the distribution are interpreted as follows:

- the **coarse** mode (over 1 or 2.5 μm, depending on the adopted convention). Generally this mode has the highest volume (or mass) concentration. Particles in this mode are mainly formed by natural mechanical processes, such as erosion of the earth surface (mineral dust) and of other materials, including the ocean surface (sea spray), but also processes of anthropogenic origin such as the abrasion on tyres and on brakes of motor vehicles. The chemical composition reflects that of the source originating the particles: if aerosol has a coastal or marine origin, it is mainly constituted by minerals and NaCl (Hueglin *et al.*, 2005); a component having organic origin is also present (e.g., Cass *et al.*, 1982), and most of the components having biological origin, such as pollen and spores, is in this interval. Although coarse mode is dominated by primary particles, also secondary particles formed by the chemical interaction of gases with primary particles of crustal and marine origin can be found in this mode;
- the **accumulation** mode generally has the highest number concentration and includes particles in the range between 0.08 and 1-2 μm; these particles are formed by coagulation of small size particles and by condensation of gaseous species on the surface of pre-existing particles. Their chemical composition comprehends lots of organic substances and insoluble inorganic salts such as NH_4^+, NO_3^- and SO_4^{2-};
- **Aitken nuclei** mode includes particles having diameter between 0.07 and 0.08 μm, originated by heterogeneous reactions of gas-particle conversion (condensation) and in the combustion processes at high temperatures. They act as condensation nuclei for water vapour and for gaseous species with low vapour pressure;
- the **nucleation** mode includes particles having equivalent diameter below 0.01 μm, which are formed by the homogeneous nucleation of precursor gases and from combustion processes. The size limit that allows distinguishing these particles from big sizes molecules is in reality not certain (US EPA, 2004).

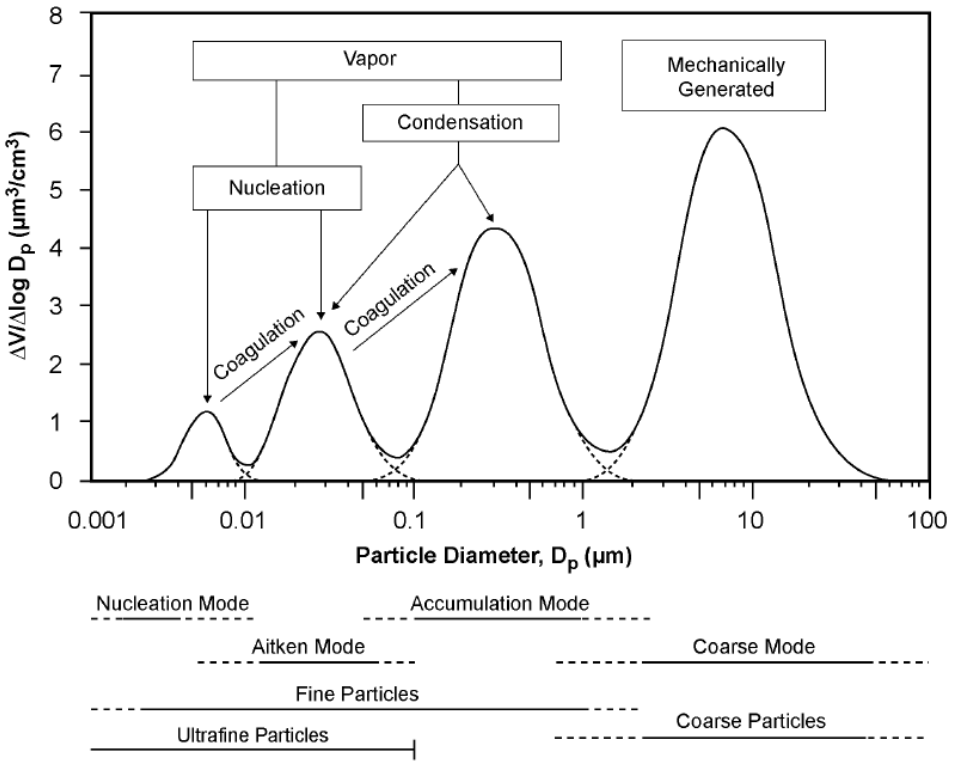

Figure 1.2 *Typical size distribution of atmospheric aerosol and origin of particulate matter (US EPA, 2004).*

Other classifications often employed distinguish among (Oberdörster, 2000):

- coarse particles, diameter larger than 2.5 or 1 μm;
- fine particles, diameter between 0.1 and 1 μm;
- ultrafine particles or nano-aerosol, diameter shorter than 0.1 μm (that can be further divided into ultrafine particles, with at least one of the three dimensions shorter than 100 nm, and nanoparticles, with all the three dimensions shorter than 100 nm).

Ultrafine particles (UFP) comprehend particles of nucleation mode and most of Aitken nuclei. Although they are so small that do not contribute in a significant way to the total mass, they make up more than 80% of the atmospheric aerosol, as can be seen in Figure 1.3. UFP are also very important from the sanitary point of view, both because of reduced dimensions and of their concentration.

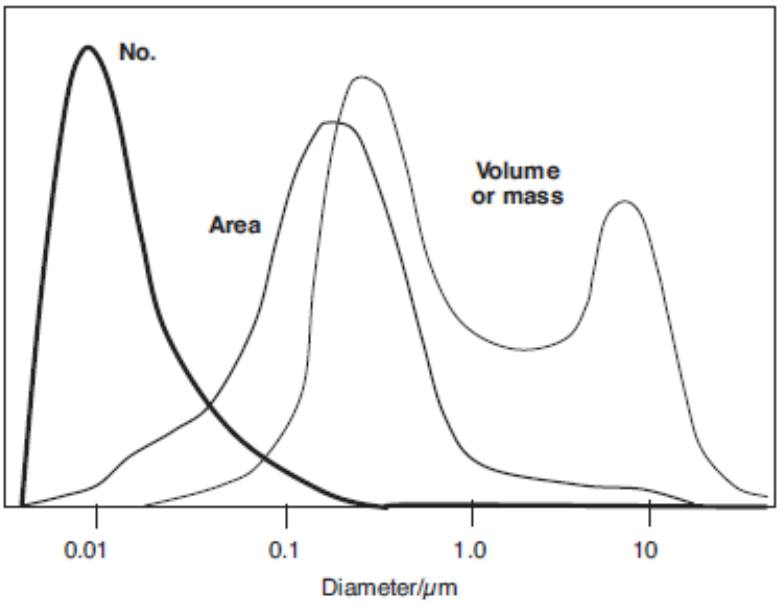

Figure 1.3 *Simplified comparison among number, area and volume of particles as a function of the logarithm of the particles diameter (Tiwary and Colls, 2002).*

The residence time of particles in the atmosphere depends also on their size. After the production/emission, particles undergo redistribution and transport processes through the atmosphere, and are finally removed by wet and dry deposition. The most efficient removal mechanism of PM is wet scavenging, which corresponds to 80% of the total removal processes and is formed by transport processes to the ground through precipitations (rain, snow, hail, but also "hidden" precipitations such as fog, frost and dew). The main mechanisms of wet deposition are:

- **rainout**, that is removal in between the cloud (also called in-cloud processes);
- **washout** or below-cloud processes, in which a particle is absorbed in a pre-existing falling droplet. This process is less efficient than rainout as there is a limited probability of collision between the droplet and the particle during the fall of the droplet.

There are three main mechanisms of dry deposition: gravitational settling, diffusive deposition and contact with surfaces. Owing to the effect of gravity, coarse particles are rapidly removed from the air by sedimentation (residence time between some minutes and some hours). Particles in the nucleation mode are rapidly transformed into coarser particles by coagulation processes and then are also removed by sedimentation. The highest residence time in the atmosphere (up to some weeks) is shown by particles in the accumulation mode, which are too large to have sufficient Brownian diffusivity and too light to be removed by gravitational settling; these particles can be easily transported by the wind up to thousands of kilometres far from the area where they are formed. Usually aerosol particles in accumulation size mode are less effectively washed out and prone to remain distributed in the atmosphere even after a spell of heavy rainfall (Chate, 2005). Dry deposition

of particles in the accumulation mode is due to collision with surfaces, even if wet deposition is the most efficient removal mechanism. The residence time of particles in the accumulation mode varies from some days to some weeks depending on climatic conditions and altitude. The term "accumulation interval" is due to the long life-time with respect to other classes of particles and to the dependence of the removal by meteorological phenomena (Baird and Cann, 2008). The residence time of Aitken nuclei is short, due to the rapid coagulation. The residence time is also a function of the injection height: with increasing injection height, the residence time increases. Aerosols from volcano eruptions which reached stratosphere may stay there for about one year.

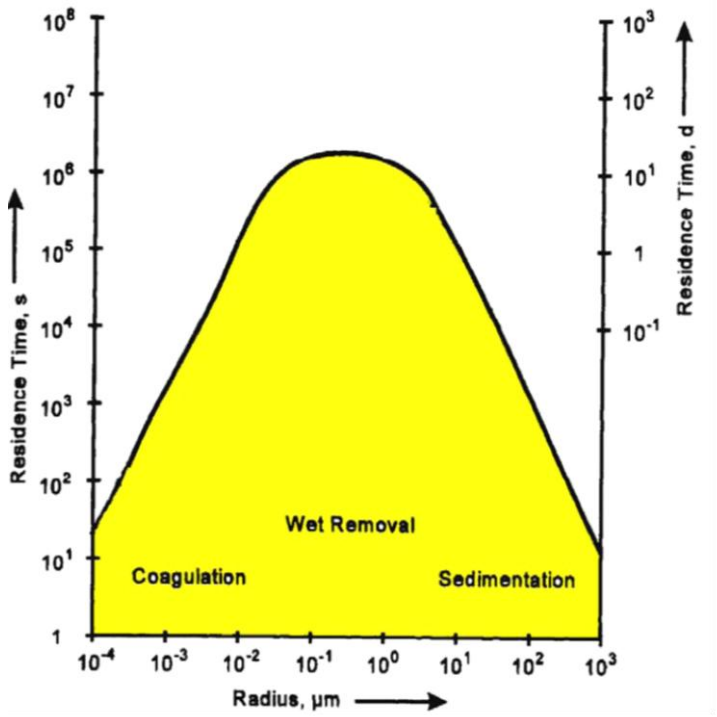

Figure 1.4 *Residence time of particles as a function of their dimensions (Prospero et al, 1983; Jaenicke, 1980).*

1.1.2 Sources of atmospheric aerosol

Sources of particulate matter can be natural or anthropogenic. Naturally occurring particles are produced by volcanoes, sea spray, grassland fires, desert dust and by a variety of biological sources (pollen, bacteria, fungal spores, fragments of vegetable organisms and animals). Anthropogenic particles derive from human activities, such as the burning of fossil fuels in vehicles, domestic heating, power plants and industrial processes. The composition of PM reflects that of the source from which it is originated.

Table 1.1 summarizes natural and anthropogenic sources for the main constituents of primary and secondary aerosol for fine and coarse particles. It also highlights that, on a global scale, estimated fluxes of anthropogenic origin are overall equivalent to those of natural origin.

Source	Estimated Flux (Tg yr^{-1}) Low	High	Best	Particle Size Category[a]
NATURAL				
Primary				
Soil dust (mineral aerosol)	1000	3000	1500	Mainly coarse
Sea salt	1000	10000	1300	Coarse
Volcanic dust	4	10000	30	Coarse
Biological debris	26	80	50	Coarse
Secondary				
Sulfates from biogenic gases	80	150	130	Fine
Sulfates from volcanic SO_2	5	60	20	Fine
Organic matter from biogenic VOC	40	200	60	Fine
Nitrates from NO_x	15	50	30	Fine and coarse
Total natural	2200	23500	3100	
ANTHROPOGENIC				
Primary				
Industrial dust, etc. (except soot)	40	130	100	Fine and coarse
Soot	5	20	10	Mainly fine
Secondary				
Sulfates from SO_2	170	250	190	Fine
Biomass burning	60	150	90	Fine
Nitrates from NO_x	25	65	50	Mainly coarse
Organics from anthropogenic VOC	5	25	10	Fine
Total anthropogenic	300	650	450	
Total	2500	24000	3600	

[a]Coarse and fine size categories refer to mean particle diameter above and below 1 μm, respectively.

Note: Sulfates and nitrates are assumed to occur as ammonium salts. Flux unit: Tg yr^{-1} (dry mass).

Source: Kiehl and Rodhe (1995).

Table 1.1 *Estimate of fluxes (Tg*yr^{-1}) of particulate matter as a function of the source, natural and anthropogenic (Seinfeld and Pandis, 2006).*

One of the main sources of natural primary particles is the formation and resuspension of dusts from soil and rocks erosion operated by winds and other atmospheric agents (physical and chemical weathering). It depends from wind and atmospheric agents, but also from the structure and chemical composition in the location, variable depending on climate, geology, geography and topography (sea, mountain, desert …). Generally particles originated by these processes are coarse-sized and constituted by silicates such as quartz, clays (most of all kaolinite, illite, feldspars, carbonates and dolomite) and to a less extent calcium sulphates (gypsum) and iron oxides. The most common chemical elements (both in soil and in rocks) are Si, Al, Fe and soluble elements such as Ca^{2+}, Mg^{2+}, Na^{+} and K^{+}, in form of minerals. Organic material is also present in soils, in different percentages depending on environmental conditions in the area.

Another important natural source of aerosol is represented by seas and oceans (sea-spray). Sea-spray is considered the second largest contributor in the global aerosol budget and reflects the composition of seawater, consisting mainly of sodium chloride (NaCl) and sulphates (Na_2SO_4, $MgSO_4$, K_2SO_4). This kind of aerosol is mainly originated by sea foam produced by wind, that generates lots of sea droplets that are suspended in the atmosphere and there remain as solid particles after evaporation processes. These particles are both coarse and fine-sized. Sea-spray can have a deep influence on the composition of PM in coastal areas and on islands.

Volcanic emissions are another natural source of primary mineral particles but also gases (most of all sulphur dioxide, carbon dioxide and water vapour). The contribution of volcanic emissions is generally localized and variable in time.

Natural PM comprehends also a biogenic fraction, generally made up by vegetal debris, pollen, spores and microorganisms (e.g., bacteria, viruses, fungi and seaweeds). While viruses and bacteria have dimensions less than 2 μm, vegetal debris, pollen and spores are generally in the coarse size (Pòsfai and Molnàr, 2000).

Natural sources do not originate only primary aerosol, but also gaseous precursors of secondary aerosol; for instance SO_2 emitted by volcanoes, but most of all dimethyl sulphide [$(CH_3)_2S$] of biogenic marine (and biomass) origin, that once diffused from the marine surface to the atmosphere, is oxidised to SO_2. SO_2 is further oxidized by OH· radical, forming H_2SO_4 (sulphuric acid). This acid component is neutralized by gaseous ammonia emitted by natural cycle of nitrogen. The acid-base reaction forms $(NH_4)_2SO_4$, a salt that represents one of the most abundant components of secondary aerosol (Finlayson-Pitts and Pitts, 1999).

Also a small part of nitrates coming from NO_x in the nitrogen cycle (Roelle *et al.*, 2001) and from lightning (Price *et al*., 1997a, b) are part of natural aerosol. Their presence is as important as that of NaCl, since water vapour can condensate (formation of clouds and precipitation) only owing to their hygroscopicity and to their ability of absorption/adsorption[1] in the form of ultrafine crystals. In fact it is well known that, because of low pressure and rarefaction of gases with height in the atmosphere, it would be extremely hard for water vapour to meet the necessary thermodynamic conditions to homogenous condensation, despite low temperatures.

A carbonaceous fraction is also part of secondary natural PM, constituted by both elemental carbon produced by natural combustion of forests and by organic substances emitted by vegetation (Harrison

[1] Absorption is the process by which one substance melts in the mass of a particle, whereas adsorption is the process by which molecules of a substance, such as a gas or a liquid, collect on the surface of another substance. In the case of adsorption, the molecules are attracted to the surface but do not enter the solid's minute spaces as in absorption; an important example is adsorption of big organic molecules on carbon molecules (soot).

et al., 2001). Vegetal biosphere releases in the atmosphere many organic unsaturated molecules such as isoprene and terpenes (generally called bio-VOC's) whose oxidation originates more polar organic compounds, characterized by a reduced vapour pressure and by a higher probability to undergo nucleation processes that form secondary aerosol (Christoffersen *et al.*, 1998; Koch *et al.*, 2000).

The main anthropogenic sources are mostly localized in urban and industrial areas. Generally, anthropogenic sources contribute mostly to the secondary fraction, associated to the huge quantities of gaseous precursors emitted by combustion processes both from stationary (electric energy production, industries, incinerators, heating) and mobile sources (light and heavy duty, off-road, air and ship traffic). Also catalytic converters installed inside internal combustion engines with the aim at cutting down harmful emissions of exhausts, promoting (through catalysts) their complete oxidation and in particular converting unburned hydrocarbons, nitrogen oxides NO_x, carbon monoxide CO to CO_2, H_2O and N_2, emit platinum-palladium in the form of PM. Moreover, the excess of operation of catalytic converters caused increased emissions of ammonia in PM.

In urban environment primary PM is generated by erosion processes of roads operated by traffic and by wear of motor vehicles' mechanical components (engine, brakes, tyres). Moreover in exhaust carbonaceous particles are also present (most of all elemental carbon, EC), of primary origin and typically submicron-sized.

Also industrial activities, such as concrete production, mineral industries, ceramic and building materials manufacture, are typically sources of coarse particles, but associated with emissions of gaseous precursor which can generate secondary aerosol.

Secondary anthropogenic PM is mainly formed by sulphates, ammonium nitrates and organic carbon. Sulphur dioxide is emitted by coal and diesel oil combustion, fuels by which sulphur impurities are only partially removed before sale and use. In the past the extensive use of coal as fuel caused serious episodes of atmospheric pollution, in particular linked to acid rains. In fact coal is a fuel containing elevated amounts of sulphur; the concentration of sulphur dioxide in the atmosphere was so elevated that ammonia was no more able to neutralize sulphuric acid, very hygroscopic. Wet deposition produced precipitations with very acid pH (with values up to 3-4 units), and consequent serious damages to entire ecosystems. Nowadays SO_2 levels are strongly reduced thanks to the use of fuels containing reduced concentrations of sulphur, such as diesel and fuel oil, and to the phase out of coal's production. In Figure 1.5 the historic series of SO_2 concentrations in Milan is reported: a notable decrease of this gas since the end of '50s due to the decrease of the coal's use is observed (Cazzuli *et al.*, 2005). A similar decrease was observed in all developed countries. Anyway, in many areas, most of all in developing countries such as China and India, acid rains still occur due to high local industrialization (Wenche *et al.*, 2006; Larssen *et al.*,

2006; Muthukumara *et al.*, 2012). Driven by the rapid economic development, SO_2 emissions from India and China have been continuously increasing over the past two decades (Garg *et al.*, 2006; Lu *et al.*, 2011; JRC/PBL, 2013; Kurokawa *et al.*, 2013). According to a new analysis of data from NASA's Aura satellite (Lu *et al.*, 2013), emissions of sulphur dioxide from power plants in India increased by more than 60% between 2005 and 2012, due to the rapid growth of electricity demand and the absence of regulations.

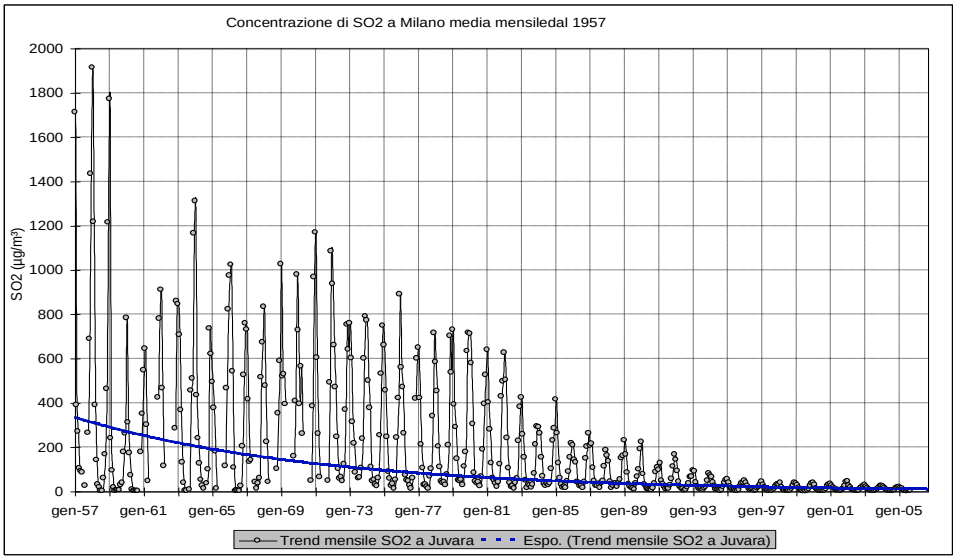

Figure 1.5 *Historic series of SO_2 concentrations in Milan since 1957 until 2005 (Cazzuli et al., 2005).*

Nitrogen oxides are among other gaseous precursors formed during combustion processes. An elevated temperature is needed to combine atmospheric nitrogen and oxygen (Finlayson-Pitts and Pitts, 1999), and therefore nitrogen oxides are mostly emitted by urban traffic and industrial processes at high temperatures. NO_x are oxidized in the atmosphere by OH· to HNO_3 and, similarly to H_2SO_4, after the neutralization with NH_3 form condensed vapour droplets and/or crystal salts (condensation nuclei).

Even in the case of anthropogenic sources precursors of secondary PM exist. These are mainly fugitive emissions, which are the fractions of volatile hydrocarbons emitted by vehicles because of evaporation, and organic solvents widely used both in industry as well as in daily life. VOCs (Volatile Organic Compounds) are compounds with high vapour pressure and low solubility in water. They include a great variety of chemical substances, some of which can have adverse effects on health. Many VOCs are produced and used in the production of paints, pharmaceutical and cooling substances. Typically VOCs are industrial solvents such as trichlorethylene, fuel additives such as MTBE or by-products generated by chlorine addition to water such as chloroform.

On a global scale, the most important anthropogenic sources of VOCs are associated to extended cultivated areas and to forests combustion, an activity linked to large scale variations of land use in behalf of farm areas (Odum *et al.*, 1996; 1997a, b). Same as bio-VOCs, even these substances can be oxidized in the atmosphere and transformed in more polar and condensable species.

While 80-90% of PM emitted by combustion is less than 1 μm diameter, less than 10% of the mass of dust from geologic material is $PM_{2.5}$.

1.1.3 Effects of aerosols

It is widely recognized that atmospheric PM influence climate through at least two main pathways: its effect on both the absorption and scattering of solar radiation (**direct** effect) and its role in cloud formation processes (**indirect** effect). In fact, as an indirect effect, aerosols in the lower atmosphere can modify the size of cloud particles, changing how the clouds reflect and absorb sunlight, thereby affecting the Earth's energy budget.

In the atmosphere, when particles are sufficiently large, we notice their presence as they scatter and absorb sunlight. Their scattering of sunlight can reduce visibility and redden sunrises and sunsets.

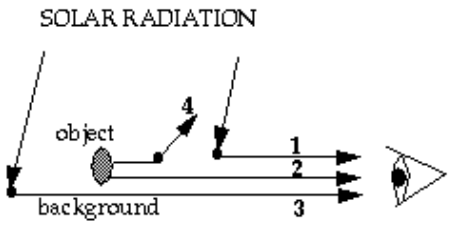

Figure 1.6 *Reduction of visibility by aerosols. The visibility of an object is determined by its contrast with the background (2 vs. 3). This contrast is reduced by aerosol scattering of solar radiation into the line of sight (1) and by scattering of solar radiation from the object out of the line of sight (4) (http://acmg.seas.harvard.edu/people/faculty/djj/book/bookchap8.html#20531).*

Earth's climate is influenced not only by greenhouse gases which heat up the planet absorbing the infrared component of the Earth's radiation and re-emitting it towards the Earth's surface. The action of aerosols on climate is more complex: they can behave such as greenhouse gases and produce a heating effect or act as cooling, depending on their chemical-physical characteristics (D'Alessio *et al.*, 2005; Mitra *et al.*, 2002).

The interaction of aerosol particles with the solar radiation depends on their chemical composition. Some components of the aerosol can scatter incoming solar radiation reducing its flux to the Earth's surface, and are thus capable of reducing the heating due to greenhouse gases (for example, sulphate). Other components, such as elemental carbon, have a continuous absorbing

spectrum that extends to IR, and can contribute to the heating effect. The ability of the atmospheric aerosol to influence the way solar radiation is transmitted through the atmosphere has relevant consequences in terms of radiation budget and thus in terms of climate change.

Figure 1.7 represents mean global radiative forcing for year 2011 starting from a pre-industrial situation of 1750 (IPCC, 2013) and aggregated uncertainties for the main drivers of climate change. Values are global average radiative forcing (RF) partitioned according to the emitted compounds or processes that result in a combination of drivers. The best estimates of the net radiative forcing are shown as black diamonds with corresponding uncertainty intervals; the numerical values are provided on the right of the figure, together with the confidence level in the net forcing (VH-very high, H-high, L-low, VL-very low). Aerosols result to have a "cooling" effect on climate, by scattering sunlight and by leading to smaller but more numerous cloud droplets, which makes clouds brighter and extends their lifetimes (IPCC, 2007; IPCC, 2013). However, the net effect of all contributes on climate is positive in agreement with the trend of atmospheric temperature observed in the troposphere. The net effect of aerosol, which includes cloud adjustments due to aerosols, is negative (-0.9 W m^{-2}, medium confidence) and it is a balance of positive forcing mainly due to "black carbon" absorption of solar radiation and a negative forcing of reflecting aerosol from most aerosols. Despite its importance for climate, atmospheric nucleation is poorly understood (Almeida *et al.*, 2013). There is high confidence that aerosols and their interactions with clouds have offset a substantial portion of global mean forcing from well-mixed greenhouse gases. They continue to contribute the largest uncertainty to the total RF estimate (IPCC, 2013). The forcing from stratospheric volcanic aerosols can have a large impact on the climate some years after volcanic eruptions. Several small eruptions have caused a radiative forcing of -0.11 W m^{-2} for the years 2008-2011, which is approximately twice as strong as during the years 1999-2002 (IPCC, 2013).

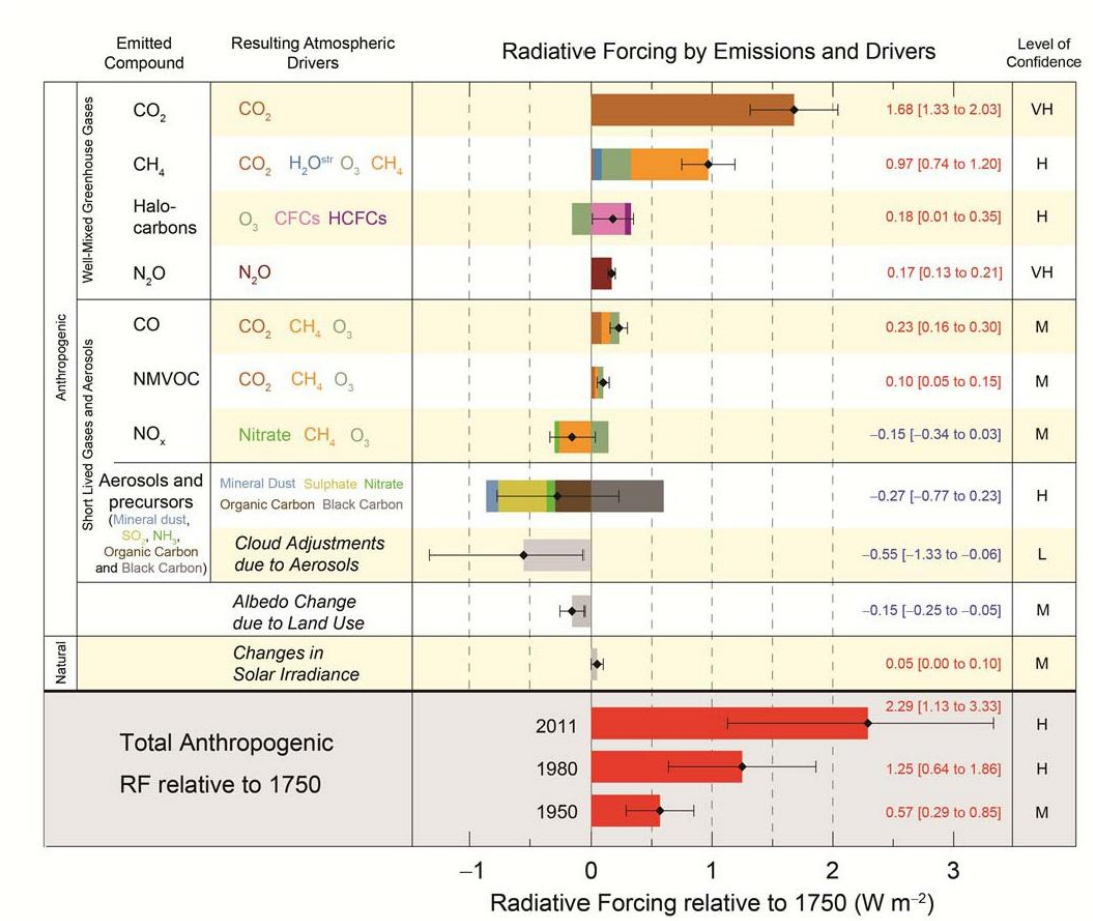

Figure 1.7 *Radiative forcing estimates in 2011 relative to 1750 and aggregate uncertainties for the main drivers of climate change. Values are global average radiative forcing (RF) partitioned according to the emitted compounds or processes that result in a combination of drivers. The best estimates of the net radiative forcing are shown as black diamonds with corresponding uncertainty intervals; the numerical values are provided on the right of the figure, together with the confidence level in the net forcing (VH-very high, H-high, L-low, VL-very low). Albedo forcing due to black carbon on snow and ice is included in the black carbon aerosol bar. Total anthropogenic radiative forcing is provided for three different years relative to 1750. The net effect of aerosol includes cloud adjustments due to aerosols is negative (-0.9 W m^{-2}, medium confidence) and it is a balance of positive forcing mainly due to "black carbon" absorption of solar radiation and a negative forcing of reflecting aerosol from most aerosols. There is high confidence that aerosols and their interactions with clouds have offset a substantial portion of global mean forcing from well-mixed greenhouse gases. They continue to contribute the largest uncertainty to the total RF estimate (IPCC, 2013. Figure 5 from Approved Summary for Policymakers).*

PM deposition exerts a significant influence on aquatic and terrestrial ecosystems. Deposition of acid pollutants such as sulphuric acid contributes to soil acidification with adverse effects on forests and crop cultivation and on the economy. Enhanced rates of nitrates deposition, instead, contributes to eutrophication of aquatic ecosystems, causing a negative impact on the life of aquatic animals.

The relationship between ecosystems and particulate depends on size, origin and chemical composition of particles; the effects of acid rains strongly depend on soil composition.

Deposition of particulate matter on plants can have direct effects if it resides long time on leaves or indirect effects in the case in which it is deposited to soil, where it can be absorbed by roots. When particulate permeate in soil spread by dry and wet depositions, the environmental impact is increased as chemical composition is modified by deposition.

Acid rains can damage forests and slow their growth strongly modifying the acidity of the soil, ruining leaves, solving nutritive substances and releasing toxic substances for plants (e.g., aluminium, easily absorbed by plants). When pH of soil is reduced, nutritive substances such as potassium, calcium and magnesium are exchanged with H^+ and are washed. Soil has a natural ability to neutralize acidity, on the basis of chemical composition and of rocky underlayer (US EPA, 2012).

Acid components in soil can penetrate deep into it and reach aquifers, rivers and lakes, adding to the direct effect of precipitation. Rivers and lakes completely acidify when both water and soil are no more able to neutralize the acid component: pH can be reduced from normal values of 6-8 units to 2-4 units. In acidified lakes elevated concentrations of Al^{3+} in solution are normally found. Aluminum comes from washing of rocks by H^+: in neutral pH conditions aluminum ions are blocked into rocks thanks to their reduced solubility. Acid pH and aluminum released by soil into waters are extremely dangerous to aquatic ecosystems, and in particular for ichthyic species (US EPA, 2012).

Materials exposed to air and atmospheric agents are naturally subject to degradation processes due to the effects of heat, humidity, oxidative capacities of the atmosphere and presence of microorganisms. The presence of aggressive pollutants can speed up already existing degrading processes and activate new ones. The main pollutants responsible for such acceleration are SO_x, NO_x, CO_2, O_3 and derivatives, and PM_x (Vandini *et al.*, 2000). Acid aerosol can attack cultural heritage and construction materials, altering their chemical composition.

The effects of PM on human health have been widely studied in the last twenty years and include asthma, lung cancer and cardiovascular issues. An important relationship has been found between current PM_{10} concentration in ambient air and the number of hospitalizations and deaths due to respiratory and cardiovascular diseases (Pope *et al.*, 1995; Dockery and Pope, 1996). The threat of atmospheric particles to health depends on their size, shape, and chemical composition. In particular, researches demonstrated that the most important parameter determining the toxicity of particles is its size, as it is correlated to the ability of penetration into the respiratory system: while PM_{10} is able to

penetrate in the bronchi, $PM_{2.5}$ can reach the lungs and nanoparticles are able to pass through the lungs and enter the circulatory system (Dockery and Stone, 2007; Pérez *et al.*, 2009).

In fact, inhalation constitutes the main exposition pathway to particulate. For this reason, a concentration limit under which there is no adverse effect on health does not exist (WHO, 2002).

Human respiratory system acts a "filter" against foreign bodies: before reaching the lungs, particles have to pass through a series of natural barriers, as shown in Figure 1.8:

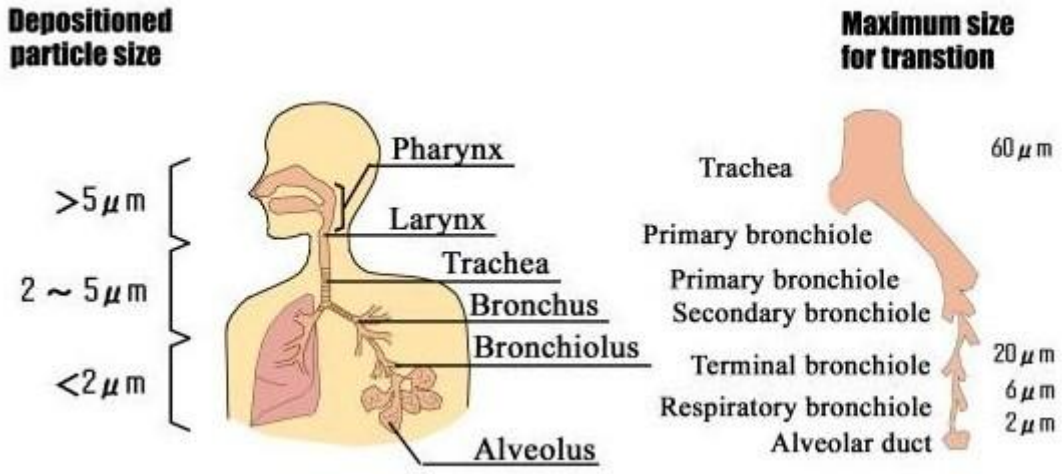

Figure 1.8 *Depositioned particle size in respiratory tract (http://www.tus.ac.jp/rist/lab/introduction/2research-centers/906.html).*

Particles having sizes higher than 1 μm are easily intercepted and deposited in nose and throat, from where are then thrown out; those having size in the range 1 μm – 100 nm can deposit in bronchioles, and then be carried into the throat and thrown out in about two hours.

Ultrafine particulate is the most dangerous as it can reach alveoli and be transported by circulatory system to different organs of respiratory system. It is removed in a slower and less complete way: it can escape phagocytosis of macrophages of pulmonary alveoli and can reach lymphatic system, epithelial tissues and pulmonary pits causing wounds, inflammations and preventing gaseous exchanges with blood. Moreover, due to the particular surface structure, particles can adsorb carcinogenic chemical substances, toxic or reactive substances that are deposited on cells with which they interact (Oberdörster, 2000).

The specialized cancer agency of the World Health Organization (WHO), the International Agency for Research on Cancer (IARC), recently announced that it has classified outdoor air as carcinogenic to humans (IARC, 2013). Particulate matter, a major component of air pollution, was evaluated separately and was also classified as carcinogenic to humans (IARC, 2013). The IARC evaluation showed an increasing risk of lung cancer with increasing levels of exposure to outdoor

air pollution and particulate matter.

Anenberg *et al.* (2010) published an estimate of the global health effects of air pollution based on a single atmospheric model. More recently, Silva *et al.* (2013) improved these calculations by using results from a range of atmospheric different models—six in all—rather than relying on just one. They concluded that 2.1 million deaths occur worldwide each year as a direct result of fine particulate matter.

The map of Figure 1.9 shows the model estimate of the average number of deaths per 1,000 square kilometers (386 square miles) per year due to air pollution. The researchers used the difference in pollution levels between 1850 and 2000 as a measure of human-caused air pollution. Dark brown areas have more premature deaths than light brown areas. Blue areas have experienced an improvement in air quality relative to 1850 and a decline in premature deaths. Fine particulate matter takes an especially large toll in eastern China, northern India, and Europe—all areas where urbanization has added considerable quantities of $PM_{2.5}$ to the atmosphere since the start of the Industrial Revolution. A few areas—such as the southeastern United States—saw $PM_{2.5}$ concentrations decline relative to pre-industrial levels (shown in blue). In the southeastern United States, the decrease in $PM_{2.5}$ is likely related to a decline in local biomass burning that has occurred over the last 160 years.

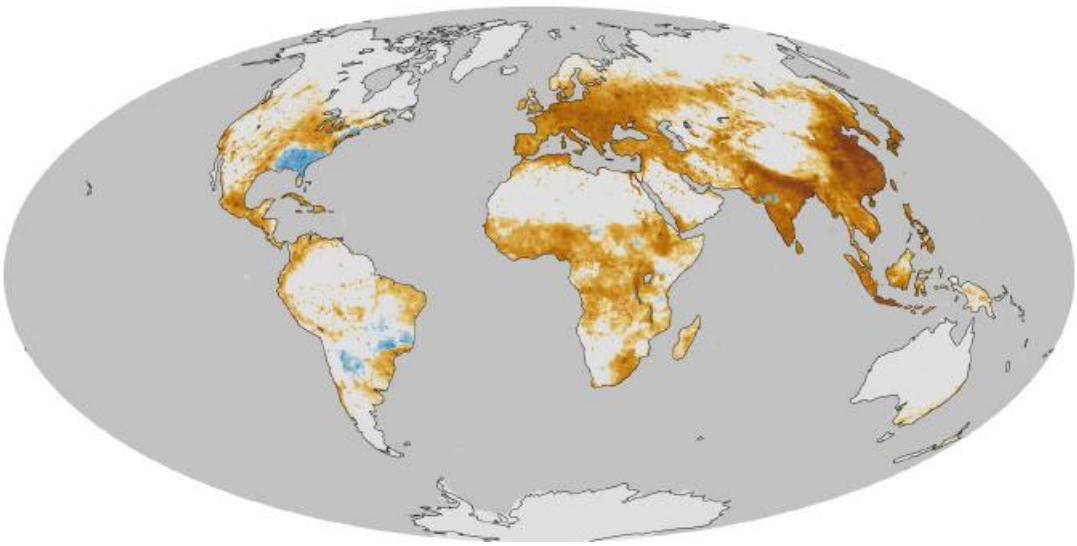

Figure 1.9 *Model estimate of the average number of deaths per 1000 square kilometers per year due to air pollution. The researchers used the difference in pollution levels between 1850 and 2000 as a measure of human-caused air pollution. Dark brown areas have more premature deaths than light brown areas. Blue areas have experienced an improvement in air quality relative to 1850 and a decline in premature deaths.* (http://earthobservatory.nasa.gov/IOTD/view.php?id=82087&src=eoa-iotd)

Some metals such as Fe, Cu and Mn in contact with pulmonary tissues can produce chemical reactions adverse on human health (Fenton reactions) (Harrison *et al.*, 2001). Moreover, metals can undergo oxidation-reduction reactions or act as catalysts of chemical reactions, forming free

radicals such as OH· radical, well-known for its inflammatory capabilities (Harrison *et al.*, 2000).

Ultrafine particles are also supposed to directly interact with central nervous system, being deposited on nasal mucous membrane and diffused through olfactory nerve to the brain: this can lead to adverse neurotoxic effects (Oberdörster *et al.*, 2004).

1.1.4 Chemical composition

Particulate matter is extremely complex in terms of size and formation mechanisms and for this reason is extremely heterogeneous also from the chemical point of view. Emission and formation processes affect not only the size distribution of particles, but also their chemical composition (Raes *et al.*, 2000). Figure 1.10 reports a schematic representation of the main mechanisms of formation of particles of atmospheric particles together with their corresponding chemical components.

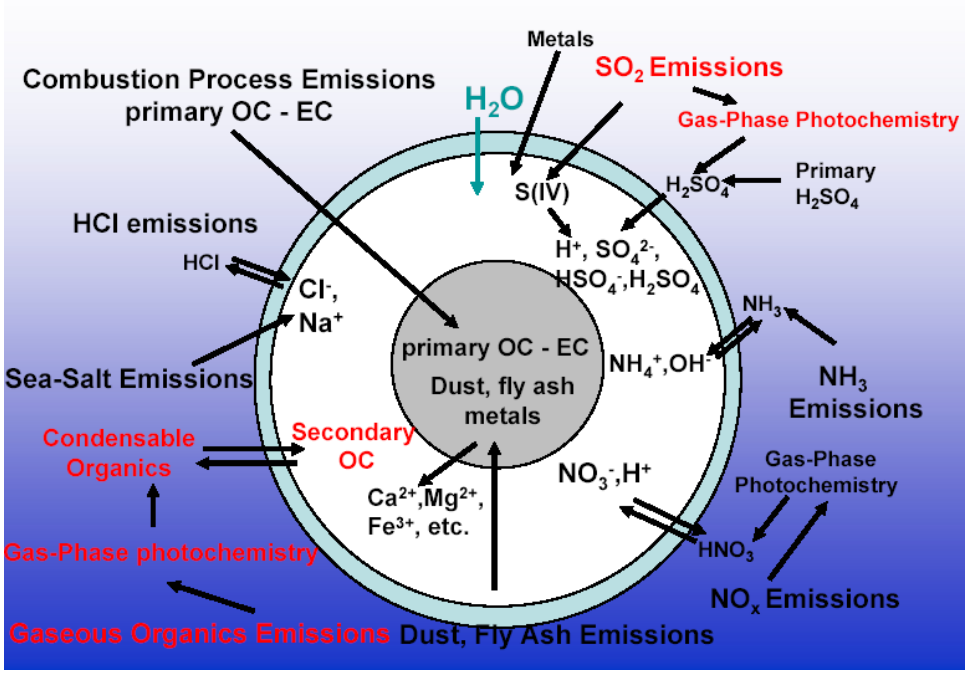

Figure 1.10 *Chemical composition of atmospheric aerosol (elaboration of the scheme of Seinfeld, Brice Temine, Department of Chemistry, UCC http://crac.ucc.ie/tour/Brice1.pdf)*

During recent years, substantial improvements have been carried out in the chemical characterization and identification of the main atmospheric aerosol components (Viana *et al.*, 2008). All the individual inorganic species, typically representing more than 1% of the total PM mass, can be easily determined and their main sources identified: crustal elements (silicon, aluminium, calcium, carbonate), sea-salt aerosol (sodium chloride), inorganic secondary species (nitrate, sulphate, ammonium), primary anthropogenic species (elemental carbon).

Much more complex is the situation for organic compounds, as this class constitutes a relevant fraction of PM mass (20-60%) but includes a wide variety of individual species, each one at very low concentration levels. Organic matter can be measured as a whole, but only a small part of the species that constitute this group can be determined individually; for this reason the monitoring of organic species in PM is generally addressed only to harmful (toxic and carcinogenic) compounds or to specific species that can be considered tracers of specific PM emission sources.

Chemical components constituting PM are not homogeneously distributed on all size fractions, but tend to accumulate in specific intervals, as a function of the source and the corresponding formation mechanism (Raes *et al.*, 2000).

Generally speaking, sulphates, ammonium, hydrogen ions, elemental carbon, the organic component and trace elements are mainly present in the fine fraction, while crustal (calcium, aluminium, silicon, magnesium and iron) and biological material (spores, pollen, organic fragments) are in the coarse fraction (Chiari *et al.*, 2004; Hueglin *et al.*, 2004; Moreno *et al.*, 2004).

Sulphates, nitrates and ammonium are among the most abundant components in PM. In gaseous phase sulphur dioxide and nitrogen dioxide react with OH· radical producing sulphuric and nitric acid (Finlayson-Pitts and Pitts, 1999). As of Figure 1.11, sulphuric acid then reacts with ammonia and form ammonium sulphate, while HNO_3 is neutralized by reaction with calcium carbonate of crustal origin or by substitution with marine NaCl.

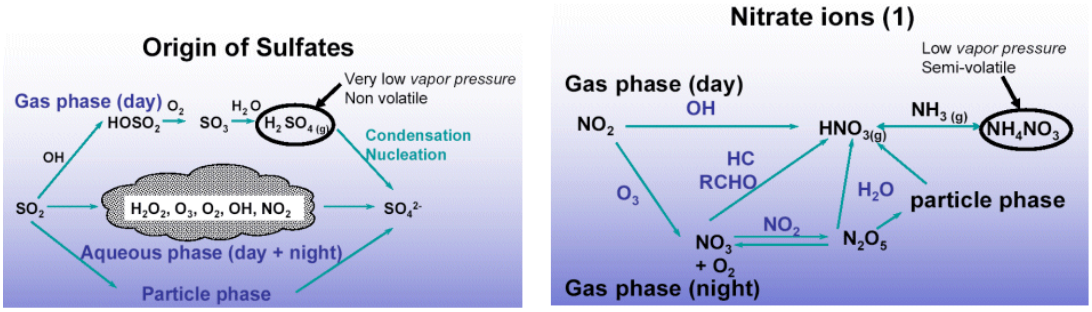

Figure 1.11 *Formation processes of nitrates and sulfates (Brice Temine, Department of Chemistry UCC, http://crac.ucc.ie/tour/Brice1.pdf)*

Neutralization by ammonia is not always complete: in strongly man-made environments a sub-stoichiometric concentration of ammonia is often observed, which determines a typical acid character of PM. Sometimes acidity can be more than neutralized, such as in Saharan Dust, due to the typically basic composition of minerals that form this natural aerosol.

Nitric acid is more volatile and as a consequence significant concentrations are in form of gas, while sulfuric acid has a very low vapor pressure in environmental conditions and exist in form of particles in aerosol phase (Hewitt, 2001).

The carbonaceous fraction of aerosol is formed by elemental carbon (or black carbon), organic molecules and carbonates (about 5% as estimated by Fermo *et al.*, 2006). These compounds are present in elevated amounts in atmospheric dusts, especially of anthropogenic origin. Carbonates are typically compounds of crustal origin.

Researches carried on urban and rural aerosol show that aerosol of the shortest size is mainly constituted by carbonaceous material (Putaud *et al.*, 2004). A considerable fraction of EC and OC (organic carbon) comes from combustion not only through fossil fuels, but also by forest fires that affect on planetary scales extended surfaces of forests (equatorial band, boreal forests, Mediterranean area). EC are present in amorphous or crystalline form and is the component of atmospheric aerosol which can mostly absorb solar radiation. It is also responsible of the notable reduction of visibility in industrial districts. Concentrations are extremely variable depending on the locations and seasons: in rural areas it is usually in the range 0.2-2 $\mu g\ m^{-3}$, whereas in urban areas its range is 1.5-20 $\mu g\ m^{-3}$. OC can be directly emitted to the atmosphere both as primary OC, or formed by condensation and/or oxidation of low volatility products by photo-oxidation of hydrocarbons (secondary OC). OC derives mostly from oxidation of combustion products, such as VOCs (Volatile Organic Compounds) and their successive condensation, dissolution in aqueous phase, adsorption (mainly on EC particles) or absorption (Seigneur, 2001). The organic fraction in urban and rural aerosol is a complex mixture of organic compounds (Jacobson *et al.*, 2000; Baltensperger *et al.*, 2005). Tropospheric particulate contains a significant and variable amount of organic material (10-70% in mass of fine particulate depending on the location), which has an important impact of physical and chemical properties of aerosol (McFiggans *et al.*, 2005). OC represent 90 to 97% of total carbon present in the fine fraction in rural areas, while the remaining is attributed to elemental carbon (Tagliavini *et al.*, 2000). PAHs (Polycyclic Aromatic Hydrocarbons), a class of compounds notably toxic and carcinogenic, are among the minority of carbonaceous fraction. They are formed by incomplete combustion of organic substance (coal, oil, wood, gasoline). PAHs, adsorbed on the surface of particles generated by combustion, are released in atmosphere together with other pollutants (nitrates, sulfates, ozone, PAN and radicals). In these conditions PAHs are subject of chemical transformations that can lead to degradation and formation of more polar compounds. PAHs can react with nitrogen dioxide to form nitro-PAHs that can be oxidized by ozone or photo-degraded and oxidized to quinons (US EPA, 1997).

Metals and other elements are present in the aerosol to low levels of concentration and represent a reduced of the mass of PM (2-3 %). Some elements are considered “tracers” of the sources by which are emitted (Mitra *et al*., 2002; Tositti and Sandrini, 2007), such as those shown in Table 1.2:

Tracer	Source
Al, Fe, Si, K, Mn	Rocks, soil
Na, Cl	Marine aerosol
Br, Pb, Ba	Vehicular traffic
V, Ni	Fuel oil
Se, As, Cr, Co, Cu	Coal combustion
Zn, Sb, Cu, Cd, Hg	Waste incinerator

Table 1.2 *Trace elements and sources (table elaborated by Mitra et al., 2002).*

Lead, zinc, bromine, nickel, vanadium, potassium and sulfur are mainly in the fine fraction of particulate, while sodium, iron, chromium, silicon, aluminum and magnesium are in the fine and coarse fraction (Ariola *et al.*, 2002). Figure 1.12 reports yearly emission fluxes of some trace elements particularly relevant from the environmental and toxicological point of view and the estimates for global cumulative sources. The comparison between the two kinds of sources, together with the fact that in the atmosphere metals and non-metals (with few exceptions) travel attached to particulate or in crystalline matrices show how these species are present everywhere and how a unique identification of the emission sources can be problematic (Pacyna and Pacyna, 2001).

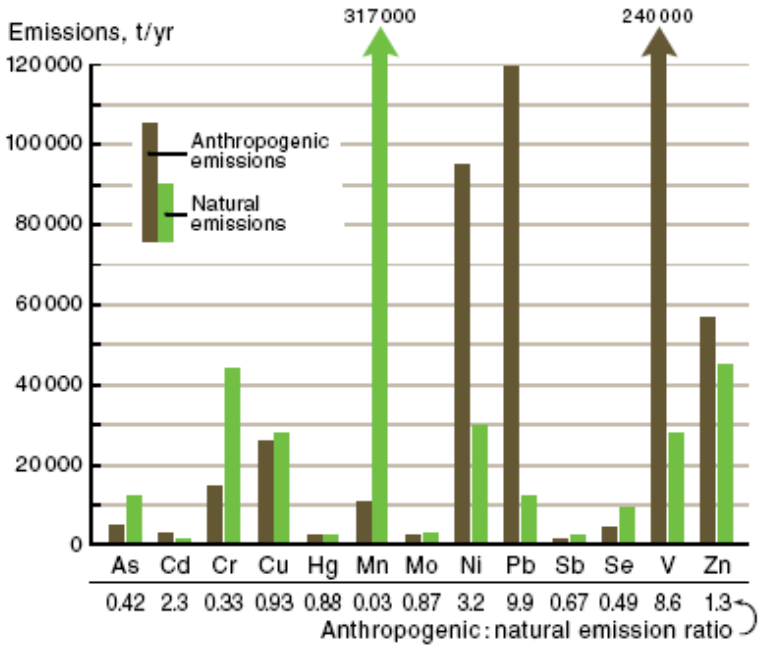

Figure 1.12 *Global estimated anthropogenic emissions of metals compared to estimated natural sources (Nriagu and Pacyna, 1989).*

1.2 Environmental radiotracers

Natural and artificial, radioactive, water-soluble, aerosol-borne tracers are an ideal tool to study atmospheric transport processes. The source distribution of these elements is relatively well known, they are removed from the atmosphere only by radioactive decay as well as by wet and dry deposition, and many observations exist to be compared with transport model results. Radioactive tracers in the atmosphere may be divided into three groups (Junge, 1963):

I. Natural radioactivity from emissions out of the Earth's surface, that include the three families of natural radioactive decay (^{238}U, ^{235}U and ^{232}Th) (Table 1.3) and some primordial radionuclides of which the most abundant is ^{40}K (0.0119% of the natural isotopic mixture of elemental potassium);

II. Natural radioactivity produced by cosmic radiation (bombardment of stable nuclides by cosmic rays);

III. Artificial radioactivity produced by nuclear weapon tests.

Figure 1.13 reports a schematic view of the main radionuclides in the atmosphere:

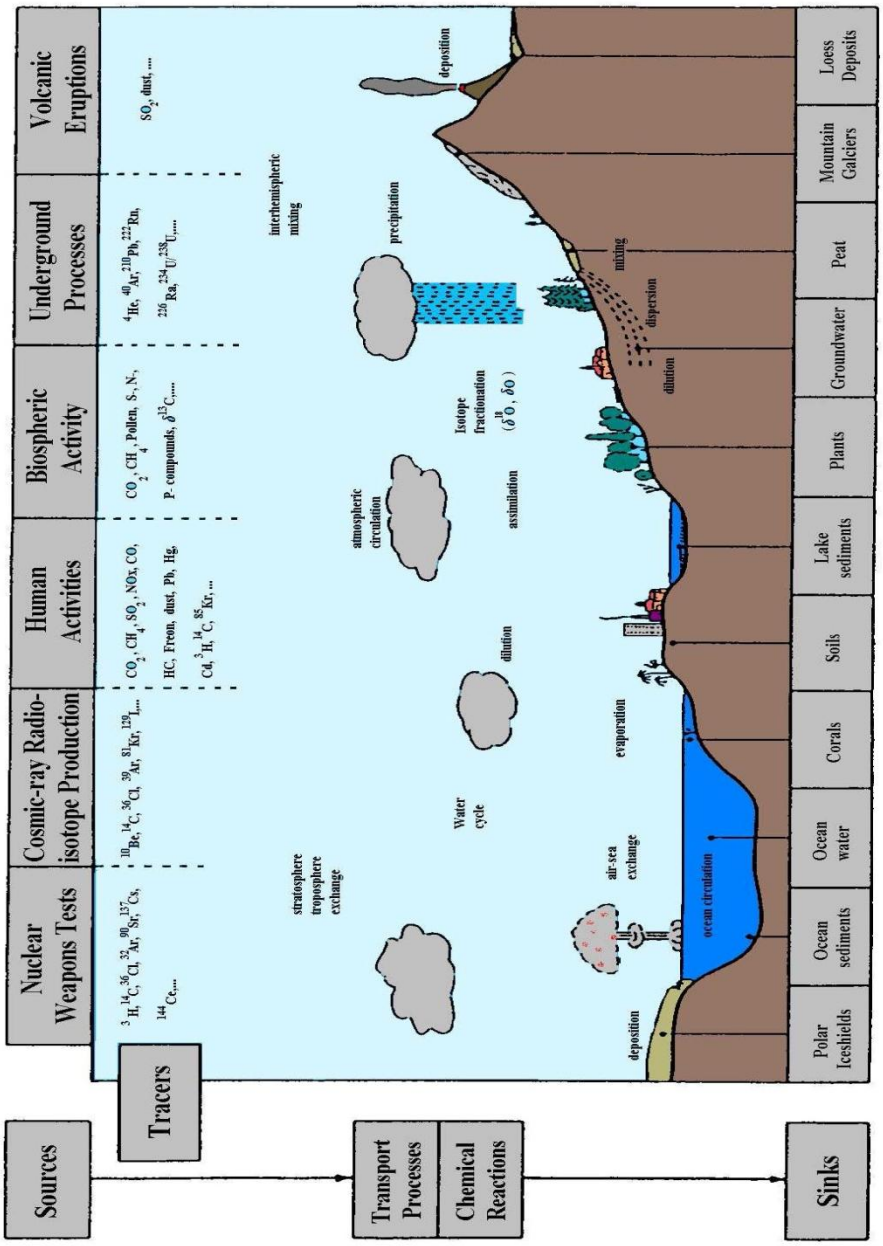

Figure 1.13 *Schematic view of the main radionuclides in the atmosphere.*

Radon isotopes are members of the natural decay series: the ^{238}U decay series (^{222}Rn, half-life 3.8 days), the ^{232}Th decay series (^{220}Rn, also called thoron, half-life 56 s) and the 235U series (^{219}Rn, also called actinon, half-life 3.9 s). Almost all radon in the atmosphere is produced in soils and rocks by radioactive decay of the respective precursor (Table 1.3), from which it is released and transported by diffusion. In atmospheric studies using radon isotopes, ^{222}Rn plays a dominant role, as its longer half-life facilitates a greater diffusive transport and an atmospheric concentration that is 100 times higher than that of ^{220}Rn. The atmospheric activity concentration of ^{219}Rn is relatively negligible.

Nuclide	Half-life	Radiation
Uranium series		
^{226}Ra	1,622 years	α,γ
^{222}Rn	3.8 days	α,γ
^{218}Po	3.05 min	α
^{214}Pb	26.8 min	β,γ
^{218}At	1.5–2.0 s	α
^{214}Bi	19.7 min	β,α
^{214}Po	1.64×10^{-4} s	α,γ
^{210}Tl	1.3 min	β,γ
^{210}Pb	22 years	β,γ
^{210}Bi	5.0 days	β,α
^{210}Po	138 days	α,γ
^{206}Tl	4.2 min	β
^{206}Pb	Stable	
Thorium series		
^{224}Ra	3.64 days	α,γ
^{220}Rn	55.6 s	α,γ
^{216}Po	0.145 s	α
^{212}Pb	10.6 h	β,γ
^{212}Bi	60.5 min	β,α,γ
^{212}Po	3.04×10^{-7} s	α
^{208}Tl	3.1 min	β,γ
^{208}Pb	Stable	
Actinium series		
^{223}Ra	11.4 days	α,γ
^{219}Rn	4.0 s	α,γ
^{215}Po	1.77×10^{-3} s	α,β
^{211}Pb	36.1 min	β,γ
^{215}At	$\sim 10^{-4}$ s	α
^{211}Bi	2.16 min	α,β,γ
^{211}Po	0.52 s	α,γ
^{207}Tl	4.79 min	β,γ
^{207}Pb	Stable	

Table 1.3 *Partial decay series starting from Radium isotopes in the three main radioactive decay series (Sykora and Froehlich, 2010).*

About 99% of ^{222}Rn in the atmosphere originates in soils and rocks, where it is produced by radioactive decay of its parent nuclide ^{226}Ra. Once released to the atmosphere, it remains there until its radioactive decay. As it is a chemically inert gas, physical or chemical processes cannot remove it from the atmosphere. Therefore, it is suitable to trace atmospheric mass transport and to identify air masses derived from the continental boundary layer. Furthermore, atmospheric ^{222}Rn is the source of its decay products (^{214}Bi, ^{214}Pb, ^{210}Pb, ^{210}Bi, and ^{210}Po) in the atmosphere, which are also suitable to identify air masses from the continental boundary layer.

In particular, atmospheric ^{210}Pb is mainly produced within the atmosphere by decay of ^{222}Rn; its direct precursor is ^{214}Po (Table 1.3). The produced ^{210}Pb atoms are attached to aerosols in the diameter size range between 0.1 and 0.5 μm (accumulation mode) (Papastefanou and Ioannidou,

1995; Winkler *et al.*, 1998; Gaffney *et al.*, 2004; Ioannidou *et al.*, 2005). For particles of this size, precipitation is the main mechanism of removal from the atmosphere. ^{210}Pb is a minor constituent of this aerosol type (one ^{210}Pb-containing aerosol particle in about 10^4 aerosol particles) and, thus, it is useful to trace their atmospheric transport and to determine their atmospheric residence time (Lambert *et al.*, 1990; Koch *et al.*, 1996). Figure 1.14 shows an example of the spatial distribution of ^{210}Pb in air over the Pacific. The sampling sites belong to the network of the SEAREX (sea/air exchange). Generally, an increase of the concentration with latitude north is observed, and it is correlated with the size of the land-mass upwind from the sampling sites (Turekian and Graustein, 2003).

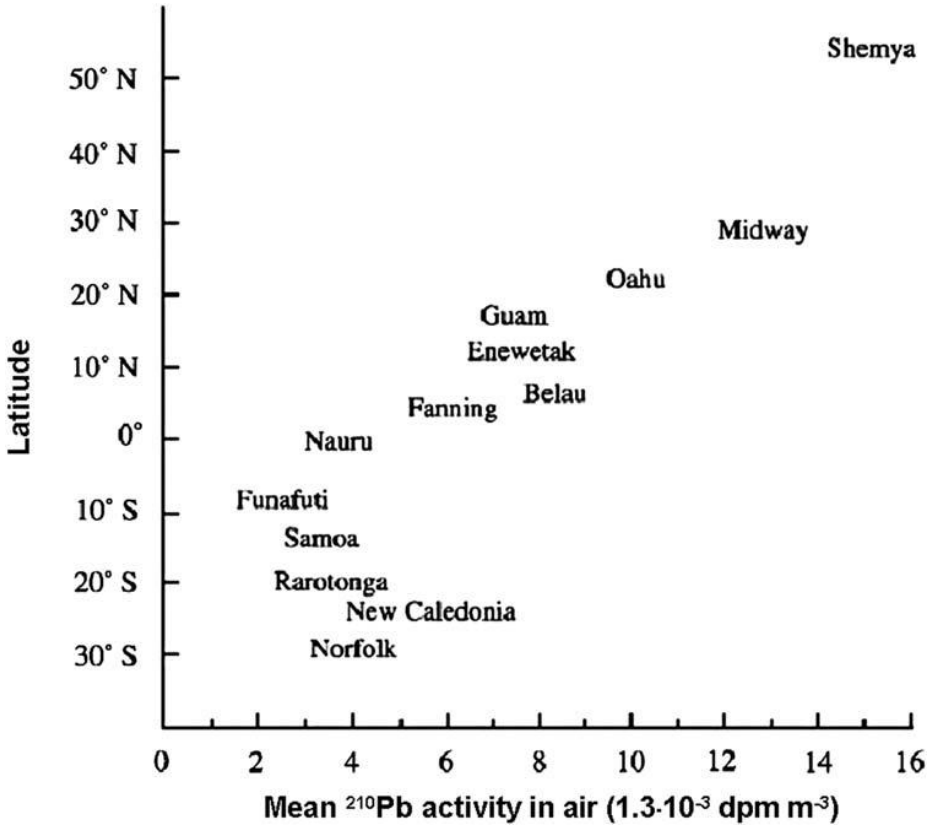

Figure 1.14 *Distribution of ^{210}Pb in air at stations of the SEAREX network. The site name is centered over the point representing the data. The length of the name approximates to the error of the mean. (from Turekian and Graustein, 2003; Sykora and Froehlich, 2010).*

Cosmogenic radionuclides are produced by the interaction of cosmic rays (composed of protons of very high energy, of galactic or solar origin) with the atoms that form the atmosphere, and their rate of production depends primarily on the cosmic-ray particle flux (Masarik, 2010), but is also linked to the Earth's magnetic field (Turekian and Graustein, 2003). Cosmic radiation penetrates all of the space, the source being primarily outside our solar system. The primary cosmic radiation consists of very high-energy heavy particles, photons and muons. The interactions of cosmic-ray particles with the

Earth's atmosphere and the Earth's surface produce a cascade of secondary particles and a variety of cosmogenic nuclides. The concentration of cosmogenic nuclides is the result of the interplay between four processes: production, decay, transport and deposition. Examples of cosmogenic nuclides are radioactive isotopes of the elements beryllium, carbon, aluminum, chlorine, calcium, and iodine. Their lifetimes range from seconds to thousands and even millions of years, and some of the isotopes are stable.

Lal *et al.* (1958), Lal and Peters (1962, 1967), Masarik and Beer (1999) and Nagai *et al.* (2000) have published reviews on the production and distribution of cosmogenic radionuclides. Table 1.4 is a compilation of the cosmogenic radionuclides, of which ^{14}C, ^{3}H, ^{7}Be and ^{10}Be are the most frequently used in atmospheric studies.

Nuclide	Half-life	Production rate (atoms $cm^{-2} s^{-1}$)		Global inventory
		Troposphere	Total atmosphere	
^{3}He	Stable	6.7×10^{-2}	0.2	3.2×10^{3} t
^{10}Be	1.5×10^{6} years	1.5×10^{-2}	4.5×10^{-2}	260 t
^{26}Al	7.1×10^{5} years	3.8×10^{-5}	1.4×10^{-4}	1.1 t
^{81}Kr	2.3×10^{5} years	5.2×10^{-7}	1.2×10^{-5}	8.5 kg
^{36}Cl	3.0×10^{5} years	4×10^{-4}	1.1×10^{-3}	15 t
^{14}C	5,730 years	1.1	2.5	75 t
^{39}Ar	268 years	4.5×10^{-3}	1.3×10^{-2}	52 kg
^{32}Si	140 years	5.4×10^{-5}	1.6×10^{-4}	0.3 kg
^{3}H	12.36 years	8.4×10^{-2}	0.25	3.5 kg
^{22}Na	2.6 years	2.4×10^{-5}	8.6×10^{-5}	1.9 g
^{35}S	87 days	4.9×10^{-4}	1.4×10^{-3}	4.5 g
^{7}Be	53 days	2.7×10^{-2}	8.1×10^{-2}	3.2 g
^{37}Ar	35 days	2.8×10^{-4}	8.3×10^{-4}	1.1 g
^{33}P	25.3 days	2.2×10^{-4}	6.8×10^{-4}	0.6 g
^{32}P	14.3 days	2.7×10^{-4}	8.1×10^{-4}	0.4 g

Table 1.4 *Production rates and global inventory of cosmogenic radionuclides (from Turekian and Graustein, 2003; Sykora and Froehlich, 2010).*

The decay of ^{7}Be (half-life 53 days) to ^{7}Li by electron capture is associated with the emission of a 477.6 keV gamma ray that facilitates measurement of its activity by low-level germanium detector. Lal and Peters (1962, 1967) have shown that the ^{7}Be production rate decreases with atmospheric depth (Figure 1.13). Most ^{7}Be resides in the stratosphere. Its production rate reaches a maximum in the upper stratosphere at about 20 km (Masarik and Beer, 1999) and decreases with decreasing altitude down to ground level due to Stratosphere-to-Troposhere Exchange (STE) (e.g., Stohl *et al.*, 2000). The relatively high production rates of ^{7}Be in the upper troposphere, combined with its transport from the lower stratosphere to the upper troposphere, normally maintain a steep vertical concentration gradient between the upper and lower troposphere (Feely *et al.*, 1989).

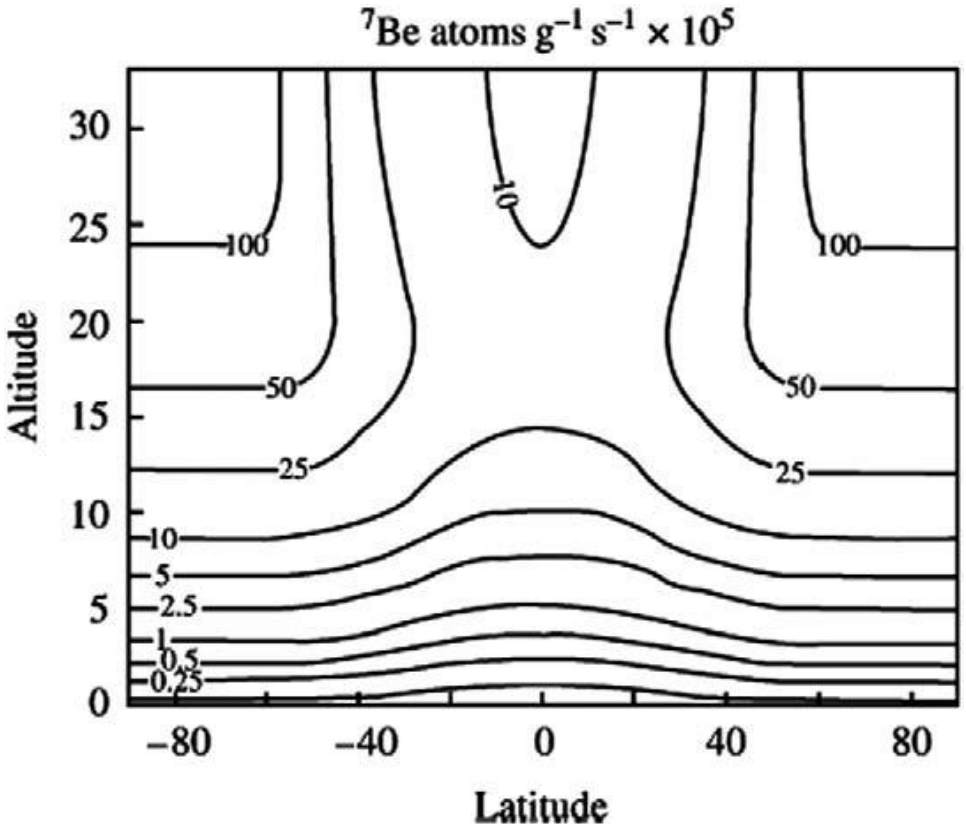

Figure 1.15 *Production of ^{7}Be in the atmosphere as a function of latitude and altitude (from Turekian and Graustein, 2003; Sykora and Froehlich, 2010).*

The source functions of cosmogenic radionuclides depend mainly on latitude and altitude (Benioff, 1956; Lal *et al*., 1958; Lal and Peters, 1962; O'Brien, 1979; Masarik and Beer, 1999). Considering ^{7}Be, only 33% is produced in the troposphere, particularly in the upper troposphere, while the rest is produced in the stratosphere (Figure 1.15).

Natural radionuclides from terrestrial and upper atmospheric sources (^{222}Rn, ^{220}Rn, ^{212}Pb, ^{210}Pb, ^{7}Be, ^{10}Be, etc.) and of anthropogenic origin are widely used as tracers to examine atmospheric processes relevant to air quality and climate and to validate atmospheric models simulating transport, transformation and removal processes of gases and aerosols. The validation and calibration of such models require accurate experimental data on source functions and temporal and spatial variation of relevant radionuclides. Yet, the effective use of such data is still limited, especially due to the insufficient accuracy of radionuclide source functions.

Measurements at different locations carried out by, e.g., Papastefanou and Ioannidou (1995), Takayuki *et al.* (1996), El-Hussein *et al.* (2001) and Gerasopoulos *et al.* (2001) have shown that the ^{7}Be concentration in air at ground level depends on latitude, altitude and on local meteorological conditions. At middle latitudes, ^{7}Be values are generally higher than at high latitudes (Feely *et al.*, 1989; Baeza *et al.*, 1996; Todorovic *et al.*, 1999; Al-Azmi *et al.*, 2001; Aldahan *et al.*, 2001). In

Bratislava (latitude about 48°N), measurements from 2001 to 2005 yielded a monthly average ^{7}Be activity concentration in ground air of 2.85 mBq m^{-3} (Sykora *et al.*, 2005); during the period from 1981 to 1995, the monthly average was 3.12 mBq m^{-3} at nearly the same location (Durana *et al.*, 1996). These values are remarkably lower than the value of 5.06 mBq m^{-3} derived from daily measurements during the period 1982 to 2002 in Palermo, Italy (39°N), and the value of 5.21 mBq m^{-3} obtained in Kuwait (29°N) during 1994–1998 by Al-Azmi *et al.* (2001). The larger values at the latter two stations, which are located close to the sea, may be attributed to enhanced vertical air mass exchange at coastal stations compared to inland stations such as Bratislava. Figure 1.16 illustrates the latitudinal effect of ^{7}Be measured at various ground-level stations. The global average tropospheric ^{7}Be is 12.5 mBq m^{-3} (UNSCEAR, 2000).

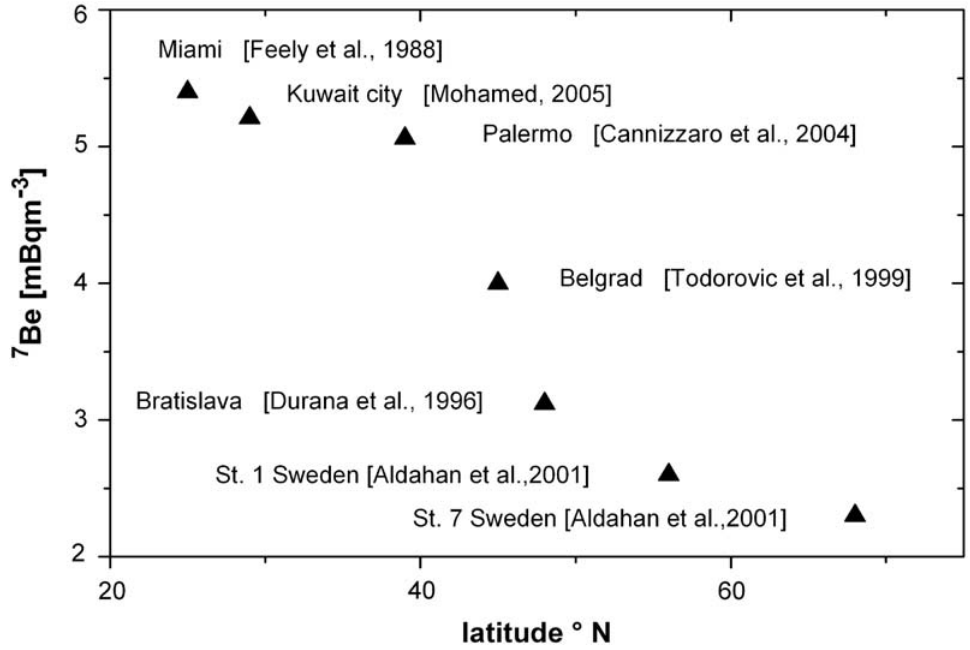

Figure 1.16 *Annual ^{7}Be concentrations at various locations as function of latitude (Sykora and Froehlich, 2010).*

In Figure 1.17 a compilation of data of ^{7}Be in surface air in Northern Hemisphere is represented (Kulan *et al.*, 2006). Higher concentrations are found at middle latitudes and lower concentrations are towards the Pole and the Equator. The production rate of ^{7}Be is highest in the stratospheric air at high latitudes (Beer *et al.*, 2012). Mixing of this stratospheric air into the upper troposphere occurs along the tropopause discontinuity in mid latitude regions. Subsequently, convective mixing within the troposphere will bring ^{7}Be rich air masses from upper tropospheric or lower stratospheric origin into the planetary boundary layer and to the Earth's surface. Stohl *et al.* (2003) highlighted the importance of events of rapid deep stratospheric intrusions. As one of the preferred destinations of such intrusions they identified the Mediterranean region. This might explain why the highest

concentrations of ^{7}Be in ground level air shown in the N-S transect of Figure 1.17 were observed at latitudes around 35-40°N.

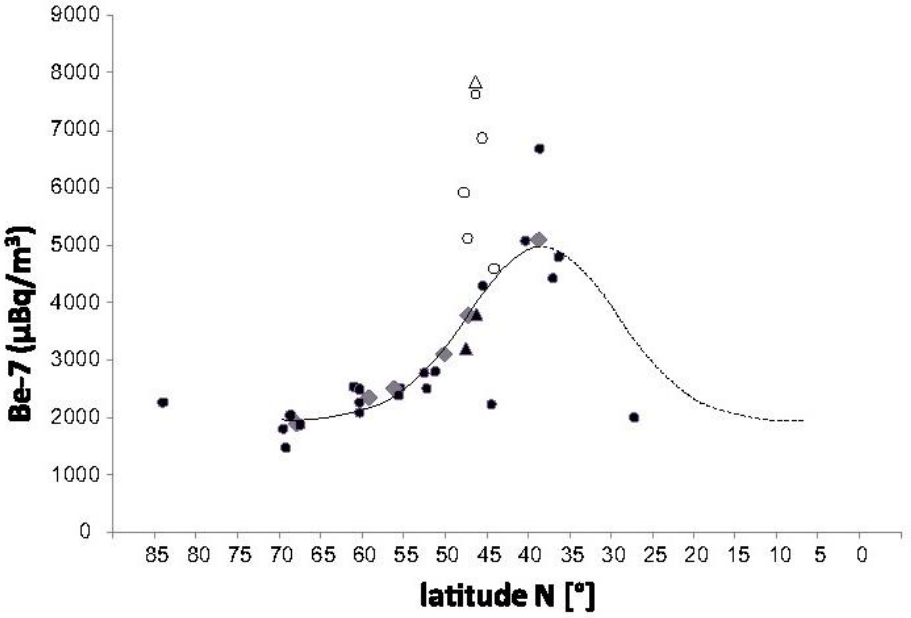

Figure 1.17 *Long term averages of ^{7}Be concentrations in ground level air for the northern hemisphere between 17°W and 30°E. Filled symbols represent data from sampling stations located within the atmospheric boundary layer. Open symbols show data from high altitude sites which lay typically above the ABL. Triangles correspond to data from this paper. Diamonds and the fitted lines (solid and stippled lines) are according to Kulan et al. (2006). Additional data points (circles) are from: Dutkiewicz and Husain (1985), Kolb (1992), El-Hussein et al. (2001), Gerasopoulos et al. (2001), Azahra et al. (2003), Ioannidou et al. (2005), Todorovic et al. (2005), Cristofanelli et al. (2006), Daish et al. (2006), Likuku (2006), Leppänen et al. (2010), Bourcier et al. (2011), Dueñas et al. (2011), Pham et al. (2011), Leppänen et al. (2012). Results from Steinmann et al. (2013) are represented as open circles (Jungfraujoch, Switzerland, average 2006-2011), filled triangles (average ratios of four other locations at ground level in Switzerland) (Steinmann et al., 2013).*

Like ^{210}Pb, also^{7}Be once produced is rapidly attached to submicron-sized particles (Papastefanou and Ioannidou, 1995; Winkler *et al.*, 1998; Gaffney *et al.*, 2004; Ioannidou *et al.*, 2005). As ^{7}Be and ^{210}Pb share the same Winkler fate of aerosol, useful information about transport, removal and residence time of aerosols in the atmosphere can be obtained from combined measurements of ^{7}Be and ^{210}Pb. ^{7}Be is produced in the stratosphere and upper troposphere, and ^{210}Pb in the lowermost metre of the atmosphere over continents and islands. While ^{7}Be is mixed downward, ^{210}Pb is mixed upward, but both are removed from the atmosphere by precipitation. Thus, changes in the ^{7}Be/^{210}Pb ratio in space and time reflect both vertical and horizontal transport in the atmosphere. Virtually, all

^{210}Pb is transported from the continent, which makes the ^{7}Be/^{210}Pb ratio an excellent indicator of continental sources of local aerosols: low values of the ratio due to high ^{210}Pb reflect high continental influence, while low values point to relative isolation from continental sources.

The pair ^{210}Pb and ^{7}Be is also useful to test global atmospheric models for wet and dry deposition (Liu *et al.*, 2001). Long-term data records of ^{210}Pb (Preiss *et al.*, 1996) and ^{7}Be (Feely *et al.*, 1989; Larsen and Sanderson, 1995) are available from worldwide networks and provide good constraints for model validation. ^{7}Be and ^{210}Pb have also been used to validate global numerical models describing other processes, such as transport of continental air over the oceans (Turekian *et al.*, 1989; Balkanski *et al.*, 1993), transport from the stratosphere (Rangarajan and Gopalakrishnan, 1970; Viezee and Singh, 1980; Sanak *et al.*, 1985; Dibb *et al.*, 1992, 1994; Rehfeld and Heimann, 1995) and subsidence in the troposphere (Feely *et al.*, 1989; Koch *et al.*, 1996).

The ratio ^{7}Be/^{210}Pb can also be used to determine the sources of chemical species in the lower free troposphere such as ozone and nitrate. Graustein and Turekian (1990) have correlated the ozone concentration with a function of ^{7}Be and ^{210}Pb measured at Izania, Tenerife, and found that the primary source of ozone in the lower free troposphere of this eastern Atlantic region was the upper troposphere.

Long-term records of monthly mean surface air concentration of ^{210}Pb, ^{7}Be and O_3 measured at New York City, USA (Lee, 2004), indicate that the summer maximum of ozone corresponds well with the summer minimum of ^{210}Pb and maximum of ^{7}Be. ^{7}Be and ozone concentrations measured during summer campaigns in free tropospheric air at Mt. Fuji, Japan, showed a clear correlation between ^{7}Be and ozone, which indicates transport from the lowermost stratosphere and uppermost troposphere. The ozone values at low ^{7}Be concentration represented instead a photochemical component of ozone produced in the troposphere. Based on these measurements, the ozone influx from the stratosphere has been estimated to be about 0.9-10^{11} molecules cm^{-2} s^{-1} (Lee, 2004).

In summary, the use of ^{7}Be and ^{210}Pb in order to trace tropospheric aerosol resides on their well-known properties:

- they have distinct and well known sources and sinks;
- they can be measured with accuracy without risks of contamination during the manipulation of the sample;
- they have a chemistry in the atmosphere which is easier than that of other stable substances transported by aerosol particles, and for this reason are able to give information on basic processes in which aerosol is involved.

1.3 Receptor modelling

Tools called **receptor models** are applied to obtain information on the sources of air pollutants from the measured airborne concentrations. Information about the identification of the sources of materials emitted into the air, the quantitative estimation of the emission rates of the pollutants, the understanding of the transport of the substances from the sources to downwind locations, and the knowledge of the physical and chemical transformation processes that can occur during that transport is needed to the management of air quality. The name receptor models or receptor-oriented models arises from the fact that these methods are focused on the behavior of the ambient environment at the point of impact as opposed to the source-oriented dispersion models that focus on the emissions, transport, dilution and transformations that occur beginning at the source and following the pollutants to the sampling or receptor sites. While source-oriented models are predictive models that may be applied both to PM and gaseous species and calculate ambient concentrations starting from source emissions and atmospheric dispersion models, receptor models are diagnostic models, which identify the sources and calculate their contribution starting from measured concentrations of PM mass and chemical compounds in the sampling site (receptor). The traditional source-oriented approach consists in solving dispersion model equations forward in time for given sources of pollutant (Astitha *et al.*, 2005). As a result, a time- and space-dependent concentration field C is obtained. In many practical applications, air pollution at a given receptor is of primary interest, and alternative receptor-oriented modeling can be a more effective approach (Astitha *et al.*, 2005). Air quality at the receptor is characterized by an integral of pollution concentration over the modelling domain and time of simulation. In the receptor-oriented approach, starting from backward trajectories (or puffs, when Lagrangian Particle Dispersion Models are used), an influence function C* is determined instead of concentration. The influence function calculated for a given receptor depends on meteorology and transformation of pollutant in the atmosphere, but it is independent of emission sources (Astitha *et al.*, 2005). The receptor-oriented approach is useful for emission control, planning locations of new emission sources, and assessing the contributions from different sources to air pollution in a given area.

The source-receptor relationship is an important concept in air quality modeling. It describes the sensitivity of a "receptor" element *y* to a "source" *x* (Seibert and Frank, 2004). Typically receptor models use the chemical composition data for airborne particulate matter samples and result in the identification of the pollution source types and in estimates of the contribution of each source type to the observed concentrations (Hopke and Thurston, 1984; Thurston and Spengler, 1985; Hopke, 2009). Some models have also been developed to identify the locations of the sources through the use of ensembles of air parcel back trajectories. In fact the chemical and physical composition of an

air mass is inherently related to its path through the atmosphere and in order to get the maximum information out of long term time series of composition measurements, data are often divided according to air mass history (Fleming *et al.*, 2012).

1.3.1 Back trajectories

Atmospheric composition measurements have been interpreted using wind speed and direction measurements as a marker for air mass history for many years, but this resulted in poor attribution of the sources. In meteorology, trajectories are defined as the paths of infinitesimally small particles (Dutton, 1986). The fluid particle, marked at a certain point in space at a given time, can be traced forward or backward in time along its trajectory. In trajectory models, this is done by integrating the trajectory equation $\Delta x_i = v_i \Delta t$ (where Δx is the position increment during a time step Δt resulting from the wind v; the index i runs from 1 to 3 and denotes the three dimensions of space), using mean (non-turbulent) horizontal and vertical winds from a meteorological model.

While forward trajectories describe where a particle will go, backward trajectories (or back trajectories) indicate where it came from. Therefore, they can be used to interpret measurements of atmospheric trace substances, in order to establish relationships between their sources and their receptors (Stohl, 1998). Large data-sets are often investigated using back trajectories, allowing statistical analyses to be made (e.g., Moody and Galloway, 1988; Brankov *et al.*, 1998; Eleftheriadis *et al.*, 2009; Tarasova *et al.*, 2009).

Inaccuracies in the input wind fields are the largest errors in trajectory calculations (Stohl, 1998). Other sources of errors are the interpolation of the wind velocity from grid points to actual trajectory positions (Rolph and Draxler, 1990; Doty and Perkey, 1993; Stohl *et al.*, 1996), and truncation errors which occur in the numerical solution of the trajectory equation (e.g., Walmsley and Mailhot, 1983; Seibert, 1993). Total trajectory position errors result from all the above sources, but are difficult to determine and normally unknown. In a survey of results from previous studies, Stohl (1998) suggested that average trajectory errors are on the order of 15-20% of the distance travelled after a few days. In critical flow situations errors up to 100% are also possible. The accuracy of an individual trajectory being limited by these errors, it is virtually impossible to describe transport phenomena in turbulent flows by calculating single trajectories. The limitations and uncertainties that apply to individual trajectories may, to some extent, be overcome by a statistical classification approach, aggregating a large number of trajectories over a long time period, since potential errors tend to average out; in particular, errors are reduced when daily trajectories are categorized according to the common path air parcels followed (Brankov *et al.*, 1998; Stohl, 1998).

1.3.2 Source-receptor models incorporating back trajectories

Using a model of atmospheric transport, the position of the air being sampled backward in time from the receptor site from various starting times throughout the sampling interval can be calculated. With back trajectories it is possible to examine source-receptor relationships and the timescales of long-range and local transport and its effect on the observed composition (Fleming *et al.*, 2012). As outlined in previous paragraph, many uncertainties and limitations apply to individual trajectories, but they are generally overcome when a large number of back trajectories is calculated and is grouped into the common paths followed by air parcels. In particular there are two major ways to visualize air quality data: the first one is cluster analysis where the data is split into a number of groups representing distinct fetch areas and atmospheric transport patterns. The second one is to produce a probability map which identifies areas around the receptor site that contribute to the pollution observed at the site. This is done using the trajectories in Residence Time Analysis (RTA) (Poirot and Wishinski, 1986; Poirot *et al.*, 2001), Areas of Influence Analysis (AIA) (Malm *et al.*, 1990), Quantitative Bias Trajectory Analysis (QTBA) (Keeler and Samson, 1989), Potential Source Contribution Function (PSCF) (Ashbaugh *et al.*, 1985), and Residence Time Weighted Concentrations (RTWC) (Stohl, 1996).

In Chapters 2 and 6, the PSCF receptor model, which is the most widely used of the trajectory ensemble methods, will be used; cluster analysis will instead be applied in Chapter 5. The two methods are briefly described in the following sections.

Cluster analysis of back trajectories

The application of clusters to back trajectories analysis was introduced by Moody (1986) and Moody and Galloway (1988), who recognised its ability to simultaneously account for variations in wind speed and direction (Harris and Kahl, 1990).

Cluster analysis is a categorization method used to separate the data in classes or clusters, such that objects in the same cluster are similar to each other and different from objects located in further clusters (Manly, 1994). Individual trajectories of an ensemble are grouped into a smaller number of clusters, and in this way the errors in the individual trajectories tend to average out. It has been demonstrated that clusters of back trajectories arriving at a specific location can serve as surrogates for different synoptic circulation patterns (Dorling *et al.*, 1992).

Clusters are groups with similar distributions: in the case of back trajectories, similar directions and lengths of a combination of trajectory pathways and composition. In general, trajectories are grouped by a statistical technique and then the concentrations of some atmospheric compounds at the receptor site are analysed for each trajectory classification to see whether each classification is

chemically distinct. Cluster analysis thus provides an objective means of grouping trajectories whilst giving information about the history of the air mass and the air pollution climatology of a site, helping to determine source-receptor relationships (Fleming *et al.*, 2012). However, it has been pointed out by, e.g., Stohl (1998) that in reality cluster analysis is not completely objective, since the selection of the clustering algorithm and the specification of the distance measure and of the number of clusters used is subjective. Anyway, the result of a cluster analysis is similar to a flow climatology, but cluster analysis is more objective and accounts for variations in transport speed and direction simultaneously (Stohl, 1998).

In cluster analysis, each data is treated as a point in an *n*-dimensions space. The coordinate axes of this space are defined by the measurements used to characterize the data (in the case of trajectories, latitude and longitude). The analysis defines the degree of similarity between the data measuring the distances between the points in space (Lavine, 2000). Similar data will be close to each other, while different data will be far away. The choice of the metric to be used for the distance depends on the kind of measured variables. Euclidean distances are commonly used for continuous variables, but in our case the great-circle distance, i.e., the shortest distance measured along the surface of the sphere, was chosen, since the computation of Euclidean distances with geographical coordinates as planar would lead to errors that might not be acceptable at high latitudes.

There are two differently types of clustering algorithms, hierarchical and non-hierarchical clustering:

- *Hierarchical clustering* partitions data following a series of steps either by grouping or by separating the objects one by one in each step. These algorithms do not construct a single partition with *k* clusters but deal with all values of *k* in the same run (Kaufman and Rousseeuw, 2005). All the classified objects are considered at each step of the hierarchical clustering and the process is determined by the construction of an agglomeration tree. The two closest clusters are merged in each step, starting the procedure with singleton clusters and ending with a single cluster that contains all the objects. This approach is commonly used when the number of clusters is not known. Examples of this clustering procedure are Ward's method[2], average-linkage [3](which calculates the distance between all pairs of points and the cluster) and centroid methods.
- *Non-hierarchical clustering* attempts to directly decompose the data set into a set of disjoint clusters by minimising the measure of dissimilarity in the trajectories within each cluster,

[2] In Ward's method at each step the deviances associated to all possible groupings is calculated and the group associated to the minimum deviance is chosen (Lavine, 2000).

[3] In average linkage method the distance of all pairs of points in which a member of each pair belong to the cluster is calculated. The average of these distances is used to calculate the similarity between the points and the cluster (Lavine, 2000).

whilst maximising the dissimilarity of different clusters. These methods are applied if one wants to classify the objects into *k* clusters, where *k* is fixed. In general, the algorithm tries to find a "good" partition in the sense that objects of the same cluster should be close or related to each other, whereas objects of different clusters should be far apart or very different (Kaufman and Rousseeuw, 2005). The *k*-means procedure is the most commonly used for trajectories classification (e.g., Sharma *et al.*, 2006; Eneroth *et al.*, 2007; Huang *et al.*, 2010; Dueñas *et al.*, 2011) and is also used in Chapter 5.

The *k*-means is an iterative algorithm that used a specified number of clusters *k* to partition the data by comparing each object to the arithmetic mean of all the members of each of the *k* clusters (cluster centres). The selection of the optimal number of clusters that best describes the different air flow patterns is performed by computing the percentage change in within-cluster variance, as a function of the number of clusters (Dorling *et al.*, 1992). The assignment of members (trajectories) to a given group (cluster) is carried out by minimising the internal variability within the group of trajectories and maximising the external variability between different groups based on the trajectory coordinates. It uses the Root Mean Square Deviation (RMSD) of all individual clusters from their cluster mean trajectory against the number of clusters retained until a "break" is reached, indicating that two clusters have been merged which are unacceptably different. Alternatively, if a threshold percentage change in RMSD is exceeded at any particular point in the clustering process, this is also taken as an indication that an optimum number of clusters have been reached. The *k*-means clustering method is often quoted as the Dorling method in climatological clustering research and is well suited for large databases because of its relatively small computational requirements (see for example Dorling and Davies, 1995).

Potential Source Contribution Function

The method was originally developed by Ashbaugh *et al.* (1985) and Malm *et al.* (1986). Air parcel back trajectories ending at a receptor site are represented by segment endpoints. Each endpoint has two coordinates (latitude and longitude) representing the central location of an air parcel at a particular time. To calculate the PSCF, the whole geographic region covered by the trajectories is divided into an array of grid cells whose size is dependent on the geographical scale of the problem so that the PSCF is a function of locations as defined by the cell indices *i* and *j*.

Let *N* be the total number of trajectory segment endpoints during the whole study period, *T*. If n_{ij} is the number of trajectory segment endpoints that fall in the *ij*th cell during the *T* time period, then the probability of this event, *A*, is given by

$$P[A_{ij}] = \frac{n_{ij}}{N} \tag{1.2}$$

where $P[A_{ij}]$ is a measure of the residence time of a randomly selected air parcel in the *ij*th cell relative to the time period *T*.

In the same *ij*th cell there exists a subset of m_{ij} segment endpoints for which the corresponding trajectories arrive at a receptor site at the time when the measured concentrations are higher than a pre-specified criterion value. The probability of these high concentration events B_{ij} is then given by

$$P[B_{ij}] = \frac{m_{ij}}{N} \tag{1.3}$$

where $P[B_{ij}]$is again a measure of the residence time but for contaminated air parcels.

The PSCF is defined as

$$P_{ij} = \frac{P[B_{ij}]}{P[A_{ij}]} = \frac{m_{ij}}{n_{ij}} \tag{1.4}$$

and is the conditional probability that an air parcel which passed through the *ij*th cell had a high concentration upon arrival at the trajectory endpoint. That is, cells with high PSCF values are indicative of areas of "high potential" contribution (Wang *et al.*, 2006). They do not necessarily make a large contribution to long-term air pollutant concentrations, since this also depends on the frequency at which air parcels actually travel over that region (Stohl, 1998). The error associated with the trajectory segment increases with increasing distance from the receptor sites (Stohl, 1996). In this trajectory approach the method looks at the collective properties of a large number of end points. Although the trajectory segment endpoints are subject to uncertainty, a sufficient number of endpoints should provide accurate estimates of the source locations if the location errors are random and not systematic (Begum *et al.*, 2005; Hopke, 2009). Cells containing emission sources would be identified with conditional probabilities close to one if trajectories that have crossed the cells effectively transport the emitted contaminant to the receptor site. The PSCF model thus provides a means to map the source potentials of geographical areas. It does not apportion the contribution of the identified source area to the measured receptor data (Begum *et al.*, 2005; Hopke, 2009).

1.3.3 Source apportionment

From a general point of view, source apportionment is the estimation of the contributions to the airborne concentrations of some atmospheric species (generally, a pollutant; primarily, airborne particulate matter) that arise from the emissions of natural and anthropogenic sources.

Such kind of models have been applied to the study of PM since the '70s and reconstruct the sources estimating contributes starting from chemical-physical of atmospheric aerosol measured in one or more receptor sites using different mathematical tools (US EPA, 2004).

The basic idea of source apportionment is that aerosol particles retain elemental-chemical composition characteristic of their origin: the PM composition at the receptor site is a combination

of the compositions of the aerosols emitted by the different sources. The main hypothesis is then that mass conservation can be assumed and a mass balance analysis can be used to identify and apportion sources of airborne particulate matter in the atmosphere. The common approach is to obtain a data set constituted by a large number of chemical constituents such as elemental concentrations in a number of samples. The assumption is that the measured concentrations derive from the summation of the mass contributions of a number of independent sources or source types (Hopke, 2009). The mathematical expression of the mass balance equation that accounts for all *m* chemical species in the *n* samples, as contributions from *p* independent sources is

$$x_{ij} = \sum_{k=1}^{p} g_{ik} f_{kj} \quad (1.5)$$

where $i = 1,..., n$ samples, $j = 1,\ldots, m$ species and $k = 1, \ldots, p$ sources.

Receptor models based on the mass balance equation require the validity of the following assumptions (Watson *et al.*, 2002):

1) all the sources that give a significant contribution have been identified (otherwise the mass reconstruction is poor);
2) source chemical profiles are constant in time (or at least during the sampling period);
3) source chemical profiles are constant in space, i.e., they do not change during transport from the source to the receptor site;
4) source profiles are each other linearly independent (not collinear), in order to correctly disentangling the corresponding source contributions.

Equation (1.5) can be solved in a number of different ways, depending on the information that is available. The problem can be divided into two classes: the case in which the source profiles are known and the case in which the source profiles are unknown.

If the sources profiles in the region are a priori known, the problem can be rewritten as a regression problem where the profiles and the ambient concentrations are known

$$x_j = \sum_{k=1}^{p} g_k f_{kj} + e_j \quad (1.6)$$

where the equation is now written for one sample at a time.

This approach was first suggested by Winchester and Nifong (1971) and Miller *et al.* (1972), and the common solution to this problem is achieved through an effective-variance least squares method (Cooper *et al.*, 1984), now generally referred to as the Chemical Mass Balance (CMB) model (Watson *et al.*, 1990). The CMB model is most useful for primary emissions where the chemical characteristics of the particles permit their apportionment. Secondary particles are difficult since they are the result of chemical transformations of gaseous emissions into particles and are generally treated as specific chemical species such as sulphate, nitrate, and ammonium or ammonium sulphate and ammonium nitrate. Of course the key issues in the application of CMB are the

knowledge of the profiles. Misspecification of the profiles in the model can be a major problem even though one may apparently get a good fit to the data. In the following a description of two multivariate methods that deal with the most general case in which the source profiles are not known and that have been used in one of the following works will be given.

A number of methods have been developed that deal with the most general case in which the source profiles are not known. In general, these methods are form of factor analysis, in which the source apportionment is simultaneously extracted from the whole data matrix. These methods attempt to apportion the sources on the basis of interpretations (internal correlations) at the receptor site alone (Viana *et al.,* 2008). The wide family of all "Factor Analysis" techniques comprehends Target Transformation (TTFA), Principal Component Factor Analysis (PCFA), Positive Matrix Factorization (PMF).

Principal components and factor analysis are names given to several of the variety of forms of eigenvector analysis. A great deal of confusion exists in the literature in regard to the terminology of eigenvector analysis. Various changes in the way the method is applied has resulted in it being called factor analysis, principal component analysis, principal components factor analysis, empirical orthogonal function, etc., depending on the way the data are scaled before analysis or how the resulting vectors are treated after the eigenvector analysis is completed. All of the methods have the objective to compress data into fewer dimensions and the identification of the structure of interrelationships that exist between the variables measured or the cases studied. Principal components analysis (PCA) is a multivariate statistical technique that attempts to identify a new set of variables as linear combinations of the measured variables so that the observed variations in the system can be reproduced by a smaller number of these causal factors. The new variables, commonly known as principal components (PCs), are orthogonal and uncorrelated to each other.

Since PCA can only be performed on a set of samples in which the various sources contribute different amounts of particles to each sample, the mass balance needs to be expanded to a matrix equation

$$X = GF + E \tag{1.7}$$

where X is the m x n pollutant concentration data matrix, G is the m x p matrix containing the p source profiles, F is the p x n matrix of source contributions, E is the residual matrix, the part of variance not explained by the model.

The methods of Factor Analysis/Multiple Linear Regression (FA/MLRA) and Positive Matrix Factorization, which are used in Chapter 7, will be described in the remainder of this paragraph.

Factor Analysis/Multiple Linear Regression

Factor Analysis/Multiple Linear Regression (FA/MLRA) is a technique that consists of two following steps: a first procedure to identify sources of PM through Factor Analysis and a second

one in which contributions of different sources are estimated by multiple linear regression. The first objective of FA is to investigate how an elevated number *p* of correlated variables (analyzed chemical species) can be linked to a lower number of independent not observed variables (factors) and then to solve the matrix using a number of factors far lower than *p*. There is the possibility to find a number *k* of factors lower than *p* if every observed data $x_i = (x_1, x_2, \ldots, x_i, \ldots, x_p)$ can be written as

$$x_j = \sum_{l=1}^{k} \lambda_{jl} f_l + \mu_l \qquad (1.8)$$

where f_l with $l = 1, \ldots, k$ are the factors, λ_{jl} are the loadings and μ_l are error terms (specific factors) (Tucker and Mac Callum, 1997; Härdle and Simar, 2003).

In this way each calculated factor is a linear combination of the original variables and expresses a maximum of variability in the original data but is also uncorrelated with the rest of data. Loadings represent the degree of correlation between the variables and the single calculated factors; they are linked to the composition of the source (Henry *et al.*, 1984; Hopke and Thurston, 1984; Salvador *et al.*, 2004).

In particular the elements with higher loadings in each factor are interpreted as fingerprints of the source that they represent. For this reason in order to identify in a unique way a single source with a single factor particular compounds characteristic of that source have to be identified. Normally, loadings in the range 0.4-0.6 are considered high (Lv *et al.*, 2006), even if the association of compounds to sources represent the delicate step of the analysis.

By design, the eigenvector analysis compresses the information content of the data set into as few eigenvectors as possible. Thus, in considering the number of factors to be used to describe the system, it is necessary to carefully examine the problems of reconstructing both the variability within the data and the actual data itself. Following the diagonalization of the correlation or covariance matrix, it is necessary to make the difficult choice of the number of factors, *p*, to use in the subsequent analysis. This problem occurs in any application of an eigenvector analysis of data containing noise. In the absence of error, the eigenvalues beyond the true number of sources become zero except for calculation error. The choice becomes more difficult depending on the error in the data. Several approaches have been suggested (Hopke *et al.*, 1980; Dresser *et al.*, 1988). A large relative decrease in the magnitude of the eigenvalues is one indicator of the correct number of factors. It can often be useful to plot the eigenvalues as a function of factor number and look for sharp breaks in the slope of the line (Cattell, 1966). If the eigenvalue is a measure of the information content of the corresponding eigenvector, then only sufficiently "large" eigenvalues need to be retained in order to reproduce the variation initially present in the data. One of the most commonly used and abused criteria for selecting the number of factors to retain is retaining only

those eigenvalues greater than 1 (Guttman, 1954). The argument is made that the normalized variables each carry one unit of variance. Thus, if an eigenvalue is less than one, then it carries less information than one of the initial variables and is therefore not needed. However, Kaiser and Hunka (1973) made a strong argument that although eigenvalue greater than one does set a *lower* limit on the number of factors to be retained, it does not set a simultaneous upper bound. Thus, there must be at least as many factors as there are eigenvalues greater than one, but there can be more than that number that are important to the understanding of the system's behavior. Hopke (1982) has suggested a useful empirical criterion for choosing the number of retained eigenvectors. In a number of cases of airborne particulate matter composition source identification problems, Hopke found that choosing the number of factors containing variance greater than one *after* an orthogonal rotation provided a stable solution. Because the matrices produced by the diagonalization process have been calculated in a way to maximize the amount of variance contained in each factor, they may not reflect the pattern of variables representative of a particle source. Thus, the factors are rotated generally to achieve what is termed "simple structure" (Hopke *et al.*, 1976). A varimax rotation is most commonly used in such analyses. With this axes rotation few variables with high loadings exist for each factor and an elevated number of variables have instead loadings close to zero.

Even though the choice of the model dimension and the search for non-negative solutions by axis rotations can be based entirely on mathematical criteria, it has been suggested that factor analysis attempts to get more information out of atmospheric data than is really there (Henry, 1987).

Prior to FA, the variables have to be normalized: generally in the study of PM the standardization is used (Thurston and Spengler, 1985; Swietlicki *et al.*, 1996; Marcazzan *et al.*, 2003), which converts real x_{ij} values to displacements from a normal distribution using the following transformation

$$z_{ij} = \frac{x_{ij} - \overline{x_i}}{\sigma_i} \tag{1.9}$$

where $i = 1, 2, \ldots, n$ is the total number of elements in the analysis, $j = 1, 2, \ldots,$ m is the total number of observations, z_{ij} the standardized value of the ith element for the jth observation; x_{ij} the concentration of that element for that observation, $\overline{x_i}$ the average concentration on all concentrations of ith element and σ_i the standard deviation of the concentrations of ith element. The result of the standardization is a distribution of average value equal to zero and standard deviation equal to one.

After the identification of the sources of PM, next step is to derive the contributions of each source. Contributions are obtained through MLRA using Absolute Factorial Scores (AFS) as independent variables and PM as dependent variable (Thurston and Spengler, 1985; Harrison *et al.*, 1997). AFS are calculated inserting daily values of each element in the factor equations and are the new

coordinates of samples calculated respect the new *k* axes represented by the *k* extracted factors. As the values of the original matrix have been normalized, also factorial scores are referred to normalized values. Thurston and Spengler (1985) proposed to obtain the score of an artificial sample with null concentrations for each *p* variable. After the application of FA, factorial scores of this sample are subtracted from the factorial scores of real observations, and new factorial scores referred to the real zero, not normalized, are obtained (Thurston and Spengler, 1985; Salvador *et al.*, 2004).

Estimated daily contributions of each source are obtained as products of daily AFS with multilinear regression coefficients. The result of the regression of PM concentrations on AFS is an interception constant, representing (if higher than zero) the quantity of PM not explained by identified sources.

The source profiles for each element are then obtained by regression of daily concentrations on estimated daily contributions of sources, obtained as product of absolute factorial scores with the coefficients of multilinear regression. The estimated daily concentration of PM is obtained as sum of daily contributions of the sources:

$$PM = \varsigma_0 + \sum_{j=1}^{k} \varsigma_j \cdot AFS_j \qquad (1.10)$$

with ζ_0 the interception constant contribution of sources not considered in the model, ζ_i the coefficients of regression, AFS_j absolute factorial scores, *j* the number of factors extracted by FA.

Positive Matrix Factorization

Positive Matrix Factorization (PMF) (Paatero, 1997, 1999) is based on a different approach to the factor analysis problem from the prior form of factor analysis. While all other methods are based on eigenvector analysis and singular value decomposition, PMF is based on an explicit least-square approach with individual data points weights.

The *X* matrix of Eq. 1.7 can also be defined as

$$X = USV' = \bar{U}\bar{S}\bar{V}' + E \qquad (1.11)$$

where $\bar{U}$ and $\bar{V}'$ are the first *p* columns of the *U* and *V* matrices. The *U* and *V* matrices are calculated from eigenvalue-eigenvector analyses of the *XX'* and *X'X* matrices, respectively. It can be shown (Lawson and Hanson, 1974; Malinowski, 1991) that the second term on the right side of Eq. 1.7 estimates *X* in the least-squares sense that it gives the lowest possible value for

$$\sum_{i=1}^{m}\sum_{j=1}^{n} e_{ij} = \sum_{i=1}^{m}\sum_{j=1}^{n}\left[x_{ij} - \sum_{p=1}^{p} g_{ip} f_{pj}\right] \qquad (1.12).$$

An eigenvector analysis is an implicit least-squares analysis as it is minimizing the sum of squared residuals for the model. Paatero and Tapper (1993) showed that in effect in PCA there is scaling of the data by column or by row and that this scaling will lead to distortions in the analysis. They further showed that optimum scaling of the data would be to scale each data point individually so as

to have more precise data having more influence on the solution than points that have higher uncertainties. However, they showed that point-by-point scaling result in a scaled data matrix that cannot be reproduced by a conventional factor analysis based on singular value decomposition.

In particular the main limits of FA/MLRA that have been solved by PMF are:

- uncertainties on measured data are not taken into account, and concentrations of all chemical species are equally weighted independently from the accuracy of their measurements;
- some factor loadings may be negative (which means anti-correlation among factors and measured species);
- as components are by definition uncorrelated, the model cannot describe real collinear sources (due for example to meteorological factors);
- the model outputs are given without uncertainty or with uncertainties that do not take into account the experimental uncertainties on input data.

PMF takes the approach of an explicit least squares in which the method minimizes the object function:

$$Q = \sum_{j=1}^{n} \sum_{i=1}^{m} \left(\frac{x_{ij} - \sum_{p=1}^{p} g_{ip} f_{pj}}{s_{ij}} \right) \quad (1.13)$$

where s_{ij} is an estimate of the "uncertainty" in the *j*th variable measured in the *i*th sample. The factor analysis problem is then to minimize *Q(E)* with respect to G and F with the constraint that each of the elements of *G* and *F* is to be non-negative (Paatero and Tapper, 1993, 1994).

A correctly weighted least squares formulation of the factor problem leads to an optimum fitting of the data matrix. Moreover, the possibility to input each data with a specific weight allows a correct and effective use of all the information contained in the dataset, as it is possible also to use "problematic" data (missing data, lower or near detection limit values, …). The weight makes *Q* a dimensionless quantity that is invariant for scale changes (optimal scaling).

In the way it is built, this method works in robust mode, i.e., it excludes outliers so that they do not affect the calculations of the contributions. The errors in the F matrix are estimated from the concentrations and assuming that other matrices are not affected by errors. Each matrix is treated in a similar way in turn, so that each element of matrix has an associated uncertainty.

In the PMF model, it is suggested that variables associated to elevated errors in the measurements or to a lot of missing data are not considered (US EPA, 2005). It is possible to verify if a variable should be included or not calculating the signal to noise ratio (SNR) for each variable (Paatero and Hopke, 2003):

$$SNR = \frac{1}{2}\sqrt{\frac{\sum_{i=1}^{n} x_{ij}^2}{\sum_{i=1}^{n} \sigma_{ij}^2}} \quad (1.14)$$

with x_{ij} the concentrations of the species and s_{ij} the uncertainty associated to the *i*th variable in the *j*th observation. The value of the ratio can be:

1. strong, in the case in which noise is low or the signal is elevated, and then that variable is robust and can be inserted into the model;
2. bad, when there are too many missing values or the errors are elevated, and the variable should be removed from the elaborations;
3. weak, if the variable is not robust but can be inserted in the model, even if with a lower weight than the others (uncertainty three times higher).

References

Al-Azmi D., Sayed A.M., and Yatim H.A., 2001. Variations in ^{7}Be concentrations in the atmosphere of Kuwait during the period of 1994 to 1998. *Applied Radiation and Isotopes* 55, 413–417.

Aldahan A., Possnert G., and Vintersved I., 2001. Atmospheric interactions at northern high latitudes from weekly Be isotopes in surface air. *Applied Radiation and Isotopes* 54, 345–353.

Almeida J., et al., 2013. Molecular understanding of sulphuric acid-amine particle nucleation in the atmosphere. *Nature* 502, 359-370.

Anenberg S.C., Horowitz L.W., Tong D.Q., West J.J., 2010. An Estimate of the Global Burden of Anthropogenic Ozone and Fine Particulate Matter on Premature Human Mortality Using Atmospheric Modelling. *Environmental Health Perspectives* 118, 1189-1195.

Ariola V., Campajola L., D'Alessandro A., Del Carmine P., Gagliardi F., Lucarelli F., Mandò P.A., Marcazzan G., Moro R., Nava S., Prati P.,Valli G., Vecchi R., Zucchiatti A., 2002. *Nuclear Instruments and Methods in Physics Research B* 190, 471-476.

Ashbaugh L.L., Malm W.C., Sadeh W.Z. 1985. A residence time probability analysis of sulfur concentrations at Grand Canyon National Park. *Atmospheric Environment* 19, 1263–1270.

Astitha M., Kallos G., Mihapoulos N., 2005. Analysis of Air Quality Observations with the Aid of the Source-Receptor Relationship Approach. Journal of the Air & Waste Management Association 55(4), 523-535, doi:10.1080/10473289.2005.10464628

Azahra M., Camacho-García A., González-Gómez C., López-Peñalver J.J., El Bardouni T., 2003. Seasonal ^{7}Be concentrations in near-surface air of Granada (Spain) in the period 1993-2001. 59, 159-164.

Baeza A., Delrio L.M, Jimenez A., Miro C., Paniagua J.M., and Rufo M., 1996. Analysis of the temporal evolution of atmospheric beryllium as a vector of the behavior of other radionuclides in the atmosphere. *Journal of Radioanalytical and Nuclear Chemistry*, 207(2), 331–344.

Baird C., Cann M., 2008. Environmental Chemistry. Ed. Freeman & Co (Sd), 650 pp, 4th Edition.

Balkanski Y.J., Jacob D.J., Gardner G.M., Graustein W.C., Turekian K.K., 1993. Transport and residence times or tropospheric aerosols inferred from a global three-dimensional simulation of ^{210}Pb. *Journal of Geophysical Research* 98, 20573-20586.

Baltensperger U., et al., 2005. Secondary organic aerosols from anthropogenic and biogenic precursors. *Royal Society of Chemistry* 130, 265-278.

Beer J., McCracken K., von Steiger R., 2012. Cosmogenic radionuclides. Springer, Heidelberg, pp.426.

Begum B.A., Kim E., Jeong C.H., Lee D.H., Hopke P.K. 2005. Evaluation of the potential source contribution function using the 2002 Quebec forest fire episode. *Atmospheric Environment* 39(20), 3719–3724.

Benioff P.A., 1956. Cosmic ray production rate and mean removal time of Beryllium-7 from the atmosphere. *Physical Review*, 104, 1122–1130.

Bourcier L., Masson O., Laj P., Pichon J.M., Paulat P., Freney E., Sellegri K., 2011. Comparative trends andseasonalvariationof ^{7}Be, ^{210}Pb and ^{137}Cs at two altitude sites in the central part of France. *Journal of Environmental Radioactivity* 102, 294-301

Brankov E., Rao S.T., Porter P.S., 1998. A trajectory-clustering correlation methodology for examining the long-range transport of air pollutants. *Atmospheric Environment* 32 (9), 1525-1534.

Brice T., et al., 2004. CRAC - The Centre for Research into Atmospheric Chemistry, UCC, Cork; http://crac.ucc.ie/tour/Brice2.pdf

Camuffo D., Van Grieken R., Busse H.J., Sturaro G., Valentino A., Bernardi A., Blades N., Shooter D., Gysels C., Deutsch F., Wieser M., Kim O., Ulrych U., 2001. Environmental monitoring in four European museums. *Atmospheric Environment* 35, S127-S140.

Cannizzaro F., Greco G., Raneli M., Spitale M., Tomarchio E., 2004. Concentration measurements of ^{7}Be at ground level air at Palermo, Italy – Comparison with solar activity over a period of 21 years. *Journal of Environmental Radioactivity* 72, 259-271.

Cass G.R., Boone P.M., Macias E.S, 1982. Emissions and air quality relationships for atmospheric carbon particles in Los Angeles. In: Wolff G.T. and Klimisch R.L. (Ed.), Particulate Carbon, Springer US, pp. 207-243, doi:10.1007/978-1-4684-4154-3_13

Cattell R.B., 1966. Handbook of Multivariate Experimental Psychology. Rand McNally, Chicago, pp. 174-243.

Cazzuli O., Lanzani G., Giudici A., Tebaidi G., 2005. La qualità dell'aria in Lombardia: l'analisi delle serie storiche e l'evoluzione degli indicatori di pressione. ARPA Lombardia, Milano.

Chate D.M., 2005. Study of scavenging of submicron-sized aerosol particles by thunderstorms rain events. *Atmospheric Environment* 39, 6608-6619.

Chiari M., Del Carmine P., Lucarelli F., Marcazzan G., Nava S., Paperetti L., Prato P., Valli G., Vecchi R., Zucchiatti A., 2004. Atmospheric aerosol characterization by Ion Beam Analysis techniques: recent improvements at the Van de Graaf laboratory in Florence. *Nuclear Instruments and Methods in Physical Research B* 219-220, 166-170.

Christoffersen T.S., Hjort J., Horie O., Jensen N.R., Kotzias D., Molander L.L., Neeb P., Ruppert L., Winterhalter R., Virkulla A., Wirtz K., Larsen B., 1998. Cis-Pinic Acid, a possible precursor of organic aerosol formation from ozonolysis of alpha-pinene. *Atmospheric Environment* 32, 1657-1661.

Cooper J.A., Watson J.G., Huntzicker J.J., 1984. The effective variance weighting for least squares calculations applied to the mass balance receptor model. *Atmospheric Environment* 18, 1347-1355.

Cristofanelli P., Bonasoni P., Tositti L., Bonafé U., Calzolari F., Evangelisti F., Sandrini S., Stohl A., 2006. A 6-year analysis of stratospheric intrusions and their influence on ozone at Mt. Cimone (2165 m above sea level). *Journal of Geophysical Research*, 111. D03306. doi:10.1029/2005JD006553.

Crutzen P.J., 1973. A discussion to the chemistry of some minor constituents in the stratosphere and troposphere. *Pure and Applied Geophysics* 106, 1385–1399.

Crutzen P.J., Lawrence M.G., Poschl U., 1999. On the background photochemistry of tropospheric ozone. *Tellus* Ser. AB, 51, 123– 146.

Cuevas E., Gonzalez Y., Rodríguez S., Guerra J.C., Gómez-Peláez A.J., Alonso-Pérez S., Bustos J., Milford C., 2013. Assessment of atmospheric processes driving ozone variations in the subtropical North Atlantic free troposphere. *Atmospheric Chemistry and Physics* 13, 1973-1998.

Daish, S.R., Dale, A.A., Dale, C.J., May, R., Rowe, J.E., 2005. The temporal variations of ^{7}Be, ^{210}Pb and ^{210}Po in air in England. *Journal of Environmental Radioactivity* 84, 457-467.

D'Alessio A., D'Anna A., Ciajolo A., Faravelli T., Ranzi E., 2005. Particolato fine e ultrafine. Emissione da processi di combustione. *La chimica e l'Industria*, anno 87 n.1, pp 16-24 (in Italian)

Davidson C.I., Phalen R.F., Solomon P.A., 2005. Airborne particulate matter and human health: A Review. *Aerosol Science and Technolgy* 39(8), 737-749.

Dibb J.E., Talbot R.W., Gregory G.L., 1992. Beryllium 7 and lead 210 in the western hemisphere Arctic atmosphere: Observations from three recent aircraft-based sampling programs. *Journal of Geophysical Research* 97, 16709-16715.

Dibb J.E., Meeker L.D., Finkel R.C., Southon J.R., Caffee M.W., and Barrie L.A., 1994. Estimation of stratospheric input to the Arctic troposphere. ^{7}Be and ^{10}Be in aerosols at Alert, Canada. *Journal of Geophysical Research*, 99, 12855–12864.

Dockery D.W., Stone P.H., 2007. Cardiovascular risks from particulate air pollution. *The New England*

Journal of Medicine 356, 511-513.

Dockery D., Pope A., 1996. Epidemiology of acute health effects: Summary of time-series studies. In: Particles in our air: concentration and health effects. Wilson R., Spengler JD (Eds), Cambridge, MA, USA, Harvard University Press, pp. 123-147.

Dorling S.R., Davies T.D., Pierce C.E., 1992. Cluster analysis: a technique for estimating the synoptic meteorological controls on air and precipitation chemistry-method and applications. *Atmospheric Environment* 26A (14), 2575-2581.

Dorling S.R., Davies T.D., 1995. Extending cluster-analysis-Synoptic meteorology links to characterize chemical climates at 6 northwest European monitoring stations. *Atmospheric Environment* 29, 145-167.

Doty K.G., Perkey D.J., 1993. Sensitivity of trajectory calculations to the temporal frequency of wind data. *Monthly Weather Review* 121, 387–401.

Dueñas C., Orza J.A.G., Cabello M., Fernández M.C., Cañete S., Pérez M., Gordo E., 2011. Air mass origin and its influence on radionuclide activities (^{7}Be and ^{210}Pb) in aerosol particles at a coastal site in the western Mediterranean. *Atmospheric Research* 101, 205-214.

Dresser D.L., Baird B.K., 1988. A dispersion and receptor Model Analysis of the Wintertime PM10 Problem in Telluride, Colorado. In: PM10: Implementation of Standards. Mathai C.V., Stonefield D.H. (Ed.), APCA Transactions series TR-13, Air Pollution Control Association, Pittsburgh, PA, pp. 458-469.

Duncan B.N., West J.J., Yoshida Y., Fiore A.M., Ziemke J.R., 2008. The influence of European pollution on ozone in the Near East and northern Africa. *Atmospheric Chemistry and Physics* 8, 2267-2283, doi:10.5194/acp-8-2267-2008.

Durana L., Chudy M., and Masarik J., 1996. Investigation of ^{7}Be in the Bratislava atmosphere. *Journal of Radioanalytical and Nuclear Chemistry*, Articles, 207(2), 345–356.

Dutkiewicz V.A., Husain L., 1985. Stratospheric and tropospheric components of ^{7}Be in surface air. *Journal of Geophysical Research Atmospheres* 90(D3), 5783-5788.

Dutton J.A., 1986. The Ceaseless Wind an Introduction to the Theory of Atmospheric Motion. Dover, New York, 617 pp.

Eleftheriadis K., Vratolis S., Nyeki S., 2009. Aerosol black carbon in the European Arctic: Measurements at Zeppelin station, Ny-Ålesund, Svalbard from 1998-2007. *Journal of Geophysical Research* 36, L02809, doi:10.1029/2008GL035741.

El-Hussein A., Mohamemed A., Abd El-Hady M., Ahmed A.A., Ali A.E., Barakat A., 2001. Diurnal and seasonal variation of short-lived radon progeny concentration and atmospheric temporal variations of Pb-210 and Be-7 in Egypt. *Atmospheric Environment* 35, 4305-4313.

Eneroth K., Holmen K., Berg T., Schmidbauer N., Solberg S., 2007. Springtime depletion of tropospheric ozone, gaseous elemental mercury and nonmethane hydrocarbons in the European Arctic, and its relation to atmospheric transport. *Atmospheric Environment* 41, 8511–8526.

Feely H.W., Larsen R.J., Sanderson C.G., 1989. Factors that cause seasonal variations in ^{7}Be concentrations in surface air. *Journal of Environmental Radioactivity* 9, 223-249.

Fermo P., Piazzalunga A., Vecchi R., Valli G., Cerini M., 2006. A TGA/FT-IR study for measuring OC and EC in aerosol samples. *Atmospheric Chemistry and Physics* 6, 255-266.

Finlayson-Pitts B.J., Pitts J.N., 1999. Chemistry of the upper and lower atmosphere. Theory, experiments and applications. Academic Press, 969 pp.

Fischer H., Kormann R., Klüpfel T., Gurk Ch., Königstedt R., Parchatka U., Mühle J., Rhee T.S., Brenninkmeijer C.A.M., Bonasoni P., Stohl A., 2003. Ozone production and trace gas correlations during the June 2000 MINATROC intensive measurement campaign at Mt Cimone. *Atmospheric Chemistry and Physics* 3, 725-738.

Fleming Z.L., Monks P.S., Manning A.J., 2012. Untangling the influence of air-mass history in interpreting observed atmospheric composition. *Atmospheric Research* 104-105, 1-39.

Forster P., et al., 2007. Changes in atmospheric constituents and in radiative forcing. In: Solomon S., Qin D., Manning M., Chen Z., Marquis M., et al. (ed.) Climate Change 2007: The Physical Science Basis, Contribution of Working Group I to the Fourth Assessment Report of the Intergovernmental Panel on Climate Change. Cambridge University Press, Cambridge, UK, and New York, USA.

Fuhrer J, Booker F., 2003. Ecological issues related to ozone: agricultural issues. *Environment International* 29, 141–154.

Gaffney J.S, Marley N., Cunningham M.M., 2004. Natural radionuclides in fine aerosols in the Pittsburgh area. *Atmospheric Environment* 38, 3191-3200.

Garg A., Shukla P.R., Kapshe M., 2006. The sectoral trends of multigas emissions inventory of India. *Atmospheric Environment* 40, 4608-4620.

Gauss M., et al., 2003. Radiative forcing in the 21st century due to ozone changes in the troposphere and the lower stratosphere. *Journal of Geophysical Research* 108(D9), 4292, doi:10.1029/2002JD002624.

Gerasopoulos E., Zanis P., Stohl A., Zerefos C.S., Papastefanou C., Ringer W., Tobler L., Hübener S., Gäggeler H.W., Kanter H.J., Tositti L., Sandrini S., 2001. A climatology of ^{7}Be at four high-altitude stations at the Alps and the Northern Apennines. *Atmospheric Environment* 35, 6347-6360

Godoi R.H.M., Kontozova V., Van Grieken R., 2006. The shielding effect of the protective glazing of historical stained glass windows from an atmospheric chemistry perspective: case study Saint Chapelle, Paris. *Atmospheric Environment* 40, 1255-1265.

Graustein W.C., and Turekian K.K., 1990. ^{222}Rn fluxes from soils to the atmosphere measured by ^{210}Pb–^{226}Ra disequilibrium in soils. *Geophysical Research Letters*, 17, 841–844.

Guttman L., 1954. Some Necessary Conditions for Common Factor Analysis. *Psychometrika* 19, 149-161.

Härdle W., Simar L., 2003. Applied Multivariate Statistical Analysis. pp. 488. (http://www.stat.wvu.edu/~jharner/courses/stat541/mva.pdf)

Harris J.M., Kahl J.D., 1990. A descriptive atmospheric transport climatology for the Mauna Loa observatory, suing clustered trajectories. *Journal of Geophysical Research* 95, 13651-13667.

Harris J.M., Draxler R.R., Oltmans S.J., 2005. Trajectory model sensitivity to differences in input data and vertical transport method. *Journal of Geophysical Research* 110, D14109.

Harrison R.M., Smith D.J.T., Pio C.A., Castro L.M., 1997. Comparative receptor modelling study of airborne particulate pollutants in Birmingham (United Kingdom), Coimbra (Portugal) and Lahore (Pakistan). *Atmospheric Environment* 31(20), 3309-3321.

Harrison R.M., Yin J., 2000. Particular matter in the atmosphere: which particle proprieties are important for its effects on health? *Science of the Total Environment* 249(1-3), 85-101

Harrison D., Hunter M.C., Lewis A.C., Seakins P.W., Nunes T.V., Pio C.A., 2001. Isoprene and Monoterpene emission from the coniferous species Abies Borigiis-regis – implications for regional air chemistry in Greece. *Atmospheric Environment* 35, 4687 4698.

Haynes P.H., Marks C.J., McIntyre M.E., Shepherd T.G., Shine K.P., 1991. On the "Downward Control" of extra-tropical diabatic circulations by eddy-induced mean zonal forces. *Journal of Atmospheric Science* 48, 651–678.

Henry R.C., 1987. Current factor analysis receptor models are ill-posed. *Atmospheric Environment* 21, 1815-1820.

Henry R.C., Lewis C:W., Hopke P.K., Williamson H.J., 1984. Review of receptor model fundamentals. *Atmospheric Environment* 18, 1507-1515.

Hesselbjerg J., et al., 2013.Chapter 14: Climate Phenomena and their Relevance for Future Regional Climate Change. In: Working Group I Contribution to the IPCC Fifth Assessment Report Climate Change 2013: The Physical Science Basis. Technical Summary. Fyfe J., Kwon W.-T., Trenberth K., Wratt D., (Ed.), 145 pp.

Heyder J., Gebhart J., Stahlhofen W., 1974. Diameters of airborne particles. *Water, air and soil pollution* 3(4), 567-572.

Hewitt C.N., 2001. The atmospheric chemistry of sulphur and nitrogen in power station plumes. *Atmospheric Environment* 35, 1155-1170.

Hoek, G., Fisher P., Brunekreef B., Lebret E., Hofsschreuder P., Mennen M.G., 1993. Acute effects of ambient ozone on pulmonary function of children in the Netherlands. *The American Review of Respiratory Disease*, 147, 11– 117.

Holton J.R., Haynes P.H., McIntyre M.E., Douglass A.R., Rood R.B., and Pfister L., 1995. Stratosphere-troposphere exchange. *Review of Geophysics*, 33, 403–439.

Hopke P.K., Gladney E.S., Gordon G.E., Zoller W.H., Jones A.G., 1976. The Use of Multivariate Analysis to Identify Sources of Selected Elements in the Boston Urban Aerosol. *Atmospheric Environment* 10, 1015-1025.

Hopke P.K., Lamb R.E., Natusch D.F.S., 1980. Multielemental Characterization of Urban Roadway Dust. *Environmental Science and Technology* 14, 164-172.

Hopke P.K., 1982. Comments on 'Trace Element Concentrations in Summer Aerosols at Rural Sites in New York State and Their Possible Sources' by P. Parekh and L. Husain and 'Seasonal Variations in the Composition of Ambient Sulfur-Containing Aerosols' by R. Tanner and B. Leaderer. *Atmospheric Environment* 16, 1279-1280.

Hopke P.K., Thurston G.D., 1984. Inter-laboratory comparison of source apportionment procedures. *Atmospheric Environment* 18, 1517-1537.

Hopke P.K., 2009. Theory and application of source apportionment. In: Developments in Environmental Science, Volume 9. Legge, A.H. (Ed.), Elsevier Ltd. doi:10.1016/S1474-8177(08)00201-5

Huang L., Gong S.L., Sharma S., Lavoue D., Jia C.Q., 2010. A trajectory analysis of atmospheric transport of black carbon aerosols to Canadian high Arctic in winter and spring (1990–2005). *Atmospheric Chemistry and Physics* 10, 5065–5073.

Hueglin C., Gehrig R., Baltensperger U., Gysel M., Monn C., Vonmont H., 2005. Chemical characterization of PM2.5, PM10 and coarse particles at urban, near-city and rural sites in Switzerland. *Atmospheric environment* 39(22), 637-651

IARC (International Agency for Research on Cancer), 2013. Air Pollution and Cancer. IARC Scientific Publication n.61. Edited by Kurt Straif, Aaron Cohen, and Jonathan Samet. ISBN 978-92-832-2161-6 ISSN 0300-5085.

Ioannidou A., Manolopoulou M., Papastefanou C., 2005. Temporal changes of ^{7}Be and ^{210}Pb concentrations in surface air at temperate latitudes (40°). *Applied Radiation and Isotopes* 63(2), 277-284.

IPCC, 2007. Climate Change 2007: the Physical Science Basis. Contribution of Working Group I to the Fourth Assessment Report of the Intergovernmental Panel on Climate Change. Cambridge University Press.

IPCC, 2013. Working Group I Contribution to the IPCC Fifth Assessment Report. Climate Change 2013: The Physical Science Basis. Approved summary for policy makers. Twelfth Session of Working Group I.

Jacobson M.C., Hansson H.-C., Noone K.J., Charlson R.J., 2000. Organic atmospheric aerosols: review and state of the science. *Reviews of Geoophysics* 38, 267-294.

Jacobson M.Z., 2002. Atmospheric Pollution: history, science and regulation. Cambridge University Press, Cambridge, 375 pp.

Jaenicke R., 1980. Atmospheric aerosols and global climate. *Journal of Aerosol Science*, 11, 577-588.

John W., 2001. Size Distribution Characteristics of Aerosol. In: Baron P.A., Willeke K., Aerosol Measurement, New York.

JRC (Joint Research Centre)/PBL (Netherlands Environmental Assessment Agency), 2013. Emission Database for Global Atmospheric Research (EDGAR) release version 4.2; http://edgar.jrc.ec.europa.eu, accessed January 08, 2014.

Junge C.E., 1963. Air chemistry and radioactivity. Academic Press, New York and London. 382 pp.

Kaiser H.F., Hunka S., 1973. Some Empirical Results with Guttman's Stronger Lower Bound for the Number of Common Factors, *Educational and Psychological Measurement* 33, 99-102.

Kaufman L., Rousseeuw P.J., 2005. Finding Groups in Data. An Introduction to Cluster Analysis. Wiley & Sons, Inc., Hoboken, New Jersey, 355 pp.

Keeler G.J., Samson P.J. 1989. Spatial representativeness of trace element ratios. *Environmental Science and Technology* 23, 1358–1384.

Kinney P.L., 1993. A meta-analysis of repeated FEV1 data from six summercamp studies: Mean effect of ozone and response heterogeneity. *The American Review of Respiratory Disease* 147, A636.

Koch D.M., Jacob J., Graustein W.C., 1996. Vertical transport of tropospheric aerosols as indicated ^{7}Be and ^{210}Pb in a chemical tracer model. *Journal of Geophysical Research* 101: 18651-18666.

Koch S., Winterhalter R., Uherek E., Kolloff A., Neef P., Moortgat G.K., 2000. Formation of new particles in the gas-phase ozonolysis of monoterpenes. *Atmospheric Environment* 34, 4031-4042.

Kolb W., 1992. Aktivitätskonzentrationen von Radionukliden in der bodennahen Luft Norddeutschlands und Nordnorwegens im Zeitraum von 1963 bis 1990. PTB-Berichte Radioaktivität, PTB-Ra-29, pp. 122.

Kulan A., Aldahan A., Possnert G., Vintersved I., 2006. Distribution of ^{7}Be in surface air of Europe. *Atmospheric Environment* 40, 3855-3868.

Kurokawa J., Ohara T., Morikawa T., Hanayama S., Greet J.M., Fukui T., Kawashima K.., Akimoto H., 2013. Emissions of air pollutants and greenhouse gases over Asian regions during 2000-2008: Regional Emission Inventory in ASia (REAS) version 2. *Atmospheric Chemistry and Physics Discussion* 13, 10049-10123.

Lal D., Malhotra P.K., Peters B., 1958. On the production of radioisotopes in the atmosphere by cosmic radiation and their application to meteorology. *Journal of Atmospheric and Terrestrial Research* 12, 306-328.

Lal D., and Peters B., 1962. Cosmic ray isotopes and their application to problems in geophysics, Progress in Cosmic Ray Physics, Vol. 6, No. 3. N. Holland Publishing Co., Amsterdam.

Lal D., and Peters B., 1967. Cosmic ray produced radioactivity on Earth, Encyclopedia of Physics, Vol. 46, No. 2, Springer, New York, pp. 551–612.

Lambert R.J., Ardouin B., Sanak J., 1990. Atmospheric transport of trace elements toward Antartica. *Tellus Ser. B* 42, 76-82.

Larsen R.J., and Sanderson C.G., 1995. EML surface air sampling program, 1990–1993 data. Environmental Measurement Laboratory Report EML-572. US Department of Energy, New York, USA.

Larssen T., et al., 2006. Acid Rain in China. *Environmental Science and Technology* 40, 418-425.

Lavine B.K., 2000. Clustering and Classification of Analytical Data. Encyclopedia of Analytical Chemistry, R.A. Meyers (Ed.).

Lawson C.L., Hanson R.J. 1974. Solving least-squares problems. Prentice-Hall, Englewood Cliffs, NJ.

Lee H. N., 2004. Issues and challenges of using natural radionuclides as tracer for atmospheric studies. In: 1st International Expert Meeting on Sources and Measurements of Natural Radionuclides Applied to Climate and Air Quality Studies. World Meteorological Organization Technical Document No. 1201, pp. 30–34.

Leppänen A.-P., Pacini A.A., Usoskin I.G., Aldahan A., Echer E., Evangelista H., Klemola S., Kovaltsov G.A., Mursula K., Possnert G., 2010. Cosmogenic Be-7 in air: a complex mixture of production and transport. *Journal of Atmospheric and Solar-Terrestrial Physics* 72, 1036-1043.

Leppänen A-P, Usoskin I.G., Kovaltsov G.A., Paatero J., 2012. Cosmogenic ^{7}Be and ^{22}Na in Finland: Production, observed periodicities and the connection to climatic phenomena. *Journal of Atmospheric and Solar-Terrestrial Physics* 74, 164-180.

Lelieveld J., et al., 2002. Global air pollution crossroads over the Mediterranean. *Science* 298, 794-799.

Likuku, A.S., 2006. Factors influencing ambient concentrations of ^{210}Pb and ^{7}Be over the city of Edinburgh (55.9°N, 03.2°W). *Journal of Environmental Radioactivity* 87, 289-304.

Liu H., Jacob D.J., Bey I., Yantosca R.M., 2001. Constraints from the ^{210}Pb and ^{7}Be on wet deposition and transport in a global three-dimensional chemical tracer model driven by assimilated meteorological fields. *Journal of Geophysical Research* 106, D11, 12109-12128.

Lu Z., Zhang Q., Streets D.G., 2011. Sulfur dioxide and primary carbonaceous aerosol emissions in China and India, 1996-2010. *Atmospheric Chemistry and Physics* 11, 9839-9864.

Lu Z., Streets D.G., de Foy B., Krotkov N.A., 2013. Ozone Monitoring Instrument Observations of Interannual Increases in SO_2 Emissions from Indian Coal-Fired Power Plants during 2005-2012. *Environmental Science and Technology* 47, 13993-14000. doi:10.1021/es4039648

Lv W., Wang Y., Querol X., Zhuang X., Alastuey A., López A., Viana M., 2006. Geochemical and statistical analysis of trace metals in atmospheric particulates in Wuhan, central China. *Environmental Geology* 51, 121-132.

Malinowski E.R. 1991. Factor analysis in chemistry (second ed.). Wiley, New York.

Malm W.C., Johnson C.E., Bresch J.F. 1986. Application of principal component analysis for purposes of identifying source-receptor relationships. In: Pace T.G. (ed.) Receptor methods for source apportionment. Air Pollution Control Association, Pittsburgh, PA, pp. 127–148.

Malm W.C., Gebhart K.A., Henry R.C. 1990. An investigation of the dominant source regions of fine sulfur in the western United States and their areas of influence. *Atmospheric Environment* 24A, 3047–3060.

Manahan E.S., 2000. Chimica dell'ambiente. Ed. Piccin.

Manly B.F.J., 1994. Multivariate Statistical Methods: A Primer. Chapman and Hall/CRC, London, pp. 129-133.

Marcazzan G.M., Valli G., Vecchi R., 2002. Factors influencing mass concentration and chemical composition of fine aerosols during a PM high pollution episode. *Science of the Total Environment* 298, 65-79.

Marinoni A., Cristofanelli P., Calzolari F., Roccato F., Bonafè U., and Bonasoni P., 2008. Continuous measurements of aerosol physical parameters at the Mt. Cimone GAW Station (2165 m asl, Italy). *Science of the Total Environment*, 391, 241-251.

Masarik J., and Beer J. 1999. Simulation of particle fluxes and cosmogenic nuclide production in the Earth's atmosphere. *Journal of Geophysical Research* 104, 12099–12111.

Masarik J., 2010. Origin and Distribution of Radionuclides in the Continental Environment. In: Radioactivity in the environment, Volume 16, chapter 1, 1-25. Elsevier B.V.

McFiggans G., Coe H., Burgess R., Allan J., Cubison M., Alfarra M. R., Saunders R., Saiz-Lopez A., Plane J. M. C., Wevill D. J., Carpenter L. J., Rickard A. R., and Monks P.S., 2004. Direct evidence for coastal iodine particles from Laminaria macroalgae – Linkage to emissions of molecular iodine. *Atmospheric Chemistry and Physics* 4, 701–713.

Millàn M., Sanz J., Salvador R., Mantilla E., 2006. Atmospheric dynamics and ozone cycles related to nitrogen deposition in the western Mediterranean. *Environmental Pollution* 118, 167-186.

Miller M.S., Friedlander S.K., Hidy G.M., 1972. A chemical element balance for the Pasadena aerosol. *Journal of Colloidal Interface Science* 39, 65-176.

Mitra A.P., Morawska L., Sharma C., Zhang J., 2002. Chapter two: methodologies for characterization of combustion sources end for quantification of their emissions. *Chemosphere* 39, 903-922.

Moody J.L., 1986. The influence of meteorology on precipitation chemistry at selected sites in the Eastern United States. Ph.D. Thesis, Univ. of Mich., Ann Arbor, 176 pp.

Moody J.L., Galloway J.N., 1988. Quantifying the relationship between atmospheric transport and the chemical composition of precipitation on Bermuda. *Tellus* B 40, 463-479.

Monks P.S., et al., 2009. Atmospheric composition change – global and regional air quality. *Atmospheric Environment* 43, 5268-5350.

Moreno T., Jones T.P., Richards R.J., 2004. Characterization of aerosol particulate matter from urban and industrial environment: examples from Cardiff and Port Tablot, South Wales, UK. *Science of the Total Environment* 334-335, 337-346.

Muthukumara M., Markandya A., Sagar A., Sahin S., 2012. India's Economic Growth and Environmental Sustainability: What Are the Tradeoffs? Policy Research Working Paper 6208. The World Bank South Asia Region. Disaster Risk Management and Climate Change (Ed.) 41 pp.

Myhre G., et al., 2013. Chapter 8: Anthropogenic and Natural Radiative Forcing. In: Working Group I Contribution to the IPCC Fifth Assessment Report Climate Change 2013: The Physical Science Basis. Technical Summary. Jacob D., Ravishankara A.R., Shine K., (Ed.), 139 pp.

Nagai H., Tada W., and Kobayashi T., 2000. Production rates of ^{7}Be and ^{10}Be in the atmosphere. *Nuclear Instruments and Methods in Physics Research Section B: Beam Interactions with Materials and Atoms*, 172(1–4), 796–801.

Nava S., Becherini F., Bernardi A., Bonazza A., Chiari M., García-Orellana I., Lucarelli F., Ludwig F., Migliori A., Sabbioni C., Udisti R., Valli G., Vecchi R., 2010. An integrated approach to assess air pollution threats to cultural heritage in a semi-confined environment: The case study of Michelozzo's Courtyard in Florence (Italy). *Science of the Total Environment* 408, 1403-1413.

Nriagu J.O, Pacyna J.M., 1988. Quantitative assessment of worldwide contamination of air, water and soils with trace metals. *Nature* 333, 134-139.

Oberdörster G., Finkelstein J.N., Johnston C., Gelein R., Cox C., Baggs R., Elder A.C.P., 2000. Acute Pulmonary Effects of Ultrafine Particles in Rats and Mice. HEI (Health Effects Institute) Research Report 96.

Oberdörster G., Zharp Z., Atudorei V., Elder A., Gelein R., Kreyling W., Cox C., 2004. Translocation of Inhaled Ultrafine Particles to the Brain. *Inhalation Toxicology* 16(6-7), 437-445.

O'Brien K., 1979. Secular variations in the productions of cosmogenie isotopes in the atmosphere. *Journal of Geophysical Research* 84, 42–43.

Odum J.R., Hoffman T., Bowman F., Collin D., Flagan R.C., Seinfield J.H., 1996. Gas/particle partitioning and secondary organic aerosol yields. *Environmental Science and Technology* 30, 2580-2585.

Odum J.R., Jungkamp T.P.W., Griffin R.J., Flagan R.C., Seinfield J.H., 1997a. The atmospheric aerosol-formation potential of whole gasoline vapour. *Science* 276, 96-99.

Odum J.R., Jungkamp T.P.W., Griffin R.J., Flagan R.C., Seinfield J.H., 1997b. Aromatics, refounded gasoline, and atmospheric aerosol. *Environmental Science and Technology* 31, 1890-1897.

Paatero P., Tapper U. 1993. Analysis of different modes of factor analysis as least squares fit problems. *Chemometrics & Intelligent Laboratory Systems* 18, 183–194.

Paatero P., Tapper U., 1994. Positive Matrix Factorization: a non-negative factor model with optimal utilization of error estimates of data values. *Environmetrics* 5, 111-126.

Paatero P., 1997. Least squares formulation of robust, non-negative factor analysis. *Chemometrics & Intelligent Laboratory Systems* 37, 23-35.

Paatero P., 1999. The multilinear engine-a table driven least squares program for solving multilinear problems, including the n-way parallel factor analysis model. *Journal of Computational and Graphical Statistics* 8, 854-888.

Paatero P., Hopke P.K., 2003. Discarding or downweighting high-noise variables in factor analytic models. *Analytica Chimica Acta* 490, 277-289.

Pacyna J.M., Pacyna E.G., 2001. An assessment of global and regional emissions of trace metals to the atmosphere from anthropogenic sources worldwide. *Environmental Reviews* 9, 269-298.

Papastefanou C., Ioannidou A., 1995. Aerodynamic size association of ^{7}Be in ambient aerosols. *Journal of Environmental Radioactivity* 26, 273-282.

Pérez L., Medina-Ramón M., Künzli N., Alastuey A., Pey J., Pérez N., García R., Tobías A., Querol X., Sunyer J., 2009. Size fractionate particulate matter, vehicle traffic, and case-specific daily mortality in Barcelona (Spain). *Environmental Science and Technology* 43, 4707-4714.

Pham M.K., Betti M., Nies H., Povinec P.P., 2011. Temporal changes of ^{7}Be, ^{137}Cs and ^{210}Pb activity concentrations in surface air at Monaco and their correlation with meteorological parameters. *Journal of Environmental Radioactivity* 102, 1045-1054.

Poirot R.L., Wishinski P.R. 1986. Visibility, sulfate, and air mass history associated with the summertime aerosol in northern Vermont. *Atmospheric Environment* 20, 1457–1469.

Poirot R.L., Wishinski P.R., Hopke P.K., Polissar A.V. 2001. Comparative application of multiple receptor methods to identify aerosol sources in northern Vermont. *Environmental Science and Technology* 35, 4622–4636.

Pope A.C. III, Thun M.G., Namboodiri M.M., Dockery D.W., Evans J.S., Speizer F.E., Health J.C.W., 1995. Particulate air pollution as a predictor of mortality in a prospective study of US adults. *American Journal of Respiratory and Critical Care Medicine* 151, 669-674.

Pope C.A., Dockery D.W., 2006. Health effects of fine particulate air pollution: lines that connect. *Journal of the Air & Waste Management Association* 56, 709–742.

Pope C.A. III, Ezzati M., Dockery D.W., 2009. Fine-particulate air pollution and life expectancy in the United States. *Northern England Journal of Medicine* 360, 376-386.

Pöschl U., 2005. Atmospheric aerosols: composition, transformation, climate and health effects. *Angewandte Chemie International Edition* 44, 7520-7540.

Pòsfai M., Molnàr A., 2000. Aerosol particles in the troposphere: a mineralogical introduction. In: Environmental Mineralogy. Edited by David J. Vaughan and Roy A. Wogelius, pp. 434

Preiss P.J., Melieres M.-A., and Pourchet M., 1996. Use of a new database of lead-210 for global aerosol model validation. *Journal of Geophysical Research* 101(25), 325–347, 357.

Price C., Penner J., Prather M., 1997a. NOx from lightning: 1. Global distribution based on lightning physics. *Journal of Geophysical Research* 102(D5), 5929-5941.

Price C., Penner J., Prather M., 1997b. NOx from lightning: 2. Constraints from the global atmospheric electric circuit. *Journal of Geophysical Research* 102(D5), 5943-5951.

Prospero J., Charlson R.J., Mohnen V., Jaenicke R., Delany A.C., Moyers J., Zoller W., Ruhn K., 1983. The atmospheric aerosol system: an overview. *Reviews of Geophysics* 21(7), 1607-1629, doi:10.1029/RG021i007p01607

Putaud J.-P., Raes F., Van Dingenen R., Brüggemann E., Facchini M.C., et al., 2004. A European aerosol phenomenology—2: chemical characteristics of particulate matter at kerbside, urban, rural and background sites in Europe. *Atmospheric Environment* 38 (16), 2579-2595.

Raes F., Van Dingeren R., Vignati E., Wilson J., Putaud J.P., Seinfield J.H., Adams P., 2000. Formation and cycling of aerosols in the global troposphere. *Atmospheric Environment* 34, 4215-4240.

Ramaswamy V., Boucher O., Haigh J., Hauglustaine D., Haywood J., Myhre G., Nakajima T., Shi G.Y., and Salomon S., 2001. Radiative forcing of climate change, in Climate Change 2001: The Scientific Basis—Contribution of Working Group I to the Third Assessment Report of The Intergovernmental Panel on Climate Change. Houghton J. T. et al. (Ed.), pp. 349– 416, Cambridge Univ. Press, New York.

Rangarajan C., and Gopalakrishnan S.S., 1970. Seasonal variation of beryllium7 relative to caesium137 in surface air at tropical and sub-tropical latitudes. *Tellus* 22, 115–121.

Rehfeld S., and Heimann M., 1995. Three dimensional atmospheric transport simulation of the radioactive tracers ^{210}Pb, ^{7}Be, ^{10}Be, and ^{90}Sr. *Journal of Geophysical Research* 100(D12), 26141–26161.

Roelle P.A., Baek B.H., Aneja S., Aneja V.P., 2001. Nitric oxide emissions from biosolid amended soils. *Hydrological Science and Technology Journal* 17, 306-316

Rolph G.D., Draxler R.R., 1990. Sensitivity of three-dimensional trajectories to the spatial and temporal densities of the wind field. *Journal of Applied Meteorology* 29, 1043–1054.

Salvador P., Artiñano B., Alonso D.G., Querol X., Alastuey A., 2004. Identification and characterisation of sources of PM_{10} in Madrid (Spain) by statistical methods. *Atmospheric Environment* 38, 435-447.

Sanak J., Lambert G., and Ardouin B., 1985. Measurements of stratosphere-to-troposphere exchange in Antarctica by using short-lived cosmonuclides. *Tellus B* 37 (2), 109–115.

Scebba F, Canaccini F, Castagna A, Bender J, Weigel H-J, Ranieri A., 2006. Physiological and biochemical stress responses in grassland species are influenced by both early-season ozone exposure and interspecific competition. *Environmental Pollution* 142, 540–548.

Seibert P., 1993. Convergence and accuracy of numerical methods for trajectory calculations. *Journal of Applied Meteorology* 32, 558–566.

Seibert P., Frank A., 2004. Source-receptor matrix calculation with a Lagrangian particle dispersion model in backward mode. *Atmospheric Chemistry and Physics* 4, 51-63.

Seigneur C., 2001.Current status of air quality models for particulate matter. *Journal of Air & Waste Management Association* 51, 1508-21.

Seinfeld J.H., Pandis S.N., 2006. Atmospheric Chemistry and Physics: From Air Pollution to Climate Change, 2nd Edition. Wiley, New York, 1232 pp. ISBN: 978-0-471-72018-8

Sharma S., Andrews E., Barrie L.A., Ogren J.A., Lavoue D., 2006. Variations and sources of the equivalent black carbon in the high Arctic revealed by long-term observations at Alert and Barrow: 1989–2003. *Journal of Geophysical Research-Atmospheres*, 111.

Silva R.A., et al., 2013. Global premature mortality due to anthropogenic outdoor air pollution and the contribution of past climate change. *Environmental Research Letters* 8(3), doi:10.1088/1748-9326/8/3/034005

Staehelin J, Thudium J, Buheler R, Volz-Thomas A, Graber W., 1994. Trends in surface ozone concentrations at Arosa (Switzerland). *Atmospheric Environment* 28, 75–78.

Steinmann P., Zeller M., Beuret M., Ferreri G., Estier S., 2013. Cosmogenic ^{7}Be and ^{22}Na in ground level air in Switzerland. *Journal of Environmental Radioactivity* 124, 68-73.

Stohl A., 1996. Trajectory statistics—a new method to establish source-receptor relation- ships of air pollutants and its application to the transport of particulate sulfate in Europe. *Atmospheric Environment* 30, 579–587.

Stohl A., 1998. Computation, accuracy and applications of trajectories-a review and bibliography. *Atmospheric Environment* 32, 947-966.

Stohl A., Wotawa G., Seibert P., Kromp-Kolb H., 1995. Interpolation errors in wind fields as a function of spatial and temporal resolution and their impact on different types of kinematic trajectories. *Journal of Applied Meteorology* 34, 2149–2165.

Stohl A., Spoichtinger-Rakowsky N., Bonasoni P., Feldmann H., Memmesheimer M., Scheel H.E., Trickl T., Hübener S., Ringer W., Mandl M., 2000. The influence of stratospheric intrusions on alpine ozone concentrations. *Atmospheric Environment* 34, 1323-1354.

Stohl A., Wernli H., James, P., Borqui M., Forster C., Liniger M.A., Seibert P., Sprenger M., 2003. A new perspective of stratosphere-troposphere exchange. American Meteorological Society, 1565-1573 doi:10.1175/BAMS-84-11-1565

Sykora I., Meresova J., and Holy K., 2005. Radioactivity of Bratislava atmosphere in 2004. Progress Report, KJFB FMFI UK-144/05, May 2005, Bratislava.

Sykora I., and Froehlich K., 2010. Radionuclides as tracers of atmospheric processes. In: Radioactivity in the environment, Volume 16, chapter 3, 51-88. Elsevier B.V.

Swietlicki W., Puri S., Hansson B.G., Kristiansson P., 1996. Urban air pollution source apportionment using a combination of aerosol and gas monitoring techniques. *Atmospheric Environment* 30, 2795-2809.

Tagliavini E., Decesari S., Facchini M.C., Matta E., Lettini F., Ricrea M., Fuzzi S., Putaud J.-P., 2000. Chemical features and seasonal variation of fine aerosol water-soluble organic compounds in the Po valley, Italy. *Atmospheric Environment* 35, 3691-3699.

Takayuki, T., Y. Kenji, H. Koh, and T. Shizuo. (1996). Seasonal variations of residence time and upper atmospheric contribution of aerosols studied with Pb-210, Bi-210, Po-210 and Be-7. *Tellus* 48(B), 690–702.

Tarasova O.A., Senik I.A., Sosonkin M.G., Cui J., Staehelin J., Prevot A.S.H., 2009. Surface ozone at the Caucasian site Kislovodsk High Mountain Station and the Swiss Alpine site Jungfraujoch: data analysis and trends (1990-2006). *Atmospheric Chemistry and Physics* 9, 4157-4175.

Thurston G.D., Spengler J.D., 1985. A quantitative assessment of source contributions to inhalable particulate matter pollution in metropolitan Boston. *Atmospheric Environment* 19, 9-25.

Tiwary A., Colls J., 2002. Air Pollution, measurement, modelling and mitigation. Ed. Routledge, pp. 60.

Todorovic, D., D. Popovic, M. Radenkovic, and G. Djuric, 1999. Concentration measurements of ^{7}Be and ^{137}Cs in ground level air in Belgrade city area. *Environment International* 25(1), 59–66.

Todorovic D., Popovic D., Djuric G., Radenkovic M., 2005. ^{7}Be to ^{210}Pb concentration ratio in ground level air in Belgrade area. *Journal of Environmental Radioactivity* 79, 297-307

Tositti L., Sandrini S., 2007. Variabilità spazio-temporale dei livelli di aerosol ambientale (frazione PM10) in provincia di Ferrara –Parte I, Ferrara, Arpa Emilia Romagna-Sezione di Ferrara, 1-98.

Tositti L., Riccio A., Sandrini S., Brattich E., Baldacci D., Parmeggiani S., Cristofanelli P., Bonasoni P., 2013. Short-term climatology of PM10 at a high altitude background station in southern Europe. *Atmospheric Environment* 65, 145-152.

Tucker L., MacCallum E., 1997. Exploratory Factor Analysis, p. 459. [http://www.unc.edu/~rcm/book/factornew.htm]

Turekian K.K., Graustein W.C., and Cochran J.K., 1989. Lead-210 in the SEAREX program: An aerosol tracer across the Pacific. In: Chemical Oceanography (Ed. J. P. Riley). Academic Press, London, pp. 51–81

Turekian K.K., and Graustein,W.C., 2003. Natural Radionuclides in the Atmosphere. Treatise on Geochemistry, Volume 4. In:Ralph Keeling F. (Ed.). Executive Editors: Heinrich D. Holland and Karl K. Turekian. pp. 347. ISBN 0-08-043751-6. Elsevier, p.261-279

UNSCEAR (United Nations Scientific Committee on the Effects of Atomic Radiation), 2000. Sources and Effects of Ionizing Radiation. United Nations, New York.

US EPA (Environmental Protection Agency), 1997. National ambient air quality standards for particulate matter, Final Rule. Washington, USEPA. *Fed Reg*, 62, 38652-760.

US EPA (Environmental Protection Agency), 2004. Air Quality Criteria for Particulate Matter, vol. I.

US EPA (Environmental Protection Agency), 2005 EPA PMF 1.1 User's Guide. US-EPA, pp. 32. [http://www.epa.gov/heasd/products/pmf/users_guide.pdf]

US EPA (Environmental Protection Agency), 2012. Acid Rain. http://www.epa.gov/acidrain/

Usher C.R., Michel A.E., Grassian V.H., 2003. Reactions on mineral dust. *Chemical Review* 103, 4883-4939

Vandini M., Fiori C., Lorusso S., 2000. Il deterioramento dei materieli lapidei di interesse storico-artistico: effetti dell'inquinamento atmosferico. Arie di città. LA qualità dell'aria in ambiente urbano. I quaderni di Arpa. pp 503-507

vanLoon G.W., Duffy S.J., 2000. Environmental chemistry. A global perspective. Oxford University Press, 492 pp.

Viana M., et al., 2008. Source apportionment of particulate matter in Europe: A review of methods and results. *Journal of Aerosol Science* 39, 827-849.

Viezee W., and Singh H.B., 1980. The distribution of Be-7 in the troposphere; implications for stratospheric/tropospheric exchange. *Geophysical Research Letters*, 7, 805–808.

Volz-Thomas A., et al., 2002. Tropospheric ozone and its control, in Towards Cleaner Air for Europe-Science, Tools and Applications. Part 1: Results from the EUROTRAC-2; Synthesis and Integration (S&I) Project, Builtjes P.J.-H. et al. (Ed.), Chap. 3, pp. 73– 122, Int. Sci. Secr., Munich, Germany.

Walmsley J.L., Mailhot J., 1983. On the numerical accuracy of trajectory models for long-range transport of atmospheric pollutants. *Atmospheric Ocean* 21, 14–39.

Wang Y.Q., Zhang X.Y., Arimoto R., 2006. The contribution from distant dust sources to the atmospheric particulate matter loadings at XiAn, China during spring. *Atmospheric Environment* 368, 875-883.

Watson J.G., Robinson N.F., Chow J.C., Henry R.C., Kim B.M., Pace T.G., Meyer E.L., Nguyen Q., 1990. The USEPA/DRI chemical mass balance receptor model. CMB 7.0. *Environmental Software* 5, 38-49.

Watson J.G., Zhu T., Chow J.C., Engelbrecht J., Fujita E.M., Wilson W.E., 2002. Receptor modelling application framework for particle source apportionment. *Chemosphere* 49, 1093-1136.

Wenche A., Min S., Lei J., Thorjørn L., Dawei Z., Renjun X., Jinhong Z., Jinsong X., Lei D., 2006. Air concentrations and wet deposition of major inorganic ions at five non-urban sites in China, 2001–2003. *Atmospheric Environment* 41, 1706–1716.

WHO (World Health Organization), 2002. Guidelines for concentration and exposure-response measurement of fine and ultrafine particulate matter for use in epidemiologic studies. WHO Dietrich Schwela, Lidia Morawska, QUT, Dimitrios Kotzias, EC JRC. Published on behalf of the European Commission.

Winchester J.W., Nifong G.D., 1971. Water pollution in Lake Michigan by trace elements from pollution aerosol fallout. *Water, Air & Soil Pollution* 1, 50-64.

Winkler R., Dietl F., Frank G., Thiersch J., 1998. Temporal variation of ^{7}Be and ^{210}Pb size distributions in ambient aerosols. *Atmospheric Environment* 32, 983-991.

Wotawa G., Kröger H., Stohl A., 2000. Transport of ozone towards the Alps – results from trajectory analyses and photochemical model studies. *Atmospheric Environment* 34, 1367-1377.

CHAPTER 2 — Short-Term Climatology of PM_{10} at Mt. Cimone

2.1 Introduction[1]

Air pollution by airborne particulate matter (from now on named PM) represents an environmental problem of primary concern whose role in air quality and climatic issues is well recognised (EMEP, 2000; WHO, 2000; IPCC, 2007; JRC, 2010; IPCC, 2013).

In fact, owing to its remarkable complexity, great efforts are being exerted in order to fill a number of gaps in the knowledge of PM phenomenology, ranging from the source apportionment to the complete resolution of the chemical mixtures according to particle size up to transformation and transport processes in which PM is involved. Though the collection of experimental data and the understanding of the atmospheric system are in continuous and tremendous progress, its inherent complexity and continuous evolution of sources still points out its incomplete knowledge and consequently the need for continuous monitoring and updating (Monks *et al*., 2009; Colbeck and Lazaridis, 2010).

In order to fulfil the need for regulating aerosol concentration levels, PM metrics have long been introduced internationally into air quality legislation. The progress in this field of research has also stimulated the evolution of PM gravimetric standards leading to a shift toward lower cut-off sizes in connection with health issues such as $PM_{2.5}$, PM_1 and $PM_{0.1}$ (particulate matter with mean aerodynamic diameter < 2.5, 1, 0.1 μm, respectively) or even suggesting the shift towards the adoption of a totally different PM standard i.e., air particles number density (USEPA, 2004; Johansson *et al.*, 2006).

[1] Part of this chapter consists of a paper by Tositti L. (Dept. of Chemistry "G. Ciamician" Università di Bologna), Riccio A. (Dept. of Applied Science, University of Napoli "Parthenope"), Sandrini S. (Dept. of Chemistry "G. Ciamician" Università di Bologna), Brattich E. (Dept. of Biological, Geological and Environmental Sciences-Section of Geology, Università di Bologna), Baldacci D. (Dept. of Chemistry "G. Ciamician" Università di Bologna), Parmeggiani S. (Dept. of Chemistry "G. Ciamician" Università di Bologna), Cristofanelli P. (Institute of Atmospheric Sciences and Climate of the Italian National Research Council ISAC-CNR), Bonasoni P. (Institute of Atmospheric Sciences and Climate of the Italian National Research Council ISAC-CNR), 2013. Short-term climatology of PM10 at a high altitude background station in Southern Europe. *Atmospheric Environment* 65, 142-152. doi:10.1016/j.atmosenv.2012.10.051. Section 2.3.5 regarding the Saharan Dust episode happened in March 2004 has been presented at 7th International Workshop on Sand/Duststorms and Associated Dustfall, 2-4/12/2013, ESA/ESRIN, Frascati (Rome), Italy.

As a result, the use of PM_{10} standard may presently appear as a somewhat dated reference metric for air particulate; nevertheless it is recognised that for environmental purposes PM_{10} is still a very informative index since to date there is a wealth of data concerning this aerosol fraction available from datasets, providing a tool for large scale comparison and analysis. Instead the attention towards the finest fractions is required for health protection purposes as well as for investigating microphysical processes.

The PM_{10} metric is also very useful in areas affected by large-scale volcanic plumes and, especially in association with $PM_{2.5}$, is a more predictive tool able to efficiently detect coarse-to-fine variations typical of natural events, such as mineral dust transport toward southern Europe. As such, PM_{10} vs. $PM_{2.5}$ relationships may help to adequately identify PM_{10} exceedances on an event basis.

Aside from scientific research and investigations within academic institutions, air quality networks provide basic information on pollution levels including PM_{10} (and now even $PM_{2.5}$) within the single countries with the objective of safeguarding population, cultural heritage and environment, as required by the European legislation. In this complex framework there emerges an increasing awareness of the importance of mixing of natural and anthropogenic PM sources influencing both the background PM levels and affecting at different levels countries in the north and south of the European continent (Querol *et al.*, 2009 and references therein; Pey *et al*., 2010).

In Italy, PM_{10} measurements are available with a good temporal and spatial coverage, especially in the northern and central regions of the peninsula, where it is measured within the air quality networks managed by the national system of environmental agencies at regional and national scale (ISPRA, 2010). For this reason most of PM_{10} data is focussed on urban sites with limited information on background stations, though recent upgrades in Italian air quality legislation is trying to fill this relevant gap. Under urban/industrial conditions where attention is mainly addressed to population safeguard, PM_{10} levels detected in the national air quality network are usually very high, especially in the Po valley where, owing to the large degree of urban development and to the low capacity of pollution dispersal (Van Dingenen *et al.*, 2004; Vecchi *et al*., 2004), air quality suffers from high frequency/high criticality PM pollution episodes, occurring mainly in winter. The average situation is such that, without suitable chemical speciation, local source intensity may mask other background contributions associated with large-scale circulation affecting the Italian peninsula throughout the year.

Moreover it has long been recognised how Italy is often downwind of African mineral dust plumes which may significantly enhance PM_{10} levels producing mass loads above the EC objective value of 50 $\mu g\ m^{-3}$, especially during the summer season, when ground level stations experience much lower seasonal averages (Balkanski *et al*., 2003; Fischer *et al*., 2003; Bonasoni et al., 2004;

Cristofanelli and Bonasoni, 2009). In other cases the influence from the European continent has been pointed out suggesting the influence of transboundary pollution (Marenco *et al.*, 2006; Riccio *et al*., 2007, 2009; EMEP, 2011).

In this Chapter the PM_{10} data time series collected over the years 1998-2011 at Mt. Cimone observatory, a high altitude station on the top of the Italian Northern Apennines, is analysed. This site is considered representative of the European continental background conditions (Bonasoni *et al.*, 2000; Marinoni *et al.*, 2008), and due to its altitude and geographical position southwards of the Alps and the Po valley, as well as being in the core of the Mediterranean region, it is suitable to study a wide spectrum of atmospheric processes. In particular, owing to its remoteness with respect to the intense pollution sources, densely clustered over the Italian territory, it offers the unique opportunity to observe background influence of airborne particulate sources, usually overshadowed by local sources at ground level.

This chapter will therefore include:

- description of the average behaviour of PM_{10} at this site based on basic statistics and on the meteorological framework;
- analysis of PM_{10} data at Mt. Cimone in connection with PM_{10} data on the regional scale collected by the local networks North and South of the Apennine range;
- analysis of PM_{10} data in association with fine and coarse particles number density;
- source apportionment of PM_{10} based on back-trajectories clustering technique.

2.1.1 Site description

Mt. Cimone station (44°11' N, 10°42' E, 2165 m asl) is located on the highest summit of the Northern Apennines experiencing both regional and long-range transport of air masses (Bonasoni *et al.*, 1997, 2000; Cristofanelli *et al.*, 2006; Cristofanelli and Bonasoni, 2009) (Figure 2.1). The station is maintained by the Italian Meteorological Office managed by the Italian Air Force since 1941 and hosts the research platform "Ottavio Vittori" managed by ISAC-CNR[2]. Its main meteorological features can be briefly summarized as follows: an annual mean temperature of about 2°C, with a winter mean and minimum respectively of -4°C and -22°C and a summer mean and maximum of about 10°C and 18°C. Snow cover usually lasts from November to late May. Mt. Cimone is the windiest site among the Italian meteorological stations, with wind speeds reaching intensities of 216 km h^{-1}. During the year prevailing winds blow from S-SW in the warm season and N-NE in the cold one. More details on the station are available at http://www.isac.cnr/cimone/.

[2] Institute of Atmospheric Sciences and Climate of the Italian National Research Council

Figure 2.1 *Location of Mt. Cimone station in the northern Italian Apennines (Planiglobe, kk&w - digital cartography, http://www.planiglobe.com/).*

2.2 Experimental

Ambient aerosol is systematically collected at Mt. Cimone since 1998 with a high volume PM_{10} sampler by General Metal Works collecting aerosol particles with a mean aerodynamic diameter lower than 10 μm. Filters are manually changed every two or three days.

The equipment has been adapted in order to overcome the harsh meteorological conditions of the site, frequently characterised by high relative humidity, strong winds and low temperatures often leading to sudden and quick frosting. The sampling head has thus been equipped with a heating system by an electric resistance to prevent inlet icing in case of harsh meteorological conditions. Sampling operations (with exception PC interface of filter change) are remotely controlled from

Bologna facilities at ISAC-CNR allowing the recording of mean meteorological and sampling parameters during air filtration.

The average flow rate is about 1.13 m^3 min^{-1} at standard temperature and pressure (STP), with an average volume of air collected on each filter equal to 3000-4000 m^3 during approximately 48 hours samplings (115-175 samples per year), depending on weather conditions, failures of the sampling equipment and/or of the power supply and personnel on site. A total of 839 two-day samples were collected during the period 1998-2011 (53% of the total collected samples).

The PM_{10} data collected at ground stations, used in Subsection 2.3.2 to describe the regional framework, were gravimetrically determined by the Environmental Protection Agencies networks of Emilia Romagna and Tuscany according to the European Standard EN 12341 (CEN, 1998), absorbed in the Italian Ministerial decree n.60 (DM 60/02).

The uncertainty associated with the sampled volume has been estimated by the manufacturer to be around 5%. Aerosol is collected on rectangular glass-fiber filters (Whatman, 20 cm x 25 cm). According to the product specification the collection efficiency of the filters is more than 99% for the inhalable fraction of aerosol with diameter between 0.1 and 10 μm.

Once delivered to the University of Bologna, aerosol mass load on filters is determined gravimetrically by an electronic microbalance with a sensitivity of 0.0001 g after 24 hours filter conditioning at controlled temperature (22-24 °C) and relative humidity (around 30%) inside a desiccator. After weighing, the PM_{10} samples are subjected to non-destructive high-resolution γ-spectrometry with HPGe detectors for the determination of airborne radiotracers lead-210 and beryllium-7, only marginally treated in this work, but already partially investigated in other papers (Gerasopoulos *et al.*, 2001; Cristofanelli *et al.*, 2006; Lee *et al.*, 2007) and treated in following Chapters 3, 4, 5 and 6 of this thesis.

At Mt. Cimone, since 2000, concentration and size distribution of particles with optical diameter between 0.30 and 20 μm have been continuously recorded by ISAC-CNR in 15-size channels by using an optical particle counter (OPC, Mod. GRIMM 1.108). These measurements allow the determination of a fine mode (0.3 μm ≤ Dp < 1 μm) and a coarse mode (1 μm ≤ Dp ≤ 20 μm) of particles with a 1-minute time resolution. The instrument is based on the quantification of the 90° scattering of light by aerosol particles. According to the specifications, the reproducibility of the OPC in particle counting is ±2% (Putaud *et al.*, 2004). A heated non-selective sampling head at 9 m above the ground draws air in the OPC inlet. The sampling head heating system, together with the laboratory temperature, constant at about 20°C for the whole year, prevents size counting bias at high relative humidity levels affecting hygroscopic growth.

Prior to the analysis, all the concentrations have been normalized at 25°C and 1 atm.

2.2.1 Trajectory model description and source apportionment technique

In order to evaluate the effects of short-term climatology on PM_{10} concentrations, back trajectories were calculated by means of the HYSPLIT model (version 4.9; Draxler, 1999).

HYSPLIT is a well-known trajectory model, updated several times over the last two decades (Draxler and Taylor, 1982; Draxler, 1992; Draxler, 1999; Draxler and Rolph, 2011) and now is a complete system for computing simple trajectories for complex dispersion and deposition simulations using either puff or particle approaches. It has already been used to cluster trajectories arriving at several sites in Northern (Dorling and Davies, 1995) and Southern Europe (Escudero *et al.*, 2006).

Gridded meteorological data from the NCAR/ARL website were used. NCAR data consist of a large set of global meteorological data, stored at a spatial resolution of 2.5° × 2.5° in a 6-hours archive starting from 1948. These data originate from the operational series of computer forecasts and analysis undertaken by the National Centers for Environmental Prediction.

Four back trajectories for each day were computed, covering the whole monitoring period. Trajectories arrive at synoptic times (00, 06, 12, and 18 UTC) at the height of 1000 m above the measurement site, and were integrated backward in time by interpolating the 4-D wind records to the current particle positions up to five days back.

A review by Stohl (1998) revised the limitations and advantages which apply to trajectory calculations; the uncertainties involved in any analyzed meteorological field, the interpolation to trajectory position and the lack of representation of small-scale effects (e.g., turbulence) inevitably limit the significance of analysis based on backward trajectories. Typical trajectory errors are about 10–20% of the travel distance, but individual trajectories can have much larger errors depending on the meteorological situation (Harris *et al.*, 2005); moreover, the analysis of backward trajectories is known to generate "ghost sources" in the wake of real emission sources (Wotawa and Kröger, 1999; Maione *et al.*, 2008) since it implicitly assumes that concentrations measured at the receptor site are smeared out along all the associated trajectories; Vasconcelos *et al*. (1996 a, b) investigated the spatial resolution of the method, and found that the angular resolution was good, but that the radial resolution was poor, so that caution is needed in the interpretation of results from back-trajectories.

However, the limitations and uncertainties that apply to individual trajectories may, to some extent, be overcome by a statistical classification approach, aggregating a large number of trajectories over a long time period, since potential errors tend to average out. Notwithstanding their limitations, trajectory classification approaches have been used to analyze source-receptor relationships in a large number of studies: Keeler and Samson (1989), Seibert *et al*. (1994), Stohl (1996), Cape *et al*. (2000), Lui *et al*. (2003), Bonasoni *et al*. (2004), Marinoni *et al*. (2008), and many others of similar vein.

In this work a source-receptor approach has been applied. Ashbaugh (1983) and Ashbaugh *et al.* (1985) originally developed this approach and much work has been done to add to this basic method (Seibert *et al.*, 1994; Stohl, 1996).

According to Ashbaugh *et al.* (1985), a conditional probability (CP) was reconstructed by exploiting the residence time of each trajectory; to this aim, the European domain was discretized using grid cells, each one of 1.0° × 1.0° side length, and the "high incident trajectories" (HITs), i.e., trajectories arriving at the receptor site during a measurement period at or above the 50th percentile, were selected, which means that the concentration values residing in the highest 50% of all measured concentrations were considered. The time spent by HITs in each grid cell was calculated, and a CP was assigned to each grid cell by means of the formula

$$CP_{ij} = \frac{HIT_{ij}}{T_{ij}} \tag{2.1}$$

where HIT_{ij} is the residence time of 'hits' in the (i, j) grid cell and T_{ij} the time spent by all trajectories in the same grid cell.

The resulting field may exhibit small-scale variations that are not necessarily statistically significant and should not be shown in a contour plot. On the other hand, a simple smoothing is not completely justified, since it can remove significant features. In order to remove small-scale variations in the concentration field, while retaining the most statistically significant features, HIT_{ij} was filtered using a binomial test with a 95% confidence level. HIT_{ij} values which did not significantly exceed 50% were set to zero. This value was chosen since the high incident days were defined as those at, or above, the 50th percentile. The test was applied to the CP_{ij}s of each cell, assuming that individual values were independent from each other.

The CP field is related to most relevant emission source areas (Seibert *et al.*, 1994; Stohl, 1996); however, it should be stressed that the actual spatial distribution of emission sources may be different because meteorological conditions (and thus also the emission, transformation and removal processes) are specific for the pathways towards Mt. Cimone, and the resulting CP field has to be interpreted as a map of source fields contributing specifically to the concentration at this site.

The vertical transport is not considered in this methodology, therefore here the contributions from upper troposphere and lower troposphere are not distinguished.

2.3 Results and discussion

2.3.1 PM_{10} trend

The dataset depicted in Figure 2.2 (light dots) consists of the PM_{10} mass load concentrations measured at Mt. Cimone from 1998 to 2011.

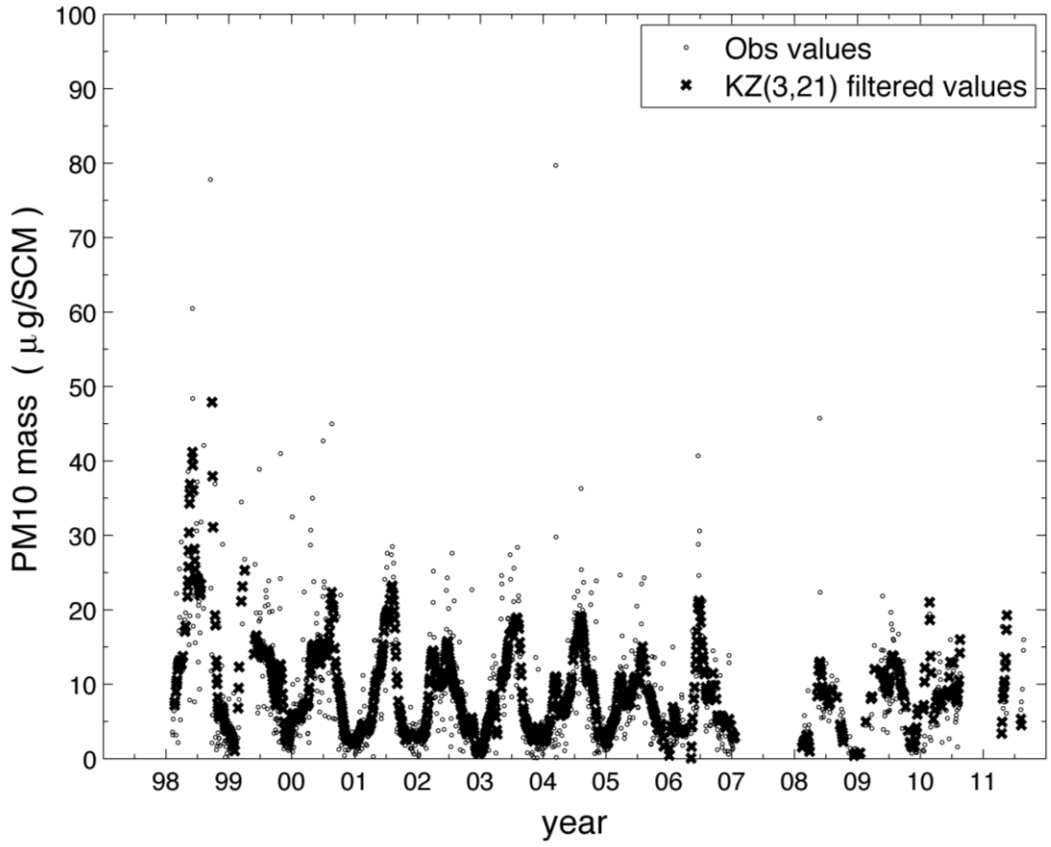

Figure 2.2 *PM_{10} concentration (small dots). The thicker markers are the seasonal fluctuations, as estimated by the KZ(3,21) filter. 'SCM' stands for Standard Cubic Meter, i.e., concentration normalized at 1 atm and 25 °C.*

The large gap presented by the data in 2007 is due to technical problems with the aerosol sampler. Owing to manual filter change at the station, sampling time is not uniform (though most samples are collected over 48 hours), therefore in order to safely apply statistical techniques data have been firstly homogenised by selecting only those samples referring to an averaging period no longer than 48 hours. The selection of only two-days averaged samples is also required by the analysis of source-receptor relationships; values referring to a sampling period longer than two days may be associated with fast changing synoptic conditions, so that back trajectories may derive from very different source areas, "blurring" the resulting images and adding an additional source of

uncertainty into the interpretation of source-receptor relationships. All data referring to the PM_{10} mass accumulated over a longer time period have been neglected in any further analyses.

PM_{10} displays a marked intra-annual variation, with winter minima and summer maxima (see Figure 2.2); to highlight anomalies, i.e., the synoptically influenced deviations from the seasonal cycle, the original time series was de-seasonalized by means of the Kolmogorov-Zurbenko filter (Zurbenko, 1986), denoted as *KZ*(*m*,*n*). This filter is based upon the calculation of a moving average $\bar{z}_t$ centered over a time window of *n* values (*n* is an odd integer), i.e.,

$$\bar{z}_t = \frac{1}{n} \sum_{i=t-(n-1)/2}^{t+(n-1)/2} y_i \tag{2.2}$$

The moving average is then iterated *m* times. A detailed discussion of the KZ filter, as well as comparisons with other separation techniques, can be found in Eskridge *et al.* (1997) and Rao *et al.* (1997).

The de-seasonalized time series (Figure 2.3) was obtained by:

$$PM = PM^{MCT} \frac{\overline{PM}}{PM^{KZ}} \tag{2.3}$$

where PM^{MCT} is the original time series measured at the Mt. Cimone site, $\overline{PM}$ is the mean concentration, evaluated over the whole monitoring period, and PM^{KZ} is the seasonal fluctuation obtained after the application of the *KZ*(3,21) filter, i.e., the moving average applied three times over a time windows of twenty-one days (thicker markers in Figure 2.2); this filter was chosen because it guarantees an almost perfect separation of the seasonal and synoptic time scales, as evaluated from the spectral response of the filter (Rao *et al.*, 1997). The de-seasonalized time series is shown in Figure 2.3. Summer maxima of the seasonal deviation will be discussed in more details later on in this Section.

The resulting time-series is characterised by remarkable variability between samples. In this framework the variations of PM_{10} concentrations mostly reflect the balance between sources and removal by meteorological processes whose time-scale is of the order of 3-5 days, i.e., a quasi-synoptic timescale. The mass load concentrations mainly fall below 10 μg m^{-3} and may occasionally exceed 20 μg m^{-3} (10% of cases). Fluctuations over the mean periodical behaviour show the occurrence of relative minima associated mainly with wet removal of PM throughout the year and/or with limited exchange with ground-level sources, most typical during the winter. Relative maxima are widely scattered throughout the year though the most significant increases tend to be more frequent in the warm season.

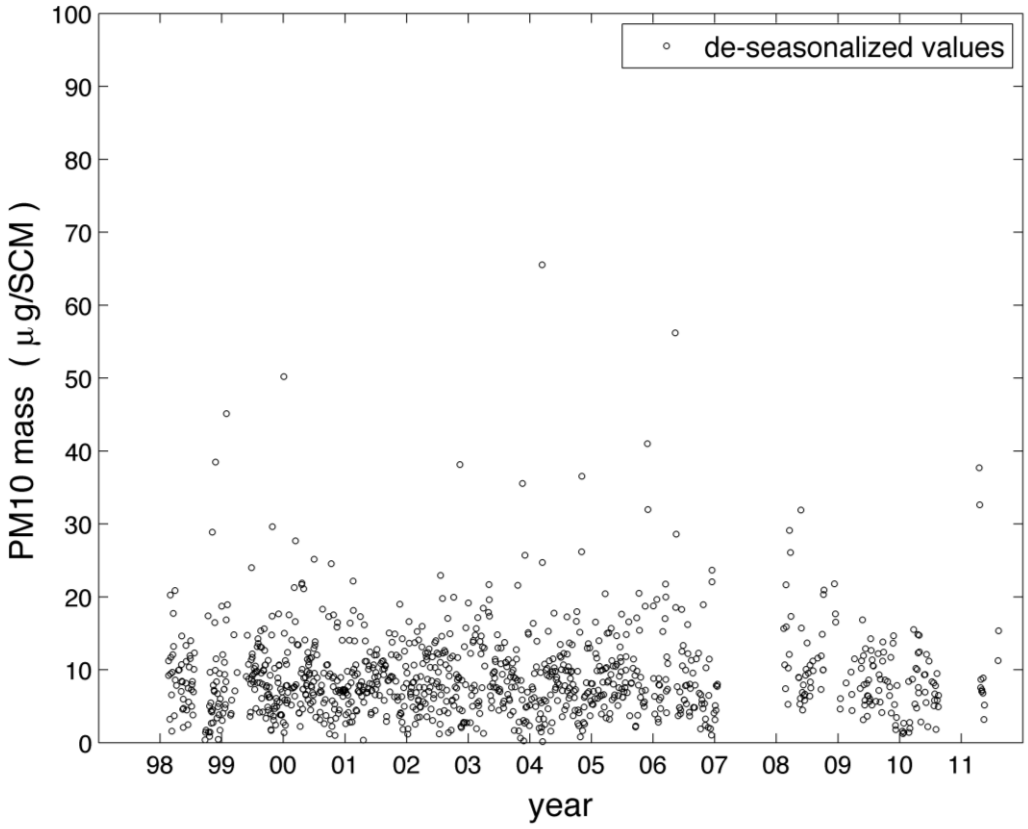

Figure 2.3 *De-seasonalized PM_{10} time series obtained by eqn. (2.3).*

An analysis of basic statistics results obtained on the rough data (number of observations = 1586) yields an arithmetic mean of 8.8 ± 8.0 µg m^{-3} (geometric mean = 6.0 µg m^{-3}; min = 0.1 µg m^{-3}; max = 79.7 µg m^{-3}); a skewness level of 2.6 indicates asymmetry in the data distribution, as clearly evident from the probability density function (pdf) in Figure 2.4. The distribution shows its maximum around 4 -6 µg m^{-3} suggesting the geometric mean as a more representative parameter rather than arithmetic mean.

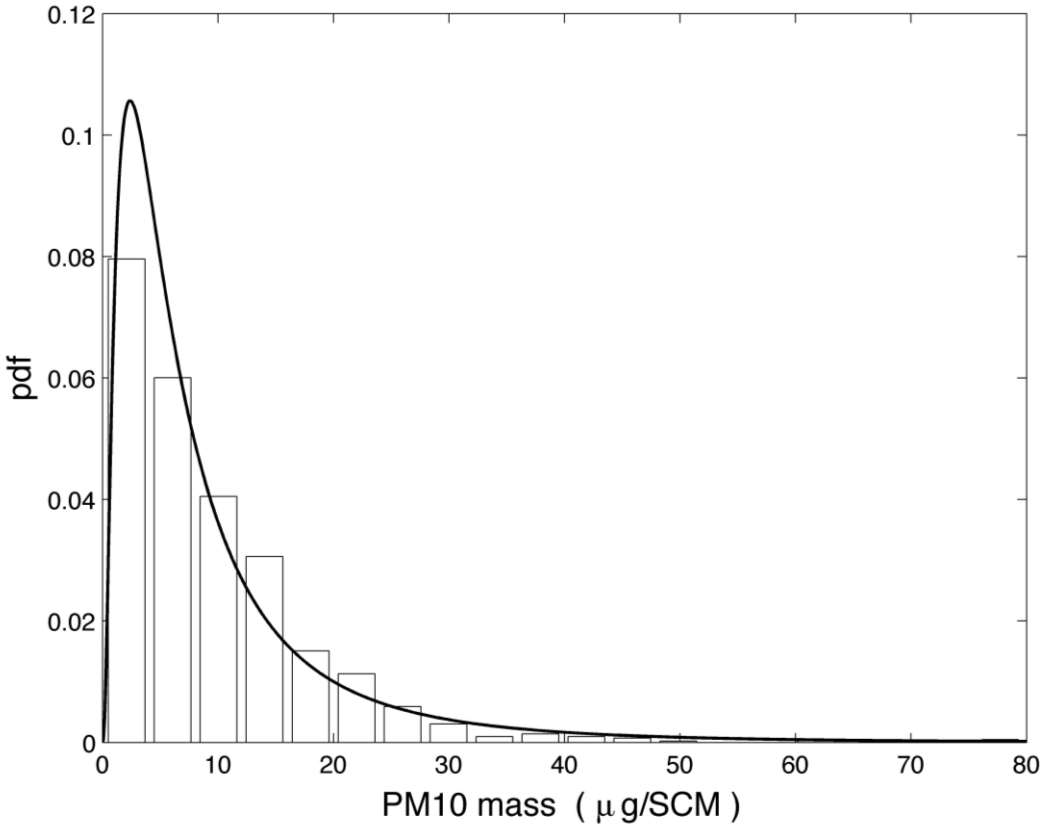

Figure 2.4 *Empirical probability density function of PM_{10} concentration (bars). The solid line is the maximum likelihood estimation of a log-normal pdf fitted to the data.*

2.3.2 The regional framework

High values of PM mass loads at this high altitude station were analysed in a doctoral thesis by Baldacci (2005) based on the comparison of PM_{10} relative maxima with the corresponding values of ^{210}Pb measured in the samples, the fine and coarse particle number density, Atmospheric Optical Thickness (AOT) and back trajectories analysis on an event basis. In summary, highest PM_{10} data can be attributed on average to three classes of events:

- Saharan dust transports from the northern African deserts, which act as an important source of mineral dusts for both the western (Prospero, 1996; Barnaba and Gobbi, 2004; Bonasoni *et al.*, 2004; Escudero *et al.*, 2005; Cristofanelli *et al.*, 2009), central (Di Sarra *et al.*, 2001; Barkan *et al.*, 2005) and eastern Mediterranean area (Papayannis *et al.*, 2005);
- uplift of polluted air masses from the Italian areas north of the Apennines range (i.e., Po Valley), especially during intrusion events from the boundary layer favoured by deep convection (Crosier *et al.*, 2007; Carbone *et al.*, 2010);
- advection of PM_{10} enriched air masses from the European continent North and East of the Italian peninsula.

Interannual variations are also observed as a result of dominating meteorological conditions in single years. Comparison of annual means is depicted in Figure 2.5, reporting box and whiskers plot of collected PM_{10} and grouped by year. The annual means show largest variability at higher concentration levels; in principle this effect is mostly ascribed to Saharan dust incursions, often observed at Mt. Cimone (Bonasoni *et al*., 2004, Marinoni *et al*., 2008; Riccio *et al*., 2009) and whose frequency is rather unpredictable while they lead to remarkable increments in PM_{10} mass load as described in Baldacci (2005).

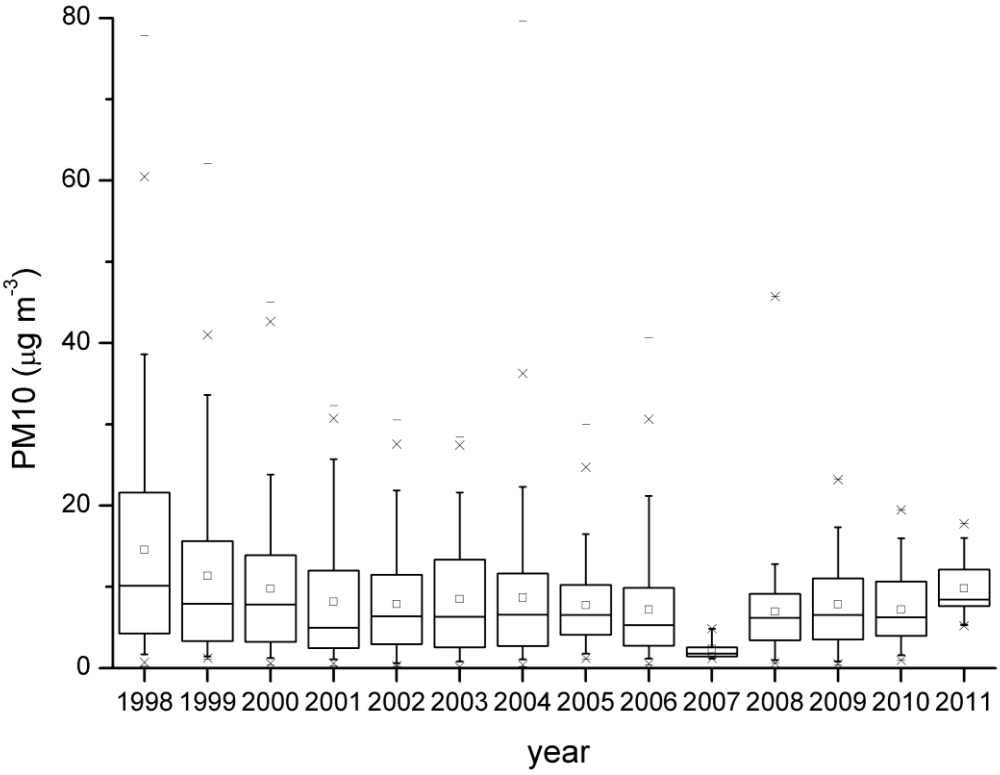

Figure 2.5 *Box and whiskers plot of the PM_{10} collected at Mt. Cimone and grouped by year (1998-2011). The boxes contain the range 25^{th}-75^{th} percentile of the data; the whiskers represent the 5^{th} and 95^{th} percentile, while the square and the line inside the boxes denote the arithmetic mean and the median, respectively. Crosses and external lines represent the outliers and extreme values (minima and maxima), respectively.*

As previously discussed, PM_{10} time series shows a pronounced seasonal fluctuation with winter minima and summer maxima. This seasonal behaviour has been evaluated on the basis of frequency analysis on data grouped by single month (Figure 2.6). Asymmetry in the frequency distribution is preserved in all the months, though summer months' concentrations are distributed over a broader interval compared to the other months. It is observed that PM_{10} concentration reaches maximum levels in July and minimum in December. This behaviour is attributed to the seasonal fluctuation of the mixed layer height, as well as to the intense vertical exchange in the lower troposphere occurring in the warm season at this latitude, as reported by Baltensperger (1997), Baldacci (2005), Cristofanelli *et al.* (2006, 2009). The importance of vertical motion and of the resulting lower troposphere mixing has been already discussed in a previous paper concerning the behaviour of the $^{7}Be/^{210}Pb$ ratio at Mt. Cimone (Lee *et al.*, 2007), a parameter which is known to efficiently describe this transport component within the troposphere as a result of the mixing of natural radionuclides whose reservoirs are located respectively in the stratosphere/upper troposphere (^{7}Be) and in the mixed layer (^{210}Pb).

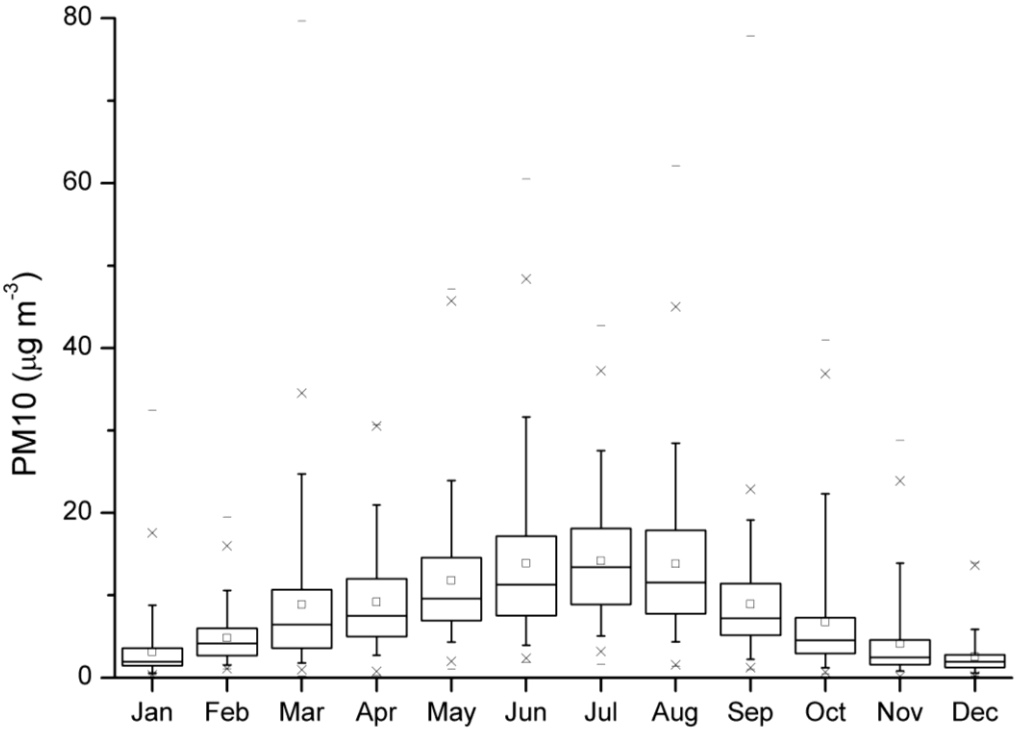

Figure 2.6 *Box and whiskers plot of the PM_{10} collected at Mt. Cimone (1998-2011) and grouped by months.*

As previously reported (Bonasoni *et. al.*, 2000; Fischer *et al*, 2003), during the cold season background free-troposphere conditions are often accomplished at Mt. Cimone top, whereas during the warm season the top of Mt. Cimone is enveloped into a fluctuating mixed layer, a phenomenology characterized by a daily modulation which, as a result of solar heating, is particularly intense during

this period (Marinoni *et al.*, 2008). The overall seasonal effect is a combination of upward motion due to mixed layer expansion, thermal convection and mountain/valley breeze regime, altogether resulting into the uplift of airborne particulate from the lower troposphere and the substantial increase of mass load observed during the warm season. Nucleation at this height may be relevant as promoted by the favourable physico-chemical conditions, but its contribution in term of mass load is negligible, therefore the source of airborne particulate mass is mainly attributed to transport from sources at the regional and synoptic scale, as previously mentioned. This behaviour is further confirmed by the good agreement between PM_{10} and ^{210}Pb (Pearson's correlation coefficient R = 0.56; Spearman's correlation coefficient R = 0.70), suggesting that they share source and timing in connection with the prevailing accumulation (fine) mode fraction (Lee *et al.*, 2007).

The influence of the efficient vertical exchange, driven by thermal convection in the warm season and causing the uplift of PM from ground level sources to Mt. Cimone top, is observed even at the Jungfraujoch in Switzerland, i.e., at higher altitude and latitude with respect to Mt. Cimone (Baltensperger, 1997; Tomasi *et al.*, 2003). On the regional scale the PM_{10} increase at Mt. Cimone summit during the warm season is in phase-opposition with stations at ground level, both northward (Po Valley) and southward of the Apennine range, where maxima are recorded during the winter (i.e., when stable conditions inhibit the uplift of PM emitted at ground level).

It is worth to note that, in agreement with the above observations, PM_{10} at Mt. Cuccolino, a semirural monitoring station (presently discontinued) of the Regional Environmental Protection Agency (ARPA Emilia-Romagna), at about 200 m asl on the hills close to Bologna, corresponds to an intermediate height between the behaviour in the free troposphere and in the mixed layer, showing a very weak seasonality and PM concentrations between ground stations and Mt. Cimone (see Figure 2.7).

The analyzed regional data of PM_{10}, on a daily sampling time basis, allows for further observations. The 2004 PM_{10} data at ground stations were determined gravimetrically on daily samples collected on filters at stations of the Environmental Protection Agencies networks of Emilia Romagna and Tuscany (mostly covering urban stations and a few rural and semirural stations). Figure 2.7 shows that, while the seasonal behaviour is opposite due to the winter decoupling from the CBL and the summer upward expansion of CBL over Mt. Cimone, on the lower timescale a strong correlation between all the stations in certain dates can be noted.

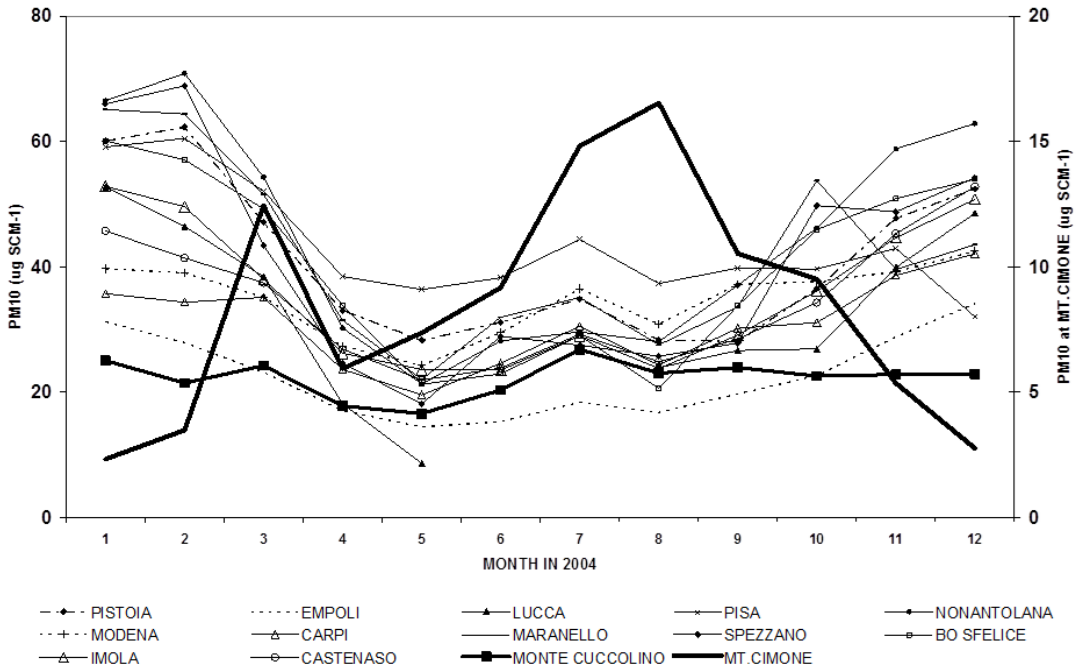

Figure 2.7 *PM_{10} monthly means at various stations south and north Mt. Cimone in 2004. Southern stations are located in Tuscany (Empoli, Lucca, Pisa, Pistoia,), while Northern stations are located in Emilia-Romagna (Bologna S. Felice, Carpi, Castenaso, Imola, Maranello, Modena, Monte Cuccolino, Nonantolana, Spezzano). The Mt. Cimone average value during March shows the influence of a huge Saharan dust outbreak, whose effect is very strong, suggesting a high elevation transport episode, which will be discussed with details in following Section 2.3.5.*

2.3.3 PM_{10} vs. OPC densities

In order to obtain a more detailed characterization of PM_{10} fluctuations at Mt. Cimone, the data were compared with number densities of fine (< 1 μm) and coarse (>1 μm) particles simultaneously measured at this site since 2000 with an Optical Particle Counter. The latter data were extensively discussed in Van Dingenen *et al*., (2005) and Marinoni *et al*. (2008).

Figures 2.8(a,b) depict the trend of PM_{10} and, respectively, fine particles (a) and coarse (b) particles for the year 2005, in which the number density series is less patchy.

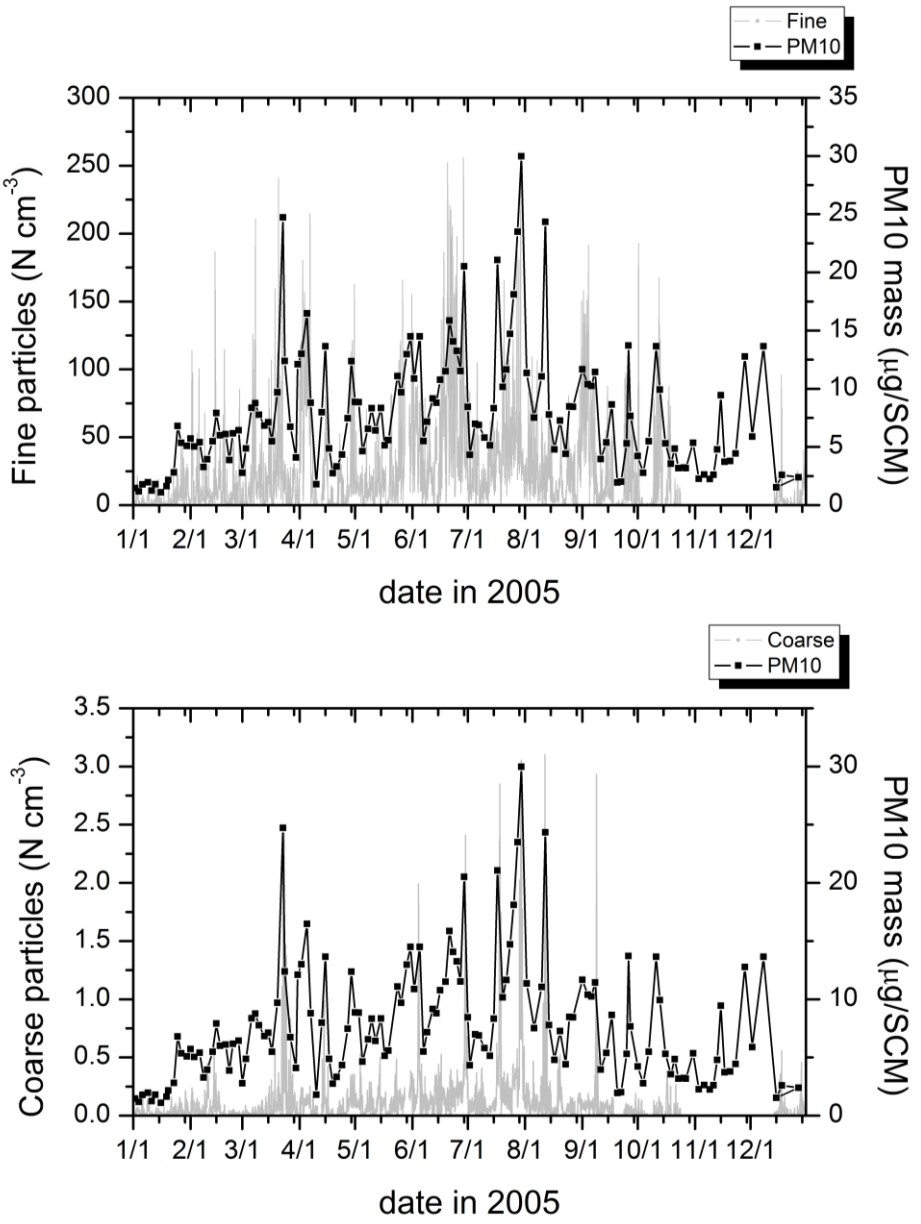

Figure 2.8(a,b) *Trend of PM_{10} and fine particles (0.3 μm ≤ Dp < 1 μm) (a) and coarse particles (1 μm ≤ Dp ≤ 20 μm) (b) for the year 2005 at Mt. Cimone.*

During the periods in which all the above observations were available the trend is very similar, showing a good agreement between fine and coarse fractions, according to the expected behaviour of airborne particulate and its relationships. The pattern of PM_{10} and number densities are in excellent overall agreement showing that the adopted sampling strategy of PM_{10} is able to efficiently capture a large fraction of its variance, even at this theoretically poor time resolution.

In order to analyse the correlations between PM_{10} mass loadings and OPC data, number densities were averaged over the same time interval of PM_{10} sampling. This allowed to obtain the scatter plots presented in Figure 2.9, reporting respectively PM_{10} vs. fine particles (Figure 2.9 a), PM_{10} vs. coarse particles (Figure 2.9 b) and coarse vs. fine particles (Figure 2.9 c).

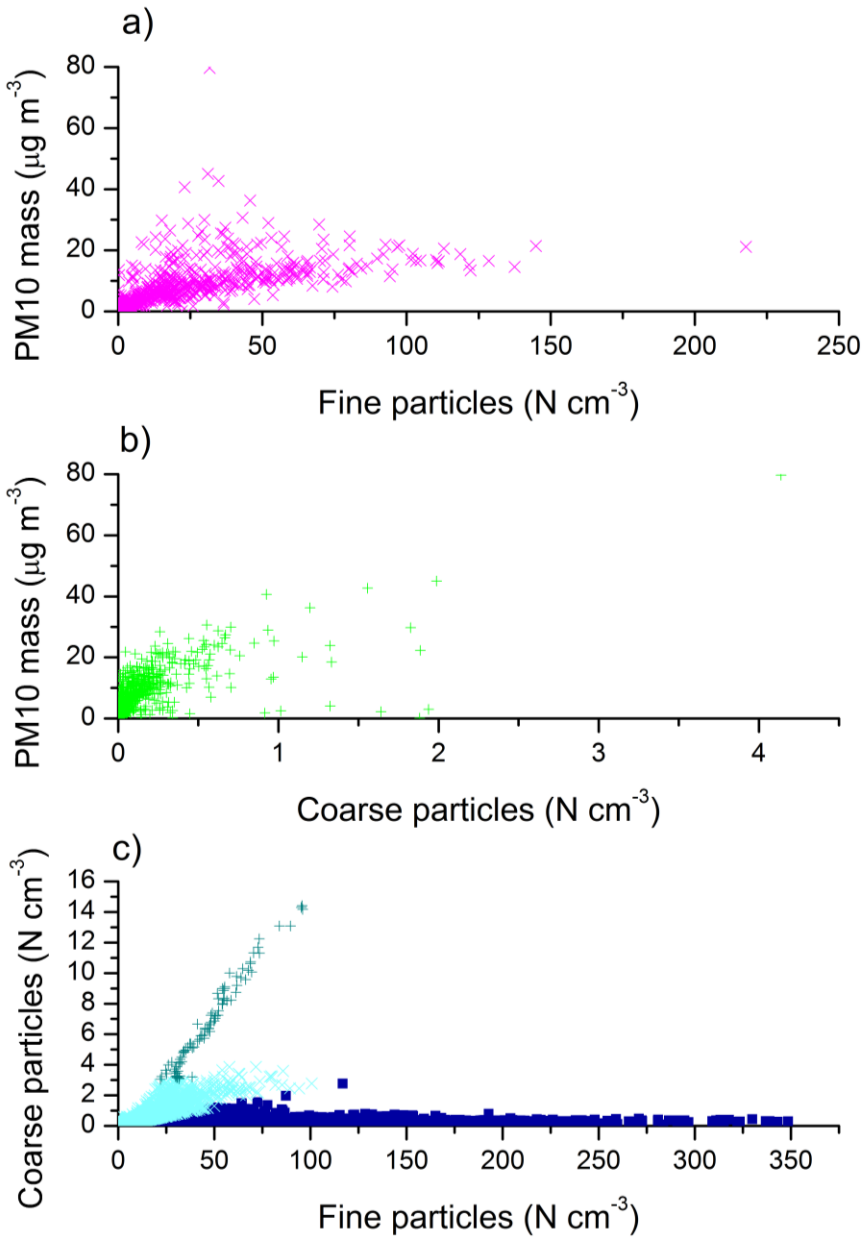

Figure 2.9(a,b,c) *Scatter plot of a) PM_{10} vs. fine particles b) PM_{10} vs. coarse particles and c) coarse vs. fine particles. In Figure 2.9 c data have been classified in three clusters; clusters are indicated by different symbols and colors, i.e., dark cyan "pluses", cyan "crosses" and blue small dots.*

As previously observed, high PM_{10} can be produced not only by Saharan Dust episodes carrying high coarse fractions, but also by the uplift of polluted air masses enriched in secondary aerosol.

The plot of coarse vs. fine particles (Figure 2.9 c) clearly shows the presence of three main classes of events; "*k*-means" analysis have been exploited to cluster these classes using the cosine similarity as aggregation criteria. The first cluster (dark cyan plus symbols) is characterized by high values of the coarse fraction: most of data present in this cluster belong to an exceptional event of

Saharan dust transport occurred from 13 to 15 March 2004, which was already reported by Beine *et al.* (2005). A second cluster (cyan crosses) is characterized by significant loadings of the coarse fraction (normally between 2 and 4 particles cm^{-3}), with a small contribution from the fine fraction. The visual inspection of satellite aerosol optical depth maps (MODIS and SeaWIFS) and model data (DREAM) shows that most of these events are attributable to Saharan dust events. Finally, the last cluster (blue small dots) shows data with small loadings of the coarse fraction (less than 2 particles cm^{-3}) but significant fine loadings, suggesting events of anthropogenic pollution.

Another interesting feature in Figures 2.9 a and 2.9 b is that PM_{10} peaks appear to be associated either with coarse plus fine particle peaks as a consequence of Saharan dust incursions or uniquely to fine particles peaks when air masses originate in air sheds enriched in secondary pollutants.

It is remarkable to note that during Saharan dust events not only the coarse fraction but also the finer fraction typically increase (Marinoni *et al.*, 2008), as already observed by other authors (Prospero *et al.*, 2001; Zauli Sajani *et al.*, 2011). Therefore, while polluted air masses can be characterised by simultaneous increases of fine particles number and PM_{10}, Saharan dust events are traced by the simultaneous increase of coarse plus fine mass loadings.

Moreover, as reported in Baldacci (2005), PM_{10} increase due to polluted air masses uplift is accompanied by a simultaneous increase of ozone and ^{210}Pb, a good proxy for secondary aerosol from the lower troposphere layer (Graustein and Turekian, 1996; Arimoto *et al.*, 1999; Hammer *et al.*, 2007; Dombrowski-Etchevers *et al.*, 2009), for which back trajectories suggest source areas in the Balkans or in northern central Europe or even in the Po Valley as reported by Bonasoni *et al.* (2004) and Marinoni *et al.* (2008), and with greater details in Chapter 6. Instead in the case of Saharan Dust, ozone has been found to decrease, as reported in Figure 2.10, where de-seasonalized PM_{10} and O_3 time series acquired at Mt. Cimone from 1998 till 2003 are reported. O_3 decreases are linked to a double effect: reduced sources of pollution in Northern Africa together with O_3- destroying reactions on the surface of mineral particles probably through catalytic mechanisms due to their chemical-physical structure (Usher *et al.*, 2003; Bonasoni *et al.*, 2004). This suggests that a multitracer approach (Bonasoni *et al.*, 2004) seems to better constrain the behaviour of certain kinds of transports.

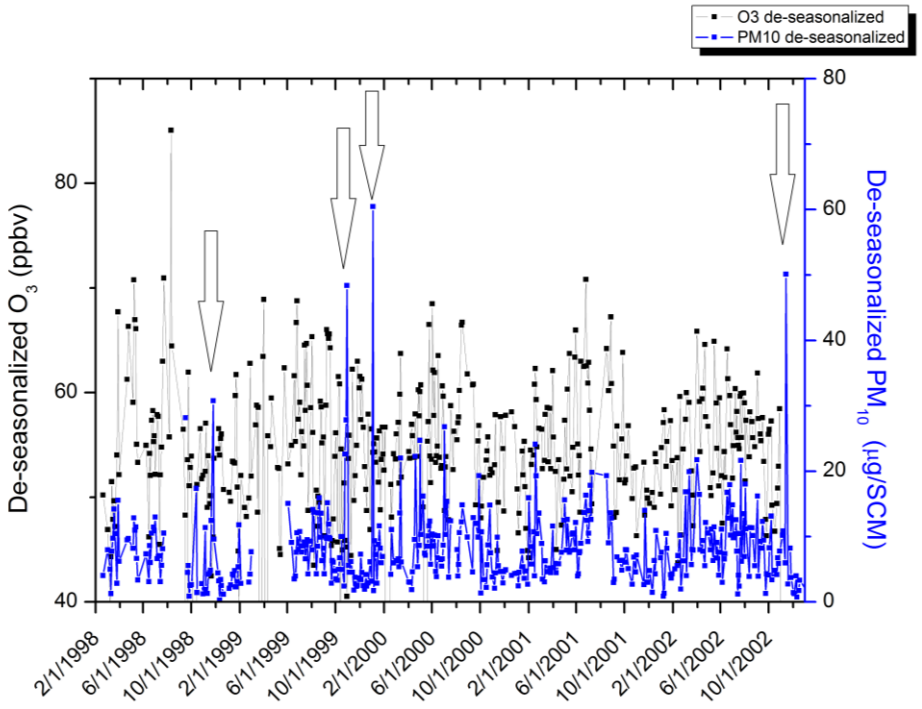

Figure 2.10 *De-seasonalized O_3 and PM_{10} time series acquired at Mt. Cimone from 1998 till 2003. Arrows indicate events identified as Saharan Dust incursions, where increases of PM_{10} and decreases of O_3 are observed.*

As concerns ^{210}Pb, its role in association with Saharan Dust is not straightforward; this aspect is presently under investigation since ^{210}Pb occurrence in mineral dust seems to be affected both by geographical origin of resuspended material and by grain-size.

2.3.4 Source apportionment by Hysplit back trajectories

As described in Subsection 2.2.1, back trajectories were calculated by means of the HYSPLIT4 model, and used to evaluate the conditional probability in eqn. (2.1).

Figure 2.11 shows the conditional probability map, obtained by eqn. (2.1). This figure highlights the direction of arrival of the most important contributions to the measured PM_{10} at Mt. Cimone. Apart from the expected contributions from the nearby Italian regions, important contributions come from Northern African, and Eastern European regions, confirming that Mt. Cimone station, at the centre of the Mediterranean basin, could be the ideal experimental platform for observing the "crossroads" of pollution transports, as outlined by the modelling work of Lelieveld *et al*. (2002).

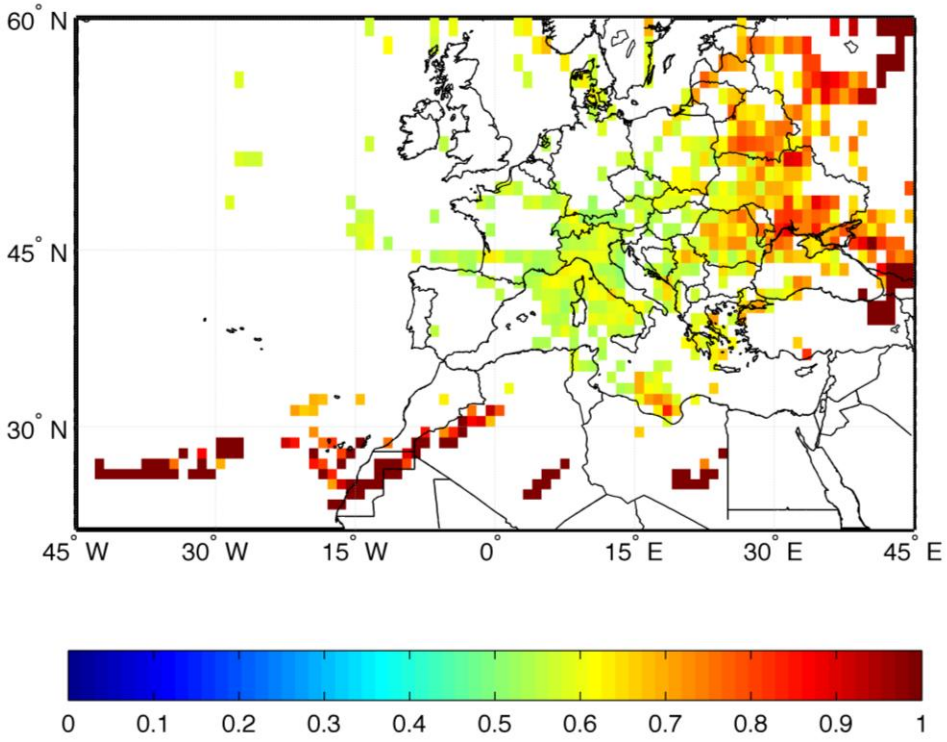

Figure 2.11 *Source-receptor relationships, as evaluated by the conditional probability map defined by eqn. (2.1). Non-significant sources were filtered by using a binomial test at a 95% significance level.*

These results are comparable to those obtained by equivalent analyses. Using the Absorbing Aerosol Index (AAI) derived from TOMS (Total Ozone Mapping Spectrometer) on the Nimbus 7 satellite, Prospero *et al*. (2002) characterized the major dust sources in the world. In the African continent the most active dusty areas are made by an extensive system of salt lakes and dry lakes found in the lowlands south of the Tell Atlas, the Eastern Libyan Desert and Egypt, and a quasi-permanent dusty area extending from the coast of Mauritania deep into Algeria, the so-called "dust belt". It is worthwhile to note that the analysis of residence times ascribes to some of these areas the contribution to the most severe PM episodes recorded at Mt. Cimone.

As the trajectory statistics applied in this work attributes the same weight to all segments of the trajectory and not to the segment corresponding to the actual location of emissions (Stohl, 1996), then artificial emission sources can be localized in regions where several back trajectories during high concentration events have passed through, before passing over the actual source region. The maximum of conditional probability east of the Canary Islands and Morocco coastline is associated with trajectories passing first over the Atlantic Ocean and then north-eastward over North Africa, where dust is actually mobilized, toward the Mediterranean basin, in agreement with Israelevich *et al.* (2012). Due to the equal weight assumption, the source-receptor analysis assigns a high conditional probability to the segments passing off the Atlantic coasts, too, so that this maximum

can be probably ascribed as a fictitious result. The same reasoning also applies to the relative maximum off the Libyan coast, over the Gulf of Sirte, where trajectories are usually associated with an anticyclonic pathway from the Libyan Desert or from Egypt.

The analysis of residence times highlights the contribution from eastern European countries. While PM (and its precursors) emissions have declined in western countries during the last decade, it is expected not to be reduced as quickly, or even to increase, in eastern European and former Soviet Union (FSU) countries: the total PM emissions from FSU countries from mobile sources will probably exceed those from western European countries from 2015 onwards, before eventually declining (WBCSD, 2004). The map in Figure 2.11 reveals that trajectories from the Eastern sector usually load a high level of PM mass and are associated with the highest PM concentrations at the receptor site.

2.3.5 The dust episode in March 2004

Dust outbreaks are very common throughout the year, with a peak frequency in spring (March, April, May) towards the Atlantic Ocean, or in late spring/summer (May, June, July) towards the Mediterranean Sea (even if winter and especially autumn events, though less frequent, are usually very intense) (Prospero *et al*., 2002; Baldacci, 2005; Barkan *et al*., 2005). Every year strong winds blowing over the Sahara desert lift hundreds of millions of tons of dust high into the sky over North Africa.

In 2004, from 13 to 15 March, as reported by Beine *et al*. (2005), a severe PM episode was observed at Mt. Cimone. Figure 2.12(a-e), showing the 2004 time series of PM_{10}, ^{210}Pb, number densities of fine and coarse particles, and ^{7}Be, highlights a clear increase of all these parameters during the Saharan Dust episode (per cent increase with respect to monthly mean of March 2004: +540% PM_{10}, +73% ^{210}Pb, +54% number density of fine particles, +360% number density of coarse particles, +32% ^{7}Be; per cent increase with respect to yearly mean of 2004: +820% PM_{10}, +33% ^{210}Pb, +42% number density of fine particles, + 1257% number density of coarse particles). Reasons for this and other ^{7}Be more relevant increases connected to transports from the Northern Africa regions will be given in following Chapters 5 and 6, which will specifically deal with the characterization of advection patterns and their impact on variations in atmospheric composition observed at Mt. Cimone. Here it can be briefly anticipated that some episodes of transport from North-Africa seem to be connected not only to uplift of crustal particles and increases of PM_{10} and ^{210}Pb, but also to strong downdrafts from the upper troposphere and to increases in ^{7}Be, in agreement, for instance, with Dueñas et al. (2011). A contemporary decrease of O_3 (Figure 2.12 f) was also observed (per cent decrease with respect to monthly mean of March 2004 equal to -9%; per cent decrease with respect to yearly mean of 2004 equal to -5%), for the reasons previously

explained in Subsection 2.3.3. In particular, the most relevant increases were observed for PM_{10} and for coarse particles: PM_{10} concentration reached 80 μg m^{-3}, a value seven times higher than the mean level during the preceeding and subsequent days, and the maximum PM_{10} concentration recorded at Mt Cimone in more than 12 years observations. This episode has been ascribed to a long lasting Saharan dust outbreak, as confirmed by back trajectories calculated for the period and by the results of the DREAM model (Figure 2.13 shows examples of the results obtained for 15th March 2004), starting at the beginning of March, and first impacting the Atlantic Ocean and then the Mediterranean area.

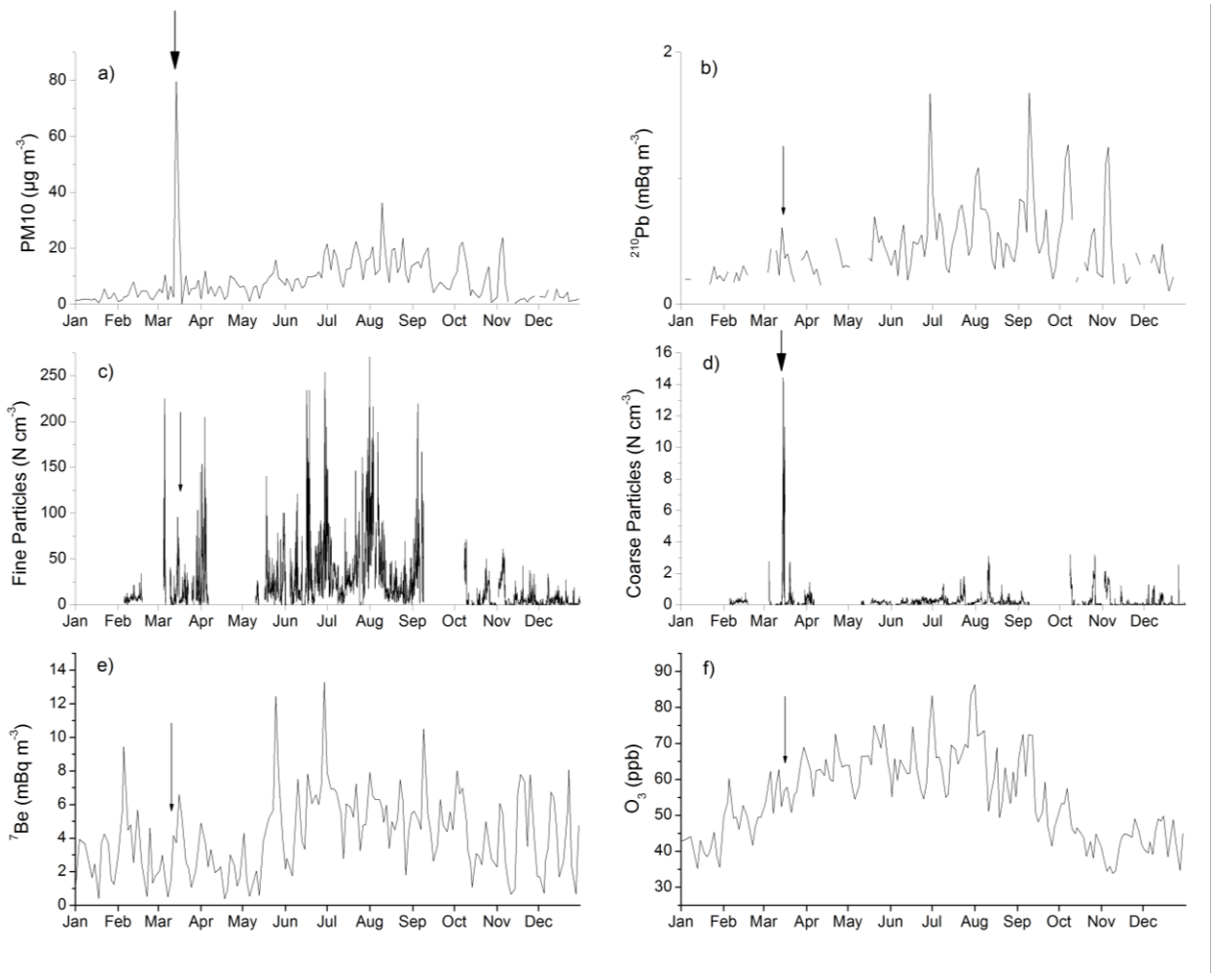

Figure 2.12(a,b,c,d,e,f) *Time series of PM_{10} (a), ^{210}Pb (b), number density of fine particles (c), number density of coarse particles (d), ^{7}Be (e) and ozone (f) for the year 2004 at Mt. Cimone. Arrows indicate the observed increase (in the case of PM_{10}, ^{210}Pb, fine and coarse particles number densities, ^{7}Be) and decrease in the case of O_3, connected to the outstanding Saharan Dust transport of March 2004.*

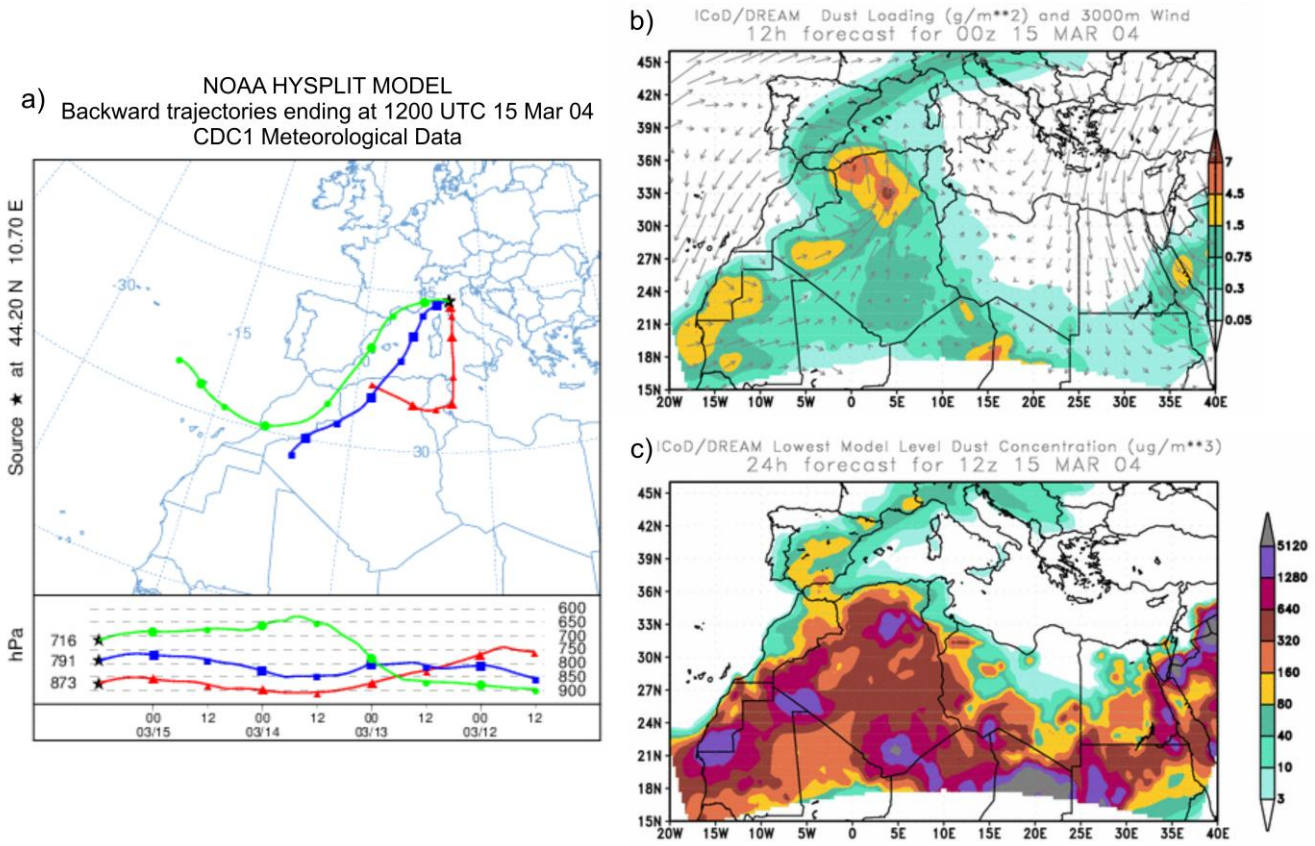

Figure 2.13(a,b,c) *a) Back-trajectories (96-hours backward) calculated by Hysplit-4 model ending at Mt. Cimone on 15th March 2004, 12 UTC and for three arrival heights: 1400, 2200 and 3000 m asl; b) Dust loading from the dust regional model DREAM for the day 15th March 2004, 00 UTC; c) Lowest model level dust concentration resulting from the dust regional model DREAM (images from the BSC-DREAM8b (Dust REgional Atmospheric Model) model, operated by the Barcelona Supercomputing Center, http://www.bsc.es/projects/earthscience/DREAM/) for the day 15th March 2004, 12 UTC.*

The first part of this episode has been described in details elsewhere (Knippertz and Fink, 2006). This event originated from the Bodele depression in northern Chad, a remarkable source of dust (Koren *et al.*, 2006); the analysis of aerosol optical depth (Figure 2.16) revealed that dustiness conditions occurred along the entire ITCZ. On 5th March 2004 images from the visible channel of the SeaWIFS satellite (Figure 2.14) show a huge, dense, meridionally oriented dust plume off the northwest African coast from west of Madeira to Cape Verde, sustained by hazy and prolonged Harmattan conditions. This plume spread laterally, moved westward and formed an arc for over 5000 km from Guinea to the northern tip of Morocco. The plume crossed the Atlantic Ocean and impacted onto the Caribbean region (Knippertz and Fink, 2006).

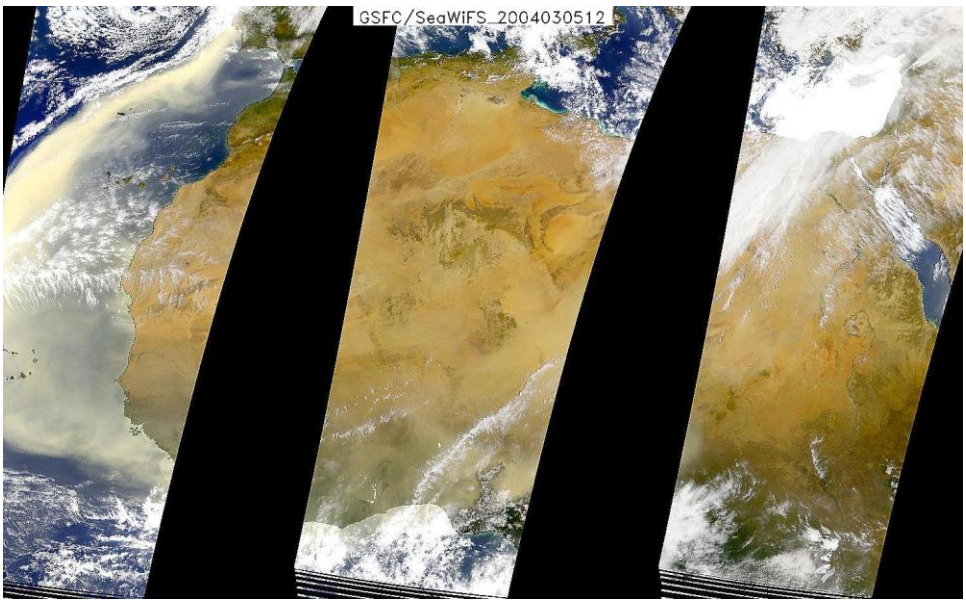

Figure 2.14 *The SeaWIFS image for 15 March 2004 shows a major dust outbreak from Western Africa across the Atlantic. The massive storm formed a huge arc of thick dust reaching Cape Verde Islands and the shores of Western Europe; during the following days, the dust plume continued to spread southwards and westwards. (Image courtesy of the SeaWIFS Project, NASA Goddard Space Flight Center).*

At the end of this extraordinary episode, the sequence of two main meteorological patterns: 1) the penetration of an upper-level trough to low latitudes with a minimum centered over the NW Algerian coast; and 2) a Sahara high extending all over the Mediterranean Sea with an elongated north-eastward tongue, mobilized dust to the south of the northern Atlas Mountains in Morocco and western Algeria. The inception of a steep gradient pressure between a trough and a Saharan high along the Western Sahara and the western Mediterranean basin is a typical condition during which dust is efficiently transported toward the central Mediterranean (Barkan *et al*., 2005).

The synoptic conditions characterizing the mid-March period is represented by the NCEP-based map of 700 mbar level (Figure 2.15). The chart shows the relative position of the two geopotential maxima/minima, and the NE high extending toward the western Mediterranean basin. Figure 2.16 shows the aerosol optical depth at the beginning of the second dust outbreak (on 13th March, 2004) and the average over the period 10-15 March, 2004. These images clearly show the severe dust outbreaks across the Atlantic and the Northern part of Italy: during this event the monitoring site at Mt. Cimone was located exactly along the main axis of the dust plume trajectory, leading to a PM_{10} record maximum of 80 μg m^{-3}.

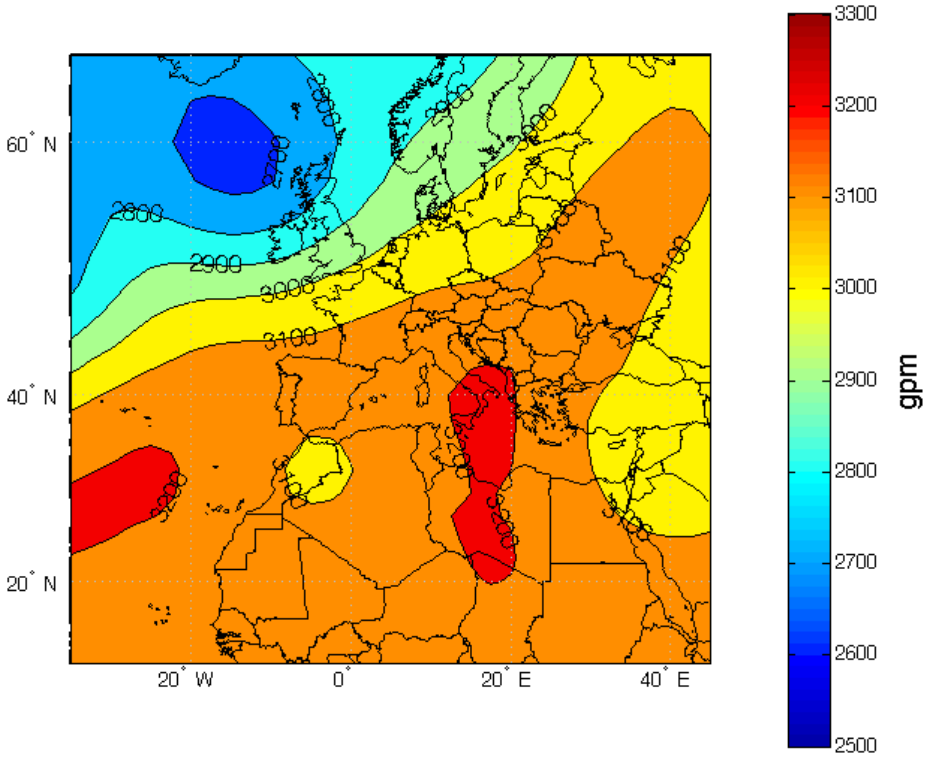

Figure 2.15 *The geopotential height at 700 mbar for 14 March 2004, 12 UTC. Data from the NCEP/DOE AMIP-II Reanalysis project (Image provided by the NOAA-ESRL Physical Sciences Division, Boulder Colorado from their Web site at http://www.esrl.noaa.gov/psd/).*

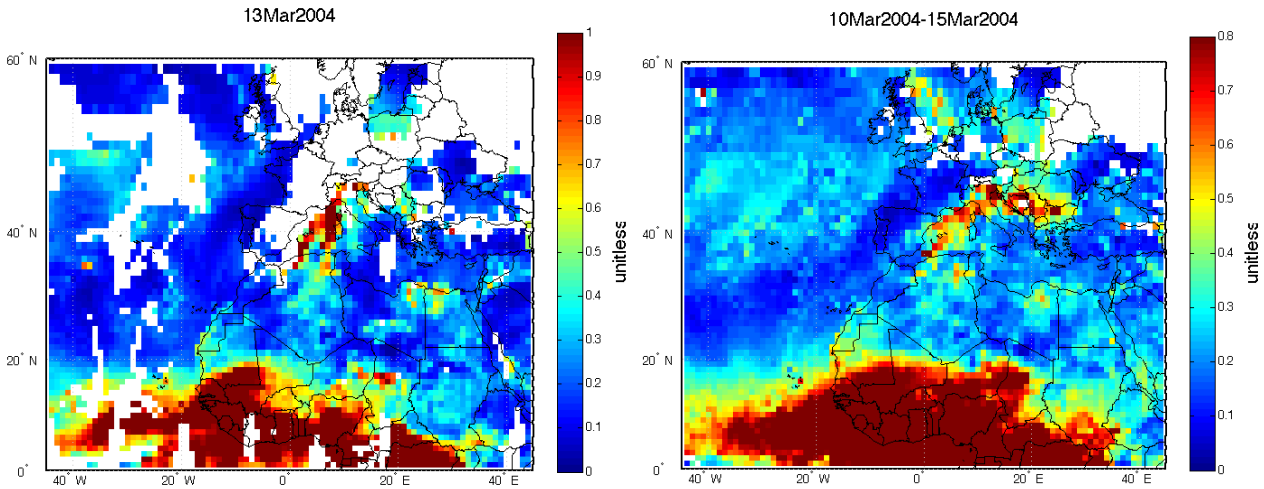

Figure 2.16 *Aerosol optical depth at 0.55 μm, daily average on 13th March 2004 (left), and time averaged over the period 10-15 March 2004 (right). Every image is the average over data from the MODIS Terra and Aqua satellites (MOD08_D3.051 and MYD08_D3.051 collections). Deep Blue retrievals are included into the average. (Image courtesy of MODIS instrument team, NASA Goddard Space Flight Center).*

2.4 Conclusions

The analysed PM_{10} data series collected at Mt. Cimone over the years 1998-2011 was found to be characterized by a marked intra-annual variation as well as by a seasonal cycle with winter minima and summer maxima. The latter phenomenology is caused both by the seasonal fluctuation of the mixed layer height and by the intense vertical exchange during the warm season, as well as mountain/valley breeze regimes. Average PM_{10} value at this high elevation site amounts to 8.8 $\mu g\ m^{-3}$, the whole data-set being characterized by a lognormal distribution.

The de-seasonalized time series showed a remarkable variability between samples, due to the balance between sources and removal processes.

A complex effect of different processes and different sources on the PM_{10} time series at the receptor site is revealed by the use of different kinds of measurements, statistical and source apportionment techniques.

The highest PM_{10} concentrations were found to be connected with three different kinds of processes, such as Saharan dust transports from the Northern African deserts, uplift of polluted air masses from the Italian areas north of the Apennines range and advection of PM_{10} enriched air masses from the European continent. In fact, the source apportionment conducted through back trajectories statistical techniques recognised high contributions from the nearby Italian regions as expected, but also from Northern Africa (mineral dust) and Eastern Europe (highly polluted air masses from less developed countries).

The analysis of PM_{10} data in connection with coarse and fine particle number revealed that while during Saharan dust events both the fine and the coarse fraction usually increase, during uplifts of polluted air masses only the rise up of the fine fraction is usually observed.

A detailed analysis of the synoptic conditions during an exceptional Saharan dust event observed during March which led to the extremely high concentration of 80 $\mu g\ m^{-3}$ at Mt. Cimone was also presented.

It is confirmed that the location hosting the research activity herein reported provides an ideal platform for the observation of aerosol transport from source areas including both well-recognized and less investigated regions.

Acknowledgements

Italian Air Force Meteorological Office is gratefully acknowledged for hosting ISAC-CNR atmospheric research platform, therefore allowing for the collection of precious compositional datasets.

ISAC-CNR is gratefully acknowledged for providing aerosol size distribution and ozone data, besides infrastructural access at the WMO-GAW Global Station Italian Climate Observatory "O. Vittori" at Mt. Cimone. The Italian Climate Observatory "O. Vittori" is supported by MIUR and DTA-CNR throughout the Project of National Interest NextData.

We acknowledge NOAA (http://www.esrl.noaa.gov/) for providing the HYSPLIT trajectory model (available at http://ready.arl.noaa.gov/HYSPLIT.php) and the NCEP/NCAR reanalysis data used in this study (images available at http://www.esrl.noaa.gov/psd/). The Barcelona Supercomputing Center is acknowledged for providing images from the BSC-DREAM8b (Dust REgional Atmospheric Model) model http://www.bsc.es/projects/earthscience/DREAM/. PLANIGLOBE (http://www.planiglobe.com/) is acknowledged for providing the map for locating Mt. Cimone. NASA Goddard Space Flight Center is acknowledged for providing satellite images of MODIS (Terra and Aqua) and SeaWIFS.

References

Arimoto R., Snow J.A., Graustein W.C., Moody J.L., Ray B.J., Duce R.A., Turekian K.K. and Maring H.B., 1999. Influences of atmospheric transport pathways on radionuclide activities in aerosol particles from over the North Atlantic. *Journal of Geophysical Research* 104, D17, 21301-21316, doi:10.1029/1999JD900356.

Ashbaugh L.L., 1983. A statistical trajectory technique for determining air pollution source regions. *Journal of the Air Pollution Control Association* 33, 1096-1098.

Ashbaugh L.L., Malm W.C., Sadeh W.Z., 1985. A residence time probability analysis of sulfur concentrations at Grand Canyon National Park. A statistical trajectory technique for determining air pollution source regions. *Atmospheric Environment* 19, 1263-1270.

Baldacci D., 2005. Identificazione delle sorgenti di aerosol atmosferico e influenza sui livelli di PM10 a Monte Cimone a Bologna. PhD Thesis in Earth and Environmental Sciences, University of Bologna (tutor: Prof. Tositti Laura).

Balkanski Y., Bauer S.E., Van Dingenen R., Bonasoni P., Schulz M., Fischer H., Gobbi G.P., Hanke M., Hauglustaine D.A., Putaud J.-P., Stohl A., Raes F., 2003. The Mt Cimone, Italy, free tropospheric campaign: principal characteristics of the gaseous and aerosol composition from European pollution, Mediterranean influences and during African dust events. *Atmospheric Chemistry and Physics Discussion* 3, 1753–1776.

Baltensperger U., Gäggeler H. W., Jost D. T., Lugauer M., Schwikowski M., Weingartner E., and Seibert P. 1997. Aerosol climatology at the high-alpine site Jungfraujoch, Switzerland. *Journal of Geophysical Research* 102(D16), 19,707–19,715, doi:10.1029/97JD00928.

Barkan J., Alpert P., Kutiel H., Kishcha P., 2005. Synoptics of dust transportation days from Africa toward Italy and central Europe. *Journal of Geophysical Research* 110, 7208–7221, D07208, doi:10.1029/2004JD005222.

Barnaba F. and Gobbi G.P., 2004. Aerosol seasonal variability over the Mediterranean region and relative impact of maritime, continental and Saharan dust particles over the basin from MODIS data in the year 2001. *Atmospheric Chemistry and Physics* 4, 2367-2391.

Beine H.J., Amoroso A., Esposito G., Sparapani R., Ianniello A., Georgiadis T., Nardino M., Bonasoni P., Cristofanelli P., and Dominé F., 2005. Deposition of atmospheric nitrous acid on alkaline snow surfaces. *Geophysical Research Letters* 32, L10808, doi:10.1029/2005GL022589.

Bonasoni P., Calzolari F., Colombo T., Corazza E., Santaguida R., Tesi G., 1997. Continuous CO and H_2 measurements at Mt. Cimone (Italy): preliminary results. *Atmospheric Environment*, 31, No.7, 959-967.

Bonasoni P., Stohl A., Cristofanelli P., Calzolari F., Colombo T., Evangelisti F., 2000. Background ozone variations at Mt. Cimone Station. *Atmospheric Environment* 34, 5183–5189.

Bonasoni P., Cristofanelli P., Calzolari F., Bonafé U., Evangelisti F., Stohl A., Zauli Sajani S., van Dingenen R., Colombo T., Balkanski Y., 2004. Aerosol-ozone correlations during dust transport episodes. *Atmospheric Chemistry and Physics* **4**, 1201–1215.

Cape J.N., Methven J, and Hudson L.E., 2000. The use of trajectory cluster analysis to interpret trace gas measurements at Mace Head, Ireland. *Atmospheric Environment* 34, 3651–3663, doi: 10.1016/S1352-2310(00)00098-4.

Carbone C., Decesari S., Mircea M., Giulianelli L., Finessi E., Rinaldi M., Fuzzi S., Marinoni A., Duchi R., Perrino C., Sargolini T., Vardè M., Sprovieri F., Gobbi G.P., Angelini F., Facchini M.C., 2010. Size-resolved aerosol chemical composition over the Italian Peninsula during typical summer and winter conditions. *Atmospheric Environment* 44(39), 5269-5278.

CEN (Comité Européen de Normalisation), 1998. Air Quality Determination of the PM10 fraction of suspended particulate matter. Reference method and field test procedure to demonstrate reference equivalence of measurement methods. Ref. No. EN12341:1998.

Colbeck I., and Lazaridis M., 2010. Aerosols and environmental pollution. *Naturwissenschaften* 97:2, 117-131.

Cristofanelli P., Bonasoni P., Tositti L., Bonafè U., Calzolari F., Evangelisti F., Sandrini S. and Stohl A., 2006. A 6-years analysis of stratospheric intrusions and their influence on ozone at Mt. Cimone (2165 m above sea level). *Journal of Geophysical Research* 111, D03306, doi: 10.1029/2005JD006553.

Cristofanelli P. and Bonasoni P., 2009. Background ozone in the southern Europe and Mediterranean area: Influence of the transport processes, *Environmental Pollution* 157, 1399–1406.

Cristofanelli P., Marinoni A., Arduini J., Bonafè U., Calzolari F., Colombo T., Decesari S., Duchi R., Facchini M. C., Fierli F., Finessi E., Maione M., Chiari M., Calzolai G.; Messina P., Orlandi E., Roccato F., and P. Bonasoni, 2009. Significant variations of trace gas composition and aerosol properties at Mt. Cimone during air mass transport from North Africa – contributions from wildfire emissions and mineral dust. *Atmospheric Chemistry and Physics Discussion* 9, 7825-7872.

Crosier J., Allan, J.D., Coe, H., Bower, K.N., Formenti, P., Williams, P.I., 2007. Chemical composition of summertime aerosol in the Po Valley (Italy), northern Adriatic and Black Sea. *Quarterly Journal of the Royal Meteorological Society* 133, 61-75.

Di Sarra A., Di Iorio T., Cacciani M., Fiocco G., and Fua D., 2001. Saharan dust profiles measured by lidar at Lampedusa. *Journal of Geophysical Research* 106, 10335–10347.

DM 60/02, Decreto Ministeriale n.60 del 02/04/2002. Decreto Ministeriale n° 60 del 02/04/2002 Recepimento della direttiva 1999/30/CE del Consiglio del 22 aprile 1999 concernente i valori limite di qualità dell'aria ambiente per il biossido di zolfo, il biossido di azoto, gli ossidi di azoto, le particelle e il piombo e della direttiva 2000/69/CE relativa ai valori limite di qualità aria ambiente per il benzene ed il monossido di carbonio.

Dombrowski-Etchevers I., Peuch V.-H., Josse B. and Legrand M., 2009. Evaluation of the parametrized transport of lead-210 in high-altitude European sites. *Geoscientific Model Development Discussion* 2, 247-278.

Dorling S.R., and Davies T.D., 1995. Extending cluster analysis-synoptic meteorology links to characterize chemical climates at six Northwest European monitoring stations. *Atmospheric Environment* 29, 145-167.

Draxler R.R., and Taylor A.D., 1982. Horizontal dispersion parameters for long-range transport modeling. *Journal of Applied Meteorology* 21, 367-372.

Draxler R.R., 1992. Hybrid single-particle Lagrangian integrated trajectories (HYSPLIT): Version 3.0 -- User's guide and model description. NOAA Tech. Memo. ERL ARL-195, 26 pp. and Appendices.

Draxler R.R., 1999. HYSPLIT4 user's guide. NOAA Tech. Memo. ERL ARL-230, NOAA Air Resources Laboratory, Silver Spring, MD.

Draxler R.R. and Rolph G.D., 2011. HYSPLIT (HYbrid Single-Particle Lagrangian Integrated Trajectory) Model access via NOAA ARL READY Website (http://ready.arl.noaa.gov/HYSPLIT.php). NOAA Air Resources Laboratory, Silver Spring, MD.

Dueñas C., Orza J.A.G., Cabello M., Fernández M.C., Cañete S., Pérez M., Gordo E., 2011. Air mass origin and its influence on radionuclide activities (^{7}Be and ^{210}Pb) in aerosol particles at a coastal site in the western Mediterranean. *Atmospheric Research* 101, 205-214.

EMEP Co-operative Programme for Monitoring and Evaluation of the Long Range Transmission of Air Pollutants, 2000. Status Report with respect to Measurements, Modelling and Emissions of Particulate Matter in EMEP: An Integrated Approach. Joint CCC and MSC-W Report 2000. Available at http://www.nilu.no/projects/ccc/reports/emep5-2000.pdf, last accessed May 10, 2012.

EMEP Co-operative Programme for Monitoring and Evaluation of the Long Range Transmission of Air Pollutants, 2011. Status Report 4/2011 Transboundary particulate matter in Europe. CCC & MSC-W & ceip & ciam Report 2011. Available at http://www.nilu.no/projects/ccc/reports/emep4-2011.pdf, last accessed May 10, 2012.

Eskridge R.E., Ku J.Y., Rao S.T., Porter P.S., and Zurbenko I.G., 1997. Separating different scales of motion in time series of meteorological variables. *Bullettin of the American Meteorological Society* 78, 1473–1483.

Escudero M., Castillo S., Querol X., Avila A., Alarcón M., Viana M.M., Alastuey A., Cuevas E., and Rodríguez S., 2005. Wet and dry dust episodes over Eastern Spain. *Journal of Geophysical Research* 110, D18S08, doi:10.1029/2004JD004731.

Escudero M., Stein A., Draxler R.R, Querol X., Alastuey A., Castillo S., and Avila A., 2006. Determination of the contribution of northern Africa dust source areas to PM10 concentrations over the central Iberian Peninsula using the Hybrid Single-Particle Lagrangian Integrated Trajectory model (HYSPLIT) model. *Journal of Geophysical Research* 111, D06210, doi:10.1029/2005JD006395.

Fischer H., Kormann R., Klupfel T., Gurk C., Konigstedt R., Parchatka U., Muhle J., Rhee T.S., Brenninkmeijer C.A.M., Bonasoni P., and Stohl A., 2003. Ozone production and trace gas correlations during the June 2000 MINATROC intensive measurement campaign at Mt. Cimone. *Atmospheric Chemistry and Physics* **3**, 725–738.

Gerasopoulos E., Zanis P., Stohl A, Zerefos C.S., Papastefanou C., Ringer W., Tobler L., Huebener S., Kanter H.J., Tositti L. and Sandrini S., 2001. A climatology of ^{7}Be at four high-altitude stations at the Alps and the Northern Apennines. *Atmospheric Environment* 35/36, 6347-6360.

Graustein W.C. and Turekian K.K., 1996. ^{7}Be and ^{210}Pb indicate an upper troposphere source for elevated ozone in the summertime subtropical free troposphere of the eastern North Atlantic. *Geophysical Research Letters* 23, 539-542.

Hammer S., Wagenbach D., Preunkert S., Pio C.A., Schlosser C. and Meinhardt F., 2007. Lead-210 observations within CARBOSOL: a diagnostic tool for assessing the spatiotemporal variability of related chemical aerosol species? *Journal of Geophysical Research* 112, D23S03.

Harris J.M., Draxler R.R. and Oltmans S.J., 2005. Trajectory model sensitivity to differences in input data and vertical transport method. *Journal of Geophysical Research* 110 D14109, doi:10.1029/2004JD005750.

IPCC (Intergovernmental Panel on Climate Change), Fourth Assessment Report, 2007. Climate Change 2007: The Physical Science Basis. Available at http://www.ipcc.ch, last accessed May 10, 2012.

IPCC (Intergovernmental Panel on Climate Change), 2013. Working Group I Contribution to the IPCC Fifth Assessment Report. Climate Change 2013: The Physical Science Basis. Approved summary for policy makers. Twelfth Session of Working Group I. Available at http://www.climatechange2013.org/images/uploads/WGI_AR5_SPM_brochure.pdf, last accessed 24th November 2013

ISPRA (Istituto Superiore per la Ricerca e la Protezione Ambientale), 2010. Annuario dei dati ambientali (in Italian). Available online at http://annuario.apat.it/, Last accessed May 10, 2012.

Israelevich P., Ganor E., Alpert P., Kishcha P., and Stupp A., 2012. Predominant transport paths of Saharan Dust over the Mediterranean Sea to Europe. *Journal of Geophysical Research* 117, D02205, doi:10.1029/2011JD016482.

Johansson C., Norman M., Gidhagen L., 2006. Spatial and temporal variations of PM10 and particle number concentrations in urban air. *Environmental Monitoring and Assessment* 127,477-487, doi:10.1007/s10661-006-9296-4.

JRC (European Commission Joint Research Centre Institute for Environment and Sustainability) Scientific and Technical Reports, 2010. Climate and air quality impacts of combined climate change and air pollution policy scenarios. Available online at http://publications.jrc.ec.europa.eu/repository/bitstream/111111111/15085/1/lbna24572enc.pdf, last accessed May 10, 2012.

Keeler G.J. and Samson P.J., 1989. Spatial representativeness of trace element ratios, *Environmental Science and Technology*, 23 (11), 1358–1364.

Knippertz P., and Fink A.H., 2006. Synoptic and dynamic aspects of an extreme springtime Saharan dust outbreak. *Quarterly Journal of the Royal Meteorological Society* 132, 1153–1177.

Koren I., Kaufman Y.J., Washington R., Todd M.C., Rudich Y., Martins J.V., Rosenfeld D., 2006. The Bodele depression: a single spot in the Sahara that provides most of the mineral dust to the Amazon forest. *Environmental Research Letters* 1(1), doi:10.1088/1748-9326/1/1/014005

Lee H. N., Tositti L., Zheng X. D., Bonasoni P., 2007. Analyses and comparisons of ^{7}Be, ^{210}Pb and activity ratio $^{7}Be/^{210}Pb$ with ozone observations at two GAW stations from high mountains. *Journal of Geophysical Research* **112**, 1 – 11.

Lelieveld J., Berresheim H., Borrmann S., Crutzen P.J., Dentener F.J., Fischer H., Feichter J., Flatau P.J., Heland J., Holzinger R., Korrmann R., Lawrence M.G., Levin Z., Markowicz K.M., Mihalopoulos N., Minikin A., Ramanathan V., De Reus M., Roelofs G.J., Scheeren H.A., Sciare J., Schlager H., Schultz M., Siegmund P., Steil B., Stephanou E.G., Stier P., Traub M., Warneke C., Williams J., Ziereis H., 2002. Global air pollution crossroads over the Mediterranean. *Science* 298 (5594), 794–799.

Lui W., Hopke P.K., Han Y., Yi S., Holsen T.M., Cybart S., Kozlowski K. and Milligan M., 2003. Application of receptor modeling to atmospheric constituents at Potsdam and Stockton, NY. *Atmospheric Environment* 37, 4997–5007.

Maione M., Giostra U., Arduini J., Belfiore L., Furlani F., Geniali A., Mangani G., Vollmer M.K., Reimann S., 2008. Localization of source regions of selected hydrofluorocarbons combining data collected at two European mountain stations. *Science of the Total Environment* 391, 232-240.

Marenco F., Bonasoni P., Calzolari F., Ceriani M., Chiari M., Cristofanelli P., D'Alessandro A., Fermo P., Lucarelli F., Mazzei F., Nava S., Piazzalunga A., Prati P., Valli G., and Vecchi R., 2006. Characterization of atmospheric aerosols at Monte Cimone, Italy during summer 2004: Source

apportionment and transport mechanisms. *Journal of Geophysical Research* 111, D24202, doi:10.1029/2006JD007145.

Marinoni A., Cristofanelli P., Calzolari F., Roccato F., Bonafè U. and Bonasoni P., 2008. Continuous measurements of aerosol physical parameters at the Mt. Cimone GAW Station (2165 m asl, Italy). *Science of the Total Environment* 391, 241-251.

Monks P.S., Granier C., Fuzzi S., Stohl A., Williams M.L., Akimoto H., Amann M., Baklanov A., Baltensperger U., Bey I., Blake N., Blake R.S., Carslaw K., Cooper O.R., Dentener F., Fowler D., Fragkou E., Frost G.J., Generoso S., Ginoux P., et al., 2009. Atmospheric composition change – global and regional air quality. *Atmospheric Environment* 43(33), 5268-5350.

Papayannis A., Balis D., Amiridis V., Chourdakis G., Tsaknakis G., Zerefos C., Castanho A.D.A., Nickovic S., Kazadzis S., Grabowski J., 2005. Measurements of Saharan dust aerosols over the Eastern Mediterranean using elastic backscatter-Raman lidar, spectrophotometric and satellite observations in the frame of the EARLINET project. *Atmospheric Chemistry and Physics* 5, 2065-2079.

Pey J., Querol X., Alastuey A., 2010. Discriminating the regional and urban contributions in the North-Western Mediterranean: PM levels and composition. *Atmospheric Environment* 44, 1587-1596.

Prospero J. M., 1996. Saharan dust transport over the North Atlantic Ocean and the Mediterranean, in: The Impact of Desert Dust Across the Mediterranean, edited by S. Guerzoni and R. Chester, Springer, New York pp. 133-151.

Prospero J.M., Olmez I., and Ames M., 2001. Al and Fe in PM2.5 and PM10 suspended particles in south-central Florida: the impact of the long range transport of African mineral dust. *Water Air and Soil Pollution* 125, 291-317.

Prospero J.M., Ginoux P., Torres O., Nicholson S.E., and Gill T.E., 2002. Environmental characterization of global sources of atmospheric soil dust identified with the Nimbus 7 Total Ozone Mapping Spectrometer (TOMS) absorbing aerosol product. *Review of Geophysics* 40, 2-1:2-31.

Putaud J.-P., Raes F., Van Dingenen R., Bruggemann E., Facchini M.-C., Decesari S., Fuzzi S., Gehrig R., Huglin C., Laj P., Lorbeer G., Maenhaut W., Mihalopoulos N., Muller K., Querol X., Rodriguez S., Schneider J., Spindler G., ten Brink H., Torseth K., Wiedensohler A., 2004. A European aerosol phenomenology—2: chemical characteristics of particulate matter at kerbside, urban, rural and background sites in Europe. *Atmospheric Environment* 38, 2579–2595.

Querol X., Alastuey A., Pey J., Cusack M., Perez N., Mihalopoulos N., Theodosi C., Gerasopoulos E., Kubilay N., and Koçak M., 2009. Variability in regional background aerosols within the Mediterranean, *Atmospheric Chemistry and Physics* 9, 4575-4591.

Rao S.T., Zurbenko I.G., Neagu R., Porter P.S., Ku J.Y., and Henry R.F., 1997. Space and time scales in ambient ozone data. *Bulletin of the American Meteorological Society* 78, 2153–2166.

Riccio A., Giunta G., Chianese E., 2007. The application of a trajectory classification procedure to interpret air pollution measurements in the urban area of Naples (Southern Italy), *Science of the Total Environment* 376, 198 - 214, doi 10.1016/j.scitotenv.2007.01.068.

Riccio A., Chianese E., Tositti L., Baldacci D., and Sandrini S., 2009. Modeling the transport of Saharan dust toward the Mediterranean region: an important issue for its ecological implications. *Ecological Questions* 11, 65 – 72.

Seibert P., Kromp-Kolb H., Baltensperger U., Jost D.T., Schwikowski M., Kasper A., Puxbaum H., 1994. Trajectory analysis of aerosol measurements at high Alpine sites. In Transport and Transformation of Pollutants in the Troposphere (edited by Borrell P.M., Borrell P, Cvitas T and Seiler W.). Academic Publishing, Den Hag, pp. 689-693.

Stohl A., 1996. Trajectory statistics-A new method to establish source-receptor relationships of air pollutants and its application to the transport of particulate sulfate in Europe. *Atmospheric Environment* 30, 579-587.

Stohl A., 1998. Computation, accuracy and applications of trajectories - A review and bibliography. *Atmospheric Environment* 32, 947-966.

Tomasi C., Lupi A., Marani S., and Vitale V., 2003. Water vapour absorption effects on solar radiation in an Apennine valley from hygrometric measurements of precipitable water taken at various altitudes. *Il Nuovo Cimento* C, vol. 026, Issue 01, p.91.

Usher C.R., Michel A.E., Grassian V.H., 2003. Reactions on mineral dust. *Chemical Reviews* 103, 4883-4939.

USEPA (United States Environmental Protection Agency), 2004. Air Quality Criteria for Particulate Matter (Final Report, Oct 2004). Volume I of II. National Center for Environmental Assessment Research Triangle Park, NC. Available at http://cfpub.epa.gov/ncea/cfm/recordisplay.cfm?deid=87903#Download, last accessed May 10, 2012.

Van Dingenen R., et al., 2004. A European aerosol phenomenology-1: physical characteristics of particulate matter at kerbside, urban, rural and background sites in Europe. *Atmospheric Environment* 38, 2561-2577.

Van Dingenen R., Putaud J.P., Martins-Dos Santos S. and Raes F., 2005. Physical aerosol properties and their relation to air mass origin at Monte Cimone (Italy) during the first MINATROC campaign. *Atmospheric Chemistry and Physics* 5, 2203–2226.

Vasconcelos L. A. P., Kahl J. D. W., Liu D., Macias E. S., White, W. H., 1996a. Spatial resolution of a transport inversion technique. *Journal of Geophysical Research* 101, 19,337–19,342.

Vasconcelos L.A.P., Kahl J.D.W., Liu D., Marcias E.S. and White W.H., 1996b. A tracer calibration of back trajectory analysis at the Grand Canyon. *Journal of Geophysical Research* 101 (D14), 19329–19335, doi:10.1029/95JD02609.

Vecchi R., Marcazzan G., Valli G., Ceriani M. and Antoniazzi C., 2004. The role of atmospheric dispersion in the seasonal variation of PM1 and PM2.5 concentration and composition in the urban area of Milan (Italy). *Atmospheric Environment* 38, 4437–4446.

WBCSD (World Business Council for Sustainable Development), 2004. Mobility 2030: Meeting the challenges to sustainability, report of the World Business Council for Sustainable Development. The Sustainable Development Project; Overview 2004. Available at http://www.wbcsd.org/pages/edocument/edocumentdetails.aspx?id=69, last accessed May 10, 2012.

WHO (World Health Organization), 2000. Air quality guidelines for Europe, 2nd ed. Copenhagen, World Health Organization Regional Office for Europe, 2000 (WHO Regional Publications, European Series, No.91). Available online at http://www.euro.who.int/__data/assets/pdf_file/0005/74732/E71922.pdf, last accessed May 10, 2012.

Wotawa, G. and Kröger, H., 1999. Testing the ability of trajectory statistics to reproduce emission inventories of air pollutants in cases of negligible measurement and transport errors, *Atmospheric Environment* 33, 3037–3043.

Zauli Sajani S., Miglio R., Bonasoni P., Cristofanelli P., Marinoni A., Sartini C., Goldoni C.A., De Girolamo G., and Lauriola P., 2011. Saharan dust and daily mortality in Emilia-Romagna (Italy). *Occupational and Environmental Medicine* 68, 446-451, doi:10.1136/oem.2010.058156.

Zurbenko I.G., 1986. The Spectral Analysis of Time Series. North-Holland, Amsterdam.

Mt. Cimone GAW global station internet site, http://www.isac.cnr.it/cimone/, last accessed 06 September 2013.

CHAPTER 3 – Temporal Changes of ^{7}Be and ^{210}Pb Activity Concentrations at Mt. Cimone

3.1 Introduction[1]

In the course of the last decades airborne radionuclides have long been investigated within the framework of atmospheric science. Initially the focus concerned the emission of artificial radioactivity during weapon testing (see for example chapter 9 of Eisenbud and Gesell, 1997; Pállson *et al.*, 2013) which pointed out to the scientists both the safety issues connected with radioactivity hazard as well as the remarkable efficiency of atmospheric transport processes at the global scale. It was soon recognized that atmospheric radioactivity had also a not negligible background component capable to trace both the gaseous and the particulate phases enabling the quantitative description of fundamental processes of atmospheric dynamics. Airborne radioactivity has long been playing a relevant role in the study of atmospheric transport processes as detectable from the frequency of scientific publications (Burton and Stewart, 1960; Junge, 1963; Reiter *et al.*, 1971; Gaggeler, 1995; Arimoto *et al.*, 1999; Turekian and Graustein, 2003; WMO-GAW, 2004; Dibb, 2007; Papastefanou, 2008; Rastogi and Sarin, 2008; Sykora and Froehlich, 2010; Froehlich and Masarik, 2010; Lozano *et al.*, 2011).

At present nuclear safety is still a basic issue at the global scale as demonstrated by the follow up of Chernobyl and Fukushima accidents (see for example chapter 12 of Eisenbud and Gesell, 1997; Papastefanou *et al.*, 1988; Hötzl *et al.*, 1992; Davison *et al.*, 1993; Vakulovsky *et al.*, 1994; Masson *et al.*, 2011; Diaz Leon *et al.*, 2011; Lozano *et al.*, 2011; Manolopoulou *et al.*, 2011; Pittauerová *et al.*, 2011; Tositti *et al.*, 2012 –Appendix II–; Ioannidou *et al.*, 2013) or as a result of episodic cases such as the fall of nuke-fed satellites (Cosmos 954, Kosmos 1402, see for example chapter 12 of Eisenbud and Gesell, 1997) or the accidental melting of orphan sources/metals scraps in high temperature processes (e.g., Algeciras accident, Krysta and Bocquet, 2007; on this occasion ^{137}Cs, a radionuclide which is usually below detection limit at Mt. Cimone, was detected at this site in two samples at very low levels). Moreover the need for monitoring potential violations of the Nuclear

[1] This chapter consists of a paper by Tositti L. (Dept. of Chemistry, Università di Bologna), Brattich E. (Dept. of Biological, Geological and Environmental Sciences-Section of Geology, Università di Bologna), Cinelli G. (Dept. of Biological, Geological and Environmental Sciences-Section of Geology, Università di Bologna; now at European Commission, DG JRC, Institute for Transuranium Elements, Via E Fermi 2749, I-21027 Ispra (VA), Italy), Baldacci D. (Dept. of Chemistry, Università di Bologna), 2014. 12 years of ^{7}Be and ^{210}Pb data in Mt. Cimone, and their correlation with meteorological parameters. *Atmospheric Environment* 87C, 108-122. doi:10.1016/j.atmosenv.2014.01.014

Ban Treaty has recently promoted the constitution of a global network for artificial radioactivity whose efficiency has been successfully tested following the recent Fukushima emergency (Masson *et al*., 2011; Hernández-Ceballos *et al*., 2012; Thakur *et al.*, 2013).

Cosmogenic and naturally occurring radionuclides have long been investigated either per se or as normalizing and reference factors in the study of artificial radioactivity or again both as efficient tracers in environmental science and as geochronometers. Altogether this field of research has been crucial to the comprehension of several basic processes such as interhemispheric transport, stratosphere-to-troposphere exchange (STE) and time scales of atmospheric dynamics, while posing the basis for basic concepts in environmental science such as biogeochemistry, environmental monitoring management and exposure/dosimetry concepts presently extended to stable "classic" pollutants such as for example ozone and/or airborne particulate matter.

At present though the application of radiotracers constitutes a niche approach, the simultaneous use of artificial and natural radiotracers still provides a solid background for the characterization of atmospheric transport (Arimoto *et al.*, 1999; Paatero and Hatakka, 2000; Dueñas *et al.*, 2011), the testing of atmospheric models (Koch *et al.*, 1996; Liu *et al*., 2001, 2004; Heinrich and Jamelot 2011; Christoudias and Lelieveld, 2013), as well as in supporting source apportionment of pollutants (Li *et al*., 2002; Cuevas *et al*., 2013).

Among the most used naturally occurring radionuclides there are ^{7}Be, ^{210}Pb, ^{222}Rn and others included in the group of the key atmospheric components that should be routinely monitored within the WMO-GAW network (WMO-GAW, 2004). In particular the importance of ^{210}Pb and ^{7}Be relies upon their distinct natural sources. ^{210}Pb (half-life, $T_{1/2}$ = 22.1 years) is supplied to the atmosphere at ground level by the radioactive decay of its precursor, ^{222}Rn ($T_{1/2}$ = 3.83 days). As the ^{222}Rn flux from the ocean is negligible, ^{210}Pb is considered a continental tracer of air masses (Balkanski *et al.*, 1983; Turekian *et al.*, 1983; Baskaran, 2011). In contrast, ^{7}Be is a relatively short lived ($T_{1/2}$ = 53.3 days) radionuclide of cosmogenic origin, produced by cosmic ray spallation reactions with light atmospheric nuclei of nitrogen and oxygen (Usoskin *et al.*, 2009): most of the ^{7}Be production (~ 75%) occurs in the stratosphere while the remaining part (~ 25%) is produced in the troposphere, and particularly in the upper troposphere (Johnson and Viezee, 1981; Usoskin and Kovaltsov, 2008). The production rate of ^{7}Be has a latitudinal dependence (Ioannidou *et al.*, 2005), while it has a negligible dependence from season and longitude, but a remarkable variation due to the 11-year solar cycle (Hötzl *et al.*, 1991; Megumi *et al*., 2000; Cannizzaro *et al*., 2004; Ioannidou *et al.*, 2005; Leppänen *et al*., 2012). Once formed, ^{7}Be and ^{210}Pb undergo rapid association onto submicron-sized aerosol particles both peaking in the accumulation mode (Papastefanou and Ioannidou, 1995; Winkler *et al*., 1998; Gaffney *et al.*, 2004; Ioannidou *et al.*, 2005). Thereafter, ^{7}Be and ^{210}Pb are removed from the

atmosphere by wet and dry scavenging of the carrier aerosol (Feely *et al.*, 1989; Kulan *et al.*, 2006). Most of the ^{7}Be produced in the stratosphere does not readily reach the troposphere because of its short half-life compared to the longer residence times of aerosols in the stratosphere (which, depending on the size of the particles, is equal to one or more years as estimated from Hamill *et al.*, 1997 and Rasch *et al.*, 2008). In fact, the relatively high production rates of ^{7}Be in the upper troposphere (UT), combined with transport from the lower stratosphere (LS) to the upper troposphere, usually maintain a steep vertical concentration gradient between the upper and the lower troposphere (Feely *et al.*, 1989). Nevertheless, the UT–LS may cause high ^{7}Be concentrations in the surface air, easily detectable at a high altitude stations such as for example Mt. Cimone station (Bonasoni *et al.*, 1999, 2000a, b; Cristofanelli *et al.*, 2003, 2006, 2009a).

Due to the similar physico-chemical behaviour, variations in the ^{7}Be/^{210}Pb ratios reflect both vertical and horizontal transport in the atmosphere. Because of the different origins of the two radionuclides, the use of the combination of ^{7}Be and ^{210}Pb as activity ratio has been shown to provide clearer information about the origin of the air masses (Graustein and Turekian, 1996; Bonasoni *et al.*, 2000a, b, 2004; Zheng *et al.*, 2005), and its seasonal variability over continents has been studied for examining vertical exchange transport processes (Koch *et al.*, 1996). The simultaneous measurements of ^{7}Be and ^{210}Pb, together with their ratio can provide useful information about the vertical motion of air masses as well as on convective activity in the troposphere (Brost *et al.*, 1991; Koch *et al.*, 1996; Tositti *et al.*, 2004; Lee *et al.*, 2004, 2007).). Recently, Lozano *et al.* (2012) studied the different synoptic patterns and air masses types associated to ranges of ^{7}Be and ^{210}Pb activity concentrations in the southwestern Iberian Peninsula, indicating the differences between the arrival of maritime and continental air masses and confirming that both radionuclides can be used as two independent atmospheric transport markers.

In this Chapter a basic overview of the time series of ^{7}Be and ^{210}Pb collected at the WMO GAW station of Mt. Cimone from 1998 until 2011 is presented. This activity has been already the object of several papers devoted to specific topics, in particular the use of ^{7}Be in STE (Stratosphere – to – Troposphere Exchange), a rather classic application of this radionuclide, though not thoroughly understood yet (Bonasoni *et al.*, 1999; Bonasoni *et al.*, 2000a, b; Cristofanelli *et al.*, 2003, 2006, 2009a). The follow up of Fukushima accident was also investigated at this station and results have been recently published either at the European scale in a collective paper by Masson *et al.* (2011) or at the regional scale comparing the radionuclidic pool at two nearby stations including Mt. Cimone (Tositti *et al.*, 2012, presented in Appendix II of this thesis). Finally another recent paper concerned the PM_{10} matrix in which pioneristically all the radionuclides herein treated are measured since the beginning of this experiment, providing a long-term overview of PM_{10} behavior in the core of the

Mediterranean region (Tositti *et al.*, 2013, presented in previous Chapter 2 of this thesis). This work presents and discusses a statistical analysis of frequency distributions, seasonality, interannual variation, correlations of the ^{7}Be, ^{210}Pb (and their ratio) data of acquired from 1998 to 2011 at the WMO-GAW station of Mt. Cimone, with the purpose of gaining better insights into the different physical mechanisms at the basis of their variability.

3.2 Material and methods

3.2.1 Measurement site

Mt. Cimone station (44°12' N, 10°42' E) is located on top of the highest peak of the Italian Northern Apennines (2165 m asl). The station is a global WMO-GAW managed by the Meteorological Office of the Italian Air Force and by the Institute of atmospheric and climate science of the National Council of Research (ISAC–CNR). It has a 360° free horizon and is fairly off main pollution sources such as cities and industrialized areas in the north (Po valley) and south (Tuscan plain) of the Apenninic range; Mt. Cimone has an elevation such that the measurement site hosted by "O. Vittori" station lies above the planetary boundary layer during most of the year, so that it can be considered representative for the South-European free troposphere (Bonasoni *et al.*, 2000b; Fischer *et al.*, 2003), even if an influence of the innermost layer cannot be completely ruled out, in particular during warm months because of the increased vertical mixing (thermal convection) and mountain/valley breeze regimes (Fischer *et al.*, 2003; Cristofanelli *et al.*, 2007). For these reasons, the measurement site is a suitable location to investigate the influence of regional and long-range transport of polluted air masses on the background free troposphere (Tositti *et al.*, 2013; Cristofanelli *et al.*, 2013), located at the center of the Southern Europe and the Mediterranean basin, a region which is recognized as a hot-spot both in terms of climate change and air-quality.

Unlike the surrounding area (temperate-continental) the climate of the mountaintop is classified as alpine, due to its height. The mean yearly temperature is about 2°C, with a winter minimum of -22°C and a summer maximum of 18°C (Colombo *et al.*, 2000). Mt. Cimone is the windiest site among the Italian meteorological stations, with wind speeds reaching intensities of 216 km h^{-1}, with a mean daily wind speed of 40 km h^{-1} during winter, probably due to the isolated position of the site. In the region the precipitations are maximum during November (secondary maximum in spring) and minimum in July (secondary minimum in January). At this station, the annual average precipitation amounts (L) to 696.3 mm (period 1964-2004; Şerban *et al.*, 2007), which is much lower than the one recorded in the period 1961-1980, equal to 744.7 mm (Rapetti and Vittorini, 1989). The annual average precipitation during the period 1998-2011 (corresponding to the sampling of PM_{10} and atmospheric radiotracers) is

even lower and equal to 381.2 mm. During the year prevailing winds blow from S-SW in the warm season and N-NE in the cold one. Generally speaking, typical synoptical circulations in Emilia-Romagna are characterized by winter fluxes originating N-NE and fast currents from S-SW all over the rest of the year. In the first case the presence of an anticyclone on the Eastern Europe or of a depression centred on the Southern Italy or on the Central Adriatic can determine the access in the Po Valley of air masses that reach the Adriatic slope of the Tuscan-Emilian Apennines; the most frequent case is the second one, in which high streams from SW associated to a depression in the Gulf of Genoa affect the Tuscan-Emilian Apennines. In fact, Mt. Cimone can be affected by intense cyclogenetic activity often originating in the near Gulf of Genoa area (Buzzi *et al.*, 1984; Davies and Schuepbach, 1994). This phenomenology has been widely connected with STE events relevant to the well-known increases of both ozone and ^{7}Be (Tosi *et al.*, 1987; Aebischer and Schär, 1998; Stohl *et al.*, 2000).

The Italian Air Force, which is in charge for the meteorological service in Italy, is responsible for the facility which hosts and integrates the research activity led by ISAC–CNR. Besides meteorology, the Italian Air Force – General Bureau for Meteorology – manages the collection of atmospheric CO_2 data presently constituting the longest time series of this fundamental greenhouse gas in Europe, dating back to 1979. It is to note that in the past this station served also as one of the Italian monitoring sites for weapon test fallout (Argiero *et al.*, 1961; Dietrich *et al.*, 1997), an activity dismissed in the 90's.

Several scientific programs have been established at Mt. Cimone with the scope of studying both climatologically relevant gases and the physical-chemical characteristics of atmospheric aerosols (see web page http://www.isac.cnr/cimone/).

3.2.2 Experimental

At Mt. Cimone station ^{7}Be, ^{210}Pb and aerosol mass loading in the form of PM_{10} have been measured since the early 1990's, but measurements became regular only since 1998 following the acquisition of a PM_{10} high volume sampler. Aerosol sampling has been carried out with a time resolution of about 48 h by using a Thermo-Environmental PM_{10} high-volume sampler with a flow rate of 1.13 m^3 min^{-1}. PM_{10} is collected on rectangular glass fiber filters (Whatman, 20.3 cm x 25.4 cm). The PM_{10} sampler collects airborne particulate matter with a mean aerodynamic diameter lower than 10 μm that carries the radionuclides, which tend to populate the fine fraction (< 1.0 μm) (Winkler *et al.*, 1998; Gaffney *et al.*, 2004), as a consequence of their physical origin. Samples are transferred to the Laboratory of Environmental Chemistry and Radiochemistry of Bologna University, where they are conditioned for 24 h at constant temperature (22-24°C) and relative

humidity (30%) inside a desiccator. The net mass load on filters is determined gravimetrically by an electronic microbalance with a sensitivity of 0.0001 g (Ohaus). After weighing, the PM_{10} samples are subjected to non-destructive high-resolution γ-spectrometry with two Hyper Pure Germanium crystal detectors (HPGe) for the determination of airborne radiotracers ^{7}Be and ^{210}Pb, respectively at 477.6 and 46.5 keV. The characteristics of the two detectors are the following ones: one p-type coaxial detector by Ortec/Ametek with a relative efficiency of 32.5% and FWHM 1.8 keV at 1332 keV and one planar DSG detector with an active surface of 1500 mm^2 and FWHM 0.73 keV at 122 keV, for higher and lower energy ranges (100-2000 keV and 0-900 keV), respectively.

Spectra are accumulated for at least one day and then processed with a specific software package (GammaVision-32, Ortec). Efficiency calibration is determined on both detectors with a blank glass fiber filter traced with accurately weighted aliquots of a standard solution of mixed radionuclides (QCY48, Amersham) supplemented with ^{210}Pb, homogeneously dispersed dropwise over the filter surface. Once dried under a hood under ambient conditions, the calibration filter is folded into a polystyrene container in the same geometry as the unknown samples. Quantitative analysis on samples is carried out by subtracting the spectrum of a blank filter in the same geometry, while uncertainty on peaks (k = 1, 68% level of confidence) is calculated propagating the combined error over the efficiency fit previously determined with the counting error. Minimum detectable activity is calculated making use of the Traditional ORTEC method with a peak cut-off limit of 40%. Activity data is corrected to the midpoint of the time interval of collection and for the decay during spectrum acquisition.

In addition to the standard procedures to test laboratory performances (to determine efficiency calibration, to determine uncertainty on peaks and minimum detectable activity and to correct for the radioactive decay during the sampling and during spectrum acquisition), accuracy and precision of ^{7}Be measurements were evaluated within an intercomparison exercise involving several European research groups (Tositti *et al.*, 2004).

Prior to all the analyses, all the concentrations have been normalized at 25°C and 1 atm.

3.3 Results and discussion

3.3.1 Seasonality and interannual variability

Figure 3.1(a,b,c) shows the time series of ^{7}Be and ^{210}Pb and of the $^{7}Be/^{210}Pb$ ratio measured at Mt. Cimone from 1998 to 2011. As previously observed in Chapter 2, the large gap presented by the data in 2007 is due to technical problems with the aerosol sampler. Besides interannual variabilities, a distinct seasonal pattern can be observed for the two tracers, which will be discussed

further on in the paper: while ^{7}Be exhibits two seasonal maxima, one during the cold season and one during the warm one, ^{210}Pb presents only one peak during the summer months. Because of the simultaneous occurrence of the ^{7}Be and ^{210}Pb peaks during the warm season, their ratio time series exhibits only one peak during the cold season.

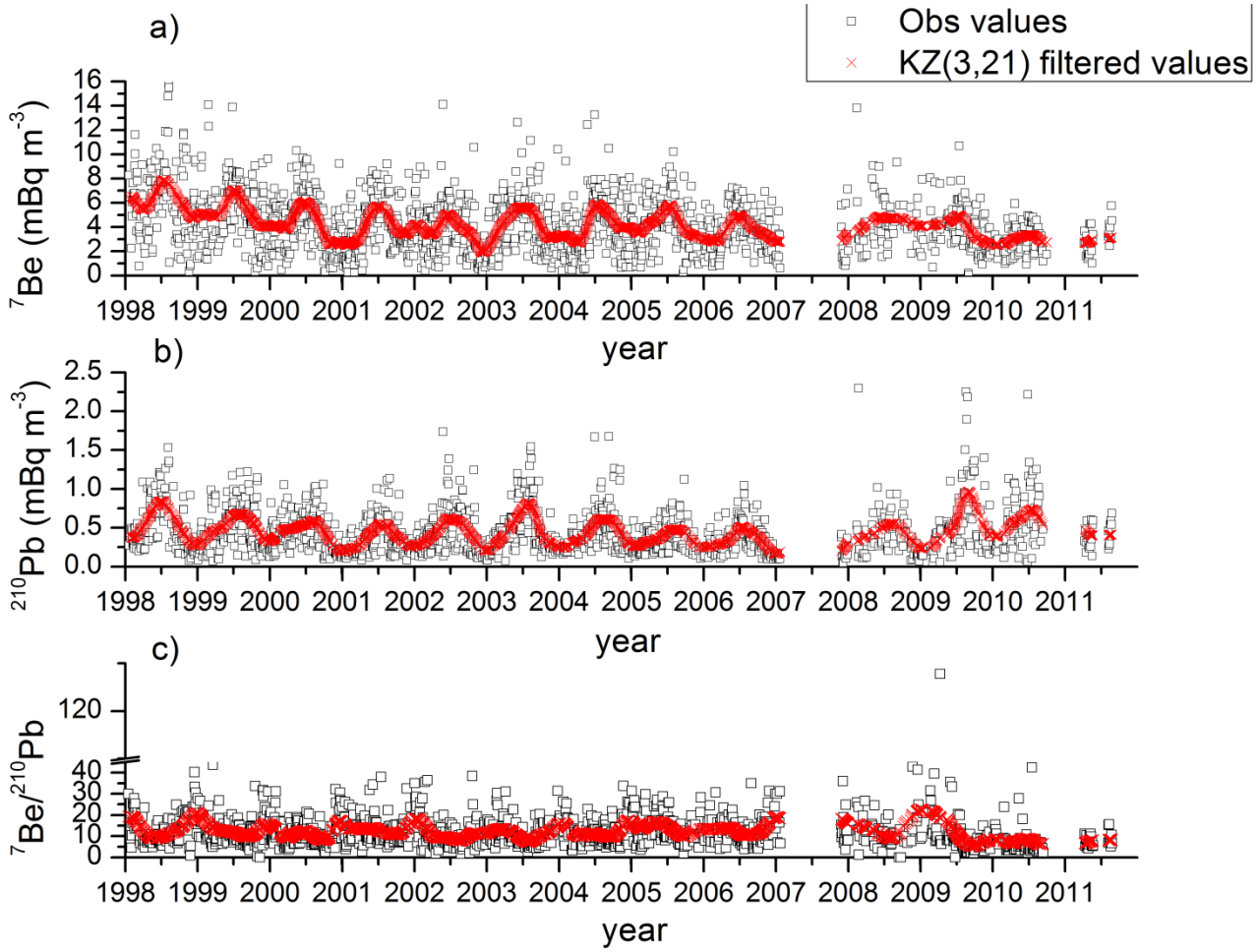

Figure 3.1(a,b,c) *Time series of the data acquired at Mt. Cimone from 1998 to 2011 (black squares) and seasonal fluctuation of the variables obtained after the application of the KZ(3,21) filter (red line): a) ^{7}Be; b) ^{210}Pb; c) ^{7}Be/^{210}Pb.*

Similar to what has been previously reported for PM_{10} dataset of Mt. Cimone in previous Chapter 2 of this thesis (Tositti *et al.*, 2013), radiotracers as well as ^{7}Be-to-^{210}Pb ratio show remarkable sample to sample fluctuations ("anomalies") overlapped to a lower frequency periodicity linked to seasonality. These anomalies, defined as the "synoptically influenced deviations from the seasonal cycle", are highlighted in Figure 3.1(a,b,c) following the application of the Kolmogorov–Zurbenko filter (Zurbenko, 1986), denoted as KZ(*m*,*n*). This filter is based upon

the calculation of a moving average $\overline{z_t}$ centred over a time window of *n* values (with *n* odd integer), i.e.,

$$\overline{z_t} = \frac{1}{n} \sum_{i=t-(n-1)/2}^{t+(n-1)/2} y_i$$

The moving average is then iterated *m* times. The reader is referred to Eskridge *et al.* (1997) and Rao *et al.* (1997) for a detailed description of this filter. The seasonal fluctuation was obtained after the application of the KZ(3,21) filter, i.e., the moving average applied three times over a time window of 21 days (crosses in Figure 3.1): the number of iterations as well as the time window of the filter were chosen evaluating the spectral response of the filter, which guarantees an almost perfect separation of the seasonal and synoptic time-scales (Rao *et al.*, 1997).

Interannual variations of ^{7}Be, ^{210}Pb and of the ^{7}Be/^{210}Pb ratio are reported in Figure 3.2(a,b,c). The vertical box encloses the middle 50% of the data. The median is the horizontal line inside the box and the square represents the mean value. Whiskers cover the range 10^{th}-90^{th} percentile. Minimum and maximum values are plotted as individual points with a line, whereas a cross indicates the 1^{st} and 99^{th} percentiles. Annual changes are commonly ascribed to different factors, especially meteorological conditions, such as the amount of precipitation, atmospheric stability, relative humidity, temperature (Ioannidou *et al.*, 2005; Dueñas *et al.*, 2009; Pham *et al.*, 2011; Carvalho *et al.*, 2013) and, in the case of ^{7}Be, also the 11-year solar cycle (Ioannidou *et al.*, 2005; Kulan *et al.*, 2006; Steinmann *et al.*, 2013).

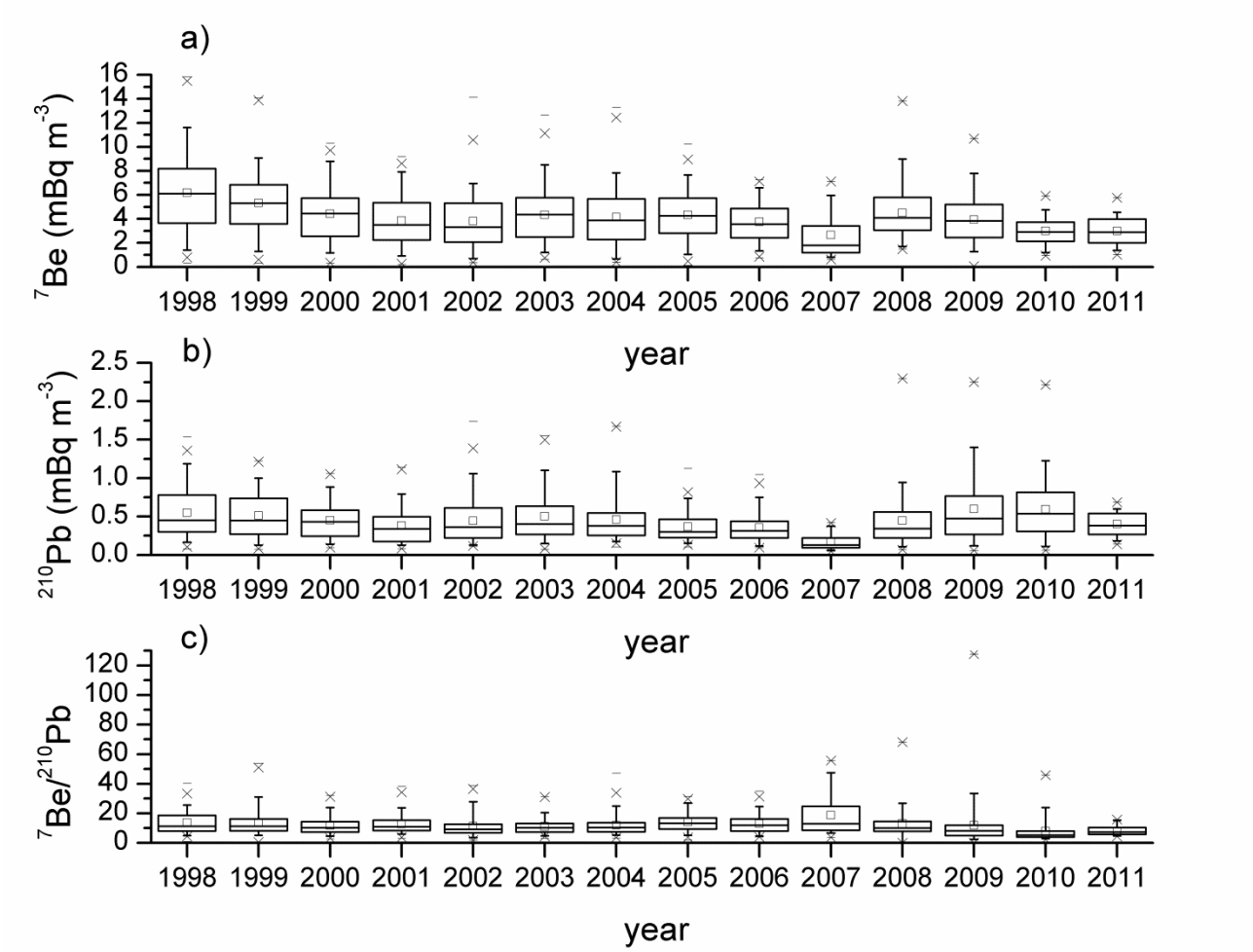

Figure 3.2(a,b,c) *Interannual variations at Mt. Cimone during the sampling period 1998-2011, represented by box and whiskers plots, of: a) ^{7}Be; b) ^{210}Pb; c) ^{7}Be/^{210}Pb.). The boxes contain the range 25th-75th percentile of the data; the whiskers represent the 5th and 95th percentile, while the square and the line inside the boxes denote the arithmetic mean and the median, respectively. Crosses and external lines represent the outliers and extreme values (minima and maxima), respectively.*

For instance, the decrease in ^{7}Be and ^{210}Pb mean activity (and in PM_{10} concentration, reported in Chapter 2, Figure 2.2) from 1998 to 1999 could be tentatively attributed to the increased total amount of precipitation (total precipitation in 1998 equal to 296 mm, whereas in 1999 the total precipitation was equal to 641 mm), whereas the increase in ^{7}Be and ^{210}Pb activity from 2002 to 2003 (similar amount of precipitation: 2002 total precipitation equal to 328 mm, 2003 total precipitation equal to 308 mm) might be due to the extremely high temperature recorded in the whole European region, possibly contributing to enhanced convection and radon exhalation, especially during the summer months (Pace *et al.*, 2005; Cristofanelli *et al.*, 2009b) and connected also to anomalous high ozone concentrations at Mt. Cimone as reported by Cristofanelli *et al.* (2007).

The effect due to the frequency and trends of different air mass transports, such as Saharan Dust incursions for instance, cannot be completely ruled out, however, and it will be the focus of Chapter 5.

Figure 3.3(a,b,c) depicts box and whiskers plots with seasonal variations of ^{7}Be, ^{210}Pb and of the ^{7}Be/^{210}Pb ratio.

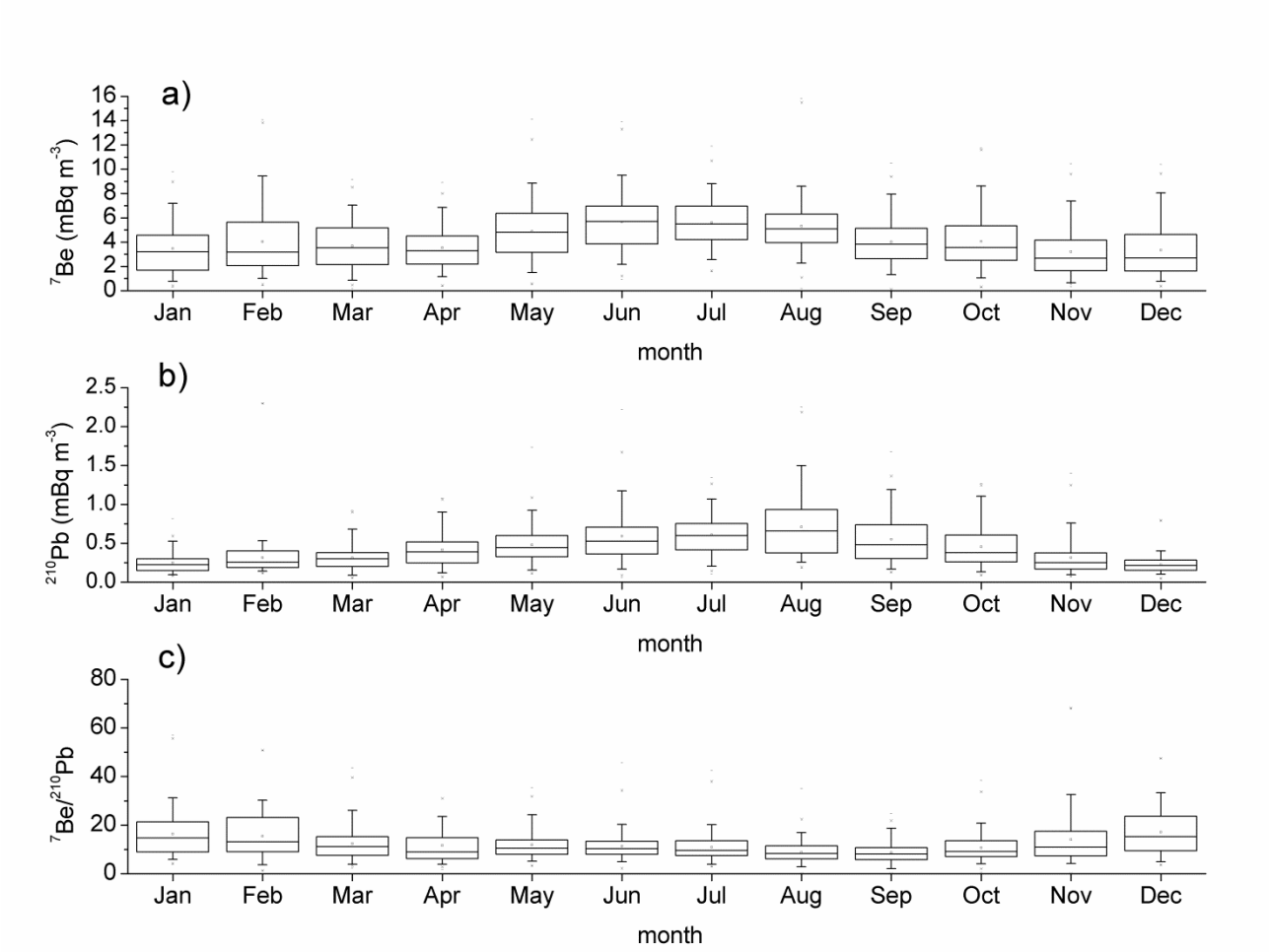

Figure 3.3(a,b,c) *Seasonal variations at Mt. Cimone during the sampling period 1998-2011, represented by box and whiskers plot, of: a) ^{7}Be; b) ^{210}Pb; c) ^{7}Be/^{210}Pb.*

The ^{7}Be concentration starts to increase during the warm period from May to August, with a maximum during the months of June–July. The seasonal variation is higher for ^{7}Be, as highlighted by maximum and minimum values, as well as by 1st and 99th percentile, which in the case of ^{7}Be with larger deviations from the mean value than for ^{210}Pb. Anyway, the variability is high for both tracers during the sampling period, with a percent standard deviation from the mean of 55% for ^{7}Be and 65% for ^{210}Pb. A secondary maximum for ^{7}Be is observed during the cold period from November to February.

^{210}Pb shows instead a simpler seasonal behaviour, with an increase starting during spring and reaching its summer maximum in August. The minimum values are observed during the cold

months, behaviour analogous to that of PM_{10} in previous Chapter 2, Figure 2.6 (Tositti *et al.*, 2013), with which ^{210}Pb shares a large part of the source term, i.e., the Earth's crust, as distinguished by ^{7}Be whose main source terms are located in the stratosphere and upper troposphere. Similarly to $PM_{10,}$ during the cold season ^{210}Pb is not uplifted to Mt. Cimone top owing to the decoupling of the Continental Boundary Layer from the free troposphere. As a result mean ^{210}Pb values at Mt. Cimone in the cold season should be representative of background free-troposphere concentrations for this tracer.

^{7}Be/^{210}Pb shows maximum values during the cold months from November to February, while the spring and summer season are characterized by lower values. The variability of the ratio is lower during the summer season and secondarily during winter (percent standard deviation from the mean equal to 53% and to 57%, respectively), while the variability is maximum during the transition seasons (standard deviation percent from the mean equal to 67% and to 72%, respectively for autumn and spring). The winter maximum of the ^{7}Be/^{210}Pb ratio at the height of Mt. Cimone is mainly caused by the scarce availability of ^{210}Pb and of its precursor ^{222}Rn, whose lift up above the PBL (Planetary Boundary Layer) is inhibited by the limited thermal convection in the cold season.

The summer maxima of ^{7}Be and ^{210}Pb, and the consequent minimum of their ratio during this season, are due to enhanced vertical mixing, thermal convection and mountain/valley breezes during this period of the year. As already highlighted by Baltensperger *et al.* (1997), Cristofanelli *et al.* (2003), Lee *et al.* (2007) and in Chapter 2 (Tositti *et al.*, 2013) during the warm season the mixing height reaches high levels, while thermal convection leads to intense vertical exchange in the troposphere. Rising warm air from the boundary layer brings about high values of ^{210}Pb, being somehow counterbalanced by cold air sinking from the upper troposphere enriched in ^{7}Be. As shown in Figure 3.3(a,b) the warm period maxima of ^{7}Be and ^{210}Pb are not completely simultaneous, though. While ^{7}Be shows a maximum during the months of June-July, a behaviour which, as reported in previous Chapter 2 (Figure 2.6), is shared by PM_{10}, ^{210}Pb shows its maximum during August. PM_{10} and ^{210}Pb share similar sources and one would expect their concentrations follow similar trends. A detailed analysis of the seasonality of air flows at this site is the objective of Chapter 5 and Chapter 6, however it can be anticipated that during the summer months the prevailing flows are short range transports from North Western Europe and from West, even if the major influence of Saharan Dust during spring and summer, especially linked to ^{210}Pb and PM_{10}, cannot be completely ruled out. In particular, our results indicate that the influence of Saharan Dust on the PM_{10} concentration is maximum during the summer season (about 49% of the peaks/events are due to this source) with a slight decrease in the transition seasons (about 44% during spring and 43% during autumn), while during winter the African source contribution to aerosol transport is significantly lower (11%), as

well as the mean concentration of PM_{10} ascribed to this source. Even if Saharan Dust transports have a seasonal frequency maximum during spring-autumn, it is during the summer season that Saharan Dust mass load contribution is especially high, with effects on the monthly averages which are rather unpredictable due to different amounts in the coarse fractions lifted up and transported away from the source region. In this respect while the influence of Saharan Dust events is mainly reflected by the relevant contribution to mass loadings due to the importance of the coarse fraction typical of these transports, the influence on ^{210}Pb is not straightforward and needs further investigations. In fact, while for regional scale transports we believe (as explained in Chapter 2; Tositti *et al.*, 2013) that there is a close connection between thermal convection (a dominant dynamical condition during the warm season in the investigated area), fine fraction and ^{210}Pb as derived from exhaled radon (the so-called excess or "unsupported ^{210}Pb), the decoupling of ^{210}Pb and PM_{10} peak concentration may have different reasons. In particular, we speculate that the amount of the coarse fraction transported by Saharan Dust which is a fairly stochastic or rather event-based factor in terms of efficiency in the lifted up and transported amounts of mineral dust, may affect the concentration of ^{210}Pb in several ways: geochemistry (mineral dust composition is not uniform in the whole northern African region, as suggested e.g., by Moreno *et al.*, 2006, Formenti *et al*., 2008, and Formenti *et al.*, 2011, affecting also the content in natural radionuclides – still scarcely known– while Saharan Dust source regions are known to fluctuate in longitude during the year, as observed by, for example, Barkan and Alpert, 2008 and Israelevich *et al.*, 2012), secondly different amounts of suspended mineral dust, and finally the occurrence of both supported (associated with the coarse mineral particles) and unsupported ^{210}Pb. All the effects so far discussed though reasonable cannot be definitely interpreted on the basis of the available data, but need to be clarified by further investigations and measurements suitably designed to the scope.

The secondary maximum of ^{7}Be during the cold months (December, January, February and March) is due to an increase in Stratosphere-to-Troposphere events during this season, as already reported by e.g., James *et al.* (2003), Stohl *et al.* (2003), Trickl *et al.* (2010). Moreover Cristofanelli *et al.* (2009a) introduced a stratospheric index based on ^{7}Be, relative humidity and ozone measurements at Mt. Cimone enabling the assessment of a higher incidence of STE events during the period from October to February with respect to the warm season, when thermal convection and the rising of the tropopause promote vertical mixing which acts as confounding factor in STE detection. As reported by James *et al.* (2003) the reason of this behaviour is mostly the seasonal differences of rapid descent within the troposphere itself, rather than the differences in Stratosphere to Troposphere Transports (STT).

The higher frequency of rapid subsidence in winter at mid-latitudes Northern Hemisphere can be ascribed to the intensity of baroclinic systems which is greatest in wintertime. In fact, well-developed tropopause folds and rapid deep intrusions are most likely to occur in the wake of intense cyclogenesis, usually limited to the wintertime storm track regions (James *et al*., 2003).

Previously, Elbern *et al*. (1997), identified a principal late winter maximum and a secondary maximum around September and October, with clear minima during early summer for deep stratospheric intrusions at the Zugspitze (2962 m asl, Germany) and Wank (1776 m asl, Germany) summits, widespread on the mesoscale. Cyclones developing in the Gulf of Genoa, which are well known to have a close link to STE (e.g., Aebischer and Schär, 1998; Stohl *et al.*, 2000), are a constant feature over the whole year (Trigo *et al*., 2002; Campins *et al.*, 2006), a feature which could be somehow in contrast with the above statement. However, even if they are more frequent during summer, it is during winter that they are deeper and connected to more severe weather (Trigo *et al.*, 2002). In the Gulf of Genoa both orography and dynamical processes (upper level troughs) play the most important cyclogenetic roles (Anagnostopoulou *et al.*, 2006): the upper-level dynamics seem to be more important in spring and autumn, while the orographic effect seems to contribute more significantly in winter and spring (Campins *et al.*, 2006), but during winter there is also the further influence of the thermal contrast between seawater and air (Maheras *et al*., 2002), which is at its maximum during this season (Reiter, 1975a).

The activity of the two radionuclides normalized on the PM_{10} concentration (not shown) shows maxima during the cold months (from October to February, and especially in December and January) and seasonal minima during summer for both radionuclides as a result of the lower and higher aerosol loads available for their association.

The seasonal variations of both ^{7}Be and ^{210}Pb are modulated even by seasonal precipitation patterns. As typical of mid-latitudes, summer months are usually associated to lower rates of precipitation with respect to the transition seasons and winter: as already outlined before, in the region the precipitations are maximum during November (secondary maximum in spring) and the absolute minimum appears in July, even if speaking about a mountain site precipitation includes both rain and snow.

As an example Figure 3.4a depicts PM_{10} (to which radionuclides are associated) and precipitation patterns in 2002: it can be easily seen that precipitation (bars in the Figure) events bring about PM_{10} minima as a result of wet removal, as well as maxima in RH% (Figure 3.4b).

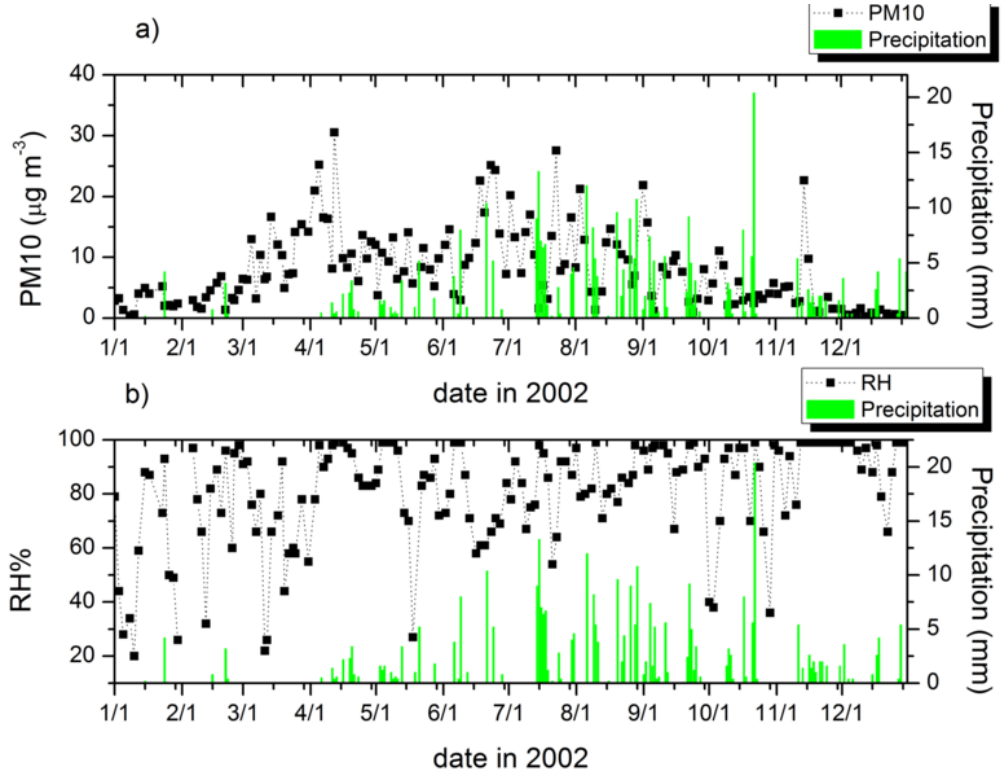

Figure 3.4(a,b) *a) Precipitation (bar) and PM_{10} (dotted line and square) patterns in 2002 at Mt. Cimone; b) Precipitation (green bar) and relative humidity (dotted line and square) patterns in 2002 at Mt. Cimone.*

3.3.2 Basic statistics

Table 3.1 presents basic statistics results obtained on the overall radionuclides and ratio dataset (1609 observations for ^{7}Be and 1443 observations for ^{210}Pb) including arithmetic mean (AM), geometric mean (GM), median (ME), minimum and maximum values (Min, Max), standard deviation (SD), 10th percentile (PC10), 90th percentile (PC90), skewness (SK) and kurtosis (KU).

	AM	GM	ME	Min	Max	SD	PC10	PC90	SK	KU
^{7}Be (mBq m^{-3})	4.3	3.6	4.0	0.05	15.8	2.3	1.5	7.3	0.9	1.3
^{210}Pb (mBq m^{-3})	0.46	0.38	0.38	0.05	2.30	0.30	0.16	0.87	1.65	4.39
^{7}Be/^{210}Pb	12.2		10.3	0.5	127.8	8.0	5.2	21.3	3.7	35.1

Table 3.1 *Statistical parameters for the ^{7}Be, ^{210}Pb and ^{7}Be/^{210}Pb time series: arithmetic mean (AM), geometric mean (GM), median (ME), minimum and maximum values (Min, Max), standard deviation (SD), 10th percentile (PC10), 90th percentile (PC90), skewness (SK) and kurtosis (KU).*

The skewness levels obtained for the three parameters suggest asymmetries in their frequency distributions, though less pronounced in the case of ^{7}Be. Kurtosis is a measure of the sharpness of the distribution of variable: taking the kurtosis of the normal distribution equal to zero, the high

kurtosis of the three variables and in particular of the $^{7}Be/^{210}Pb$ ratio, indicates a distribution sharper than the normal one and possibly the presence of significant tails. Figure 3.5(a,b,c) depicts the frequency distribution for the three time series.

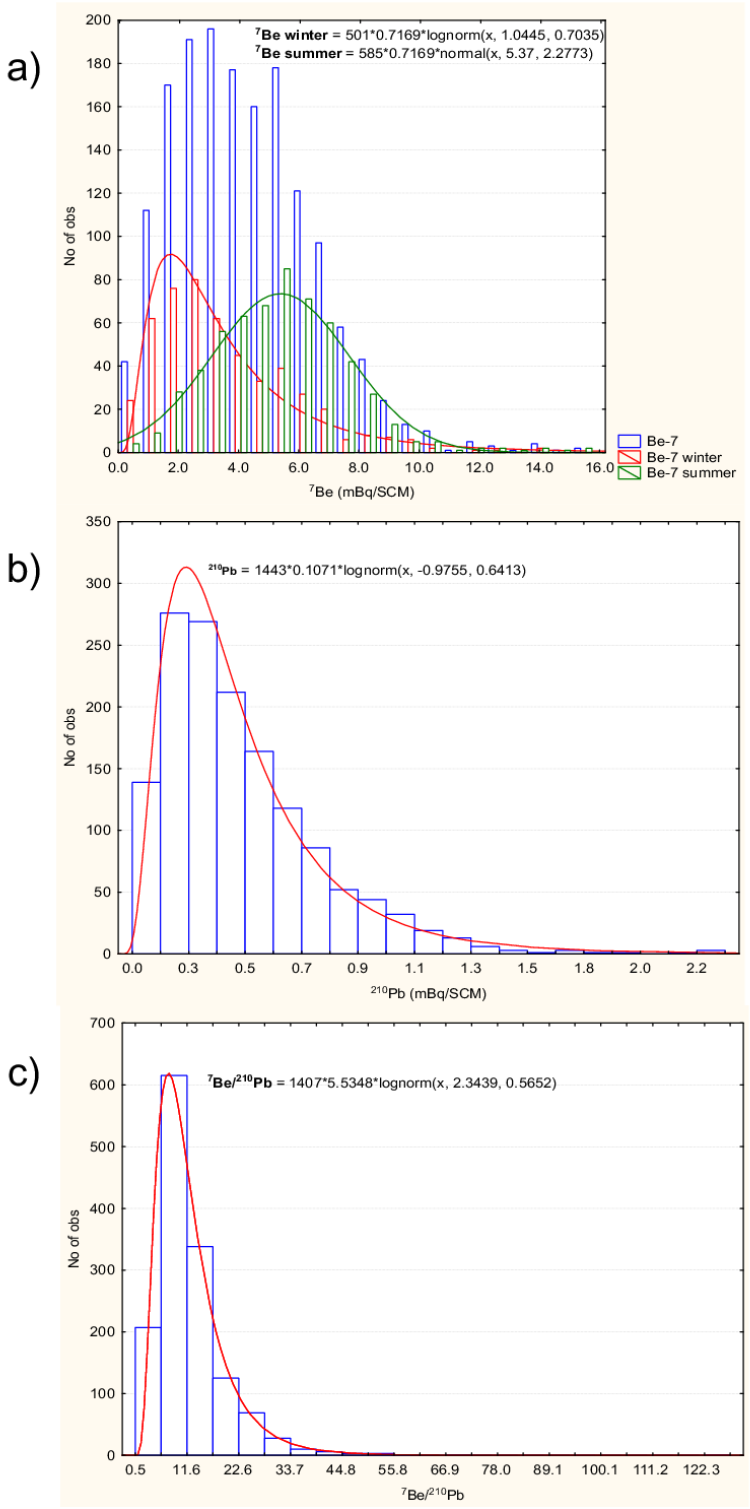

Figure 3.5(a,b,c) *Frequency distributions of a) ^{7}Be (blue distribution) and ^{7}Be during the cold (November, December, January and February, red distribution) and warm season (May, June, July, August, green distribution), fitted by a lognormal (red curve) and a normal distribution (green curve), respectively; b) ^{210}Pb, fitted by a lognormal distribution; c) $^{7}Be/^{210}Pb$, fitted by a lognormal distribution.*

While ^{210}Pb and ^{7}Be/^{210}Pb ratio data are very well fitted by log-normal distributions (Shapiro–Wilk *W* test equal to 0.997, with probability *p* less than 0.01, for the distribution of the natural logarithm of ^{210}Pb and of ^{7}Be/^{210}Pb), the ^{7}Be frequency distribution is bi-modal. This behaviour is attributed to the presence of two distinct seasonal maxima for this tracer, respectively during the cold and warm season as confirmed by decomposing the dataset into two major seasonal subsets ranging respectively between November and February (extended winter) and between May and August (extended summer) as reported in Figure 3.5a. While the winter distribution, which gives rise to the lower mode of the distribution at 3 mBq m^{-3}, is well fitted by a lognormal function (Shapiro–Wilk *W* test of the natural logarithm = 0.985, $p < 0.01$), the summer distribution corresponds to a normal distribution peaking at about 6 mBq m^{-3}. The skewness values for the two distributions during the two seasons are different: while during the cold period the skewness for ^{7}Be is equal to 1.21, highlighting once again the asymmetry of the distribution during this period, the value during the warm period is equal to 0.81, showing a larger degree of symmetry which is well recognizable in the distribution of Figure 3.5a. The kurtosis value is higher during summer than during winter (equal to 2.05 and 1.84, respectively), probably because of the presence of heavier tails in the distribution of the warm period. In the case herein treated the pronounced observed asymmetry suggests that the geometric mean or the median should be used instead of the mean to characterize average values of the three time series investigated (Wilks, 2006).

Bimodality in the frequency distribution of ^{7}Be has already been observed at four high-altitude stations including Mt. Cimone (Gerasopoulos *et al.*, 2001) and by Lee *et al.* (2007) at the Mt. Cimone and Mt. Waliguan GAW stations. In order to understand the physical origin of the bimodality of the ^{7}Be distribution Gerasopoulos *et al.* (2001) proposed to apply a simple statistical treatment based on *t*-test over separation values among ^{7}Be bins in order to split the data into major groupings as a function of distinct meteorological and atmospheric conditions. It is to note that at the time of the above mentioned publication ^{7}Be dataset from Mt. Cimone was included in the paper, but was insufficient for this elaboration. In brief ^{7}Be was distributed into bins in the range from 1 to 11 mBq m^{-3}: each bin represents a separation value, for which it is possible to form two classes of meteorological and atmospheric data, linked, respectively, to values lower and higher than the separation one. The Student's *t*-test value is then calculated to check for the difference between the means of the two classes. Figure 3.6(a-f) reports the results of this analysis performed for relative humidity, specific humidity, tropopause height, pressure, temperature and wind speed.

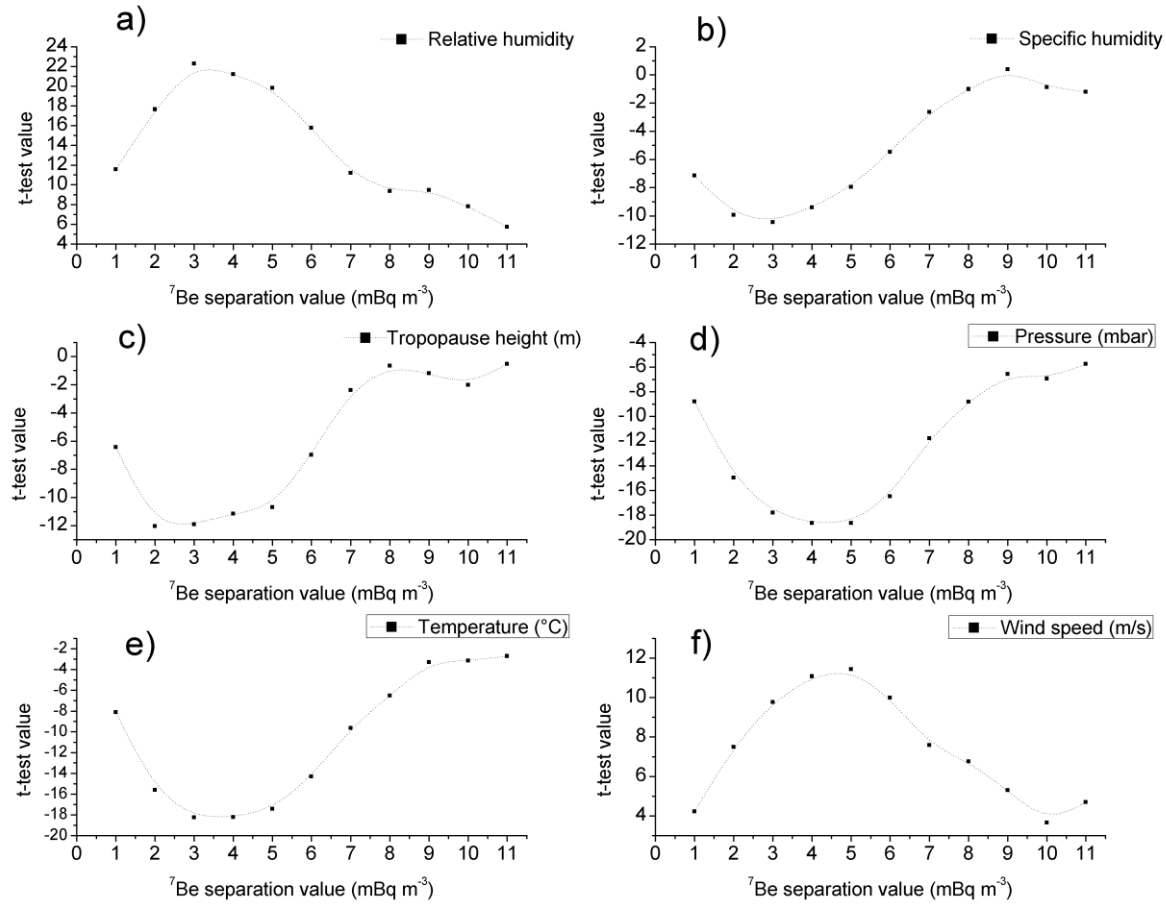

Figure 3.6(a,b,c,d,e,f) *t-test values for the significance of the difference between the means of meteorological and atmospheric parameters , when sorted according to a separation value of ^{7}Be: a)relative humidity; b) specific humidity; c) tropopause height; d) pressure; e) temperature; f) wind speed. Lines connecting the values are polynomial b-splines.*

In all the curves a transition class in the *t*-test values at 3-4 mBq m^{-3} of ^{7}Be can be observed. A second maximum at 9-10 mBq m^{-3} (8 mBq m^{-3} for tropopause height and relative humidity) is also shown by the presented curves for atmospheric/meteorological variables. This result might suggest the presence of a third mode for values of ^{7}Be above 8 mBq m^{-3}. Data so far available at Mt. Cimone do not allow further verifications of this hypothesis, as the values above 8 mBq m^{-3} are only the 6% of the total case, but this would be in agreement with Reiter *et al.* (1983) who showed that the total ogive of the frequency distribution of ^{7}Be at Zugspitze at a higher altitude than Mt. Cimone, is composed of three modes, of which the first corresponds to a distribution of the tropospheric values without stratospheric influx, the second one to a distribution of the values influenced by stratospheric intrusions and the third to a distribution of high values originated from deep stratospheric intrusions (Elbern *et al.*, 1997; Bonasoni *et al.*, 1999; Bonasoni *et al.*, 2000a, b; Stohl *et al.*, 2000, 2003; James *et al.*, 2003; Zanis *et al.*,

2003; Cristofanelli *et al.*, 2003, 2006, 2007, 2009a; Trickl *et al.*, 2010) in proximity of the station, with limited shear and therefore with minimal path. The positive sign of the *t*-test values for relative humidity and wind speed can be attributed to the anti-correlation between these two variables and ^{7}Be, due to removal and dispersion of particles during high relative humidity/wind speed conditions, or maximum ^{7}Be associated to minima of relative humidity during STE. On the contrary, the negative sign of the *t*-test values for other variables (tropopause height, specific humidity, pressure and temperature) reveals a positive correlation between ^{7}Be and these variables.

Ozone has been routinely monitored at the Mt Cimone station since 1996 by ISAC–CNR (Institute of Atmospheric Sciences and Climate of the Italian National Research Council): data are available at http://ds.data.jma.go.jp/gmd/wdcgg/ (World Data Centre for Greenhouse Gases, WDCGG).

As shown in Figure 3.7, ozone shares the bimodality of ^{7}Be. It has already been shown that O_3 increases in the troposphere are due to two different mechanisms, particularly at a high-altitude station such as Mt. Cimone: 1) continental emissions in the PBL and transports in the troposphere (associated to ^{210}Pb transports) (Arimoto *et al.*, 1999; Li *et al.*, 2002; Liu *et al.*, 2004); 2) transport from the stratosphere/upper troposphere, where it is known to be present a large ozone reservoir (associated to ^{7}Be transports) (Monks, 2000; Li *et al.*, 2002; James *et al.*, 2003; Cuevas *et al.*, 2013). Even if the seasonality of this trace gas (Figure 3.8) is associated to an increase starting during late spring (April–May) and continuing during summer, the bimodality of its distribution clearly resembles the one of ^{7}Be. In fact, over the Mediterranean region and in southern Europe, the tropospheric seasonal cycle of O_3 is usually dominated by the presence of a broad spring-summer peak (Bonasoni *et al.*, 2000b; Kouvarakis *et al.*, 2002; Ribas and Peñuelas, 2004; Nolle *et al.*, 2005; Di Carlo *et al.*, 2007; Cristofanelli and Bonasoni, 2009), due to the superposition of the hemispheric-scale spring maximum (April–May) and the increased photochemical production of O_3 that characterises the lower troposphere during summer (Pochanart *et al.*, 2001; Lelieveld *et al.*, 2002). Moreover, typical summer fair weather conditions, besides contributing to an increase in O_3 production from anthropogenic precursors, can also favour the export of polluted air masses from the boundary layer to the free troposphere of the continental Europe (Henne *et al.*, 2005; Cristofanelli *et al.*, 2007) and over the Mediterranean basin (Kouvarakis *et al.*, 2002; Lelieveld *et al.*, 2002; Gerasopoulos *et al.*, 2005a). The spring O_3 maximum was attributed to STE (Monks, 2000; Vingarzan, 2004) and long-range transport of O_3 precursors accumulating during winter in the northern hemispheric free troposphere, and its ensuing in situ photochemical production. In the free troposphere, the presence of the yearly O_3 double peak, frequently integrated in a broad spring-summer peak, was already evidenced for measurements carried out in high mountain areas by

Cristofanelli and Bonasoni (2009). O_3 distributions during extended winter and extended summer are well fitted by normal distribution (Shapiro–Wilk W test = 0.984, $p < 0.0006$ winter distribution; Shapiro–Wilk W test = 0.957, $p < 0.000001$ summer distribution).

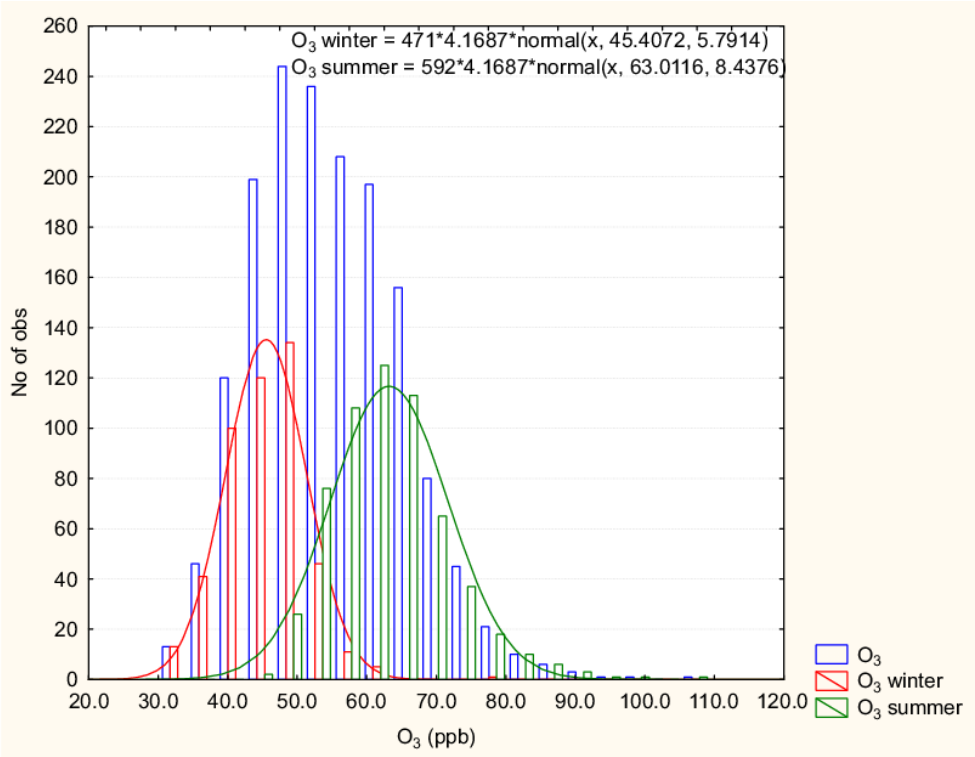

Figure 3.7 *Frequency distributions O_3 (blue distribution) and O_3 during the cold (November, December, January and February, red distribution) and warm season (May, June, July, August, green distribution), fitted by two normal distributions.*

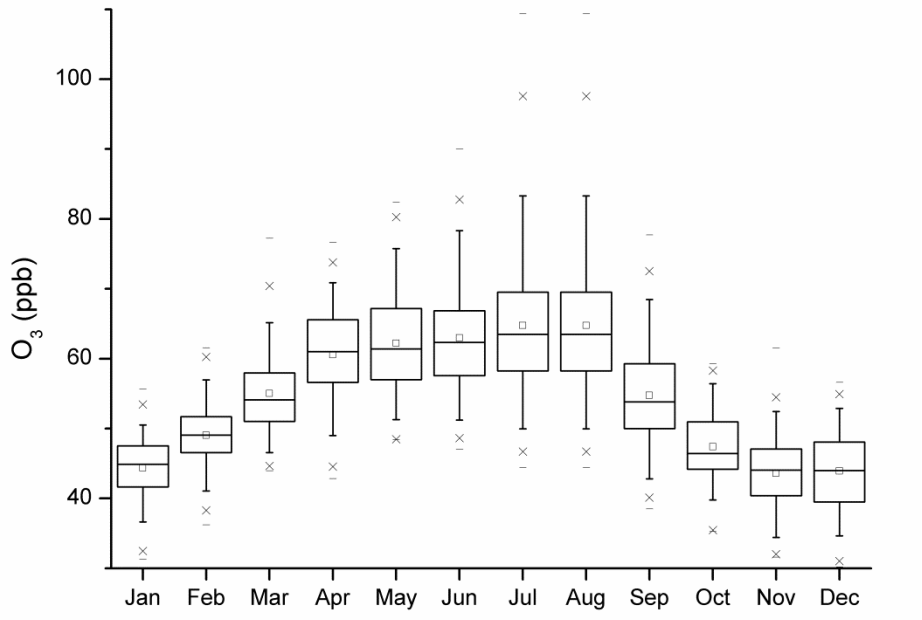

Figure 3.8 *Seasonal variations of O_3 at Mt. Cimone during the sampling period 1998-2011, represented by box and whiskers plot.*

The same approach of the *t*-test over separation values can be applied on O_3 bins in order to split the data into major groupings related to different meteorological and atmospheric conditions (Figure 3.9(a-f)).

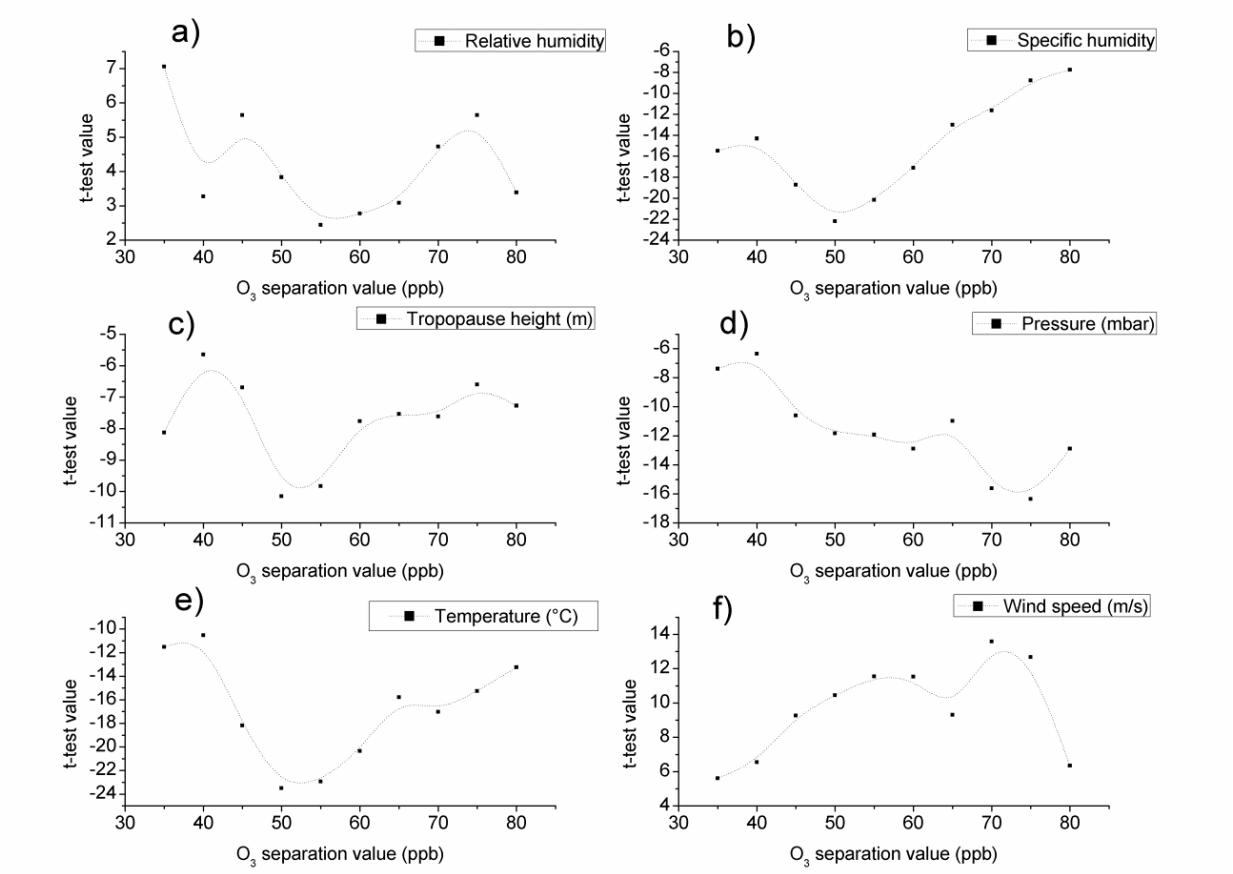

Figure 3.9(a,b,c,d,e,f) *t-test values for the significance of the difference between the means of meteorological and atmospheric parameters , when sorted according to a separation value of O_3: a)relative humidity; b) specific humidity; c) tropopause height; d) pressure; e) temperature; f) wind speed. Lines connecting the values are polynomial b-splines.*

The presence of at least two modes (even three in the case of tropopause height and relative humidity) is clear also in the case of O_3.

Even in this case, the positive sign of the *t*-test highlights the presence of anti-correlation of ozone with relative humidity and wind speed; the negative sign instead highlights its correlation with the tropopause height (same as ^{7}Be, as the lower tropopause height during winter is associated with increased STE and transports of both O_3 and ^{7}Be from the UT–LS, but also the higher tropopause during summer is associated to the maximum seasonal O_3, transported from the polluted boundary layer), pressure (anticyclonic conditions are associated to increased photochemical

activities and therefore to increased ozone production) and temperature (increased photochemical production of ozone during summer with increased temperatures).

3.3.3 Correlations with other atmospheric species

In order to investigate the potential use of ^{7}Be and ^{210}Pb as atmospheric tracers Spearman's rank correlation coefficients of ^{7}Be and ^{210}Pb and of PM_{10} concentrations with a series of meteorological and compositional parameters such as a set of trace gases and black carbon among those monitored at Mt. Cimone have been calculated and results are presented in Table 3.2.

	p (mbar)	T (°C)	RH %	SH (kg kg^{-1})	TH (m)	WS (m s^{-1})	O_3 (ppb)	CO_2 (ppm)	BC (μg m^{-3})	CO (ppb)	^{7}Be (mBq m^{-3})	^{210}Pb (mBq m^{-3})	PM_{10} (μg m^{-3})	FP (N cm^{-3})	CP (N cm^{-3})	^{7}Be/^{210}Pb
^{7}Be (mBq m^{-3})	0.49	0.46	-0.56	0.21	0.34	-0.32	0.47	-0.36	0.47	-0.12	1.00	0.56	0.51	0.36	0.07	0.31
^{210}Pb (mBq m^{-3})	0.45	0.61	-0.25	0.51	0.43	-0.28	0.55	-0.35	0.62	-0.12	0.56	1.00	0.70	0.54	0.28	-0.54
PM_{10} (μg m^{-3})	0.37	0.60	-0.22	0.54	0.32	-0.23	0.64	-0.33	0.74	-0.07	0.51	0.70	1.00	0.65	0.29	-0.31
^{7}Be/^{210}Pb	-0.05	-0.25	-0.24	-0.38	-0.17	0.04	-0.16	0.05	-0.26	0.01	0.31	-0.54	-0.31	-0.27	-0.26	1.00

Table 3.2 *Spearman's rank correlation coefficients of ^{7}Be, ^{210}Pb, PM_{10} and ratio ^{7}Be/^{210}Pb with meteorological/atmospheric variables (pressure P, temperature T, relative humidity RH%, specific humidity SH, tropopause height TH, wind speed WS), trace gases (ozone O_3, carbon dioxide CO_2, carbon monoxide CO), black carbon (BC) and fine and coarse particles number densities (FP and CP, respectively).*

In general the relationship between ozone and ^{7}Be is widely recognized as a traditional field on investigation concerning STE (see for example Reiter, 1975b; Dutkiewicz, and Husain, 1979; Reiter, 1983; Dutkiewicz and Husain, 1985; Tremblay *et al.*, 1993; Allen *et al.*, 2003; Gerasopoulos *et al.*, 2005b; Trickl *et al.*, 2010). The approach was extended to the relationships between ozone and ^{7}Be and/or ^{210}Pb due to the complex source terms of O_3 which can be successfully intercepted by both the radionuclides representing two of the major sources for this fundamental gaseous component i.e., the stratosphere and the PBL (see for example Prospero *et al.*, 1995; Graustein and Turekian, 1996; Arimoto *et al.*, 1999; Li *et al.*, 2002; Liu *et al.*, 2004; Lee *et al.*, 2007; Cuevas *et al.*, 2013).

Less frequent is the use of the radiotracers with other gases apart from CO_2 (Zheng *et al.*, 2011) or Hg (Lamborg *et al.*, 2000). In this work we have taken into account the following atmospheric species measured at Mt. Cimone observatory i.e., O_3, CO_2, CO by IAFMS (Italian Air Force) and ISAC–CNR (Institute of Atmospheric Sciences and Climate of the Italian National Research Council) available the World Data Centre for Greenhouse Gases (at http://ds.data.jma.go.jp/gmd/wdcgg/) while black carbon and fine ($0.3\ \mu m \leq Dp < 1\ \mu m$) and coarse

particle (1 μm ≤ Dp ≤ 20 μm) number densities are available at EBAS database (at http://ebas.nilu.no/). Measurements at Mt. Cimone from different research groups, as well as meteorological and atmospheric parameters, such as temperature, pressure, relative humidity, wind speed and tropopause height (determined from radiosoundings at S. Pietro Capofiume station, the closest ground based station in the Po Valley for which this observational activity is available) were retrieved together and averaged to the same time resolution of two-days as PM_{10} and radionuclides for statistical homogenization of data.

The non-parametric Spearman's rank correlation coefficients have been applied instead of Pearson's approach, because, as previously observed, the parameters herein discussed are not normally distributed and therefore the former method is preferable (Wilks, 2006). Except for carbon monoxide, whose measurement started only in 2007 and therefore has a poor statistics, all the correlation coefficients are significant at $p < 0.05$.

An elevated correlation is found for ^{210}Pb and PM_{10} with temperature, suggesting the role of thermal convection during the warmer months in increasing vertical mixing within the troposphere. During the warm season the combination of an upward motion due to mixed layer expansion, thermal convection and mountain/valley breeze regime, results in an uplift of ^{210}Pb, PM_{10} and other substances from the polluted boundary layer (ozone, elemental carbon, all positively correlated with ^{210}Pb and PM_{10}). Relative humidity is negatively correlated with all the particulate associated parameters suggesting the effect of wet scavenging. As of Figure 3.4b maxima of relative humidity are associated with precipitation leading to minima in aerosol load due to wet scavenging. However the anti-correlation between ^{7}Be and relative humidity is much stronger than for the other parameters indicating the role of downward transport from the extremely dry UT–LS air causing simultaneous increases of ^{7}Be (and ozone) and decrease of relative humidity due to stratosphere depletion in water vapour. Both ^{7}Be and ozone show bimodal frequency distributions with behaviours slightly different for each of them. In this framework it is to note that specific humidity and relative humidity are not completely equivalent: in principle, specific humidity would be preferable for the identification of stratospheric intrusions being conserved in an air mass. However, stratospheric air masses usually mix with tropospheric ones during the descent to the lower troposphere, and since specific humidity in tropospheric air is highly variable (lower values in winter and at high altitudes and higher values in summer and close to the surface), the use of specific humidity as a tracer for stratospheric intrusions would result in the identification of excess STE during winter and at higher stations (Stohl *et al.*, 2000). This is the reason why the observational climatology of stratospheric intrusions is generally based on relative humidity instead of specific humidity.

Table 3.3 reports again Spearman's rank correlation coefficients in this case calculated on a seasonal basis: winter (December January February), spring (March April May), summer (June July August) and

autumn (September October November). In this case it was chosen to study the correlations on a "normal" four seasons basis, which was preferred to the use of the two extended winter/summer periods used for the distribution of ^{7}Be, in order to better study the difference between the two transition seasons, too.

WINTER	p (mbar)	T (°C)	RH %	SH (kg kg^{-1})	TH (m)	WS (m s^{-1})	O_3 (ppb)	CO_2 (ppm)	BC (μg m^{-3})	CO (ppb)	^{7}Be (mBq m^{-3})	^{210}Pb (mBq m^{-3})	PM_{10} (μg m^{-3})	FP (N cm^{-3})	CP (N cm^{-3})	^{7}Be/^{210}Pb
^{7}Be (mBq m^{-3})	0.50	0.15	-0.64	-0.46	0.22	-0.19	0.44	-0.29	-0.08	-0.09	1.00	0.49	0.13	-0.43	-0.15	0.68
^{210}Pb (mBq m^{-3})	0.24	-0.03	-0.29	-0.30	0.03	-0.19	0.36	-0.24	-0.07	-0.15	0.49	1.00	0.40	-0.51	-0.10	-0.26
PM_{10} (μg m^{-3})	0.01	-0.26	-0.12	-0.24	-0.20	0.00	0.19	-0.02	-0.18	-0.37	0.13	0.40	1.00	-0.52	-0.09	-0.22
^{7}Be/^{210}Pb	0.33	0.24	-0.45	-0.18	0.24	-0.07	0.18	-0.20	-0.01	-0.20	0.68	-0.26	-0.22	-0.22	-0.13	1.00
SPRING																
^{7}Be (mBq m^{-3})	0.53	0.46	-0.59	0.17	0.39	-0.32	0.40	-0.28	0.15	0.10	1.00	0.51	0.55	0.06	0.25	0.40
^{210}Pb (mBq m^{-3})	0.41	0.39	-0.28	0.27	0.24	-0.20	0.37	-0.28	0.28	0.18	0.51	1.00	0.59	0.00	0.25	-0.53
PM_{10} (μg m^{-3})	0.53	0.43	-0.35	0.29	0.36	-0.23	0.35	-0.27	0.05	0.14	0.55	0.59	1.00	0.18	0.29	-0.14
^{7}Be/^{210}Pb	0.00	0.00	-0.22	-0.11	0.03	-0.03	-0.04	0.01	-0.16	-0.21	0.40	-0.53	-0.14	0.02	-0.02	1.00
SUMMER																
^{7}Be (mBq m^{-3})	0.21	0.34	-0.43	-0.05	0.02	-0.15	0.36	-0.27	-0.07	0.13	1.00	0.52	0.62	0.09	-0.07	0.24
^{210}Pb (mBq m^{-3})	0.43	0.63	-0.37	0.42	0.31	-0.16	0.37	-0.18	0.04	0.09	0.52	1.00	0.61	0.11	0.06	-0.64
PM_{10} (μg m^{-3})	0.33	0.57	-0.41	0.28	0.11	-0.06	0.30	-0.31	-0.01	0.05	0.62	0.61	1.00	0.05	-0.09	-0.16
^{7}Be/^{210}Pb	-0.28	-0.44	0.07	-0.53	-0.32	0.07	-0.14	-0.02	-0.08	-0.04	0.24	-0.64	-0.16	0.01	-0.09	1.00
AUTUMN																
^{7}Be (mBq m^{-3})	0.50	0.38	-0.59	-0.09	0.25	-0.31	0.40	-0.25	-0.05	0.12	1.00	0.54	0.40	0.04	0.01	0.33
^{210}Pb (mBq m^{-3})	0.48	0.57	-0.25	0.32	0.34	-0.21	0.44	-0.17	0.08	0.03	0.54	1.00	0.67	0.19	0.07	-0.50
PM_{10} (μg m^{-3})	0.35	0.49	-0.15	0.38	0.20	-0.10	0.39	-0.28	0.21	0.00	0.40	0.67	1.00	-0.12	-0.19	-0.42
^{7}Be/^{210}Pb	-0.03	-0.26	-0.33	-0.45	-0.08	-0.08	-0.05	-0.06	-0.28	-0.02	0.33	-0.50	-0.42	-0.13	0.08	1.00

Table 3.3 *Spearman's rank correlation coefficients of ^{7}Be, ^{210}Pb, PM_{10} and activity ratio ^{7}Be/^{210}Pb with meteorological/atmospheric variables (pressure P, temperature T, relative humidity RH%, specific humidity SH, tropopause height TH, wind speed WS), trace gases (ozone O_3, carbon dioxide CO_2, carbon monoxide CO), black carbon (BC) and fine and coarse particles (FP and CP, respectively) for each season (winter, spring, summer, autumn).*

The table highlights how the correlation can be significantly different during the seasons. During summer ^{210}Pb shows its maximum correlation with temperature (0.63) and specific humidity (0.42), while its maximum correlation with pressure is shown during autumn (0.48), when the maximum ^{210}Pb–PM_{10} correlation (0.67) and ^{210}Pb–O_3 are also found. During spring ^{210}Pb shows its maximum correlation with temperature (0.46).

Fine particles show maximum correlation coefficients with ^{7}Be, ^{210}Pb and PM_{10} during winter, while during the other seasons no simple correlation is found for this variable.

PM_{10} is correlated with temperature during summer (0.63), while a partial correlation with pressure can be found during spring.

^{7}Be shows its maximum anti-correlation with relative humidity during winter (-0.64), decreasing during the transition seasons and showing its minimum value during summer. During the cold season anti-correlation (-0.46) is found also in respect with specific humidity, emphasizing the role of active STE in the cold period. Gerasopoulos *et al.* (2001) reported an analogous correlation pattern for ^{7}Be and relative-specific humidity: they explained that the elevated correlation between the above parameters respectively throughout the year and during cold months with the dominating effect of wet scavenging during the warm period, while in the cold period vertical transport becomes important as previously explained.

In the cold season the highest $^{7}Be–O_3$ correlation is also observed, which could highlight the same UT–LS origin of these two parameters during this season when ozone photochemistry and transport from PBL are limited; this observation is in agreement with Cristofanelli *et al.* (2009a). In summer the high correlation among temperature, ^{210}Pb and PM_{10} confirms the influence of enhanced convective vertical mixing, affecting simultaneously the concentrations of ^{7}Be (downward motion), ^{210}Pb, PM_{10} and other trace gases all uplifted to Mt. Cimone from the polluted boundary layer as mentioned before.

In Figures 3.10, 3.11 and 3.12 some scatterplots of special interest between the treated variables are presented; in fact low values of the correlation coefficients are not necessarily due to lack of correlation between couples of variables, but could be due to the presence of bivariance as found in this work, which in turn might be due to different seasonal correlation patterns or to other different mechanisms promoting different covariance in the atmosphere (see for example the scatterplot between the $^{7}Be/^{210}Pb$ ratio vs. O_3, Figure 3.10a).

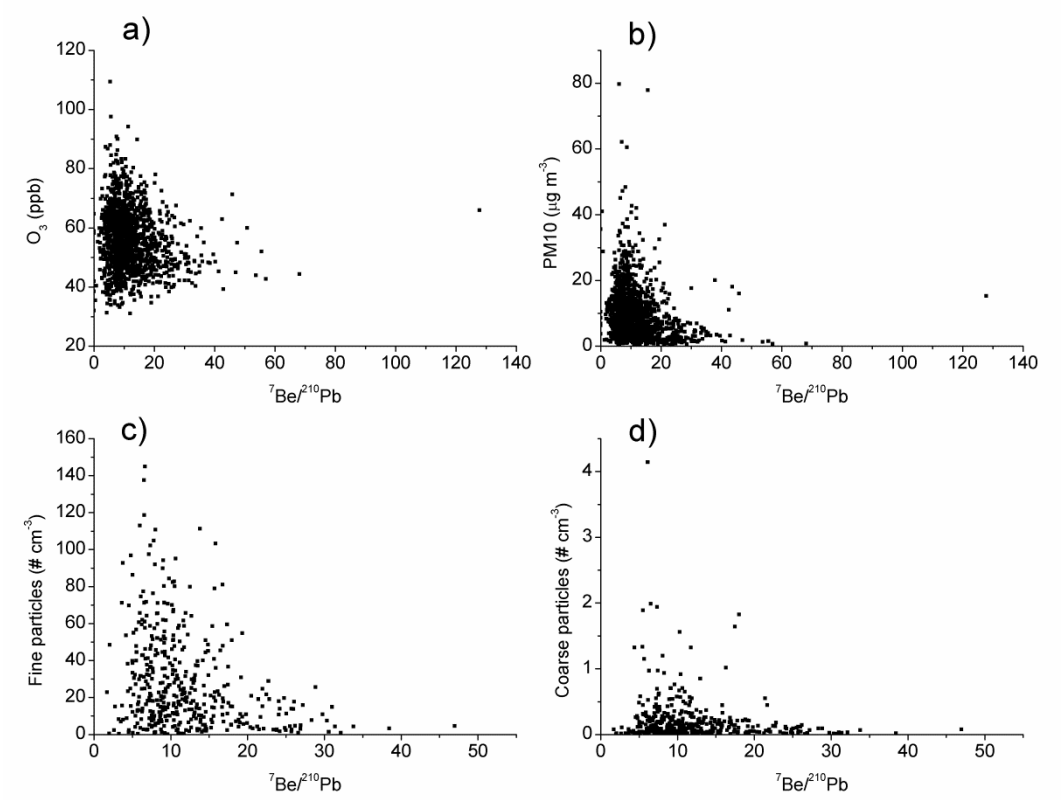

Figure 3.10(a,b,c,d) *Scatterplots of $^{7}Be/^{210}Pb$ vs. : a) O_3; b) PM_{10}; c) number density of fine particles (0.3 μm ≤ Dp < 1μm); d) number density of coarse particles (1 μm ≤ Dp ≤ 20 μm).*

As previously highlighted, ozone increase can be due both to transports of air pollution from the boundary layer (correlation with ^{7}Be and ^{210}Pb, low $^{7}Be/^{210}Pb$ ratio, especially during the warm months; see Arimoto *et al.*, 1999; Bonasoni *et al.*, 2004; Liu *et al.*, 2004; Marinoni *et al.*, 2008; Tositti *et al.*, 2013) as well as from transports from the UT–LS (correlation with ^{7}Be only, elevated $^{7}Be/^{210}Pb$ ratio, especially during the cold period; see Bonasoni *et al.*, 1999, 2000a, b; Cristofanelli *et al.*, 2006, 2009a; Liu *et al.*, 2004).

The pattern highlighted in the scatterplots of $^{7}Be/^{210}Pb$ (Figure 3.10b,c,d) clearly show how an elevated ratio can be linked both to increases as well as to decreases in aerosol mass load, and in the number densities of both fine and coarse particles.

Marinoni *et al.* (2008) suggested North Italy, west Europe and east Europe as source regions for black carbon and number density of fine particles; moreover, they reported the seasonal cycle of fine and coarse particles as characterized by the highest values in spring-summer and the lowest values in autumn-winter. The bivariance in the scatterplot of ^{210}Pb vs. black carbon and carbon monoxide (Figure 3.11a,c) show that they share some source regions/seasonalities, but not all of them: the likely influence of Saharan Dust transports as source of increases of ^{210}Pb but not of black carbon (and carbon monoxide) depending on the occasional occurrence of biomass burning in that region might be the cause of the bivariance in the scatterplots.

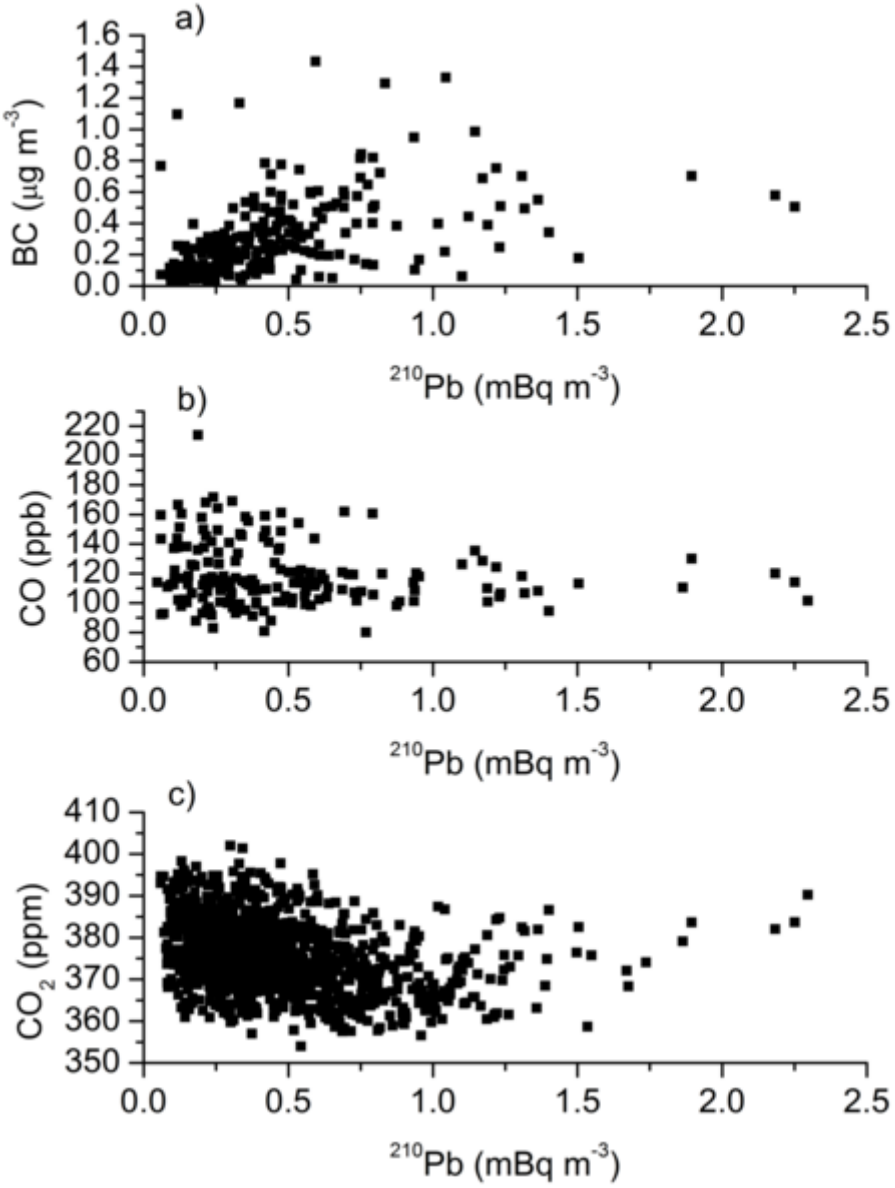

Figure 3.11(a,b,c) *Scatterplots of ^{210}Pb vs.: a) black carbon; b) carbon monoxide; c) carbon dioxide.*

The bivariance of the scatterplot of ^{210}Pb vs. CO_2 (Figure 3.11b) could be due instead to the different seasonal behaviour of the two variables: while ^{210}Pb at Mt. Cimone has been shown to exhibit a summer maximum, CO_2 presents the typical Northern Hemisphere seasonal pattern with a winter maximum and a summer minimum, which are known to be due to the seasonal modulation in carbon fluxes (Cleveland and Kaufmann, 2007).

Finally, the scatterplot in Figure 3.12 highlights that besides the summer thermal convection giving rise to both ^{7}Be and fine particles increases, other mid-scale transports can be responsible of only fine particles (Western/Eastern Europe, for instance, in agreement with the results of Tositti *et al.*, 2013, presented in Chapter 2).

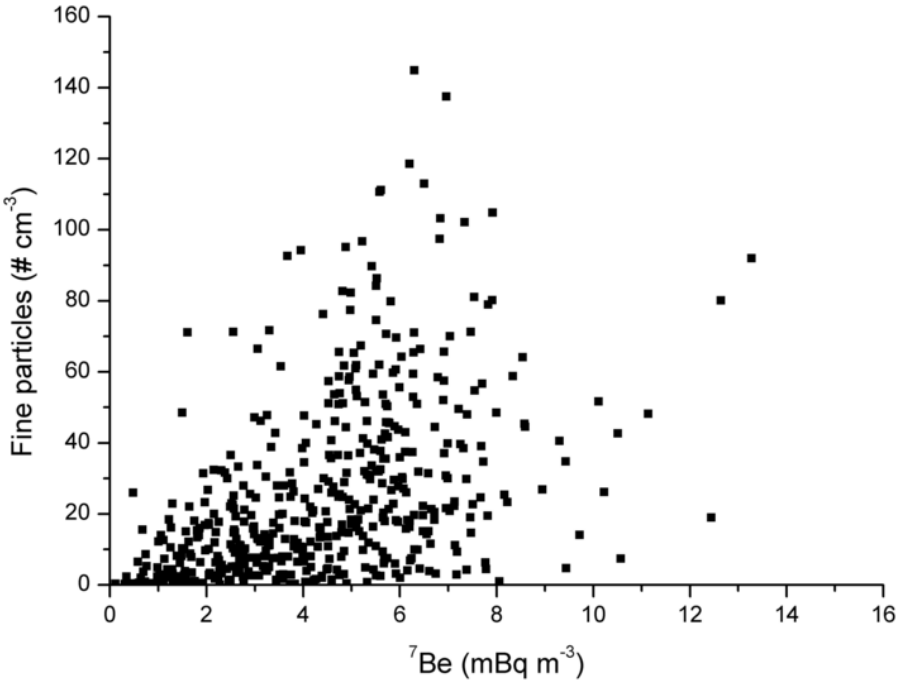

Figure 3.12 *Scatterplot of ^{7}Be vs. number density of fine particles (0.3 μm ≤ D_p < 1 μm).*

3.4 Summary and conclusions

This work reports the results of a study concerning temporal variations and statistical analysis for the atmospheric radiotracers ^{7}Be, ^{210}Pb and of their activity ratio at the WMO–GAW station of Mt. Cimone from 1998 to 2011.

1. Both radiotracers similarly to PM_{10} discussed in Chapter 2 (Tositti *et al.*, 2013), have a marked seasonal variation. Interannual variations are ascribed to amounts of overall precipitation, atmospheric stability, relative humidity, mean temperature. On a first approximation all of the three parameters have a winter minimum and a summer maximum.
2. Frequency distributions of the two radionuclides and of their ratio reveal a lognormal distribution for ^{210}Pb and for the ratio ^{7}Be/^{210}Pb, while a bimodal distribution is associated to ^{7}Be. The bimodality of the ^{7}Be distribution reflects the different seasonal behaviour of this tracer, and is further investigated with the help of a statistical *t*-test over separation values among ^{7}Be as a function of distinct meteorological and atmospheric conditions. In fact, while ^{210}Pb summer maximum is mainly due to the higher mixing height and enhanced uplift from the boundary layer as a result of thermal convection, the seasonal fluctuation of ^{7}Be is more complex, being characterized by two relative maxima, one during the cold season, which is associated to Stratosphere-to-Troposphere transport and one in the warm season, mainly (but not exclusively) associated to tropospheric subsidence balancing low tropospheric air masses

ascent occasionally accompanied by STE. $^{7}Be/^{210}Pb$ ratio presents a seasonal maximum during the cold period due to the intensity of baroclinic systems during this period. The resulting modes and data sub-grouping found with the help of *t*-test are associated respectively to the tropospheric values without stratospheric influx, while ^{7}Be modes with a tail above 8 mBq m^{-3} shows a strong influence from STE events suggesting the presence of a third mode in the distribution, potentially associated with deep stratospheric intrusions.

3. Frequency distribution was determined also for ozone, one of the main tropospheric trace gases which, besides in situ photochemical production is known to be due to two different transport mechanisms (from the polluted boundary layer like ^{210}Pb, and from UT–LS like ^{7}Be). Similarly to ^{7}Be, ozone, also presents a bimodal distribution, which is not strictly linked to its seasonal pattern, but is confirmed by the *t*-test approach, too: two or even three modes were found for ozone with this method, connected with different meteorological/atmospheric conditions, which in turn might be linked to different mechanisms causing increases in the trace gas.
4. The correlation patterns of the radionuclides and of their ratio with physical and compositional variables, namely particulate matter, ozone, and other gases such as CO_2, CO, black carbon and particles in the fine and coarse ranges, are examined, both on a total as well as on a seasonal basis. The role of thermal convection leading to increases in both the radionuclides (high correlation with temperature, tropopause height), and of wet scavenging as the most efficient removal mechanism (anti-correlation with relative humidity) is stressed. The anti-correlation of ^{7}Be with relative humidity is further emphasized by downward transport from the extremely dry UT–LS. Ozone is correlated with ^{7}Be during the cold season when they are both contributed by STE, while in the warm season it is highly correlated with ^{210}Pb, PM_{10} and trace gases all uplifted from the polluted boundary layer.
5. Finally, bivariance between $^{7}Be/^{210}Pb$ vs. O_3, PM_{10}, fine and coarse particle number density, ^{210}Pb vs. black carbon, CO and CO_2, ^{7}Be vs. fine particles number density is introduced suggesting other less conventional but potentially promising applications of the studied radiotracers in atmospheric investigations, useful in the complex framework of climate change and consequent modifications of circulation patterns.

Acknowledgements

Italian Air Force Meteorological Office (IAFMS) is gratefully acknowledged for hosting ISAC–CNR atmospheric research platform, therefore allowing for the collection of precious compositional datasets.

IAFMS is gratefully acknowledged for providing meteorological and carbon dioxide data; ISAC–CNR is gratefully acknowledged for providing aerosol size distribution, carbon monoxide, black carbon and ozone data, besides infrastructural access at the WMO-GAW Global Station Italian Climate Observatory "O. Vittori" at Mt. Cimone. The Italian Climate Observatory "O. Vittori" is supported by MIUR and DTA-CNR throughout the Project of National Interest NextData. We thank two anonymous referees for their valuable suggestions and comments, which improved the quality of our paper.

References

Argiero L., Manfredini S., Palmas G., 1961. Measurements of air radioactivity on Italy and their relation to the first Sahara atomic explosion. *Nature* 190, 618-619.

Aebischer U., Schär C., 1998. Low-Level Potential Vorticity and Cyclogenesis to the Lee of the Alps. *Journal of the Atmospheric Sciences* 55, 186-207.

Allen D.J., Dibb J.E., Ridley B., Pickering K.E., Talbot R.W., 2003. An estimate of the stratospheric contribution to springtime tropospheric ozone maxima using TOPSE measurements and beryllium-7 simulations. *Journal of Geophysical Research Atmospheres* 108(D4). doi:10.1029/2001JD001428

Anagnostopoulou C., Tolika K., Flocas H., Maheras P., 2006. Cyclones in the Mediterranean region: present and future climate scenarios derived from a general circulation mode (HadAM3P). *Advances in Geosciences* 7, 9-14.

Arimoto R., Snow J.A., Graustein W.C., Moody J.L., Ray B.J., Duce R.A., Turekian K.K., Maring H.B., 1999. Influences of atmospheric transport pathways on radionuclide activities in aerosol particles from over the North Atlantic. *Journal of Geophysical Research* 104(D17), 301-321.

Balkanski Y.J., Jacob D.J., Gardner G.M., Graustein W.C., Turekian K.K., 1983. Transport and residence times or tropospheric aerosols inferred from a global three-dimensional simulation of ^{210}Pb. *Journal of Geophysical Research* 98, 20573-20586.

Baltensperger U., Gäggeler H.W., Jost D.T., Lugauer M., Schwikowski M., Weingartner E., Seibert P., 1997. Aerosol climatology at the high-alpine site Jungfraujoch, Switzerland. *Journal of Geophysical Research* 102 (D16), 19,707-19,715. http://dx.doi.org/10.1029/97JD00928.

Barkan J., Alpert P., 2008. Synoptic patterns associated with dusty and non-dusty seasons in the Sahara. *Theoretical and Applied Climatology* 94, 153-162, doi:10.1007/s00704-007-0354-9.

Baskaran M., 2011. Po-210 and Pb-210 as atmospheric tracers and global Pb-210 fallout: a review. *Journal of Environmental Radioactivity* 102, 500-513.

Bonasoni P., Evangelisti F., Boanfé U., Feldmann H., Memmesheimer M., Stohl A., Tositti L., 1999. Stratosphere-troposphere exchanges: case studies recorded at Mt. Cimone during VOTALP project. *Physics and Chemistry of the Earth* (C) 24(5), 443-446.

Bonasoni P., Evangelisti F., Bonafé U., Ravegnani F., Calzolari F., Stohl A., Tositti L,. Tubertini O., Colombo T., 2000a. Stratospheric ozone intrusion episodes recorded at Mt. Cimone during VOTALP project: Case studies. *Atmospheric Environment* 34, 1355-1365.

Bonasoni P., Stohl A., Cristofanelli P., Calzolari F., Colombo T., Evangelisti F., 2000b. Background ozone variations at Mt Cimone station. *Atmospheric Environment* 34, 5183-5189.

Bonasoni P., Cristofanelli P., Calzolari F., Bonafé U., Evangelisti F., Stohl A., Zauli Sajani S., van Dingenen R., Colombo T., Balkanski Y., 2004. Aerosol-ozone correlations during dust transport episodes. *Atmospheric Chemistry and Physics* 4, 12501-1215.

Brost R.A., Feichter J., Heimann M., 1991. Three-dimensional simulation of ^{7}Be in a global climate model. *Journal of Geophysical Research* 96, 22423-22445.

Burton W.M., Stewart N.G., 1960. Use of long-lived natural radioactivity as an atmospheric tracer. *Nature* 186, 584-589.

Buzzi A., Giovannelli G., Nanni T., Tagliazucca M., 1984. Study of high ozone concentrations in the troposphere associated with lee cyclogenesis during ALPEX. Beiträge zur Physik der Atmosphäre, 57, 380-392.

Campins J., Jansà A., Genovés A., 2006. Three-dimensional structure of western Mediterranean cyclones. *International Journal of Climatology* 26, 323-343.

Cannizzaro F., Greco G., Raneli M., Spitale M., Tomarchio E., 2004. Concentration measurements of ^{7}Be at ground level air at Palermo, Italy – Comparison with solar activity over a period of 21 years. *Journal of Environmental Radioactivity* 72, 259-271.

Carvalho A.C., Reis M., Silva L., Madruga M.J., 2013. A decade of ^{7}Be and ^{210}Pb activity in surface aerosols measured over the Western Iberian Peninsula. *Atmospheric Environment* 67, 193-202.

Christoudias T., Lelieveld J., 2013. Modelling the global atmospheric transport and deposition of radionuclides from the Fukushima Dai-ichi nuclear accident. *Atmospheric Chemistry and Physics* 13: 1425-1438. doi:10.5194/acp-13-1425-2013

Cleveland C.J., Kauffmann R., 2007. Mauna Loa Curve. In: The Encyclopedia of Earth, available at http://www.eoearth.org/view/article/154520/ Last accessed 31 July 2013.

Colombo T., Santaguida R., Capasso A., Calzolari F., Evangelisti F., Bonasoni P., 2000. Biospheric influence on carbon dioxide measurements in Italy. *Atmospheric Environment* 34, 4963-4969.

Cristofanelli P., Bonasoni. P., Collins W., Feichter J., Forster C., James P., Kentarchos A., Kubik P.W., Land C., Meloen J., Roelofs G.J., Siegmund P., Sprenger M., Schnabel C., Stohl A., Tobler L., Tositti L., Trickl T., and Zanis P., 2003. Stratosphere-to-troposphere transport: A model and method evaluation. *Journal of Geophysical Research* 108(D12), 8525, doi:10.1029/2002JD002600

Cristofanelli P., Bonasoni P., Tositti L., Bonafé U., Calzolari F., Evangelisti F., Sandrini S., Stohl A., 2006. A 6-year analysis of stratospheric intrusions and their influence on ozone at Mt. Cimone (2165 m above sea level). *Journal of Geophysical Research* 111. D03306. doi:10.1029/2005JD006553.

Cristofanelli P., Bonasoni P., Carboni G., Calzolari F., Casarola L., Zauli Sajani S., Santaguida R., 2007. Anomalous high ozone concentrations recorded at a high mountain station in Italy in summer 2003. *Atmospheric Environment* 41, 1383-1394.

Cristofanelli P., Calzolari F., Bonafé U., Duchi R., Marinoni A., Roccato F., Tositti L., Bonasoni P., 2009a. Stratospheric intrusion index (SI^2) from baseline measurement data. *Theoretical and Applied Climatology* 97, 317-325.

Cristofanelli P., Marinoni A., Arduini J., Bonafé U., Calzolari F., Colombo T., Decesri S., Duchi R., Facchini M.C., Fierli F., Finessi E., Maione M., Chiari M., Calzolai G., Messina P., Orlandi E., Roccato F., Bonasoni P., 2009b. Significant variations of trace gas composition and aerosol properties at Mt. Cimone during air mass transport from North Africa – contributions from wildfire emissions and mineral dust. *Atmospheric Chemistry and Physics* 9, 4603-4619.

Cristofanelli P. and Bonasoni P., 2009. Background ozone in the southern Europe and Mediterranean area: Influence of the transport processes. *Environmental Pollution* 157, 1399–1406.

Cristofanelli P., Fierli F., Marinoni A., Calzolari F., Duchi R., Burkhart J., Stohl A., Maione M., Arduini J., Bonasoni P., 2013. Influence of biomass burning and anthropogenic emissions on ozone, carbon monoxide and black carbon at the Mt. Cimone WMO-GAW global station (Italy, 2165 m a.s.l.). *Atmospheric Chemistry and Physics* 13, 15-30. doi:10.5194/acp-13-15-2013

Cuevas E., Gonzalez Y., Rodríguez S., Guerra J.C., Gómez-Peláez A.J., Alonso-Pérez S., Bustos J., Milford C., 2013. Assessment of atmospheric processes driving ozone variations in the subtropical North Atlantic free troposphere. *Atmospheric Chemistry and Physics* 13, 1973-1998.

Davies T.D., Schuepbach E., 1994. Episode of high ozone concentrations at the earth's surface resulting from transport down from the upper troposphere/lower stratosphere: a review and case studies. *Atmospheric Environment* 28, 53-68

Davison W., Hilton J., Hamilton-Taylor J., Kelly M., Livens F., Rigg E., Carrick T.R., Singleton D.L., 1993. The transport of Chernobyl-derived radiocaesium through two freshwater lakes in Cumbria, UK. *Journal of Environmental Radioactivity* 19(2), 125-153.

Diaz Leon J., Jaffe D.A., Kaspar J., Knecht A., Miller M.L., Robertson R.G.H., Schubert A.G., 2011. Arrival time and magnitude of airborne fission products from the Fukushima, Japan, reactor incident as measured in Seattle, WA, USA. *Journal of Environmental Radioactivity* doi:10.1016/j.envrad.2011.06.005.

Dibb J.E., 2007. Vertical mixing above Summit, Greenland: insights into seasonal and high frequency variability from the radionuclide tracers ^{7}Be and ^{210}Pb. *Atmospheric Environment* 41, 5020-5030.

Di Carlo P., Pitari G., Mancini E., Gentile S., Pichelli E., Visconti G., 2007. Evolution of surface ozone in central Italy based on observations and statistical model. *Journal of Geophysical Research* 112, D10316, doi:10.1029/2006JD007900.

Dietrich E., Favale B., Passamonti V., 1997. Trentasei anni di misure di radioattività beta nell'aria sull'Italia al livello del suolo. Valori medi mensili dal 1957 al 1992. CNR-IFA Internal Report 97-15.

Dueñas C., Fernández M.C., Cañete S., Pérez M., 2009. ^{7}Be to ^{210}Pb concentration ratio in ground level air in Màlaga(36.7°N, 4.5°W). *Atmospheric Research* 92, 49-57.

Dueñas C., Orza J.A.G., Cabello M., Fernández M.C., Cañete S., Pérez M., Gordo E., 2011. Air mass origin and its influence on radionuclide activities (^{7}Be and ^{210}Pb) in aerosol particles at a coastal site in the western Mediterranean. *Atmospheric Research* 101, 205-214.

Dutkiewicz V.A., Husain L., 1979. Determination of stratospheric ozone at ground level using ^{7}Be/ozone ratios. *Geophysical Research Letters* 6(3), 171-174. doi:10.1029/GL006i003p00171

Dutkiewicz V.A., Husain L., 1985. Stratospheric and tropospheric components of7Be in surface air. *Journal of Geophysical Research Atmospheres* 90(D3), 5783-5788.

Eisenbud M., Gesell T. 1997. Environmental Radioactivity. From Natural, Industrial and Military Sources. 4th edition Academic Press. 656 pp, ISBN 0-12-235154-1

EBAS database http://ebas.nilu.no/, last accessed 01 August 2013.

Elbern H., Kowol J., Sládkovic R., Ebel A., 1997. Deep stratospheric intrusions: a statistical assessment with model guided analyses. Atmospheric Environment, 31(19), 3207-3226.

Eskridge R.E., Ku J.Y., Rao S.T., Porter P.S., Zurbenko I.G., 1997. Separating different scales of motion in time series of meteorological variables. *Bulletin of the American Meteorological Society* 78, 1473-1483.

Feely H.W., Larsen R.J., Sanderson C.G., 1989. Factors that cause seasonal variations in ^{7}Be concentrations in surface air. *Journal of Environmental Radioactivity* 9, 223-249.

Fischer H., Kormann R., Klüpfel T., Gurk Ch., Königstedt R., Parchatka U., Mühle J., Rhee T.S., Brenninkmeijer C.A.M., Bonasoni P., Stohl A., 2003. Ozone production and trace gas correlations during the June 2000 MINATROC intensive measurement campaign at Mt Cimone. *Atmospheric Chemistry and Physics* 3, 725-738.

Formenti P., Rajot J.L., Desboeufs K., Caquineau S., Chevaillier S., Nava S., Gaudichet A., Journet E., Triquet S., Alfaro S., Chiari M., Haywood J., Coe H., Highwood E., 2008. Regional variability of mineral dust from western Africa: Results from the AMMA SOP0/DABEX and DODO field campaigns. *Journal of Geophysical Research Atmospheres* 113(D23), doi:10.1029/2008JD009903

Formenti P., Schütz L., Balkanski Y., Desboeufs K., Ebert M., Kandler K., Petzold A., Scheuvens D., Weinbruch S., Zhang D., 2011. Recent progress in understanding physical and chemical properties of African and Asian mineral dust. *Atmospheric Chemistry and Physics* 11, 8231-8256.

Froehlich K., Masarik J., 2010. Radionuclides as tracers and timers of processes in the continental environment – Basic concepts and methodologies. In: Radioactivity in the Environment 16, Chapter 2: 27-49. Edited by Elsevier. Doi:10.1016/S1569-4860(09)01602-7

Gaffney J.S, Marley N., Cunningham M.M., 2004. Natural radionuclides in fine aerosols in the Pittsburgh area. *Atmospheric Environment* 38, 3191-3200.

Gaggeler H.W., 1995. Radioactivity in the atmosphere. *Radiochimica Acta* 70-71, 345-353

Gerasopoulos E., Zanis P., Stohl A., Zerefos C.S., Papastefanou C., Ringer W., Tobler L., Hübener S., Gäggeler H.W., Kanter H.J., Tositti L., Sandrini S., 2001. A climatology of ^{7}Be at four high-altitude stations at the Alps and the Northern Apennines. *Atmospheric Environment* 35, 6347-6360

Gerasopoulos E., Kouvarakis G., Vrekoussis M., Kanakidou M., Mihalopoulos N., 2005a. Ozone variability in the marine boundary layer of the eastern Mediterranean based on 7-year observations. *Journal of Geophysical Research* 110, D15309, doi:10.1029/2005JD005991.

Gerasopoulos E., Zanis P., Papastefanou C., Zerefos C.S., Ioannidou A., Hernli H., 2005. Deep stratosphere-to-troposphere transport (STT) over SE Europe: a complex case study captured by enhanced ^{7}Be concentrations at the surface of a low topography region. *Atmospheric Chemistry and Physics Discussion* 5, 101-129.

Graustein W.C., Turekian K.K., 1996. ^{7}Be and ^{210}Pb indicate an upper troposphere source for elevated ozone in the summertime subtropical free troposphere of the eastern North Atlantic. *Geophysical Research Letters* 23, 539-542.

Hamill P., Jensen E.J., Russell P.B., Bauman J.J., 1997. The Life Cycle of Stratospheric Aerosol Particles. *Bulletin of the American Meteorological Society* 78, 1395-1410.

Heinrich P., Jamelot A., 2011. Atmospheric transport simulation of ^{210}Pb and ^{7}Be by the LMDz general circulation model and sensitivity to convection and scavenging parameterization. *Atmospheric Research* 101, 54-66.

Henne S., Furger M., Prévôt A.S.H., 2005. Climatology of mountain venting-induced elevated moisture layers in the lee of Alps. *Journal of Applied Meteorology* 44, 620–633.

Hernández-Ceballos M.A., Hong G.H., Lozano R.L., Kim Y.I., Lee H.M., Kim S.H., Yeh S.W., Bolívar J.P., Baskaran M., 2012. Tracking the complete revolution of surface westerlies over Northern Hemisphere using radionuclides emitted from Fukushima. *Science of the Total Environment* 438, 80-85.

Hötzl H., Rosner G., Winkler R., 1991. Correlation of ^{7}Be concentrations in surface air and precipitation with the solar cycle. Naturwissenschaften 78, 215-217.

Hötzl H., Rosner G., Winkler R., 1992. Sources of present Chernobyl-derived caesium concentrations in surface air and deposition samples. *Science of the Total Environment* 119, 231-242.

Ioannidou A., Manolopoulou M., Papastefanou C., 2005. Temporal changes of ^{7}Be and ^{210}Pb concentrations in surface air at temperate latitudes (40°). *Applied Radiation and Isotopes* 63(2), 277-284.

Ioannidou A., Giannakaki E., Manolopoulou M., Stoulos S., Vagena E., Papastefanou C., Gini L., Manenti S., Groppi F., 2013. An air-mass trajectory study of the transport of radioactivity from Fukushima to Thessaloniki, Greece and Milan, Italy. *Atmospheric Environment* 75, 163-170.

Israelevich P., Ganor E., Alpert P., Kishcha P., Stupp A., 2012. Predominant transport paths of Saharan dust over the Mediterranean Sea to Europe. *Journal of Geophysical Research: Atmospheres* 117(D2), doi:10.1029/2011JD016482

James P, Stohl A., Forster C., Eckhardt S., Seibert P., Frank A., 2003. A 15-year climatology of stratosphere-troposphere exchange with a Lagrangian particle dispersion model 2. Mean climate and seasonal variability. *Journal of Geophysical Research* 108(D12), 8522. doi:10.1029/2002JD002639

Johnson W., Viezee W., 1981. Stratospheric ozone in the lower troposphere-I. Presentation and interpretation of aircraft measurements. *Atmospheric Environment* 15, 1309–1323.

Junge C.E., 1963. Air chemistry and radioactivity. Academic Press, New York and London. 382 pp.

Koch D.M., Jacob J., Graustein W.C., 1996. Vertical transport of tropospheric aerosols as indicated ^{7}Be and ^{210}Pb in a chemical tracer model. *Journal of Geophysical Research* 101, 18651-18666.

Kouvarakis G., Vrekoussis M., Mihalopoulos N., Kourtidis K., Rappenglueck B., Gerasopoulos E., Zerefos C., 2002. Spatial and temporal variability of tropospheric ozone in the boundary layer above the Aegean Sea (eastern Mediterranean). *Journal of Geophysical Research* 107 (D18), 8137, doi:10.1029/2000JD000081.

Krysta M., Bocquet M., 2007. Source reconstruction of an accidental radionuclide release at European scale. *Quarterly Journal of the Royal Meteorological Society* 133(623), 529-544.

Kulan A., Aldahan A., Possnert G., Vintersved I., 2006. Distribution of ^{7}Be in surface air of Europe. *Atmospheric Environment* 40, 3855-3868.

Lamborg C.H., Fitzgerald W.F., Graustein W.C., Turekian K.K., 2000. An examination of the atmospheric chemistry of mercury using ^{210}Pb and ^{7}Be. *Journal of Atmospheric Chemistry* 36, 325-338.

Lee H.N., Wan G., Zheng X., Sanderson C.G., Josse B., Wang S., Yang W., Tang J., Wang C., 2004. Measurements of ^{210}Pb and ^{7}Be in China and their analysis accompanied with global model calculations of ^{210}Pb. *Journal of Geophysical Research* 109, D22203. doi:10.1029/2004JD005061

Lee H.N., Tositti L., Zheng X., Bonasoni P., 2007. Analyses and comparisons of variations of ^{7}Be, ^{210}Pb and $^{7}Be/^{210}Pb$ with ozone observations at two Global Atmosphere Watch stations from high mountains. *Journal of Geophysical Research* 112, D05303. doi:10.1029/2006JD007421

Lelieveld J., et al., 2002. Global air pollution crossroads over the Mediterranean. *Science* 298, 794–799.

Leppänen A.-P., Usoskin I.G., Kovaltsov G.A., Paatero J., 2012. Cosmogenic ^{7}Be and ^{22}Na in Finland: Production, observed periodicities and the connection to climatic phenomena. Journal of Atmospheric and Solar-Terrestrial Physics 74, 164-180.

Li Q., Jacob D.J., Fairlie T.D., Liu H., Martin R.V., Yantosca R.M., 2002. Stratospheric versus pollution influences on ozone at Bermuda: Reconciling past analyses. *Journal of Geophysical Research* 107, D22, 4611. doi:10.1029/2002JD002138

Liu H., Jacob D.J., Bey I., Yantosca R.M., 2001. Constraints from the ^{210}Pb and ^{7}Be on wet deposition and transport in a global three-dimensional chemical tracer model driven by assimilated meteorological fields. *Journal of Geophysical Research* 106, D11, 12109-12128.

Liu H., Jacob D.J., Dibb J.E., Fiore A.M., Yantosca R.M., 2004. Constraints on the sources of tropospheric ozone from ^{210}Pb-^{7}Be-O_3 correlations. *Journal of Geophysical Research* 109, D07306. doi:10.1029/2003JD003988.

Lozano R.L., Hernández-Ceballos M.A., Adame J.A., Casas-Ruíz M., Sorribas M., San Miguel E.G., Bolívar J.P., 2011. Radioactive impact of Fukushima accident on the Iberian Peninsula: evolution and plume previous pathway. *Environment International* 37, 1259-1264.

Lozano R.L., Hernández-Ceballos M.A., San Miguel E.G., Adame J.A., Bolívar J.P., 2012. Meteorological factors influencing the ^{7}Be and ^{210}Pb concentrations in surface air from the southwestern Iberian Peninsula. *Atmospheric Environment* 63, 168-178.

Maheras P., Flocas H.A., Anagnostopoulou C., Patrikas I., 2002. On the vertical structure of composite surface cyclones in the Mediterranean region. *Theoretical and Applied Climatology* 71, 199-217.

Manolopoulou M., Vagena E., Stoulos S., Ioannidou A., Papastefanou C., 2011. Radioiodine and radiocesium in Thessaloniki, Northern Greece due to Fukushima nuclear accident. *Journal of Environmental Radioactivity* 102, 796-797.

Marinoni A., Cristofanelli P., Calzolari F., Roccato F., Bonafé U., Bonasoni P., 2008, Continuous measurements of aerosol physical parameters at the Mt Cimone GAW Station (2165 m asl, Italy*). Science of the Total Environment* 391, 241-251.

Masson O., et al., 2011. Tracking of airborne radionuclides from the damaged Fukushima Dai-Ichi nuclear reactors by European Networks. *Environmental Science and Technology* 45, 7670-7677. doi:10.1021/es2017158. 28323, 28332.

Megumi K., Matsunami T., Ito N., Kiyoda S., Mizohata A., Asano T., 2000. Factors, especially sunspot number, causing variations in surface air concentrations and depositions of ^{7}Be in Osaka, Japan. *Geophysical Research Letters* 27(3), 361-364.

Monks P.S., 2000. A review of the observations and origins of the spring ozone maximum. *Atmospheric Environment* 34, 3545-3561.

Moreno T., Querol X., Castillo S., Alastuey A., Cuevas E., Herrmann L., Mounkaila M., Elvira J., Gibbons W., 2006. Geochemical variations in aeolian mineral particles from the Sahara-Sahel Dust corridor. *Chemosphere* 65(2), 261-270.

Mt. Cimone web site, http://www.isac.cnr/cimone/ Last accessed 01 august 2013.

Nolle M., Ellul R., Ventura F., Güsten H.A., 2005. Study of historical surface ozone measurements (1884-1900) on the island of Gozo in the central Mediterranean. *Atmospheric Environment* 39, 5608–5618.

Paatero J., Hatakka J., 2000. Source areas of airborne ^{7}Be and ^{210}Pb in Northern Finland. *Health Physics* 79(6), 691-696.

Pace G., Meloni D., di Sarra A., 2005. Forest fire aerosol over the Mediterranean basin during summer 2003. *Journal of Geophysical Research* 110, D21202. doi:10.1029/2005JD005986

Pállson S.E., Howard B.J., Bergan T.D., Paatero J., Isaksson M., Nielsen S.P., 2013. A simple model to estimate deposition based on a statistical reassessment of global fallout data. *Journal of Environmental Radioactivity* 121, 75-86.

Papastefanou C., Manolopoulou M., Charalambous S., 1988. Radiation measurements and radioecological aspects of fallout from the Chernobyl reactor accident. *Journal of Environmental Radioactivity* 7(1), 49-64.

Papastefanou C., Ioannidou A., 1995. Aerodynamic size association of ^{7}Be in ambient aerosols. *Journal of Environmental Radioactivity* 26, 273-282.

Papastefanou C., 2008. Radioactive aerosols. In: Radioactivity in the Environment, Volume 12 Chapter 2. Edited by Elsevier B.V. pp. 11-58. doi:10.1016/S1569-4860(07)12002-7

Pham M.K., Betti M., Nies H., Povinec P.P., 2011. Temporal changes of ^{7}Be, ^{137}Cs and ^{210}Pb activity concentrations in surface air at Monaco and their correlation with meteorological parameters. *Journal of Environmental Radioactivity* 102, 1045-1054.

Pittauerová D., Hettwig B., Fischer H.W., 2011. Fukushima fallout in Northwest German environmental media. *Journal of Environmental Radioactivity* 102, 877-880.

Pochanart P., Akimoto H., Maksyutov S., Staehelin J., 2001. Surface ozone at the Swiss Alpine site Arosa: the hemispheric background and the influence of largescale anthropogenic emissions. *Atmospheric Environment* 35, 5553–5566.

Prospero J.M., Schmitt R., Cuevas E., Savoie D.L., Graustein W.C., Turekian K.K., Volz-Thomas A., Diaz A., Oltmans S.J., Levy II H., 1995. Temporal variability of summer-time ozone and aerosols in the free troposphere over the eastern North Atlantic. *Geophysical Research Letters* 22, 2925-2928.

Rao S.T., Zurbenko I.G., Neagu R., Porter P.S., Ku J.Y., Henry R.F., .1997. Space and time scales in ambient ozone data. *Bulletin of the American Meteorological Society* 78, 2153-2166.

Rapetti F., Vittorini S., 1989. Aspetti del clima nei versanti tirrenico ed adriatico lungo l'allineamento Livorno-Monte Cimone-Modena. *Atti della Società Toscana di Scienze Naturali, Memorie,* Serie A 96, 159-192.

Rasch P.J., Tilmes S., Turco R.P., Robock A., Oman L., Chen C., et al., 2008. An overview of geoengineering of climate using stratospheric sulfate aerosols. *Philosophical Transactions of the Royal Society A-Mathematical Physical and Engineering Sciences* 366(1882), 4007-4037.

Rastogi N., Sarin M.M., 2008. Atmospheric ^{210}Pb and ^{7}Be in ambient aerosols over low- and high-altitude sites in 34 semiarid regions: Temporal variability and transport processes. *Journal of Geophysical Research*, 113, doi:10.1029/2007JD009298

Reiter R., Sladkovich K., Pötzl K., Carnuth W., Kanter H.J., 1971. Studies on the influx of stratospheric air into the lower troposphere using cosmic-ray produced radionuclides and fallout. Archiv für Meteorologie, Geophysik und Bioklimatologie, Serie A, Vol.20(3), 211-246.

Reiter E.R., 1975a. Weather phenomena of the Mediterranean basin. Part 1. General description of the meteorological processes. In: Handbook for forecasters in the Mediterranean basin. Environment Prediction Research Facility. Naval Postgraduate School, Monterey, California. U.S. Department of Commerce. Available at http://www.dtic.mil/cgi-bin/GetTRDoc?AD=ADA024271 Last accessed 01 August 2013.

Reiter E.R., 1975b. Stratospheric-Tropospheric Exchange Processes. *Review of Geophysics and Space Physics* 13(4), 459-474.

Reiter R., Munzert K., Kanter H.J., Potzl K., 1983. Cosmogenic radionuclides and ozone at a mountain station at 3.0 km a.s.1. Archiv fur Meteorologie, Geophysik und Bioclimatologie, Serie B 32, 131–160.

Ribas A., Peñuelas J., 2004. Temporal patterns of surface ozone levels in different habitats of the North Western Mediterranean basin. *Atmospheric Environment* 38, 985–992.

Şerban E., Santaguida R., Lauria L., 2007. The pluviometric surplus and deficit, as climatic risk phenomena at Monte Cimone weather station, Italy. *Seminarul Geografic "D. Cantemir*" 28, 33-42.

Steinmann P., Zeller M., Beuret M., Ferreri G., Estier S., 2013. Cosmogenic ^{7}Be and ^{22}Na in ground level air in Switzerland. *Journal of Environmental Radioactivity* 124, 68-73.

Stohl A., Spoichtinger-Rakowsky N., Bonasoni P., Feldmann H., Memmesheimer M., Scheel H.E., Trickl T., Hübener S., Ringer W., Mandl M., 2000. The influence of stratospheric intrusions on alpine ozone concentrations. *Atmospheric Environment* 34, 1323-1354.

Stohl A., Wernli H., James, P., Borqui M., Forster C., Liniger M.A., Seibert P., Sprenger M., 2003. A new perspective of stratosphere-troposphere exchange. *American Meteorological Society*, 1565-1573 doi:10.1175/BAMS-84-11-1565

Sykora I., Froehlich K., 2010. Radionuclides as tracers of atmospheric processes. In: Radioactivity in the Environment 16, Chapter 3: 51-88. Edited by Elsevier. doi:10.1016/S1569-4860(09)01603-9

Thakur P., Ballard S., Nelson R., 2013. An overview of Fukushima radionuclides measured in the northern Hemisphere. *Science of the Total Environment* 458-460, 577-613.

Tosi E., Smith R.B., Bradford M.L., 1987. Aerial Observations of Stratospheric Descent in a Gulf of Genoa Cyclone. *Meteorology and Atmospheric Physics* 36, 141-160.

Tositti L., Hübener S., Kanter H.J., Ringer W., Sandrini S., Tobler L., 2004. Intercomparison of sampling and measurement of ^{7}Be in air at four high-altitude locations in Europe. *Applied Radiation and Isotopes* 61, 1497-1502.

Tositti L., Brattich E., Cinelli G., Previti A., Mostacci D., 2012. Comparison of radioactivity data measured in PM10 aerosol samples at two elevated stations in northern Italy during the Fukushima event. *Journal of Environmental Radioactivity* 114, 105-112.

Tositti L., Riccio A., Sandrini S., Brattich E., Baldacci D., Parmeggiani S., Cristofanelli P., Bonasoni P., 2013. Short-term climatology of PM10 at a high altitude background station in southern Europe. *Atmospheric Environment* 65, 145-152

Tremblay J., Servranckx R., 1993. Beryllium-7 as a tracer of stratospheric ozone: A case study. *Journal of Radioanalytical and Nuclear Chemistry* 172(1), 49-56.

Trickl T., Feldmann H., Kanter H.-J., Scheel H.-E., Sprenger M., Stohl A. Wenli H., 2010. Forecasted deep stratospheric intrusions over central Europe: case studies and climatologies. *Atmospheric Chemistry and Physics* 10, 499-524.

Trigo I.F., Bigg G.R., Davies T.D., 2002. Climatology of Cyclogenesis Mechanisms in the Mediterranean. *Monthly Weather Review* 130, 549-569.

Turekian K.K., Benninger L.K., Dion E.P., 1983. ^{7}Be and ^{210}Pb total deposition fluxes at New Haven Connecticut and at Bermuda. *Journal of Geophysical Research* 88, 5411-5415.

Turekian K.K., Graustein W.C., 2003. Natural radionuclides in the atmosphere. In: The Atmosphere. Ed RF Keeling, Vol 4. Treatise on Geochemistry (Eds HD Holland and KK Turekian) Elsevier-Pergamon, Oxford: 261-279.

Usoskin I., Kovaltsov. G., 2008.Production of cosmogenic ^{7}Be isotope in the atmosphere: full 3D modelling. *Journal of Geophysical Research* 113, D12107.

Usoskin I.G., Field C.V., Schmidt G.A., Leppänen A-P, Aldahan A., Kovaltsov G.A., Possnert G., Ungar R.K., 2009. Short-term production and synoptic influences on atmospheric ^{7}Be concentrations. *Journal of Geophysical Research* 114, D06108. doi:10.1029/2008JD011333

Vakulovsky S.M., Nikitin A.I., Chumichev V.B., Katrich I.Y., Voitsekhovich O.A., Medinets V.I., Pisarev V.V., Bovkum L.A., Khersonsky E.S., 1994. Cesium-137 and strontium-90 contamination of water bodies on the areas affected by releases from the Chernobyl nuclear power plant accident: an overview. *Journal of Environmental Radioactivity* 23(2), 103-122.

Vingarzan R., 2004. A review of surface ozone background levels and trends. *Atmospheric Environment* 38, 3431–3442.

Wilks D., 2006. Statistical methods in the Atmospheric Sciences. International Geophysics Series. Second Edition Academic Press

Winkler R., Dietl F., Frank G., Thiersch J., 1998. Temporal variation of ^{7}Be and ^{210}Pb size distributions in ambient aerosols. *Atmospheric Environment* 32, 983-991.

WMO-GAW (World Meteorological Organization, - Global Atmosphere Watch) Report No. 155, 2004. 1st International Expert Meeting on Sources and Measurements of Natural Radionuclides Applied to Climate and Air Quality Studies, (Gif-sur-Yvette, France, 3-5 June 2003) (WMO TD No. 1201), [available at ftp://ftp.wmo.int/Documents/PublicWeb/arep/gaw/gaw155.pdf, last accessed 01 August 2013]

World Data Centre for Greenhouse Gases (WDCGG), http://ds.data.jma.go.jp/gmd/wdcgg/ Last accessed 01 August 2013.

Zanis P., Gerasopoulos E., Priller A., Schnabel C., Stohl A., Zerefos C., Gäggeler H.W., Tobler L., Kubik P.W., Kanter H.J., Kanter H.J., Scheel H.E., Luterbacher J., Berger M., 2003. An estimate of the impact of stratosphere-to-troposphere transport (STT) on the lower free tropospheric ozone over the Alps using ^{10}Be and ^{7}Be measurements. *Journal of Geophysical Research* 108(D12), 8520. doi:10.1029/2002JD002604

Zheng X., Wang G., Tang J., Zhang X., Yang W., Lee H.N., Wang C., 2005. ^{7}Be and ^{210}Pb radioactivity and implications on sources of surface ozone at Mt. Waliguan. *Chinese Science Bulletin* 50(2), 167-171.

Zheng X.D., Wan G., Tang J., 2011. Source characteristics of O_3 and CO_2 at Mt. Waliguan Observatory, Tibetan Plateau implied by using ^{7}Be and ^{210}Pb. *Science China Earth Sciences* 54(4), 550-560.

Zurbenko I.G., 1986. The Spectral Analysis of Time Series. North-Holland, Amsterdam.

CHAPTER 4 – Processes Controlling the Seasonal Variations of ^{210}Pb and ^{7}Be at Mt. Cimone: A Model Analysis

4.1. Introduction[1]

The use of atmospheric radionuclides to understand atmospheric dynamics, pollutant dispersion and pollutant removal processes has a long history punctuated by the number of relevant scientific publications (e.g., Junge, 1963; Reiter *et al.*, 1971; Gaggeler, 1995; Arimoto *et al*., 1999; Turekian and Graustein, 2003; WMO-GAW, 2004; Dibb, 2007; Papastefanou, 2008; Rastogi and Sarin, 2008; Froehlich and Masarik, 2010; Sykora and Froehlich, 2010; Lozano *et al*., 2011; Lozano *et al*., 2012). In the beginning, radionuclides in the atmosphere were monitored to understand the effects of atmospheric nuclear bomb fallout, which occurred mostly from tests in the 1960s. Natural radionuclides were measured simultaneously with anthropogenic radionuclides in fallout (Junge, 1963). Atmospheric chemistry, air pollution and climate-related issues became prominent after the 1970s. During the past three decades, the largely separate communities conducting observations and modeling of natural radionuclides and chemical constituents began to merge, and the value of natural radionuclide tracers in atmospheric chemistry research and assessment has been recognized (WMO-GAW, 2004).

As routine measurements of naturally occurring radionuclides in a global monitoring network for atmospheric composition support global climate change and air quality research, natural radionuclides are measured at many of the regional, global and contributing-partner stations in the Global Atmosphere Watch (GAW) network of the World Meteorological Organization (WMO) (WMO-GAW, 2004). In particular, ^{210}Pb and ^{7}Be natural radionuclides are helpful in the understanding of the roles of transport and scavenging in controlling the behaviors of radiatively active trace gases and aerosols (Balkanski *et al.*, 1993; Koch *et al.*, 1996), as well as their anthropogenic (vs. natural) origin (e.g., Graustein and Turekian, 1996; Arimoto *et al*., 1999; Liu *et al.*, 2004; Cuevas *et al.*, 2013). It is therefore recommended that they are routinely monitored at WMO-GAW stations around the world (Lee *et al.*, 2004). Although ^{210}Pb and ^{7}Be have long (1998-

[1] This chapter consists of a manuscript in preparation by Brattich E. (Dept. of Biological, Geological and Environmental Sciences-Section of Geology, Università di Bologna), Hongyu Liu (National Institute of Aerospace, Hampton, Virginia, USA), Tositti L. (Dept. of Chemistry, Università di Bologna).

2011) been measured at the Global WMO-GAW station of Mt. Cimone (Italy), their seasonal behaviour has not been thoroughly elucidated (Lee *et al.*, 2007; Tositti *et al.*, 2014, presented in Chapter 3). Here we apply a state-of-the-art global chemistry and transport model (CTM) to the simulation of ^{210}Pb and ^{7}Be, with an objective to better understand the roles of transport and precipitation scavenging processes in controlling their seasonal variations at Mt. Cimone.

Because of their contrasting natural origins, ^{210}Pb and ^{7}Be have been used as a pair to study the vertical transport and scavenging of aerosols (Koch *et al.*, 1996). ^{210}Pb (half-life $\tau_{1/2}$ = 22.3 years) is the decay daughter of ^{222}Rn ($\tau_{1/2}$ = 3.8 days), emitted from soils by decay of ^{226}Ra (Turekian *et al.*, 1977). The oceanic input of ^{222}Rn is about two orders of magnitude less than the continental input and, because of the continental origin of ^{222}Rn, ^{210}Pb is considered as a tracer of air masses with continental origin (Baskaran, 2011). ^{7}Be ($\tau_{1/2}$ = 53.3 days) is a cosmogenic radionuclide generated by cosmic ray spallation reactions with nitrogen and oxygen (Lal *et al.*, 1958). Most (~67%) of ^{7}Be is produced in the stratosphere and the remaining (~33%) is generated in the troposphere, particularly in the upper troposphere (Johnson and Viezee, 1981; Usoskin and Kovaltsov, 2008). ^{7}Be is thus considered a tracer of stratospheric influence (Viezee and Singh, 1980; Dibb *et al.*, 1992, 1994; Liu *et al.*, 2004) and subsidence (Feely *et al.*, 1989; Koch *et al.*, 1996; Liu *et al.*, 2004). Once produced, both radionuclides rapidly attach onto aerosol particles in the fine fraction (Papastefanou and Ioannidou, 1995; Winkler *et al.*, 1998; Gaffney *et al.*, 2004; Ioannidou *et al.*, 2005), and are removed from the atmosphere mainly by wet and secondarily dry deposition (Kulan *et al.*, 2006). The concentrations of these radionuclides in surface air thus depend on their sources, wet and dry removal, radioactive decay (in the case of ^{7}Be), and transport (Beer *et al.*, 2012).

In the past, several observational studies of factors influencing surface ^{210}Pb and ^{7}Be concentrations in Europe, Middle East and North Africa have been made. With compiled data of ^{7}Be in ground level air over Europe, Kulan *et al.* (2006) showed that higher concentrations are present at middle latitudes (20-50°N) because of the mixing of stratospheric air into the upper troposphere along the tropopause discontinuity in midlatitude regions and subsequent convective mixing within the troposphere, which brings ^{7}Be-rich air masses into the planetary boundary layer and to the earth's surface. Lower ^{7}Be concentrations are towards the pole and presumably, as interpolated in the work of Steinmann *et al.* (2013) who complemented that of Kulan *et al.* (2006) with some more recent literature data from Europe and some low latitude sites, towards the equator. Lozano *et al.* (2012) examined the meteorological factors influencing the ^{210}Pb and ^{7}Be concentrations in surface air in the south-western Iberian Peninsula (El Arenosillo) and concluded that different synoptic patterns are associated with the ranges of ^{210}Pb and ^{7}Be activity concentrations. The low values of ^{210}Pb are strongly linked to air masses from the Atlantic Ocean,

whereas the highest values are associated with air masses clearly under the influence of continents, such as the Iberian Peninsula and North of Africa. As for ^{7}Be, they determined that the highest ^{7}Be activity concentrations over south-western Iberian Peninsula are related with the arrival of air masses from middle latitudes, and in particular from the Canary Islands, western Mediterranean Basin and the north of Africa, an observation in agreement with Dueñas *et al.* (2011). North and Atlantic advection patterns are instead associated with low ^{7}Be concentrations. High ^{7}Be concentrations in the Canary Islands were observed by Hernández *et al.* (2008) and were attributed to downward transport from the stratosphere. The amount of precipitation associated with each range of activity concentrations generally indicates larger influence on ^{210}Pb than on ^{7}Be concentrations (Koch *et al.*, 1996; Caillet *et al.*, 2001; Likuku, 2006; Dueñas *et al.*, 2009; Lozano *et al.*, 2012).

There are a number of studies that examined the seasonal behavior of ^{210}Pb and ^{7}Be at European mid-latitude surface sites (e.g., Cannizzaro *et al.*, 2004; Ioannidou *et al.*, 2005; Daish *et al.*, 2005; Todorovic *et al.*, 2005; Likuku, 2006; Dueñas *et al.*, 2009; Pham *et al.*, 2011; Carvalho *et al.*, 2013; Steinmann *et al.*, 2013). Higher monthly mean ^{210}Pb concentrations during autumn (October-November) and lower concentrations during spring (March-April) were observed in Thessaloniki (Ioannidou *et al.*, 2005). The higher values of ^{210}Pb during autumn were attributed to the frequent inversion conditions of the surface layers, resulting in a build-up of radon and its decay products in ground-level air, while the minimal values during spring were linked to higher washout due to the larger amount of precipitation during this period at that site (Ioannidou *et al.*, 2005). Generally speaking, high levels of ^{210}Pb during summer and low levels in winter reflect the differing rates of ^{222}Rn emanation from soil above the European land mass during winter (wet or snow covered soil) and summer (dry soil) (Hötzl and Winkler, 1987; Caillet *et al.*, 2001; Ioannidou *et al.*, 2005; Daish *et al.*, 2005). The spring ^{210}Pb maximum observed, for example, in England by Likuku (2006) and Daish *et al.* (2005) was not completely explained, but possible explanations were suggested: 1) a "pulse" of radon was held back by winter conditions, followed by release during thawing of the snow-cap; 2) it could arise from anthropogenic sources such as the use of fertilisers during spring soil conditioning; and 3) the folding of the tropopause in spring could bring a high-altitude ^{210}Pb component in precipitation, as shown in Tokieda *et al.* (1996), where its contribution is about 12% in spring compared to about 2% in winter. However, this last factor could explain only an increase of ^{210}Pb wet-deposition fluxes, whereas precipitation needs to be evaporated to increase ^{210}Pb airborne concentration because of this high-altitude component. Daish *et al.* (2005) did not explain whether or not this is the case.

At European mid-latitude surface sites, monthly ^{7}Be averages are characterized by a well-defined annual cycle with lower values during winter and higher values during summer. Generally, the increase of ^{7}Be in ground level air from March to May is ascribed to the more efficient stratosphere-to-troposphere exchange (STE) and higher frequency of tropopause folding, whereas the further increase of ^{7}Be during summer is due to the stronger convective mixing and higher tropopause. Convection brings the ^{7}Be in the upper troposphere (rather than direct input of stratospheric air) down to the lower troposphere and ground level (Gerasopoulos *et al.*, 2001; Ioannidou *et al.*, 2005; Likuku *et al.*, 2006; Steinmann *et al.*, 2013; Ioannidou *et al.*, 2014).

High-elevation sites such as Jungfraujoch (Switzerland), Zugspitze (Germany), Mt. Cimone (Italy), lying typically above the planetary boundary layer (PBL), are characterized by higher ^{7}Be due to direct influences of air masses from the free troposphere and lower ^{210}Pb concentrations (Zanis *et al.*, 2000). Reiter *et al.* (1983) analyzed 12 years of ^{7}Be data for Zugspitze (2962 m asl, Germany) and found that the seasonality of this radionuclide is characterized by higher values in summer due to convection-forced exchange with the upper troposphere, and reduced values from April to June, due to the precipitation pattern at that site. Gerasopoulos *et al.* (2001) analyzed the ^{7}Be data obtained from 1996 to 1998 at four high-altitude stations (Jungfraujoch-Switzerland, Zugspitze-Germany, Sonnblick-Austria, and Mt. Cimone-Italy). They found that the monthly means showed an annual cycle with a late-summer maximum at all stations, which was attributed to the higher tropopause that lead to more efficient vertical transport from the upper troposphere to the lower troposphere. It is generally observed that at high-altitude sites a secondary maximum of ^{7}Be during cold months (December-March) is due to an increase in stratosphere-to-troposphere events during this season (e.g., James *et al.*, 2003; Stohl *et al.*, 2003; Trickl *et al.*, 2010). The higher frequency of rapid subsidence in winter at Northern Hemisphere mid-latitudes can be ascribed to the intensity of baroclinic systems, which is greatest in wintertime. In fact, well-developed tropopause folds and rapid deep intrusions are most likely to occur in the wake of intense cyclogenesis, usually limited to the wintertime storm track regions (James *et al.*, 2003).

^{210}Pb and ^{7}Be data from October 2004 to July 2008 at Puy de Dome (1465 m asl, France) and Opme (660 m asl, France) were analyzed by Bourcier *et al.* (2011). They observed similar ^{210}Pb concentrations at the two sites, indicating that the vertical transport is efficient enough to consider the atmosphere well mixed on the scale of ^{210}Pb lifetime, consistent with the study of Abe *et al.* (2010). It also indicates that short-term observations of varying airborne profiles do not represent long-term observations of ^{210}Pb in the atmosphere. The seasonal ^{210}Pb pattern was characterized by maximum concentrations in the spring and autumn and minimum concentrations in winter, due to higher radon emissions during the dry season than during the wet seasons, and lower PBL height

during winter (weaker vertical transport means a decrease of ^{210}Pb concentrations at high-altitude sites). ^{7}Be concentrations at the two sites were instead characterized by a maximum in summer and a minimum in winter, at both altitudes: this seasonal behaviour was ascribed to stronger vertical mixing during summer compared to winter, with an increased feeding of the PBL from the upper troposphere.

Studies using 1-D models to determine the levels of surface ^{7}Be showed higher concentrations at high-altitude sites (Jasiulionis and Wershofen, 2005; Simon *et al.*, 2009) but also suggested that the diffusion of ^{7}Be was affected by the seasonal variation of meteorological conditions. In a global 3-D transport model study, Rehfeld and Heimann (1995) compared the simulated seasonal pattern of surface ^{210}Pb and ^{7}Be concentrations with the observations at several sites in both hemispheres. They found that at Mauna Loa (19.47N, 155.6W, 3400 m asl, Hawaii) ^{210}Pb seasonality was characterized by high concentrations in spring and summer and lower ones in winter, as opposed to the seasonal pattern found at higher latitudes. They attributed this behaviour to the elevation of the site, representative of conditions of the middle troposphere rather than those in the PBL. As for ^{7}Be, the comparison between the model and the observations at Rexburg (43.8N, 111.83W, USA) showed systematically lower modelled values, due to the much higher precipitation rate used in the model. The seasonality of ^{7}Be was characterized by a summer maximum, caused by higher convective activity by which much more ^{7}Be aerosols are transported downward out of their source region (Feely *et al.*, 1988) and a winter minimum. Balkanski *et al.* (1993) examined the transport of ^{210}Pb in a global 3-D model and reported a weak decrease of ^{210}Pb concentrations between the continental mixed layer and the free troposphere: simulated concentrations at 6-km altitude were about 50% of continental mixed-layer over much of the Northern Hemisphere in summer, and over large areas of the tropics year around, a result consistent with the few observations available for the free troposphere (Moore *et al.*, 1973).

The measurements of ^{7}Be at Mt. Cimone have already been the objective of previous studies, mainly concerning its use in the study of the role of STE in surface ozone increases (Bonasoni *et al.*, 1999, 2000a, b; Cristofanelli *et al.*, 2003, 2006; Lee *et al.*, 2007; Cristofanelli *et al.*, 2009a), and in the framework of EU project such as VOTALP (Vertical Ozone Transport in the Alps) and STACCATO (influence of Stratosphere-Troposphere exchange in A Changing Climate on Atmospheric Transport and Oxidation capacity). Previous studies led to the assessment of a higher incidence of STE events during the period from October to February relative to the warm season, when thermal convection and the rising of the tropopause promote vertical mixing, which acts as a confounding factor in STE detection. Lee *et al.* (2007) studied the seasonal patterns and frequency

distributions of ^{210}Pb and ^{7}Be measured at the station and highlighted higher concentrations of both radionuclides in the summertime, due to the higher mixing height and horizontal transport by regional airflows; the latter also led to increases in O_3. During winter, a general increase in ^{7}Be is associated with a decrease in ^{210}Pb, due to the dominating effect of STE and subsidence in the free troposphere. At the time of this work, no modelling study of the radionuclides has been conducted for the site.

In this Chapter, we conduct simulations of ^{210}Pb and ^{7}Be at Mt. Cimone with a state-of- the-art global 3-D chemistry and transport model (GMI CTM) driven by assimilated meteorological fields for the year of 2005. Our objectives are a better elucidation of the seasonal variations of ^{210}Pb and ^{7}Be concentrations and an improved understanding of the roles of transport and precipitation scavenging processes in their seasonalities at Mt. Cimone.

The remainder of this Chapter is organized as follows. Section 4.2 describes the measurement site, the radioactivity measurements at Mt. Cimone, and the GMI CTM. Section 4.3 evaluates the model performance in reproducing the observed wind and precipitation fields. Section 4.4 evaluates the seasonal ^{210}Pb and ^{7}Be concentrations in the model with those observed. Section 4.5 examines the sources and seasonal variations in the simulated radionuclide activities, followed by summary and conclusions in section 4.6.

4.2 Data and methods

4.2.1 Radionuclide measurements at Mt. Cimone

Mt. Cimone station (44°12’ N, 10°42’ E, 2165 m asl) is a global WMO-GAW station managed by the Meteorological Office of the Italian Air Force, which hosts the research platform “Ottavio Vittori” of the Institute of Atmospheric and Climate Science of the National Council of Research (ISAC-CNR). The station is located on top of the highest peak of the Italian northern Apennines, with a 360° free horizon and an elevation such that the station lies above the PBL during most of the year: the Mt. Cimone measurements are considered representative for the southern Europe/Mediterranean free troposphere (Bonasoni *et al.*, 2000a; Fischer *et al.*, 2003; Cristofanelli *et al.*, 2007), even though during the warmer months an influence of PBL can be detected both due to convective processes and mountain/valley breeze regimes (Fischer *et al.*, 2003; van Dingenen *et al.*, 2005; Tositti *et al.*, 2013; see also Chapters 2 and 3). Note in this framework that southern Europe and Mediterranean basin are considered as a hot-spot region in terms of both climate change (e.g., Forster *et al.*, 2007) and air quality (Monks *et al.*, 2009), as well as a major crossroad of different air mass transport processes

(see previous Chapter 2 and following Chapters 5 and 6; Li *et al.*, 2001; Lelieveld *et al.*, 2002; Millàn *et al.*, 2006; Duncan *et al.*, 2008; Tositti *et al.*, 2013).

At Mt. Cimone station, ^{210}Pb, ^{7}Be, and aerosol mass load in the form of PM_{10} have been regularly measured since 1998 with a Thermo-Environmental PM_{10} high volume sampler. Details of the sampling of PM_{10} and ^{210}Pb and ^{7}Be have been given in previous Chapters 2 and 3.

For our analysis, we used monthly averages of ^{210}Pb and ^{7}Be data at Mt. Cimone in 2005.

4.2.2 GMI Model

The GMI (Global Modeling Initiative, http://gmi.gsfc.nasa.gov) is a NASA-funded project aiming at improving assessments of anthropogenic perturbations to the Earth system; in this framework a CTM appropriate for stratospheric assessments was developed (Rotman *et al.*, 2001). It was firstly used to evaluate the potential effects of stratospheric aircraft on the global stratosphere (Kinnison *et al.*, 2001) and on the Antarctic lower stratosphere (Considine *et al.*, 2000). The recent version of the GMI CTM includes a nearly full treatment of both stratospheric and tropospheric photochemical and physical processes and is also capable of simulating atmospheric radionuclides ^{222}Rn, ^{210}Pb, ^{7}Be, and ^{10}Be throughout the troposphere and stratosphere (Considine *et al.*, 2004; Rodriguez *et al.*, 2004; Considine *et al.*, 2005; Liu *et al.*, 2013). Details of the model are described in Duncan *et al.* (2007, 2008), Strahan *et al.* (2007) and Considine *et al.* (2008).

In this work a version of the GMI model with the same basic structure as described by Considine *et al.* (2005) and Liu *et al.* (2013) was used, including parameterizations of the important tropospheric physical processes such as convection, wet scavenging, dry deposition and planetary boundary layer mixing were also included. Meteorological data used to drive the CTM, e.g., horizontal winds, convective mass fluxes and precipitation fields, are taken from the output of the assimilated data set MERRA (Modern ERA Retrospective Analysis for research and applications) from the NASA Global Modeling and Assimilation Office (GMAO). MERRA is a reanalysis for the satellite era using a major new version of the Goddard Earth Observing System Data Assimilation System Version 5 (GEOS-5.2.0).

The flux-form semi-Lagrangian advection scheme and a convective transport algorithm from the CONVTRAN routine in NCAR CCM3 physics package are used in the model. The wet deposition scheme is the same of Liu *et al.* (2001): it includes scavenging in wet convective updrafts, and first-order rainout and washout from both convective anvils and large-scale precipitations. The gravitational settling effect of cloud ice particles included in Liu *et al.* (2001) is not considered

here. Dry deposition of aerosols is computed using the resistance-in-series approach. For the simulations of radionuclides, each simulation was run for six years, recycling the meteorological data for each year of the simulation; the sixth year output was used for analysis.

A uniform ^{222}Rn emission of 1.0 atom cm^{-2} s^{-1} from land under nonfreezing conditions is assumed (Liu *et al.*, 2001). Following Jacob and Prather (1990), the flux is reduced by a factor of 3 under freezing conditions. The flux from oceans and ice is null. Although a large variability of ^{222}Rn emission from land is observed, the above emission estimate is thought to be accurate to within 25% globally (Turekian *et al.*, 1977) and to within a factor of 2 regionally (Wilkening *et al.*, 1975; Schery *et al.*, 1989; Graustein and Turekian, 1990; Nazaroff, 1992; Liu *et al.*, 2001).

Following Brost *et al.* (1991) and Koch *et al.* (1996), the Lal and Peters (1967) ^{7}Be source for 1958 (solar maximum year) is used, as it best simulated stratospheric ^{7}Be concentrations measured from aircraft (Liu *et al.*, 2001). Stratospheric ^{7}Be concentrations are determined by a balance between production and radioactive decay. For this reason, the stratospheric ^{7}Be observations are used as a constraint on the ^{7}Be source. The ^{7}Be production rate is inversely correlated with solar activity (e.g., Lal and Peters, 1967; Koch and Mann, 1996). At high solar activity, the deflection of cosmic rays away from the solar system lowers the ^{7}Be production rate. No interannual variability in the ^{7}Be source is considered in the model (Liu *et al.*, 2001). This may lead to an underestimate of tropospheric ^{7}Be concentrations, especially at high latitudes during a solar minimum (or near minimum) year. Lal and Peters (1967) reported that the relative amplitude of the ^{7}Be production rate over an 11-year solar cycle is about 13% below 300 hPa at latitudes above 45 degree.

Because of the coarse resolution of the model (2° latitude by 2.5° longitude), the model representation of the topography at the site is poor. The elevation of Mt. Cimone in the model is only 298 m, whereas in reality the mountain is 2165 m (asl) high (Figure 4.1). For this reason, the model output was not sampled at ground level, but at the gridbox corresponding to the elevation of the site. In order to see the sensitivity of model-observation comparisons to spatial sampling, the model was sampled not only at the grid ("ij") corresponding to the latitude and longitude of Mt. Cimone, but also for the 8 adjacent grids ("ip1jm1", "ijm1", "im1jm1", "ip1j", "im1j", "ip1jp1", "ijp1", "im1jp1", where "p" stands for "plus" and "m" stands for "minus"). To better understand the sources and seasonality of radiotracers in the model, we examine model output not only for ^{210}Pb ^{7}Be, and their ratio ^{7}Be/^{210}Pb (an indicator of vertical transport, Koch *et al.*, 1996), which can be directly compared to the measurements taken at Mt. Cimone, but also for other radiotracers and quantities, e.g., ^{222}Rn, ^{10}Be, stratospheric ^{210}Pb, stratospheric ^{7}Be, stratospheric ^{10}Be, stratospheric ^{7}Be/total ^{7}Be (i.e., fraction of ^{7}Be coming from the stratosphere), and ^{10}Be/^{7}Be (a STE tracer, Zanis *et al.*, 2003).

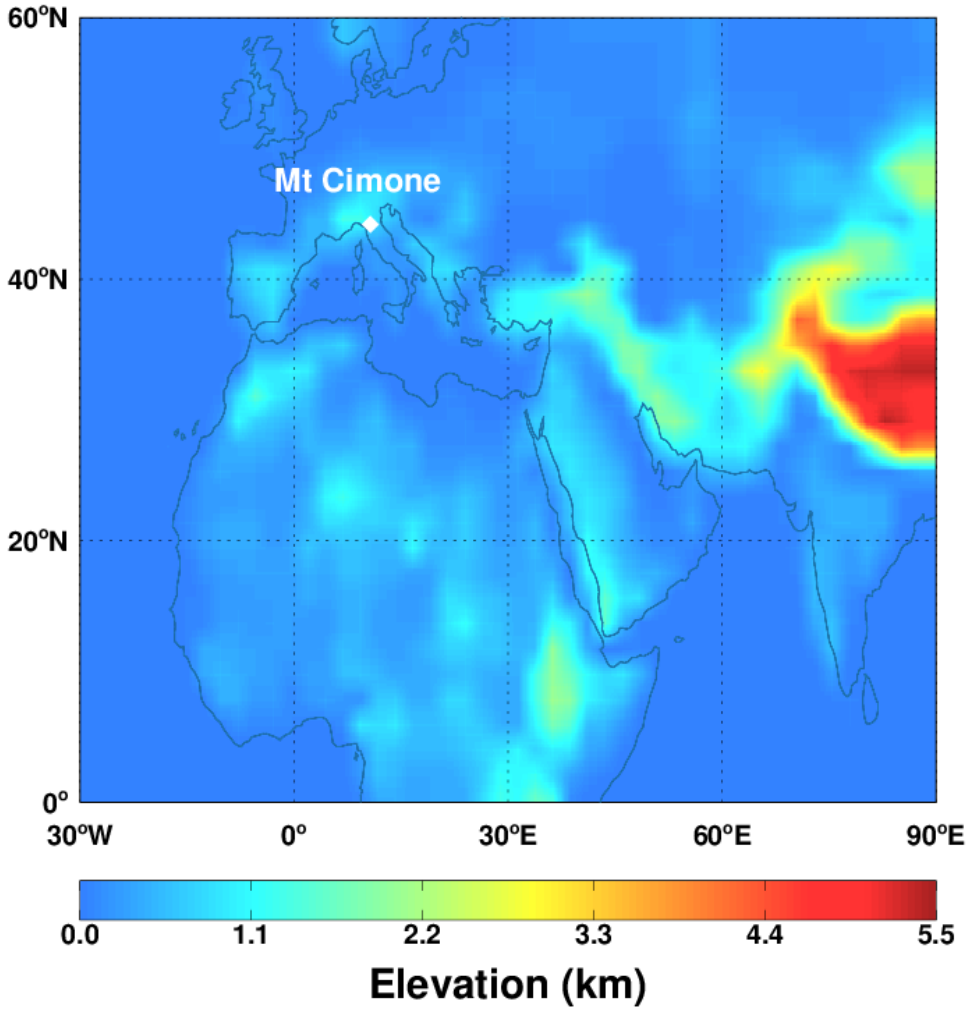

Figure 4.1 *Surface elevations (km) in the GMI model.*

Year 2005 was chosen for analysis because of the availability of observational data and model output at the start of this collaborative work. Monthly averages of ^{210}Pb and ^{7}Be data at Mt. Cimone were calculated for comparison with model results. To compare the seasonalities of ^{210}Pb and ^{7}Be between the model and the observations, the annual mean concentration was subtracted from the monthly mean concentrations and then divided by the annual mean (i.e., monthly percentage deviations from the annual mean concentration were calculated).

4.3 Seasonal variations of transport and precipitation at Mt. Cimone: observations vs. model simulations

Seasonal transport in the model was studied and reported in Figure 4.2(a,b). In the model Mt. Cimone appears to be in a location where there is a large horizontal gradient of wind (transport). The seasonal wind can be briefly summarized as follows:

- Fast N-NW: January and December
- Slower (but not slow) N-NW: March and August
- N: February
- Slow W: April, May and July
- Slow W-NW: June
- Very slow/calm: September
- Slow S-SW: October
- Slow W-SW: November

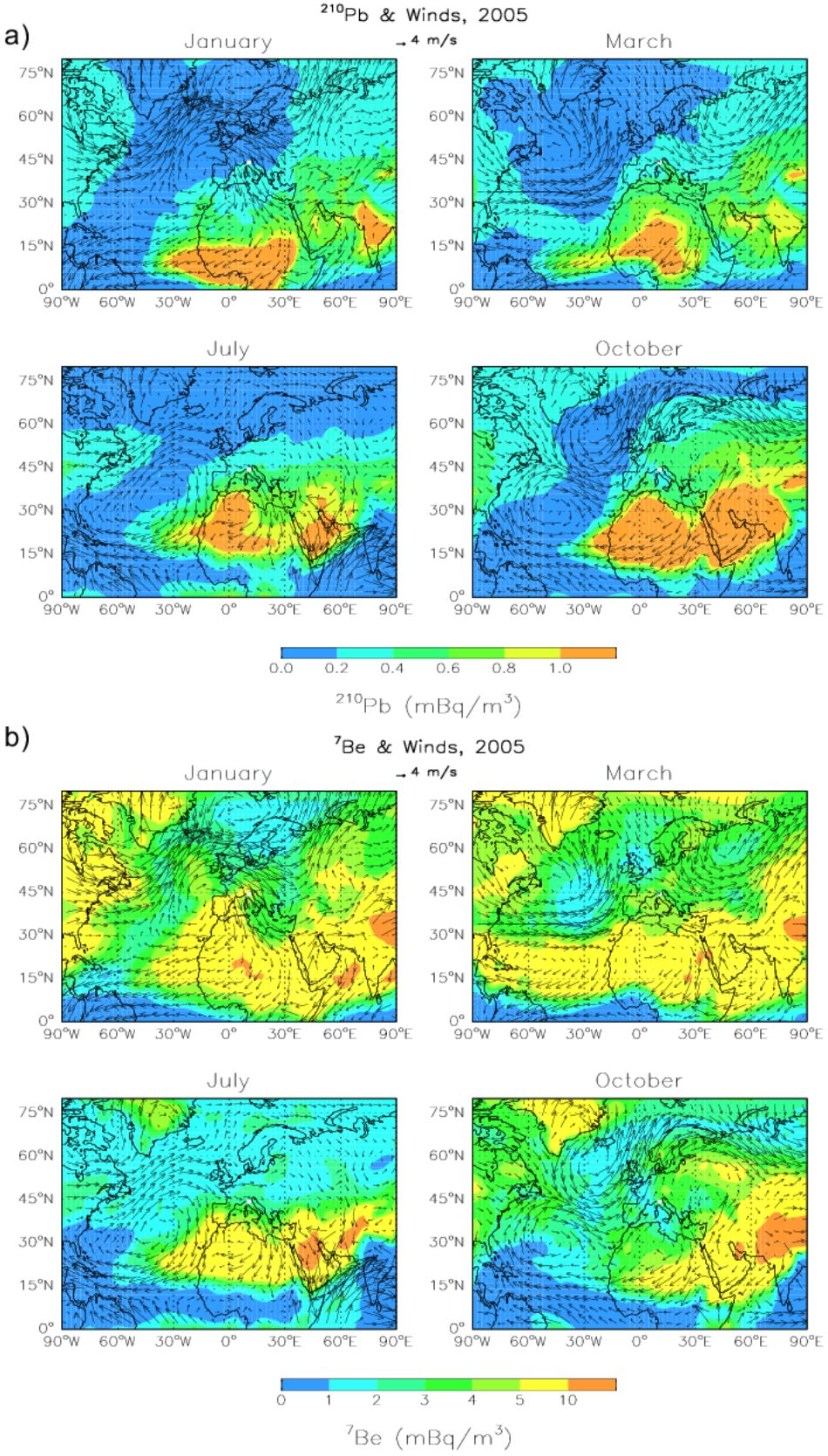

Figure 4.2(a,b) *Seasonality of winds in the MERRA meteorological data, at the elevation of Mt. Cimone. Color images show the GMI simulated monthly mean ^{210}Pb (a) and ^{7}Be (b) concentrations. The white dot indicates the location of Mt. Cimone (44°12' N, 10°42' E, 2165 m asl).*

The most frequent situations in the circulation patterns in the Emilia-Romagna region are characterized by the fluxes from NE (Karst plateau) or fast currents from SW (Giuliacci, 1988). In the first case (NE) the presence of an anticyclone on the eastern Europe or of a depression centered on the southern Italy or on the central Adriatic Sea can allows air masses originating in the Karstic and Dinaric Alps to enter in the Po Valley. The second case (SW) is most frequent and characterized by jets from SW associated with a depression on the Ligurian Sea or on the northern Tyrrhenian Sea. Moreover, in cases of slow general circulation (typical, for example, of the warm period), because of the presence of the Alpine barrier, atmospheric layers of the Po Valley are mainly influenced by circulations due to thermal differences with different baric situations during the day and during the night (Giuliacci, 1988). Synoptic scale breezes are then formed, and do not directly affect Mt. Cimone. They are able to influence the characteristics of the wind, which are then described by a NE direction during the day and a SW direction during night on the northern Apennines.

Mt. Cimone is the windiest meteorological station in Italy and the prevailing winds blow from S-SW and N-NE directions (Ciattaglia *et al.*, 1987; Colombo *et al.*, 2000). The analyses of wind observations at Mt. Cimone during the period of 1998-2011 agree with previous studies from Italian Air Force (Ciattaglia, 1983; Ciattaglia *et al.*, 1987; Colombo *et al.*, 2000) analysing the climatology of local wind intensity and direction during the period of 1946-1999. N-NE directions are more significant during the cold period, when an equivalent decrease of fluxes from SW is recorded. This situation is strictly linked to the different synoptic situation of the cold season, which is characterized by the influence of the intense anticyclone on eastern Europe. The presence of this anticyclone can favour the development of low-pressure systems over central Europe, to the north-east of Italy, generating cold streams from this quadrant. Ciattaglia (1983) indicated that NE winds are a consequence of the N-S component shifted by the Alps mountain chains. While winds blowing from the S-SW sector generate a sea air inflow, a continental air inflow is observed when winds come from the N-NE sector (Ciattaglia *et al.*, 1987).

Wind roses during the different seasons of 2005 partially follow the general description of winds at Mt. Cimone. Prevailing winds during the winter season are fast NNE-NE, but also slower W-SW, while on the contrary summer winds are described by slow WSW-W. The transition seasons show as expected an intermediate character, with prevailing W-SW winds during spring and fast NNE but also slower W-S (and all directions falling in between) during autumn.

The difference between local wind roses and model winds (Figure 4.2) might reflect the fact that, even though the mountaintop is very elevated and completely free of orographic obstacles, the wind observations are more or less localized especially compared to those in a coarse-resolution model (2° X 2.5°). In particular, the NE direction, which is commonly observed during winter and autumn

at Mt. Cimone, is missing from the assimilated winds. More important for this kind of comparison is the difference in the N-S direction between model-observations, which arises in particular during summer and, to a lesser extent, during transition seasons.

The model is able to capture relevant features of pressure systems and seasonal circulation patterns of the North Atlantic/Mediterranean/African region. The semi-permanent high pressure system located in the North Atlantic with different positions during different seasons is the Bermuda/Azores high. The Siberian High, a semi-permanent system of high pressure centred in northeastern Siberia during the colder half of the year, originating from the intense cooling of the surface layers of air over the continent, is well discernible in the simulated winds in the January-April plots. The ITCZ is also well discernible in the summer/autumn season. The Siberian High is discernible in the simulated winds, too. In northern Europe there are approximately two main states for the atmosphere, the westerly or zonal flows modulated by the advection of Atlantic lows, and the long-lived blocking anticyclonic configurations over North Sea or Scandinavia (easterly) (Burlando *et al.*, 2008). According to Huschke's nomenclature (1959), in the Mediterranean and surrounding regions there are more than 50 wind systems (Burlando, 2009). Most of them are local-scale wind systems (Burlando, 2009); they are thus not captured by a global meteorological model such as MERRA. Etesian winds, prevailing north-easterly in the northern Aegean, northerly in the central and southern Aegean (Kotroni *et al.*, 2001) during summer, originating as part of the Asian monsoon system, from the high pressure over the Balkans and the development of a thermal low over the Anatolian plateau, are observed in simulated winds in the eastern Mediterranean. Also the Mistral, a strong north/north-westerly wind system blowing in winter from southern France into the Gulf of Lyon (Huschke, 1959; Reiter, 1975; Jiang *et al.*, 2003), is resolved by the model. Also simulated are the westerly winds commonly observed in the western Mediterranean as a result of a deep low pressure to the north over the British Isles, or depressions moving eastward across the Iberian Peninsula, whereas in the eastern Mediterranean the recurrent pattern besides the Etesian wind is a north-westerly flow, due to a low pressure extending over the Middle East and the African continent and a higher pressure system over the Balkans and the Aegean sea (Burlando, 2009). North-African lows and Sahara depressions (also referred to as Atlas lee depressions) and the resulting S-SW wind in advance (Sirocco) (Reiter, 1975), appear to be an important feature missing/underrepresented in the model, where they appear only during October/November.

Trigo *et al.* (2002) reported an updated climatology of the cyclogenesis activity in the Mediterranean on a seasonal basis. They showed that the cyclogenetic mechanisms for winter and for summer/spring are different: while in winter cyclogenesis mainly occur in the northern Mediterranean coast, in summer

cyclogenesis occur over land. In winter they identified three main cyclogenetic regions corresponding to the Gulf of Genoa, the Aegean Sea, and the Black Sea, and they concluded that the cyclones developing in these regions are essentially sub-synoptic lows (thus not resolved by a global model), triggered by the major North-Atlantic synoptic systems affected by the local topography of the northern Mediterranean coast (Trigo *et al.*, 2002). In summer, the main cyclogenetic regions are located in the Iberian Peninsula, North Africa and Middle East because of thermal effects, and in Sahara also being affected by orography (Atlas Mountains) and by the increase in low-level thermal gradients (Campins *et al.*, 2006). Those features seem to be partly captured by the model.

Important to the model performance in reproducing the observed seasonal behavior of ^{210}Pb and ^{7}Be is the accuracy of precipitation fields used in the model. We compare here the MERRA precipitation with those from the GPCP (Global Precipitation Climatology Project, http://www.gewex.org/gpcp.html) satellite and surface observations in 2005.

We compared each month's precipitation on the global scale and the comparison was then restricted to the region defined by 0-75°N and 90° W – 90°E (Figure 4.3). A good agreement between GPCP and MERRA precipitations was found for both comparisons.

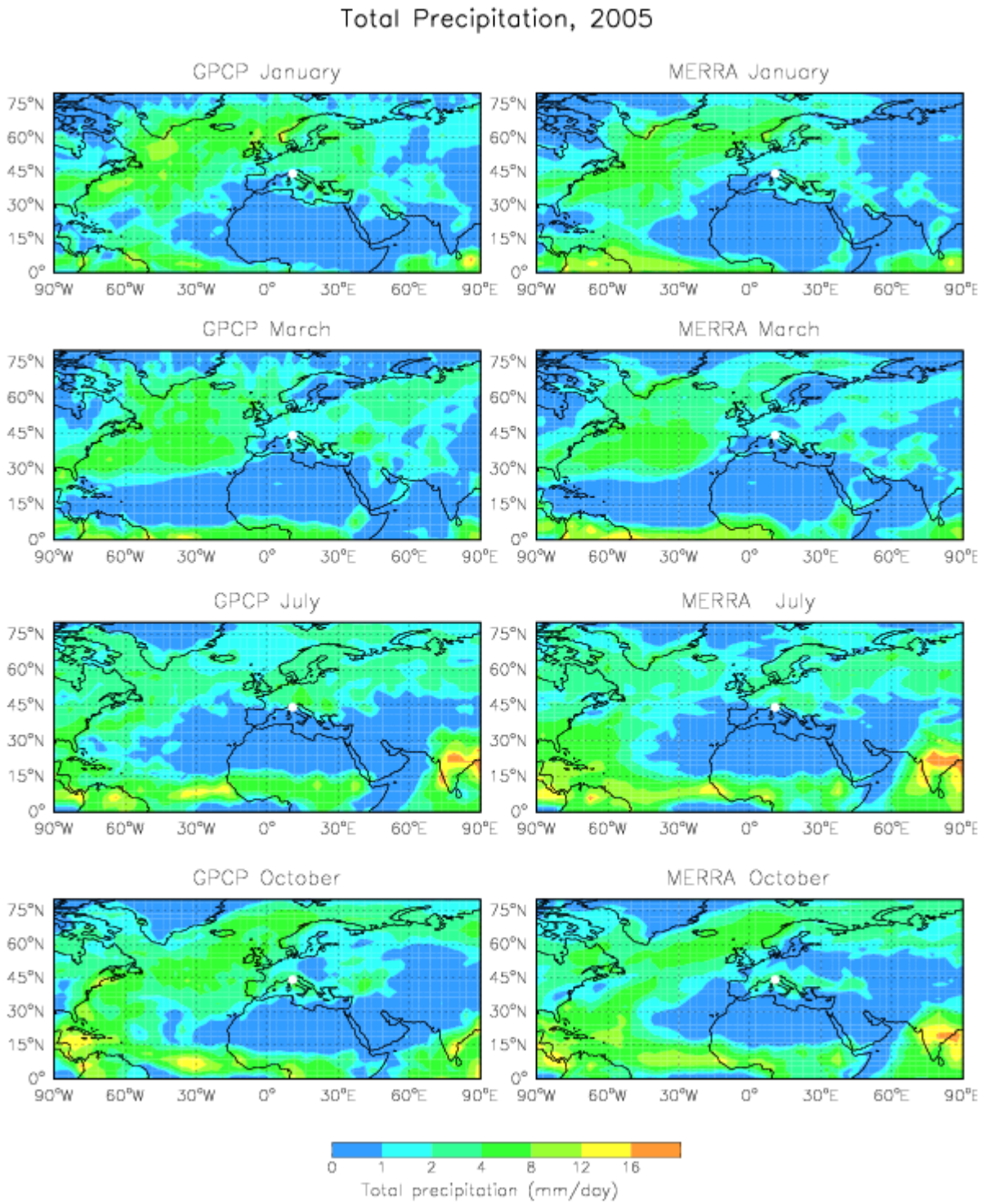

Figure 4.3 *Comparison of the regional precipitation patterns (latitude: 0-75° N, longitude: 90°W-90° E) during January, March, July and October in the GPCP observations and in the MERRA meteorological data set. The white dot indicates the location of Mt. Cimone (44°12' N, 10°42' E, 2165 m asl).*

We also compared the GPCP/MERRA precipitation seasonality for each of the 9 grids surrounding Mt. Cimone (Figure 4.4, only "ij" and "ijm1" grids are shown). The agreement

between model and satellite observations is reasonable, especially for the "im1jm1" and "ip1jp1" grids (not shown). Summer precipitation patterns are very similar in the model/GPCP observations. However, there are large differences between these values and those observed at the surface of Mt. Cimone (not shown). This difference may very well reflect again the fact that the observed surface precipitation is very localized, whereas the satellite/model precipitations are for larger scales (MERRA: 2° X 2.5°; GPCP: 2.5° X 2.5° global grid). Moreover, as Colombo *et al.* (2000) previously pointed out, different from the surrounding area where the climate is defined as temperate-continental, the climate at the mountaintop is classified as alpine because of the high elevation. In the region the observed precipitations show maxima during November (secondary maximum in spring) and absolute minimum in July (secondary minimum in January), but on the top of the mountain the precipitations are maxima during summer. Simulated precipitations show increased amounts during April and the period August-December, with minimum in June-July.

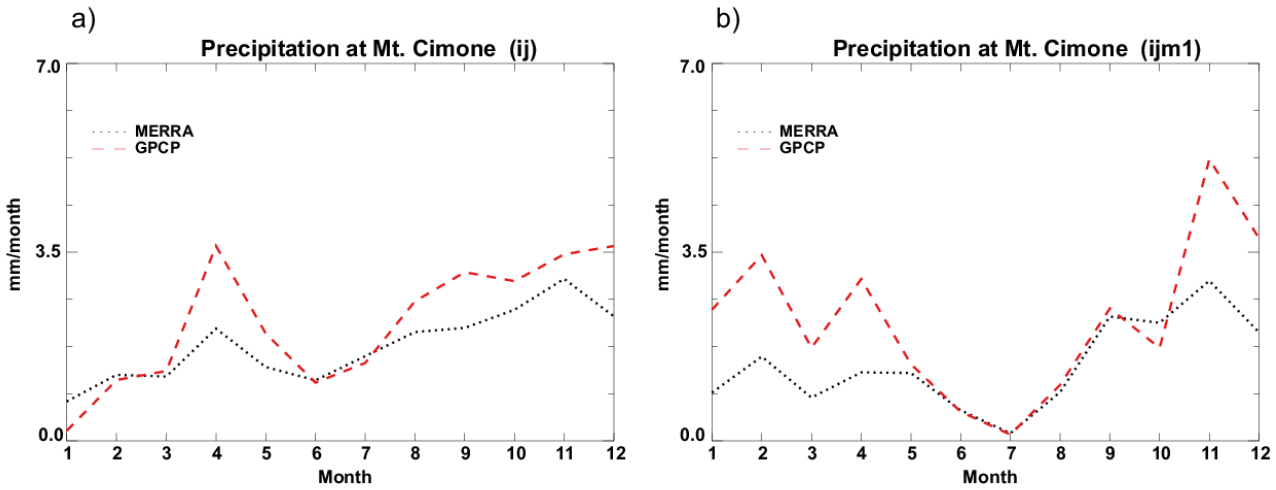

Figure 4.4 *Comparison of the seasonal precipitation in the MERRA meteorological data set with that in the GPCP satellite observations for (a) the model gridbox ("ij") corresponding to the latitude and longitude of Mt. Cimone; (b) the model gridbox ("ijm1") to the west of "ij".*

4.4 Seasonal variations of ^{210}Pb and ^{7}Be at Mt. Cimone: observations vs. model simulations

Low ^{210}Pb areas (Figure 4.2a) are seen over the Atlantic Ocean, due to the negligible flux of ^{222}Rn from the oceans, and in northern and western Europe especially during the cold season. High ^{210}Pb concentrations appear over the Sahara desert and North Africa, as a result of low precipitation in this area, and over Middle East/Asia. ^{210}Pb concentrations over southern Europe appear higher during the transition seasons and peak during summer.

Low ^{7}Be concentrations (Figure 4.2b) are simulated along the Equator, where convective scavenging is strongest. High ^{7}Be concentrations are seen over the Sahara desert, due to a combination of low precipitation and subsidence in this region. Elevated values also occur over the Middle East, North American, and Greenland.

The seasonality and frequency distributions of ^{210}Pb and ^{7}Be concentrations measured at the Mt. Cimone station were previously studied by Lee *et al.* (2007), while a more recent analysis was presented in Chapter 3 (Tositti *et al*., 2014). Generally, both radionuclides show a marked seasonal maximum in the summertime, a behaviour shared by PM_{10} and O_3. While ^{210}Pb summer maximum is mainly due to the higher mixing height and enhanced uplift from the boundary layer as a result of thermal convection, the seasonal fluctuation of ^{7}Be is more complex and characterized by two relative maxima, one during the cold season associated with stratosphere-to-troposphere transport, and one during the warm season mainly (but not exclusively) associated with tropospheric subsidence balancing lower-tropospheric air masses ascent occasionally accompanied by STE (Chapter 3; Tositti *et al.*, 2014). The measurements in 2005 are in agreement with this description (Figure 4.5, 4.6 and 4.7, solid lines): ^{210}Pb concentrations are characterized by two maxima during the warm period (July and September), while ^{7}Be concentrations are characterized by one absolute maximum during summertime (July) and one secondary maximum during the cold period (March).

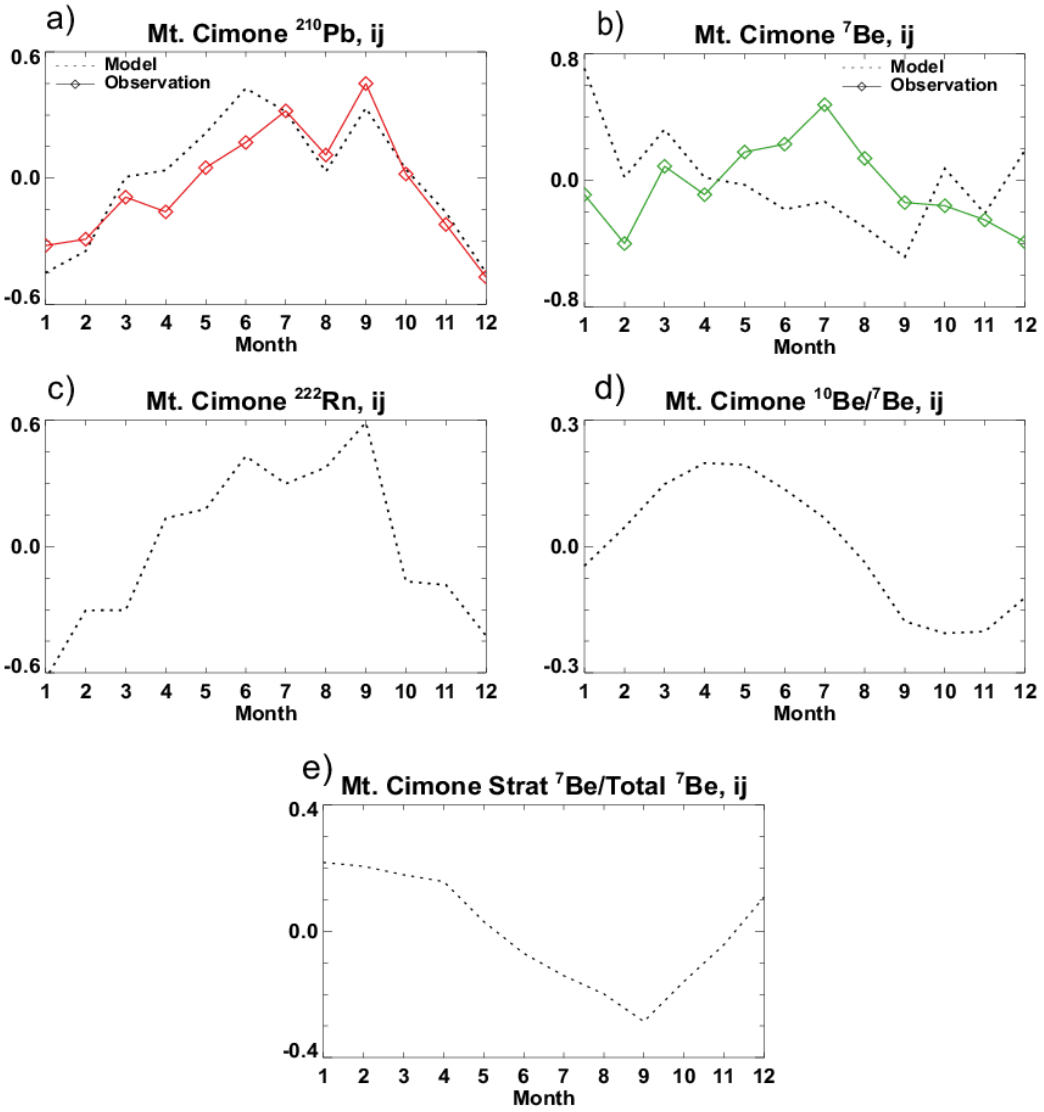

Figure 4.5 *Comparison of GMI simulated (black dotted line) percentage deviations (X 100) of ^{210}Pb (a) and ^{7}Be (b) concentrations from the annual means at the "ij" grid with those observed at Mt. Cimone (solid lines). Also shown are GMI simulated monthly fluctuations of ^{222}Rn activities (c), ^{10}Be/^{7}Be ratios (d) and strat ^{7}Be/total ^{7}Be ratios (e) at the "ij" grid.*

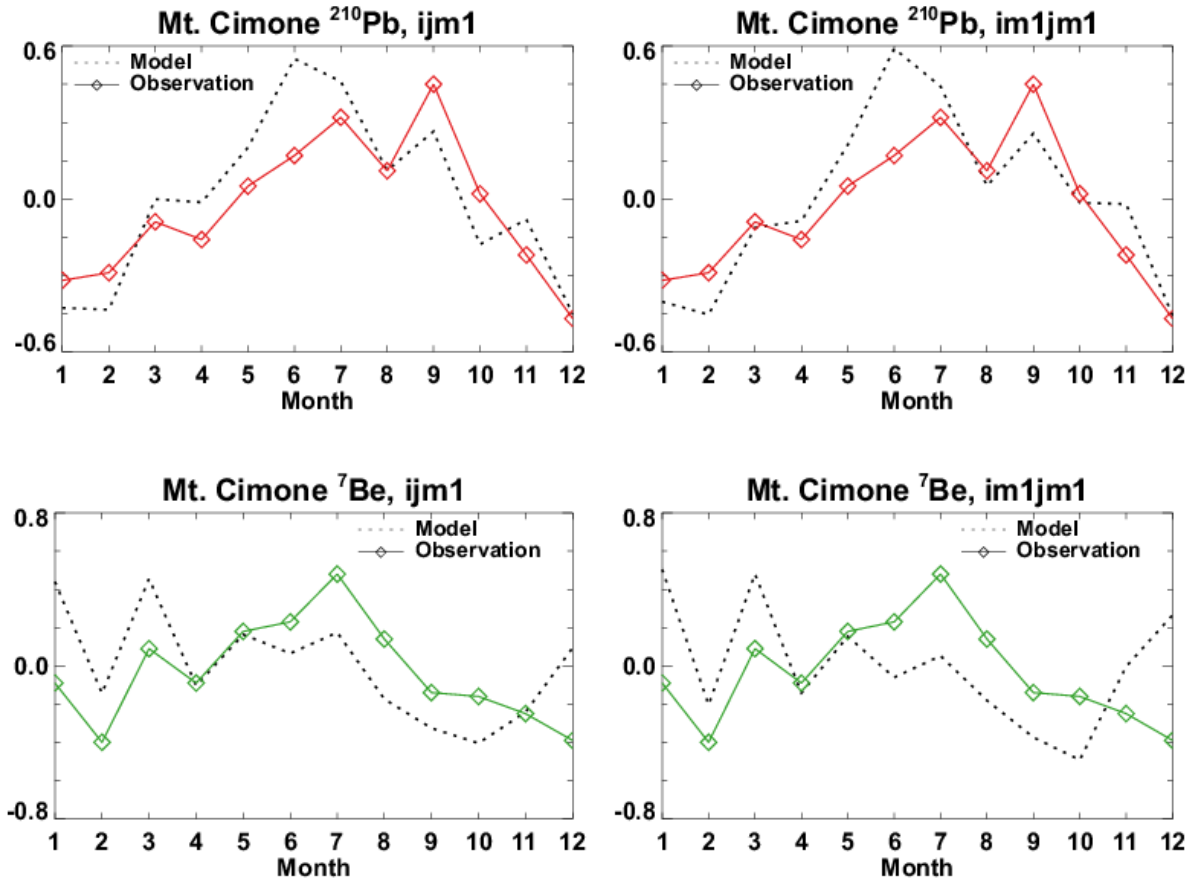

Figure 4.6 *Same as Figure 4.5(a, b), but for the "ijm1" and "im1jm1" grids. In these grids, a better agreement for ^{7}Be in summer was found.*

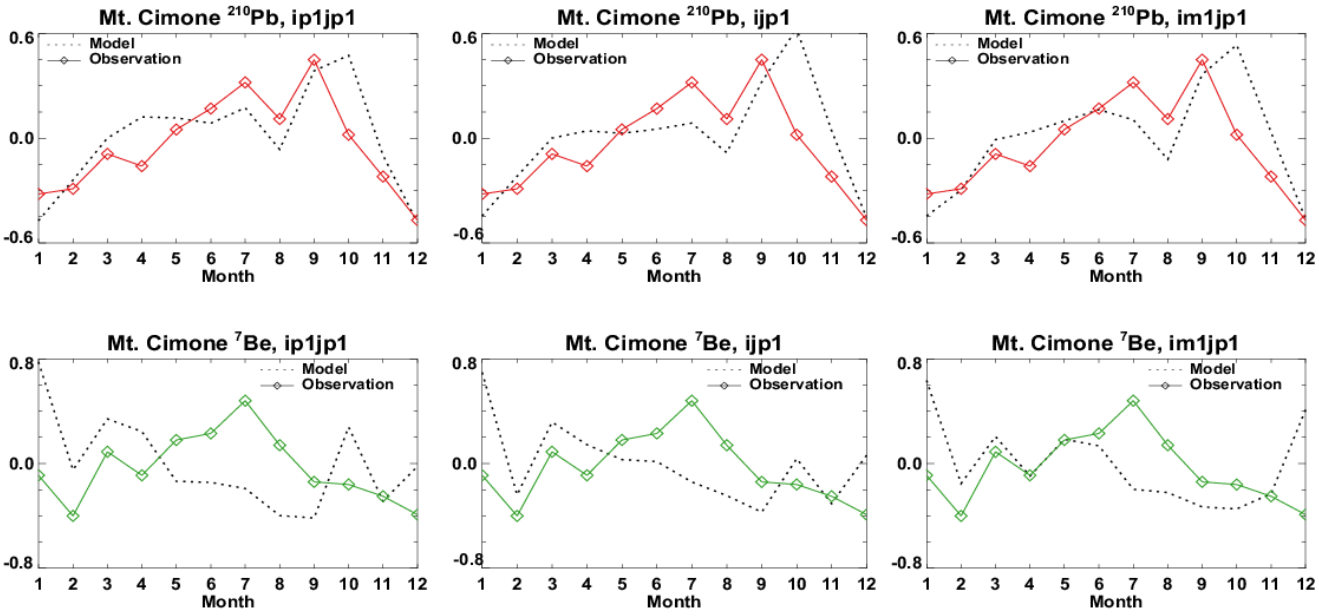

Figure 4.7 *Same as Figure 4.5(a,b), but for "ip1jp1" "ijp1", "im1jp1" grids. In these grids, a better agreement for ^{7}Be in winter was found.*

In Figures 4.5, 4.6 and 4.7 the simulated ^{210}Pb and ^{7}Be activities are compared with the observations at Mt. Cimone. The seasonality of ^{210}Pb is well captured by the GMI model driven by the MERRA meteorological fields, although slightly underestimated in spring. The model reproduces the presence of two seasonal maxima observed in the measurements, with the maximum observed in July in the measurements shifted to June in the simulation.

As for ^{7}Be, the model well captures the March maximum and the general seasonal pattern during the cold and transition seasons. During the warm period, the simulated ^{7}Be concentrations show a month-to-month variability similar to that in the observations, but are significantly lower than the observed. A better agreement was found at some adjacent model gridboxes (Figure 4.6 and Figure 4.7 vs. Figure 4.5).

4.5 Sources and seasonality of ^{210}Pb and ^{7}Be at Mt. Cimone: a model analysis

The importance of simulating the seasonality of ^{210}Pb and ^{7}Be relies in the fact that in the model their sources and governing processes are perfectly known. For instance, from Figure 4.5c one could conclude that the summer ^{210}Pb maximum is due to stronger (thermal) convection, which uplifts more ^{222}Rn from the boundary layer, as pointed out by, e.g., Lee *et al.* (2007) and in previous Chapter 3.

In a similar manner, the source of ^{7}Be March maximum can be investigated with the model simulations. Figure 4.5 also shows the simulated seasonal patterns of the fraction of ^{7}Be originating from the stratosphere (strat ^{7}Be/total ^{7}Be) and of the ^{10}Be/^{7}Be activity ratio. As both tracers exhibit a maximum during December-March, the March ^{7}Be maximum is largely due to a large stratospheric influence during winter/spring months. However, the model tends to overestimate the observed ^{7}Be concentrations during the period December-March, suggesting that STE and/or subsidence in the model is likely too fast.

The fact that the model uses the ^{7}Be production rate of Lal and Peters (1967) for a solar maximum year may partially explain the lower annual mean ^{7}Be in the model than in the observations. In fact, the sunspot number in 2005 was quite low (29.8) (slowly decreasing from 2000, solar maximum year, reaching the minimum in 2008), especially compared to the 1958 value of 184.8 (sunspot number data available from the World Data Center SILSO, Royal Observatory of Belgium, Brussels, http://sidc.oma.be/sunspot-data/).

During the winter period, associated with the simulated (Figure 4.2b) and observed ^{7}Be increases (Figure 4.5, 4.6 and 4.7), strong and long-range transport seems to dominate in the European region (Figure 4.2). In particular, transport from higher latitude regions (Arctic, northern Europe, and

North America), which have already been linked to STE by many authors (e.g., Bonasoni *et al.*, 1999, 2000ab), appears particularly important during the cold period (Figure 4.2).

On the contrary, during the warm period the simulated (Figure 4.2a) and observed ^{210}Pb concentrations increase. It appears to be associated with short-range and regional transport as suggested by the model simulations. As expected, long-range transport is more typical of the winter/spring season because of stronger horizontal winds, while regional effects are more important during summer when convection gets stronger.

The discrepancy between the simulations and the observations of ^{7}Be during the warm period is partly due to the sensitivity to spatial sampling in the model. As seen from the map plots of ^{210}Pb and ^{7}Be concentrations (Figure 4.2) at the elevation of Mt. Cimone, the sampling site appears to be located in a region where the N-S gradient of concentrations is large (especially for ^{7}Be). The presence of an elevated gradient in the region surrounding Mt. Cimone was also observed for winds, as expected because concentrations and transport are inherently connected. The sensitivity to spatial sampling in the model is therefore ascribed to this observed strong gradient in the N-S direction. In fact, while "ijm1" and "im1jm1" grids are better for summer ^{7}Be comparisons (Figure 4.6), the grids "ip1jp1", "ijp1", and "im1jp1" are better for winter (Figure 4.7).

The model underestimation of ^{7}Be levels during the warm months suggests looking with more details in the mixing between the PBL and the lower free troposphere: entrainment of free tropospheric air into the PBL (whose influence at Mt. Cimone is higher in summer, due to enhanced vertical mixing and mountain wind breeze regime, as reported by e.g., Fischer *et al.*, 2003 and Cristofanelli *et al.*, 2007) could be limited. A limited mixing with the PBL in the model would result in lower ^{7}Be concentrations, as even though subsidence of upper tropospheric air (which has been influenced by frequent shallow stratosphere-to-troposphere transport events) in the lower free troposphere were correctly simulated, the higher ^{7}Be air masses could not penetrate adequately the PBL.

The comparison between model/observations of radionuclides suggests that the model simulated summer ^{210}Pb and ^{7}Be concentrations are often low (more for ^{7}Be than for ^{210}Pb), but the model ^{7}Be/^{210}Pb ratio is much closer to the observed ratio (Figure 4.8). This suggests that the ratio cancels out the errors in precipitation scavenging that contribute to the underestimate of ^{210}Pb and ^{7}Be activities, as previously suggested by Koch *et al.* (1996).

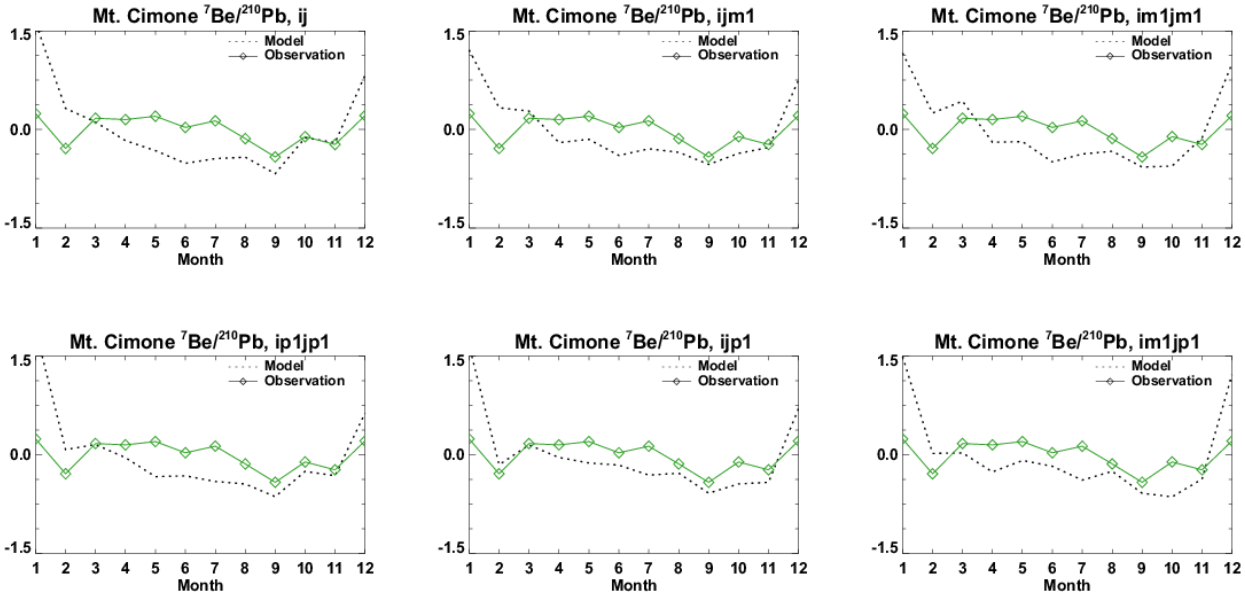

Figure 4.8 *Comparison between GMI simulated monthly fluctuations (in percentage X 100) of $^{7}Be/^{210}Pb$ ratios at the "ij", "ijm1", "im1jm1", "ip1jp1", "ijp1", and "im1jp1" grids (black dotted line) and those from the observations at Mt. Cimone (green solid line).*

If one compares the seasonality of radionuclides (Figures 4.5, 4.6 and 4.7) and precipitation at the 9 grids (Figure 4.4), the maxima/minima of precipitation appear to be in phase with minima/maxima of radionuclides activities. Moreover, in previous Chapter 3 (Tositti *et al.*, 2014) it was showed that precipitation events bring about PM_{10} minima as a result of wet removal, as well as maxima in relative humidity.

We have conducted model sensitivity experiments where convective transport/scavenging, wet scavenging (both large-scale and convective), and dry deposition processes are turned off, respectively, to examine the roles of these processes in controlling the seasonality of ^{210}Pb and ^{7}Be at Mt. Cimone. Figure 4.9 shows the results for the standard and sensitivity runs at the "ijm1" grid, for which the simulated tracer seasonal variations are similar to those observed.

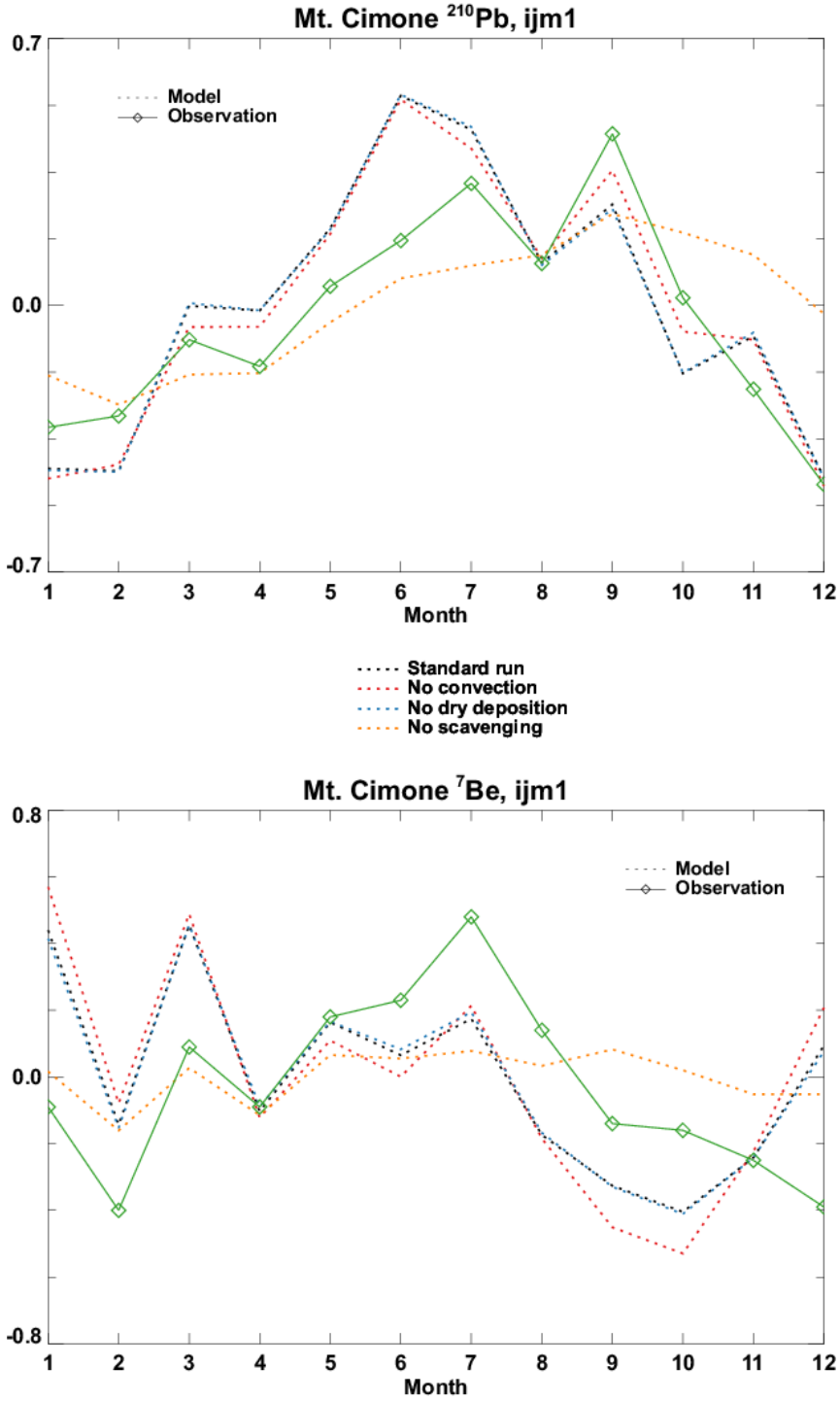

Figure 4.9 *Comparison of GMI simulated monthly fluctuations (in percentage X100) of ^{210}Pb and ^{7}Be at the "ijm1" grid between the standard (black dotted line) and the sensitivity runs at Mt. Cimone. The sensitivity runs are those without convective transport/scavenging (red dotted line), without dry deposition (blue dotted line), and without scavenging (orange dotted line). The observations are shown as green solid line.*

As expected, turning off dry deposition does not significantly change the simulated ^{210}Pb and ^{7}Be concentrations, due to the high elevation of the site (larger effects are shown at the bottom model layer).

Also turning off convection (with neither convective transport nor convective scavenging), the simulated ^{7}Be seasonality remains nearly the same. In the case of ^{210}Pb, turning off convection does not have a large effect on the simulated seasonality either. As we previously noted, convection plays a dominant role in determining the summer ^{210}Pb maximum. The fact that concentrations in the run without convection are similar to those in the standard run is probably due to the compensating effects of convective transport and convective scavenging in the free troposphere. In fact, when turning off convection, there is no convective transport of ^{222}Rn, therefore less ^{222}Rn (and ^{210}Pb) being transported to the free troposphere; on the other hand, no convective scavenging of ^{210}Pb increases its concentration in the free troposphere. A map of surface ^{222}Rn concentrations at the elevation of Mt. Cimone (not shown), as well as a map of changes in ^{210}Pb concentrations due to the convection processes (Figure 4.10) show that convection in the region is more important during summer and autumn, but also during spring when it is not completely negligible.

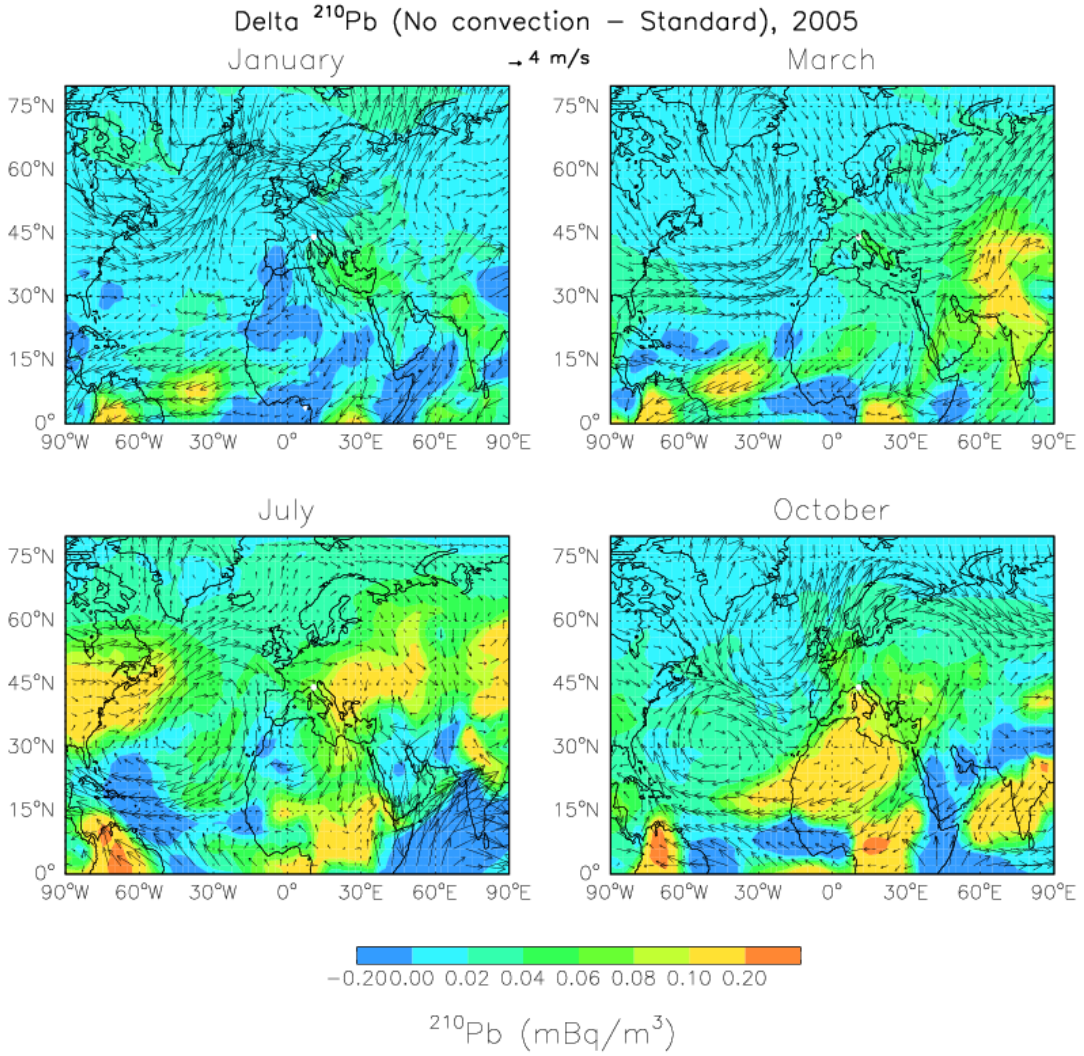

Figure 4.10 *GMI simulated difference of ^{210}Pb concentrations at the elevation of Mt. Cimone between a sensitivity run without convection and the standard run. Arrows denote MERRA winds. The white dot indicates the location of Mt. Cimone (44°12' N, 10°42' E, 2165 m asl).*

The model run without scavenging clearly suggests that wet scavenging is mainly responsible for the seasonal variation of ^{7}Be (Figure 4.9, bottom panel). For ^{210}Pb (Figure 4.9, top panel), it seems that wet scavenging plays a more important role during August-December than during January-July. This appears to be associated with the seasonality of precipitation, which shows prolonged elevated values during the period of August/September-December, as well as a maximum during April, as previously discussed (Figure 4.4). A map of changes in ^{210}Pb concentrations due to scavenging in model (Figure 4.11) confirms that the scavenging effect is larger during fall and, to a lesser extent, during summer. At Mt. Cimone, the scavenging effect is not minimal during July (month of minimum precipitation, Figure 4.4), suggesting the influence of precipitation scavenging elsewhere in the region on the site.

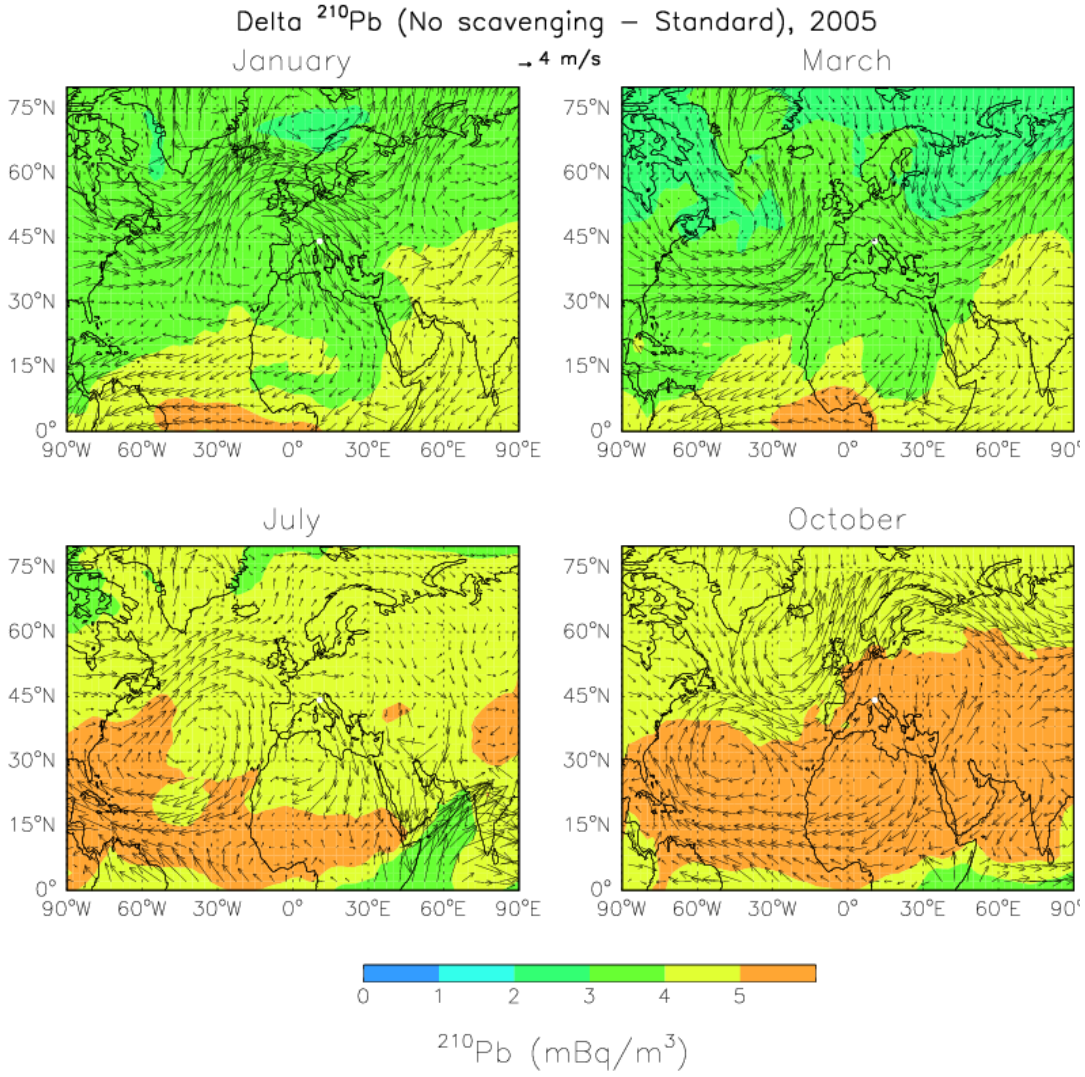

Figure 4.11 *Same as Figure 4.10, but for a sensitivity simulation where wet scavenging is turned off.*

4.6 Summary and conclusions

In this Chapter, we have tested the ability of a global 3-D model (GMI CTM) driven by MERRA assimilated meteorological data to simulate ^{210}Pb and ^{7}Be, two natural atmospheric radionuclides originating from contrasting source regions (lower troposphere and upper troposphere/lower stratosphere, respectively), attached to submicron particles, and removed from the troposphere mainly by wet deposition. Our objective was to investigate the seasonality of ^{210}Pb and ^{7}Be at the Mt. Cimone WMO-GAW station by examining the roles of horizontal advection, vertical transport (large-scale and convection), and wet scavenging. For this purpose, the model results have been compared with surface observations obtained at the station in 2005.The seasonal pattern of ^{210}Pb concentrations is characterized by the presence of maxima during the warm period, while minima during the cold period are generally observed. The seasonality of ^{7}Be seasonality is instead more complex, with two separate maxima during the warm and cold periods. The model performance in representing the transport and scavenging processes was tested by comparing model results with the observations. In particular, the MERRA precipitation field used by the model was evaluated against the GPCP satellite and surface observations, and a general good agreement was found. On the contrary, a general disagreement between the model and the local observations of winds and precipitation was observed, which was attributed to the coarse resolution of the model compared to the localized characteristics of winds and precipitation from surface measurements.

The seasonal pattern of ^{210}Pb concentrations is characterized by the presence of maxima during the warm period, while minima during the cold period are generally observed. The seasonality of ^{7}Be seasonality is instead more complex, with two separate maxima during the warm and cold periods. The model performance in representing the transport and scavenging processes was tested by comparing model results with the observations. In particular, the MERRA precipitation field used by the model was evaluated against the GPCP satellite and surface observations, and a generally good agreement was found. The model was able to capture the main circulation patterns observed in the Northern Hemisphere. Some local-scale winds/pressure systems, which may be of importance for the sampling site, were not well described in the simulations. In particular, a general disagreement between the model and the local observations of winds and precipitation was noted, which was attributed to the coarse resolution of the model compared to the localized characteristics of winds and precipitation from surface measurements.

The model well reproduced the observed ^{210}Pb seasonality: ^{210}Pb maximum during the warm period was attributed to the stronger (thermal) convection, which uplifts more ^{222}Rn (and ^{210}Pb) from the boundary layer. The seasonal pattern of ^{7}Be was instead better represented during the cold period, while the summer ^{7}Be maximum was underestimated. The model tends to overestimate the ^{7}Be observations during the cold period, probably because the STE and/or subsidence in the model

was too fast. The lower simulated annual average ^{7}Be concentration relative to the observation is instead partly attributed to the fact that the model used the ^{7}Be production rate for a solar maximum year, while in 2005 the solar activity was rather low.

By examining the wind fields and horizontal distribution of radiotracers in the model, we noted that the sampling site is in a location where there is a large gradient especially in the North-South direction. For this reason, we investigated the sensitivity of model results to spatial sampling. A better agreement between the model and the observations at some adjacent gridboxes was found. The ^{7}Be March maximum was linked to the large stratospheric influence during winter/spring. The model tends to underestimate the summertime ^{210}Pb and ^{7}Be, but the model errors due to precipitation scavenging appear to be canceled out in the ^{7}Be/^{210}Pb ratio. We have conducted a series of model sensitivity experiments to further examine and quantify the roles of wet scavenging, dry deposition, and convective transport/scavenging in controlling the seasonality of ^{210}Pb and ^{7}Be at Mt. Cimone. Dry deposition does not have a significant effect on the magnitude and seasonality of ^{210}Pb and ^{7}Be concentrations at the site. The relatively weak effects of convective transport and scavenging on the radiotracer seasonality were attributed to the compensating effects of convective transport and convective scavenging on tracer concentrations in the free troposphere (both convective transport and convective scavenging turned off in the run without convection). Convection in the region seems to be more important during summer and autumn, although it is not completely negligible during spring. Finally, scavenging is found to be the most important process controlling the seasonal variations of ^{210}Pb and ^{7}Be at Mt. Cimone. For ^{210}Pb, it was noted that scavenging seems to be more important during August-December than during January-July. This was related to the seasonality of local and regional precipitation, which shows prolonged elevated values in the period of August-December.

We have conducted a first modeling study of ^{210}Pb and ^{7}Be observations at Mt. Cimone. Our simulations demonstrated the model's capability to reproduce the seasonality, while highlighting the weaknesses of the model in reproducing local features mostly due to its coarse resolution. A future study about the interannual variability and the ^{210}Pb-^{7}Be-O_3-CO relations is also planned. Both radionuclides will prove to be very useful tracers in our future modeling studies of ^{210}Pb-^{7}Be-O_3-CO relationship, as well as the interannual variability of these tracers and other trace gases and aerosols at Mt. Cimone.

Acknowledgements

Italian Air Force Meteorological Office (IAFMS) and ISAC-CNR are gratefully acknowledged for their precious technical support at the Mt. Cimone station. In particular, ISAC-CNR is gratefully acknowledged for providing

infrastructural access at the WMO-GAW Global Station Italian Climate Observatory "O. Vittori" at Mt. Cimone. IAFMS is gratefully acknowledged for providing meteorological observations at Mt. Cimone. The Italian Climate Observatory "O. Vittori" is supported by MIUR and DTA-CNR throughout the Project of National Interest NextData. Erika Brattich thanks the National Institute of Aerospace (NIA) Visitor Program for financial support during her one month visit. Hongyu Liu is supported by NASA Modeling and Analysis Program (MAP) and NASA Atmospheric Composition Modeling and Analysis Program (ACMAP). The GMI core team at NASA GSFC is acknowledged for programming support. NASA Center for Computational Sciences (NCCS) provided supercomputing resources.

References

Abe T., Kosako T., Komura K., 2010. Relationship between variations of ^{7}Be, ^{210}Pb, and ^{212}Pb concentrations and sub-regional atmospheric transport: simultaneous observation at distant locations. *Journal of Environmental Radioactivity* 101, 113-121.

Arimoto R., Snow J.A., Graustein W.C., Moody J.L., Ray B.J., Duce R.A., Turekian K.K., Maring H.B., 1999. Influences of atmospheric transport pathways on radionuclide activities in aerosol particles from over the North Atlantic. *Journal of Geophysical Research* 104(D17), 301-321.

Balkanski Y, Jacob D.J., Gardner G.M., Graustein W., Turekian K.K., 1993. Transport and residence times of tropospheric aerosols inferred from a global three-dimensional simulation of ^{210}Pb. *Journal of Geophysical Research* 98 (D11), 20573-20586.

Baskaran M., 2011. Po-210 and Pb-210 as atmospheric tracers and global atmospheric Pb-210 fallout: a review. *Journal of Environmental Radioactivity* 102, 500-513.

Beer J., McCracken K., von Steiger R., 2012. Cosmogenic radionuclides. Springer, Heidelberg, p.426.

Bonasoni P., Evangelisti F., Bonafé U., Feldmann H., Memmesheimer M., Stohl A., Tositti L., 1999. Stratosphere-troposphere exchanges: case studies recorded at Mt. Cimone during VOTALP project. *Physics and Chemistry of the Earth* (C) 24(5), 443-446.

Bonasoni P., Evangelisti F., Bonafé U., Ravegnani F., Calzolari F., Stohl A., Tositti L,. Tubertini O., Colombo T., 2000a. Stratospheric ozone intrusion episodes recorded at Mt. Cimone during VOTALP project: Case studies. *Atmospheric Environment* 34, 1355-1365.

Bonasoni P., Stohl A., Cristofanelli P., Calzolari F., Colombo T., Evangelisti F., 2000b. Background ozone variations at Mt Cimone station. *Atmospheric Environment* 34, 5183-5189.

Bourcier L., Masson O., Laj P., Pichon J.M., Paulat P., Freney E., Sellegri K., 2011. Comparative trends and seasonal variation of ^{7}Be, ^{210}Pb and ^{137}Cs at two altitude sites in the central part of France. *Journal of Environmental Radioactivity* 102, 294-301.

Brost R.A., Feichter J., Heimann H., 1991. Three-dimensional simulation of ^{7}Be in a global climate model. *Journal of Geophysical Research* 96, 22423-22445.

Burlando M., Antonelli M., Ratto C.F., 2008. Mesoscale wind climate analysis: identification of anemological regions and wind regimes. *International Journal of Climatology* 28, 629-641.

Burlando M., 2009. The synoptic-scale surface wind climate regimes of the Mediterranean Sea according to the cluster analysis of ERA-40 wind fields. *Theoretical and Applied Climatology* 96, 69-83.

Caillet S., Arpagaus P., Monna F., Dominik J., 2001. Factors controlling ^{7}Be and ^{210}Pb atmospheric deposition as revealed by sampling individual rain events in the region of Geneva, Switzerland. *Journal of Environmental Radioactivity* 53, 241-256.

Campins J., Jansà A., Genovés A., 2006. Three-dimensional structure of western Mediterranean cyclones. *International Journal of Climatology* 26, 323-343.

Cannizzaro F., Greco G., Raneli M., Spitale M.C., Tomarchio E., 2004. Concentration measurements of ^{7}Be at ground level air at Palermo, Italy – comparison with solar activity over a period of 21 years. *Journal of Environmental Radioactivity* 84, 457-467.

Carvalho A.C., Reis M., Silva L., Madruga M.J., 2013. A decade of ^{7}Be and ^{210}Pb activity in surface aerosols measured over the Western Iberian Peninsula. *Atmospheric Environment* 67, 193-202.

Ciattaglia L., 1983. Interpretation of Atmospheric CO_2 Measurements at Mt. Cimone (Italy) Related to Wind Data. *Journal of Geophysical Research* 88(C2), 1331-1338.

Ciattaglia L., Cundari V., Colombo T., 1987. Further measurements of atmospheric carbon dioxide at Mt. Cimone, Italy: 1979-1985. *Tellus* 39B, 13-20.

Colombo T., Santaguida R., Capasso A., Calzolari F., Evangelisti F., Bonasoni P., 2000. Biospheric influence on carbon dioxide measurements in Italy. *Atmospheric Environment* 34, 4963-4969.

Considine D.B., Douglass A.R., Connell P.S., Kinnison D.E., Rotman D.A., 2000. A polar stratospheric cloud parameterization for the global modeling initiative three-dimensional model and its response to stratospheric aircraft. *Journal of Geophysical Research* 105(D3), 3955-3973.

Considine D.B., Connell P.S., Logan J.A., 2004. Simulating ozone in the near tropopause region with a new combined model of the stratosphere and troposphere, in: Quadrennial Ozone Symposium QOS 2004, edited by: Zerefos C., pp. 739-740, International Ozone Commission, Kos, Greece.

Considine D.B., Bergmann D.J., Liu H., 2005. Sensitivity of Global Modeling Initiative chemistry and transport model simulations of radon-222 and lead-210 to input meteorological data. *Atmospheric Chemistry and Physics* 5, 3389-3406.

Considine D.B., Logan J.A., Olsen M.A., 2008. Evaluation of near-tropopause ozone distributions in the Global Modeling Initiative combined stratosphere/troposphere model with ozonesonde data. *Atmospheric Chemistry and Physics* 8, 2365-2385.

Cristofanelli P., Bonasoni. P., Collins W., Feichter J., Forster C., James P., Kentarchos A., Kubik P.W., Land C., Meloen J., Roelofs G.J., Siegmund P., Sprenger M., Schnabel C., Stohl A., Tobler L., Tositti L., Trickl T., and Zanis P., 2003. Stratosphere-to-troposphere transport: A model and method evaluation. *Journal of Geophysical Research* 108(D12), 8525, doi:10.1029/2002JD002600

Cristofanelli P., Bonasoni P., Tositti L., Bonafé U., Calzolari F., Evangelisti F., Sandrini S., Stohl A., 2006. A 6-year analysis of stratospheric intrusions and their influence on ozone at Mt. Cimone (2165 m above sea level). *Journal of Geophysical Research* 111. D03306. doi:10.1029/2005JD006553.

Cristofanelli P., Bonasoni P., Carboni G., Calzolari F., Casarola L., Zauli Sajani S., Santaguida R., 2007. Anomalous high ozone concentrations recorded at a high mountain station in Italy in summer 2003. *Atmospheric Environment* 41, 1383-1394.

Cristofanelli P., Calzolari F., Bonafé U., Duchi R., Marinoni A., Roccato F., Tositti L., Bonasoni P., 2009a. Stratospheric intrusion index (SI^2) from baseline measurement data. *Theoretical and Applied Climatology* 97, 317-325.

Cristofanelli P., et al., 2009b. Significant variations of trace gas composition and aerosol properties at Mt. Cimone during air mass transport from North Africa – contributions from wildfire emissions and mineral dust. *Atmospheric Chemistry and Physics* 9, 4603-4619.

Cuevas E., Gonzalez Y., Rodríguez S., Guerra J.C., Gómez-Peláez A.J., Alonso-Pérez S., Bustos J., Milford C., 2013. Assessment of atmospheric processes driving ozone variations in the subtropical North Atlantic free troposphere. *Atmospheric Chemistry and Physics* 13, 1973-1998.

Daish S.R., Dale A.A., Dale C.J., May R., Rowe J.E., 2005. The temporal variations of ^{7}Be, ^{210}Pb and ^{210}Po in England. *Journal of Environmental Radioactivity* 84, 457-467.

Dibb J.E., Talbot R.W., Gregory G.L., 1992. Beryllium 7 and lead 210 in the western hemisphere Arctic atmosphere: Observations from three recent aircraft-based sampling programs. *Journal of Geophysical Research* 97, 16709-16715.

Dibb J.E., Meeker L.D., Finkel R.C., Southon J.R., Caffee M.W., Barrie L.A., 1994. Estimation of stratospheric input to the Arctic troposphere: ^{7}Be and ^{10}Be in aerosols at Alert, Canada. *Journal of Geophysical Research* 99, 12855-12864.

Dibb J.E., 2007. Vertical mixing above Summit, Greenland: insights into seasonal and high frequency variability from the radionuclide tracers ^{7}Be and ^{210}Pb. *Atmospheric Environment* 41, 5020-5030.

Dueñas C., Fernández M.C., Cañete S., Pérez M., 2009. ^{7}Be to ^{210}Pb concentration ratio in ground level air in Málaga (36.7°N, 4.5°W). *Atmospheric Research* 92, 49-57.

Dueñas C., Orza J.A.G., Cabello M., Fernández M.C., Cañete S., Pérez M., Gordo E., 2011. Air mass origin and its influence on radionuclide activities (^{7}Be and ^{210}Pb) in aerosol particles at a coastal site in the western Mediterranean. *Atmospheric Research* 101, 205-214.

Duncan B.N., Strahan S.E., Yoshida Y., 2007. Model study of the cross-tropopause transport of biomass burning pollution. *Atmospheric Chemistry and Physics* 7, 3713-3736.

Duncan B.N., West J.J., Yoshida Y., Fiore A.M., Ziemke J.R., 2008. The influence of European pollution on ozone in the Near East and northern Africa. *Atmospheric Chemistry and Physics* 8, 2267-2283, doi:10.5194/acp-8-2267-2008.

Feely H.W., Larsen R.J., Sanderson C.G., 1988. Annual report of the surface air sampling program. Environmental Measurements Laboratory, U.S. Department of Energy, 165 pp.

Feely H.W., Larsen R.J., Sanderson C.G., 1989. Factors that cause seasonal variations in beryllium-7 concentrations in surface air. *Journal of Environmental Radioactivity* 9, 223-249.

Fischer H., Kormann R., Klüpfel T., Gurk C., Königstedt R., Parchatka U., Mühle J., Rhee T.S., Brenninkmeijer C.A.M., Bonasoni P., Stohl A., 2003. Ozone production and trace gas correlations during the June 2000 MINATROC intensive measurement campaign at Mt. Cimone. *Atmospheric Chemistry and Physics* 3, 725-738.

Forster P., et al., 2007. Changes in Atmospheric Constituents and in Radiative Forcing, in Climate Change 2007: The Physical Science Basis. Contribution of Working Group I to the Fourth Assessment Report of the Intergovernmental Panel on Climate Change, edited by: Solomon S., Qin D., Manning M., Chen Z., Marquis M., Averyt K.B., Tignor M., Miller H.L., Cambridge University Press, Cambridge,, United Kingdom and New York, NY, USA.

Froehlich K., Masarik J., 2010. Radionuclides as tracers and timers of processes in the continental environment – Basic concepts and methodologies. In: Radioactivity in the Environment 16, Chapter 2: 27-49. Edited by Elsevier. doi:10.1016/S1569-4860(09)01602-7

Gaffney J.S, Marley N., Cunningham M.M., 2004. Natural radionuclides in fine aerosols in the Pittsburgh area. *Atmospheric Environment* 38, 3191-3200.

Gaggeler H.W., 1995. Radioactivity in the atmosphere. *Radiochimica Acta* 70-71, 345-353

Gerasopoulos E., et al., 2001. A climatology of ^{7}Be at four high-altitude stations at the Alps and the Northern Apennines. *Atmospheric Environment* 35, 6347-6360.

Giuliacci M., 1988. Climatologia fisica e dinamica della Valpadana. Ente regionale di sviluppo agricolo. Servizio meteorologico regionale, Bologna, pp. 403 (In Italian)

Graustein W.C., Turekian K.K., 1990. Radon fluxes from soils to the atmosphere measured by ^{210}Pb-^{226}Ra disequilibrium in soils. *Geophysical Research Letters* 17, 841-844-

Graustein W.C., Turekian K.K., 1996. ^{7}Be and ^{210}Pb indicate an upper troposphere source for elevated ozone in the summertime subtropical free troposphere of the eastern North Atlantic. *Geophysical Research Letters* 23, 539-542.

Hernández F., Rodríguez S., Karlsson L., Alonso-Pérez S., López-Pérez M., Hernandez-Armas J., Cuevas E., 2008. Origin of observed high ^{7}Be and mineral dust concentrations in ambient air on the Island of Tenerife. *Atmospheric Environment* 42, 4247-4256.

Hötzl H., Winkler R., 1987. Activity concentrations of ^{226}Ra, ^{228}Ra, ^{210}Pb, ^{40}K and ^{7}Be and their temporal variations in surface air. *Journal of Environmental Radioactivity* 5, 445-458.

Huschke R.G. (Ed.), 1959. Glossary of Meteorology. American Meteorological Society, Boston, USA.

Ioannidou A., Manolopoulou M., Papastefanou C., 2005. Temporal changes of ^{7}Be and ^{210}Pb concentrations in surface air at temperate latitudes (40°). *Applied Radiation and Isotopes* 63(2), 277-284.

Ioannidou A., Vasileiadis A., Melas D., 2014. Time lag between the tropopause height and ^{7}Be activity concentrations on surface air. *Journal of Environmental Radioactivity* 129, 80-85.

Jacob D.J., Prather M.J., 1990. Radon-222 as a test of boundary layer convection in a general circulation model. *Tellus* Ser. B 42, 118-134.

James P., Stohl A., Forster C., Eckhardt S., Seibert P., Frank A., 2003. A 15-year climatology of stratosphere-troposphere exchange with a Lagrangian particle dispersion model 2. Mean climate and seasonal variability. *Journal of Geophysical Research* 108(D12), 8522. doi:10.1029/2002JD002639

Jasiulionis R., Wershofen H., 2005. A study of the vertical diffusion of the cosmogenic radionuclides, ^{7}Be and ^{22}Na in the atmosphere. *Journal of Environmental Radioactivity* 79, 157-169.

Jiang Q., Smith R.B., Doyle J., 2003. The nature of the Mistral: observation and modelling of two MAP events. *Quarterly Journal of the Royal Meteorological Society* 129, 857-875.

Johnson W., Viezee W., 1981. Stratospheric ozone in the lower troposphere-I. Presentation and interpretation of aircraft measurements. *Atmospheric Environment* 15, 1309–1323.

Junge C.E., 1963. Air chemistry and radioactivity. Academic Press, New York and London, 382 pp.

Kinnison D.E., Connell P.S., Rodriguez J.M., Rotman D.A., Considine D.B., Tannahill J., Ramaroson R., Rasch P.J., Douglass A.R., Baughcum S.L., Coy L., Waugh D.W., Kawa S.R., Prather M.J., 2001. The Global Modeling Initiative assessment model: Application to high-speed civil transport perturbation. *Journal of Geophysical Research* 106(D2), 1693-1711.

Koch D.M., Jacob D.J., Graustein W.C., 1996. Vertical transport of tropospheric aerosols as indicated by ^{7}Be and ^{210}Pb in a chemical tracer model. *Journal of Geophysical Research* 101(D13), 18651-18666.

Koch D.M., Mann M.E., 1996. Spatial and temporal variability of ^{7}Be surface concentrations. *Tellus Ser. B.*, 48, 387-396.

Kotroni V., Lagouvardos K., Lalas D., 2001. The effect of Crete Island on the Etesian winds over the Aegean Sea. *Quarterly Journal of the Royal Meteorological Society* 127, 1917-1938.

Kulan A., Aldahan A., Possnert G., Vintersved I., 2006. Distribution of ^{7}Be in surface air of Europe. *Atmospheric Environment* 40, 3855-3868.

Lal D., Malhotra P.K., Peters B., 1958. On the production of radioisotopes in the atmosphere by cosmic radiation and their application to meteorology. *Journal of Atmospheric and Solar-Terrestrial Physics* 12, 306-328.

Lal D., Peters B., 1967. Cosmic ray produced radioactivity on the Earth, in Handbuch der Physik, 46/2, edited by K. Sitte, pp. 551-612, Springer-Verlag, New York.

Lee H.N., Wan G., Zheng X., Sanderson C.G., Josse B., Wang S., Yang W., Tang J., Wang C., 2004. Measurements of ^{210}Pb and ^{7}Be in China and their analysis accompanied with global model calculations of ^{210}Pb. *Journal of Geophysical Research* 109, D22203. doi:10.1029/2004JD005061

Lee H.N., Tositti L., Zheng X., Bonasoni P., 2007. Analyses and comparisons of variations of ^{7}Be, ^{210}Pb and ^{7}Be/^{210}Pb with ozone observations at two Global Atmosphere Watch stations from high mountains. *Journal of Geophysical Research* 112, D05303. doi:10.1029/2006JD007421

Lelieveld J., et al., 2002. Global air pollution crossroads over the Mediterranean. *Science* 298, 794-799.

Li Q., Jacob D.J., Logan J.A., Bey I., Yantosca R.M., Liu H., Martin R.V., Fiore A.M., Field B.D., Duncan B.N., 2001. A Tropospheric Ozone Maximum Over the Middle East. *Geophysical Research Letters* 28(17), 3235-3238.

Likuku A.S., 2006. Factors influencing ambient concentrations of ^{210}Pb and ^{7}Be over the city of Edinburgh (55.9°N, 03.2°W). *Journal of Environmental Radioactivity* 87, 289-304.

Liu H., Jacob D.J., Bey I., Yantosca R.M., 2001. Constraints from the ^{210}Pb and ^{7}Be on wet deposition and transport in a global three-dimensional chemical tracer model driven by assimilated meteorological fields. *Journal of Geophysical Research* 106, D11, 12109-12128.

Liu H., Jacob D.J., Dibb J.E., Fiore A.M., Yantosca R.M., 2004. Constraints on the sources of tropospheric ozone from ^{210}Pb-^{7}Be-O_3 correlations. *Journal of Geophysical Resea*rch 109(D07306), doi:10.1029/2003JD003988.

Liu H., Considine D.B., Horowitz L.W., Crawford J.H., Strahan S.E., Damon M.R., Rodriguez J.M., Xu X., Carouge C., Yantosca R.M,. 2013. Using beryllium-7 to assess cross-tropopause transport in global models. *Journal of Geophysical Research*, revised.

Lozano R.L., Hernández-Ceballos M.A., Adame J.A., Casas-Ruíz M., Sorribas M., San Miguel E.G., Bolívar J.P., 2011. Radioactive impact of Fukushima accident on the Iberian Peninsula: evolution and plume previous pathway. *Environment International* 37, 1259-1264.

Lozano R.L., Hernandéz-Ceballos M.A., San Miguel E.G., Adame J.A., Bolívar J.P., 2012. Meteorological factors influencing the ^{7}Be and ^{210}Pb concentrations in surface air from the southwestern Iberian Peninsula. *Atmospheric Environment* 63, 168-178.

Millàn M., Sanz J., Salvador R., Mantilla E., 2006. Atmospheric dynamics and ozone cycles related to nitrogen deposition in the western Mediterranean. *Environmental Pollution* 118, 167-186.

Monks P.S., et al., 2009. Atmospheric composition change – global and regional air quality. *Atmospheric Environment* 43, 5268-5350.

Moore H.E., Poet S.E., Martell E.A., 1973. ^{222}Rn, ^{210}Pb, ^{210}Bi, and ^{210}Po, profiles and aerosol residence times versus altitude. *Journal of Geophysical Research* 78, 7065-7075.

Nazaroff W.W., 1992. Radon transport from soil to air. *Reviews of Geophysics* 30, 137-160.

Papastefanou C., Ioannidou A., 1995. Aerodynamic size association of ^{7}Be in ambient aerosols. *Journal of Environmental Radioactivity* 26, 273-282.

Papastefanou C., 2008. Radioactive aerosols. In: Radioactivity in the Environment, Volume 12 Chapter 2. Edited by Elsevier B.V. pp. 11-58. doi:10.1016/S1569-4860(07)12002-7

Pham M.K., Betti M., Nies H., Povinec P.P., 2011. Temporal changes of ^{7}Be, ^{137}Cs and ^{210}Pb activity concentrations in surface air at Monaco and their correlation with meteorological parameters. *Journal of Environmental Radioactivity* 102, 1045-1054.

Rastogi N., Sarin M.M., 2008. Atmospheric ^{210}Pb and ^{7}Be in ambient aerosols over low- and high-altitude sites in 34 semiarid region: Temporal variability and transport processes, *Journal of Geophysical Research* 113, doi:10.1029/2007JD009298

Rehfeld S., Heimann M., 1995. Three dimensional atmospheric transport simulation of the radioactive tracers ^{210}Pb, ^{7}Be, ^{10}Be, and ^{90}Sr. *Journal of Geophysical Research* 100 (D12), 26141-26161.

Reiter R., Sladkovich K., Pötzl K., Carnuth W., Kanter H.J., 1971. Studies on the influx of stratospheric air into the lower troposphere using cosmic-ray produced radionuclides and fallout. *Archiv für Meteorologie, Geophysik und Bioklimatologie*, Serie A, Vol.20(3), 211-246.

Reiter E.R., 1975. Weather phenomena of the Mediterranean basin. Part 1. General description of the meteorological processes. In: Handbook for forecasters in the Mediterranean basin. Environment Prediction Research Facility. Naval Postgraduate School, Monterey, California. U.S. Department of Commerce. Available at http://www.dtic.mil/cgi-bin/GetTRDoc?AD=ADA024271 Last accessed 01 August 2013.

Reiter R., Munzert K., Kanter H.-J., Pötzl K., 1983. Cosmogenic radionuclides and ozone at a mountain station at 3.0 km a.s.l. *Archives for Meteorology, Geophysics and Bioclimatology* Ser.B, 32, 131-160.

Rodriguez J.M., Logan J.A., Bergmann D., Megretskaia I., Jacob D.J., Xie H., Das B., Strahan S.E., 2004. The impact of meteorological fields on tropospheric ozone distributions calculated by the Global

Modeling Initiative (GMI) chemical-transport model, in: Quadrennial Ozone Symposium QOS 2004, edited by: Zerefos C., pp.147, International Ozone Commission, Kos, Greece.

Rotman D.A., et al., 2001. Global Modeling Initiative assessment model: Model description, integration, and testing of the transport shell. *Journal of Geophysical Research* 106(D2), 1669-1691.

Schery S.D., Whittlestone S., Hart K.P., Hill S.E., 1989. The flux of radon and thoron from Australian soils. *Journal of Geophysical Research* 100, 26141-26161.

SILSO, World Data Center – Sunspot Number and Long-Term Solar Observations, Royal Observatory of Belgium, on-line Sunspot Number catalogue: http://www.sidc.be/SILSO/

Simon J., Meresova J., Sykora I., Jeskovsky M., Holy K., 2009. Modeling of temporal variations of vertical concentration profile of ^{7}Be in the atmosphere. *Atmospheric Environment* 43, 2000-2004.

Steinmann P., Zeller M., Beuret P., Ferreri G., Estier S., 2013. Cosmogenic ^{7}Be and ^{22}Na in ground level air in Switzerland (1994-2011). *Journal of Environmental Radioactivity* 124, 68-73.

Stohl A., Wernli H., James, P., Borqui M., Forster C., Liniger M.A., Seibert P., Sprenger M., 2003. A new perspective of stratosphere-troposphere exchange. *American Meteorological So*ciety, 1565-1573 doi:10.1175/BAMS-84-11-1565

Strahan S.E., Duncan B.N., Hoor P., 2007. Observationally-derived diagnostics of transport in the lowermost stratosphere and their application to the GMI chemistry transport model. *Atmospheric Chemistry and Physics* 7, 1435-2445.

Sykora I., Froehlich K., 2010. Radionuclides as tracers of atmospheric processes. In: Radioactivity in the Environment 16, Chapter 3: 51-88. Edited by Elsevier. doi:10.1016/S1569-4860(09)01603-9

Todorovic D., Popovic D., Djuric G., Radenkovic M., 2005. ^{7}Be to ^{210}Pb concentration ratio in ground level air in Belgrade area. *Journal of Environmental Radioactivity* 79, 297-307.

Tokieda T., Yamanaka K., Harada K., Tsunogai S., 1996. Seasonal variations of residence time and upper atmospheric contribution of aerosols studied with Pb-210, Bi-210, Po-210 and Be-7. *Tellus* 48B, 690-702.

Tositti L., Riccio A., Sandrini S., Brattich E., Baldacci D., Parmeggiani S., Cristofanelli P., Bonasoni P., 2013. Short-term climatology of PM10 at a high altitude background station in southern Europe. *Atmospheric Environment* 65, 145-152.

Tositti L., Brattich E., Cinelli G., Baldacci D., 2014. 12 years of ^{7}Be and ^{210}Pb in Mt. Cimone, and their correlation with meteorological parameters. *Atmospheric Environment* 87C, 108-122. doi:10.1016/j.atmosenv.2014.01.014

Trickl T., Feldmann H., Kanter H.-J., Scheel H.-E., Sprenger M., Stohl A. Wernli H., 2010. Forecasted deep stratospheric intrusions over central Europe: case studies and climatologies. *Atmospheric Chemistry and Physics* 10, 499-524.

Trigo I.F., Bigg G.R., Davies T.D., 2002. Climatology of cyclogenesis mechanisms in the Mediterranean. *Monthly Weather Review* 130, 549-569.

Turekian K.K., Nozaki Y., Benninger L.K., 1977. Geochemistry of atmospheric radon and radon products. *Annual Review of Earth and Planetary Science* 5, 227-255.

Turekian K.K., and Graustein W.C., 2003. Natural Radionuclides in the Atmosphere. Treatise on Geochemistry, Volume 4. In:Ralph Keeling F. (Ed.). Executive Editors: Heinrich D. Holland and Karl K. Turekian. pp. 347. ISBN 0-08-043751-6. Elsevier, p.261-279

Usoskin I., Kovaltsov. G., 2008.Production of cosmogenic ^{7}Be isotope in the atmosphere: full 3D modelling. *Journal of Geophysical Research* 113, D12107.

van Dingenen R, Putaud JP, Martins-Dos Santos S, Raes F, 2005. Physical aerosol properties and their relation to air mass origin at Monte Cimone (Italy) during the first MINATROC campaign. *Atmospheric Chemistry and Physics* 5, 2203-2226.

Viezee W., Singh H.B., 1980. The distribution of beryllium-7 in the troposphere. Implications on stratosphere/tropospheric air exchange. *Geophysical Research Letters* 7, 805-808.

Wilkening M.H., Clements W.E., Stanley D., 1975. Radon222 flux measurements in widely separated regions. In: The Natural Radiation Environment II, pp. 717-730, U.S. Energy and Res. Dev. Admin., Oak Ridge, Tenn.

Winkler R., Dietl F., Frank G., Thiersch J., 1998. Temporal variation of ^{7}Be and ^{210}Pb size distributions in ambient aerosols. Atmospheric Environment 32, 983-991.

WMO-GAW (World Meteorological Organization, - Global Atmosphere Watch), 2004. 1st International Expert Meeting on Sources and Measurements of Natural Radionuclides Applied to Climate and Air Quality Studies, (Gif-sur-Yvette, France, 3-5 June 2003) (WMO TD No. 1201), Report No. 155 [available at ftp://ftp.wmo.int/Documents/PublicWeb/arep/gaw/gaw155.pdf, last accessed 01 August 2013]

Zanis P., Monks P.S., Schuepbach R., Carpenter L.J., Green T.J., Mills G.P, Bauguitte S., Penkett S.A., 2000. In situ ozone production under free tropospheric conditions during FREETEX '98 in the Swiss Alps. *Journal of Geophysical Research* 105 (D1), 24223-24234.

Zanis P., et al., 2003. An estimate of the impact of stratosphere-to-troposphere transport (STT) on the lower free tropospheric ozone over the Alps using ^{10}Be and ^{7}Be measurements. *Journal of Geophysical Research* 108(D12), 8520. doi:10.1029/2002JD002604

CHAPTER 5 – Advection Patterns at the WMO-GAW Station of Mt. Cimone: Seasonality, Trends and Influence on Atmospheric Composition

5.1 Introduction[1]

The aim of this work is to find a relationship, if any, between the seasonality, trends, interannual variability in the advection patterns and the variations in the atmospheric composition observed in a long time series acquired at the WMO-GAW Mt. Cimone station (Italy). In particular, the main species which are considered to this aim, are PM_{10}, atmospheric radiotracers such as ^{7}Be and ^{210}Pb, and O_3, which have been object of a number of studies, especially, but not only, concerning the study of Stratosphere-to-Troposphere-Exchange (STE) at this high altitude site (Bonasoni *et al.*, 1999, 2000a, b; Cristofanelli *et al.*, 2003; Bonasoni *et al.*, 2004; Cristofanelli *et al.*, 2006; Lee *et al.*, 2007; Cristofanelli *et al.*, 2009a, b; Tositti *et al.*, 2012, presented in Appendix II; Cristofanelli *et al.*, 2013; Tositti *et al.*, 2013, 2014, see previous Chapters 2 and 3).

^{7}Be and ^{210}Pb are especially useful as radiotracers to investigate vertical motions in the atmosphere because of their natural contrasted origin: in fact, while ^{7}Be (half-life 53.3 days) is produced by cosmic ray spallation reactions with nitrogen and oxygen in the stratosphere (about 75%) and in the upper troposphere (Johnson and Viezee, 1981; Usoskin and Kovaltsov, 2008), ^{210}Pb (half-life 22 years) is a tracer of continental air masses (Balkanski *et al.*, 1993), being emitted as decay daughter of ^{222}Rn (half-life 3.8 days) emitted from soils (Turekian *et al.*, 1977). Once produced, both radionuclides attach to submicron-sized aerosol particles peaking in the accumulation mode (Papastefanou and Ioannidou, 1995; Winkler *et al.*, 1998; Gaffney *et al.*, 2004; Ioannidou *et al.*, 2005). Thereafter, the main removal mechanisms of ^{7}Be and ^{210}Pb from the atmosphere are wet and dry scavenging of the carrier aerosol (Feely *et al.*, 1989; Kulan *et al.*, 2006). For this reason, the simultaneous measurements of ^{7}Be and ^{210}Pb, together with their ratio, can provide useful information about the vertical motion of air masses as well as on convective activity in the troposphere (Brost *et al.*, 1991; Koch *et al.*, 1996; Tositti *et al.*, 2004; Lee *et al.*, 2004, 2007).

Backward trajectories have long been used in the study of the effect of the origin and pathway of air masses on composition change and trends. A good review of the methods useful to this aim is

[1] This chapter consists of a manuscript in preparation by Brattich E. (Dept. of Biological, Geological and Environmental Sciences-Section of Geology, Università di Bologna), Orza J.A.G. (SCOLAb, Fisica Aplicada, Miguel Hernandez University; Elche, Spain), Tositti L. (Dept. of Chemistry, Università di Bologna).

available in Fleming *et al.* (2012). While a large number of studies sort air masses by designated a priori geographical sectors, the method to cluster the trajectories with a statistical technique and then to analyse the concentrations at the receptor site for each trajectory classification, to see whether each classification is chemically distinct, is also quite common: to cite only a few examples, clusters of back trajectories were used by Huang *et al.* (2010) to study 15 years of particulate matter concentration at Alert (Greenland), monthly average ozone and mercury transport to the Arctic by Eneroth *et al.* (2007), to compare the composition for Alert and Barrow in the Arctic (Sharma *et al.*, 2006), to derive seasonal air masses origin in Beijing, China (Xia *et al.*, 2007), to study three years of ozone measurements at Mace Head, Ireland (Cape *et al.*, 2000), to identify trajectory types at various Atlantic Ocean sites (Virginia, Bermuda, Cape Point, Amsterdam Island) (Moody *et al.*, 1989), to study 10 years of tracer levels at Ny-Ålesund, Svalbard (Eneroth *et al.*, 2003), and to analyse CO and O_3 measurements at Hong Kong, China (Wang *et al.*, 2004). The variability in the occurrence of each trajectory group and the assessment of trend in association with atmospheric circulation indexes, such as the North Atlantic Oscillation index (NAOi), is less common (Orza *et al.*, 2013).

The use of both air masses classification and atmospheric radiotracers is not so usual but has already been objective of some studies. The air mass origin influence on ^{7}Be and ^{210}Pb activities in Málaga (Southern Spain) has been studied with the use of clusters of back-trajectories by Dueñas *et al.* (2011), who associated polar maritime air masses to low ^{7}Be and ^{210}Pb activities; also, for the first time an association of continental flows from Northern Africa with high concentrations of both radionuclides was underlined by this study, which might result from African dust uplifting after downward movement of air from the upper troposphere. The influence of air mass type on the ^{7}Be and ^{210}Pb concentrations in the city of Edinburgh (Scotland, UK) was studied by Likuku (2006), who used a broad a priori classification of the trajectories between continental (higher ^{210}Pb activities) and oceanic air masses, and at Bermuda by Arimoto *et al.* (1999), who associated the highest loadings for ^{7}Be and ^{210}Pb to transport from the NW of Bermuda, whereas low activities were linked to transport from E and SE. Moody *et al.* (1995) linked highest ^{7}Be values at Bermuda to subsiding flow behind surface cold fronts moving eastward over the North Atlantic. The same kind of downward transport was observed in the Northern Apennines and the Alps by Bonasoni *et al.* (2000a) and by Zanis *et al.* (2003). The source areas of ^{7}Be and ^{210}Pb in Northern Finland have been investigated by means of trajectory statistics by Paatero and Hatakka (2000), showing that the highest ^{210}Pb concentrations are associated to continental air masses originating in Central Russia, whereas high ^{7}Be activities are found in air masses from Central Russia and air masses coming from southwest during springtime. Clustering techniques have been also applied to back trajectories by Lozano *et al.* (2012) in south-western Spain to identify the origin of the air

masses giving rise to different ranges of ^{7}Be and ^{210}Pb: once again, air masses with clear continental influence are associated to the highest ^{210}Pb values, whereas air masses from middle latitudes, such as from the Canary Islands, Western Mediterranean Basin and the north of Africa bring on the highest ^{7}Be concentrations. Some events of elevated or low ^{7}Be concentrations in Canary Islands have been analysed in connection with different origin of the air masses by Hernández *et al.* (2008), who pointed out that high ^{7}Be activities are due to subsidence and may be concurrent with African dust outbreaks. Back trajectories and atmospheric radionuclides were also used to assess the impacts of stratospheric and pollution influences on ozone at Bermuda by Li *et al.* (2002). The positive correlation of surface O_3 with ^{7}Be and ^{210}Pb is due to the strong subsidence behind cold fronts, resulting in the mixing of middle-tropospheric air with continental outflow in the air arriving at Bermuda.

Back trajectories statistical methods have also already been used to study atmospheric composition at a number of high altitude sites. Salvador *et al.* (2010) investigated the influence of synoptic weather patterns and long-range transport episodes on the concentrations of several compounds related to different aerosol sources (EC, OC, SO_4^{2-}, Ca^{2+}, Na^{+}, K^{+}, ^{210}Pb and dicarboxylic acids) registered in PM_{10} or $PM_{2.5}$ aerosol samples collected at three high altitude background sites by means of clusters of back trajectories. Transport of NO_X, CO, and O_3 to four alpine GAW stations was investigated by trajectory residence time analysis (Kaiser *et al.*, 2007). Residence time of air masses was also applied to categorize surface ozone at Arosa (Switzerland) by Pochanart *et al.* (2001). The same method of residence time of trajectories was also used to study SO_2 data acquired at Sonnblick (Austria) (Tscherwenka *et al.*, 1998) and more recently to study European source and sink areas of CO_2 with a Lagrangian dispersion model at the high alpine site Jungfraujoch (Switzerland) (Uglietti *et al.*, 2011). Concentration weighted trajectory was applied to apportion the sources of black carbon over the western part of trans-Himalayas (Babu *et al.*, 2011). Air masses origin was also studied by means of back trajectories to understand the different CO concentrations found at two background sites, one of which located at a high altitude, by Scheel *et al.* (1998), to assess the influence of south foehn on the ozone mixing ratios at the high alpine site Arosa (Campana *et al.*, 2005), to corroborate the source region of a Saharan dust transport at Jungfraujoch, identified by means of mineralogical and chemical composition (Schwikowski *et al.*, 1995), and to investigate possible reasons of trends identified in long-term ozone measurements at two background mountain sites (Kislovodsk High Mountain Station in Caucasus, Russia -2070 m asl- and the Jungfraujoch in Switzerland) (Tarasova *et al.*, 2009). Gerasopoulos *et al.* (2001) examined the source regions of ^{7}Be at four high-altitude stations in Europe by means of the concentration weighted trajectory method, showing that typically very low ^{7}Be concentrations are

advected from low levels and especially from ocean areas. A path of quite high ^{7}Be activities is observed for trajectories descending 4500 m, stretching from the northwest to the measurement sites, linked to stratospheric intrusions at the mountain stations (Stohl *et al.*, 2000). Very recently, Cuevas *et al.* (2013) studied O_3 transport pathways at Izaña (Tenerife, Spain) by means of the so called "mean concentrations at receptor" method, also with the support of atmospheric radiotracers data: a positive correlation throughout the year between ozone and potential vorticity and ^{7}Be was attributed to the transport from the middle and upper troposphere.

Some trajectory statistical methods were also applied to study atmospheric composition at Mt. Cimone site. The residence time analysis suggested by Ashbaugh *et al.* (1985) was applied by Wotawa *et al.* (2000) to identify the O_3 source regions. Bonasoni *et al.* (2000b) evaluated the frequency of different air mass origins to the Mt. Cimone area as a function of trajectory starting positions within the domain 80° N, 50° W, and 20° N, 50° E, dividing the domain into six a priori identified regions (Arctic, Atlantic Ocean, Continental Europe, Eastern Europe, Mediterranean Basin and Saharan-African region) and then applied the trajectory statistics method of Seibert *et al.* (1994) to study the relation of ozone concentrations to air mass path. This a priori classification of geographical source regions was then used in all successive studies concerning air mass origin and atmospheric composition at this site (Balkanski *et al.*, 2003; Fischer *et al.*, 2003; Gobbi *et al.*, 2003; Putaud *et al.*, 2004; Cristofanelli *et al.*, 2006; Marenco *et al.*, 2006; Marinoni *et al.*, 2008; Cristofanelli *et al.*, 2007, 2009b). The trajectory statistics method of Seibert *et al.* (1994) was then used also by Marinoni *et al.* (2008) to evaluate the correlations between air mass origins and aerosol physical parameters, while the potential source contribution function (PSCF) of Ashbaugh *et al.* (1985) was applied to investigate PM_{10} transport to the site by Tositti *et al.* (2013; Chapter 2), but no cluster of back trajectories has been previously applied to study thoroughly the advection patterns at this site and the links between atmospheric composition and air mass origin.

This Chapter is dedicated to the finding of the main advection patterns at Mt. Cimone and to examine how the variations in the atmospheric composition can be related to the changes observed in the flow patterns, both from a seasonal and an interannual point of view, analysing the data acquired at Mt. Cimone from 1998 till 2011. The relationship of flow patterns and atmospheric composition with NAO is also investigated. The presence of trends in the monthly time series is carefully examined.

This Chapter consists of four sections. Section 5.2 describes the measurements techniques and the statistical methods used in the cluster analysis of back trajectories, the analysis of significant differences by advection patterns and the assessment of trends. Section 5.3 presents and discusses the results, further divided as follows: Subsection 5.3.1 describes the main advection patterns found

by the cluster analysis of back trajectories; Subsection 5.3.2 analyses the relationships between advection patterns and meteorological parameters/other atmospheric components; in Subsection 5.3.3 a temporal analysis of the monthly time series and a trend analysis is done; in Subsection 5.3.4 associations of air flow types and meteorological/atmospheric variables with NAO are examined. Finally, Section 5.4 summarizes our main conclusions.

5.2 Material and methods

Mt. Cimone (44°11' N, 10°42' E, 2165 m asl), the highest peak of the Italian northern Apennines, hosts a global WMO-GAW station maintained by the Italian Meteorological Office since 1941 and a research platform managed by the Institute of Atmospheric Sciences and Climate of the Italian National Research Council (ISAC-CNR). The main characteristics of this high-altitude background site have been already described in previous Chapters 2, 3 and 4.

As a WMO-GAW station, a number of atmospheric compounds are measured at Mt. Cimone since a long time. Besides meteorology, the Italian Meteorological Office is responsible for CO_2 data, presently constituting the longest time series of this fundamental greenhouse gas in Europe, dating back to 1979, whereas ISAC-CNR has been collecting tropospheric ozone data since 1996 and carbon monoxide since 2007 (the three datasets are available at http://ds.data.jma.go.jp/gmd/wdcgg/wdcgg.html); since 2000 ISAC-CNR has been continuously recorded concentration and size distribution of particles with optical diameter between 0.30 and 20 μm by using an optical particle counter (OPC, Mod. GRIMM 1.108). These measurements allow the determination of a fine mode (0.3 μm ≤ Dp < 1 μm) and a coarse mode (1 μm ≤ Dp ≤ 20 μm) of particles with a 1-minute time resolution (data available at EBAS database http://ebas.nilu.no/). Since July 2005 ISAC-CNR has been measuring also black carbon data (available at EBAS database http://ebas.nilu.no/).

In this framework the Department of Chemistry of the University of Bologna has measured ^{7}Be, ^{210}Pb and aerosol mass load in the form of PM_{10} (airborne particulate matter with a mean aerodynamic diameter lower than 10 μm) since the early 1990's, even if measurements became regular only since 1998 following the acquisition of a Thermo-Environmental PM_{10} high-volume sampler with average flow rate of 1.13 m^3 min^{-1} at STP. The time resolution of aerosol sampling is about 48 hours (manual change of the filter, approximately 115-175 samples per year). Details of PM_{10}, ^{210}Pb and ^{7}Be sampling and measurement at Mt. Cimone have been given in previous Chapters 2 and 3.

Measurements at Mt. Cimone from different research groups, as well as meteorological and atmospheric parameters, such as temperature, pressure, relative humidity, wind speed and tropopause height (determined from radiosoundings at S. Pietro Capofiume station, the closest ground based station in the Po valley for which this observational activity is available) were retrieved together and averaged to the same time resolution of PM_{10} and radionuclides for statistical homogenization of data.

In order to analyse the origin of the air masses arriving at the measurement site, 96-hour 3D kinematic back trajectories starting four times a day (00, 06, 12, 18 UTC) at three heights (1400, 2200 and 3000 m asl) have been calculated with the HYbrid Single-Particle Lagrangian Integrated Trajectory (HYSPLIT) model version 4.8 (Draxler and Hess, 1997, 1998; Draxler, 1999; Draxler and Rolph, 2003).

The first issue encountered in the calculation of the back trajectories was the choice of the meteorological fields: in fact, meteorological fields are associated to the strongest source of errors (Stohl *et al.*, 2001) when calculating back trajectories, and they may eventually influence the outcome of the trajectory clustering (Cabello *et al.*, 2008a).

Due to the coarse resolution of the meteorological model, the topography of Mt. Cimone is poorly modelled in all of the meteorological fields that were available to us (NCEP/NCAR reanalysis available at the NOAA Air Resources Laboratory, which considers a height of 550 m asl for Mt. Cimone; 1° resolution ERA Interim dataset, considering the topography at Mt. Cimone only 249 m asl; 1.5° ERA Interim, which considers 277 m asl for Mt. Cimone), and we concluded that our best option (still not good) was to choose the National Center for Environmental Prediction (NCEP)/National Center for Atmospheric Research (NCAR) reanalysis with a 2.5° latitude-longitude resolution, 17 pressure levels from 1000 to 10 hPa, and 6 hourly data. The vertical movement of the air parcels was calculated from the vertical velocity fields. As for the choice of the heights, we considered one height just above the monitoring site (2200 m asl), one 800 m higher (3000 m asl, just at the beginning of the free troposphere) and one 800 m below (1400 m asl, above the model terrain's height for the measurement site).

Trajectories have been classified into homogeneous groups by a robust cluster procedure based on the *k*-means algorithm (Dueñas *et al.*, 2011; Orza *et al.*, 2013; Perrone *et al.*, 2013), with hourly longitude and latitude as input variables (Moody and Galloway, 1988). The aim of the cluster analysis is to classify a large data set into non-predefined dominant groups such that variance within each cluster is minimized and variance between clusters is maximized. The great-circle distance, i.e., the shortest distance measured along the surface of the sphere, has been utilized as the similarity measure in the clustering process. The *k* – means algorithm groups a given dataset into a

pre-specified number of clusters *k*. A cluster is represented by its centroid, defined as the average over the trajectories belonging to that cluster. In a first step, *k* starting centroids are randomly chosen from the trajectory set. Once the trajectories are allocated into the cluster to which centroid they are closest, the centroids are recalculated by averaging all the trajectories belonging to the same cluster in an iterative process until no changes in cluster assignment are found. The appropriate number of clusters has been assessed following Dorling *et al.* (1992). The number of clusters *k* is successively reduced by one, from 15 down to 3 clusters, and the total within-cluster root mean squared distance (RMSD) between individual trajectories and their centroids is then examined as a function of the number of clusters. The clustering result is known to present some dependence on the selected starting centroids: thus, for each *k*, 1000 replicate clustering solutions are previously computed and the solution with the smallest total RMSD is retained as the best solution for that *k*.

This clustering procedure has already been used to identify the main advection patterns and subsequently relate air masses and aerosol size distributions at SE Spain (Cabello *et al.*, 2008b), air masses and radionuclide activities in Málaga (Dueñas *et al.*, 2011), air masses and $PM_{2.5}$ and PM_1 levels and composition in Lecce (southern Italy) (Perrone *et al.*, 2013). To detect statistically significant differences in the analysed meteorological and atmospheric parameters according to the identified clusters, without any a priori assumption of their distribution (Brankov *et al.*, 1998), the Kruskall-Wallis test has been used. Whenever significant differences among the groups were found, pairwise Mann-Whitney tests were performed to identify which pairs were significantly different. Conservatively, *p*-values in the latter were compared against adjusted significance levels α using the Dunn-Sidák correction for multiple comparisons $\alpha = 1 - (1 - \alpha_t)^{1/n}$, where $n = k\,(k-1)/2$ is the number of pair-wise comparisons done between *k* categories, with overall significance $\alpha_t = 0.05$.

The analysis of individual situations has been done with composite synoptic charts of 700, 850 and 1000 hPa geopotential height, which were computed with data from NCEP/NCAR re-analysis project database (Kalnay *et al.*, 1996), available from the Earth System Research Laboratory, Physical Sciences Division, of the USA National Oceanic and Atmospheric Administration (NOAA) at http://www.esrl.noaa.gov/psd/.

The monthly time series considered in this work have been examined for significant trends over the study period by a number of nonparametric statistical methods, mainly based on the Mann-Kendall (M-K) tau test to assess the significance of monotonic trends and the Theil-Sen (T-S) slope estimate for trend magnitude.

The significance of a trend is often overestimated by serial correlation; moreover, the presence of a trend alters the estimate of the serial correlation. A first estimation of the correlation coefficients at different lags was done by computing the autocorrelation function (ACF) for each time series, showing that they present, in general, some degree of serial correlation. In addition they show seasonality; therefore, two methods of trend analysis have been used with the aim of removing, or reducing, the influence of seasonality and lag-1 autocorrelation in the monthly data:

(1) The seasonal Kendall test (Hirsch *et al.*, 1982), which applies the M-K trend test separately for each month and then combines the results. (2) The Yue-Pilon (Y-P) procedure (Yue *et al.*, 2002) applied to the previously de-seasonalized monthly time series, to remove the influence of the month-to-month correlations in the significance of the trends. The Y-P procedure comprises several steps: the time series is linearly de-trended using the T-S slope, and the serial autocorrelation of the residuals is removed. Then, the discarded linear trend is added back to the remaining time series, and the M-K test is applied.

Seasonal-trend decomposition of the time series was used to obtain the de-seasonalized time series, which were subsequently analysed by the Y-P procedure. The decomposition technique used in this work (STL-decomposition hereafter) is based on a nonparametric regression technique (LOESS, locally weighted low-degree polynomial regression) recursively applied to the seasonal and trend components (Cleveland *et al.*, 1990). Additionally, the resulting (nonlinear) trend component has been used for the visual assessment of the long-term behaviour of the time series.

The association between the frequencies of each advection pattern and the measurements made at the sampling site, as well as their association to the NAO, has been examined for the de-trended monthly time series and for the seasonal means via least-square regression analysis with statistical significance evaluated by a two-tailed *t* test. Since relationships are not necessarily linear, the nonparametric Kendall rank test has also been used to identify any statistically significant association without any a priori assumption of their form. Spearman correlation coefficients have been computed for the cases with significant association.

5.3 Results and discussion

5.3.1 Characteristics of the main advection patterns

The number of groups in which the trajectories are found to be clustered is different at each arriving height: while at 1400 m only 6 clusters have been found, at 2200 m the trajectories are grouped in 8 clusters, and at 3000 m the trajectories can be classified into 7 groups. Figure 5.1 shows the

centroids (representative trajectory) of the clusters at 1400, 2200 and 3000 m asl and the relative percentage frequency of each flow pattern on the whole 1998-2011 period.

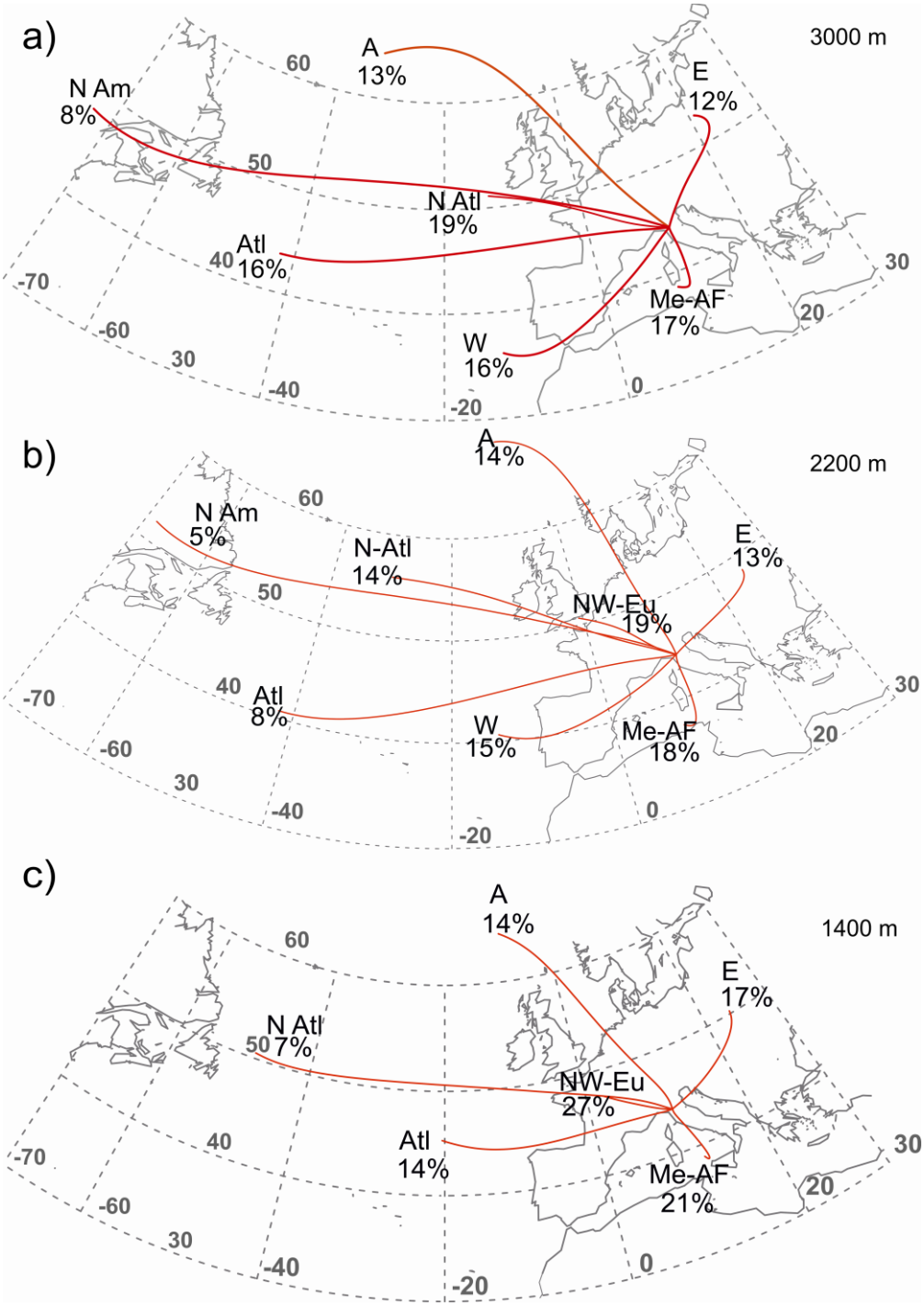

Figure 5.1(a,b,c) *Centroids of the trajectory clusters identified for trajectories arriving at: a) 3000 m asl; b) 2200 m asl; c) 1400 m asl for the 12-year study period. The flow patterns are identified as follows: A is for Arctic, E is for Eastern, Me-AF is for Mediterranean-Africa, Atl is for Atlantic, N Atl is for Northern Atlantic, N Am is for North America, NW-Eu is for North Western-Europe. The percentage indicates the frequency of occurrence of each flow pattern in the whole 1998-2011 period.*

Most of the trajectories at each height correspond to westerly flows; the name assigned to each flow pattern depends on its region of provenance (rather than from associated wind speeds or particular airmass type). At 3000 m westerly trajectories are classified into Northern Atlantic (N Atl), North America (N Am), Atlantic (Atl), and Western (W), together representing the 59% of the flows. The remaining trajectories are classified into Arctic (A), Eastern (E), Mediterranean-Africa (Me-Af), representing the 13%, 12% and 17% of the flows, respectively. At 2200 m a further flow type classified as North Western-Europe (NW-Eu) is identified, separating slow continental north-westerly flows from faster air masses coming from the Atlantic Ocean. This further classification represents the 19% of the trajectories and is decreasing the importance of the Atlantic air masses to 8% at this height. The frequency of other flow types is only slightly changed from the 3000 m height. At 1400 m the number of clusters is reduced to six and this appears mainly as the result of joining the Northern Atlantic with the North America pattern and the Atlantic with the West cluster. At this height slow flow patterns such as North Western-Europe, Eastern and Mediterranean-Africa gain importance with respect to fast flow patterns such as Northern Atlantic and Atlantic. The height of 1400 m is not further analysed in the following sections as it is neither the real topography height nor the model one.

Figure 5.2 shows the mean heights of the representative trajectories that reach the study site at 2200 m versus end-point time. The Arctic and North-American trajectories reach the most elevated heights, even if the North American ones go to lower heights when approaching the site, and again to higher heights before finally reaching it, in order to overcome the Alps. North Western-Europe and Eastern flows do not change very much their height during their travel, whereas Western, Atlantic and (more specifically) Mediterranean-Africa trajectories generally arrive from very low levels.

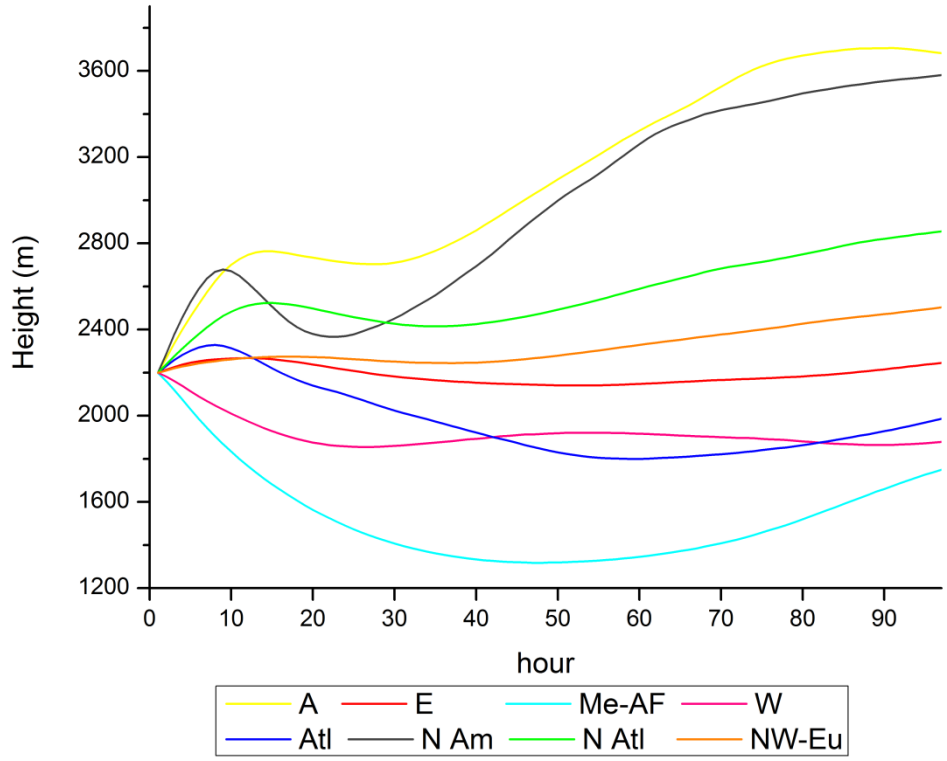

Figure 5.2 *Plot of the heights of the representative trajectories at 2200 m asl vs. end-point time.*

Figure 5.3 represents the monthly variation of the air mass patterns arriving at 3000 and 2200 m asl. A summary of the major characteristics of the identified advection patterns is as follows:

- A: advection of fast and high air masses originating in the Arctic/polar regions. This trajectory type, more frequent in autumn and winter, is found at each of the three arrival heights with a rather stable percentage frequency (13% at 3000 m, 14% at 2200 m and 1400 m).
- E: advection of relatively slow and low air masses from East. This flow type is more frequent in April, May and September and groups the 12% of the 3000 m trajectories, 13% of the 2200 m, gaining importance at the lowest 1400 m level.
- Me-Af: relatively short and low Mediterranean and North-African air masses. This kind of trajectories is frequent all-yearlong but most of all in spring and autumn; this group is associated with 17% of the 3000 m trajectories, 18% of the 2200 m ones, being more important (21% of the trajectories) at 1400 m.
- W: advection of relatively slow and low air masses from West, more frequent in July and August. This flow pattern is identified only at 3000 (16% of the trajectories) and 2200 m (15% of the trajectories).
- Atl: relatively fast and low air masses coming from the Atlantic Ocean. This advection pattern is mostly occurring from October to April. It groups the 16% of the trajectories at 3000 m

and the 14% of the trajectories at 1400 m, whereas at the midlevel of 2200 m only the 8% of the trajectories fall into this category.

- N-Am: polar fast and high air masses that originate as continental air over North America. This air mass type is almost non-existent in summer months, mostly occurring from October to April. This advection pattern is not identified at the lowest 1400 level; at higher levels is anyway a "rare" flow pattern (8% of the trajectories at 3000 m and 5% at 2200 m).
- N-Atl: relatively fast but not very high air masses coming from the Northern-Atlantic Ocean. Frequent all-yearlong but most of all in July. This group of trajectory is more important at higher levels (19% at 3000 m, 14% at 2200) whereas at 1400 m only the 7% of the trajectories fall into this category.
- NW-Eu: slow and not very high continental air masses coming from North Western-Europe. More frequent in summer months. This flow pattern is identified only at 2200 and 1400 m, where it is also very frequent (27% of the trajectories; only 19% at 2200).

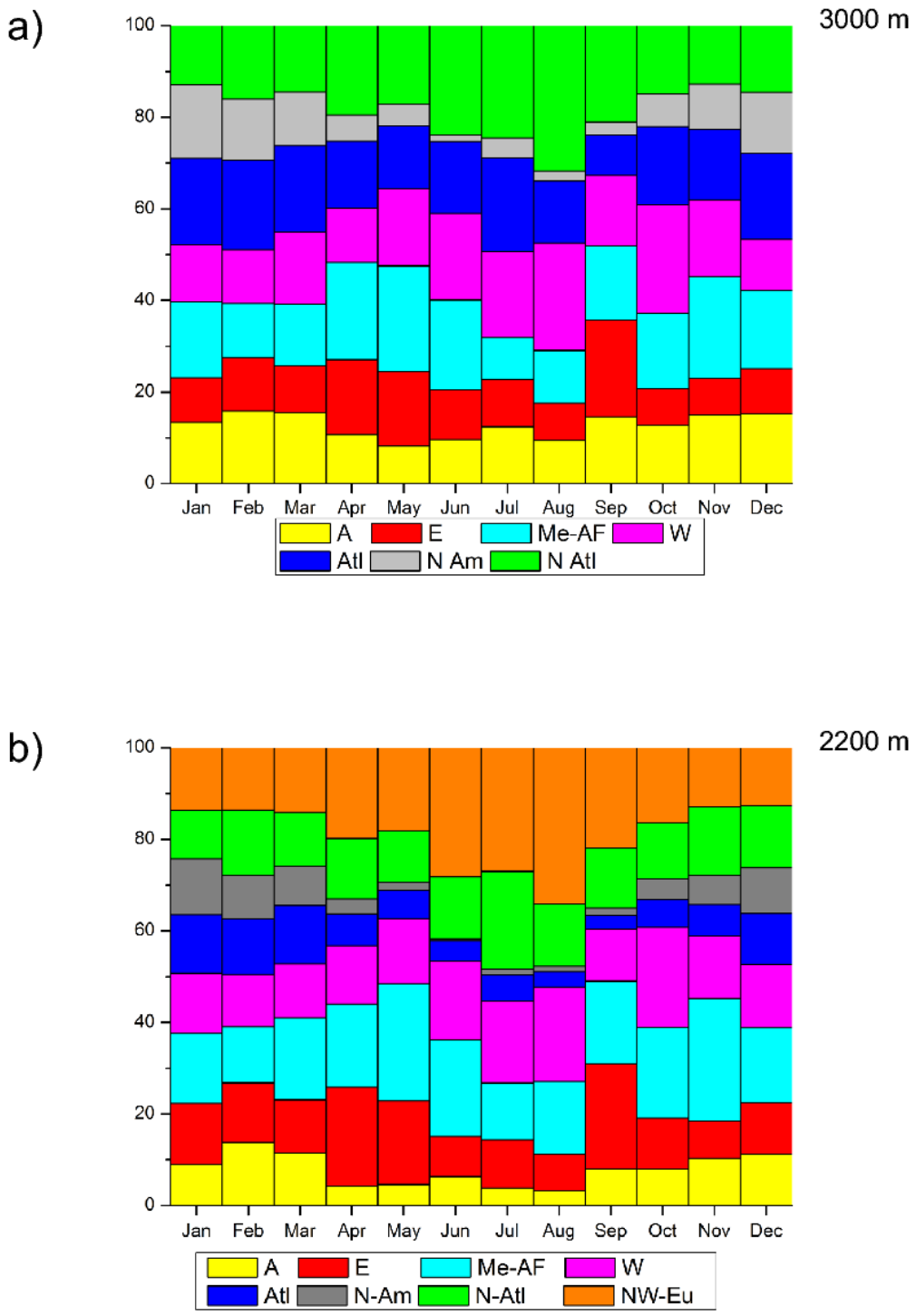

Figure 5.3(a,b) *Monthly variation of the frequencies of the identified advection patterns at a) 3000 m asl; b) 2200 m asl.*

5.3.2 Atmospheric and meteorological parameters by advection pattern

The next step of the research is to analyse the values of atmospheric compounds and meteorological parameters associated to each advection pattern. As the PM_{10} filters at the station are manually changed, sampling time is not uniform. Anyway as most of the samples were collected over

48 hours (sampling approximately 3250 m^3 of air), in order to safely apply statistical techniques data have been firstly homogenized by selecting only those samples which collected a volume between 2700 and 3700 m^3. One sample was attributed to one advection pattern only if at least the 60% of the calculated trajectories ending at the site during the sampling corresponded to that advection pattern. However, the case of fast and frequent change of the flows during the sampling has also been carefully examined.

Figure 5.4 and 5.5 show box plots of meteorological parameters such as pressure, wind speed, relative humidity, precipitation, temperature, tropopause height (Figure 5.4) and atmospheric compounds (Figure 5.5), such as CO_2, CO, O_3, PM_{10}, atmospheric radiotracers ^{7}Be and ^{210}Pb, fine and coarse particles number densities, black carbon as well as some interesting ratios such as $^{7}Be/^{210}Pb$, $^{7}Be/PM_{10}$, $^{210}Pb/PM_{10}$ representing mean, median, minimum and maximum values, 5^{th} and 95^{th} percentile values, associated to each flow pattern at 2200 m and at 3000 m asl. Table 5.1 (2200 m) and Table 5.2 (3000 m) report a summary statistics of each variable by advection pattern, reporting arithmetic mean (AM), standard deviation (SD), skewness and kurtosis (Skew and Kurt), minimum, maximum and percentiles (25^{th}, 50^{th} and 75^{th}). Last column indicates the statistically different flows identified through Mann-Whitney tests with the Dunn-Sidák correction applied to the α_t values (0.05). Figure 5.4 and 5.5, as well as Table 5.1 and 5.2, refer to the "pure cases", i.e., the samples attributed to only one advection pattern (when the 60% of the trajectories ending at Mt. Cimone during the sampling belong to that advection pattern): this way, the flow patterns can be better characterized.

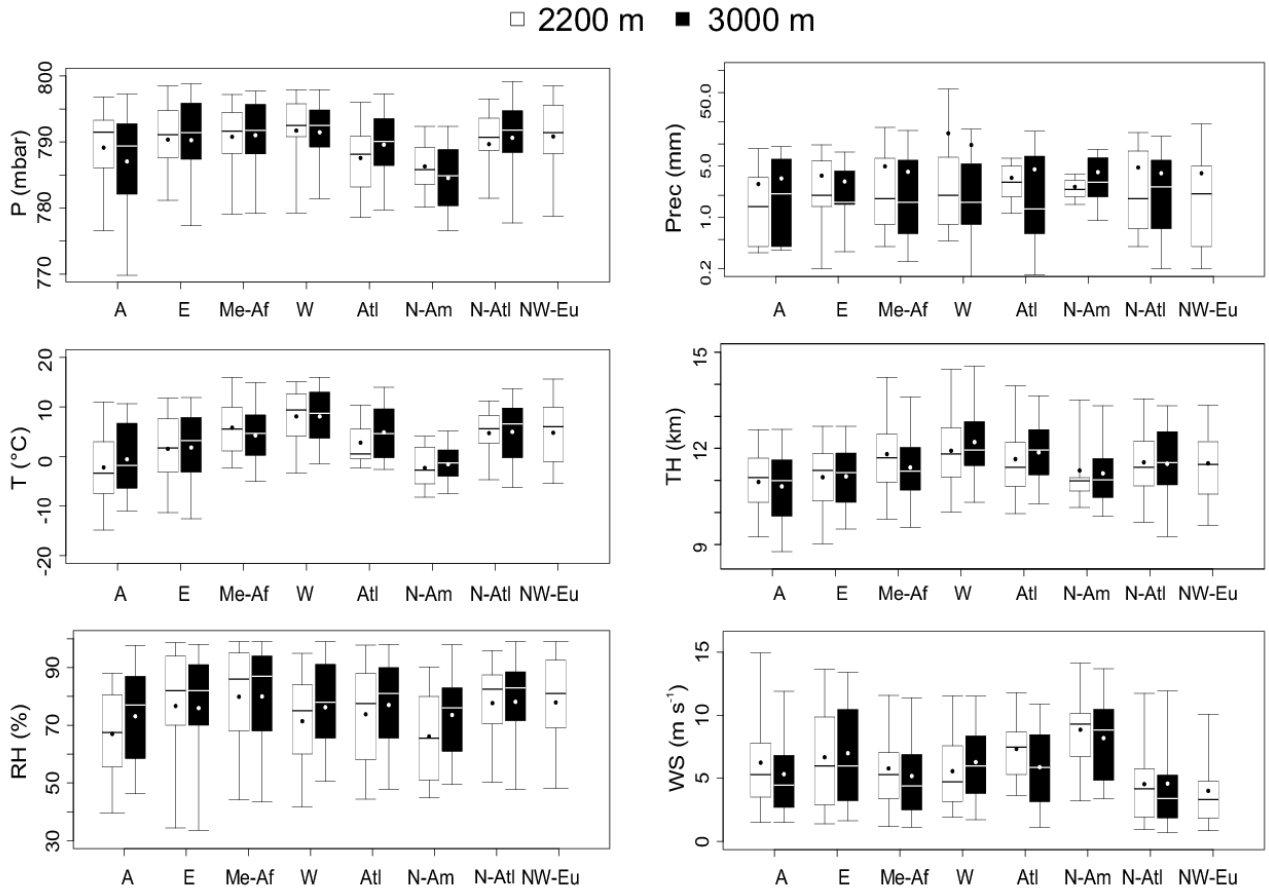

Figure 5.4 *Box plots of meteorological variables (P = pressure, T = temperature, RH =relative humidity, TH = tropopause height, WS = wind speed) versus air flows arriving at 2200 m (white box plots) and at 3000 m asl (black box plots). The horizontal bold line in each box represents the 50th percentile (median), the circle represents the mean value, lower and upper boundaries locate the 5th and 95th percentile of the values and whiskers locate the minimum and maximum values.*

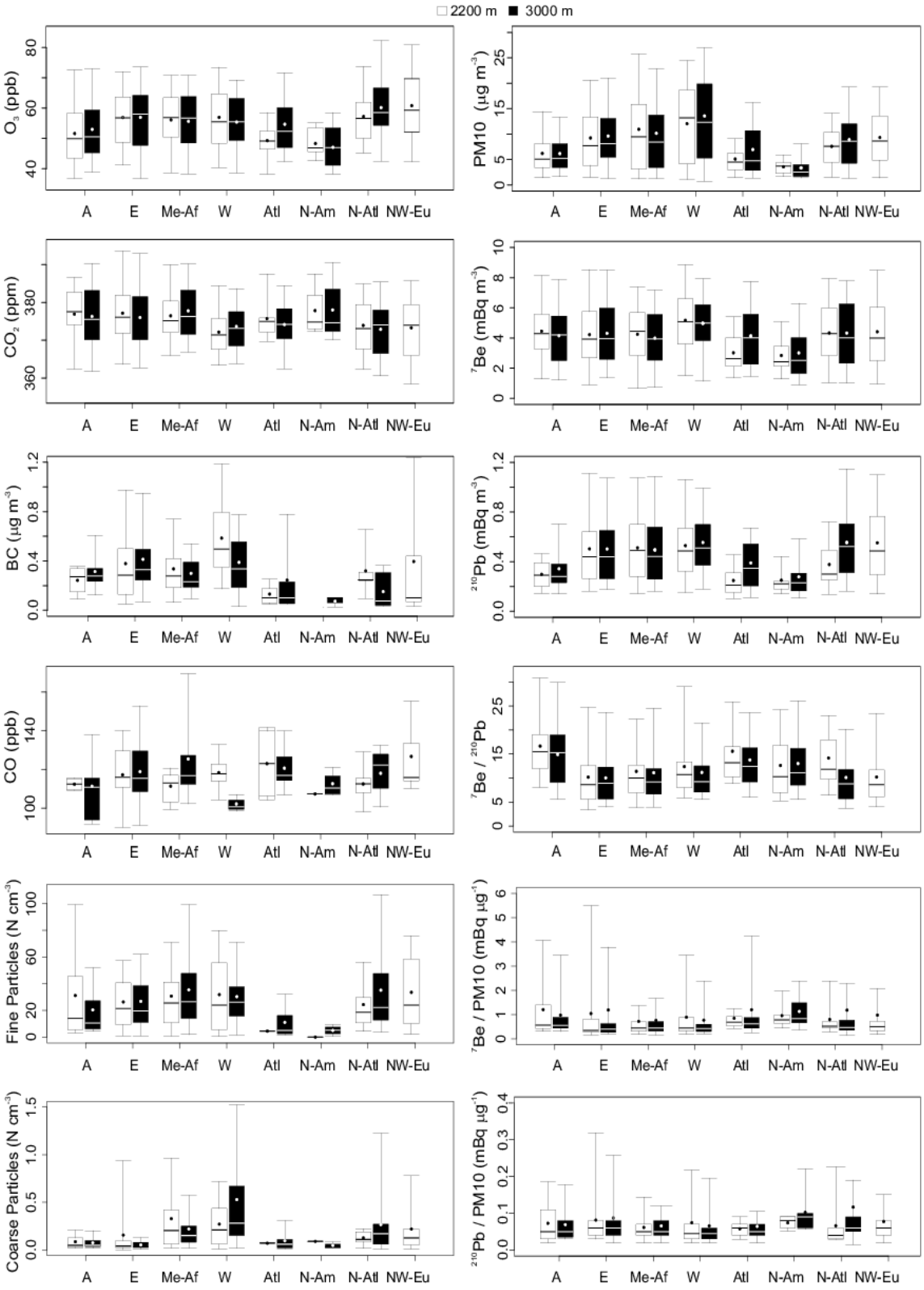

Figure 5.5 *Same as Figure 5.4, but for atmospheric gases (O_3, CO_2, CO), black carbon (BC), fine and coarse particles number densities, PM_{10}, atmospheric radiotracers ^{7}Be and ^{210}Pb, ratio $^{7}Be/^{210}Pb$, ratio $^{7}Be/PM_{10}$, ratio $^{210}Pb/PM_{10}$, versus air flows arriving at 2200 (white box plots) and at 3000 m asl (black box plots).*

8 clusters - 2200 m											
		AM	SD	Skew	Kurt	Min	Pct25	Pct50	Pct75	Max	Diff (α = 0.0064)
P (mbar)	A (37)	789	7	-1.0	3.0	771	786	792	793	799	a,b,c
	E (74)	790	6	-1.6	8.1	761	788	791	795	800	a,b,c
	Me-Af (102)	791	5	-1.0	3.6	776	788	792	794	800	a
	W (53)	792	6	-1.6	6.1	769	791	793	796	802	a
	Atl (26)	788	6	0.0	2.5	778	784	788	791	800	c
	N-Am (10)	786	4	0.0	2.1	779	784	786	789	793	b,c
	N-Atl (45)	790	7	-2.6	11.7	759	789	791	794	798	a,b,c
	NW-Eu (83)	791	6	-1	3.9	772	788	791	796	800	a,b
T (°C)	A (37)	-2.2	7.8	0.2	2.4	-17.8	-7.5	-3.4	3.0	13.4	d
	E (74)	1.5	7.2	-0.3	2.7	-15.4	-3.1	1.7	7.5	17.0	c,d
	Me-Af (102)	5.8	5.8	0.0	2.5	-11.2	1.1	5.6	9.9	17.2	a,b
	W (53)	8.1	5.8	-0.7	2.6	-6.0	4.1	9.4	12.6	16.2	a
	Atl (26)	2.8	4.9	1.3	4.2	-2.9	-0.5	0.5	5.4	17.5	c,d
	N-Am (10)	-2.3	4.6	0.3	2.0	-8.8	-5.4	-2.8	1.2	5.7	d
	N-Atl (45)	4.7	5.2	-0.7	2.8	-8.6	2.6	5.6	8.3	12.7	b,c
	NW-Eu (83)	4.8	7.1	-0.1	2.0	-10.3	-1.1	6.0	10.0	18.2	b,c
RH (%)	A (36)	67	17	-0.5	3.2	19	57	68	80	99	c
	E (69)	77	22	-1.4	4.4	10	70	82	94	100	a,b
	Me-Af (102)	80	18	-0.9	2.7	35	68	86	95	100	a
	W (53)	71	17	-0.6	3.0	26	60	75	84	99	b,c
	Atl (26)	74	19	-0.5	2.2	32	59	78	88	99	a,b,c
	N-Am (10)	66	17	0.3	2.2	41	52	66	79	98	a,b,c
	N-Atl (44)	78	14	-0.9	3.5	36	71	83	87	99	a,b
	NW-Eu (83)	78	17	-0.7	2.8	34	69	81	93	99	a,b
Prec (mm)	A (7)	2.8	3.7	1.4	3.7	0.3	0.4	1.4	3.5	10.4	a
	E (19)	3.7	3.3	0.8	2.4	0.2	1.4	2.0	5.9	10.8	a
	Me-Af (43)	5.0	6.5	2.1	7.1	0.4	0.8	1.8	6.4	27.5	a
	W (15)	14.0	40.6	3.4	12.8	0.2	0.8	2.0	6.6	160	a
	Atl (4)	3.5	2.6	0.6	2.1	0.8	2.5	3.0	4.0	7.0	a
	N-Am (3)	2.6	1.3	0.3	1.5	1.4	1.9	2.4	3.2	4.0	a
	N-Atl (9)	4.8	5.9	1.5	4.1	0.4	0.7	1.8	8.0	18.4	a
	NW-Eu (38)	4.0	5.5	2.3	7.7	0.1	0.5	2.1	4.9	23.6	a
TH (m)	A (37)	10951	1056	-0.3	2.5	8543	10313	11092	11698	12712	b
	E (60)	11099	1108	-0.5	2.6	8500	10360	11312	11832	13042	b
	Me-Af (89)	11820	1366	0.9	4.3	9232	10950	11703	12444	16325	a
	W (50)	11925	1400	0.6	3.6	9137	11125	11824	12614	15785	a
	Atl (25)	11665	1325	0.8	3.4	9438	10817	11406	12182	15133	a,b
	N-Am (9)	11310	1273	1.3	3.8	9876	10672	10986	11086	14125	a,b
	N-Atl (42)	11564	1138	0.1	3.2	8979	10866	11411	12228	14167	a,b
	NW-Eu (75)	11532	1324	0.5	3.5	8726	10579	11502	12241	15455	a,b

WS ($m\ s^{-1}$)	A [37]	6.2	4.3	1.6	5.7	0.6	3.5	5.3	7.8	20.7	a,b,c
	E [73]	6.7	4.6	1.2	5.6	0.5	2.9	6.0	9.9	26.3	a,b,c
	Me-Af [102]	5.8	3.6	1.2	5.1	0.1	3.4	5.3	7.0	18.1	a,b,c
	W [53]	5.6	3.4	1.1	4.1	0.3	3.2	4.7	7.6	17.0	b,c
	Atl [26]	7.3	2.9	0.6	3.1	2.4	5.3	7.5	8.6	14.6	a
	N-Am [10]	8.9	3.8	-0.2	2.2	3.0	7.1	9.3	10.1	14.4	a,b
	N-Atl [45]	4.5	3.3	1.0	3.5	0.2	1.9	4.2	5.8	13.0	c,d
	NW-Eu [83]	4.0	3.1	1.6	5.8	0.4	1.8	3.3	4.8	16.2	d

		AM	**SD**	**Skew**	**Kurt**	**Min**	**Pct25**	**Pct50**	**Pct75**	**Max**	**Diff (α = 0.0064)**
O_3 (ppb)	A [37]	52	12	1.0	3.7	34	43	50	58	83	b,c
	E [72]	57	11	0.7	4.8	34	49	57	64	98	a,b
	Me-Af [97]	56	10	-0.2	2.9	34	50	57	63	82	a,b
	W [52]	57	11	0.7	3.5	39	49	55	65	90	a,b
	Atl [26]	49	7	0.2	3.6	35	46	49	52	66	c
	N-Am [9]	48	5	0.4	1.6	42	46	47	54	55	b,c
	N-Atl [44]	57	8	0.4	2.7	41	50	57	62	75	a
	NW-Eu [80]	61	13	0.6	4.2	35	52	59	70	109	a
CO_2 (ppm)	A [34]	377	7	-0.6	2.7	361	374	378	383	390	a
	E [69]	377	9	0.1	2.9	354	372	376	382	396	a
	Me-Af [93]	376	7	0.5	2.8	362	372	375	380	396	a
	W [50]	372	6	0.6	3.4	358	368	371	376	389	b
	Atl [23]	376	5	1.4	4.2	369	372	375	376	390	a,b
	N-Am [10]	378	6	0.8	2.3	372	373	375	382	389	a,b
	N-Atl [38]	374	8	0.3	2.7	362	368	373	379	392	a,b
	NW-Eu [67]	373	9	-0.1	2.1	357	366	374	379	390	a,b
BC ($\mu g\ m^{-3}$)	A [4]	0.2	0.1	-0.6	1.9	0.07	0.2	0.3	0.3	0.4	a,b
	E [14]	0.4	0.3	1.5	5.0	0.02	0.1	0.3	0.5	1.3	a,b
	Me-Af [18]	0.3	0.2	0.8	2.8	0.04	0.2	0.3	0.4	0.8	a,b
	W [8]	0.6	0.4	0.8	2.6	0.1	0.4	0.5	0.7	1.3	a
	Atl [5]	0.13	0.09	0.7	1.9	0.05	0.06	0.1	0.2	0.3	b
	N-Atl [5]	0.32	0.25	1.0	2.7	0.06	0.2	0.2	0.3	0.7	a,b
	NW-Eu [9]	0.4	0.5	1.2	3.2	0.02	0.07	0.1	0.4	1.4	a,b
CO (ppb)	A [2]	112	4	0.0	1.0	109	111	112	114	116	a
	E [7]	117	20	-0.4	2.5	83	111	116	130	141	a
	Me-Af [10]	111	8	-0.5	1.8	98	105	113	117	121	a
	W [5]	118	12	0.1	2.2	102	114	118	123	135	a
	Atl [2]	123	26	0.0	1.0	104	114	123	132	142	a
	N-Am [1]	107	NA	NA	NA	107	107	107	107	107	a
	N-Atl [7]	113	12	0.4	3.1	94	108	113	115	134	a
	NW-Eu [5]	127	21	0.9	2.3	109	114	116	134	161	a

^{7}Be (mBq m^{-3})	A [37]	4.5	2.1	0.7	3.7	1.3	3.3	4.3	5.6	10.4	a,b,c
	E [71]	4.2	2.4	0.8	4.0	0.4	2.7	3.9	5.7	12.6	a,b,c
	Me-Af [97]	4.3	2.1	-0.1	2.2	0.1	2.8	4.5	5.7	8.3	a,b
	W [51]	5.2	2.4	0.8	4.4	0.9	3.6	5.1	6.6	13.3	a
	Atl [25]	3.0	1.4	0.5	2.1	0.9	2.1	2.6	4.0	5.7	c
	N-Am [8]	2.8	1.5	0.9	3.4	0.9	2.2	2.4	3.3	5.8	b,c
	N-Atl [44]	4.3	2.1	0.3	2.1	0.5	2.8	4.3	6.0	8.2	a,b,c
	NW-Eu [83]	4.4	2.4	0.4	2.4	0.6	2.5	4.0	6.0	11.1	a,b,c
^{210}Pb (mBq m^{-3})	A [33]	0.30	0.12	0.9	4.3	0.14	0.20	0.29	0.39	0.70	c
	E [70]	0.50	0.29	1.0	3.4	0.12	0.27	0.44	0.64	1.32	a,b
	Me-Af [89]	0.51	0.29	0.7	2.8	0.08	0.28	0.49	0.70	1.30	a,b
	W [48]	0.53	0.30	1.4	6.0	0.12	0.33	0.49	0.67	1.67	a,b
	Atl [17]	0.25	0.13	0.9	3.1	0.08	0.15	0.21	0.31	0.55	c
	N-Am [6]	0.25	0.13	1.4	3.7	0.13	0.19	0.22	0.24	0.51	a,b,c
	N-Atl [40]	0.38	0.19	1.0	3.7	0.12	0.25	0.30	0.49	0.97	b,c
	NW-Eu [76]	0.55	0.32	0.7	2.8	0.06	0.30	0.49	0.76	1.50	a

		AM	SD	Skew	Kurt	Min	Pct25	Pct50	Pct75	Max	Diff (α = 0.0064)
PM_{10} (μg m^{-3})	A [34]	6.2	3.8	0.9	3.4	0.9	3.5	5.1	8.1	15.9	c,d,e
	E [68]	9.2	6.7	1.3	5.3	0.4	3.9	7.7	13.2	35.0	a,c
	Me-Af [98]	10.9	9.3	1.4	5.2	0.3	3.2	9.5	15.6	45.7	a,b,c,d
	W [49]	12.0	8.1	0.1	1.7	0.7	4.1	13.2	18.7	26.1	a,b
	Atl [22]	5.1	3.9	2.4	9.9	1.3	3.1	4.5	5.9	19.5	c
	N-Am [8]	3.6	1.6	0.4	2.5	1.4	2.4	3.7	4.2	6.5	b,d,e
	N-Atl [44]	7.6	4.1	0.2	2.2	1.1	4.5	7.6	10.3	15.7	a,b,c,d,e
	NW-Eu [80]	9.3	6.0	0.7	3.2	0.4	4.9	8.6	13.5	28.4	a,c
Fine Particles (N cm^{-3})	A [16]	31.2	35.5	1.2	3.0	1.2	5.8	14.1	42.7	110.7	a
	E [23]	26.4	21.0	0.8	3.0	0.3	9.5	21.4	40.6	80.1	a
	Me-Af [42]	30.7	25.9	1.2	4.6	0.3	10.9	25.6	41.1	118.6	a
	W [15]	31.9	30.4	0.7	2.1	0.7	5.5	24.0	55.6	92.0	a
	N-Atl [16]	24.4	19.6	1.4	4.8	4.4	12.0	18.6	29.5	78.9	a
	NW-Eu [34]	33.6	28.0	0.9	3.1	0.5	10.1	24.1	56.0	113.0	a
Coarse Particles (N cm^{-3})	A [16]	0.09	0.07	1.0	2.9	0.02	0.03	0.05	0.11	0.26	b
	E [23]	0.16	0.33	2.9	9.8	0.002	0.03	0.04	0.10	1.33	b
	Me-Af [42]	0.33	0.43	2.6	10.0	0.01	0.07	0.21	0.40	1.94	a
	W [15]	0.27	0.25	0.7	2.3	0.01	0.06	0.21	0.44	0.76	a,b
	N-Atl [16]	0.13	0.07	0.0	1.9	0.01	0.09	0.11	0.19	0.23	a,b
	NW-Eu [34]	0.22	0.34	3.2	12.8	0.003	0.05	0.13	0.22	1.64	a,b
^{7}Be/PM_{10} (mBq μg^{-1})	A [34]	1.2	1.4	2.1	7.0	0.3	0.4	0.6	1.3	6.0	a
	E [65]	1.0	2.1	4.2	21.6	0.09	0.3	0.4	0.8	13.5	b,c
	Me-Af [93]	0.7	1.4	6.3	44.6	0.01	0.3	0.4	0.7	11.2	c
	W [47]	0.9	1.1	2.4	7.7	0.1	0.3	0.4	0.9	4.9	a,b,c
	Atl [21]	0.8	0.7	3.1	13.4	0.1	0.5	0.7	0.9	3.6	a,b
	N-Am [7]	1.0	0.6	1.5	3.9	0.4	0.6	0.8	1.0	2.3	a,b,c

	N-Atl (43)	0.8	0.9	3.4	13.8	0.2	0.5	0.5	0.7	4.7	a,b,c
	NW-Eu (80)	1.0	2.3	6.1	42.3	0.07	0.3	0.5	0.7	18.1	a,b,c
$^{210}Pb/PM_{10}$ ($mBq\ \mu g^{-1}$)	A (30)	0.07	0.06	1.1	2.6	0.02	0.03	0.05	0.10	0.2	a
	E (64)	0.08	0.09	3.1	12.4	0.01	0.04	0.06	0.08	0.5	a
	Me-Af (85)	0.06	0.05	2.8	12.9	0.01	0.04	0.05	0.07	0.3	a
	W (44)	0.07	0.10	4.0	19.3	0.02	0.03	0.05	0.07	0.6	a
	Atl (14)	0.06	0.02	-0.5	3.2	0.01	0.04	0.06	0.07	0.1	a
	N-Am (5)	0.07	0.02	-0.4	1.4	0.05	0.06	0.08	0.09	0.1	a
	N-Atl (39)	0.07	0.08	3.3	13.8	0.02	0.03	0.04	0.06	0.4	a
	NW-Eu (74)	0.08	0.09	5.9	42.4	0.004	0.04	0.06	0.08	0.8	a
$^{7}Be/^{210}Pb$	A (33)	16.7	7.0	0.8	2.7	8.0	11.9	15.5	19.1	31.4	a
	E (67)	10.2	6.2	1.2	4.0	2.0	5.6	8.6	12.6	28.6	c
	Me-Af (87)	11.4	9.3	4.1	23.6	0.5	6.9	10.0	12.7	68.1	c
	W (47)	12.4	7.1	1.9	6.3	5.4	8.0	10.7	13.4	36.5	b,c
	Atl (17)	15.6	10.4	3.1	12.1	7.9	10.2	13.2	16.6	53.7	a,b
	N-Am (6)	12.6	8.0	0.9	2.6	4.7	7.7	10.3	15.3	26.7	a,b,c
	N-Atl (39)	14.2	7.5	2.2	10.7	3.5	9.7	11.8	18.0	47.0	a,b
	NW-Eu (76)	10.2	6.8	2.6	12.5	1.9	6.1	8.6	11.7	45.9	c

Table 5.1 *Summary statistics of the variables by flow pattern at 2200 m asl (AM = arithmetic mean, SD = standard deviation, Skew = skewness, Kurt = kurtosis, Min = minimum, Pct25 = 25th percentile, Pct50 = 50th percentile, Pct75 = 75th percentile, Max = maximum). The number of cases associated to each air-flow is given in brackets as superscript. For each variable, equal letters in last column indicate groups with no significant differences (identified by a multiple comparison test with overall significance α_t=0.05).*

7 clusters - 3000 m

		AM	SD	Skew	Kurt	Min	Pct25	Pct50	Pct75	Max	Diff (α = 0.0073)
P (mbar)	A (53)	787	9	-1.1	3.9	759	782	789	793	800	b,c
	E (61)	790	8	-2.4	11.8	750	787	791	796	800	a,b
	Me-Af (76)	791	5	-0.8	3.1	777	788	792	796	800	a,b
	W (71)	791	5	-1.1	5.1	773	789	793	795	802	a
	Atl (59)	790	6	-0.6	2.8	775	786	790	794	798	a,b
	N-Atl (59)	791	7	-1.2	4.7	769	788	792	795	801	a,b
	N-Am (23)	785	6	-0.1	1.8	775	780	785	789	793	c
T (°C)	A (53)	-0.6	7.5	0.1	1.9	-15.6	-6.4	-1.8	6.7	13.4	c
	E (61)	1.8	7.8	-0.5	2.7	-17.8	-3.2	3.2	7.9	17.0	b,c
	Me-Af (76)	4.3	6.0	0.0	2.7	-11.2	0.3	4.7	8.4	16.7	b
	W (71)	8.1	5.7	-0.4	2.0	-3.7	3.7	8.7	13.0	17.2	a
	Atl (59)	4.9	5.6	0.3	1.8	-3.2	-0.3	4.6	9.6	15.4	b
	N-Atl (59)	5.0	6.8	-0.4	2.4	-10.3	-0.3	6.6	9.8	18.2	a,b
	N-Am (23)	-1.6	4.3	0.5	3.4	-8.8	-4.0	-1.3	1.3	9.5	c

RH (%)	A [52]	73	17	-0.6	3.1	19	59	77	87	99	a
	E [57]	76	21	-1.3	4.2	10	70	82	91	100	a
	Me-Af [75]	80	18	-1.0	2.7	35	68	87	94	99	a
	W [71]	76	16	-0.4	2.3	35	66	78	91	100	a
	Atl [59]	77	17	-0.7	2.7	32	66	81	90	99	a
	N-Atl [59]	78	16	-1.1	3.7	34	72	83	89	99	a
	N-Am [23]	74	16	-0.2	2.1	41	61	76	83	99	a
Prec (mm)	A [12]	3.4	3.6	1.0	-0.4	0.3	0.4	2.1	5.3	10.4	a
	E [15]	3.1	2.6	1.0	-0.1	0.2	1.5	1.6	4.3	8.6	a
	Me-Af [26]	4.2	6.0	2.7	8.0	0.2	0.6	1.6	5.9	26.7	a
	W [26]	9.7	31.0	4.9	24.7	0.1	0.8	1.6	5.0	160.0	a
	Atl [14]	4.5	7.0	2.7	8.2	0.1	0.6	1.3	6.5	26.4	a
	N-Atl [27]	4.0	4.3	1.7	3.0	0.1	0.7	2.6	6.0	17.2	a
	N-Am [11]	4.1	2.9	0.5	-1.3	0.8	1.9	3.0	6.5	8.8	a
TH (m)	A [52]	10814	1297	0.1	2.7	7833	9901	10996	11607	13929	d
	E [51]	11126	1050	-0.3	2.3	8722	10320	11246	11854	13042	c,d
	Me-Af [62]	11404	1336	0.8	5.2	8500	10714	11288	12009	16325	b,c,d
	W [69]	12196	1313	0.9	4.0	9980	11462	11950	12835	16318	a
	Atl [57]	11876	1141	0.2	3.1	9309	11177	11948	12586	14712	a,b
	N-Atl [50]	11520	1340	-0.2	3.0	8306	10944	11555	12458	14844	a,b,c
	N-Am [22]	11220	1064	0.8	2.7	9840	10479	11020	11667	13504	b,c,d
WS ($m\ s^{-1}$)	A [53]	5.3	3.7	1.8	7.4	0.6	2.7	4.5	6.8	20.7	b,c
	E [61]	7.0	4.6	1.2	5.9	0.5	3.2	6.0	10.4	26.3	a,b
	Me-Af [75]	5.2	3.5	1.1	4.3	0.1	2.5	4.4	6.9	17.7	b,c
	W [71]	6.3	3.4	1.0	4.5	0.7	3.8	6.0	8.4	18.1	a,b
	Atl [59]	5.9	3.3	0.4	2.5	0.9	3.2	5.9	8.5	14.6	a,b
	N-Atl [59]	4.6	3.9	1.5	4.9	0.4	1.9	3.4	5.3	17.8	c
	N-Am [22]	8.2	3.4	0.1	1.9	3.0	5.0	8.8	10.4	14.4	a

		AM	**SD**	**Skew**	**Kurt**	**Min**	**Pct25**	**Pct50**	**Pct75**	**Max**	**Diff (α = 0.0073)**
O_3 (ppb)	A [53]	53	11	0.6	3.3	31	45	51	59	83	b,c
	E [60]	57	12	0.5	4.0	34	48	58	64	98	a,b
	Me-Af [74]	56	10	-0.1	2.5	34	49	57	64	82	a,b
	W [69]	55	10	-0.1	2.3	35	49	55	63	77	a,b
	Atl [57]	55	10	0.9	3.8	39	47	52	60	88	a,b
	N-Atl [57]	60	12	0.4	2.8	37	54	59	67	87	a
	N-Am [22]	47	7	0.2	2.1	35	41	47	52	59	c
CO_2 (ppm)	A [47]	376	9	0.0	2.1	361	370	376	383	395	a,b
	E [54]	376	9	0.2	3.1	354	370	375	381	396	a,b
	Me-Af [73]	378	8	0.3	2.0	365	372	376	383	396	a
	W [68]	374	7	0.5	3.7	362	369	373	378	396	b
	Atl [51]	374	6	0.0	2.7	362	370	374	378	389	a,b
	N-Atl [42]	373	8	-0.1	2.3	358	367	374	378	388	b
	N-Am [23]	378	8	0.6	2.0	368	372	375	384	392	a,b

BC ($\mu g\ m^{-3}$)	A [8]	0.31	0.19	1.3	4.3	0.07	0.24	0.28	0.33	0.74	a
	E [15]	0.41	0.32	1.6	5.7	0.07	0.25	0.33	0.50	1.33	a
	Me-Af [16]	0.30	0.16	0.6	3.3	0.02	0.19	0.28	0.39	0.69	a
	W [12]	0.39	0.26	0.1	2.1	0.02	0.24	0.39	0.54	0.84	a
	Atl [7]	0.24	0.34	1.8	4.6	0.05	0.06	0.10	0.23	0.99	a
	N-Atl [6]	0.15	0.15	0.7	1.7	0.03	0.04	0.08	0.25	0.38	a
	N-Am [3]	0.07	0.05	-0.7	1.5	0.02	0.06	0.10	0.10	0.10	a
CO (ppb)	A [6]	111	20	0.8	2.7	91	98	111	115	146	a
	E [8]	119	23	0.4	2.9	83	109	115	125	161	a
	Me-Af [14]	125	28	2.3	8.0	101	112	117	126	214	a
	W [3]	102	5	0.5	1.5	98	99	101	104	108	a
	Atl [7]	121	13	0.6	2.1	104	114	117	127	142	a
	N-Atl [3]	118	18	-0.4	1.5	98	110	122	128	134	a
	N-Am [5]	113	7	0.5	1.7	107	107	110	117	122	a
^{7}Be ($mBq\ m^{-3}$)	A [51]	4.2	2.3	0.6	3.2	0.5	2.5	4.2	5.5	10.5	a,b
	E [58]	4.3	2.4	0.9	3.9	0.5	2.6	4.0	6.0	12.6	a,b
	Me-AF [71]	4.0	2.0	0.0	2.0	0.5	2.5	4.0	5.6	8.2	b
	W [69]	5.0	2.1	-0.2	2.9	0.4	3.8	5.0	6.2	10.2	a
	Atl [55]	4.1	2.1	0.2	2.0	0.9	2.3	4.0	5.6	8.5	a,b
	N-Atl [58]	4.3	2.3	0.4	2.7	0.1	2.4	4.0	6.2	11.1	a,b
	N-Am [21]	3.0	1.8	0.6	2.1	0.6	1.6	2.5	4.0	6.4	b
^{210}Pb ($mBq\ m^{-3}$)	A [47]	0.34	0.25	3.7	19.9	0.12	0.23	0.28	0.38	1.70	c
	E [57]	0.50	0.28	1.0	3.5	0.13	0.26	0.44	0.65	1.32	a,b
	Me-Af [64]	0.49	0.29	0.7	2.6	0.08	0.26	0.44	0.67	1.14	a,b
	W [65]	0.55	0.26	0.7	3.4	0.14	0.37	0.51	0.70	1.30	a
	Atl [44]	0.39	0.22	0.9	4.3	0.08	0.21	0.35	0.54	1.15	b,c
	N-Atl [54]	0.55	0.32	0.8	3.4	0.06	0.31	0.52	0.70	1.50	a
	N-Am [15]	0.28	0.17	1.5	4.9	0.11	0.17	0.23	0.31	0.75	c

		AM	**SD**	**Skew**	**Kurt**	**Min**	**Pct25**	**Pct50**	**Pct75**	**Max**	**Diff (α = 0.0073)**
PM_{10} ($\mu g\ m^{-3}$)	A [50]	6.2	3.8	1.0	3.6	1.1	3.5	5.2	8.0	17.2	c
	E [56]	9.6	6.7	1.4	5.8	0.4	5.5	8.1	13.0	35.0	a,b
	Me-Af [73]	10.1	9.0	1.9	7.6	0.4	3.4	8.4	13.8	45.7	a,b,c
	W [68]	13.6	11.5	2.8	16.9	0.1	5.7	12.3	19.8	79.7	a
	Atl [55]	7.0	5.5	1.2	3.9	0.4	2.8	4.8	10.7	25.6	b,c
	N-Atl [56]	8.9	5.9	0.9	4.0	0.2	4.3	8.6	11.8	28.4	a,b,c
	N-Am [19]	3.3	2.3	1.3	3.7	1.4	1.7	2.5	4.0	9.1	d
Fine Particles ($N\ cm^{-3}$)	A [19]	343.9	368.1	2.4	8.6	46.2	150.3	218.6	372.4	1611.3	a,b
	E [17]	634.0	452.0	0.7	2.1	44.8	275.2	554.4	796.5	1450.3	a,b
	Me-Af [26]	293.8	298.1	1.5	5.2	20.4	60.3	187.5	453.7	1262.7	a
	W [29]	160.9	201.0	2.8	11.1	1.4	55.5	93.1	174.4	978.3	a
	Atl [14]	168.0	127.4	1.7	5.2	58.3	90.1	122.8	203.8	520.0	b
	N-Atl [23]	442.3	690.7	2.4	7.9	22.3	79.8	149.5	500.9	2695.0	a
	N-Am [3]	202.8	229.3	0.4	1.5	1.0	78.2	155.3	303.7	452.1	a,b

Coarse Particles (N cm^{-3})	A [19]	0.07	0.06	1.2	3.5	0.01	0.04	0.05	0.10	0.22	c,d
	E [17]	0.05	0.05	1.1	3.6	0.002	0.03	0.03	0.08	0.17	d
	Me-Af [26]	0.22	0.27	3.0	12.9	0.02	0.08	0.15	0.25	1.33	a,b
	W [29]	0.53	0.80	3.4	15.5	0.01	0.15	0.28	0.67	4.14	a
	Atl [14]	0.10	0.14	2.6	8.9	0.01	0.02	0.06	0.11	0.53	b,c,d
	N-Atl [23]	0.27	0.40	2.6	8.8	0.003	0.06	0.17	0.27	1.64	a,b,c
	N-Am [3]	0.05	0.04	0.7	1.5	0.02	0.03	0.03	0.06	0.09	a,b,c,d
^{7}Be/PM_{10} (mBq μg^{-1})	A [48]	1.0	1.2	2.9	11.2	0.1	0.4	0.6	0.9	6.0	a,b,c
	E [53]	1.2	3.1	4.5	22.8	0.1	0.3	0.4	0.6	18.1	a
	Me-Af [68]	0.8	1.3	4.8	25.7	0.01	0.3	0.4	0.7	7.9	c,d
	W [66]	0.8	1.5	5.7	38.7	0.1	0.3	0.4	0.6	11.2	d
	Atl [51]	1.2	2.1	4.7	28.2	0.1	0.4	0.6	0.9	13.8	a,b
	N-Atl [55]	1.2	3.9	6.9	50.2	0.01	0.4	0.5	0.8	29.2	b,c,d
	N-Am [18]	1.1	0.7	1.1	3.0	0.4	0.7	0.8	1.4	2.8	a
^{210}Pb/PM_{10} (mBq μg^{-1})	A [44]	0.07	0.05	1.4	3.9	0.02	0.04	0.05	0.08	0.19	a,b,c
	E [52]	0.09	0.12	4.2	21.4	0.01	0.04	0.06	0.08	0.78	b,c
	Me-Af [61]	0.07	0.06	3.9	20.0	0.01	0.04	0.05	0.08	0.38	b,c
	W [62]	0.07	0.09	4.6	25.6	0.01	0.03	0.05	0.06	0.60	c
	Atl [40]	0.06	0.06	4.2	22.7	0.01	0.04	0.05	0.07	0.41	b,c
	N-Atl [51]	0.12	0.31	6.6	46.2	0.004	0.05	0.06	0.09	2.24	a,b
	N-Am [13]	0.10	0.06	1.4	3.6	0.05	0.06	0.09	0.10	0.22	a
^{7}Be/^{210}Pb	A [45]	14.9	7.4	0.8	3.1	4.3	9.1	15.3	19.0	35.0	a
	E [54]	10.0	6.0	1.3	4.3	2.0	5.6	8.9	12.3	28.6	b
	Me-Af [63]	11.1	9.3	4.0	23.9	0.5	6.6	9.2	12.0	68.1	b
	W [64]	11.2	7.8	3.9	21.6	4.5	7.1	9.3	12.4	57.0	b
	Atl [44]	13.8	7.1	2.4	11.8	2.7	9.3	12.4	16.2	47.0	a
	N-Atl [53]	10.1	6.8	2.9	15.3	1.9	5.7	8.8	11.8	45.9	b
	N-Am [15]	13.0	6.6	0.9	2.9	4.7	8.6	11.1	16.2	26.7	a,b

Table 5.2 *Same as Table 5.1, but for the variables by flow pattern at 3000 m asl (AM = arithmetic mean, SD = standard deviation, Skew = skewness, Kurt = kurtosis, Min = minimum, Pct25 = 25th percentile, Pct50 = 50th percentile, Pct75 = 75th percentile, Max = maximum).*

From the point of view of meteorological variables, Arctic air masses are very cold, dry especially at 2200 m, and associated to low tropopause heights and low wind speeds in the surrounding of the sampling station. Eastern advection pattern is associated with high pressures, high relative humidity, low tropopause heights and low wind speeds.

Mediterranean-Africa air masses are warm and very humid, associated with low wind speeds. Western air masses are also very warm and associated to high tropopause height and slow wind speeds. Atlantic air masses are moderately warm and humid (more at 3000 m), and show moderate wind speeds (especially at 2200 m). Flows from North America present the lowest pressure levels

both at 2200 and at 3000 m; they are also very cold, dry (especially at 2200 m), and associated with low tropopause heights and moderate winds. North-Atlantic air masses are moderately warm and very humid, connected to slow wind speeds. Flows from North Western-Europe (cluster found only at 2200 m) present usually higher temperatures, high relative humidity and slow wind speeds.

Overall, Arctic and North America trajectories, both more frequent in the cold period, are subsiding flows related to the lowest temperature and (particularly the Arctic advections) relative humidity. Quite contrasting features are found for the Mediterranean-Africa trajectories, which pass over the Mediterranean at low altitudes and are warm and humid flows. The purely continental Eastern flows present no significant differences in temperature with respect to the cold advections, though humidity takes intermediate values that differ significantly from both the cold and warm groups. The lowest pressure at the surface and higher wind speed are associated to the Atlantic and North America advections, while Northwest- Europe flows present the lowest wind speed and high pressure, frequently related to blocking situations in summertime. Relatively low values of the tropopause height are found for Arctic and Eastern flows, which present significant differences with respect to Western and Mediterranean-Africa flows at 2200 m and Western, Atlantic and North Atlantic ones at 3000 m.

From the point of view of the atmospheric compounds, North American air masses are usually very clean (low O_3, black carbon, CO, PM_{10}, fine and coarse particles). Eastern, Western and North Western flows generally carry on elevated values of atmospheric compounds: in particular, Western air masses carry on elevated values of O_3, PM_{10}, fine and coarse particles, while Eastern and North Western-Europe air masses bring lower concentrations of particulate matter, but associated to higher loadings of fine particles than coarse particles, as previously observed in Chapter 2 (Tositti *et al.*, 2013). Mediterranean-Africa air flows also bring PM_{10} as associated to Saharan Dust transports: this kind of transport is associated to elevated loadings of both the fine and coarse sized particles. Black carbon is higher in Western air masses, even though also flows from East and North Western-Europe largely contribute to its increase. Arctic, Atlantic, North-American and North Atlantic air masses show low contributions to black carbon. Carbon monoxide is low with flows from Arctic, North-America, North Atlantic; Eastern, Western and North Western-Europe flows show elevated concentrations of this gas, even if at 3000 m the contribution of Western air masses is greatly decreased, whereas Mediterranean-Africa and North Atlantic advection patterns contribute more at higher height.

North Atlantic and North West Europe advections, both passing over the British Isles and France, present the highest levels of O_3 with no significant differences with the concentrations for Eastern, Mediterranean-Africa and Western flows. In turn, Atlantic as well as North America and Arctic are

associated with low O_3 values, which points out the influence of precursor levels. At 3000 m, the significant differences in O_3 are reduced, with North Atlantic (high values) significantly different from North America and Arctic flows, and North America flows differing from all other advection types except Arctic. CO_2 values are quite homogeneously distributed over the flow types: at 2200 m significant differences are found only between Western (associated to low CO_2 values) and Eastern, Arctic and Mediterranean-Africa flows, while at 3000 m only significant differences between Mediterranean-Africa and North Atlantic, Western associated to lower CO_2 values are found. For black carbon only one significant difference at 2200 m between Western (high levels) and Atlantic (low levels) is found; at 3000 m no significant difference between flow types is found. For carbon monoxide no significant difference is found either at 2200 or at 3000 m. Also from the point of view of the number densities of fine particles, flows are not significantly different from each other at 2200 m, while at 3000 m Atlantic air masses, which are associated with a low number of fine particles, are significantly different from North Atlantic, Mediterranean-Africa and Western, which on the contrary are rich in fine particles. Coarse particles are transported mostly by Mediterranean-Africa flows, which at 2200 m are significantly different from Eastern and Arctic, while at 3000 m significant differences between Arctic (low number density of coarse particles) and Mediterranean-Africa, Western (higher loadings of coarse particles) and between Eastern (low number of coarse particles) and North Atlantic, Mediterranean-Africa, Western (rich in coarse particles) can be found. Further significant differences for coarse particles at this height can be found between Western, rich in coarse particles, and Atlantic air masses. As for PM_{10}, clean Atlantic air masses present significant differences at 2200 m with Eastern, Western, Mediterranean-Africa and North Western-Europe which are related to higher PM_{10} values, while North American flows, which are also clean from this point of view, are significantly different from North Western-Europe air masses. Arctic flows, associated to low PM_{10} values, are significantly different from Western air masses.

From the point of view of atmospheric radiotracers, Arctic air masses are associated to high ^{7}Be and low ^{210}Pb (high $^{7}Be/^{210}Pb$); this kind of transport, in agreement with previous papers about stratospheric intrusions at Mt Cimone (Bonasoni *et al.*, 1999, 2000a, b), is in fact frequently associated to STE. In fact, the production rate of ^{7}Be is highest in the stratospheric air at high latitudes (Beer *et al.*, 2012), even if the mixing of stratospheric air into the upper troposphere occurs along the tropopause discontinuity in mid-latitude regions. Stohl *et al.* (2003) already highlighted the importance of events of rapid deep stratospheric intrusions which tend to have as a more frequent destination the Mediterranean region. Both radionuclides present low activities when the air mass comes from the Atlantic and North America. ^{210}Pb present low values with the arrival of air masses from the ocean (Atlantic, North America and Northern America), while the highest values are linked

to flows with a clear continental origin such as Mediterranean-Africa, Western, Eastern and North Western-Europe. This behaviour is of course due to ^{210}Pb continental origin, as ^{222}Rn flux from the oceans into the atmosphere is negligible (Balkanski *et al.*, 1993; Baskaran, 2011). At 2200 m Atlantic and Arctic air masses, being associated with low values of ^{210}Pb, are significantly different from Eastern, Mediterranean-Africa, North Western-Europe and Western, as well, while North Atlantic flows are significantly different from North Western-Europe. At 3000 m Arctic and North American flows are significantly different from other flow types except from Atlantic, which are significantly different from North Atlantic, Western, Mediterranean-Africa and Eastern (higher values of ^{210}Pb). A further significant difference is also found for Atlantic with North Atlantic and Western, associated to higher ^{210}Pb values. ^{7}Be low values are connected to Atlantic and Northern American air masses, while Western flows are related to the highest values, probably associated to Gulf of Genoa and Gulf of Lion cyclogenesis, which are well known to be associated with STE (e.g., Aebischer and Schär, 1998; Stohl *et al.*, 2000). Western air masses, being linked to high ^{7}Be values at 2200 m, are significantly different from Atlantic and North American flows which are associated with lower values of this tracer. Atlantic air masses being associated to low ^{7}Be values are significantly different from Mediterranean-Africa. At 3000 m significant differences are found between Western and Mediterranean-Africa, North American flows.

Similarly to Dueñas *et al.* (2011), Mediterranean-Africa air masses are linked to high activities of both ^{7}Be and ^{210}Pb, due to the combination of African dust uplifting and downward movement from the upper troposphere. ^{7}Be/^{210}Pb as well as ^{7}Be/PM_{10} and ^{210}Pb/PM_{10} ratios associated to this kind of advection pattern are not very high, as due to the simultaneous transport of particulate matter and radionuclides. As for ^{7}Be/PM_{10}, differences are significant only between Mediterranean-Africa and Atlantic, Arctic flows, being Arctic also significantly different from Eastern and Mediterranean-Africa air masses (higher activity on a lower number of particles). At 3000 m the number of significant differences is more elevated: North American air masses are significantly different from Western, North Atlantic, Eastern and Mediterranean-Africa, which are also significantly different from Atlantic, while Arctic and Atlantic air masses are significantly different from Eastern and Western flows. As for ^{210}Pb/PM_{10}, no significant difference is found at 2200 m, while at 3000 m North American air masses, associated with high values, are significantly different from Western, Atlantic, Eastern and Mediterranean-Africa, while North Atlantic flows, instead related to low values, are significantly different from Western. As for ^{7}Be/^{210}Pb, Eastern flows, which are associated to the lowest values at 2200 m, are significantly different from Atlantic, Arctic and North Atlantic; Arctic flows, linked to high ^{7}Be/^{210}Pb values, are significantly different from Eastern, Western, Mediterranean-Africa and North Western-Europe; Atlantic and North Atlantic flows are significantly different from Mediterranean-

Africa, Eastern and North Western-Europe (lower $^{7}Be/^{210}Pb$ values). At 3000 m, Arctic and Atlantic air masses are significantly different from North Atlantic, Mediterranean-Africa, Eastern and Western, which are related to lower values of the ratio $^{7}Be/^{210}Pb$.

When considering longer back trajectories at 2200 m asl (6-day instead of 4-day trajectories), the resulting number of clusters is reduced from eight to seven. One of these clusters, composed by south-easterly flows, is very low populated; and another one, which should be named as Eastern Atlantic, appears as the result of joining most of the Western and North Western-Europe flows identified in the 4-day trajectories. The subsequent analysis of significant differences in atmospheric compounds and meteorological parameters by advection pattern detects a smaller number of pair-wise comparisons with significant differences for the longer (6-days) trajectories. Moreover, a lower number of significant differences are revealed if the best 8 clusters solution for the 6-day trajectories were considered. This suggests that these longer trajectories may lose part of their specific features.

As shown in Figure 5.6 and as previously highlighted in Chapters 3 (Tositti *et al.*, 2014) and 4, the seasonal behaviour of ^{210}Pb is characterized by the presence of one summer maximum mainly due to higher mixing height and enhanced uplift from the boundary layer, while ^{7}Be seasonal variations are more complex, being characterized by two relative maxima, one during the cold season associated to an increased frequency of STE (James *et al.*, 2003; Stohl *et al.*, 2003) and one in the warm season mainly (but not exclusively) associated to tropospheric subsidence balancing low tropospheric air masses ascent occasionally accompanied by STE (Cristofanelli *et al.*, 2009a).

Ioannidou *et al.* (2014) recently pointed out that the high ^{7}Be activity values observed during warm months can be well explained by the solar heating of the Earth-atmosphere system. In fact, the solar heating of the surface of the Earth results in the heating of air masses in contact with the surface while turbulent eddies transport the surface air to higher altitudes. This produces a convective circulation, carrying surface air upward and bringing downward air from upper levels (Zanis *et al.*, 1999). This phenomenon is accompanied by an increase of tropopause height during the warm summer months, induced by a deep penetration of convection: the positive correlation between tropopause height and ^{7}Be activity concentrations reflects both downward transport of dry upper tropospheric air within anticyclonic conditions as well as lower scavenging rates (Paatero and Hatakka, 2000; Gerasopoulos *et al.*, 2001, 2005). In fact, as Ioannidou *et al.* (2014) pointed out, during low relative humidity events condensation is not intense and accordingly particles tend to remain small-sized, with lower scavenging and as a result higher ^{7}Be activity concentrations (Ioannidou *et al.*, 2011). Figure 5.6 highlights, however, that the seasonality of air mass transports cannot be completely ruled out as a factor influencing the seasonality of radionuclides. In fact, while ^{7}Be winter maximum can be linked to the seasonal behaviour of Arctic and North-Atlantic air masses (as Atlantic and North American air

masses, showing also a simultaneous peak with ^{7}Be, are associated to lower ^{7}Be values in the boxplots), ^{7}Be summer maximum can be associated to Mediterranean-Africa, Western and North Atlantic air masses seasonal pattern. ^{210}Pb summer maximum seems to be well related with the seasonality of Western and North Western-Europe flows. However this analysis at the monthly level cannot separate the contributions of advection patterns occurring in the same month.

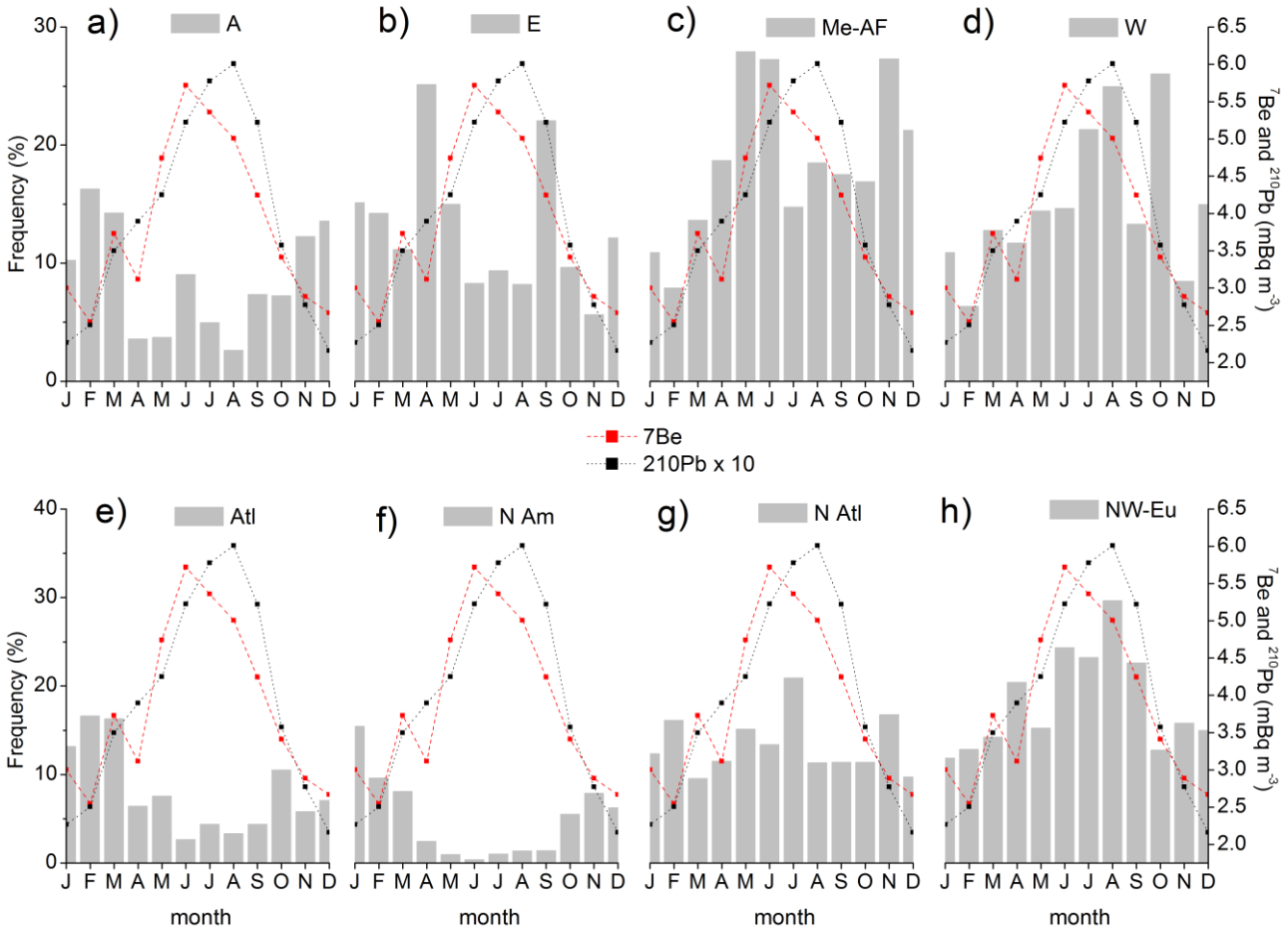

Figure 5.6 *Monthly medians activities of ^{7}Be (right scale, red line) and ^{210}Pb (right scale, black line) and their relationship with the seasonal frequency of air flows (left scale, grey bar) from: a) Arctic; b) East; c) Mediterranean-Africa; d) West; e) Atlantic; f) North America; g) North Atlantic; h) North Western-Europe.*

Figure 5.7 similarly analyses the PM_{10} seasonal pattern, already studied in Chapter 2 (Tositti *et al.*, 2013); similarly to ^{210}Pb, PM_{10} show minimum values during the cold season whereas maxima are reached during summer months, when it is uplifted from the boundary layer due to thermal convection and increased mixing height. The seasonal pattern of PM_{10} might be, however, influenced by the seasonal pattern of advection patterns bringing about elevated mass loads of particles, such as Mediterranean-Africa, Western, North Atlantic and North Western-Europe air masses. In particular, while the seasonal maximum frequency of Mediterranean-Africa in June could be contributing to the first PM_{10} increase

observed during this month, July values could be related to the contribution of North Atlantic flows, while August elevated values might be linked to the seasonal pattern of Western and North Western-Europe advections. In both Figure 5.6 and 5.7 we decided to characterize the seasonality of variables with monthly medians, and not with monthly means, as the distributions of PM_{10} and of atmospheric radiotracers are remarkably non-Gaussian (see Chapter 2 Figure 2.4 for PM_{10}, and Chapter 3, Figure 3.5 for ^{7}Be and ^{210}Pb; Tositti *et al.*, 2013, 2014), and in this case it is known that the median has to be preferred to the arithmetic mean, as less sensitive to the influence of outliers (e.g., Wilks, 2006).

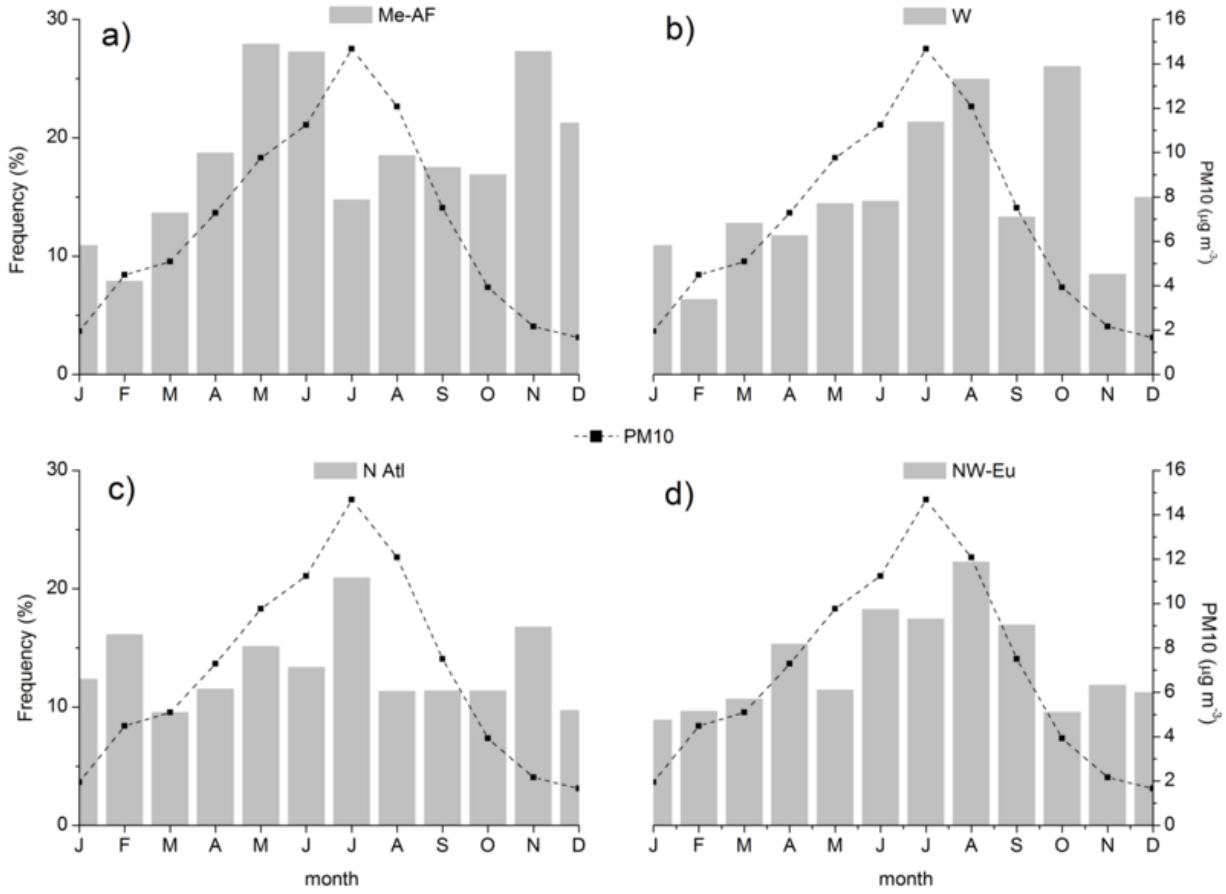

Figure 5.7 *Monthly medians concentrations of PM_{10} (right scale, black dashed line) and relationship with the seasonal frequency of air flows (left scale, grey column) from: a) Mediterranean-Africa; b) West; c) North Atlantic; d) North Western-Europe.*

However, the seasonal frequency of events is only a part of the story: in fact, also rare events might contribute a lot to increases of the variables during certain seasons. For this reason, Figure 5.8 reports boxplots of the median $^{7}Be/^{210}Pb$ contribution per number of episodes for each season. This Figure highlights that summer Arctic flows, and also summer North-American flows, in spite of being quite rare events, can contribute a lot to increases of ^{7}Be (and not of ^{210}Pb) during the summer period. Their average contribution to high $^{7}Be/^{210}Pb$ during summertime is higher than during winter when they are

more frequent. From this Figure it is also highlighted that the main contributors to winter $^{7}Be/^{210}Pb$ increases are Arctic, North Atlantic, North-American and Western flows. A further interesting observation of this Figure is that Mediterranean-Africa flows can be regarded as important contributors not only of ^{210}Pb and PM_{10}, but also of ^{7}Be. This feature, already briefly introduced in Chapter 2 when the outstanding Saharan dust transport of March 2004 was presented, was already highlighted by Hernández *et al.* (2008), who attributed episodes of high ^{7}Be concentrations in Canary Islands to subsidence concurrent with Saharan Dust outbreaks and by Dueñas *et al.* (2011), who highlighted that a combination of African dust uplifting and downward movement from the upper troposphere can in some cases cause increases in both ^{7}Be and ^{210}Pb activities. This analysis highlights also once more how fast changing synoptic transitions are relevant to characterize the measurements.

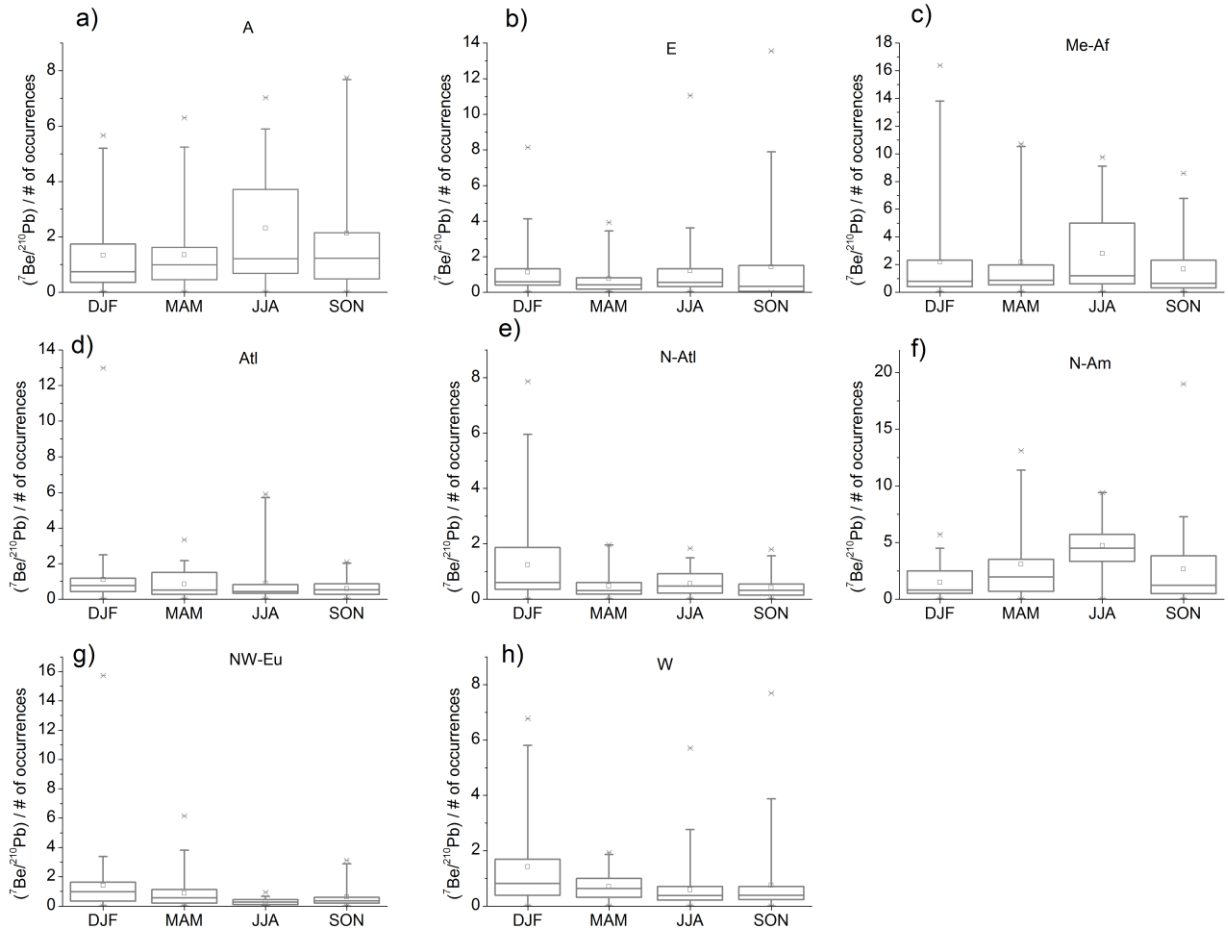

Figure 5.8 *Seasonal boxplots showing the contribution to $^{7}Be/^{210}Pb$ per number of events of each flow type: a) Arctic; b) Eastern; c) Mediterranean-Africa; d) Atlantic e) North-Atlantic; f) North-America; g) North Western-Europe; h) Western. The horizontal bold line in each box represents the 50th percentile (median), the square represents the mean value, lower and upper boundaries locate the 25th and 75th percentile of the values and whiskers locate the 5th and 95th percentile values. Crosses and horizontal lines outside the boxes further indicate 1st and 99th percentile and minimum and maximum values, respectively.*

5.3.3 Temporal analysis of transport patterns and atmospheric composition

The seasonal nature of the advection patterns, as well as of the analysed atmospheric variables, is also evidenced by the periodic behaviour of the ACF of their monthly frequencies of occurrence (in the case of flows) and medians (in the case of atmospheric variables), with maxima and minima beyond bounds of significance (95% confidence) and a full cycle of 12 months. Figure 5.9 shows for example the ACF of North American flows before and after the removal of the seasonal component using STL decomposition, and after further removal of the linear trend from the T-S slope.

The pattern of the ACF reveals also for instance the typical Northern Hemisphere seasonal pattern of CO_2 (Figure 5.9) superimposed on a rising trend, with a winter maximum and a summer minimum (Chapter 3, Subsection 3.3.3; Tositti *et al.*, 2014) which are known to be mainly due to the seasonal growth in land vegetation (e.g., Keeling *et al.*, 1996), as well as the seasonal pattern of ^{210}Pb, PM_{10}, associated to maxima during the warm season and minima during the cold season (Chapter 2, Figure 2.6 for PM_{10} and Chapter 3, Figure 3.3b for ^{210}Pb; Tositti *et al.*, 2013, 2014) and that of ^{7}Be, which is characterized by a summer maximum and a secondary winter maximum (Chapter 3, Figure 3.3a; Tositti *et al.*, 2014). In all of these cases the decomposition into seasonal, trend and remainder components using STL allowed the estimation of their relative contributions, and the removal of the seasonal component enable the removal of the periodic structure in the ACF for further analysis.

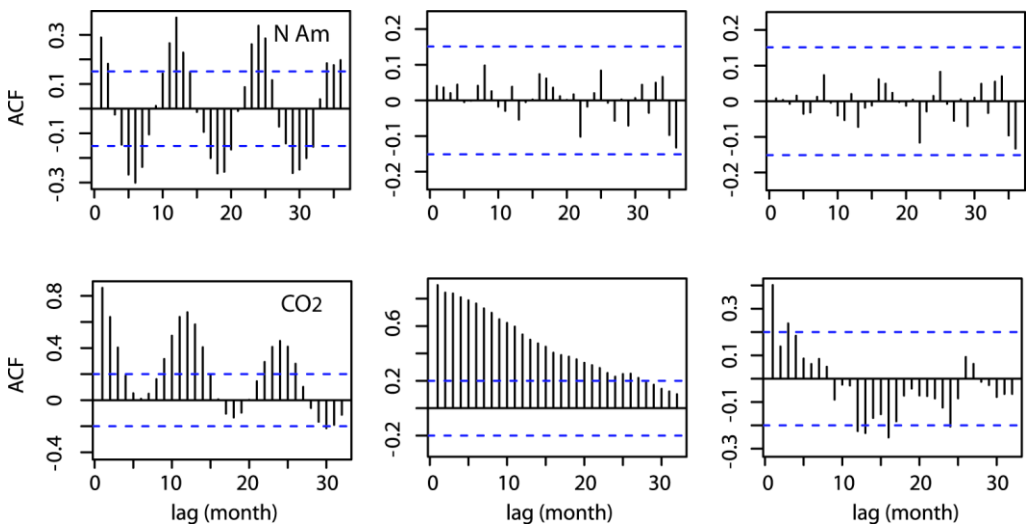

Figure 5.9 *Autocorrelation function of the monthly frequency of North American flows (upper panels) and the monthly median of CO_2 (bottom panels). From left to right they correspond to the time series, the de-seasonalized series from the STL decomposition and to the de-seasonalized and further de-trended series from the T-S slope estimate. One major difference between the two original time series is that CO_2 presents a strong trend which is evidenced by the shape of the ACF. The de-seasonalized and de-trended CO_2 time series needs further removal of the month-to-month correlation to obtain a good estimation of the significance of the trend, following the Y-P procedure.*

The assessment of the existence of temporal trends in the frequencies of the air flow types, as well as in monthly medians of the variables and in NAO indexes time series has taken into account the presence of seasonality and serial correlations in the time series (Figure 5.9). The analysis revealed significant trends in only a few cases, which in general show small trend magnitudes. Even though some differences exist in the results of the two nonparametric methods (Table 5.3), they consistently detect significant downward trends for Atlantic and North-American flows reaching Mt. Cimone at 2200 m, and for the monthly medians of ^{210}Pb and PM_{10} measured at the station in the period 1999-2006 (Figure 5.9). The mean annual change of the original monthly time series are equal to -0.008 mBq m^{-3} $year^{-1}$ and -0.15 μg m^{-3} $year^{-1}$, respectively, while for the de-seasonalized monthly series they are equal to -0.01 mBq m^{-3} $year^{-1}$ and -0.30 μg m^{-3} $year^{-1}$. A strong upward trend for CO_2 is also revealed, in agreement with longer records at Mauna Loa (Machta, 1972; Thoning *et al.*, 1989; Randerson *et al.*, 1997). The mean annual change over the time period 1999-2006 of the CO_2 measurements is equal to +1.80 ppm $year^{-1}$ for the original time series, while it is equal to +1.90 ppm $year^{-1}$ for the de-seasonalized series. Significant upward trends are also revealed by both methods for monthly precipitation for the period 1998-2011. The mean annual change over the period 1998-2011 is equal to +1.27 mm $year^{-1}$ for the original time series, while it is equal to +1.19 mm $year^{-1}$ for the de-seasonalized series. A significant upward trend is also found by the seasonal Mann-Kendall test for tropopause height for the period 1999-2006. In this case the mean annual change of the original time series is equal to 0, while it is equal to +99.6 m $year^{-1}$ for the de-seasonalized time series. The Yue-Pilon procedure results in a trend which is only weakly significant for this variable. Other advection patterns present no significant trends, despite the T-S slope being downward for Arctic and Western, and upward for Eastern, North Atlantic and North Western-Europe. Eastern advection pattern present a weakly significant trend resulting from the Yue-Pilon procedure. As for other atmospheric variables, no other significant trend is revealed, despite the T-S slopes being positive for pressure, temperature, ozone, and for the ratio $^{7}Be/PM_{10}$, while it is negative for relative humidity and ^{7}Be.

	Monthly frequencies	
NAO Index	Seasonal K	De-seasonalized Y-P
Hurrell_Stat_NAOi	0.7156/0.00	0.8877/-0.001
Hurrell_PC_NAOi	0.1104/-0.03	0.3368/-0.02
CPC_Stat_NAOi	*0.0519/-0.04*	0.1454/-0.04
CRU_Stat_NAOi	*0.0767/-0.08*	*0.0561-/0.07*
	Monthly frequencies	
Flow Type	Seasonal K	De-seasonalized Y-P
A	0.1598/-0.17	0.1025/-0.20
E	0.1718/+0.21	*0.0742/+0.31*
Me-Af	0.7736/0.00	0.7387/-0.004
W	0.3411/-0.13	0.2553/-0.25
Atl	**0.039/-0.37**	**0.0062/-0.40**
N-Am	**0.0008/-0.14**	**0.0096/-0.23**
N-Atl	0.1098/+0.27	0.1446/+0.30
NW-Eu	0.1626/+0.23	0.234/+0.33
	Monthly medians	
Variable	Seasonal K	De-seasonalized Y-P
p (mbar)	0.1237/+0.32	0.2317/+0.13
T (°C)	0.1855/+0.3	0.1024/+0.17
RH %	0.1234/-0.26	0.4996/-0.34
TH (m)	**0.0268/0.00**	*0.0749/+99.6*
WS (m s^{-1})	0.1336/0.00	0.2292/+0.12
Prec (mm)	**0.0051/+1.27**	**0.0215/+1.19**
O_3 (ppbv)	0.1320/+0.28	0.1806/+0.29
CO_2 (ppm)	**0.0000/+1.80**	**0.0000/+1.90**
^{7}Be (mBq m^{-3})	0.2840/-0.08	0.1984/-0.09
^{210}Pb (mBq m^{-3})	**0.0450/-0.008**	**0.0135/-0.01**
PM_{10} (mg m^{-3})	**0.0053/-0.15**	**0.0083/-0.30**
$^{7}Be/PM_{10}$ (mBq mg^{-1})	0.1851/+0.007	0.1616/+0.01
^{210}Pb/PM10 (mBq mg^{-1})	0.7921/0.00	0.9839/0.00
$^{7}Be/^{210}Pb$	0.6678/+0.1	0.3612/+0.08

Table 5.3 *Results of the seasonal Kendall test for the monthly time series and the Yue-Pilon (Y-P) procedure on the de-seasonalized monthly series for the detection of monotonic trends. For each case, the results are presented as: p value/ mean change per year from the Theil-Sen slope. In bold when significant at the 0.05 level, in italic when the trend is only weakly significant, i.e., significant at the 0.1 level.*

It has to be noted, however, that for Atlantic flows, monthly precipitation, tropopause height and CO_2 even a simple linear regression already found significant trends (downward for the frequency of Atlantic flows, upward for CO_2, monthly precipitation and tropopause height). Of course this method

is not appropriate as it assumes the residuals (the differences between the measured and calculated values) are independent and normally distributed with a constant variance, which is not the case.

A common measure of the NAO phase is the so called NAO index (NAOi) that is determined by the strength and the location of the semi-permanent Icelandic low and Azores high pressure systems (Walker, 1924; Walker and Bliss, 1932). The NAOi is commonly defined as the difference in normalized seas level pressure (SLP) anomalies between either Lisbon (Portugal) or Ponte Delgada (Azores), and Stykkisholmur/Reykjavik (Iceland) (Hurrell, 1995). The key strengths of this index are that station-based indexes extend back to the mid-19th century or earlier and that is simple to construct and understand. However, this definition of NAO is limited since the stations are fixed in space and thus may not track the movement of the NAO centres through the annual cycle (Pausata *et al.*, 2012), and individual pressure readings can be noisy due to small-scale and transient meteorological phenomena unrelated to NAO (Hurrell, 2013). Alternative definitions of NAOi exist: a first one is based on the empirical orthogonal function (EOF) analysis of the SLP field. The NAOi in this case is identified as the leading eigenvector (the first Principal Component, PC1) computed from the time variation of the SLP field (Hurrell, 1995; Wallace, 2000; Hurrell et al., 2003). The associated PC1 is used to evaluate the temporal evolution of the NAO in any season. The spatial pattern representing the NAO is given by the leading EOF (EOF1). The advantage of using EOF analysis of the SLP field is that the PC1 provides a more accurate representation of the NAO pattern taking into account the shifting of the NAO centres of action throughout the year (Pausata *et al.*, 2012). This index may be also less noisy than the station-based indexes. The two indexes present a significant correlation coefficient equal to 0.81. The NAOi time series (both the station-based and the Principal Components-based) over the study period shows no significant trend according to the tests, despite both the original and de-seasonalized time series present a negative T-S slope. For completeness, the results for another alternative NAO index are also reported: the CRU station-based NAOi calculated as the difference between the normalised SLP over Gibraltar and the normalised SLP over southwest Iceland (Jones *et al.*, 1997), which presents weakly significant trends resulting from both the seasonal Kendall and the Yue-Pilon procedure, as reported in Table 5.3. This index presents a significant correlation coefficient with the other two (equal to 0.80 with Hurrell station-based NAOi, and equal to 0.79 with Hurrell principal components-based NAOi).

A visual inspection of the time series and their trend components obtained from the seasonal-trend decomposition analysis (Figure 5.10) suggests that Atlantic flows downward trend was very significant in 2002-2004 and then after 2008; in the case of North American flows, instead, the decreasing trend can be appreciated in the period 1999-2006, and it levelled off after 2006 until at least 2010. While CO_2 is constantly increasing over the time period, the increasing trend of tropopause height is well seen in the period 2002-2004. For ^{210}Pb and PM_{10} the decreasing trend is better appreciated after 2001. The

increasing trend for monthly precipitation seems to be connected mostly to increases in the period 2009-2011, while the maximum yearly precipitation was reached in 1999. This upward trend in precipitation seems to be mostly connected with an increase of the proportion of rainy days.

An overall increasing trend in tropopause height is found in the period 1999-2006. However, the evolution is not monotonic: The increasing trend of tropopause height is better appreciated in the period 1999-2002; after that a slight decreasing trend is observed in the period 2002-2005, and then again an increase can be appreciated. An upward trend of tropopause height has been already observed globally using radiosonde data (Seidel *et al.*, 2001; Añel *et al.*, 2006; Seidel and Randel, 2006; Brocard *et al.*, 2013), GPS radio occultation data (Schmidt *et al.*, 2008), optimal combinations of observations and numerical weather forecast reanalyses (Highwood *et al.*, 2000; Randel *et al.*, 2000), and climate models forced by combined anthropogenic and natural effects (Santer *et al.*, 2003a, 2004; Gettelman *et al.*, 2009, 2010). Previous analyses of reanalysis data indicate that the greatest increases of tropopause height have occurred in the extratropics in both hemispheres (Santer *et al.*, 2003a; Añel *et al.*, 2006; Seidel and Randel, 2006). Tropopause height has been indicated as an alternative detection variable of climate change (Hoskins, 2003; Santer *et al.*, 2003a, b, 2004; Añel *et al.*, 2006). In fact, the increase of atmospheric CO_2 has been shown to cause tropospheric warming and stratospheric cooling (e.g., Ramaswamy *et al.*, 1996, 2001; Hansen *et al.*, 2002; Santer *et al.*, 2003a, b; Bindoff *et al.*, 2013; Myhre *et al.*, 2013; Previdi *et al.*, 2013; Santer *et al.*, 2013); moreover, the stratospheric cooling is also due to anthropogenically induced depletion of stratospheric ozone (e.g., see Chapter 5 of WMO, 2007; Myhre *et al.*, 2013; Santer *et al.*, 2013). These temperature changes tend both to increase tropopause height (Shepherd, 2002; Hoskins, 2003; Santer *et al.*, 2003b, 2004; Gettelman and Birner, 2007; Gettelman *et al.*, 2011). The increasing trend of tropopause height and stratospheric cooling are also connected to the meridional extent and width of the Hadley cell (Frierson *et al.*, 2007; Lu *et al.*, 2007; Seidel *et al.*, 2008; Allen *et al.*, 2012), which has been observed to shift poleward by some authors (Hu and Fu, 2007; Lu *et al.*, 2007; Seidel *et al.*, 2008; Allen *et al.*, 2012; Hu *et al.*, 2013) as well as to strengthen (Chen *et al.*, 2002; Hu *et al.*, 2005; Mitas and Clement, 2005). The Hadley cell has already been observed to have an important effect on ^{7}Be activity in Oceania (Doering *et al.*, 2014). The presence of a similar influence at Mt. Cimone has not yet been clarified and needs to be further investigated.

A decreasing trend of PM_{10} in the period late 90's-2010 was observed in many stations in Europe, most of all regional background stations (Pérez *et al.*, 2008; Barmpadimos *et al.*, 2011; Colette *et al.*, 2011; Barmpadimos *et al.*, 2012). Generally, these studies attribute this PM_{10} drop both to a decrease in anthropogenic emissions, due to the emission management strategies, as well as to different meteorological processes or cycles, such as the frequency and intensity of Saharan

dust episodes (Pérez *et al.*, 2008). Both Colette *et al.* (2011) and Barmpadimos *et al.* (2012) showed that the decrease in anthropogenic emissions seems to be more important than meteorology as a driving factor for the observed decrease. However, as in our case we observe a contemporary decreasing trend of ^{210}Pb at this remote background site, which cannot be ascribed to a decrease in anthropogenic emissions, the role of meteorology in these drops cannot be ruled out and would probably need further investigations. The upward trend of precipitation is best appreciated in the period 2009-2011, and therefore cannot be linked to the downward trend of ^{210}Pb and PM_{10}.

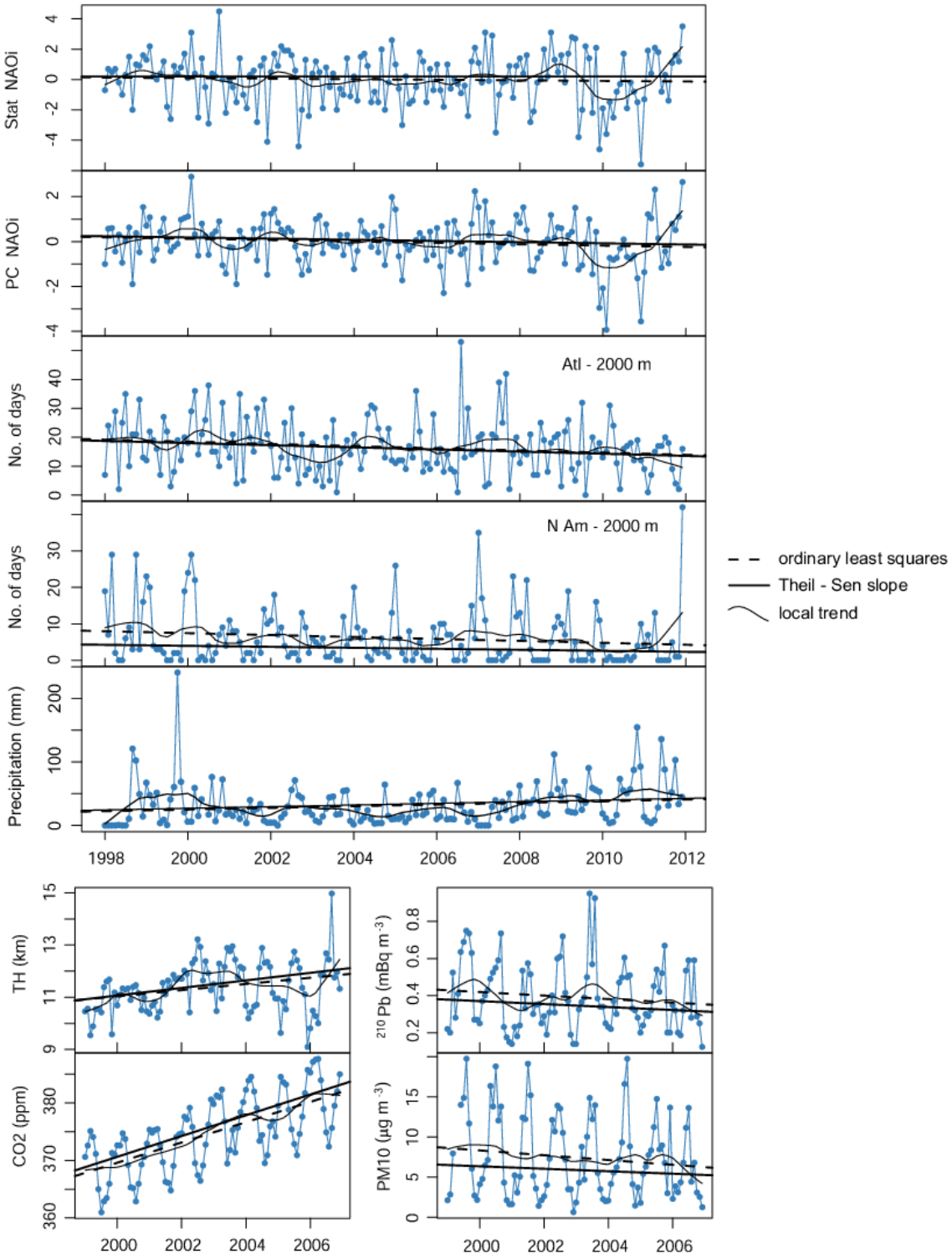

Figure 5.10 *(first five plots) Evolution of the monthly frequency of occurrence of the Atlantic and North American flow types, which show significant trends over the whole study period, evolution of the Hurrell station- and principal components-based NAO indexes, evolution of the monthly precipitation time series. (last four plots) Evolution of the monthly medians of variables which show significant trends over the period 1999-2006 (tropopause height, CO_2, ^{210}Pb and PM_{10}). Dashed lines are the linear regressions, solid lines are the Theil-Sen slope estimates, and black solid curved lines are the local trends from the seasonal-trend decomposition analysis.*

The increase in ^{210}Pb activity from 2002 to 2003 might be due to the extremely high temperature recorded in the whole European region, especially during the summer months (Cristofanelli *et al.*, 2009b; Pace *et al.*, 2005) and connected also to anomalous high ozone concentrations at Mt. Cimone as reported by Cristofanelli *et al.* (2007). In PM_{10} this increase is masked by the 2004 maximum also connected to an exceptional Saharan dust episode reported by Beine *et al.* (2005) and described in Chapter 2, Subsection 2.3.5 (Tositti *et al.*, 2013) which resulted in a concentration reaching 80 μg m^{-3}. As previously highlighted in Chapter 2, this event was characterized by significant loadings of the coarse fraction with a small contribution of the fine fraction (to which radionuclides attach). As pointed out in Chapter 2, the ^{210}Pb increase during this event was not as relevant as that of PM_{10}: as a matter of facts, the per cent increase of ^{210}Pb with respect to the monthly mean was equal to +73% for ^{210}Pb, while for PM_{10} it was equal to +540%. Moreover, the per cent increase of ^{210}Pb with respect to the yearly mean was equal to +33%, while it was equal to +820% for PM_{10}.

The analysis of the magnitude of the seasonal and trend components of the time series revealed that the seasonal component dominates over the trend component and the small-time scale variations in almost all the measured atmospheric variables (the only exceptions are RH, ^{7}Be/^{210}Pb, TH and WS), weighting about twice the trend component. In turn, the small scale variations dominate both the NAO indexes, the monthly precipitation and the frequencies of the different advection patterns, with the only exception of the North American flows that present the strongest seasonal patterns as they are almost absent in summertime.

5.3.4 Association of air flow types and meteorological/atmospheric parameters with NAO

The NAO is often regarded as a winter phenomenon, since winter months are dynamically the most active and present the largest SLP amplitude anomalies. The winter season is also associated to the strongest interdecadal variability. For this reason the extended winter period (DJFM) is frequently used in the literature of NAO.

Table 5.4 shows the linear correlation coefficients for the cases presenting significant association to NAOi during the DJFM months. NAO is strongly related to North-American flows, while it is weakly anti-correlated to Western flows and very weakly to Mediterranean-Africa flows. As a matter of facts, it is recognized that the positive NAO phase corresponding to a stronger than usual subtropical high pressure centre and deeper than normal Icelandic low results in more and stronger winter storms crossing the Atlantic Ocean on a more northerly track, while the negative phase is connected to fewer and weaker winter storms crossing on a more west-east pathway. An anti-correlation of westerly flows reaching three Mediterranean sites with NAOi was also observed by Orza *et al.* (2013): as they explained, this is connected with the fact that the location of the

subtropical high at lower latitudes during the negative phase of the NAO facilitates the entrance of westerlies (W)/south-westerlies (Me-AF) to the Mediterranean. This is also shown in Figure 5.11, where the ratio between the residence time of air parcels reaching Mt. Cimone during positive and negative phases of NAO (NAOi higher and lower than +0.5 and -0.5, respectively) during the extended winter period is depicted. From the plot it is evident that south-westerlies and lower speed westerlies from the westernmost part of Northern Africa and southern Spain are more frequent during the negative phase of the NAO. On the contrary, flows from Lybia and surrounding regions, also part of the Mediterranean-Africa flows, are more common during the positive phase of NAO. Moreover, trajectories coming from North-America are more frequent during the positive phase of NAO, as indicated by the correlation of North-American flows with NAO. Also North-Eastern flows seem to be more usually observed during the positive NAO phase, even if this was not readily observed from the correlation analysis of Table 5.4.

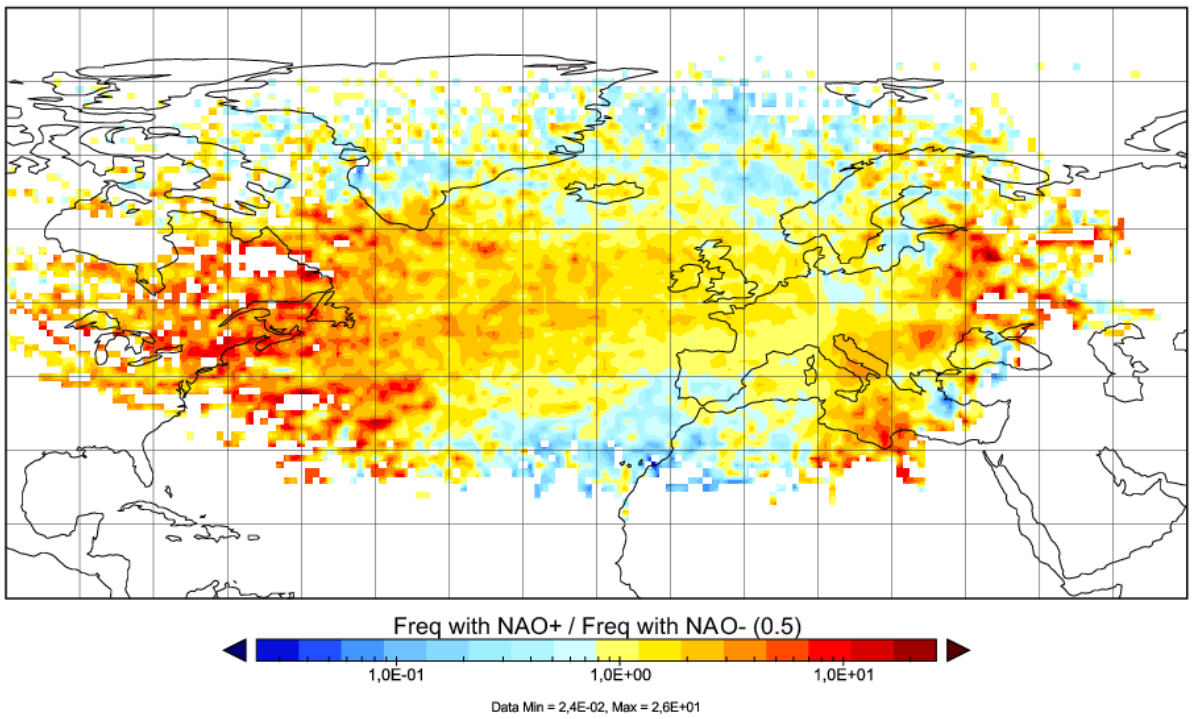

Figure 5.11 *Ratio of residence time of air parcels reaching Mt. Cimone in the positive and negative phase of NAO (NAOi higher than +0.5 and lower than -0.5, respectively) in the extended winter DJFM period.*

	Hurrell_Stat_NAOi	Hurrell_PC_NAOi	CRU_Stat_NAOi
A			
E			
Me-Af	-0.16		-0.25
W	*-0.31*	-0.25	
Atl			
N-Am	**0.48**	**0.41**	**0.49**
N-Atl			
NW-Eu			
p (mbar)		**0.48**	*0.38*
T (°C)			
RH (%)		-0.29	
TH (m)		*0.35*	*0.38*
WS (m s^{-1})			
Prec (mm)		*-0.28*	*-0.29*
O_3 (ppb)			
CO_2 (ppm)			
BC (μg m^{-3})			
CO (ppb)		*-0.77*	*-0.68*
^{7}Be (mBq m^{-3})			
^{210}Pb (mBq m^{-3})			
PM_{10} (μg m^{-3})			
Fine Particles (N cm^{-3})			
Coarse Particles (N cm^{-3})			
$^{7}Be/PM_{10}$ (mBq μg^{-1})			
$^{210}Pb/PM_{10}$ (mBq μg^{-1})			
$^{7}Be/^{210}Pb$			

Table 5.4 *Spearman correlation coefficients in the extended winter DJFM period for the cases with significant association between NAOi (Hurrell Station-based and principal components based, CRU station-based on the difference between SLP at Gibraltar and Southwest Iceland) and the frequencies of air flow types arriving at Mt. Cimone at 2200 m (first part of the table). In the second part of the table Spearman correlation coefficients in the extended winter DJFM period for the cases with significant association between NAOi and monthly medians of the atmospheric variables are reported. The correlation coefficient is bold when both linear and Kendall tests are significant at 0.01 level, italic when both tests are significant at 0.05 level; other values are significant at 0.1 level at least in one of the tests.*

A strong correlation of NAOi with pressure is also revealed; positive values of NAO are typically associated with milder weather over Western Europe (increased pressures). This results also in increased tropopause heights during this phase (weakly significant correlation of NAOi with this variable) and in anti-correlation with relative humidity (not very significant, though).

Westerlies were observed to bring on high values of CO in Figure 5.5, and this explains the observed anti-correlation of CO with NAOi.

Table 5.5 similarly reports the linear Spearman correlation coefficients for the cases presenting significant associations between monthly medians of the variables and frequencies of air flow types during the extended winter period (DJFM). Most of these associations were already observed in Figure 5.5 and in Table 5.1. Arctic flows anti-correlation with ^{210}Pb and fine particles appears mainly as the result the continental origin of ^{210}Pb and of Arctic air masses being very clean from the point of view of particles, even if they contribute more to fine than coarse-sized particles. The correlation of Arctic flows with temperature, which could be a striking feature of Table 5.5, could arise from the decreasing trend which was observed for North-American flows. In fact, North-American flows are the coldest air masses (Figure 5.4 and Table 5.1), and their decreasing trend could result in an increasing temperature and the resulting anti-correlation with Arctic flows which are not the coldest ones. This is also the cause of the correlation of Mediterranean-Africa flows with temperature. The second striking feature of Table 5.5 is the anti-correlation of Arctic flows with ^{7}Be, which seems quite in contradiction with the results of Figure 5.5 and Table 5.1. This results contrasting seasonal pattern of the two variables, thus deriving purely from mathematics and not from physics: in fact, when in Figure 5.6 we reported the seasonality of air flows and the seasonality of ^{7}Be and ^{210}Pb, it was quite clear that the seasonality of Arctic flows is just the opposite of that of ^{7}Be. Arctic flows are more frequent when ^{7}Be is low (from November to March) and ^{7}Be is higher in the central part of the year, when Arctic flows are less frequent, with the exception of June. In spite of the anti-correlation found between the frequency of Arctic flows and ^{7}Be activity, it was observed that they can contribute a lot to ^{7}Be increases (Figure 5.8), and moreover their contribution is generally higher during spring and summer than during winter, despite their higher frequency during the cold season. In any case, it seems that even if Arctic flows are associated to high ^{7}Be, the seasonality is masking that in the correlations. The association of Mediterranean-Africa flows to elevated values of black carbon and PM_{10} seems to be related to the occasional influence of biomass burning in that region (e.g., Cristofanelli *et al.*, 2009b) and to the influence of Saharan-Dust transports on PM_{10} values. The correlation of western air masses to temperature could be connected to the fact that these air masses travel not very high. Atlantic air masses coming from the ocean bring low values of fine particles and this explains the anti-correlation of these flows with fine particles number densities. North-American flows correlation to $^{7}Be/PM_{10}$ is due to the fact that this flow type is associated to high ^{7}Be but contemporary low PM_{10} values as being generally associated to low values of particles (both fine and coarse-sized, as from Figure 5.5). North Western-Europe flows are instead associated with higher anthropogenic pollution values and this is the reason of the elevated correlation coefficients with fine and coarse number densities.

	A	E	Me-Af	W	Atl	N-Am	N-Atl	NW-Eu
p (mbar)	-0.28							
T (°C)	*0.33*		*-0.37*	*0.42*				
RH (%)								
TH (m)								
WS (m s^{-1})								
Prec (mm)								
O_3 (ppb)								
CO_2 (ppm)								
BC (μg m^{-3})			*0.73*					
CO (ppb)								
^{7}Be (mBq m^{-3})	**-0.41**		0.29					
^{210}Pb (mBq m^{-3})	*-0.36*							
PM_{10} (μg m^{-3})			*0.30*					
Fine Particles (N cm^{-3})	*-0.68*				-0.57			0.57
Coarse Particles (N cm^{-3})								0.57
^{7}Be/PM_{10} (mBq μg^{-1})						0.26		
^{210}Pb/PM_{10} (mBq μg^{-1})								
^{7}Be/^{210}Pb								

Table 5.5 *Same as Table 5.4, but for the cases with significant association between monthly frequencies of flows of air flow types arriving at Mt. Cimone at 2200 m and monthly medians of the atmospheric variables.*

Even if the NAO is often regarded as a winter phenomenon, Barnston and Livezey (1987) showed that the NAO has a year-round influence on weather conditions in Europe with pronounced seasonal variation in location of the high and low pressure centres, and strong climate anomalies can also be detected outside the winter season (Pausata *et al.*, 2012). For this reason, the association between NAOi and frequencies of air flow types and between NAOi and monthly medians was further analysed by season. It was already observed by Pausata *et al.* (2012) that station-based indices being fixed in space cannot account for the seasonal migration of the NAO centres of action; instead the PC-based NAOi provides a more accurate representation of the NAO pattern in any season. Figure 5.12 reports the seasonal correlation coefficients of Hurrell Station and PC-based NAOi with flows. Figure 5.13 similarly reports seasonal correlation coefficients of Hurrell Station and PC-based NAOi with monthly medians.

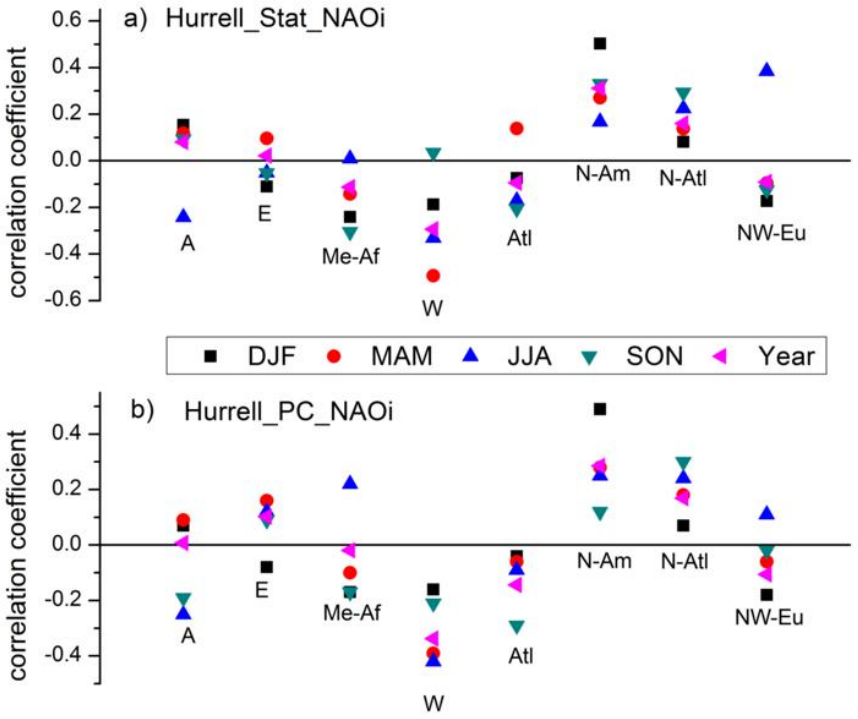

Figure 5.12 *Spearman correlation coefficients between the frequency of occurrence of the different air flow types and the NAOi (a) Hurrell station-based index; b) Hurrell PC-based index, by season and for the full year.*

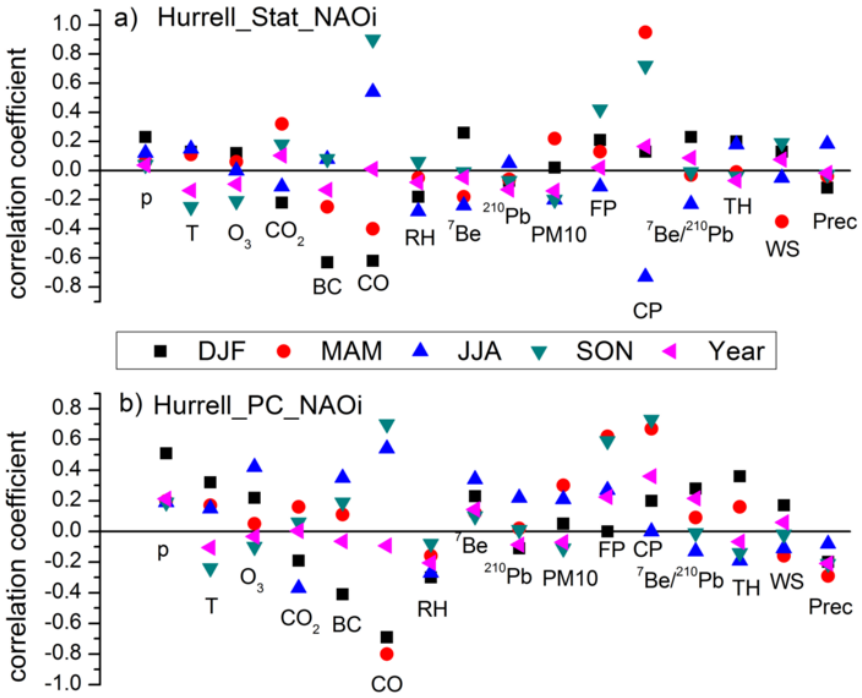

Figure 5.13 *Spearman correlation coefficients between the monthly medians of variables and the NAOi (a) Hurrell station-based index; b) Hurrell PC- based index, by season and for the full year. Capital letters indicate the variables: p = Pressure, T = temperature, O_3 = ozone, CO_2 = carbon dioxide, BC = black carbon, CO = carbon monoxide, RH = relative humidity, ^{7}Be, ^{210}Pb, PM_{10}, FP = fine particles, CP = coarse particles, $^{7}Be/^{210}Pb$, TH = tropopause height, WS = wind speed, Prec = precipitation.*

Considering winter instead of the extended winter period the correlation/anti-correlation coefficients are generally a bit higher. Anyway, the difference seems not very significant. The association between each air flow type and the NAO is similar during the different seasons but with some exceptions, namely Arctic, Eastern, Mediterranean-Africa (only in the PC-based NAOi), Atlantic and North Western-Europe. Arctic flows are negatively correlated to NAOi during summer, and weakly positively correlated during other seasons. Eastern flows are always weakly correlated to NAOi: as reported by Orza *et al.* (2013), the frequency of easterly flows in the Mediterranean is not connected to NAOi. The weak negative correlation of Mediterranean-Africa flows to NAOi which was observed during the extended winter period is present also during autumn, while during summer the PC-based NAOi (which provides a more accurate representation of the NAO pattern during this season) is positively correlated to this flow type. The anti-correlation with western flows is not restricted only to the winter period, but also to other seasons, being especially important during spring and summer (especially for the PC-based NAOi). Also Atlantic flows are negatively correlated to NAOi, even if a weak positive correlation of the station-based index is observed during spring. The correlation of NAOi with North-American flows is present throughout the year, being especially important during winter and less important during summer. It has to be remembered, however, that North-American flows are typical of the cold period, and almost non-present during the other seasons. North-Atlantic patterns, which on the contrary are present all-year long, are less correlated to NAOi but reach the highest correlation during autumn. North Western-Europe flows are positively correlated to NAOi during spring and weakly negatively correlated to NAOi during other seasons. A map similar to that of Figure 5.11 depicting the fraction of time that the air parcels stay in a grid point during the positive NAO phase with respect to the time spent in the same grid point during the negative NAO phase during the whole year (not shown) shows similar features (but not completely identical) to the ones that have been illustrated for the extended winter period. Anyway, the main features observed in the map are that the arrival of North-American air masses is more common during the positive phase of NAO, while westerlies/south-westerlies are on the contrary more frequent during the negative phase of NAO. Flows from the central-Eastern Mediterranean and Lybia are also more frequent during the positive phase of NAO.

Concerning the seasonal correlations of NAOi to atmospheric variables, the most appealing features of Figure 5.12 are the marked positive correlation of CO during autumn and less marked during summer, while during spring and winter a strong anti-correlation is observed. Because of this different correlation pattern during different seasons, no correlation is observed during the whole year time series. The anti-correlation of CO to NAOi during winter was explained as the

negative phase of NAO facilitates the entrance of westerlies to the Mediterranean, and this flow type is associated to high values of CO at Mt. Cimone. Anyway from this analysis it is also clear that during autumn and summer the positive phase of NAO is associated to higher values of CO; from the previous analysis it was observed that during autumn and spring NAO was linked to North Western-Europe and Northern-Atlantic flows, and these flows were also associated to high CO values in the boxplots. Coarse particles are positively correlated to NAO during the transition seasons, while during summer the station-based index is negatively correlated to coarse particles. Coarse particles are mostly transported by Western and Mediterranean-Africa, and to a lesser extent by North Western-Europe. The negative phase of NAO being associated to more westerlies/south-westerlies entering to the Mediterranean, the reason of the anti-correlation of coarse particles is easily understood. Positive NAO phases are associated to drier weather conditions in the Mediterranean area, corresponding to more relevant uplift of particles from the ground and this could explain the positive correlation during other seasons. Black carbon presents a pattern which is similar to CO, even if the positive correlation during the transition seasons is lower and observed only in the PC-based NAOi. However, the reasons of these associations are also connected to the negative phase of NAO facilitating the entrance of westerlies bringing high levels of BC. An association of the PC-based NAOi to O_3 was observed also by Pausata *et al.* (2012). This is fairly clear as the drier conditions in the Mediterranean area associated to the positive NAO phase result in the build-up of O_3 because of photochemical processes. The transport of O_3 enriched air masses from the Atlantic Ocean cannot be completely ruled out, however, and was also observed by Pausata *et al.* (2012). The weak positive correlation of NAO to ^{7}Be (which for the station-based NAOi is observed only during winter) can be associated to the shift of the storm track and associated SI events. An association of SI events at Mt. Cimone with NAO was already observed by Cristofanelli *et al.* (2009a). The positive correlation of NAO to TH should be linked to the higher tropopause connected to drier weather during the positive NAO phase. Other variables do not present relevant correlations to NAOi.

5.4 Summary and conclusions

This Chapter focused on finding relationships between the advection patterns and atmospheric composition observed in a long time series acquired at the WMO-GAW station of Mt. Cimone (Italy). Advection patterns were identified by a cluster analysis of back trajectories arriving at Mt. Cimone at three different heights; the cluster analysis identified 8 groups at the height of 2200 m, roughly corresponding to the altitude of the station. The results reflect strong seasonal patterns with

prevalence of westerlies as typical of mid-latitude Northern Hemisphere sites. The main features of these flow patterns, both from the meteorological and from the atmospheric composition point of view, were analysed by means of boxplots and significant differences. The results indicate that North-American flows are related to low pressures and tropopause heights, cold, and dry air masses, and linked to high wind speeds. These flows are almost non-existent during summertime, and are also generally related to low values of atmospheric pollutants such as BC, CO, O_3, PM_{10}, but also of atmospheric radionuclides ^{7}Be and ^{210}Pb. Arctic flows are also cold and more typical of the cold season. These flows are also connected to low values of atmospheric gases such as CO, O_3, BC, but also of particulate matter and ^{210}Pb. On the contrary, this flow type is associated with high ^{7}Be and seems connected to SI events. Continental flows from North-Western Europe, Eastern Europe, Western and Mediterranean-Africa are generally linked to higher values of atmospheric components; in particular, NW-Europe, Western and Eastern flows are related to "pollution" events, being associated with high levels of CO, BC, O_3 and fine particles number densities, causing also increases in PM_{10}. Because of their continental origin, these flows are also linked to high ^{210}Pb levels. Mediterranean-Africa flows being related to Saharan Dust events are related to high PM_{10} values, and increases in both the fine and coarse fraction of particles. Interestingly, this flow type was not only associated with high ^{210}Pb values, but also high ^{7}Be, which could be connected to the combination of African dust uplifting and downward movement from the upper troposphere.

The association of the seasonality of air mass transports with the seasonality of radionuclides and particulate matter was also studied. In fact, while ^{7}Be winter maximum can be linked to the seasonal behaviour of Arctic and North-Atlantic air masses, ^{7}Be summer maximum can be connected to the seasonal pattern of Mediterranean-Africa, Western and North Atlantic air masses. ^{210}Pb summer maximum seems to be well related with the seasonality of Western and North Western-Europe flows, whereas the seasonal pattern of PM_{10} might be, however, influenced by the seasonal pattern of advection types bringing about elevated mass loads of particles, such as Mediterranean-Africa, Western, North Atlantic and North Western-Europe flows.

Downward temporal trends were detected by means of non-parametric techniques for the monthly frequencies of Atlantic and North-American flows reaching Mt. Cimone at 2200 m, as well as for the monthly medians of ^{210}Pb and PM_{10} measured at the station in the period 1999-2006. These contemporary decreasing trends of both ^{210}Pb and PM_{10} cannot be ascribed to a decrease in anthropogenic emissions only, highlighting the potential role of meteorology, which would require further investigations to be carefully examined. Upward temporal trends were instead detected for CO_2 and monthly precipitation. However, the analysis of the magnitude of the seasonal and trend

components of the monthly time series revealed that the largest variabilities are associated with the seasonal components, with a reduced weight of the trend component for all the series.

The association of NAOi with advection patterns and atmospheric variables was also examined. In particular, positive correlations of NAO with the frequency of North-American flows and an anti-correlation with that of Western flows were observed. As for the atmospheric composition, the most important associations of NAO are with carbon monoxide and coarse particles, which are connected to the modifications of the flows induced by the shift of the NAO phase.

The most important aspect that was studied by this work is the role of flow patterns and NAO as factors that can have a deep influence in the variations in atmospheric composition. This was possible since the time series of data acquired at the station was long enough to characterize a sort of short-term climatology of the site. This work could be extended in a number of ways. For instance, the regions where the air masses originated when high levels of some atmospheric components are observed could be studied in greater detail, as well as information on the altitude of the trajectories along the pathway could be examined, since it can be useful to better understand the relation between air flow types and other meteorological/air quality data.

Acknowledgements

Italian Air Force Meteorological Office (IAFMS) and ISAC-CNR are gratefully acknowledged for their precious technical support at the Mt. Cimone station and for the help in the collection of compositional datasets, and in particular for providing data of meteorological and atmospheric composition data useful for this research. ISAC-CNR is gratefully acknowledged for providing aerosol size distribution, carbon dioxide, black carbon and ozone data, besides infrastructural access at the WMO-GAW Global Station Italian Climate Observatory "O. Vittori" at Mt. Cimone. IAFMS is gratefully acknowledged for providing meteorological and carbon dioxide data. The Italian Climate Observatory "O. Vittori" is supported by MIUR and DTA-CNR throughout the Project of National Interest NextData. World Data Centre for Greenhouse Gases (http://ds.data.jma.go.jp/gmd/wdcgg/) and EBAS databases (http://ebas.nilu.no/) are acknowledged for making available ozone, carbon dioxide, carbon monoxide, fine and coarse particle number density and black carbon data useful for this research work. We acknowledge NOAA (http://www.esrl.noaa.gov/) for providing the HYSPLIT trajectory model (available at http://ready.arl.noaa.gov/HYSPLIT.php) and the NCEP/NCAR reanalysis data used in this study. NOAA/ESRL Physical Sciences Division, Boulder Colorado is also acknowledged for providing daily images of meteorological variables (available at http://www.esrl.noaa.gov/psd/) useful for this research. James Hurrell and the National Center for Atmospheric Research staff are acknowledged for providing NAO indexes (both station and Principal Component-based) data and metadata retrieved from https://climatedataguide.ucar.edu/climate-data/hurrell-north-atlantic-oscillation-nao-index-station-based.Tim Osborn and CRU staff are acknowledged or providing NAO indexes based on the difference between the sea level pressure over Gibraltar and the sea level pressure over Southwest Iceland retrieved from http://www.cru.uea.ac.uk/~timo/datapages/naoi.htm. Erika Brattich thanks the University Miguel Hernandez de

Elche and Prof. Orza for giving her the possibility of a three months research period to start the collaboration which posed the scientific basis of this work.

References

Aebischer U., Schär C., 1998. Low-Level Potential Vorticity and Cyclogenesis to the Lee of the Alps. *Journal of the Atmospheric Sciences* 55, 186-207.

Allen R.J., Sherwood S.C., Norris J.R., Zender C.S., 2012. Recent Northern Hemisphere tropical expansion primarily driven by black carbon and tropospheric ozone. *Nature* 485, 350-353, doi:10.1038/nature11097

Añel J.A., Gimeno L., de la Torre L., Nieto R., 2006. Changes in tropopause height for the Eurasian region determined from CARDS radiosonde data. *Naturwissenschaften* 93, 603-609.

Arimoto R., Snow J.A., Graustein W.C., Moody J.L., Ray B.J., Duce R.A., Turekian K.K., Maring H.B., 1999. Influences of atmospheric transport pathways on radionuclide activities in aerosol particles from over the North Atlantic. *Journal of Geophysical Research* 104(D17), 301-321.

Ashbaugh L.L., Malm W.C., Sadeh W.Z., 1985. A residence time probability analysis of sulfur concentrations at Grand Canyon National Park. A statistical trajectory technique for determining air pollution source regions. *Atmospheric Environment* 19, 1263-1270.

Babu S.S., Chaubey J.P., Moorthy K.K., Gogoi M.M., Kompalli S.K., Sreekanth V., Bagare S.P., Bhatt B.C., Gaur V.K., Prabhu T.P., Singh N.S., 2011. High altitude (~4250 m asl) measurements of black carbon aerosols over western trans-Himalayas: Seasonal heterogeneity and source apportionment. *Journal of Geophysical Research* 116, D24201, doi:10.1029/2011JD016722

Balkanski Y.J., Jacob D.J., Gardner G.M., Graustein W.C., Turekian K.K., 1993. Transport and residence times or tropospheric aerosols inferred from a global three-dimensional simulation of ^{210}Pb. *Journal of Geophysical Research* 98, 20573-20586.

Balkanski Y., Bauer S.E., van Dingenen R., Bonasoni P., Schulz M., Fischer H., Gobbi G.P., Hanke M., Hauglustaine D., Putaud J.P., Stohl A., Raes F., 2003. The Mt. Cimone, Italy, free tropospheric campaign: principal characteristics of the gaseous and aerosol composition from European pollution, Mediterranean influences and during African dust events. *Atmospheric Chemistry and Physics Discussion* 3, 1753-1776.

Barmpadimos I., Hueglin C., Keller J., Henne S., Prévôt A.S.H., 2011. Influence of meteorology on PM_{10} trends and variability in Switzerland from 1991 to 2008. *Atmospheric Chemistry and Physics* 11, 1813-1835.

Barmpadimos I., Keller J., Oderbolz D., Hueglin C., Prévôt A.S.H., 2012. One decade of parallel fine ($PM_{2.5}$) and coarse (PM_{10}-$PM_{2.5}$) particulate matter measurements in Europe: trends and variability. *Atmospheric Chemistry and Physics* 12, 3189-3203.

Barnston A.G., Livezey R.E., 1987. Classification, seasonality and persistence of low-frequency atmospheric circulation patterns. *Monthly Weather Review* 115, 1083-1126.

Baskaran M., 2011. Po-210 and Pb-210 as atmospheric tracers and global atmospheric Pb-210 fallout: a review. *Journal of Environmental Radioactivity* 102, 500-513.

Beer J., McCracken K., von Steiger R., 2012. Cosmogenic radionuclides. Springer, Heidelberg, p. 426.

Beine H.J., Amoroso A., Esposito G., Sparapani R., Ianniello A., Georgiadis T., Nardino M., Bonasoni P., Cristofanelli P., and Dominé F., 2005. Deposition of atmospheric nitrous acid on alkaline snow surfaces. *Geophysical Research Letters* 32, L10808, doi:10.1029/2005GL022589

Bindoff N.L., et al., 2013. Detection and Attribution of Climate Change: from Global to Regional. In: Climate Change 2013: The Physical Science Basis. Contribution of Working Group I to the Fifth Assessment Report of the Intergovernmental Panel on Climate Change. Eds: Stockler T.F., Qin D., Plattner G.-K., Tignor M., Allen S.K., Boschung J., Nauels A., Xia Y., Bex V., Midgley P.M. Cambridge University Press, Cambridge, United Kingdom and New York, NY, USA.

Bonasoni P., Evangelisti F., Bonafé U., Feldmann H., Memmesheimer M., Stohl A., Tositti L., 1999. Stratosphere-troposphere exchanges: case studies recorded at Mt. Cimone during VOTALP project. *Physics and Chemistry of the Earth, Part C: Solar, Terrestrial and Planetary Science* I 24(5), 443-446.

Bonasoni P., Evangelisti F., Bonafé U., Ravegnani F., Calzolari F., Stohl A., Tositti L,. Tubertini O., Colombo T., 2000a. Stratospheric ozone intrusion episodes recorded at Mt. Cimone during VOTALP project: Case studies. *Atmospheric Environment* 34, 1355-1365.

Bonasoni P., Stohl A., Cristofanelli P., Calzolari F., Colombo T., Evangelisti F., 2000b. Background ozone variations at Mt Cimone station. *Atmospheric Environment* 34, 5183-5189.

Bonasoni P., Cristofanelli P., Calzolari F., Bonafé U., Evangelisti F., Stohl A., Zauli Sajani S., van Dingenen R., Colombo T., Balkanski Y., 2004. Aerosol-ozone correlations during dust transport episodes. *Atmospheric Chemistry and Physics* 4, 12501-1215.

Brankov E., Rao S.T., Porter P.S., 1998. A trajectory-clustering correlation methodology for examining the long-range transport of air pollutants. *Atmospheric Environment* 32 (9), 1525-1534.

Brocard E., Jeannet P., Begert M., Levrat G., Philipona R., Romanens G., Scherrer S.C., 2013. Upper air temperature trends above Switzerland 1959-2011. *Journal of Geophysical Research: Atmospheres* 118, 4303-4317. doi:10.1002/jgrd.50438

Brost R.A., Feichter J., Heimann M., 1991. Three-dimensional simulation of ^{7}Be in a global climate model. *Journal of Geophysical Research* 96, 22423-22445.

Cabello M., Orza J.A.G., Galiano V., 2008a. Influence of meteorological input data on backtrajectory cluster analysis-a seven-year study for southeastern Spain. *Advances in Science and Research* 2, 65-70.

Cabello M., Orza J.A.G., Galiano V., 2008b. Air mass origin and its influence over the aerosol size distribution: a study in SE Spain. *Advances in Science and Research* 2, 47-52.

Campana M., Li Y., Staehelin J., Prevot A.S.H., Bonasoni P., Loetscher H., Peter T., 2005. The influence of south foehn on the ozone mixing ratios at the high alpine site Arosa. *Atmospheric Environment* 39, 2945-2955.

Cape J.N., Methven J., Hudson L.E., 2000. The use of trajectory cluster analysis to interpret trace gas measurements at Mace Head, Ireland. *Atmospheric Environment* 34, 3651-3663.

Chen J., Carlson B.E., Del Genio A.D., 2002. Evidence for Strengthening of the Tropical General Circulation in the 1990s. *Science* 295, 838-841, doi:10.1126/science.1065835.

Cleveland R.B., Cleveland W.S., McRae J.E., Terpenning I., 1990. STL: A seasonal-trend decomposition procedure based on Loess. *Journal of Official Statistics* 6, 3–73.

Colette A., Granier C., Hodnebrog Ø., Jakobs H., Maurizi A., et al., 2011. Air quality trends in Europe over the past decade: a first multi-model assessment. *Atmospheric Chemistry and Physics* 11, 11657-11678.

Cristofanelli P., Bonasoni. P., Collins W., Feichter J., Forster C., James P., Kentarchos A., Kubik P.W., Land C., Meloen J., Roelofs G.J., Siegmund P., Sprenger M., Schnabel C., Stohl A., Tobler L., Tositti L., Trickl T., and Zanis P., 2003. Stratosphere-to-troposphere transport: A model and method evaluation. *Journal of Geophysical Research* 108(D12), 8525, doi:10.1029/2002JD002600

Cristofanelli P., Bonasoni P., Tositti L., Bonafé U., Calzolari F., Evangelisti F., Sandrini S., Stohl A., 2006. A 6-year analysis of stratospheric intrusions and their influence on ozone at Mt. Cimone (2165 m above sea level). *Journal of Geophysical Research* 111. D03306. doi:10.1029/2005JD006553.

Cristofanelli P., Bonasoni P., Carboni G., Calzolari F., Casarola L., Zauli Sajani S., Santaguida R., 2007. Anomalous high ozone concentrations recorded at a high mountain station in Italy in summer 2003. *Atmospheric Environment* 41, 1383-1394.

Cristofanelli P., Calzolari F., Bonafé U., Duchi R., Marinoni A., Roccato F., Tositti L., Bonasoni P., 2009a. Stratospheric intrusion index (SI^2) from baseline measurement data. *Theoretical and Applied Climatology* 97, 317-325.

Cristofanelli P., et al., 2009b. Significant variations of trace gas composition and aerosol properties at Mt. Cimone during air mass transport from North Africa – contributions from wildfire emissions and mineral dust. *Atmospheric Chemistry and Physics* 9, 4603-4619.

Cristofanelli P., Fierli F., Marinoni A., Calzolari F., Duchi R., Burkhart J., Stohl A., Maione M., Arduini J., Bonasoni P., 2013. Influence of biomass burning and anthropogenic emissions on ozone, carbon monoxide and black carbon at the Mt. Cimone WMO-GAW global station (Italy, 2165 m a.s.l.). *Atmospheric Chemistry and Physics* 13, 15-30. doi:10.5194/acp-13-15-2013

Cuevas E., Gonzalez Y., Rodríguez S., Guerra J.C., Gómez-Peláez A.J., Alonso-Pérez S., Bustos J., Milford C., 2013. Assessment of atmospheric processes driving ozone variations in the subtropical North Atlantic free troposphere. *Atmospheric Chemistry and Physics* 13, 1973-1998.

Doering C., Saey P., 2014. Hadley cell influence on ^{7}Be activity concentrations at Australian mainland IMS radionuclide particulate stations. *Journal of Environmental Radioactivity* 127, 88-94.

Dorling S.R., Davies T.D., Pierce C.E., 1992. Cluster analysis: a technique for estimating the synoptic meteorological controls on air and precipitation chemistry – method and applications. *Atmospheric Environment* 26, 2575-2581.

Draxler R., Hess G.D., 1997. Description of the HYSPLIT_4 modeling system. NOAA Tech. Memo. ERL ARL-224 NOAA Air Resources Laboratory, Silver Spring, MD, 24 pp.

Draxler, R.R., and G.D. Hess, 1998. An overview of the HYSPLIT_4 modeling system of trajectories, dispersion, and deposition. *Australian Meteorological Magazine*, **47**, 295-308.

Draxler, R.R., 1999. HYSPLIT4 user's guide. NOAA Tech. Memo. ERL ARL-230, NOAA Air Resources Laboratory, Silver Spring, MD.

Draxler R.R., Rolph G.D., 2003. HYSPLIT Model. NOAA Air Resources Laboratory. http://www.arl.noaa.gov/ready/hysplit4.html

Dueñas C., Orza J.A.G., Cabello M., Fernández M.C., Cañete S., Pérez M., Gordo E., 2011. Air mass origin and its influence on radionuclide activities (^{7}Be and ^{210}Pb) in aerosol particles at a coastal site in the western Mediterranean. *Atmospheric Research* 101, 205-214.

Eneroth K., Kjellstrom E., Holmen K., 2003. A trajectory climatology for Svalbard; investigating how atmospheric flow patterns influence observed tracer concentrations. *Physics and Chemistry of the Earth* 28, 1191-1203.

Eneroth K., Holmen K., Berg T., Schmidbauer N., Solberg S., 2007. Springtime depletion of tropospheric ozone, gaseous elemental mercury and nonmethane hydrocarbons in the European Arctic, and its relation to atmospheric transport. *Atmospheric Environment* 41, 8511-8526.

Feely H.W., Larsen R.J., Sanderson C.G., 1989. Factors that cause seasonal variations in ^{7}Be concentrations in surface air. *Journal of Environmental Radioactivity* 9, 223-249.

Fischer H., Kormann R., Klüpfel T., Gurk Ch., Königstedt R., Parchatka U., Mühle J., Rhee T.S., Brenninkmeijer C.A.M., Bonasoni P., Stohl A., 2003. Ozone production and trace gas correlations during the June 2000 MINATROC intensive measurement campaign at Mt Cimone. *Atmospheric Chemistry and Physics* 3, 725-738.

Fleming Z.L., Monks P.S., Manning A.J., 2012. Review: Untangling the influence of air-mass history in interpreting observed atmospheric composition. *Atmospheric Research* 104-105, 1-39.

Frierson D.M.W., Lu J., Chen G., 2007. Width of the Hadley cell in simple and comprehensive general circulation models. *Geophysical Research Letters* 34, L18804, doi:10.1029/2007GL031115

Gaffney J.S, Marley N., Cunningham M.M., 2004. Natural radionuclides in fine aerosols in the Pittsburgh area. *Atmospheric Environment* 38, 3191-3200.

Gerasopoulos E., Zanis P., Stohl A., Zerefos C.S., Papastefanou C., Ringer W., Tobler L., Hübener S., Gäggeler H.W., Kanter H.J., Tositti L., Sandrini S., 2001. A climatology of ^{7}Be at four high-altitude stations at the Alps and the Northern Apennines. *Atmospheric Environment* 35, 6347-6360.

Gerasopoulos E., Zanis P.B., Zerefos C.S., Papastefanou C., Ringer W., Gäggeler H.W., Tobler L., Kanter H.J., 2005. Factors and processes controlling the concentration of the cosmogenic radionuclide 7Be at high altitude Alpine stations. The Natural Radiation Environment (NRE-VII), Seventh International Symposium on the Natural Radiation Environment (NRE-VII) Rhodes, Greece, 20-24 May 2002, series: Radioactivity in the Environment, V7, ISSN 1569-4860/doi 10.1016/S1569-4860(04)07108-6, edited by McLaughlin J.P., Simopoulos E.S., Steinhäusler F., Elsevier Science.

Gettelman A., Birner T., 2007. Insights on tropical tropopause layer processes using global models. *Journal of Geophysical Research* 112, D23104, doi:10.1029/2007JD008945.

Gettelman A., et al., 2009. The tropical tropopause 1960-2100. *Atmospheric Chemistry and Physics* 9, 1621-1637.

Gettelman A., et al., 2010. Multi-model assessment of the upper troposphere and lower stratosphere: Tropics and trends. Journal of Geophysical Research 115, D00M08, doi:10.1029/2009JD013638.

Gettelman A., Hoor P., Pan L.L., Randel W.J., Hegglin M.I., Birner T., 2011. The extratropical upper troposphere and lower stratosphere. *Reviews of Geophysics* 49, RG3003, doi:10.1029/2011RG000355

Gobbi G.P., Barnaba F., van Dingenen R., Putaud J.P., Mircea M., Facchini M.C., 2003. Lidar and in situ observations of continental and Saharan aerosol: closure analysis and optical properties. *Atmospheric Chemistry and Physics* 3, 2161-2172.

Hansen J., et al., 2002. Climate forcings in Goddard Institute for Space Studies SI2000. Journal of Geophysical Research 107(D18), 4347, doi:10.1029/2001JD001143.

Hernández F., Rodríguez S., Karlsson L., Alonso-Pérez S., López-Pérez M., Hernandez-Armas J., Cuevas E., 2008. Origin of observed high ^{7}Be and mineral dust concentrations in ambient air on the Island of Tenerife. *Atmospheric Environment* 42, 4247-4256.

Highwood E.J., Hoskins B.J., Berrisford P., 2000. Properties of the arctic tropopause. *Quarterly Journal of the Royal Meteorological Society* 126, 1515-1532.

Hirsch R.M., Slack J.R., Smith R.A., 1982. Techniques of trend analysis for monthly water quality data, *Water Resources Research*, 18(1), 107–121.

Hoskins, 2003. Climate Change at Cruising Altitude? *Science* 301, 469-470.

Hu Y., Tung K.K., Liu Y., 2005. A Closer Comparison of Early and Late-Winter Atmospheric Trends in the Northern Hemisphere. *Journal of Climate* 18, 3204-3216.

Hu Y., Fu Q., 2007. Observed poleward expansion of the Hadley circulation since 1979. *Atmospheric Chemistry and Physics* 7, 5229-5236.

Hu Y., Tao L., Liu J., 2013. Poleward Expansion of the Hadley circulation in CMIP5 Simulations. *Advances in Atmospheric Sciences* 30, No.3, 790-795.

Huang L., Gong S.L., Sharma S., Lavoue D., Jia C.Q., 2010. A trajectory analysis of atmospheric transport of black carbon aerosols to Canadian high Arctic in winter and spring (1990-2005). *Atmospheric Chemistry and Physics* 10, 5065-5073.

Hurrell J.W., 1995. Decadal trends in the North Atlantic oscillation: regional temperatures and precipitation. *Science* 269, 676-679.

Hurrell J.W., Kushnir Y., Ottersen G., Visbeck M., 2003. An overview of the North Atlantic Oscillation. In: The North Atlantic Oscillation: Climatic Significance and Environmental Impact, AGU monograph 13, 1-35.

Hurrell J.W., 2013. The climate data guide: Hurrell North Atlantic Oscillation (NAO) index (station-based)". National Center for Atmospheric Research staff (Eds.) Retrieved from https://climatedataguide.ucar.edu/climate-data/hurrell-north-atlantic-oscillation-nao-index-station-based, last accessed 01 October 2013.

Ioannidou A., Manolopoulou M., Papastefanou C., 2005. Temporal changes of ^{7}Be and ^{210}Pb concentrations in surface air at temperate latitudes (40°). *Applied Radiation and Isotopes* 63(2), 277-284.

Ioannidou A., Kotsopoulou E., Papastefanou C., 2011. ^{7}Be in the lower atmosphere at a mid-latitude (40°N) during the year 2009 of a particular minim of solar activity. *Journal of Radioanalytical and Nuclear Chemistry* 289, 395-400.

Ioannidou A., Vasileiadis A., Melas D., 2014. Time lag between the tropopause height and ^{7}Be activity concentrations in surface air. *Journal of Environmental Radioactivity* 129, 80-85.

James P, Stohl A., Forster C., Eckhardt S., Seibert P., Frank A., 2003. A 15-year climatology of stratosphere-troposphere exchange with a Lagrangian particle dispersion model 2. Mean climate and seasonal variability. *Journal of Geophysical Research* 108(D12), 8522. doi:10.1029/2002JD002639

Johnson W., Viezee W., 1981. Stratospheric ozone in the lower troposphere-I. Presentation and interpretation of aircraft measurements. *Atmospheric Environment* 15, 1309–1323.

Jones P.D., Jonsson T., Wheeler D., 1997. Extension to the North Atlantic Oscillation using early instrumental pressure observations from Gibraltar and South-West Iceland. *International Journal of Climatology* 17, 1433-1450.

Kaiser A., Scheifinger H., Spangl W., Weiss A., Gilge S., Fricke W., Ries L., Cemas D., Jesenovec B., 2007. Transport of nitrogen oxides, carbon monoxide and ozone to the Alpine Global Atmosphere Watch

stations Jungfraujoch (Switzerland), Zugspitze and Hohenpeissenberg (Germany), Sonnblick (Austria) and Mt. Krvavec (Slovenia). *Atmospheric Environment* 41, 9273-9287.

Kalnay E., et al., 1996. The NCEP/NCAR reanalysis 40-year project. *Bulletin of the American Meteorological Society* 77, 437-471.

Keeling C.D., Chin J.F.S., Whorf T.P., 1996. Increased activity of northern vegetation inferred from atmospheric CO_2 measurements. *Nature* 382, 146-149.

Koch D.M., Jacob J., Graustein W.C., 1996. Vertical transport of tropospheric aerosols as indicated ^{7}Be and ^{210}Pb in a chemical tracer model. *Journal of Geophysical Research* 101: 18651-18666.

Kulan A., Aldahan A., Possnert G., Vintersved I., 2006. Distribution of ^{7}Be in surface air of Europe. *Atmospheric Environment* 40, 3855-3868.

Lee H.N., Wan G., Zheng X., Sanderson C.G., Josse B., Wang S., Yang W., Tang J., Wang C., 2004. Measurements of ^{210}Pb and ^{7}Be in China and their analysis accompanied with global model calculations of ^{210}Pb. *Journal of Geophysical Research* 109, D22203. doi:10.1029/2004JD005061

Lee H.N., Tositti L., Zheng X., Bonasoni P., 2007. Analyses and comparisons of variations of ^{7}Be, ^{210}Pb and ^{7}Be/^{210}Pb with ozone observations at two Global Atmosphere Watch stations from high mountains. *Journal of Geophysical Research* 112, D05303. doi:10.1029/2006JD007421

Likuku A.S., 2006. Factors influencing ambient concentrations of ^{210}Pb and ^{7}Be over the city of Edinburgh (55.9°N, 03.2°W). *Journal of Environmental Radioactivity* 87, 289-304.

Li Q., Jacob D.J., Fairlie T.D., Liu H., Martin R.V., Yantosca R.M., 2002. Stratospheric versus pollution influences on ozone at Bermuda: Reconciling past analyses. *Journal of Geophysical Research* 107, D22, 4611. doi:10.1029/2002JD002138

Lozano R.L., Hernández-Ceballos M.A., San Miguel E.G., Adame J.A., Bolívar J.P., 2012. Meteorological factors influencing the ^{7}Be and ^{210}Pb concentrations in surface air from the southwestern Iberian Peninsula. *Atmospheric Environment* 43, 168-178.

Lu J., Vecchi G.A., Reichler T., 2007. Expansion of the Hadley cell under global warming. *Geophysical Research Letters* 34, L06805, doi:10.1029/2006GL028443

Machta L., 1972. Mauna Loa and global trends in air quality. *Bulletin of the American Meteorological Society* 53, 402-420.

Marenco F., et al., 2006. Characterization of atmospheric aerosols at Monte Cimone, Italy, during summer 2004: Source apportionment and transport mechanisms. *Journal of Geophysical Research* 111, D24202. doi:10.1029/2006JD007145

Marinoni A., Cristofanelli P., Calzolari F., Roccato F., Bonafé U., Bonasoni P., 2008, Continuous measurements of aerosol physical parameters at the Mt Cimone GAW Station (2165 m asl, Italy). *Science of the Total Environment* 391, 241-251.

Mitas C.M., Clement A., 2005. Has the Hadley cell been strengthening in recent decades? *Geophysical Research Letters* 32, L03809, doi:10.1029/2004GL021765

Moody J.L., Galloway J.N., 1988. Quantifying the relationship between atmospheric transport and the chemical composition of precipitation on Bermuda. *Tellus* 40B, 463-479.

Moody J.L., Galusky J.A., Galloway J.N., 1989. The use of atmospheric transport pattern recognition techniques in understanding variation in precipitation chemistry. Atmospheric Deposition (Proceedings of the Baltimore Symposium, May 1989). IAHS Publ. No. 179.

Moody J.L., Oltmans S.J., Levy H., Merrill J.T., 1995. Transport climatology of tropospheric ozone: Bermuda, 1988-1991. *Journal of Geophysical Research* 100, 7179-7194.

Myhre G., et al., 2013. Anthropogenic and Natural Radiative Forcing. In: Climate Change 2013: The Physical Science Basis. Contribution of Working Group I to the Fifth Assessment Report of the Intergovernmental Panel on Climate Change. Eds: Stocker T.F., Qin D., Plattner G.-K., Tignor M., Allen S.K., Boschung J., Nauels A., Xia Y., Bex V., Midgley P.M. Cambridge University Press, Cambridge, United Kingdom and New York, NY, USA.

Orza J.A.G., Cabello M., Galiano V., Vermeulen A.T., Stein A., 2013. The association between NAO and the interannual variability of the tropospheric transport pathways in western Europe. In Lagrangian Modeling of the Atmosphere (Eds Lin J., Brunner D., Gerbig C., Stohl A., Luhar A., Webley P.), AGU Geophysical Monograph Vol. 200, 127-141.

Paatero J., Hatakka J., 2000. Source areas of airborne ^{7}Be and ^{210}Pb in Northern Finland. *Health Physics* 79(6), 691-696.

Pace G., Meloni D., di Sarra A., 2005. Forest fire aerosol over the Mediterranean basin during summer 2003. *Journal of Geophysical Research* 110, D21202. doi:10.1029/2005JD005986

Papastefanou C., Ioannidou A., 1995. Aerodynamic size association of ^{7}Be in ambient aerosols. *Journal of Environmental Radioactivity* 26, 273-282.

Pausata F.S.R., Pozzoli L., Vignati E., Dentener F.J., 2012. North Atlantic Oscillation and tropospheric ozone variability in Europe: model analysis and measurements intercomparison. *Atmospheric Chemistry and Physics* 12, 6357-6376.

Pérez N., Pey J., Castillo S., Viana M., Alastuey A., Querol X., 2008. Interpretation of the variability of levels of regional background aerosols in the Western Mediterranean. *Science of the Total Environment* 407, 527-540.

Perrone M.R., Becagli S., Orza J.A.G., Vecchi R., Dinoi A., Udisti R., Cabello M., 2013. The impact of long-range-transport on PM1 and PM2.5 at a Central Mediterranean site. *Atmospheric Environment* 71, 176-186.

Pochanart P., Akimoto H., Maksyutov S., Staehelin J., 2001. Surface ozone at the Swiss Alpine site Arosa: the hemispheric background and the influence of large-scale anthropogenic emissions. *Atmospheric Environment* 35, 5553-5566.

Previdi M., Liepert B.G., Peteet D., Hansen J., Beerling D.J., Broccoli A J., Frolking S., Galloway J.N., Heimann N., Le Quéré C., Levitus S., Ramaswamy V., 2013. Climate sensitivity in the anthropocene. *Quarterly Journal of the Royal Meteorological Society* 139, 674, 1121-1131.

Putaud J.-P., van Dingenen R., Dell'Acqua A., Raes F., Matta E., Decesari S., Facchini M.C., Fuzzi S., 2004. Size-segregated aerosol mass closure and chemical composition in Monte Cimone (I) during MINATROC. *Atmospheric Chemistry and Physics* 4, 889-902.

Ramaswamy V., Schwarzkopf M.D., Randel W.J., 1996. Fingerprint of ozone depletion in the spatial and temporal pattern of recent lower-stratospheric cooling. *Nature* 382, 616-618.

Ramaswamy V., et al., 2001. Stratospheric temperature trends: Observations and model simulations. *Reviews of Geophysics* 39, 71-122, doi:10.1029/1999RG000065

Randel W.J., Wu F., Gaffen D.J., 2000. Interannual variability of the tropopause derived from radiosonde data and NCEP reanalysis. *Journal of Geophysical Research* 105, 15509-15524.

Randerson J.T., Thompson M.V., Conway T.J., Fung I.Y., Field C.B., 1997. The contribution of terrestrial sources and sinks to trends in the seasonal cycle of atmospheric carbon dioxide. *Global Biogeochemical Cycles* 11(4), 535-560.

Salvador P., Artiñano B., Pio C., Afonso J., Legrand M., Puxbaum H., Hammer S., 2010. Evaluation of aerosol sources at European high altitude background sites with trajectory statistical methods. *Atmospheric Environment* 44, 2316-2329.

Santer B.D., Sausen R., Wigley T.M.L., Boyle J.S., AchutaRao K., Doutriaux C., Hansen J.E., Meehl G.A., Roeckner E., Ruedy R., Schmidt G., Taylor K.E., 2003a. Behavior of tropopause height and atmospheric temperature in models, reanalyses, and observations: decadal changes. *Journal of Geophysical Research* 108, No.D1, 4002, doi 10.1029/2002JD002258

Santer B.D., Wehner M.F., Wigley T.M.L., Sausen R., Meehl G.A., Taylor K.E., Ammann C., Arblaster J., Washington W.M., Boyle J.S., Brüggemann W., 2003b. Contributions of Anthropogenic and Natural Forcing to Recent Tropopause Height Changes. *Science* 301, 479-483

Santer B.D., Wigley T.M.L., Simmons A.J., Kålberg P.W., Kelly G.A., Uppala S.M., Ammann C., Boyle J.S., Brüggemann W., Doutriaux C., Fiorino M., Mears C., Meehl G.A., Sausen R., Taylor K.E., Washington W.M., Wehner M.F., Wentz F.J., 2004. Identification of anthropogenic climate using a second-generation analysis. *Journal of Geophysical Research* 109, D21104, doi:10.1029/2004JD005075

Santer B.D., Painter J.F., Bonfils C., Mears C.A., Solomon S., Wigley T.M.L., Glecker P.J., Schmidt G.A., Doutriaux C., Gillett N.P., Taylor K.E., Thorne P.W., Wentz F.J., 2013. Human and natural influences on the changing thermal structure of the atmosphere.

Scheel H.E., Brunke E.G., Sladkovic R., Seiler W., 1998. In situ CO concentrations at the sites Zugspitze (47°N, 11°E) and Cape Point (34°S, 18°E) in April and October 1994. *Journal of Geophysical Research* 103, D15, 19295-19304.

Schmidt T., Wickert J., Beyerle G., Heise S., 2008. Global tropopause height trends estimated from GPS radio occultation data. *Geophysical Research Letters* 35, L11806, doi:10.1029/2008GL034012

Schwikowski M., Seibert P., Baltensperger U., Gäggeler H.W., 1995. A study of an outstanding Saharan dust event at the high-alpine site Jungfraujoch, Switzerland. *Atmospheric Environment* 29(15), 1829-1842.

Seibert P., Kromp-Kolb H., Baltensperger U., Jost D.T., Schwikowski M., Kasper A., Puxbaum H., 1994. Trajectory analysis of aerosol measurements at high alpine sites. In: Borrell P.M., Borrell P., Cvitas T., Seiler W. (Eds.), Transport and Transformations of pollutants in the Troposphere. Academic Publishing, Den Haag, pp. 689-693.

Seidel D.J., Ross R.J., Angell J.K., Reid G.C., 2001. Climatological characteristics of the tropical tropopause as revealed by radiosondes. Journal of Geophysical Research 106, No.D8, 7857-7878

Seidel D.J., Randel W.J., 2006. Variability and trends in the global tropopause estimated from radiosonde data. *Journal of Geophysical Research* 111, D21101, doi:10.1029/2006JD007363.

Seidel D.J., Fu Q., Randel W.J., Reichler T.J., 2008. Widening of the tropical belt in a changing climate. *Nature Geosciences* 1, 21-24.

Sharma S., Andrews E., Barrie L.A., Ogren J.A., Lavoue D., 2006. Variations and sources of the equivalent black carbon in the high Arctic revealed by long-term observations at Alert and Barrow: 1989-2003. *Journal of Geophysical Research* – Atmospheres, 111.

Shepherd T.G., 2002. Issues in stratosphere-troposphere coupling. *Journal of the Meteorological Society of Japan* 80, 769-792.

Stohl A., Spoichtinger-Rakowsky N., Bonasoni P., Feldmann H., Memmesheimer M., Scheel H.E., Trickl T., Hübener S., Ringer W., Mandl M., 2000. The influence of stratospheric intrusions on alpine ozone concentrations. *Atmospheric Environment* 34, 1323-1354.

Stohl A., Haimberger L., Scheele M.P., Wernli H., 2001. An intercomparison of results from three trajectory models. *Meteorological Applications*, 8, 127–135.

Stohl A., et al., 2003. Stratosphere-troposphere exchange: a review, and what we have learned from STACCATO. *Journal of Geophysical Research* 108 (D12), 8516.

Tarasova O.A., Senik I.A., Sosonkin M.G., Cui J., Staehelin J., Prevot A.S.H., 2009. Surface ozone at the Caucasian site Kislovodsk High Mountain Station and the Swiss Alpine site Jungfraujoch: data analysis and trends (1990-2006). *Atmospheric Chemistry and Physics* 9, 4157-4175.

Thoning K.W., Tans P.P., Komhyr W.D., 1989. Atmospheric carbon dioxide at Mauna Loa Observatory: 2. Analysis of the NOAA GMCC data, 1974-1985. *Journal of Geophysical Research: Atmospheres* 94(D6), doi:10.1029/JD094iD06p08549

Tositti L., Hübener S., Kanter H.J., Ringer W., Sandrini S., Tobler L., 2004. Intercomparison of sampling and measurement of ^{7}Be in air at four high-altitude locations in Europe. *Applied Radiation and Isotopes* 61, 1497-1502.

Tositti L., Brattich E., Cinelli G., Previti A., Mostacci D., 2012. Comparison of radioactivity data measured in PM10 aerosol samples at two elevated stations in northern Italy during the Fukushima event. *Journal of Environmental Radioactivity* 114, 105-112.

Tositti L., Riccio A., Sandrini S., Brattich E., Baldacci D., Parmeggiani S., Cristofanelli P., Bonasoni P., 2013. Short-term climatology of PM10 at a high altitude background station in southern Europe. *Atmospheric Environment* 65, 145-152.

Tositti L., Brattich E., Cinelli G., Baldacci D., 2014. 12 years of ^{7}Be and ^{210}Pb data at the WMO-GAW station of Mt. Cimone (2165 m a.s.l., 44°12'N 10°42'E) and their correlation with meteorological parameters. *Atmospheric Environment* 87C, 108-122. doi:10.1016/j.atmosenv.2014.01.014

Tscherwenka W., Seibert P., Kasper A., Puxbaum H., 1998. On-line measurements of sulphur dioxide at the 3 km level over central Europe (Sonnblick observatory, Austria) and statistical trajectory source analysis. *Atmospheric Environment* 32(23), 3941-3952.

Turekian K.K., Nozki Y., Benninger L.K., 1977. Geochemistry of atmospheric radon and radon products. *Annual Review of Earth and Planetary Science*, 5, 227-255.

Uglietti C., Leuenberger M., Brunner M., 2011. European source and sink areas of CO_2 retrieved from Lagrangian transport model interpretation of combined O2 and CO2 measurements and the high alpine research station Jungfraujoch. *Atmospheric Chemistry and Physics* 11, 8017-8036.

Usoskin I., Kovaltsov. G., 2008.Production of cosmogenic ^{7}Be isotope in the atmosphere: full 3D modelling. *Journal of Geophysical Research* 113, D12107.

Yue S., Pilon P., Phinney P., Cavadias G., 2002. The influence of autocorrelation on the ability to detect trend in hydrological series. *Hydrological Processes* 16(9), 1807-1829.

Walker G.T., 1924. Correlation in seasonal variation of weather, IX: A further study of world weather. *Memoirs of the India Meteorological Department* 24, 275-332.

Walker G.T., Bliss E.W., 1932.World Weather V. *Memoirs of the Royal Meteorological Society* IV(36), 53-84.

Wallace M., 2000. North Atlantic Oscillation/annular mode: Two paradigms-one phenomenon. *Quarterly Journal of the Royal Meteorological Society* 126, 791-805.

Wang T.J., Lam K.S., Tsang C.W., Kot S.C., 2004. On the variability and correlation of surface ozone and carbon monoxide observed in Hong Kong using trajectory and regression analyses. *Advances in Atmospheric Sciences* 21, 141-152.

Wilks D., 2006. Statistical methods in the Atmospheric Sciences. International Geophysics Series. Second Edition Academic Press.

Winkler R., Dietl F., Frank G., Thiersch J., 1998. Temporal variation of ^{7}Be and ^{210}Pb size distributions in ambient aerosols. *Atmospheric Environment* 32, 983-991.

WMO (World Meteorological Organization), 2007. Scientific Assessment on Ozone Depletion. 2006, Global Ozone Research Monitoring Project-Report, No.50, Geneva Switzerland.

Wotawa G., Kröger H., Stohl A., 2000. Transport of ozone towards the Alps – results from trajectory analyses and photochemical studies. *Atmospheric Environment* 34, 1367-1377.

Xia X., Chen H., Zhang W., 2007. Analysis of the dependence of column-integrated aerosol properties on long-range transport of air masses in Beijing. *Atmospheric Environment* 41, 7739-7750.

Zanis P., Schuepbach E., Gäggeler H.W., Huebener S., Tobler L., 1999. Factors controlling Beryllium-7 at Jungfraujoch in Switzerland. *Tellus* 51 (4), 789-805.

Zanis P., et al., 2003. An estimate of the impact of stratosphere-to-troposphere transport (STT) on the lower free tropospheric ozone over the Alps using ^{10}Be and ^{7}Be measurements. *Journal of Geophysical Research* 108(D12), 8520. doi:10.1029/2002JD002604

CHAPTER 6 – Influence of Stratospheric Air Masses on Radiotracers and Ozone at Mt. Cimone

6.1 Introduction[1]

Although measurements of both radionuclides ^{7}Be and ^{210}Pb and the study of stratospheric intrusions have a long term tradition at the global WMO-GAW station of Mt. Cimone (44°11'N, 10°42'E, 2165 m asl), at present only few of these studies made use of the simultaneous measurements of both atmospheric radiotracers, e.g., as activity ratio, while most of them used only ^{7}Be. Research activities carried out at Mt. Cimone within EU projects VOTALP and STACCATO (Bonasoni *et al.*, 1999, 2000a, b; Fischer *et al.*, 2003; Cristofanelli *et al.*, 2003, 2006, 2009) led to the introduction of a Stratospheric Index based on the use of ^{7}Be, relative humidity and ozone (Cristofanelli *et al.*, 2009), and to the study of the seasonality and of short-term climatology of stratospheric intrusions at Mt. Cimone. In agreement with comprehensive studies of Stratosphere-to-Troposphere-Exchange (STE) in the Northern Hemisphere mid-latitudes (James *et al.*, 2003a, Sprenger and Wernli, 2003; Stohl *et al.*, 2003; Trickl *et al.*, 2010), as well as with studies carried on at other mountain sites in Europe, such as Zugspitze (2962 m asl, Germany) (Elbern *et al.*, 1997), Jungfraujoch (3580 m asl, Switzerland) and Sonnblick (3106 m asl, Austria) (Stohl *et al.*, 2000), stratospheric intrusions at Mt. Cimone are characterized by a maximum from October to February with a minimum in July (Cristofanelli *et al.*, 2006, 2009). During the warm season the efficient vertical mixing enhances the downward transport of air masses from the upper troposphere (Feely *et al.*, 1989; Gerasopoulos *et al.*, 2001, 2003), which can lead to erroneous stratospheric intrusions (SI) identifications. SI can be considered as a specific aspect of STE: the irreversible downward transport of stratospheric air relatively deep into troposphere (James *et al.*, 2003a). A number of different mechanisms can promote SI, acting on different geographical and temporal scales (Stohl *et al.*, 2000): fronts or high-pressure systems at the surface (Davies and Schuepbach, 1994; Zanis *et al.*, 1999), tropopause folding (Lamarque and Hess, 1994; Holton *et al.*, 1995; Reed, 1995; Elbern *et al.*, 1997;) and cut-off lows (Vaughan and Price, 1989; Zanis *et al.*, 2003a).

These events are characterized by tongues of anomalously high potential vorticity (PV), high ozone, high ^{7}Be and low water vapor mixing ratio, which may be stretched out into elongated filaments or roll up to form isolated coherent structures containing high PV (cut-off lows) (Holton

[1] This chapter consists of a manuscript in preparation by Brattich E. (Dept. of Biological, Geological and Environmental Sciences-Section of Geology, Università di Bologna), Orza J.A.G. (SCOLAb, Fisica Aplicada, Miguel Hernandez University; Elche, Spain), Tositti L. (Dept. of Chemistry, Università di Bologna).

et al., 1995). In particular the analysis of in situ pressure values (Cristofanelli *et al.*, 2006) suggested that at Mt. Cimone direct SI, which are the events in which stratospheric air maintains for a large part its stratospheric properties as it reaches the lower troposphere by rapid vertical transport (Eisele *et al.*, 1999) were connected with intense fronts affecting the region; on the contrary indirect SI, i.e., events in which stratospheric air reach the lower troposphere after a sequence of transport steps, with a greater chance to mix with tropospheric air (Eisele *et al.*, 1999), were possibly connected with subsiding structures related to anticyclonic areas. Although object of a long scientific debate over the last five decades (Junge, 1962; Crutzen, 1973; Chameides and Walker, 1973; Reiter, 1975; Fabian and Pruchniewicz, 1977; Singh *et al.*, 1978; Logan, 1985; Penkett and Brice, 1986; Austin and Follows, 1991; Follows and Austin, 1992; Davies and Schuepbach, 1994; Holton *et al.*, 1995; Appenzeller *et al.*, 1996; Roelofs and Lelieveld, 1997; Harris *et al.*, 1998; Bonasoni *et al.*, 1999, 2000a, b; Lelieveld and Dentener, 2000; Monks, 2000; Stohl *et al.*, 2000; James *et al.*, 2003a, b; Sprenger and Wernli, 2003; Stohl *et al.*, 2003; Fischer *et al.*, 2003; Cristofanelli *et al.*, 2006, 2009; Trickl *et al.*, 2010), STE and especially the cross-tropopause flux of ozone are still topics of great scientific interest and not thoroughly elucidated.

Moreover, the geographical areas associated to high concentrations of atmospheric radiotracers and atmospheric SI related components measured at Mt. Cimone have not been completely assessed. Together with ^{222}Rn, atmospheric radiotracers ^{7}Be and ^{210}Pb are among the most used naturally occurring radionuclides included in the group of the key atmospheric components that should be routinely monitored within the WMO-GAW network (WMO-GAW, 2004). Their importance in the understanding of vertical transports of air masses is due to their natural contrasted origin. In fact, ^{210}Pb (half-life $T_{1/2}$ = 22.1 years) is a radionuclide of crustal origin, being produced by the radioactive decay of ^{222}Rn ($T_{1/2}$ = 3.8 days) which is supplied to the atmosphere by the Earth's crust: as stated by Baskaran *et al.* (2011), the ^{222}Rn flux from the oceans is negligible compared to the input of continental origin. ^{7}Be ($T_{1/2}$ = 53.3 days) is instead a cosmogenic radionuclide produced by cosmic-ray spallation reactions with nitrogen and oxygen (Usoskin *et al.*, 2009) and is mostly produced in the stratosphere (about 75%) and in the upper troposphere (about 25%) (Johnson and Viezee, 1981; Usoskin and Kovaltsov, 2008). Once produced, both radionuclides rapidly attach to submicron-sized particles (Papastefanou and Ioannidou, 1995; Winkler *et al.*, 1998; Gaffney *et al.*, 2004; Ioannidou *et al.*, 2005), and for this reason they share a similar tropospheric fate being removed from the atmosphere by wet and dry deposition mechanisms (Feely *et al.*, 1989; Kulan *et al.*, 2006). Due to the different origins of the two radionuclides, they are used to study the origin of the air masses and to examine vertical exchange transport processes as well as convective activity in the troposphere (Brost *et al.*, 1991; Graustein

and Turekian, 1996; Koch *et al.*, 1996; Bonasoni *et al.*, 2000a; Lee *et al.*, 2004; Tositti *et al.*, 2004; Zheng *et al.*, 2005; Cristofanelli *et al.*, 2006; Lee *et al.*, 2007).

Mountain sites are very suitable locations to study tropospheric background conditions (Wotawa *et al.*, 2000; Stohl *et al.*, 2000; Cuevas *et al.*, 2013) as well as to investigate SI events (Cristofanelli *et al.*, 2006). In fact, as mixing processes act on small and intermediate (about 100 km) scales, stratospheric air masses quickly lose their original properties (Appenzeller and Davies, 1992), making it difficult to identify originally stratospheric air masses at low altitudes.

The "Ottavio Vittori" research station GAW, located on top of Mt. Cimone, is managed by the Meteorological Office of the Italian Air Force and by the Institute of atmospheric and climate science of the National Council of Research (ISAC-CNR). This station is part of the Global Atmosphere Watch (GAW) of the World Meteorological Organization (WMO). The main meteorological and territorial features, as well as peculiarities of this high-altitude WMO-GAW station have been described in Chapters 2, 3 and 4. The study of SI is one of the activities conducted at this research station and for this reason parameters helpful to identify SI are routinely monitored at Mt. Cimone (ozone, atmospheric radiotracers ^{7}Be and ^{210}Pb, relative humidity). As briefly introduced before, only one of the many STE studies conducted at Mt. Cimone made use of both ^{7}Be and ^{210}Pb (in particular as activity ratio), and this is also one of the oldest studies (Bonasoni *et al.*, 1999), while the others made use of only ^{7}Be (Bonasoni *et al.*, 1999, 2000a, b; Fischer *et al.*, 2003; Cristofanelli *et al.*, 2006, 2009). Statistical trajectory source analyses were already used to study the specific emission areas of some compounds: for instance the concentration field method of Seibert *et al.* (1994) was applied to ozone concentrations measured at high mountain peaks within and at the fringes of the Alps, among which Mt. Cimone, in order to establish the specific emission areas (Wotawa *et al.*, 2000), and the same method was applied to study the source regions of ozone (Bonasoni *et al.*, 2000b), of black carbon and fine particles (aerodynamic diameter between 0.3 and 1 μm) (Marinoni *et al.*, 2008), while the potential source contribution function (PSCF) of Ashbaugh *et al.* (1985) was used in Chapter 2 to assess the source regions of PM_{10} (Tositti *et al.*, 2013). None of these methods has been applied to radiotracers and to clarify the potential source regions of stratospheric intrusions.

In particular, Bonasoni *et al.* (2000b) divided the domain 80°-20° N, 50°W-50° E into six a priori identified regions (Arctic, Atlantic Ocean, Continental Europe, Eastern Europe, Mediterranean Basin and Saharan-African region) and then evaluated the frequency of different air mass origins to the Mt. Cimone as a function of trajectory starting positions. After this study, all works related to atmospheric composition and air mass origin made use of this a priori classification (Balkanski *et al.*, 2003; Fischer *et al.*, 2003; Gobbi *et al.*, 2003; Putaud *et al.*, 2004; Marenco *et al.*, 2006; Cristofanelli *et al.*, 2006, 2007, 2009). In Chapter 5 (Brattich *et al.*, in preparation), a cluster

analysis of back trajectories was applied to study the main advection patterns at the site, and how the seasonality and trends of the transports might influence the compounds measured at Mt. Cimone. Cluster analysis of air mass trajectories can in fact provide the transport pathways but has difficulties locating their source regions (Stohl, 1996). Trajectory based receptor models such as potential source contribution function (PSCF) and residence time weighted concentrations (RTWC) have proven useful in identifying these source regions (Hopke *et al.*, 1993). PSCF has been successfully and extensively used, for instance, to investigate the sources of atmospheric trace elements and particulate species such as sulphate, nitrate, ozone, black carbon and mercury (Poirot and Wishinski, 1986; Zeng and Hopke, 1988; Cheng *et al.*, 1993; Stohl and Kromp-Kolb, 1994; Polissar *et al.*, 1999, 2001a; Lin *et al.*, 2001; Güllü *et al.*, 2005; Wang *et al.*, 2006; Eleftheriadis *et al.*, 2009; Kong *et al.*, 2013;), but also the transport of nitrogen oxides, carbon monoxide and ozone to the Alpine GAW stations Jungfraujoch, Zugspitze and Hohenpeissenberg (Germany), Sonnblick, and Mt. Krvavec (Slovenia) (Kaiser *et al.*, 2007). The method has also been applied to locate the sources or source categories identified by multivariate receptor models, e.g., principal component analysis, positive matrix factorization of Paatero and Tapper (1994) or Henry's UNMIX (1997) (Xie *et al*., 1999; Poirot *et al.*, 2001; Polissar *et al.*, 2001b; Cohen *et al.*, 2010; Koçak *et al.*, 2011).

The major aims of this Chapter are to identify the source areas of ozone and atmospheric radionuclides ^{7}Be (stratospheric-upper tropospheric) and ^{210}Pb (crustal) and to study the major characteristics and influence of stratospheric air masses on the measurements at Mt. Cimone.

This Chapter is divided in four sections and is organized as follows. Section 6.2 describes the measurement techniques used at Mt. Cimone, and the use of back trajectories and of the PSCF method used for the identification of the source regions, similar to the one previously used in Chapter 2, but with some additional improvements. Section 6.3 presents and discusses our major results, and is further divided in Subsection 6.3.1 which describes the source areas of atmospheric radiotracers and ozone measured at Mt. Cimone, and Subsection 6.3.2 where the source regions of high potential vorticity values and the mechanisms leading to stratospheric intrusions are analyzed. Finally section 6.4 draws the main conclusions of this Chapter.

6.2 Material and methods

Continuous monitoring of ^{7}Be and ^{210}Pb radionuclides at Mt. Cimone has been carried out since 1998 till 2011, after isolated measurements were performed in 1996 and 1997. Details of PM_{10}, ^{210}Pb and ^{7}Be sampling and measurements have already been given in Chapters 2 and 3.

Tropospheric O_3 measurements at the station have been carried out continuously since 1996 by ISAC-CNR by using a UV-photometric analyzer (Dasibi 1108). The accuracy and the quality of the measurements (time sampling: 1-min, accuracy and precision: ± 2 ppb) are guaranteed within the GAW requirements. Tropospheric O_3, as well as meteorological data such as pressure, temperature, relative humidity, wind speed and wind direction data have been downloaded at http://ds.data.jma.go.jp/gmd/wdcgg/ (World Data Centre for Greenhouse Gases, WDCGG). Before the analysis, all the data were averaged at the same time resolution of PM_{10} and radionuclides for statistical homogenization of data.

In order to evaluate the origin of air masses arriving at Mt. Cimone, 4-day three-dimensional backward trajectories were calculated by means of the HYSPLIT model, version 4.8 (Draxler and Hess, 1997, 1998; Draxler, 1999; Draxler and Rolph, 2003).

Gridded meteorological data from the NOAA/ARL website were used. NCEP/NCAR reanalysis data in format ARL are a large data set of global meteorological data stored with a 2.5° latitude-longitude resolution, 17 pressure levels in a 6-h archive starting from 1948. These data derive from the operational series of computer forecasts and analyses undertaken by the National Center for Environmental Prediction (NCEP).

Four trajectories for each day, arriving at the synoptic times (00, 06, 12 and 18 UTC) at the heights of 1400, 2200 m and 3000 m asl were calculated, and the vertical movement of the air parcels was calculated from the vertical velocity fields (kinematic hypothesis, which has been observed to produce more realistic results as for the horizontal and vertical displacements of air masses (Fuelberg *et al.*, 1996)).

Global potential vorticity data stored on 6 hourly archives on 11 isentropic surfaces (270, 280, 290, 300, 315, 330, 350, 400, 450, 550 and 650 K) were also available as a NCEP/NCAR reanalysis product at http://rda.ucar.edu/datasets/ds090.0/#metadata/detailed.html?_do=y.

For each of the 96 endpoints of a trajectory, the PV is calculated by performing a 3-D nearest-neighbor interpolation with the 11 isentropic PV levels of the NCEP reanalysis, from the latitude, longitude and potential temperature of each endpoint.

Depicting the origin of the particle, back trajectories can be used to establish relationships between the sources of atmospheric trace substances and their receptors (Stohl, 1998). The accuracy and limitations of trajectory calculations have been addressed by several researchers (Merrill *et al.*, 1985; Kahl *et al.*, 1989; McQueen and Draxler, 1994; Stunder, 1996; Kahl, 1996; Stohl, 1998). It is in fact well known that the accuracy of an individual trajectory is limited by the temporal and spatial resolutions of meteorological observations, measurement errors, analysis errors and by any simplifying assumptions used in the trajectory model (Brankov *et al.*, 1998). For instance, in his review, Stohl (1998) highlighted that the significance of analysis based on back trajectories is limited

by the uncertainties involved in analyzed meteorological fields and in the interpolation to trajectory position, as well as by the lack of representation of small-scale effects such as turbulence. Typical trajectory errors are about 10-20% of the travel distance, but depending on the meteorological situation individual trajectories can have much larger errors (Harris *et al.*, 2005). Moreover, implicitly assuming that concentrations measured at the receptor site are smeared out along all the associated trajectories, the analysis of back trajectories is known to generate "ghost sources" in the wake of real emission sources (Wotawa and Kröger, 1999; Lupu and Maenhaut, 2002; Maione *et al.*, 2008). Care is also needed in the interpretation of the results obtained from the analysis of back trajectories: the results of Vasconcelos *et al.* (1996a, b) investigating the spatial resolution of the method, highlighted that even if the angular resolution is good, the spatial resolution is poor.

Potential errors in the individual trajectories are averaged out when considering a large number of back trajectories over a long time period. Although the several limitations applying to the use of the back trajectories approach hold also for the analyses of source-receptor relationships, it has been extensively used in a number of studies (e.g., Dorling and Davies, 1995; Bonasoni *et al.*, 2000b; Wotawa *et al.*, 2000; Aalto *et al.*, 2002; Abdalmogith and Harrison, 2005; Hwang and Hopke, 2007; Riccio *et al.*, 2007; Marinoni *et al.*, 2008; Tarasova *et al.*, 2009; Baker, 2010; Ebinghaus *et al.*, 2011; Martin *et al.*, 2011; Tositti *et al.*, 2013); a recent review of the studies using air-mass history to analyze atmospheric composition is available in Fleming *et al.* (2012).

In this work the PSCF method originated from the residence time probability analysis (RTA) of Ashbaugh *et al.* (1985) was adopted. This method was developed to identify geographical regions giving rise to observed concentrations (Hopke *et al.*, 1995). The concept of this method is to combine air mass back trajectories and atmospheric composition data to produce conditional probabilities over the region, where the region of interest is subdivided into a number of grid cells. The conditional probability function describes the spatial distribution of probable geographical source locations by using trajectories. The number of trajectory endpoints falling within grid cell *i,j* over the whole set of samples, $n_{i,j}$ are counted. Then, the subset of trajectories associated with high concentration samples are identified by comparing the measured concentrations to a threshold level and the number of endpoints in each grid cell associated to these high concentrations, $m_{i,j}$, is determined. The PSCF for the grid cell *i,j* is given by (detailed derivation can be found in Chapter 1, Section 1.3.2, as well as in Hopke *et al.*, 1995)

$$PSCF_{i,j} = \frac{m_{i,j}}{n_{i,j}} = \frac{residence\ time\ of\ air\ parcel\ above\ threshold\ concentration}{residence\ time\ of\ air\ parcel} \qquad (6.1).$$

PSCF is an indication of the probability that a given region contributed to those measurements whose concentration at the receptor was higher than the selected threshold. It should be stressed that the result does not yield the emission rate for a pollutant but rather the preferred source region or transport pathways to the site. Hopke *et al.* (1995) suggested fixing the threshold level to the average value, whereas other

studies such as Crawford *et al.* (2007) used the top 25% of measurements. In this work the threshold was chosen at the 50th percentile and the study region was discretized into square grid cells of 1.0° x 1.0°.

It is likely that a problem arises because of grid cells crossed by a small number of trajectories. Having poor counting statistics often results in false positive if trajectories travelling over the true source areas extend beyond these sources. Similarly to Chapter 2, (Tositti *et al.*, 2013), in order to remove small scale variations and to minimize the influence of the grid cells with small $n_{i,j}$, the results were filtered using a binomial test with a 95% confidence level (Vasconcelos *et al.*, 1996a, b). In particular, the conditional probabilities that did not significantly exceed 50% were set to zero, where the value of 50% was chosen in correspondence with the threshold values for "high" concentrations, which was defined at the 50th percentile. In addition to this, grid cells that were visited only once during the study period were removed from the probability field before the analysis.

6.3 Results and discussion

6.3.1 Source areas of atmospheric radiotracers and ozone

Atmospheric radiotracers have been traditionally used in the study of STE and in the assessment of the stratospheric influence on O_3 increases (Reiter *et al.*, 1983; Arimoto *et al.*, 1999; Monks, 2000; Wotawa *et al.*, 2000; Stohl *et al.*, 2000; Li *et al.*, 2002; Cristofanelli *et al.*, 2003; Zanis *et al.*, 2003b; Liu *et al.*, 2004; Gerasopoulos *et al.*, 2005; Carvalho *et al.*, 2010; Cuevas *et al.*, 2013), also at Mt. Cimone where the studies of stratospheric intrusions have a long-term tradition (Bonasoni *et al.*, 1999, 2000a, b; Cristofanelli *et al.*, 2006., 2009). In this work the PSCF analysis was applied in order to locate the geographical areas which can be considered as a "source" of high ^{7}Be, ^{210}Pb, ratio ^{7}Be/^{210}Pb and O_3. Figure 6.1 shows the four conditional probability maps of ^{7}Be, ^{210}Pb, ratio ^{7}Be/^{210}Pb and O_3, highlighting the main areas of provenance of the air when high concentrations of these tracers were registered at Mt. Cimone. The scale goes from 0.50 to 1 as the high concentration days were chosen as the ones whose concentrations were equal to or above the 50th percentile.

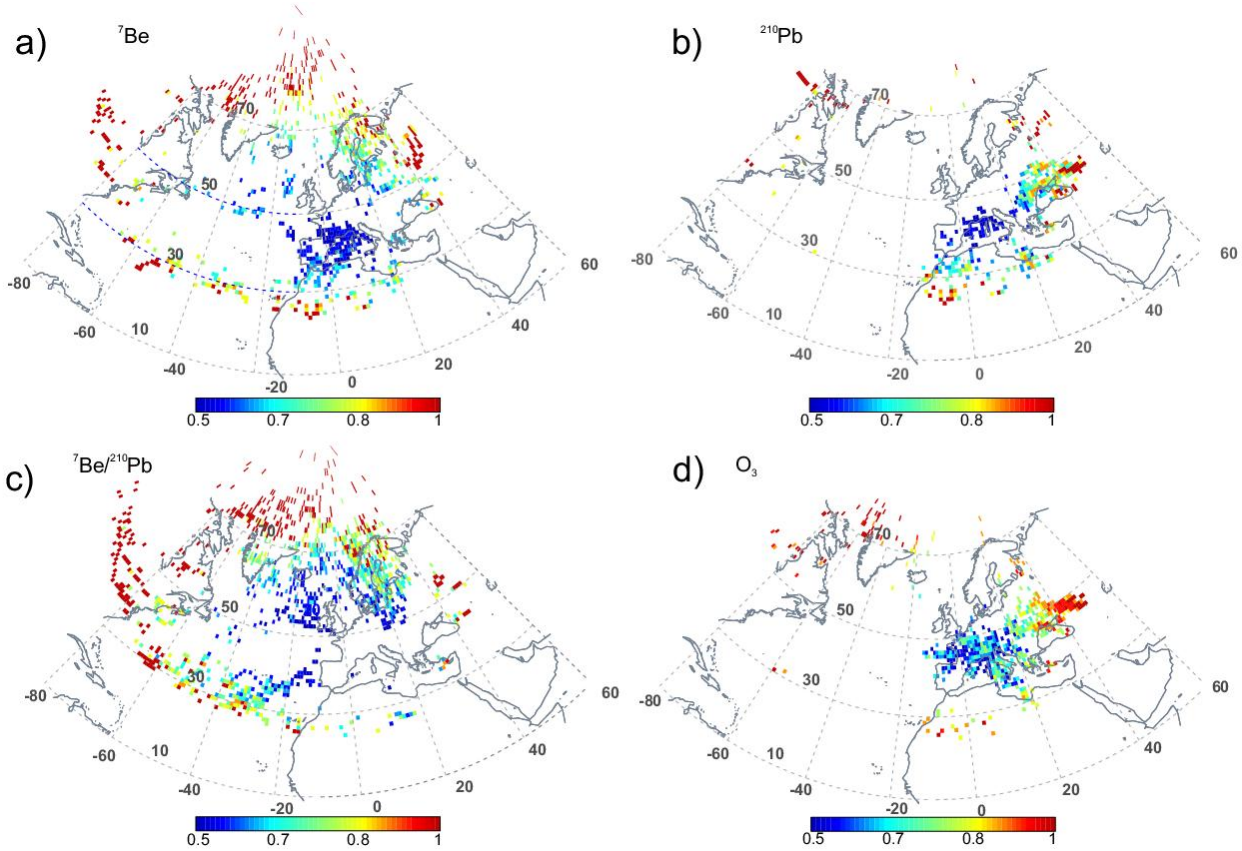

Figure 6.1(a,b,c,d) *Conditional probability maps of a) ^{7}Be; b) ^{210}Pb; c) ^{7}Be/^{210}Pb; d) O_3, evaluated by eqn. (6.1) Only significant sources are shown, while the non-significant ones were filtered by using a binomial test at a 95% confidence level. Scales go from 0.5 to 1 as the high concentration days were chosen as the ones with values equal to or above the 50th percentile. Grid cells that were visited only once during the study period were also removed from the probability field before the analysis.*

The main areas associated to high ^{7}Be are located in the Arctic region as can be seen in Figure 6.1a, whose contribution is not surprising as this origin of the air mass has been already linked to STE (high ^{7}Be, low ^{210}Pb) by many authors (e.g., Bonasoni *et al.*, 1999, 2000a, b), Northern Russia and Finland, North America. In previous Chapter 5 it has been in fact highlighted that Arctic flows are dry descending air masses arriving from high latitudes; in addition they are associated with low tropopause height in the study area. Moreover these air flows may interact with the Alps, thus they can be connected to STE in several ways. Interestingly, apart from likely "ghost sources" located east of the Canary Islands and east of Morocco, where a high conditional probability is located due to only few back trajectories during high concentration events, a high conditional probability is also located in Northern Africa, a region which so far has been connected to high ^{7}Be events only by few authors (Hernández *et al.*, 2008; Dueñas *et al.*, 2011). Menut *et al.* (2009) associated an increase in ^{7}Be, ^{210}Pb, ^{137}Cs with one intense African dust event in France.

As far as ^{210}Pb is concerned (Figure 6.1b), its main source areas are very similar to those of PM_{10} studied in Chapter 2 (Tositti *et al.*, 2013); in fact PM_{10} and ^{210}Pb share a large part of the source term (the Earth's crust), differently from ^{7}Be which originates mainly in the stratosphere-upper troposphere. Important contributions come from Eastern Europe and Northern Africa, whereas surrounding Italian and French regions show a reduced contribution. Recalling what we previously observed in Chapter 3 (Tositti *et al.*, 2014) about the decoupling of ^{210}Pb and PM_{10} summer maxima, we have carefully examined and compared their source regions, especially during the summer season when this difference was noted. In particular, we observe that while for PM_{10} there is a relevant contribution from Northern Africa (Chapter 2; Tositti *et al.*, 2013), due to Saharan Dust transport, for ^{210}Pb this source is important but seems to contribute to a lesser extent, probably since North Africa is a relevant contributor of coarse-sized particles more than fine-sized particles. Moreover, for PM_{10} the contribution of surrounding regions is more relevant (Chapter 2; Tositti *et al.*, 2013), suggesting a possible effect of particulate of secondary origin, able to influence PM_{10} increase but not ^{210}Pb. Finally, as Marinoni *et al.* (2008) observed, during summer a high contribution for PM_{10} is observed coming from the Iberian Peninsula: this region is frequently affected by forest fires and biomass burning during the summer season, and these processes are again able to affect PM_{10} concentrations rather than ^{210}Pb. The North African region seems an important contributor both for ^{7}Be as well as for ^{210}Pb: our results seem to indicate that both uplift of crustal particles and downward movement from the upper troposphere-lower stratosphere can be present when the air is coming from this region. This last mechanism might be responsible of ^{7}Be increases connected to Saharan Dust events. It is worth to note in this framework that the application of the filter which removed endpoints visited only once but linked to high concentrations recorded at Mt. Cimone was able to reduce the number of "ghost sources" with respect to Chapter 2 (Tositti *et al.*, 2013), such as the ones east of the Canary Islands and Morocco and the ones over the Gulf of Sirte.

As once produced, both ^{7}Be and ^{210}Pb radionuclides rapidly attach to submicron-sized particles (Papastefanou and Ioannidou, 1995; Winkler *et al.*, 1998; Gaffney *et al.*, 2004; Ioannidou *et al.*, 2005), they share the same fate being removed mainly by wet and secondarily by dry deposition (Feely *et al.*, 1989; Kulan *et al.*, 2006); their ratio ^{7}Be/^{210}Pb has been often used to gain insights into vertical motions of the air masses as well as on convective activity in the troposphere (Brost *et al.*, 1991; Koch *et al.*, 1996; WMO, 2001; Lee *et al.*, 2004; Tositti *et al.*, 2004; Lee *et al.*, 2007). The source areas of ^{7}Be/^{210}Pb (Figure 6.1c) are located far away from the measurement site, in the Arctic region, in North America and in the Atlantic Ocean (as already showed by Balkanski *et al.* (1993) and Baskaran (2011), the flux of ^{222}Rn from the oceans is negligible). Interestingly, these areas in the Atlantic which are highlighted as source of high ^{7}Be and low ^{210}Pb roughly correspond to the tropopause discontinuity in mid-latitude regions (a "belt" around 30 degrees is well seen) (Steinmann *et al.*, 2013), as well as to a

preferred region for cyclone formation (e.g., James *et al.*, 2003a; Stohl *et al.*, 2003). North America and Atlantic regions also correspond to locations where the polar jet stream is generally stronger. These areas will be compared to high potential vorticity regions afterwards in this Chapter.

Ozone source regions (Figure 6.1d) are more similar to ^{210}Pb than to ^{7}Be, even if the contribution of the surrounding regions seems important to this gas. Surrounding regions such as the Po Basin, southern Germany, France, greatly contribute to high concentrations of this gas, similarly to what has been previously shown by Wotawa *et al.* (2000) by means of another statistical method applied to trajectories. This does not mean, however, that increases of ozone cannot have a stratospheric influence as highlighted for instance in Figure 6.2(a,b), where the PSCF analysis on ozone was carried on separately during the cold (November to February) (Figure 6.2a) and warm season (May to August) (Figure 6.2b); on the average, however, these events contribute limitedly (but not negligibly) to the total ozone increases, as already highlighted by some authors (Bonasoni *et al.*, 1999; Stohl *et al.*, 2000; Wotawa *et al.*, 2000; Bonasoni *et al.*, 2000a,b; Monks, 2000; Zanis *et al.*, 2003b; Stohl *et al.*, 2003; Cristofanelli *et al.*, 2006). The contribution of surrounding regions is, as expected, higher during the warm season.

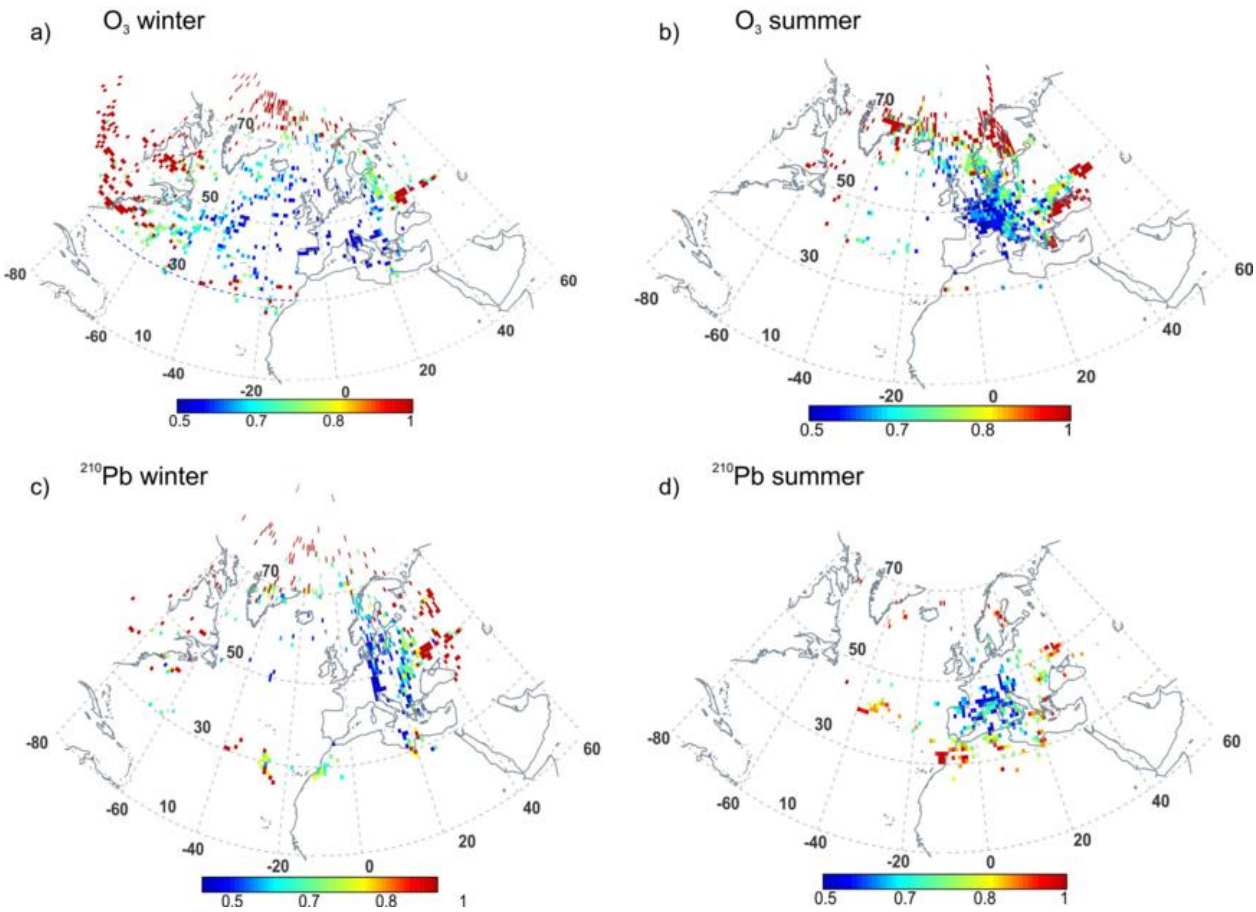

Figure 6.2(a,b,c,d) *Same as Figure 6.1, but for O_3 during the cold season (November, December, January and February) (a) and during the warm season (May, June, July, August) (b) and for ^{210}Pb during the cold (c) and warm season (d).*

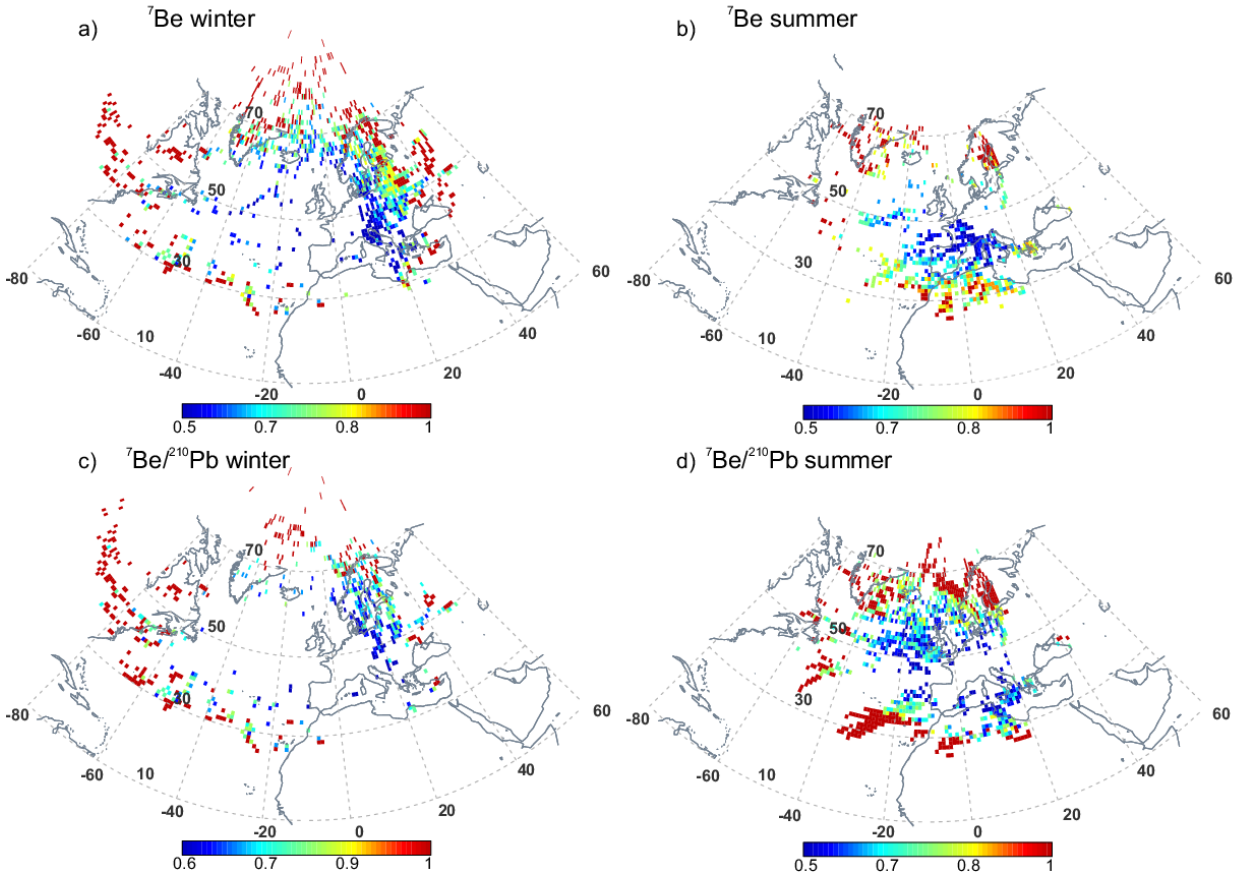

Figure 6.3(a,b,c,d) *Same as Figure 6.1, but for ^{7}Be during the cold season (November, December, January and February) (a) and during the warm season (May, June, July, August) (b) and for ^{7}Be/^{210}Pb during the cold (c) and warm season (d).*

Figure 6.2(c,d) and Figure 6.3(a,b,cd) report the same "seasonal" analysis for ^{210}Pb (Figure 6.2), ^{7}Be (Figure 6.3a,b), and ^{7}Be/^{210}Pb (Figure 6.3c,d). ^{210}Pb transport from North Africa seems to be more important during the warm season, while transport from Eastern Europe is on the contrary dominant during the cold season. Interestingly, during the warm season transport from North Africa seems to be important also for ^{7}Be transport, whereas during the cold season ^{7}Be transport is dominated by long-range transports from the Arctic and North American regions. Even if both ^{7}Be and ^{210}Pb are transported almost simultaneously from North Africa, similar seasonal patterns can be observed also in the ^{7}Be/^{210}Pb transport. The transports from North Atlantic and North Africa contribute more importantly to this tracer during the warm season. Similar to what previously observed in Chapter 4 by means of the GMI CTM, it is clear that in general the cold season is dominated by long-range transports while on the contrary during the warm season short-range transports are more important. This seasonal pattern of the transports to Mt. Cimone corresponds to what has been observed more generally in previous Chapter 5 (Brattich *et al.*, in preparation). Previously, also Marinoni *et al.* (2008) observed that long-range transport processes are more likely to produce an effect on aerosol properties during the cold season,

when the measurement site is always above the boundary layer; on the contrary, during the warm season, stronger contributions from the polluted regional boundary layer due to less aged air masses are possible. They observed that while during the cold season O_3 is almost uncorrelated with black carbon and fine-sized particles, due to the transport of aged (and well processed) air masses to the measurement site, during the warm season O_3 is instead highly correlated with black carbon and fine particles, because of the transport of polluted air masses rich in photochemically produced O_3. During the warm season, the transport of air masses from the lower troposphere is very important in determining black carbon and fine particles concentrations at the site; the vertical transport of polluted air masses from the lower troposphere is favoured by wind breeze circulations typical of summer fair weather conditions.

From our analysis the findings of Hernández *et al.* (2008), Menut *et al.* (2009), Dueñas *et al.* (2011), who associated transport from Northern Africa with increases in both ^{7}Be and ^{210}Pb are corroborated. In fact, transport from Northern Africa is connected to two different mechanisms, which are independent but may be mixed in single episodes: a strong downdraft from the upper troposphere and soil dust uplift. This way, ^{7}Be can be scavenged by African dust and transported with it. Correspondingly, ozone transported from upper levels concurrently with ^{7}Be is depleted when mixed with the dust laden air masses. Figure 6.4, representing source regions of ^{7}Be/PM$_{10}$, further highlights that Northern Africa is a source of both ^{7}Be and dust (PM$_{10}$). Recently, Belmaker *et al.* (2011) pointed out that in desert areas dry deposition is the major supply of "newly" produced cosmogenic beryllium. They observed that the concentration of ^{7}Be during a major dust storm was more than an order of magnitude higher than the regular average, and suggested that the higher the overall dust transport the higher cosmogenic ^{7}Be is scavenged. However, the physical mechanism at the basis of these findings has yet to be fully clarified.

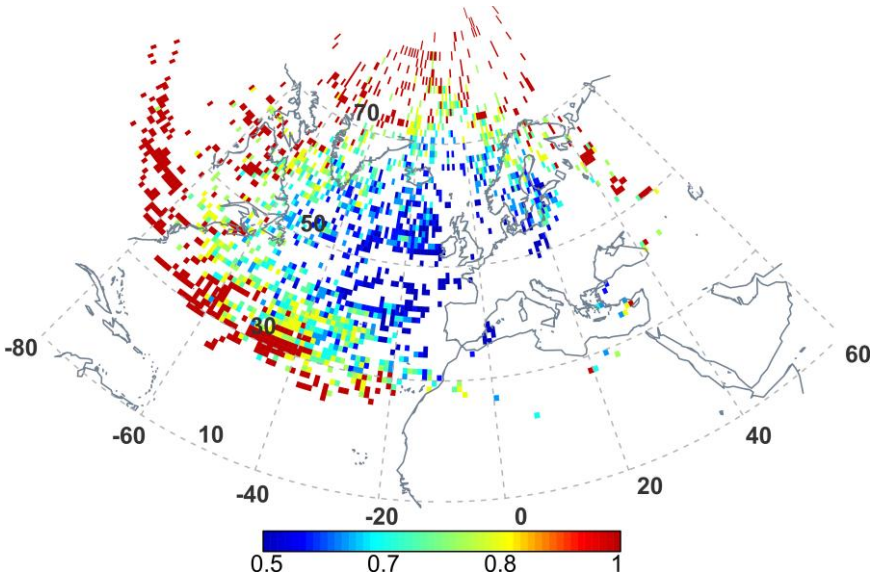

Figure 6.4(a,b,c,d) *Same as Figure 6.1, but for ^{7}Be/PM$_{10}$.*

Figure 6.5(a,b,c,d) shows the mean heights of the back trajectories when high values (higher than the 75th percentile) are registered at Mt. Cimone. It is clearly shown that high altitude back trajectories originating in the lower stratosphere come from the Arctic (where the tropopause is also lower due to limited convective overturning) and North America/Atlantic regions, with special strength over Greenland, whereas the lowest trajectories are coming from the lowest latitude regions. The highest heights are related to high $^{7}Be/^{210}Pb$ as it was expected, pointing out once more the importance of this tracer in the understanding of vertical motions and in connection with STE events.

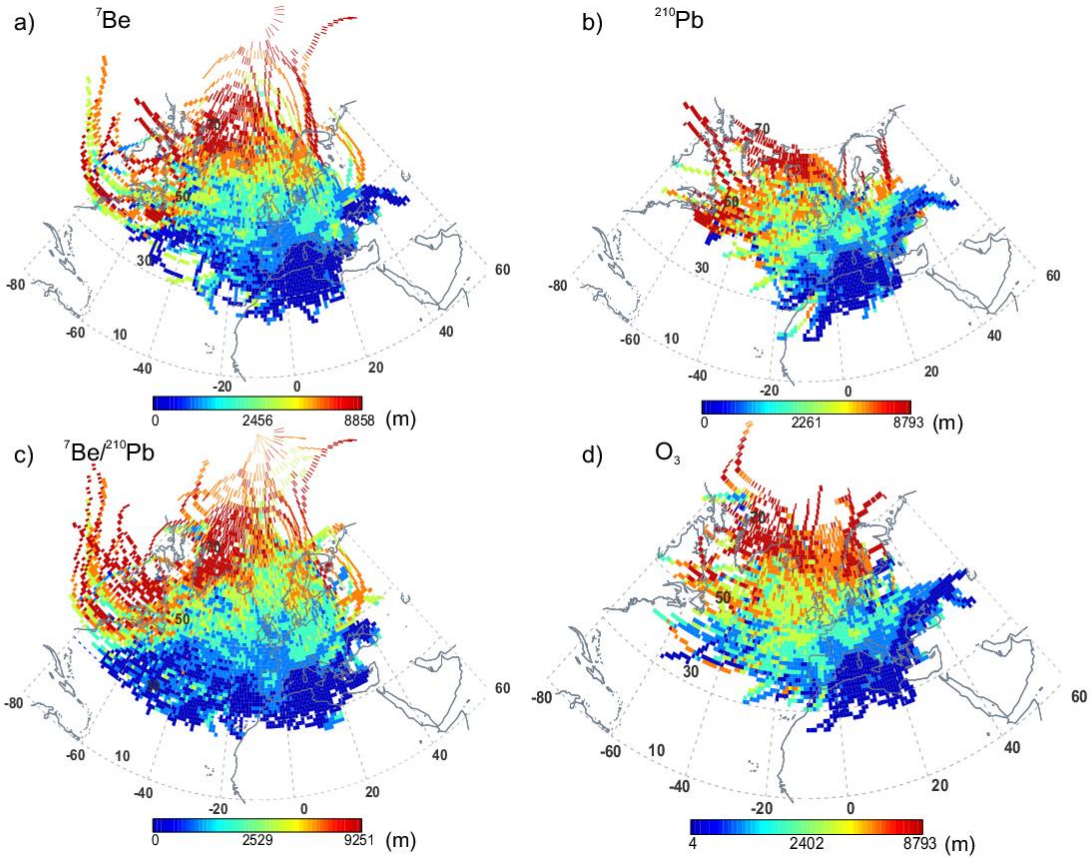

Figure 6.5(a,b,c,d) *Maps of mean back trajectory height when concentrations higher than the 75th percentile are registered at Mt. Cimone. Maps refer to: a) ^{7}Be; b) ^{210}Pb; c) $^{7}Be/^{210}Pb$; d) O_3.*

6.3.2 Analysis of potential vorticity values

Potential vorticity has been often used as a tracer of stratospheric air in the troposphere (e.g., Beekmann *et al.*, 1994; Poulida *et al.*, 1996; Cristofanelli *et al.*, 2006). In fact, the strong positive vertical gradient of potential temperature produced by the ozone layer in the stratosphere is such that the potential vorticity is there several orders of magnitude higher than in troposphere (Beekmann *et al.*, 1994). In the atmosphere above 350 hPa, PV rapidly increases with height,

reaching typical values ranging from 1.0 pvu[2] (Danielsen, 1968) to 3.5 pvu (Hoerling *et al.*, 1991; Appenzeller *et al*., 1996).

Some degree of arbitrariness in the choice of the potential vorticity threshold for stratospheric air exist: while Cuevas *et al.* (2013), for instance, used the low value of 1.0 pvu, Cristofanelli *et al.* (2006) considered the higher, even if still low, value of 1.6 pvu, justified by the fact that the trajectories may not go back all the way deeply into the stratosphere because of their limited length and also because of possible trajectory errors, while commonly the dynamical tropopause is represented by the 2 pvu surface (Holton *et al.*, 1995; Appenzeller *et al.*, 1996; James *et al.*, 2003b). It has to be known, however, that high PV values can also be generated by diabatic processes in the lower troposphere (such as strong nighttime cooling at the surface or diabatic heating due to the condensation of water vapor) (Cristofanelli *et al.*, 2006) and as such, only heights higher than 5000 m should be considered in order to be sure to identify stratospheric air masses (Olsen *et al.*, 2000). In this study we use the 1.6 pvu threshold but a sensitivity analysis is carried on afterwards to understand if and how the choice of the threshold might influence the result.

The number of times a region was linked to a potential vorticity greater than 1.6 pvu is reported in the map of Figure 6.6, from the PV values associated with each trajectory endpoint. The north Atlantic region, which has been already connected to STE events as a preferred region for cyclone formation (Stohl *et al.*, 2003; James *et al.*, 2003a; Cuevas *et al.*, 2013), and of large scale subsidence connected to the descending branch of the Hadley cell is highlighted as a potential source region of high PV. This region was in fact also observed as an area of high $^{7}Be/^{210}Pb$ levels, especially during the warm season. North Africa is also again observed as a high PV source, confirming that this region is not only associated with uplift from the Earth's crust, but also to subsidence from the upper troposphere as already reported by Dueñas *et al.* (2011). Most of the locations in this map can be related to lee cyclogenesis (Alps and Atlas mountains) and to the areas where the resulting depressions are displaced (south of the Atlas to Tunisia, the track of the cyclones formed in the lee of the Atlas). Figure 6.7 reports a map of all the trajectories having a potential vorticity greater than 1.6 pvu at a height higher than 5 km. Even if the locations associated with Northern Africa and Atlas mountains are lost in this map, because in these regions the trajectories only sporadically reach heights higher than 5000 m as previously observed in Figure 6.5, the contour of the Alps is revealed in this Figure and the importance of lee cyclogenesis as a STE promoting mechanism is well highlighted. Of course, we are aware that the resolution of the NCEP/NCAR reanalysis meteorological input fields represent large flows and cannot adequately resolve local to mesoscale phenomena such as topographically influenced flow; however, our

[2] 1 pvu = 1 x 10^{-6} m^2 K kg^{-1} s^{-1}

results point to an indication that the Alpine cyclogenetic activity, and in general lee cyclogenesis, is connected to STE, as observed by, e.g., Tosi *et al.* (1987), Aebischer and Schär (1997), Stohl *et al.* (2000). Nevertheless, mesoscale and local meteorological effects which we cannot resolve with this method, have already been observed to be very important for variations of PM_{10}, ^{7}Be and ^{210}Pb (Lozano *et al.*, 2013).

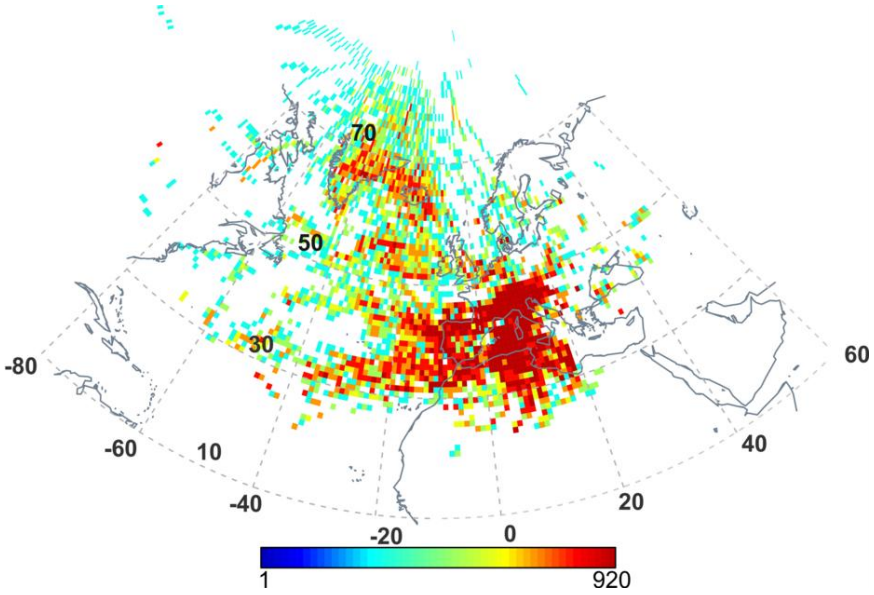

Figure 6.6 *Map showing the number of times of a potential vorticity greater than 1.6 pvu was observed along the trajectories ("source regions" of high PV).*

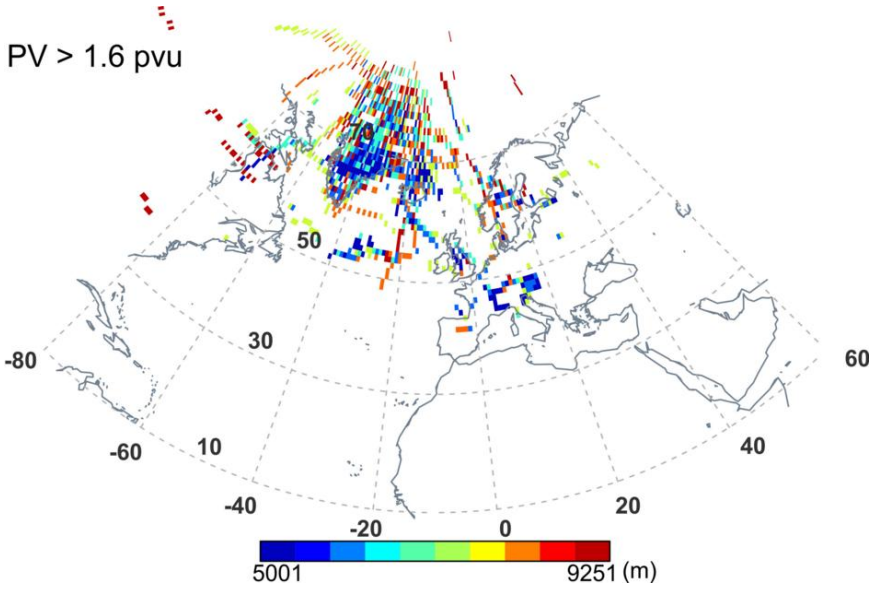

Figure 6.7 *Map showing the heights of the trajectories associated with heights greater than 5000 m and to potential vorticity higher than 1.6 pvu.*

The time spent between the moment a trajectory crosses a region of PV greater than 1.6 pvu and the time of arrival to Mt Cimone lies mainly in the range 24 to 72 hours, even if there are also some cases reaching the upper and lower extremes (the latter corresponding to a stratospheric intrusion just above the measurement site). These time intervals, along with $^{7}Be/^{210}Pb$ measurements and PV data are plotted against each other in Figure 6.8. Papastefanou and Ioannidou (1995) estimated residence times for ^{7}Be-aerosols varying between 7.4 and 8.9 days (average 8 days), while according to Liu *et al.* (2001) mean residence times in the troposphere are about 20 days for ^{7}Be (17 days including loss from radioactive decay). In any case, the mean residence time of ^{7}Be in the atmosphere is much longer than the time spent between the trajectory crossed the PV threshold of 1.6 pvu and the time of the measurement at Mt. Cimone. Only a few data belong to the range 72 to 96 hours, and for this reason it is speculated that considering longer trajectories is not going to add further insight to the analysis.

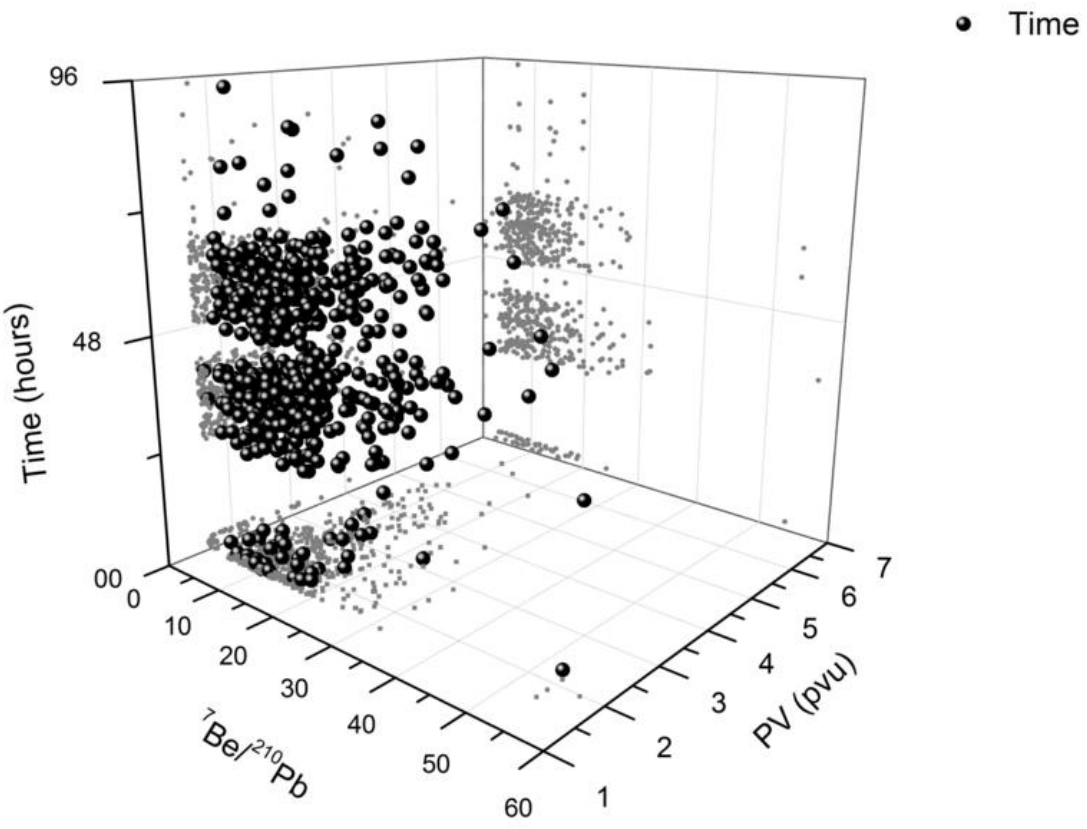

Figure 6.8 *3-d scatterplot representing as X coordinate $^{7}Be/^{210}Pb$ measurements at Mt. Cimone, Y coordinate PV data higher than 1.6 pvu and Z coordinate time interval between the crossing of the 1.6 pvu surface and the moment of the arrival of the trajectory at Mt. Cimone. Grey dots represent the projections on each surface.*

In order to examine how the results depend on the selection of the threshold used for PV, Figure 6.9 presents the results obtained with the different thresholds of 1 pvu and 2 pvu. As it could be expected, the threshold of 1 pvu seems too low to be considered, while the results obtained selecting the threshold of 2 pvu can be well compared to those with the threshold of 1.6 pvu: once more the storm track regions such as the North Atlantic and the regions connected to lee cyclogenesis are highlighted as linked to STE processes.

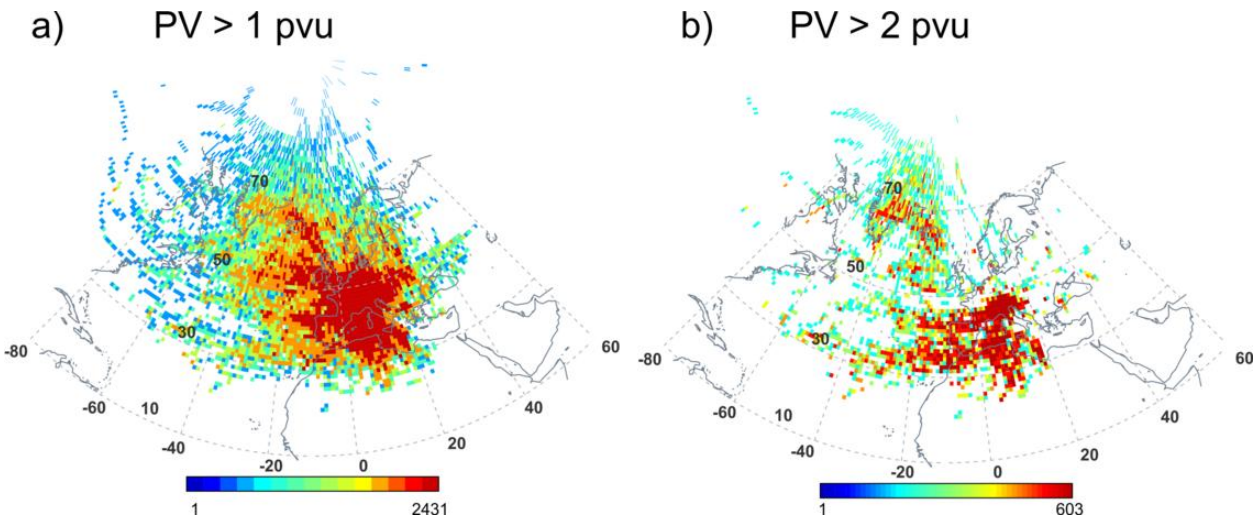

Figure 6.9(a,b). *Map showing the number of times a potential vorticity greater than 1 pvu (a) and 2 pvu (b) was observed along the trajectories.*

6.4. Summary and conclusion

The major scope of this Chapter was to examine the source areas connected to high concentrations of ^{7}Be, ^{210}Pb and O_3 in order to gain a better understanding of the processes promoting their increases, and of the source regions of SI events.

The PSCF analysis was used to this scope. The main source areas of ^{7}Be are located in the Arctic region, in Northern Russia, Finland and North America. Increases of ^{7}Be are also connected to air masses originating in Northern Africa. ^{210}Pb originates mainly in Eastern Europe and Northern Africa, with a limited contribution of surrounding Italian and French regions.

Both ^{210}Pb and PM_{10} experience a maximum in summertime, but their maxima are decoupled which points out to a possible difference in their sources. While for PM_{10} there is a relevant contribution from Northern Africa, due to Saharan Dust transport, for ^{210}Pb this source is important but seems to contribute to a lesser extent, probably since North Africa is a relevant contributor of coarse-sized particles more than fine-sized particles. Moreover, for PM_{10} the contribution of surrounding regions is more relevant than for ^{210}Pb, suggesting a possible effect of particulate of

secondary origin. Finally, during summer a high contribution for PM_{10} is observed from the Iberian Peninsula, a region which during this season is frequently affected by forest fires and biomass burning, processes again able to affect more PM_{10} concentrations rather than ^{210}Pb.

The role of the North African region as contributing both to ^{210}Pb and ^{7}Be increases is understood in terms of simultaneous uplift of crustal particles and downward movements from the upper troposphere-lower stratosphere. The ratio $^{7}Be/^{210}Pb$, useful to understand the vertical motions of the air, originates far away from the measurement site, in the Arctic region, in North America and in the Atlantic region. This last area corresponds to the tropopause discontinuity in the mid-latitudes, as well as to a preferred region for cyclone formation. North America and Atlantic region also correspond to preferred locations for a stronger polar jet-stream. The source regions of O_3 are similar to those of ^{210}Pb, even if the surrounding region, such as the Po Basin, France and southern Germany seem to give important contributions to its increase. A separate analysis for the cold and warm periods highlighted that the contributions of the surrounding regions is higher during the warm season. The PSCF analysis by season applied to ^{210}Pb show that the contribution of North Africa dominates during the warm season, while transport from Eastern Europe dominates during the cold season. As for ^{7}Be, long range transports from the Arctic and North American regions are more important during the cold period, whereas during the warm season the transport from Northern Africa is important also to ^{7}Be increases. Observing the seasonal pattern of $^{7}Be/^{210}Pb$ transport, it is clear that while transports from North Atlantic and North Africa dominate the warm season, transports from Arctic, North American and Eastern Europe interest mainly the cold period. It is clear that in general the cold season is dominated by long-range transports while on the contrary during the warm season short-range transports are more important.

The analysis of the mean heights of the back trajectories when high concentrations/activities are registered at Mt. Cimone showed that the trajectories travelled at higher altitudes on average the higher the latitudes: high altitude back trajectories originate mainly in the Arctic and North America/Atlantic regions, with special strength over Greenland, whereas the lowest trajectories are coming from the lowest latitude regions. In particular, the highest heights are connected to high $^{7}Be/^{210}Pb$, highlighting once more the importance of this tracer in the understanding of vertical motions and in connection with STE events.

A potential vorticity analysis linked to the trajectories provided information on the contribution of the lower stratosphere/upper troposphere to the study site. The North Atlantic is highlighted as a potential source region of high PV; this confirms that STE events are promoted in this region. Importantly, also northern Africa is again observed in this analysis, highlighting once more that this region can give rise not only to particles originating from the Earth's crust but also to radionuclides transported by subsidence from the upper troposphere. Most of the locations related to high PV

values are also linked to lee cyclogenesis and to the areas where the resulting depressions are displaced. The importance of lee cyclogenesis as a STE promoting mechanisms is especially highlighted when observing the heights of the trajectories having high potential vorticity and heights higher than 5000 m.

The travelling time spent between the trajectory cross of the high PV threshold and the time of the measurement at Mt. Cimone fall mainly in the range 24-72 hours. This suggests that it should not be needed to compute longer trajectories.

Finally, a sensitivity analysis carried out to understand how the choice of the threshold value for potential vorticity might influence the results showed a similar outcome for 1.6 and 2 pvu. The relevance of the North Atlantic storm track and lee cyclogenesis regions is highlighted using both thresholds.

Acknowledgements

Italian Air Force Meteorological Office (IAFMS) and ISAC-CNR are gratefully acknowledged for their precious technical support at the Mt. Cimone. ISAC-CNR is gratefully acknowledged for providing ozone data, besides infrastructural access at the WMO-GAW Global Station Italian Climate Observatory "O. Vittori" at Mt. Cimone. The Italian Climate Observatory "O. Vittori" is supported by MIUR and DTA-CNR throughout the Project of National Interest NextData. We acknowledge NOAA (http://www.esrl.noaa.gov/) for providing the HYSPLIT trajectory model (available at http://ready.arl.noaa.gov/HYSPLIT.php) and the NCEP/NCAR meteorological reanalysis data, comprehending potential vorticity at http://rda.ucar.edu/datasets/ds090.0/#metadata/detailed.html?_do=y. Erika Brattich thanks the University Miguel Hernandez de Elche and Prof. Orza for giving her the possibility of a three months research period to start the collaboration which posed the scientific basis of this work.

References

Aalto T., Hatakka J., Paatero J., Tuovinen J.P., Aurela M., Laurila T., Holmen K., Trivett N., Viisanen Y., 2002. Tropospheric carbon dioxide concentrations at a northern boreal site in Finland: basic variations and source areas. *Tellus Ser. B: Chemical and Physical Meteorology*, 54(2), 110-126, doi:10.1034/j.1600-0889.2002.00297.x

Abdalmogith S.S., Harrison R.M., 2005. The use of trajectory cluster analysis to examine the long-range transport of secondary inorganic aerosol in the UK. *Atmospheric Environment* 39, 6686-6695.

Aebischer U., Schär C., 1997. Low-Level Potential Vorticity and Cyclogenesis to the Lee of the Alps. *Journal of the Atmospheric Sciences* 55, 186-207.

Appenzeller C., Davies H.C., 1992. Structure of stratospheric intrusions into the troposphere. *Nature* 358, 570-572.

Appenzeller C., Holton J.R., Rosenlof K.H., 1996. Seasonal variation of mass transport across the tropopause. *Journal of Geophysical Research* 101(D10), 15071-15078.

Arimoto R., Snow J.A., Graustein W.C., Moody J.L., Ray B.J., Duce R.A., Turekian K.K., Maring H.B., 1999. Influences of atmospheric transport pathways on radionuclide activities in aerosol particles from over the North Atlantic. *Journal of Geophysical Research* 104(D17), 301-321.

Ashbaugh, L.L., Malm, W.C., Sadeh, W.Z., 1985. A residence time probability analysis of sulfur concentrations at ground canyon national park. *Atmospheric Environment* 19(8), 1263-1270.

Austin J.F., Follows M.J., 1991. The ozone record at Payerne: An assessment of the cross-tropopause flux. *Atmospheric Environment* 25A, 1873-1880.

Baker J., 2010. A cluster analysis of long range air transport pathways and associated pollutant concentrations within the UK. *Atmospheric Environment* 44 (4), 563-571.

Balkanski Y.J., Jacob D.J., Gardner G.M., Graustein W.C., Turekian K.K., 1993. Transport and residence times or tropospheric aerosols inferred from a global three-dimensional simulation of ^{210}Pb. *Journal of Geophysical Research* 98, 20573-20586.

Baskaran M., 2011. Po-210 and Pb-210 as atmospheric tracers and global Pb-210 fallout: a review. *Journal of Environmental Radioactivity* 102, 500-513.

Beekmann M., Ancellet G., Megie G., 1994. Climatology of tropospheric ozone in southern Europe and its relation with potential vorticity. *Journal of Geophysical Research* 99, 12841-12853.

Belmaker R., Lazar B., Stein M., Beer J., 2011. Short residence time and fast transport of fine detritus in the Judean Desert: Clues from ^{7}Be in settled dust. *Geophysical Research Letters* 38, L16714, doi:10.1029/2011GL048672

Bonasoni P., Evangelisti F., Bonafé U., Feldmann H., Memmesheimer M., Stohl A., Tositti L., 1999. Stratosphere-troposphere exchanges: case studies recorded at Mt. Cimone during VOTALP project. *Physics and Chemistry of the Earth* (C) 24(5), 443-446.

Bonasoni P., Evangelisti F., Bonafé U., Ravegnani F., Calzolari F., Stohl A., Tositti L,. Tubertini O., Colombo T., 2000a. Stratospheric ozone intrusion episodes recorded at Mt. Cimone during VOTALP project: Case studies. *Atmospheric Environment* 34, 1355-1365.

Bonasoni P., Stohl A., Cristofanelli P., Calzolari F., Colombo T., Evangelisti F., 2000b. Background ozone variations at Mt Cimone station. *Atmospheric Environment* 34, 5183-5189.

Brankov E., Rao S.T., Porter P.S., 1998. A trajectory-clustering correlation methodology for examining the long-range transport of air pollutants. *Atmospheric Environment* 32 (9), 1525-1534.

Brost R.A., Feichter J., Heimann M., 1991. Three-dimensional simulation of ^{7}Be in a global climate model. *Journal of Geophysical Research* 96, 22423-22445.

Carvalho A., Monteiro A., Ribeiro I., Tchepel O., Miranda A.I., Corrego C., Saavedra S., Souto J.A., Casares J.J., 2010. High ozone levels in the northeast of Portugal: Analysis and characterization. *Atmospheric Environment* 44, 1020-1031.

Chameides W., Walker J.C.G., 1973. A photochemical theory of tropospheric ozone. *Journal of Geophysical Research* 99, 12841-12853.

Cheng M.-D., Hopke P.K., Zeng Y., 1993. A receptor-oriented methodology for determining source regions of particulate sulfate at Dorset, Ontario. *Journal of Geophysical Research* 98, 16839-16849.

Cohen D.D., Crawford J., Stelcer E., Bac V.T., 2010. Long range transport of fine particle windblown soils and coal fired power station emissions into Hanoi between 2001 and 2008. *Atmospheric Environment* 44, 3761-3769.

Crawford J., Chambers S., Cohen D.D., Dyer L., Wang T., Zahorowski W., 2007. Receptor modeling using Positive Matrix Factorization, back trajectories and Radon-222. *Atmospheric Environment* 41, 6823-6837.

Cristofanelli P., et al., 2003. Stratosphere-to-troposphere transport: A model and method evaluation. *Journal of Geophysical Research* 108(D12), 8525, doi:10.1029/2002JD002600

Cristofanelli P., Bonasoni P., Tositti L., Bonafé U., Calzolari F., Evangelisti F., Sandrini S., Stohl A., 2006. A 6-year analysis of stratospheric intrusions and their influence on ozone at Mt. Cimone (2165 m above sea level). *Journal of Geophysical Research* 111, D03306. doi:10.1029/2005JD006553.

Cristofanelli P., Bonasoni P., Carboni G., Calzolari F., Casarola L., Zauli Sajani S., Santaguida R., 2007. Anomalous high ozone concentrations recorded at a high mountain station in Italy in summer 2003. *Atmospheric Environment* 41, 1383-1394.

Cristofanelli P., Calzolari F., Bonafé U., Duchi R., Marinoni A., Roccato F., Tositti L., Bonasoni P., 2009a. Stratospheric intrusion index (SI^2) from baseline measurement data. *Theoretical and Applied Climatology* 97, 317-325.

Cristofanelli P., Fierli F., Marinoni A., Calzolari F., Duchi R., Burkhart J., Stohl A., Maione M., Arduini J., Bonasoni P., 2013. Influence of biomass burning and anthropogenic emissions on ozone, carbon monoxide and black carbon at the Mt. Cimone WMO-GAW global station (Italy, 2165 m a.s.l.). *Atmospheric Chemistry and Physics* 13, 15-30. doi:10.5194/acp-13-15-2013

Crutzen P.J., 1973. A discussion on the chemistry of some minor constituents in the stratosphere and troposphere. *Pure and Applied Geophysics* 106-108, 1385-1399.

Cuevas E., Gonzalez Y., Rodríguez S., Guerra J.C., Gómez-Peláez A.J., Alonso-Pérez S., Bustos J., Milford C., 2013. Assessment of atmospheric processes driving ozone variations in the subtropical North Atlantic free troposphere. *Atmospheric Chemistry and Physics* 13, 1973-1998.

Danielsen E.F., 1968. Stratospheric-tropospheric exchange based on radioactivity, ozone and potential vorticity. *Journal of Atmospheric Sciences* 25, 502-518.

Davies T.D., Schuepbach E., 1994. Episodes of high ozone concentrations at the Earth's surface resulting from transport down from the upper troposphere/lower stratosphere: a review and case studies. *Atmospheric Environment* 28, 53-68.

Dorling S.R., Davies T.D., 1995. Extending cluster-analysis-Synoptic meteorology links to characterize chemical climates at 6 northwest European monitoring stations. *Atmospheric Environment* 29, 145-167.

Draxler R., Hess G.D., 1997. Description of the HYSPLIT_4 modeling system. NOAA Tech. Memo. ERL ARL-224 NOAA Air Resources Laboratory, Silver Spring, MD, 24 pp.

Draxler, R.R., and G.D. Hess, 1998: An overview of the HYSPLIT_4 modeling system of trajectories, dispersion, and deposition. *Australian Meteorological Magazine* 47, 295-308.

Draxler, R.R., 1999. HYSPLIT4 User's Guide. NOAA Tech. Memo. ERL ARL-230, NOAA Air Resources Laboratory, Silver Spring, MD. Draxler R.R., Rolph G.D., 2003. HYSPLIT Model. NOAA Air Resources Laboratory. http://www.arl.noaa.gov/ready/hysplit4.html.

Draxler R.R., Rolph G.D., 2003. HYSPLIT Model. NOAA Air Resources Laboratory. http://www.arl.noaa.gov/ready/hysplit4.html.

Dueñas C., Orza J.A.G., Cabello M., Fernández M.C., Cañete S., Pérez M., Gordo E., 2011. Air mass origin and its influence on radionuclide activities (^{7}Be and ^{210}Pb) in aerosol particles at a coastal site in the western Mediterranean. *Atmospheric Research* 101, 205-214.

Ebinghaus R., Jennings S.G., Kock H.H., Derwent R.G., Manning A.J., Spain T.G., 2011. Decreasing trends in total gaseous mercury observations in baseline air at Mace Head, Ireland from 1996 to 2009. *Atmospheric Environment* 45, 3475-3480.

Eisele H., Scheel H.E., Sladkovic R., Trickl T., 1999. High resolution lidar measurements of stratosphere-troposphere exchange. Journal of Atmospheric Sciences 56, 319-330.

Elbern H., Kowol J., Sladkovic R., Ebel A., 1997. Deep stratospheric intrusions: a statistical assessment with model guided analyses. *Atmospheric Environment* 31, 3207-3226.

Eleftheriadis K., Vratolis S., Nyeki S., 2009. Aerosol black carbon in the European Arctic: Measurements at Zeppelin station, Ny-Ålesund, Svalbard from 1998-2007. *Geophysical Research Letters* 36, L02809, doi:10.1029/2008GL035741

Fabian P., Pruchniewicz P.G., 1977. Meridional distribution of ozone in the troposphere and its seasonal variations. *Journal of Geophysical Research* 82, 2063-2073.

Feely H.W., Larsen R.J., Sanderson C.G., 1989. Factors that cause seasonal variations in ^{7}Be concentrations in surface air. *Journal of Environmental Radioactivity* 9, 223-249.

Fischer H., Kormann R., Klüpfel T., Gurk Ch., Königstedt R., Parchatka U., Mühle J., Rhee T.S., Brenninkmeijer C.A.M., Bonasoni P., Stohl A., 2003. Ozone production and trace gas correlations

during the June 2000 MINATROC intensive measurement campaign at Mt Cimone. *Atmospheric Chemistry and Physics* 3, 725-738.

Fleming Z.L., Monks P.S., Manning A.J., 2012. Review: Untangling the influence of air-mass history in interpreting observed atmospheric composition. *Atmospheric Research* 104-105, 1-39.

Follows M.J., Austin J.F., 1992. A zonal average of the stratospheric contributions to the tropospheric ozone budget. *Journal of Geophysical Research* 97(D16), 18047-18060.

Fuelberg H.E., Loring R.O. Jr., Watson M.W., Sinha M.C., Pickering K.E., Thompson A.M., Sachse G.W., Bale D.R., Scheberl M.R., 1996. TRACE - A Trajectory intercomparison: 2. Isentropic and kinematic methods. *Journal of Geophysical Research*, **101**, 23927-23939.

Gaffney J.S, Marley N., Cunningham M.M., 2004. Natural radionuclides in fine aerosols in the Pittsburgh area. *Atmospheric Environment* 38, 3191-3200.

Gerasopoulos E., Zanis P., Stohl A., Zerefos C.S., Papastefanou C., Ringer W., Tobler L., Hübener S., Gäggeler H.W., Kanter H.J., Tositti L., Sandrini S., 2001. A climatology of ^{7}Be at four high-altitude stations at the Alps and the Northern Apennines. *Atmospheric Environment* 35, 6347-6360.

Gerasopoulos E., Zerefos C.S., Papastefanou C., Zanis P., O'Brien K., 2003. Low frequency variability of beryllium-7 surface concentrations over the Eastern Mediterranean. *Atmospheric Environment* 37, 1745-1756.

Gerasopoulos E., et al., 2005. Deep stratosphere-to-troposphere transport (STT) over SE Europe: a complex case study captured by enhanced ^{7}Be concentrations at the surface of a low topography region. *Atmospheric Chemistry and Physics Discussion* 5, 101-129.

Gobbi G.P., Barnaba F., van Dingenen R., Putaud J.P., Mircea M., Facchini M.C., 2003. Lidar and in situ observations of continental and Saharan aerosol: closure analysis and optical properties. *Atmospheric Chemistry and Physics* 3, 2161-2172.

Graustein W.C., Turekian K.K., 1996. ^{7}Be and ^{210}Pb indicate an upper troposphere source for elevated ozone in the summertime subtropical free troposphere of the eastern North Atlantic. *Geophysical Research Letters* 23, 539-542.

Güllü G., Doğan G., Tuncel G., 2005. Atmospheric trace element and major ion concentrations over the eastern Mediterranean Sea: Identification of anthropogenic source regions. *Atmospheric Environment* 39, 6376-6387.

Harris J.M., Oltmans S.J., Dlugokencky E.J., Noveli P.C., Johnson B.J., Mefford T., 1998. An investigation into the source of springtime tropospheric ozone maximum at Mauna Loa Observatory. *Geophysical Research Letters* 25(11), 1895-1898.

Harris J.M., Draxler R.R. and Oltmans S.J., 2005. Trajectory model sensitivity to differences in input data and vertical transport method. *Journal of Geophysical Research* **110** D14109, doi:10.1029/2004JD005750.

Hernández F., Rodríguez S., Karlsson L., Alonso-Pérez S., López-Pérez M., Hernandez-Armas J., Cuevas E., 2008. Origin of observed high ^{7}Be and mineral dust concentrations in ambient air on the Island of Tenerife. *Atmospheric Environment* 42, 4247-4256.

Henry R.C., 1997. History and fundamentals of multivariate air quality receptor models. *Chemometrics and Intelligent Laboratory Systems* 37, 525-530.

Hoerling M.P., Schaack T.K., Lenzen A.J., 1991. Global objective tropopause analysis. *Monthly Weather Review* 119, 1816-1831

Holton J.R., Haynes P.H., McIntyre M.E., Douglass A.R., Rood R.B., Pfister L., 1995. Stratosphere-troposphere exchange. *Reviews of Geophysics* 33, 403-439.

Hopke P.K., Gao N., Cheng M.D., 1993. Combining chemical and meteorological data to infer sources areas of airborne pollutants. *Chemometrics and Intelligent Laboratory Systems* 19(2), 187-199.

Hopke P.K., Barrie L.A., Li S.M., Cheng M.D., Li C., Xie Y., 1995. Possible sources and preferred pathways for biogenic and non-sea-salt sulphur for the high Arctic. *Journal of Geophysical Research* 100, 16595-16603.

Hwang I., Hopke P.K., 2007. Estimation of source apportionment and potential source locations of PM2.5 at a west coastal IMPROVE site. *Atmospheric Environment* 41, 506-518.

Ioannidou A., Manolopoulou M., Papastefanou C., 2005. Temporal changes of ^{7}Be and ^{210}Pb concentrations in surface air at temperate latitudes (40°). *Applied Radiation and Isotopes* 63(2), 277-284.

James P, Stohl A., Forster C., Eckhardt S., Seibert P., Frank A., 2003a. A 15-year climatology of stratosphere-troposphere exchange with a Lagrangian particle dispersion model 2. Mean climate and seasonal variability. *Journal of Geophysical Research* 108(D12), 8522. doi:10.1029/2002JD002639

James P, Stohl A., Forster C., Eckhardt S., Seibert P., Frank A., 2003b. A 15-year climatology of stratosphere-troposphere exchange with a Lagrangian particle dispersion model 1. Methodology and validation. *Journal of Geophysical Research* 108(D12), 8519. doi:10.1029/2002JD002637

Johnson W., Viezee W., 1981. Stratospheric ozone in the lower troposphere-I Presentation and interpretation of aircraft measurements. *Atmospheric Environment* 15, 1309–1323.

Junge C.E., 1962. Global ozone budget and exchange between stratosphere and troposphere. *Tellus* 14, 363-377.

Kahl J.D., Harris J.M., Herbert G.A., Olson M.P., 1989. Intercomparison of three long-range trajectory models applied to Arctic haze. *Tellus* 41B, 524-536.

Kahl J.D., 1996. On the prediction of trajectory model error. Atmospheric Environment 30(17), 2945-2957.

Kaiser A., Scheifinger H., Spangl W., Weiss A., Gilge S., Fricke W., Ries L., Cemas D., Jesenovec B., 2007. Transport of nitrogen oxides, carbon monoxide and ozone to the Alpine Global Atmosphere Watch stations Jungfraujoch (Switzerland), Zugspitze and Hohenpeissenberg (Germany), Sonnblick (Austria) and Mt. Krvavec (Slovenia). *Atmospheric Environment* 41, 9273-9287.

Koçak M., Theodosi C., Zarmpas P., Im U., Bougiatoti A., Yenigun O., Mihapoulos N., 2011. Particulate matter (PM10) in Istanbul: Origin, source areas and potential impact on surrounding regions. *Atmospheric Environment* 45, 6891-6900.

Koch D.M., Jacob J., Graustein W.C., 1996. Vertical transport of tropospheric aerosols as indicated ^{7}Be and ^{210}Pb in a chemical tracer model. *Journal of Geophysical Research* 101: 18651-18666.

Kong X., He W., Qin N., He Q., Yang B., Ouyang H., Wang Q., Xu F., 2013. Comparison of transport pathways and potential sources of PM10 in two cities around a large Chinese lake using the modified trajectory analysis. *Atmospheric Research* 122, 284-297.

Kulan A., Aldahan A., Possnert G., Vintersved I., 2006. Distribution of ^{7}Be in surface air of Europe. *Atmospheric Environment* 40, 3855-3868.

Lamarque J.-F., Hess P.G., 1994. Cross-Tropopause Mass Exchange and Potential Vorticity Budget in a Simulated Tropopause Folding. *Journal of the Atmospheric Sciences* 51(15), 2246-2269.

Lee H.N., Wan G., Zheng X., Sanderson C.G., Josse B., Wang S., Yang W., Tang J., Wang C., 2004. Measurements of ^{210}Pb and ^{7}Be in China and their analysis accompanied with global model calculations of ^{210}Pb. *Journal of Geophysical Research* 109, D22203. doi:10.1029/2004JD005061

Lee H.N., Tositti L., Zheng X., Bonasoni P., 2007. Analyses and comparisons of variations of ^{7}Be, ^{210}Pb and ^{7}Be/^{210}Pb with ozone observations at two Global Atmosphere Watch stations from high mountains. *Journal of Geophysical Research* 112, D05303. doi:10.1029/2006JD007421

Lelieveld J., Dentener F., 2000. What controls tropospheric ozone. *Journal of Geophysical Research* 105(D3), 3543-3563.

Li Q., Jacob D.J., Fairlie T.D., Liu H., Martin R.V., Yantosca R.M., 2002. Stratospheric versus pollution influences on ozone at Bermuda: Reconciling past analyses. *Journal of Geophysical Research* 107, D22, 4611. doi:10.1029/2002JD002138

Lin C.-J., Cheng M.-D., Schroeder W.H., 2001. Transport patterns and potential sources of total gaseous mercury measured in Canadian high Arctic in 1995. *Atmospheric Environment* 35, 1141-1154.

Liu H., Jacob D.J., Dibb J.E., Fiore A.M., Yantosca R.M., 2004. Constraints on the sources of tropospheric ozone from ^{210}Pb-^{7}Be-O_3 correlations. *Journal of Geophysical Research* 109, D07306. doi:10.1029/2003JD003988.

Logan J.A., 1985. Tropospheric ozone: Seasonal Behavior, Trends, and Anthropogenic Influence. *Journal of Geophysical Research* 90(D6), 10463-10482.

Lozano R.L., Hernández-Ceballos M.A., Rodrigo J.F., San Miguel E.G., Casas-Ruiz M., García-Tenorio R., Bolívar J.P., 2013. Mesoscale behavior of ^{7}Be and ^{210}Pb in superficial air along the Gulf of Cadiz (south of Iberian Peninsula). *Atmospheric Environment* 80, 75-84. doi:10.1016/j.atmosenv.2013. 07.050

Lupu A., Maenhaut W., 2002. Application and comparison of two statistical trajectory techniques for identification of source regions of atmospheric aerosol species. *Atmospheric Environment* 36, 5607-5618.

Maione M., Giostra U., Arduini J., Belfiore L., Furlani F., Geniali A., Mangani G., Vollmer M.K., Reimann S., 2008. Localization of source regions of selected hydrofluorocarbons combining data collected at two European mountain stations. *Science of the Total Environment* 391, 232-240.

Marenco F., et al., 2006. Characterization of atmospheric aerosols at Monte Cimone, Italy, during summer 2004: Source apportionment and transport mechanisms. *Journal of Geophysical Research* 111, D24202. doi:10.1029/2006JD007145

Marinoni A., Cristofanelli P., Calzolari F., Roccato F., Bonafé U., Bonasoni P., 2008. Continuous measurements of aerosol physical parameters at the Mt Cimone GAW Station (2165 m asl, Italy). *Science of the Total Environment* 391, 241-251.

Martin C.L., Allan J.D., Crosier J., Choularton T.W., Coe H., Gallagher M.W., 2011. Seasonal variation of fine particulate composition in the centre of a UK city. *Atmospheric Environment* 45, 4379-4389.

McQueen T.J., Draxler R.R., 1994. Evaluation of model back-trajectories of the Kuwait oil fires smoke plume using digital satellite data. *Atmospheric Environment* 28 (13), 2159-2174.

Menut L., Masson O., Bessagnet B., 2009. Contribution of Saharan Dust on radionuclide activity levels in Europe? The 21-22 February 2004 case study. *Journal of Geophysical Research* 114, D16202, doi:10.1029/2009JD011767

Merrill J.T., Bleck R., Avila L., 1985. Modeling atmospheric transport to the Marshal Islands. *Journal of Geophysical Research* 90, 12927-12936.

Monks P.S., 2000. A review of the observations and origins of the spring ozone maximum. *Atmospheric Environment* 34, 3545-3561.

Olsen M.A., Gallus W.A., Stanford J.L., Brown J.M., 2000. Fine-scale comparison of TOMS total ozone data with model analysis of an intense Midwestern cyclone. *Journal of Geophysical Research* 105, 20,487-20,498.

Paatero P., Tapper U., 1994. Positive matrix factorization: a non-negative factor model with optimal utilization of error estimates of data values. *Environmetrics* 5, 111-126.

Papastefanou C., Ioannidou A., 1995. Aerodynamic size association of ^{7}Be in ambient aerosols. Journal of Environmental Radioactivity 26, 273-282.

Penkett S.A., Brice K.A., 1986. The spring maximum in photo-oxidant in the Northern hemisphere troposphere. *Nature* 319, 655-657.

Poirot R.L., Wishinski P.R., 1986. Visibility, sulphate and air mass history associated with the summertime aerosol in northern Vermont. *Atmospheric Environment* 20, 1457-1469.

Poirot R.L., Wishinski P.R., Hopke P.K., Polissar A.V., 2001. Comparative application of multiple receptor methods to identify aerosol sources in northern Vermont. *Environmental Science and Technology* 35, 4622-4636.

Polissar A.V., Hopke P.K., Paatero P., Kaufmann Y.J., Hall D.K., Bodhaine B.A., Dutton E.G., Harris J.M., 1999. The aerosol at Barrow, Alaska: long-term trends and source locations. *Atmospheric Environment* 33, 2441-2458.

Polissar A.V., Hopke P.K., Harris J.M., 2001a. Source regions for atmospheric aerosol measured at Barrow, Alaska. *Environmental Science and Technology* 35, 4214-4226.

Polissar A.V., Hopke P.K., Poirot R.L., 2001b. Atmospheric aerosol over Vermont: chemical composition and sources. *Environmental Science and Technology* 35, 4604-4621.

Poulida O., Dickerson R.R., Heymsfield, 1996. Stratosphere-troposphere exchange in a midlatitude mesoscale convective complex: 1. Observations. *Journal of Geophysical Research* 101(D3), 6823-6836.

Putaud J.-P., van Dingenen R., Dell'Acqua A., Raes F., Matta E., Decesari S., Facchini M.C., Fuzzi S., 2004. Size-segregated aerosol mass closure and chemical composition in Monte Cimone (I) during MINATROC. *Atmospheric Chemistry and Physics* 4, 889-902.

Reed R.J., 1995. A study of a characteristic type of upper-level frontogenesis. *Journal of Meteorology* 12, 226-237.

Reiter R., 1975. Stratospheric-Tropospheric Exchange Processes. *Reviews of Geophysics and Space Physics* 13(4), 459-474.

Reiter R., Munzert K., Kanter H.J., Potzl K., 1983. Cosmogenic radionuclides and ozone at a mountain station at 3.0 km a.s.1. *Archiv fur Meteorologie, Geophysik und Bioclimatologie*, Serie B 32, 131–160.

Riccio A., Giunta G., Chianese E., 2007. The application of a trajectory classification procedure to interpret air pollution measurements in the urban areas of Naples (Southern Italy). *Science of the Total Environment* 376, 198-214.

Roelofs G.J., Lelieveld J., 1997. Model study of the influence of cross-tropopause O3 transports on tropospheric O_3 levels. *Tellus* 49B, 38-55.

Seibert P., Kromp-Kolb H., Baltensperger U., Jost D.T., Schwikowski M., Kasper A., Puxbaum H., 1994. Trajectory analysis of aerosol measurements at high alpine sites. In: Borrell P., Cvitai T., Seiler W. (Eds.) Transport and transformation of Pollutants in the Troposphere. Academic Publishing, Den Haag, pp. 689-693.

Singh H.B., Ludwig F.L., Johnson W.B., 1978. Tropospheric ozone: concentrations and variabilities in clean remote atmospheres. *Atmospheric Environment* 12, 2185-2196.

Sprenger M., Wernli H., 2003. A northern hemispheric climatology of cross: tropopause exchange for the ERA15 time period (1979-1993). *Journal of Geophysical Research* 108(D12), 8521.

Steinmann P., Zeller M., Beuret P., Ferreri G., Estier S., 2013. Cosmogenic ^{7}Be and ^{22}Na in ground level air in Switzerland (1994-2011). *Journal of Environmental Radioactivity* 124, 68-73.

Stohl A., Kromp-Kolb H., 1994. Origin of ozone in Vienna and surroundings, Austria. *Atmospheric Environment* 28, 1255-1266.

Stohl A., 1996. Trajectory statistics – a new method to establish source-receptor relationships of air pollutants and its application to the transport of particulate sulphate in Europe. *Atmospheric Environment* 30(4), 579-587.

Stohl A., 1998. Computation, accuracy and applications of trajectories - A review and bibliography. *Atmospheric Environment* 32, 947-966.

Stohl A., Spoichtinger-Rakowsky N., Bonasoni P., Feldmann H., Memmesheimer M., Scheel H.E., Trickl T., Hübener S., Ringer W., Mandl M., 2000. The influence of stratospheric intrusions on alpine ozone concentrations. *Atmospheric Environment* 34, 1323-1354.

Stohl A., Wernli H., James, P., Borqui M., Forster C., Liniger M.A., Seibert P., Sprenger M., 2003. A new perspective of stratosphere-troposphere exchange. *American Meteorological Society*, 1565-1573 doi:10.1175/BAMS-84-11-1565

Stunder B.J.B., 1996. An assessment of the quality of forecast trajectories. *Journal of Applied Meteorology* 35, 1319-1331.

Tarasova O.A., Senik I.A., Sosonkin M.G., Cui J., Staehelin J., Prevot A.S.H., 2009. Surface ozone at the Caucasian site Kislovodsk High Mountain Station and the Swiss Alpine site Jungfraujoch: data analysis and trends (1990-2006). *Atmospheric Chemistry and Physics* 9, 4157-4175.

Tosi E., Smith R.B., Bradford M.L., 1987. Aerial Observations of Stratospheric Descent in a Gulf of Genoa Cyclone. *Meteorology and Atmospheric Physics* 36(1-4), 141-160.

Tositti L., Hübener S., Kanter H.J., Ringer W., Sandrini S., Tobler L., 2004. Intercomparison of sampling and measurement of ^{7}Be in air at four high-altitude locations in Europe. *Applied Radiation and Isotopes* 61, 1497-1502.

Tositti L., Brattich E., Cinelli G., Previti A., Mostacci D., 2012. Comparison of radioactivity data measured in PM10 aerosol samples at two elevated stations in northern Italy during the Fukushima event. *Journal of Environmental Radioactivity* 114, 105-112.

Tositti L., Riccio A., Sandrini S., Brattich E., Baldacci D., Parmeggiani S., Cristofanelli P., Bonasoni P., 2013. Short-term climatology of PM10 at a high altitude background station in southern Europe. *Atmospheric Environment* 65, 145-152.

Tositti L., Brattich E., Cinelli G., Baldacci D., 2014. 12 years of ^{7}Be and ^{210}Pb data at the WMO-GAW station of Mt. Cimone (2165 m a.s.l., 44°12'N 10°42'E) and their correlation with meteorological parameters. *Atmospheric Environment* 87C, 108-122. doi:10.1016/j.atmosenv.2014.01.014

Trickl T., Feldmann H., Kanter H.-J., Scheel H.-E., Sprenger M., Stohl A., Wernli H., 2010. Forecasted deep stratospheric intrusions over Central Europe: case studies and climatologies. *Atmospheric Chemistry and Physics* 10, 499-524.

Usoskin I., Kovaltsov. G., 2008.Production of cosmogenic ^{7}Be isotope in the atmosphere: full 3D modelling. *Journal of Geophysical Research* 113, D12107.

Usoskin I.G., Field C.V., Schmidt G.A., Leppänen A-P, Aldahan A., Kovaltsov G.A., Possnert G., Ungar R.K., 2009. Short-term production and synoptic influences on atmospheric ^{7}Be concentrations. *Journal of Geophysical Research* 114, D06108. doi:10.1029/2008JD011333

Vasconcelos L. A. P., Kahl J. D. W., Liu D., Macias E. S., White, W. H., 1996a. Spatial resolution of a transport inversion technique. *Journal of Geophysical Research* 101, 19,337–19,342

Vasconcelos L.A.P., Kahl J.D.W., Liu D., Marcias E.S. and White W.H., 1996b. A tracer calibration of back trajectory analysis at the Grand Canyon. *Journal of Geophysical Research* 101 (D14), 19329–19335, doi:10.1029/95JD02609.

Vaughan G., Price J.D., 1989. Ozone transport into the troposphere in a cut-off low event: ozone in the atmosphere. Deepak, Hampton, VA, USA, pp 415-446

Wang Y.Q., Zhang X.Y., Arimoto R., 2006. The contribution from distant dust sources to the atmospheric particulate matter loadings at XiAn, China during spring. *Atmospheric Environment* 368, 875-883.

Winkler R., Dietl F., Frank G., Thiersch J., 1998. Temporal variation of ^{7}Be and ^{210}Pb size distributions in ambient aerosols. *Atmospheric Environment* 32, 983-991.

WMO, 2001. WMO TD No. 1073, July 2001. http://www.wmo.int/pages/prog/gcos/documents/gruanmanuals/GAW/gaw143.pdf (accessed 02.09.13)

WMO-GAW (World Meteorological Organization, - Global Atmosphere Watch) Report No. 155, 2004. 1st International Expert Meeting on Sources and Measurements of Natural Radionuclides Applied to Climate and Air Quality Studies, (Gif-sur-Yvette, France, 3-5 June 2003) (WMO TD No. 1201), [available at ftp://ftp.wmo.int/Documents/PublicWeb/arep/gaw/gaw155.pdf, last accessed 01 August 2013]

Wotawa, G. and Kröger, H., 1999. Testing the ability of trajectory statistics to reproduce emission inventories of air pollutants in cases of negligible measurement and transport errors, *Atmospheric Environment* 33, 3037–3043.

Wotawa G., Kröger H., Stohl A., 2000. Transport of ozone towards the Alps – results from trajectory analyses and photochemical model studies. *Atmospheric Environment* 34, 1367-1377.

Xie Y.-L., Hopke P.K., Paatero P.,Barrie L.A., Li S.-M., 1999. Locations and preferred pathways of possible sources of Arctic aerosol. *Atmospheric Environment* 33, 2229-2239.

Zanis P., Schuepbach E., Gäggeler H.W., Hübener S., Tobler L., 1999. Factors controlling beryllium-7 at Jungfraujoch in Switzerland. *Tellus* 51B, 789-805.

Zanis P., et al., 2003a. Forecast, observation and modelling of a deep stratospheric intrusion event over Europe. *Atmospheric Chemistry and Physics Discussions* 3, 763-777.

Zanis P., et al., 2003b. An estimate of the impact of stratosphere-to-troposphere transport (STT) on the lower free tropospheric ozone over the Alps using ^{10}Be and ^{7}Be measurements. *Journal of Geophysical Research* 108(D12), 8520. doi:10.1029/2002JD002604

Zeng Y., Hopke P.K., 1988. A study of the sources of acid precipitation in Ontario, Canada. *Atmospheric Environment* 23, 1499-1509.

Zheng X., Wang G., Tang J., Zhang X., Yang W., Lee H.N., Wang C., 2005. ^{7}Be and ^{210}Pb radioactivity and implications on sources of surface ozone at Mt. Waliguan. *Chinese Science Bulletin* 50(2), 167-171.

CHAPTER 7 – Source Apportionment of Particulate Matter in a Large City of Southeastern Po Valley (Bologna, Italy)

7.1. Introduction[1]

Air pollution has long been recognized as a serious concern due to its negative influence on the biotic and abiotic compartments of the Earth at both small and large scales, including climatic change. In the last two decades airborne Particulate Matter (PM) has increasingly attracted the interest of the scientific community because, in spite of the ever improving efforts in abatement technologies, its concentration is locally still very high often exceeding the thresholds. Effects of PM hazards include damage to the environment and cultural heritage (Camuffo *et al.*, 2001; Godoi *et al.*, 2006; Nava *et al.*, 2010) through direct and indirect effects such as respectively alteration of atmospheric chemistry and reactivity, climate change and biogeochemical cycles (Charlson *et al.*, 1992; Finlayson-Pitts and Pitts, 1999; Usher *et al.*, 2003; Seinfeld and Pandis, 2006; Forster *et al.*, 2007) as well as adverse impacts on human health (Davidson *et al.*, 2005; Pope and Dockery, 2006; Pope *et al.*, 2009).

The persistence of high levels of atmospheric pollution arises from a number of figures spanning from a generalized and huge increase in all the types of transportation from vehicles to maritime and aviation (EEA, 2011), building, soil use, urbanization and atmospheric circulation at every space and time scale. In this framework complexity in aerosol chemistry and phenomenology (Van Dingenen *et al.*, 2004; Putaud *et al.*, 2004; Prather *et al.*, 2008; Putaud *et al.*, 2010; Carslaw *et al.*, 2010; Colb and Worsnop, 2012) linking PM composition to its peculiar and transient mix of sources are still a matter of basic research. Although the formation mechanisms and chemical characterization of PM are still quite challenging, valuable tools for the identification of the emission spectrum over a location have long been available. Source apportionment techniques based upon chemical speciation and

[1] This chapter consists of a paper by Tositti L. (Dept. of Chemistry, Università di Bologna), Brattich E. (Dept. of Biological, Geological and Environmental Sciences, Università di Bologna), Masiol M. (Dept. of Environmental Sciences, Informatics and Statistics, Università Ca' Foscari Venezia; now Marie Curie Research Fellow at GEES, University of Birmingham, UK), Baldacci D. (Dept. of Chemistry, Università di Bologna), Ceccato D. (LNL-INFN Legnaro & Dept. of Physics, Università di Padova), Parmeggiani S. (Dept. of Chemistry, Università di Bologna), Stracquadanio M. (ENEA Bologna), Zappoli S. (Dept. of Industrial Chemistry, Università di Bologna), 2014. Source apportionment of particulate matter in a large city of southeastern Po Valley (Bologna, Italy). *Environmental Science and Pollution Research* 21, 872-890. doi:10.1007/s11356-013-1911-7

subsequent receptor modeling provide in facts a fundamental tool in order to obtain quantitative and reliable information about the number and types of sources of PM active in a given location. Such information is of crucial importance to understand the potential emission sources and to take corrective decisions within environmental policies in a given area. In the last decade the use of these tools has provided an ever increasing application with the aim of solving PM sources mix in a innumerable series of cases (see for example, Harrison *et al*., 1997; Querol *et al.*, 2001; Marcazzan *et al*., 2003; Vallius *et al*., 2005; Kim *et al.*, 2003a;b; Viana *et al*., 2007; Viana *et al.*, 2008a;b and references therein; Yin *et al.*, 2010; Masiol *et al.*, 2012a;b; Pant and Harrison, 2012).

If the choice of PM chemical species to characterize is fairly unlimited and to some extent arbitrary, though always experimentally demanding, data treatments enabling source apportionment include a relatively limited number of statistical techniques among which the most popular and effective are presently the Principal Component Analysis followed by Multi-Linear Regression Analysis (PCA/MLRA, Thurston and Spengler, 1985; Viana *et al.*, 2006; Almeida *et al.*, 2006; Viana *et al*., 2008a;b;) and the Positive Matrix Factorization (PMF, Paatero and Tapper, 1994; Lee *et al.*, 1999; Kim *et al*., 2003a,b; Lee *et al.*, 2008).

In this Chapter we present data of chemical speciation based on major inorganic ions, trace elements and carbonaceous matter collected in Bologna within the framework of the national project SITECOS (Integrated Study on national Territory for the characterization and the COntrol on atmospheric pollutantS), covering simultaneous and coherent PM monitoring in ten locations of the Italian peninsula in association with the large meteoclimatic and environmental differences from north to south (Amodio *et al*., 2007). Bologna was one of the stations hosting SITECOS monitoring activity in the Po Valley. The whole Po Valley is recognized as one of the most polluted regions in Europe due to highest level of population and industrial density. Moreover, automotive, railing and flying transports have been regarded as important emission sources for this area (EC, 2004). Extensive agricultural activity and related food industry is highly developed in the whole region.

The air quality in the Po Valley is usually very poor not only due to the aforementioned anthropogenic emissions, but also to its topography. Alps and Apennines mountain chains act as a shield against atmospheric circulation, leading to weak winds, low mixing heights and prolonged atmospheric stabilities, causing air mass stagnation and reduced pollutant dispersal both in the cold (extreme PM average concentrations) and in the warm (extreme photosmog levels) seasons.

Several studies on PM composition and source identification have been carried out in various urban locations of the Po Valley, e.g., in Turin (Gilli *et al*., 2007), Milan (Marcazzan *et al*., 2003; Lonati *et al*., 2005), Venice-Mestre (Rampazzo *et al*., 2008), Ispra (Rodríguez *et al.*, 2005) and Bologna (Matta *et al.*, 2002). Still the whole region is a sort of large-scale laboratory deserving

attention and efforts by the scientific community. A recent overview on receptor model techniques, European studies and sources can be found in Belis *et al*. (2013).

Bologna (44°29' N; 11°20' E) (Figure 7.1) is a mid-size city (380 000 inhabitants) reaching one million people including the metropolitan area. The territory is not directly affected by large scale industrial facilities, however a recently upgraded municipal waste incinerator is active in the town outskirts and mechanical and food manufactures are densely present in the whole area, together with agricultural activities. Due to its strategic location at the crossroad between north and south of Italy as well as of the western and eastern sides of the Po Valley, it is heavily interested by large scale transportation (railway and aviation) but it is mainly affected by local and long-range light and heavy duty traffic. It is worth noting that besides the urban traffic, Bologna is an important crossroads between North and South Italy; moreover it is surrounded by much trafficked orbital roads.

Figure 7.1 *Map and location of Bologna (44°29' N, 11°20'E) in the Italian Po Valley (Planiglobe, kk&w - digital cartography).*

This Chapter mainly aims to evaluate the source contributions in an urban background site in Bologna by: (i) detecting the seasonal variations in PM chemical composition; (ii) identifying and quantifying the main emission sources using PCA/MLRA (Viana *et al.*, 2006) and PMF (Paatero and Tapper, 1994; Paatero, 1997; 1999) receptor modeling techniques; (iii) comparing the source apportionment results, and

(iv) evaluating the impact of long range transport due to Saharan dust outbreaks. The results aim at providing a clear and quantitative knowledge of the main sources of airborne particles, enhancing the effectiveness of further control policies. Remarkably though several papers have been published about Bologna airshed and its particulate matter, as far as the authors are aware, this is the first source apportionment study and for the first time trace elements have been accounted for.

7.2. Material and Methods

An urban background site (high density residential area, distance > 50 m from major streets) was placed in the courtyard of the Chemistry Dept., Bologna University, near the city center. PM_{10} and $PM_{2.5}$ were sampled on a daily simultaneous basis (24 h) in two main periods: a winter campaign and a summer campaign for a total of 84 days in 2006. Sampling was continuous within each campaign. Two preliminary short term campaigns were carried out in 2005: a very short campaign (only 9 samples) was carried out during the summer 2005, in which only $PM_{2.5}$ was sampled, whereas a simultaneous PM_{10} and $PM_{2.5}$ campaign was carried out during autumn 2005. Owing to the different experimental design these data could not be elaborated together with the former data. More details about the periods, the sampling and the analyses carried on the samples during the four campaigns are available in Table 7.1.

Campaign	Sampled Fraction	Filter Type	Type of analyses
Summer 2005 07/18-07/28/05	$PM_{2.5}$	Quartz fiber filter Ø 47 mm	½ filter for inorganic ions (IC) ¼ filter EC/OC (TGA)
Autumn 2005 09/26-10/19/05	$PM_{2.5}$	Quartz fiber filter Ø 47 mm	¼ filter for metals (ICP-MS) ¼ filter for inorganic ions (IC)
	PM_{10}	PTFE with support ring Ø 47 mm	
Winter 2006 01/23-03/05/03/06	$PM_{2.5}$	Quartz fiber filter Ø 47 mm	¼ filter EC/OC (CHN) ¼ filter inorganic ions (IC)
	PM_{10}	PTFE with support ring Ø 47 mm	whole filter for elements (PIXE)
Summer 2006 06/20/-07/20/06	$PM_{2.5}$	Quartz fiber filter Ø 47 mm	¼ filter EC/OC (CHN) ¼ filter TC (CHN)
	PM_{10}	PTFE with support ring Ø 47 mm	whole filter for elements (PIXE)

Table 7.1 *Details about the sampling campaigns and the analyses carried on the sampled filters.*

Samplings were daily performed according to European standard EN 14907 (CEN, 2005) using a HYDRA Dual (FAI, Italy) low volume sampler and started at midnight. PM_{10} was collected on PTFE (Whatman with support ring, 2 µm, Ø 47 mm) while $PM_{2.5}$ was collected on quartz fiber filters (Schleicher and Schuell, Germany, Ø 47 mm) in agreement with SITECOS shared sampling strategy.

Blank filter mass and PM mass load were determined gravimetrically after 48 hours conditioning at constant temperature and relative humidity in a drier. Filter weights were obtained as the average of at least three measurements using a microbalance (nominal precision 1 µg). Each $PM_{2.5}$ filter was cut in three aliquots. One quarter of the filter was sonicated in ultrapure water for 30 minutes and subsequently analyzed by isocratic ion chromatography with a Dionex ICS-90 for the determination of five major inorganic cations (NH_4^+, Na^+, Mg^{2+}, K^+ and Ca^{2+}) and 3 anions (Cl^-, NO_3^-, SO_4^{2-}). Cation setup: precolumn, CG12A, column CS12A 4 µm; methanesulfonic acid (20 mM) as eluant. Anion set-up: precolumn, AG14A; column, AS14A 7 µm; Na_2CO_3 (8 mM) and $NaHCO_3$ (1 mM) as eluant.

The second aliquot was analyzed for Total Carbon (TC) using an elemental analyser (CHN Flash Combustion, Termoquest, Milano), coupled to a muffle pretreatment (Nabertherm, Lilienthal) for 2 hours at 450°C. The collected samples were then analyzed for elemental carbon with a complete oxidation of OC at 350°C for 3 hours and 30 minutes. The third aliquot was stored for further analyses. Only for the autumn 2005 campaign, ICP-MS (Element 2 double focusing, with an HNO_3 pH 1.5 filter extraction) elemental analyses were performed on this third aliquot.

PM_{10} samples on PTFE membranes were analyzed by Particle Induced X-Ray Emission (PIXE) at LNL-INFN laboratories (Padua, Italy) for the non-destructive quantitative determination of 19 elements (Na, Mg, Al, Si, S, Cl, K, Ca, Ti, V, Cr, Mn, Fe, Ni, Cu, Zn, Br, Pb, P). PIXE set-up was described in detail in Mittner *et al.* (1996) and involves a 1.8 MeV proton beam and a low-energy germanium detector. X-ray spectra from PIXE were fitted using GUPIX software package (Maxwell *et al.*, 1995) to obtain concentration, minimum detection limits and % fit error for each element in each sample.

Filter blanks and field blanks were analysed together with the samples in order to subtract their contribution to samples. Detection limit (LOD) was calculated as LOD = $\overline{x_b}$ + 3.14 σ_b with $\overline{x_b}$ as the arithmetic mean of the analyte concentration in the blanks and σ_b as its standard deviation. Experimental data lower than LOD were rejected at first and then substituted by LOD/2 only before applying multivariate statistical analyses, whereas data greater than LOD were subtracted by $\overline{x_b}$. Experimental uncertainty (RDS) was detected following Miller and Miller (1993); all the uncertainties were added up following the rules for error propagation. The relative percent error was in the range 3% (for Na^+) and 13% (for Mg^{++}).

For ion chromatography, quality control was carried out by analyzing the synthetic rain water BCR®-408 and BCR®-409 (IRMM, Community Bureau of Reference of the European Community) certified reference materials. The quality and the accuracy of quantitative PIXE analyses were checked with NIST SRM 2783 Air Particulate thin film standard on Filter Media.

The influence of external PM contributions from African dust outbreaks over Bologna was investigated by the reconstruction of air mass backward trajectories using NOAA HYSPLIT v 4.9 model (Draxler, 1999; Rolph, 2003; Draxler and Rolph, 2011). HYSPLIT set-up: starting at 00:00 h local time, at 50, 500, 1000 m AGL, duration -90 h, 6 h step, model vertical velocity, GDAS1 meteorological data fields input data.

7.3. Results and Discussion

7.3.1 PM levels

A preliminary explorative data analysis was performed for each single campaign. Results are summarized in Table 7.2. Yearly, PM_{10} mass concentration levels are in the 12.4–151.5 μg m^{-3} range, with an average (mean ±standard deviation) of 44.5 ± 24.2 μg m^{-3}, while $PM_{2.5}$ ranges from 7.9 to 124.3 μg m^{-3}, with an average of 31.6 ± 21.0 μg m^{-3}.

	PM_{10}	Na	Mg	Al	Si	S	Cl	K	Ca	Ti	V	Cr	Mn	Fe	Ni	Cu	Zn	Br	Pb	P
AUTUMN 2005																				
N	24	0	0	24	0	0	0	0	0	0	24	24	24	24	24	24	24	0	24	0
mean	46	-	-	0.02	-	-	-	-	-	-	0.002	0.001	0.003	0.05	0.001	0.005	0.041	-	0.013	-
std dev	17	-	-	0.01	-	-	-	-	-	-	0.001	0.000	0.002	0.03	0.000	0.002	0.024	-	0.009	-
WINTER 2006																				
N	49	41	32	40	40	41	41	41	41	41	0	37	14	41	37	0	41	21	30	0
mean	51	0.23	0.05	0.11	0.5	1.2	1.1	0.32	1.2	0.03	-	0.006	0.02	0.67	0.006	-	0.08	0.01	0.03	-
std dev	31	0.15	0.03	0.07	0.3	0.7	0.8	0.18	0.8	0.02	-	0.003	0.01	0.37	0.004	-	0.054	0.005	0.018	-
SUMMER 2006																				
N	35	9	18	34	34	34	34	34	34	34	9	32	34	34	11	34	34	0	0	18
mean	35	0.09	0.05	0.26	0.8	1.1	0.05	0.27	1.2	0.04	0.006	0.004	0.016	0.7	0.004	0.02	0.03	-	-	0.024
std dev	11	0.07	0.03	0.24	0.6	0.4	0.11	0.13	0.5	0.03	0.003	0.001	0.007	0.4	0.002	0.006	0.008	-	-	0.007

	$PM_{2.5}$	EC	OC	NO_3^-	SO_4^{2-}	Cl^-	NH_4^+	Ca^{++}	K^+	Mg^{++}	Na^+	Cd	As	Mo	Hg
SUMMER 2005															
N	9	9	9	9	9	3	9	8	8	8	9	0	0	0	0
mean	17.7	1.7	5.7	0.40	5.8	0.11	1.93	0.19	0.15	0.03	0.13	-	-	-	-
std dev	4.3	0.4	4.8	0.09	2.5	0.04	1.08	0.07	0.07	0.01	0.05	-	-	-	-
AUTUMN 2005															
N	24	0	0	24	24	13	24	24	24	4	23	24	24	24	24
mean	33	-	-	7.3	5.0	0.53	3.8	0.11	0.21	0.013	0.075	0.0005	0.0008	0.0005	0.0007
std dev	18	-	-	6.9	2.8	0.21	2.1	0.04	0.19	0.004	0.078	0.0004	0.0005	0.0003	0.0008
WINTER 2006															
N	49	42	42	41	41	21	42	37	42	24	40	0	0	0	0
mean	41	2.7	4.1	12.1	3.9	0.94	3.6	0.19	0.31	0.03	0.06	-	-	-	-
std dev	26	1.3	2.0	9.4	2.0	0.84	2.3	0.11	0.21	0.02	0.04	-	-	-	-
SUMMER 2006															
N	35	34	34	34	34	13	34	32	34	30	0	0	0	0	0
mean	21	1.7	4.0	0.74	5.2	0.66	1.55	0.32	0.39	0.04	-	-	-	-	-
std dev	7	1.1	1.3	0.93	2.0	0.41	0.74	0.09	0.30	0.01	-	-	-	-	-

Table 7.2) *Number of days when the elements have been found (N), arithmetic mean concentration and standard deviation (μg m^{-3}) for major and trace ions and elements obtained at Bologna during the four campaign of the SITECOS project (summer 2005, autumn 2005, winter 2006 and summer 2006) in PM_{10} (a) and $PM_{2.5}$ (b).*

Annual mean of PM_{10} concentration was above the European annual PM_{10} threshold of 40 μg m^{-3} fixed by 1999/30/EC (EC, 1999), while the European 24 h PM_{10} limit value of 50 μg m^{-3} is exceeded in 9 days during September-October 2005, 18 days during January-March 2006 and 5 days during June-July 2006 campaigns. Though $PM_{2.5}$ thresholds were enforced in Italy in 2008, results from the present investigations clearly show that not only this fraction represents a considerable mass contribution to PM_{10} (up to 90% in the winter), but also $PM_{2.5}$ limits were frequently exceeded as presently regulated (EC, 2008).

Data on mixed layer height were obtained by the annual reports of the Regional Environmental Protection Agency ARPA-ER, where this parameter is evaluated based on atmospheric modeling (Calmet meteorological pre-processor (ARPA-EMR, 2013)). The mixing height typically shows

winter minima and summer maxima and is inversely correlated with the PM_{10} and $PM_{2.5}$ seasonal trend in agreement with similar findings concerning the Po Valley (Matta *et al.*, 2002; Lonati *et al*., 2008; Rampazzo *et al*., 2008).

The daily average concentrations of $PM_{2.5}$ and PM_{10} are found equal to 33 and 46 μg m^{-3} in autumn, 41 and 51 μg m^{-3} in winter, 21 and 35 μg m^{-3} in summer.

In most European sites the $PM_{2.5}$:PM_{10} ratio ranges from 0.4 to 0.9 with a slight increase from natural to urban background sites (Putaud *et al*., 2004; 2010). In this study, the ratio among the two fractions varies seasonally, with values of 0.5-0.6 during the warm season and 0.8-0.9 during the cold period. In general this difference is attributed to an increase in the coarse fraction under dryer summer conditions, due to higher resuspended dust during the warm season, as well as to different combustion source profiles in the two seasons.

7.3.2 Chemical characterization and seasonal patterns

Table 7.2 reports basic statistics of the chemical species measured in PM_{10} and $PM_{2.5}$. During the whole period, the most abundant elements in PM_{10} follow the order: Ca > S > Si > Cl > Fe > K > Na > Al > Mg > Zn > Ti > Pb > P > Br > Mn > Cu > Cr > Ni > V. These elements are mainly associated to natural sources, i.e., crustal material (Si, Al, Ca, Fe), sea spray (Na and Cl), but also to secondary inorganic aerosol (SIA) and biomass burning (S and K, respectively). Anthropogenic-related elements (Cr, Cu, Zn, Pb) exhibit values slightly lower than in other Italian urban sites (e.g., Lucarelli *et al*. 2000; Marcazzan *et al*., 2003; Rampazzo *et al*., 2008) (Table 7.3). The most abundant species in $PM_{2.5}$ are nitrate, sulfate, ammonium, and the carbonaceous fraction. These latter species present concentrations comparable with other European sites located in the Mediterranean Region (Putaud *et al*., 2004; 2010). On average, the carbonaceous fraction represents about 17-20% (cold period vs. warm period value) of $PM_{2.5}$ mass, while SIA accounts for 28% of $PM_{2.5}$ on average (warm period average value 22%, cold period average value 33%).

	Firenze Site A	Firenze Site B	Firenze Site C	Milano Winter	Milano summer	Venezia site 1	Venezia site 2	Venezia site 3	This study
PM_{10}	47000±1600	28000±1200	32000±20000	87400±37800	41500±14500	46000±32000	41000±31000	23000±15000	44500±24200
Na	670±580	620±590	780±700			460±660	1141±2770	2948±6931	202±150
Mg	140±61	73±50	100±60			346±220	324±149	174±165	53±30
Al	400±200	180±130	260±160	175±82	129±60	307±192	320±169	147±209	140±170
Si	1140±540	510±350	800±490	675±309	452±197	1074±1076	3364±10086	6055±10433	646±500
P	33±15	18±9	22±13			32±29	33±19	7±12	24±10
S	2720±1390	1850±1050	1700±930	540±206	571±202	5474±7412	5983±8190	12169±25719	1195±600
Cl	270±520	240±490	330±570	161±155	173±180				600±800
K	370±190	350±200	400±230	132±47	132±53	595±1287	736±1604	2518±6140	300±200
Ca	1880±950	910±490	1670±970	427±187	264±123	1378±1366	3118±8509	4016±10438	1197±700
Ti	52±24	25±15	37±25	20±8	14±6	45±51	87±236	128±258	35±30
V	11±6	9±5	9±6	3±2	3±2	18±43	27±68	67±169	3±2
Cr	12±4	4±3	7±4	5±2	5±3	11±11	17±38	22±37	4±3
Mn	24±9	10±5	17±10	12±5	10±4	23±16	19±8	15±10	13±10
Fe	1730±550	380±200	890±550	514±193	423±150	919±584	522±215	329±254	515±400
Ni	9±5	5±3	7±5	3±1	2±1	10±21	6±3	5±6	4±3
Cu	90±27	16±8	38±23	20±8	17±6	40±23	24±15	12±12	13±10
Zn	80±34	36±27	56±37	75±47	56±37	100±93	80±46	74±8	51±40
Br	72±28	15±10	41±26	9±4	10±4				14±5
Pb	280±99	64±46	150±97	109±48	105±44	79±51	53±31	52±38	24±20
Cd						3±3	3±3	8±11	0.5±0.4
As	10±4	4±2	7±4						0.8±0.5
Mo						3±3	2±1	2±3	0.5±0.3

Table 7.3 *Comparison between the average elemental concentrations (ng m^{-3}) observed in this study and in Firenze (Lucarelli et al., 2000), Milano (Marcazzan et al., 2003) and Venezia (Rampazzo et al., 2008).*

The analyses carried out during the project about the partitioning of TC between organic and elemental carbon reveals that about 60-70% of total carbon is composed of organic carbon while the elemental carbon account for only the 40-30% (cold vs warm value). These values are in agreement with previous European studies (Putaud *et al.*, 2010) that investigated the main chemical composition of several sites in Europe, including Bologna, and showed that total carbon in this area is mostly composed of organic carbon (69%) and secondarily of elemental component (31%). The sea-salt contribution to PM_{10} was calculated assuming that Na^+ has only a marine origin and deriving the sea-salt fraction of K^+, Mg^{++}, Ca^{++}, Cl^- and SO_4^{2-} from the typical seawater ratios respect to Na^+ (Riley and Chester, 1971): the average value was found equal to 1%.

The contribution of the crustal matter to PM_{10} was estimated on the basis of the semi-empirical equation (Chan *et al.*, 1997; Salma *et al.*, 2001):

$$c(\text{crustal matter}) = 1.16*\left(c(\text{Al}) + 2.15c(\text{Si}) + 1.41c(\text{Ca}) + 1.67c(\text{Ti}) + 2.09c(\text{Fe})\right)$$

where $c(i)$ is the concentration of element i; crustal matter contributes 13% on average, with a clear increase from the average value of 10% during the cold period to the 17% found during the warm period. This increase can be attributed to the above mentioned increase of the coarse fraction due to dryer summer conditions but also to the incursion of a Saharan Dust in June 2006, which will be described with further details in Section 7.3.6.

CO_3^{2-} were indirectly determined from the contents of Ca and Mg on the basis of the empirical relationship suggested by Querol *et al.* (1998), which assumes that the carbonate form is the dominant species for both elements; though experimentally unverified this hypothesis largely accommodates most situations including the local one where the pedological framework (alluvional plain) plus the building influence are reasonable sources of this component.

The contribution of carbonates to PM_{10} was equal to 4-5% (cold and warm value, respectively).

This first rough estimate of the PM_{10} contributions of some "a priori" known sources give us firstly an idea of the relevant contribution of SIA to particulate matter and of the high percentage due to crustal matter resuspension, increasing from winter to summer. The minor contribution of sea salt, which was expected due to the distance of Bologna from the sea, is confirmed by this first estimate.

The elemental composition largely follows the same seasonal behavior as PM_{10}, with higher values during the warm season, while S, K, Ca and Fe do not present significant seasonal differences. Crustal tracers (Si, Al, Ti) and V exhibit higher concentrations during summer, usually attributed to an increase in soil resuspension and Saharan Dust contribution. This latter contribution is further investigated. During the cold season nitrates contribute more than sulfates to $PM_{2.5}$, in good agreement with European data recorded in the last decade (Van Dingenen *et al*., 2004; Putaud *et al*., 2004; 2010). In fact, during the warm season the lower contribution of nitrates is partly due to incomplete collection of NH_4NO_3 due to its remarkable thermal instability (Schaap *et al.*, 2002; Schaap *et al*., 2004a, b; Vecchi *et al.*, 2009), while the increase of the photochemical oxidation of SO_2 leads to a relative raise of sulfates (Hewitt, 2001; Rodríguez *et al*., 2004; Vecchi *et al*., 2004).

The equivalence ratio between the experimental concentrations of $nssSO_4^{2-}$ (determined as the difference between experimental SO_4^{2-} and sea salt sulfates, estimated by the typical seawater to Na^+), NO_3^- and NH_4^+ is calculated for the campaigns of autumn 2005, winter and summer 2006 in order to assess the degree of neutralization in the analyzed aerosol samples (see Figure 7.2(a-c)). On the basis of the principle of electroneutrality, during the cold season the sum of sulfates and nitrates equivalents is not balanced by sufficient ammonium equivalents, which therefore calls for extra positive cations;

this balancing fraction is attributed to H^+ (whose measure is not straightforward) which therefore implies an acid character of aerosol (Pathak *et al.*, 2004; Squizzato *et al.*, 2013). In the warm season cation deficit is substantially balanced by calcium as often observed in the warm season when soil resuspension increases adding carbonates to atmospheric bases available for acid neutralization (Alastuey *et al.*, 2004).

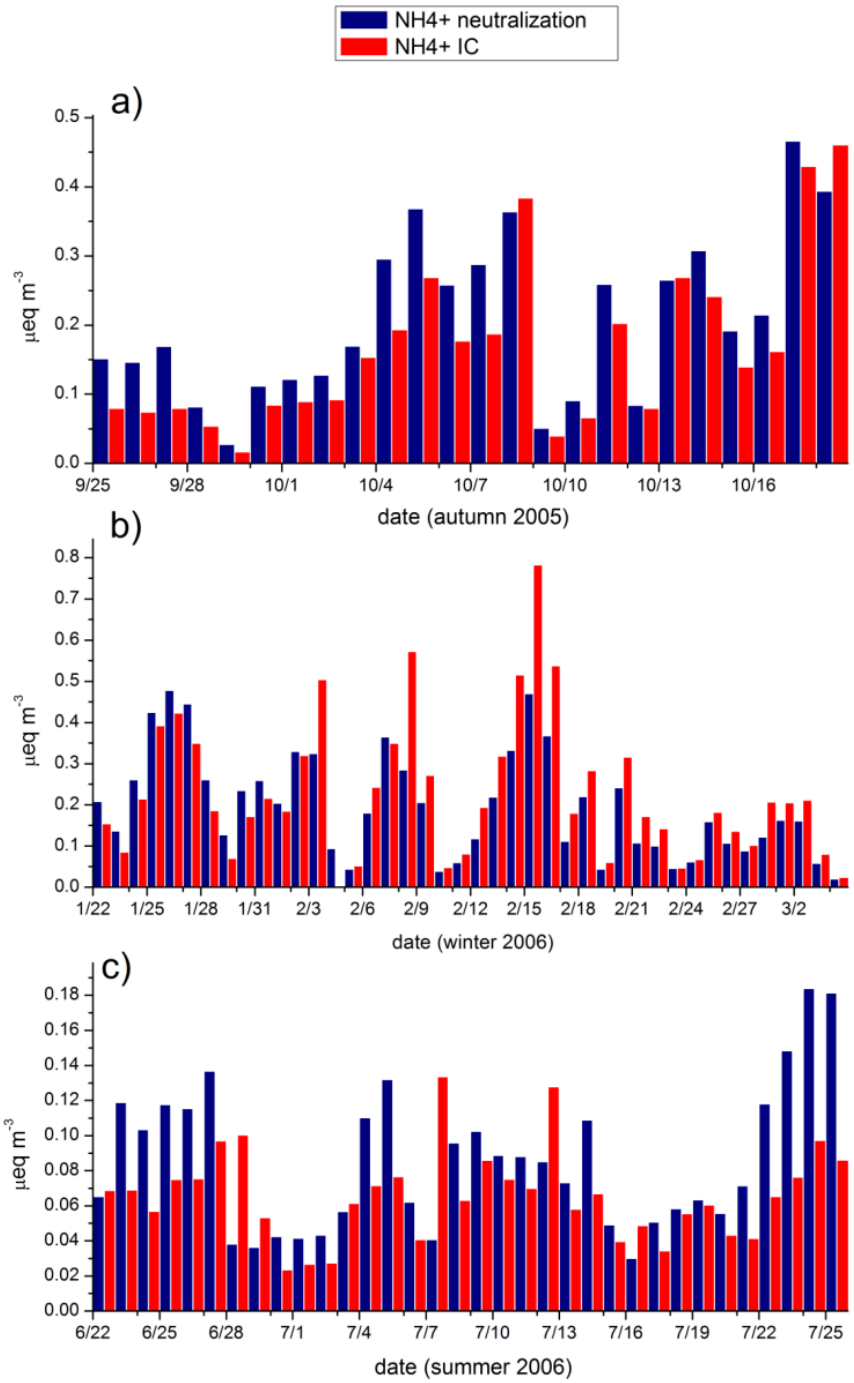

Figure 7.2(a,b,c) *Time series of the IC determined NH_4^+ moles and necessary NH_4^+ moles to complete neutralization of sulfuric and nitric acid during the periods: a) autumn 2005; b) winter 2006; c) summer 2006.*

7.3.3 Enrichment Factors

In order to acquire some preliminary information about the crustal and non-crustal sources of trace elements in particulate matter, crustal enrichment factors (EFs) were calculated during the cold and warm seasons. The enrichment factor is defined as (Lantzy and McKenzie, 1979; Voutsa *et al.*, 2002)

$EF = (C_{element}/C_{reference})_{air}/(C_{element}/C_{reference})_{crust}$

where $C_{element}$ is the concentration of any element, $C_{reference}$ is the concentration of reference element. Generally, Al, Fe or Si are chosen as reference elements. In this work the average ratio of each trace element to Al in the crust (Bowen, 1979) was used; in fact, in an urban framework real soil composition may represent an arbitrary choice due to the dominant influence of traffic related sources (vehicles and pavement) and buildings (Marcazzan *et al.*, 2003). By convention, an $EF \leq 10$ indicates a non-enriched element suggesting a crustal origin. EFs >> 10^4 indicate that the element is enriched respect to the Earth's crust; according to the local conditions this enrichment may be attributed to the influence of anthropogenic sources locally active in the area.

Figure 7.3 reports the EF average values for the two analyzed periods. Lowest EF's were found for Mg, Al, Ti, Mn, K and Fe, suggesting that these elements have a terrigenous origin. Na, Cr, Cu, Zn, but especially Cl and S are found to be enriched, particularly during the winter season. Anthropogenic sources may be relevant to these elements. The EF calculated for the data of autumn 2005 using Al as reference crustal element are presented in Figure 7.4: all the elements apart from Mn and Fe are found to be enriched, and Cu, Zn, Pb, Cd, As, Mo and Hg present very elevated EF value.

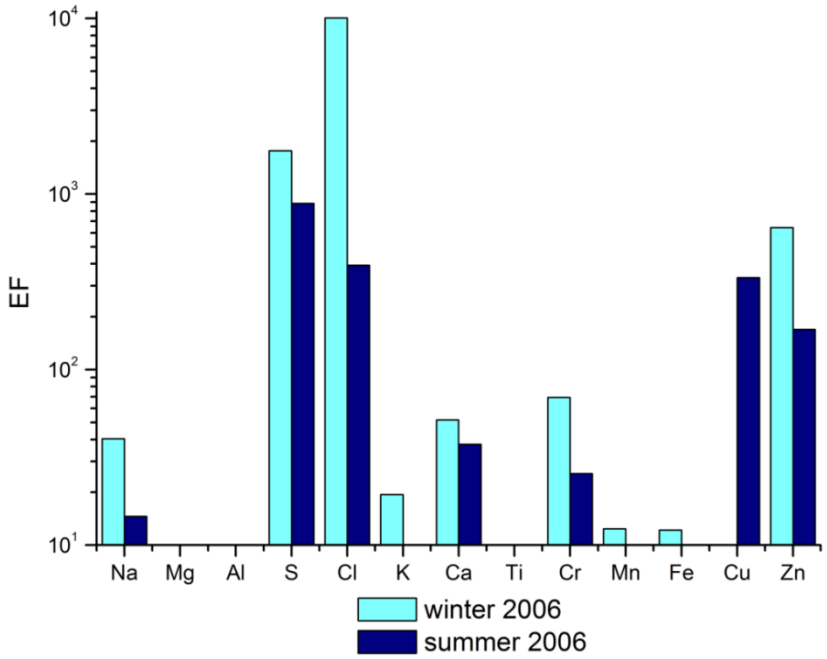

Figure 7.3 *Average values of enrichment factors of the analyzed elements during winter and summer 2006, calculated considering Si as reference crustal element.*

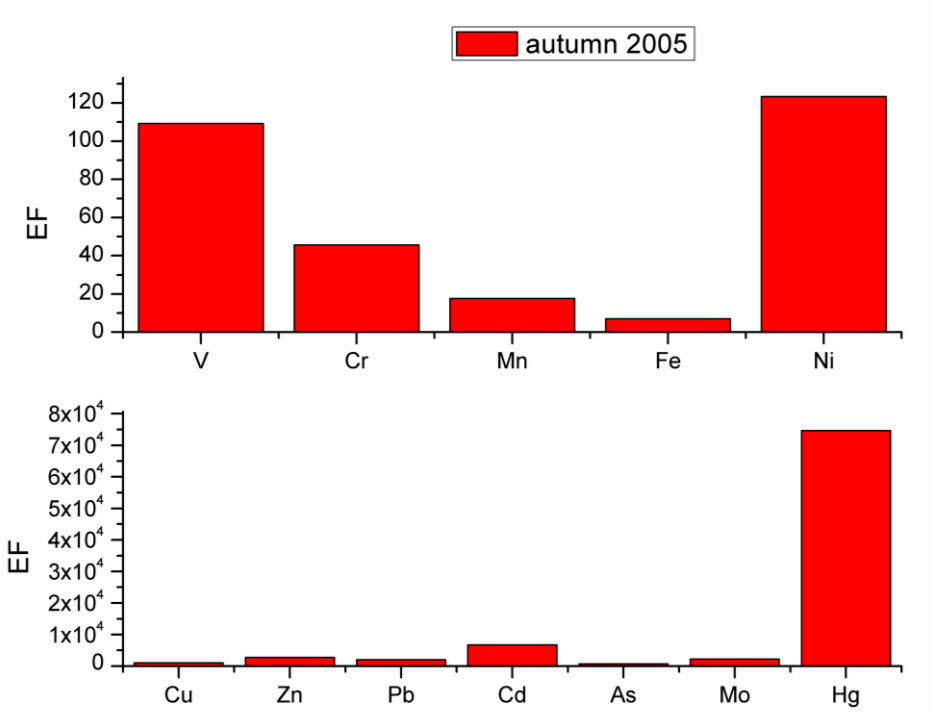

Figure 7.4 *Average values of enrichment factors of the analyzed elements during autumn 2005, calculated considering Al as reference crustal element.*

7.3.4 PCA/MLRA

PCA/MLRA receptor modeling was applied to the data of the period winter-summer 2006 (January-March and June-July 2006). As already highlighted in previous studies in the Po Valley (Matta *et al*., 2002; 2003) the major part of total aerosol mass is distributed in the fine size range. Moreover, as noted not only in the above-mentioned studies but also during a previous study carried out in Bologna on the size-segregated samples collected by means of a multi-stage high-volume cascade impactor (Andersen, Lab Automate Technologies) in this area (ARPA-EMR, 2005), inorganic ions represent a substantial part of the total mass, and are typically present in the fine fraction (< 1.5 μm). During this study it was observed that in this area nitrate dominates the fractions below 1.5 μm; nitrate is known to be a complex ion species owing to both remarkable volatility and chemical weakness when associated with ammonium and to post formation reactivity leading to displacement reactions with other aerosol species and to a size distribution shift towards coarser fractions. Crustal elements on the contrary dominate the coarse fraction, because of their mechanical origin: the coarse fraction is known to count very little in terms of number of f particles, but a lot as for the weigh (Mitra *et al*., 2002; D'Alessio *et al*., 2005). Taking into account these considerations, in this study the ions data analyzed in the $PM_{2.5}$ fraction and the elemental data measured in PM_{10} were merged together.

Before applying multivariate statistical analysis, the overall dataset was subjected to a strict selection in order to optimize modeling conditions: variables with > 10% values below the detection limit were discarded while if only a limited number of data was found lower than the LOD they were substituted by LOD/2.

Before choosing the data for the analysis, a comparison between the PIXE analyzed elements in PM_{10} and the corresponding ion analyzed in $PM_{2.5}$ was also carried on. Na, Mg and Ca were always more abundant in PM_{10} than in $PM_{2.5}$, which is reasonably linked to their mechanical (mostly crustal for Mg and Ca, marine for Na) origin. In order to prevent double counting in the working matrix PIXE data were kept for Na, Cl and Ca; for Mg, the ion data were retained, as slightly more abundant, whereas the Cl^- data were discarded as the Cl data are far more abundant (see Table 7.2 for reference about the number of data available for each variable).

A good correlation was found between SO_4^{2-} determined in IC and the calculated SO_4^{2-} concentrations in PM_{10} ($r^2 = 0.75$) which means that S analyzed in PM_{10} has a prevailing secondary origin mostly lined to the presence of ammonium sulfate. K was often higher in PM_{10} than K^+ in $PM_{2.5}$, but for 19 samples the opposite was observed. For these samples a contemporary increase of K^+ and OC and a general good correlation of K^+ with OC were observed ($r^2 = 0.78$ winter value, $r^2 = 0.40$ summer value): the overall conclusion of these observations was a probable link of K^+ to combustion sources, and in particular to biomass burning. From these considerations it was assumed that all the PM_{10} sulfur was in the sulfate form, and the IC sulfates data were kept instead of S; for K, the difference between the PIXE and IC values was calculated (K_{ins}) and K^+ and K_{ins} were treated as independent variable. A final matrix consisting of 20 variables and 76 observations was analyzed.

Results of the Varimax rotated PCA on the standardized data (mean = 0, standard deviation = 1) revealed four factors (Table 7.4 and Figure 7.5 a-d), accounting for 80% of the total variance. Communality, which represents the amount of variance of each variable explained by the model, showed high values for all the variables, except for K^+ and Mg^{++} (0.5 and 0.4, respectively), probably because of their low concentrations.

	Factor 1	Factor 2	Factor 3	Factor 4
NO_3^-	**0.92**	0.00	0.22	0.10
SO_4^{2-}	0.09	0.29	**0.81**	-0.02
NH_4^+	**0.80**	0.00	*0.40*	0.07
K^+	0.18	-0.02	**0.80**	0.06
Mg^{++}	-0.47	0.16	0.18	**0.62**
OC	*0.54*	0.29	*0.55*	-0.15
EC	**0.80**	0.01	0.13	-0.07
Na	*0.49*	-0.16	-0.25	**0.69**
Al	-0.12	**0.95**	0.12	-0.08
Si	0.01	**0.98**	0.08	-0.05
Cl	**0.67**	-0.18	0.11	*0.55*
Ca	0.38	**0.82**	-0.04	0.09
Ti	0.06	**0.98**	0.08	-0.04
Cr	**0.85**	0.37	0.09	0.01
Mn	**0.63**	**0.61**	0.10	0.12
Fe	*0.43*	**0.87**	0.04	0.02
Ni	**0.87**	0.20	0.06	0.10
Cu	**0.72**	-0.03	-0.12	-0.09
Zn	**0.90**	0.19	0.15	0.13
K ins	-0.12	**0.80**	0.22	-0.02
Eigenvalue	8.3	4.8	1.7	1.2
Variance (%)	41.7	24.1	8.4	5.8
Cumulative percent	41.7	65.8	74.2	80.0
Source	Traffic and ammonium nitrate	Crustal	Mixed combustion	"Pseudo-marine"

Table 7.4 *Results of the VARIMAX rotated PCA on the standardized data. Loadings >0.6 are marked in bold, while loadings between 0.4 and 0.6 are in italics*

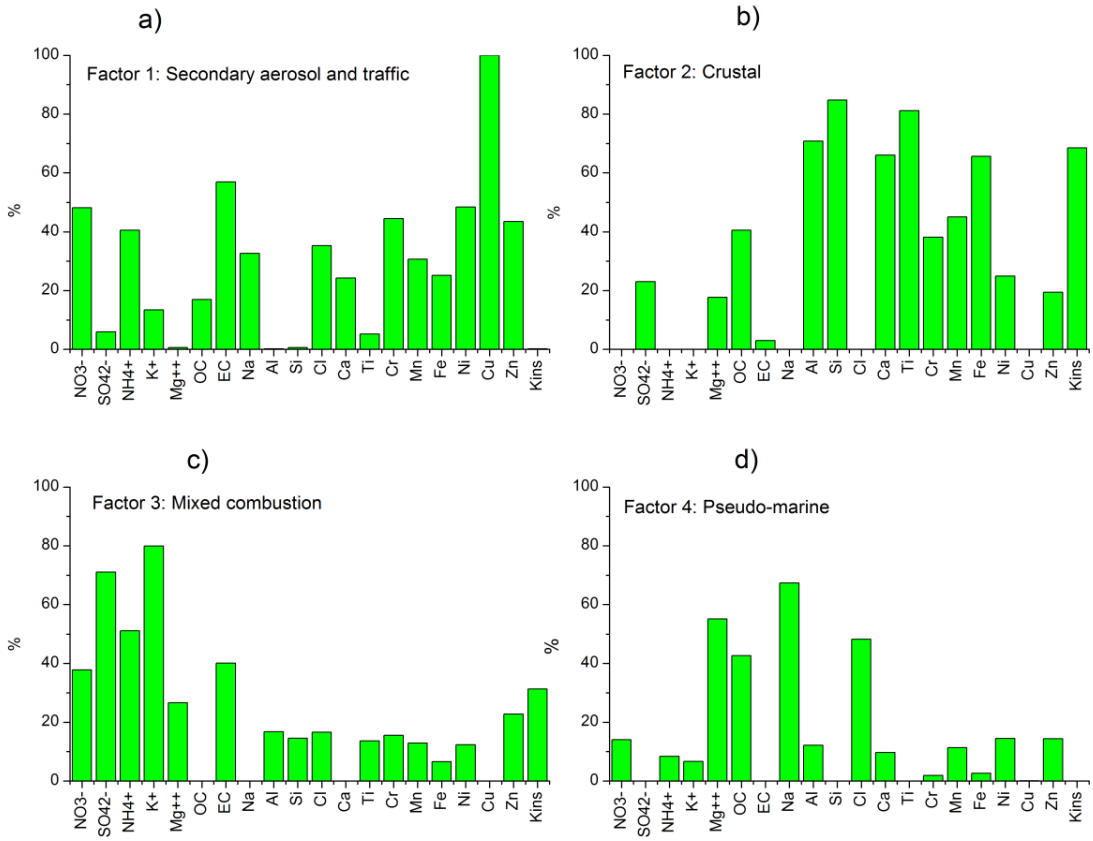

Figure 7.5(a,b,c,d) *Source profiles illustrated as percentage of the species (%) in the four identified sources by the PCA model.*

The first factor (42% of the total variance) is clearly related to an anthropogenic source, being composed of Cr, Zn, Ni, Cu, nitrate, ammonium, EC, Cl, and secondarily OC and Fe. Chromium, copper, nickel and zinc have been extensively linked to various industrial processes and mostly to traffic (abrasion and corrosion of brakes, tyres) (Wahlin *et al.*, 2006; Alastuey *et al.*, 2007; Lin *et al.*, 2008; Thorpe and Harrison, 2008; Gietl *et al.*, 2010; Koçak *et al.*, 2011), whereas NO_3^- and NH_4^+ are the main component of secondary ammonium nitrate formed through homogeneous and heterogeneous reactions from gaseous NOx and NH_3 (Schaap *et al.*, 2004a; Pathak *et al.*, 2009). This factor seems mainly associated with traffic, a relevant contribution in Bologna emissive profile, which seems to be confirmed by the results of the cluster (Figure 7.6) and factor analyses applied to the dataset of the autumn campaign in 2005 (not homogeneous with the subsequent sampling periods, as the analyses were all carried out on the $PM_{2.5}$ fraction) showing that the four variables Cr, Zn, NO_3^-, NH_4^+ are closely linked also to V, a tracer of diesel engines, widely used for both light and heavy vehicles in Italy. Since the industrial emissions in Bologna are not significantly high due to the lack of major industries (neither chemical industries nor energy production facilities are present in the territory), while the main industries are linked to manufacture activities, and since the city centre is affected by heavy traffic roads (one of which close to the

sampling site), the vehicular emissions appear as the most probable source for this association of elements. Thus, this source can be interpreted as a combination of secondary aerosol (mainly composed of nitrates coupled to ammonium) and traffic.

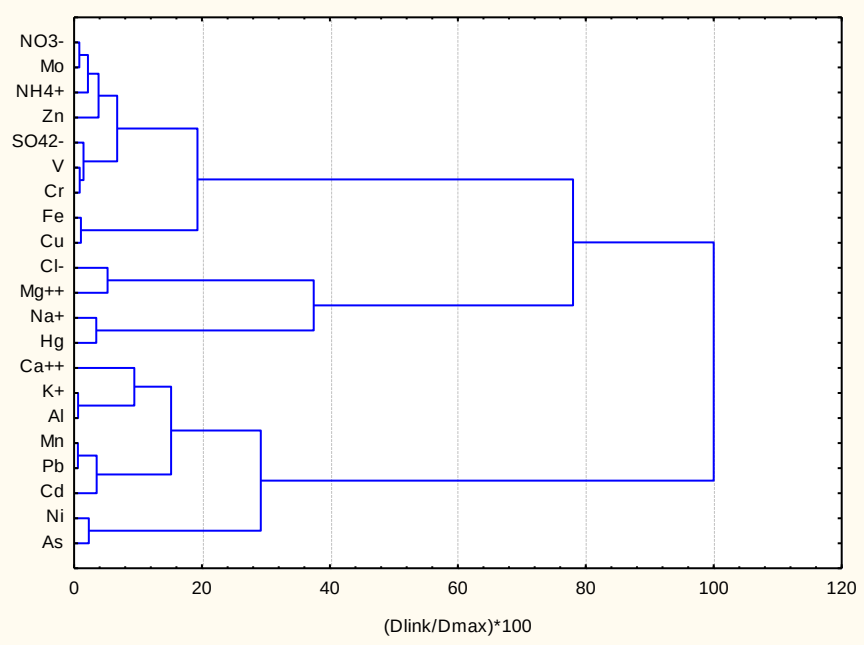

Figure 7.6 *Cluster analysis for the variables observed during the autumn 2005 campaign, calculated with Ward's agglomerative hierarchical method and squared Euclidean distances. Similarity values are normalized to* (D_{link}/D_{max} * 100)

The second factor explains about 24% of the total variance and mainly links typical crustal elements K_{ins}, Al, Si, Ca, Ti, Fe, Mn (loadings >0.6). This source was then interpreted as crustal material originated from soil resuspension (Qin *et al.*, 2006; Mazzei *et al.*, 2006; Vecchi *et al.*, 2008). The influence of road dust cannot be excluded due to the pavement wear and to the abrasion occurring on mechanical parts, such as brake lining and drums (Fe, Mn) (Garg *et al.*, 2000; Iijima *et al.*, 2008; Thorpe and Harrison, 2008; Bukowiecki *et al.*, 2009; Gietl *et al.*, 2010). A usual association of Fe with Cu is observed looking at the clusters of the single campaigns (an example of this observation can be found in Figure 7.6, referring to the period autumn 2005) and this can indicate a possible source from mechanical abrasion of vehicles (brakes). Fe also showed a significantly high linear correlation with Cu, Mn, Cr, Pb and Zn ($0.6 < R < 0.9$), all elements typically attributed to the abrasive/coarse contribution of vehicles, partly dropped from the matrix used in modeling for the reason explained, but reported as averages in Table 7.2.

The third factor (8% variance) includes K^+, SO_4^{2-}, and to a lesser extent NH_4^+, OC. While K^+ is largely linked to combustion processes, including biomass burning (Morawska and Zhang, 2002;

Mahowald *et al.*, 2005; Thurston *et al.*, 2011; Masiol *et al.*, 2012a), NH_4^+ and SO_4^{2-} are attributed to gas-to particle reactions leading to the secondary ammonium sulfate formation. According to Ramadan *et al.* (2000) and/or Begum *et al.* (2004) for example, biomass burning sources are successfully identified by K and carbonaceous parameters, an evidence recently enforced and stressed by Pachon *et al.* (2013) who confirm the relevant role of potassium as an efficient tracer of biomass burning as compared to levoglucosan, an alternative tracer widely used to this scope. It is worth noting that in the present study ionic potassium in $PM_{2.5}$ was chosen for receptor modeling, representing the soluble/fine fraction of this element as compared to total potassium by PIXE in PM_{10} available in the present data set to which the former largely contributes, as previously discussed, when high correlation between K^+ and OC was described corroborating the tight association with biomass burning.

The last source is made up of Na, Cl and Mg^{++} and accounts for 6% of the total variance, representing the marine aerosol. Although Bologna is far distant from the coast (> 100 km) and the influence of sea salt is very limited, as already highlighted by the "a-priori" PM mass balance, this factor shows evidence of the occurrence of episodic transports of sea salt aerosol mainly in the coarse fraction. Due to its distance from the Adriatic coast and to the weak circulation in this region, Bologna can rarely be reached by marine air masses, an occurrence usually more frequent in the winter, but in any case fairly unusual (Bora episodes); therefore this sea salt component is mostly attributed to the use of road de-icing practice following snowfall as often reported (e.g., Furusjö *et al.*, 2007; Belis *et al.*, 2013) and will be named from now on as "pseudo-marine".

The daily source contributions to the PM levels were then obtained by the regression of the Absolute Factorial Scores (AFS) on PM_{10} concentrations following the methodology described in Thurston and Spengler (1985). Results of ANOVA show a statistically significant relationship (at a 99% confidence level) for all the sources on PM masses. The adjusted coefficients of multiple determination indicate that the model explains 92% of the PM_{10} variability.

Figure 7.9(a) shows the percentage mass contribution of the four sources identified by PCA/MLRA to PM_{10}. On average, the "mixed combustion" source mainly contributes to PM_{10} mass, accounting for 36%, followed by traffic and ammonium nitrate source, crustal and "pseudo-marine" particles, accounting for 32%, 21% and 10%, respectively.

The time series of PM_{10} source contributions can be found in Figure 7.7. The "pseudo-marine" contribution presents higher levels during the cold periods. The crustal source presents higher contribution during the summer, as already found by the empirical calculations for the PM mass balance; this is probably due to dryer conditions favouring the resuspension of crustal material. In addition, an influence of Saharan dust outbreaks cannot be excluded. A further elaboration

including the back trajectories analysis is subsequently presented to extract helpful information on the influence of long-range transports.

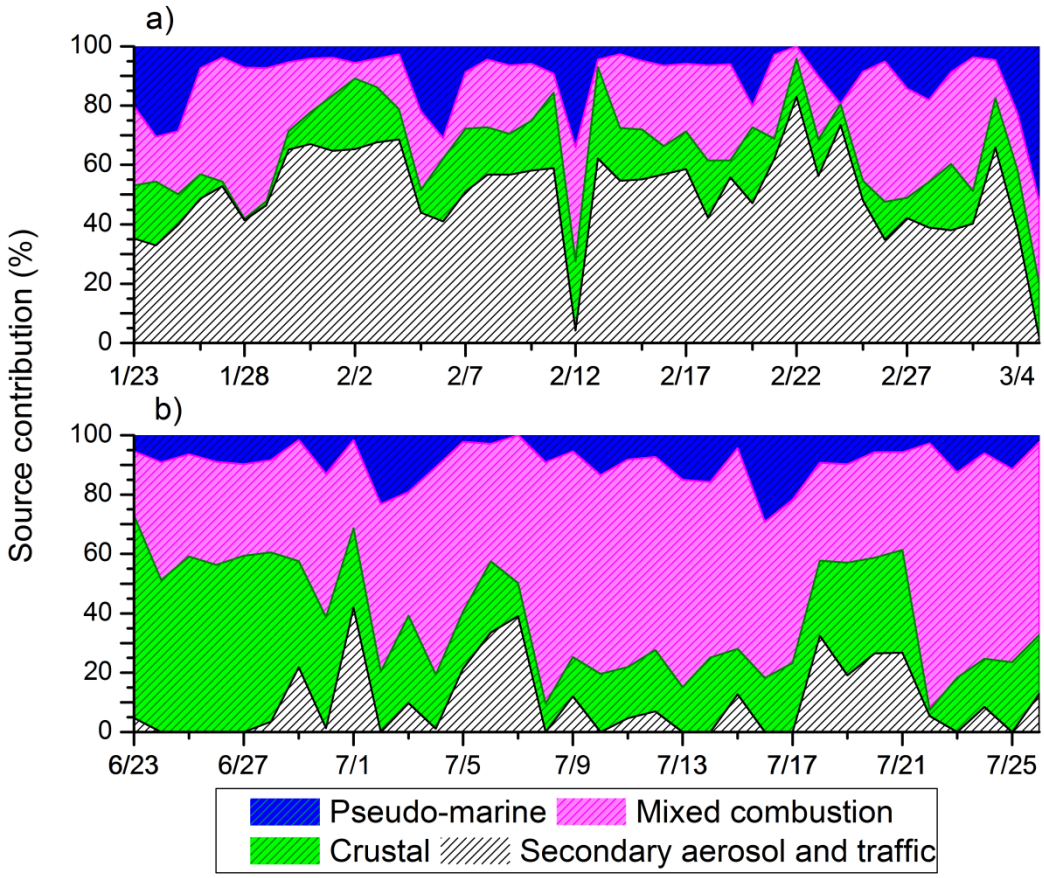

Figure 7.7(a,b) *Time series of the PM_{10} source contribution resulting from the PCA/MLRA model: a) winter 2006 campaign; b) summer 2006 campaign.*

The traffic source contributes mainly during the cold season due to marked low level atmospheric stability, while its dispersal is promoted during the warm season by marked instability and convection leading to a deeper mixed layer (Ponce *et al.*, 2005; Marenco *et al.*, 2006). The mixed combustion source is more intense during the warm period ruling out the potential role of the incinerator and of agricultural biomass burning at the end of the harvest and before the cold season rather than domestic heating typical of winter. The increase in sulfates during summer can be explained by enhanced photochemistry during the warm season: the oxidation kinetics of SO_2 (primary precursor emitted from the "mixed combustion" source) to sulfates are promoted during the warm season and have already been associated to higher levels during summer (Hewitt, 2001; Rodríguez *et al.*, 2004; Vecchi *et al.*, 2004).

7.3.5 PMF

PMF analysis was also performed on the same dataset, using the EPA PMF 3.0 software package. The final matrix used for PMF modeling consists of 20 parameters (21 with PM_{10}) x 76 observations in agreement with Pant and Harrison (2012) stating that a minimum of 50 points is suitable for the scope. The data consistency though not optimal for statistical purposes is widely coherent with published papers such as, for example, Qin and Oduyemi (2003), Furusjo *et al.* (2007), Callén *et al.* (2009). The chosen parameters are retained in order to fulfill the conditions of minimizing model uncertainty, with negligible or absent missing data.

Uncertainty was calculated as the analytical uncertainty plus one third of the LOD, in agreement with the widely used method by Reff *et al*. (2007). Missing (but higher than LOD) values were replaced by their median and the associated uncertainty was calculated as four times the species median, whereas data lower than LOD were replaced by LOD/2, while the associated uncertainty was taken as 0.83 LOD (Polissar *et al*., 1998; Reff *et al.,* 2007).

Cu was treated as a weak variable due to a low signal-to-noise ratio (< 2), therefore its uncertainty was tripled. Sodium was also added to the list of weak variables because of the presence of a large number of data below LOD during the warm season. The overall uncertainty of the dataset was also increased of a further 9% to account for sampling uncertainties and the exclusion of some further species for which observations were missing (EPA, 2008). PM_{10} was set as the "total variable" and as such considered weak by default by the software.

PMF uses algorithms in order to find a solution that minimizes $Q(\mathbf{E})$ using various random starting points. For this study 100 starting points were chosen for the elaboration of the results.

As the theoretical optimum value of *Q(E)* (E residual matrix, *Q(E)* object function to be minimized) should be roughly equal to the number of degrees of freedom for the data matrix (Qin and Oduyemi, 2003; Furusjö *et al*., 2007; Yatkin and Bayram, 2007) (1520 in this case), and the two parameters IM (maximum scaled residuals mean of the modeled variables) and IS (maximum scaled residual standard deviation of the modeled variables) show a drastic decrease when the number of factors increases up to a critical value (Lee *et al.,* 1999), the most physically feasible number of factors describing the system is 6.

The diagnostic parameters on the performance obtained by the PMF model such as intercept constant, slope of the regression line, standard error and r^2 with a factorization value of 6 were analyzed and are presented as Table 7.5.

Variable	Intercept	Slope	SE	r^2
PM_{10}	0.56	0.98	4.8	0.97
NO_3^-	0.12	0.95	2.0	0.95
SO_4^{2-}	0.30	0.89	0.7	0.88
NH_4^+	0.06	0.90	0.7	0.87
K^+	0.18	0.24	0.1	0.23
Mg^{++}	0.02	0.09	0.01	0.03
OC	0.42	0.84	0.8	0.78
EC	0.25	0.82	0.4	0.87
Na	0.01	0.75	0.05	0.84
Al	0.00	1.00	0.02	0.98
Si	-0.01	1.03	0.08	0.98
Cl	0.06	0.83	0.2	0.89
Ca	0.05	0.95	0.1	0.96
Ti	0.00	0.90	0.00	0.97
Cr	0.00	0.91	0.00	0.87
Mn	0.00	0.79	0.01	0.69
Fe	0.00	1.01	0.08	0.96
Ni	0.00	0.79	0.00	0.75
Cu	0.02	0.30	0.02	0.28
Zn	0.01	0.79	0.01	0.91
K_{ins}	0.02	0.86	0.05	0.70

Table 7.5 *Diagnostic parameters on the performance obtained by PMF model: a) intercept constant, identifying the fraction of the variable not explained by the model; b) slope of the regression line, c) standard error SE, estimate of the variability between experimental and retrieved from the model concentrations; d) r^2, correlation between experimental and retrieved from the model concentrations.*

The predicted PM_{10} mass concentrations well reproduce the measured ones ($r^2 = 0.97$) and the scaled residuals are normally distributed.

The source profiles are reported in Figure 7.8(a,b,c,d,e,f), whereas the contribution of the six identified sources on PM_{10} can be found in Figure 7.9(b). The first source (8% of PM_{10}) exhibits elevated contributions of Na and Cl clearly linked to the marine aerosol, but also to road salt in winter. The second source (35% of PM_{10}) is interpreted as "secondary aerosol and traffic emissions", with high contributions from NO_3^-, NH_4^+, Ni, Zn, K^+, Cr, Cu, OC and EC. As already pointed out discussing the results obtained by the PCA model, Ni, Cr, Cu, Zn can be linked to brakes and tyre emissions (Garg *et al.*, 2000; Wahlin *et al.*, 2006; Ijima *et al.*, 2008; Thorpe and Harrison, 2008; Bukowiecki *et al.*, 2009; Gietl *et al.*, 2010), whereas NO_3^- and NH_4^+ are the main component of secondary ammonium nitrate, formed through homogeneous reactions from gaseous NOx and NH_3. Road traffic is a major source of NOx, especially in a town like Bologna characterized by medium industries (mostly mechanical), agriculture and traffic; the increasing use of three-way catalysts on cars has presumably led to increasing emissions of NH_3 from vehicle exhausts (Sutton *et al.*, 2000; Gilbert *et al.*, 2003; Frati *et al.*, 2006), caused by the reducing

conditions inside the converter, though large scale agriculture is its main source. In the following this source will be referred to as “traffic”.

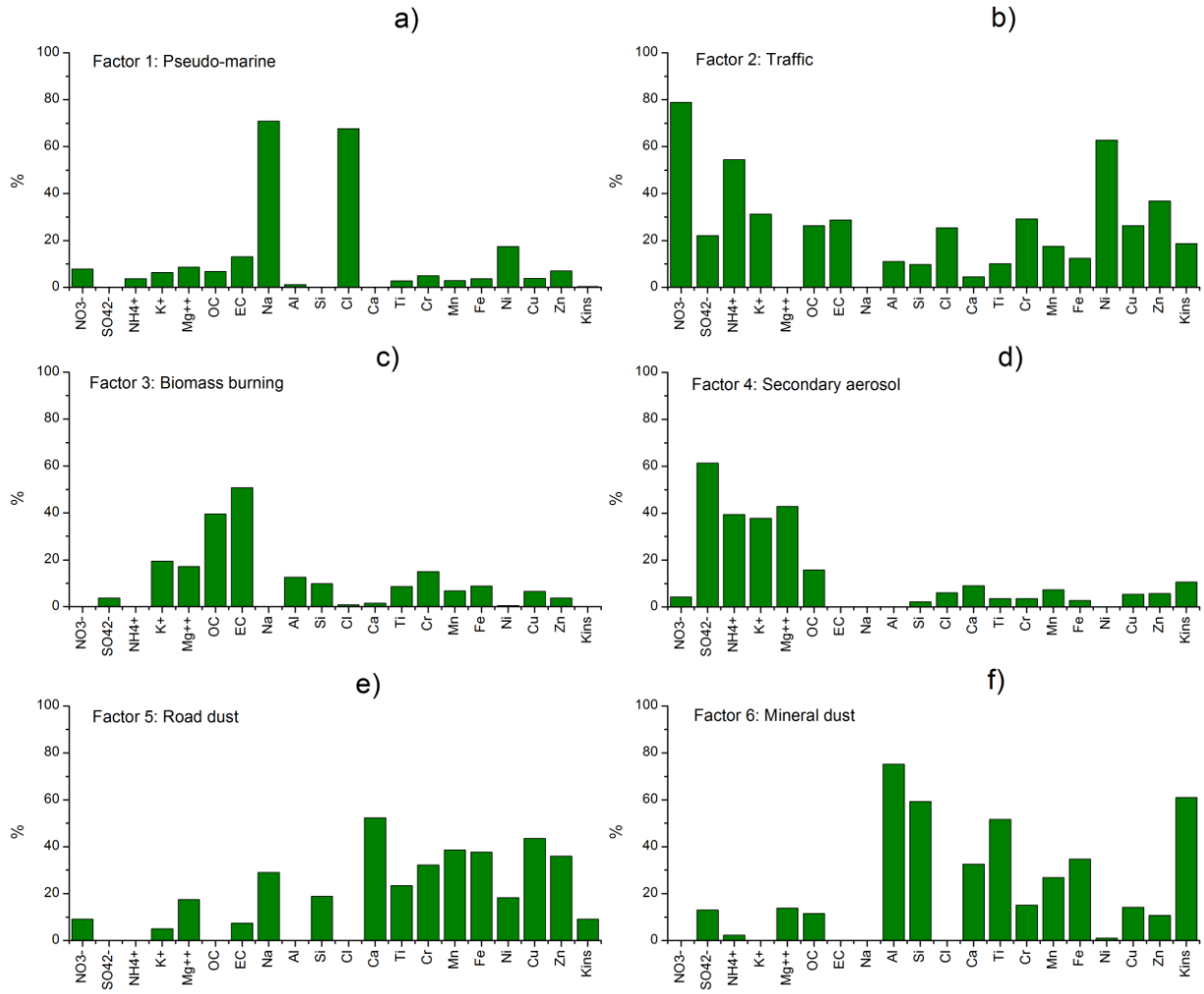

Figure 7.8(a,b,c,d,e,f) *Source profiles illustrated as percentage of the species (%) in the six identified sources by the PMF model.*

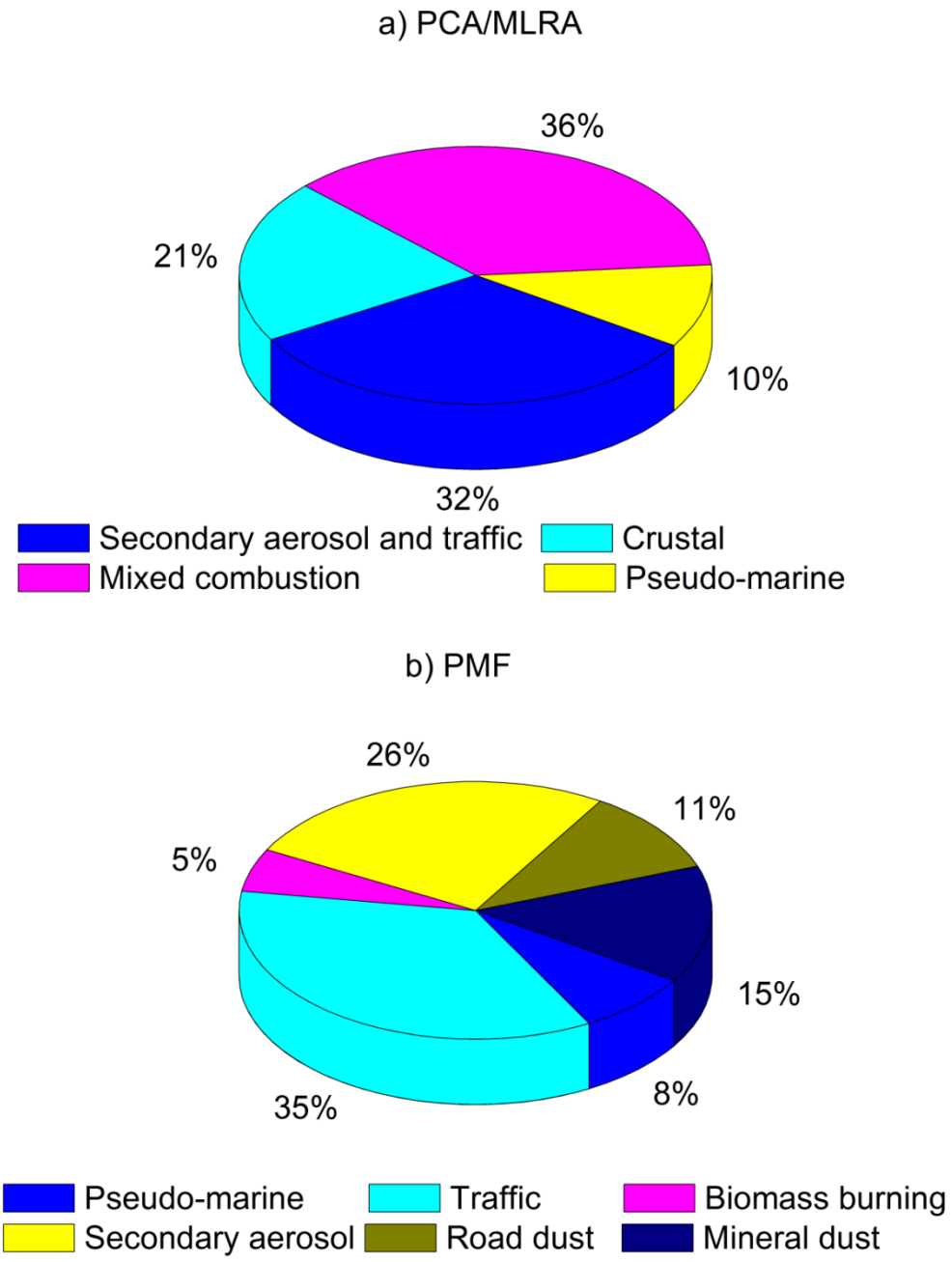

Figure 7.9(a,b) *Contribution of the sources to PM_{10} as resulting from the application of the a) PCA/MLRA model; b) PMF model.*

The third source (5% of PM_{10}) exhibits contributions from OC, EC, and K^+, Mg^{++} to a lesser extent, and represents the biomass burning source (Morawska and Zhang, 2002; Dan *et al.*, 2004; Mahowald *et al.*, 2005; Thurston *et al.*, 2011; Masiol *et al.*, 2012a; Pachon *et al.*, 2013). High linear correlation among K^+, sulfates and Cl^- ($R > 0.9$) all measured in $PM_{2.5}$ and a slower but still significant linear correlation with Zn, a multisource species, suggests a likely influence of the municipal waste incinerator, whose relative importance requires further investigations.

The fourth source (26% of PM_{10}) is linked to SO_4^{2-}, Mg^{++}, NH_4^{+}, K^{+} and represents the secondary aerosol (ammonium sulfate), mainly linked to the use of fuel oil from heavy duty vehicles, as suggested by the high good linear correlation coefficient between S/sulfates and the typical tracers of this source (V, Ni; sulfates–V R = 0.73 autumn 2005; sulfates–Ni R = 0.64 during autumn 2005 and winter 2006), whose data were not sufficient for the source apportionment but can be used for the purpose of gaining better insights as briefly outlined before going into the details of receptor modeling.

The fifth source (11% of PM_{10}) is made up of Ca, Cu, Mn, Fe, Zn, Ni, Na. This source is thus attributed to the road dust associated to the abrasion of the mechanical parts of the vehicles (brakes, pads, drums, tyres), as well as to the road dust asphalt, and is thus referred to as road dust.

The sixth source (15% of PM_{10}) presents elevated shares from typical crustal elements (Al, Si, Ti, K_{ins}, Ca, Fe, Mn) and is identified as the mineral dust source.

With respect to the PCA/MLRA, the PMF model is able to distinguish between the mineral and road dust, and to split the ammonium sulfate from the traffic source.

The reconstructed time series of the four identified sources are reported as Figure 7.10.

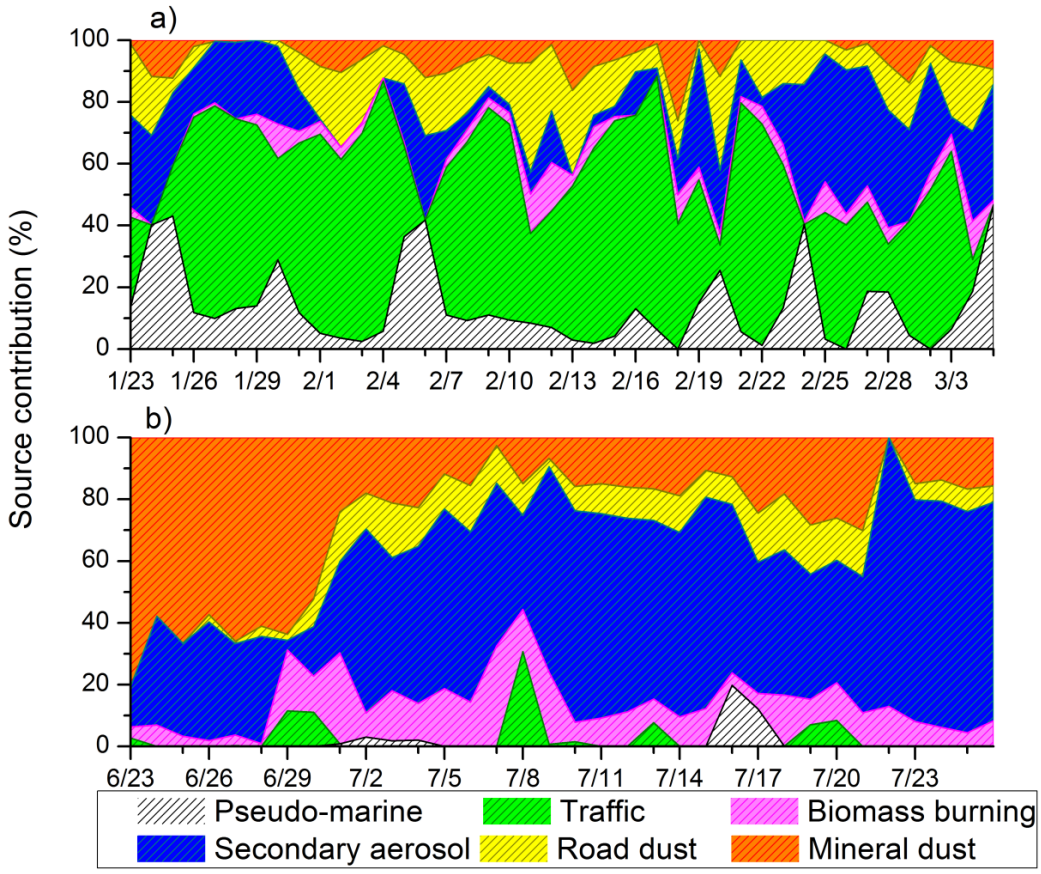

Figure 7.10(a,b) *Time series of the PM_{10} source contribution resulting from the PMF model: a) winter 2006 campaign; b) summer 2006 campaign.*

The "pseudo-marine" contribution presents higher levels during the cold periods. This is obviously also due to the winter use of sea salt as de-icing agents on the roads. The soil dust source yields a higher contribution in the warm season, in agreement with the empirical calculations for the PM mass balance and with the PCA/MLRA model as a result of enhanced resuspension under dry weather conditions. In addition, the influence of a Saharan dust transport during the summer period cannot be excluded. A further elaboration including the back trajectories analysis is subsequently presented to extract helpful information on the influence of long-range transports across the Apennine range even in northern Italy.

The traffic source contributes mainly during the cold season probably because of the influence of the ammonium nitrate, more stable at low winter temperatures: in addition the marked low level atmospheric stability promotes the higher concentrations of most PM components during the cold season, while its dispersal is promoted during the warm season owing to marked instability and convection leading to a deeper mixed layer (Ponce *et al*., 2005). The road dust source, however, also shows a slight decrease from the winter to the summer season, which possibly means that a general decrease of the traffic from the cold to the warm season cannot be completely excluded. The biomass burning source is more intense during the warm period; as a consequence it seems likely that this source is linked both to the agricultural biomass burning at the end of the harvest and possibly to the waste incinerator, rather than to domestic heating, which is instead typical of winter. The secondary aerosol (ammonium sulfate) source also shows an increase from the cold to the warm season. As pointed out before, the increase in sulfates during summer is due to enhanced photochemistry during the warm season as widely observed in the literature (Hewitt, 2001; Rodríguez *et al*., 2004; Vecchi *et al*., 2004).

7.3.6 Analysis of a case study occurred during the sampling campaigns

All the European plain zones, and in particular the Po Valley, are characterized by a typical trend of the PM concentrations, with a marked thermal gradient between summer and winter (Marcazzan *et al*., 2003; Matta *et al*., 2003). This result is mainly attributed to the variation of the thickness of the planetary boundary layer (PBL), i.e., the volume of air where the atmospheric pollutants are dispersed. The height of the PBL is directly proportional to the solar irradiance and because of the thermal expansion of the atmospheric gases and the trend of the turbulence is lower during the cold season and higher during the warm one. The overall result is a variation of the volume where the gases and PM can be dispersed. This results in the consequent rise of the winter concentrations of PM, mainly (but not only) due to the different dilution ratios. For this reason, generally, PM_{10} and $PM_{2.5}$ limit values set by the European legislation (1999/30/CE and 2008/50/CE) are frequently exceeded during the cold season in the whole Po Valley. The influence of additional sources during the cold

season, such as domestic heating, along with frequent thermal inversions can also drop the dispersion of locally emitted pollutants in the lower atmosphere. Moreover, some peculiar orographic characteristics of the Po Valley, which is surrounded by the Alps and Apennines mountain chains, can enhance the air mass stagnation with the consequent increase of the pollutants.

An interesting high PM value episode in June 2006 was investigated. This period was characterized by an anomalous series (7 subsequent days, of which 5 exceeding the European limit value) of PM_{10} concentrations in the range 46-56 µg m^{-3}. As previously recognized by for example Matassoni *et al.* (2009), Guarnieri *et al.* (2011) and Nava *et al.* (2012) this period was characterized by a Saharan dust outbreak, which strongly impacted overall Italy and in general the whole Mediterranean basin. The influence of this natural event in Bologna was quite remarkable owing both to its intensity and duration. As shown in Figure 7.11, during this period the contribution of mineral dust to PM_{10} was very high (81% on 23th June, and then ranging from 52 to 67% in the following 6 days till the end of June). Figure 7.11 reports the temporal trend of PM_{10} mass load during the period June-July 2006 in the city of Bologna and at a remote station (WMO-GAW) on Mt. Cimone (44°12' N, 10°42' E, 2165 m asl). As it lies above the PBL during most of the year (Winkler *et al.*, 1998), the Mt. Cimone background station is not influenced by common anthropogenic emissions due to cities and industrialized areas. For this reason, the measurements of atmospheric species carried out at this site can be considered representative for the South- European free troposphere (see previous Chapters 2, 3, 4, 5 and 6; Bonasoni *et al.*, 2000; Fischer *et al.*, 2000; Tositti *et al.*, 2013).

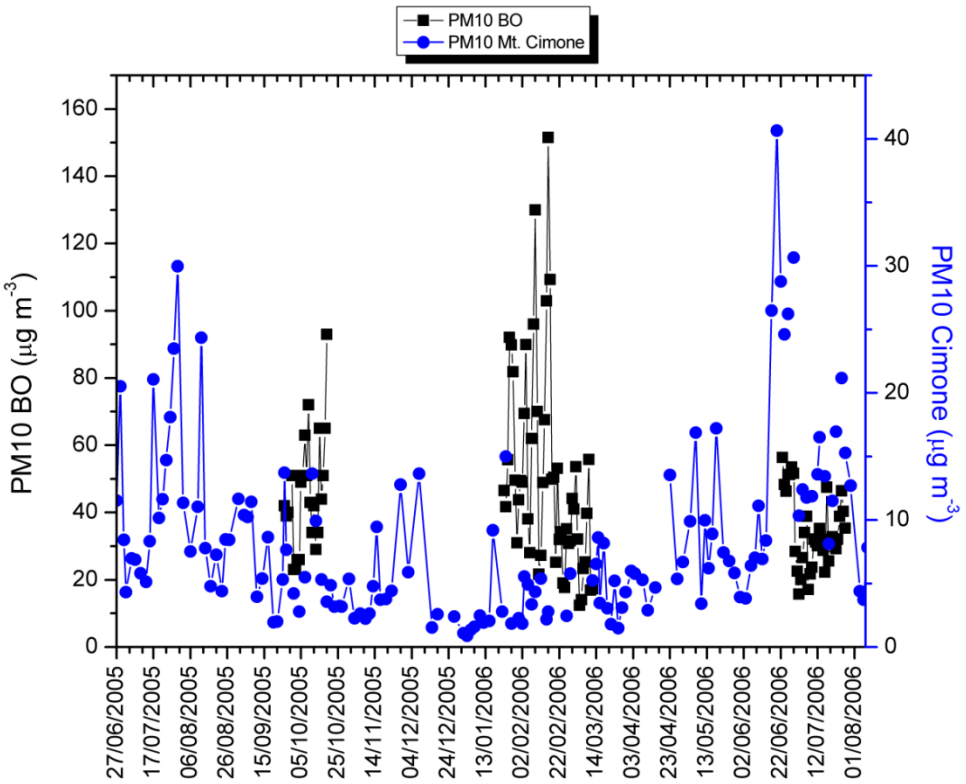

Figure 7.11 *PM_{10} mass loading (µg m^{-3}) during the year 2006 at the Mt. Cimone site and in the city of Bologna. An increase in the end of June 2006 is evident at both sites.*

In Figure 7.12(a-f) scatterplots of some elements during the joint period winter-summer 2006 are presented. The Saharan Dust event is identified by an oval in the Figure. The scatterplots highlight three clusters of elements: the first one, to whom the Al-Si, Ti-Si couples belong, groups together elements which, sharing the same crustal source, exhibit elevated correlation values and keep the same ratio even during the SD event; for the second (Ca-Si, Fe-Si) and third (Mn-Si and Zn-Si) group the ratio is different during the SD event, and specifically it is little decreased for the second group while it is largely decreased for the third one. The analysis of the EF value shows that the typical crustal elements (Al, Ti) were enriched during the SD event, while the elements that can derive also from anthropogenic sources (brake pads, drums), as for example Mn, Cu, Cr and Zn, result to be depleted.

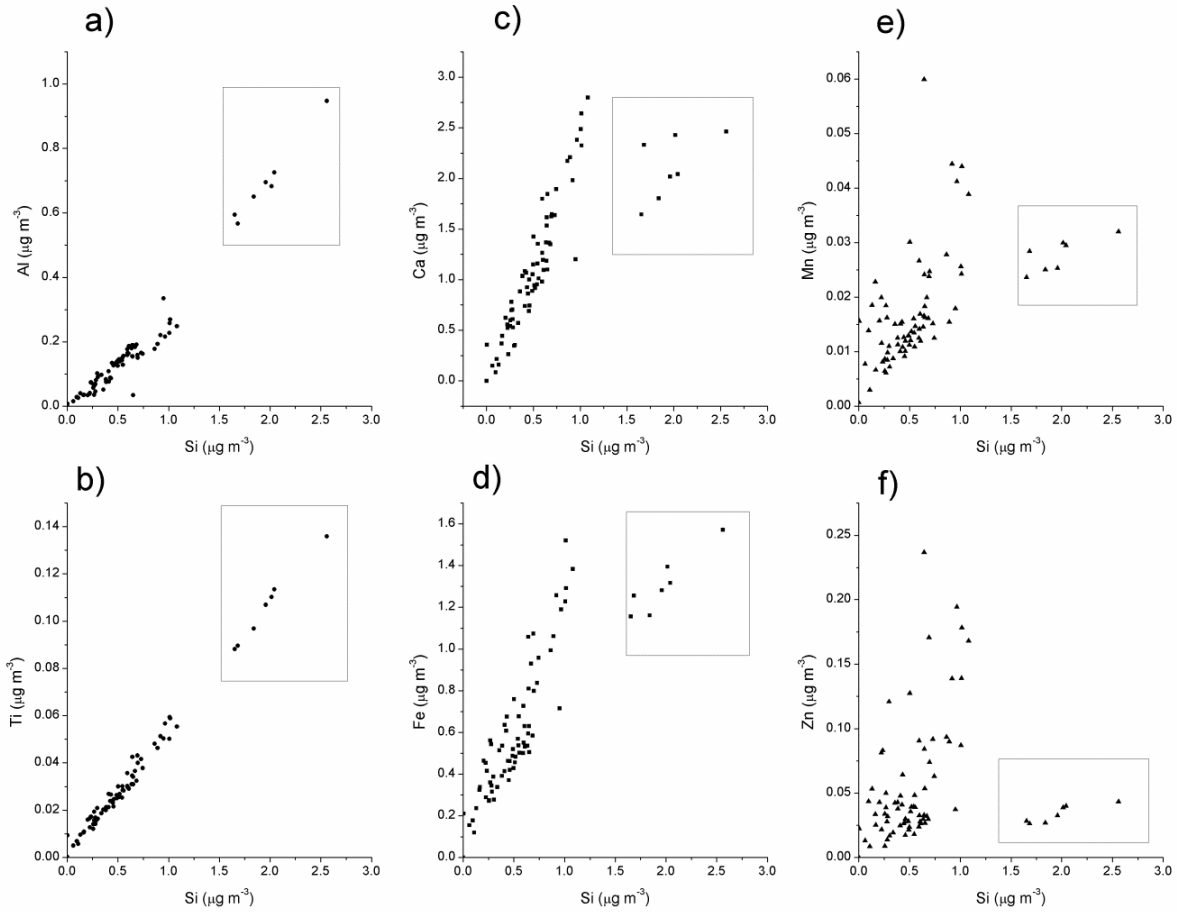

Figure 7.12(a,b,c,d,e,f) *Scatterplot of crustal elements during the period winter-summer 2006: a) Al vs. Si; b) Ti vs. Si; c) Ca vs. Si; d) Fe vs. Si; e) Mn vs. Si; f) Zn vs. Si. In the rectangle the days of the SD transport event happened at the end of June 2006 are identified.*

The air mass origin analyzed with the help of the HYSPLIT-4 model and the Dust Regional Atmospheric Model DREAM (*http://www.bsc.es/projects/earthscience/DREAM/*)(Figure 7.13 a-c), predicting the atmospheric life cycle of the eroded desert dust, show a transport of dust from the Sahara desert in that period. The synoptic situation, illustrated in Figure 7.13 (d,e), was characterized

by an extended African high pressure and not by an episode with baric minimum over the Tyrrhenian Sea, which is instead a situation more typical during the transition seasons. Escudero *et al.* (2005) showed that the transport of air masses towards the Western Mediterranean basin can be originated by four meteorological scenarios: 1) a North African high located at surface levels, 2) an Atlantic depression, 3) a North African depression, and 4) a North African high located at upper levels (Querol *et al.*, 2009b). The high pressure system on North Africa (Morocco and Algeria) and the trough West of the African coast have been observed to be a typical synoptic configuration allowing for the transports of the dust for some thousands of kilometers in a short time, directly on the Mediterranean basin and Europe (Barkan *et al.*, 2005; Meloni *et al.*, 2008). Barkan *et al.* (2005) showed that it is the joint effect of the horizontal and vertical flows formed around the front between cold air and the African warm air that causes the uplift of the dust and transportations over long distances. This phenomenon is an integral part of the West Africa monsoon system that develops starting from June (Guarnieri *et al.*, 2011).

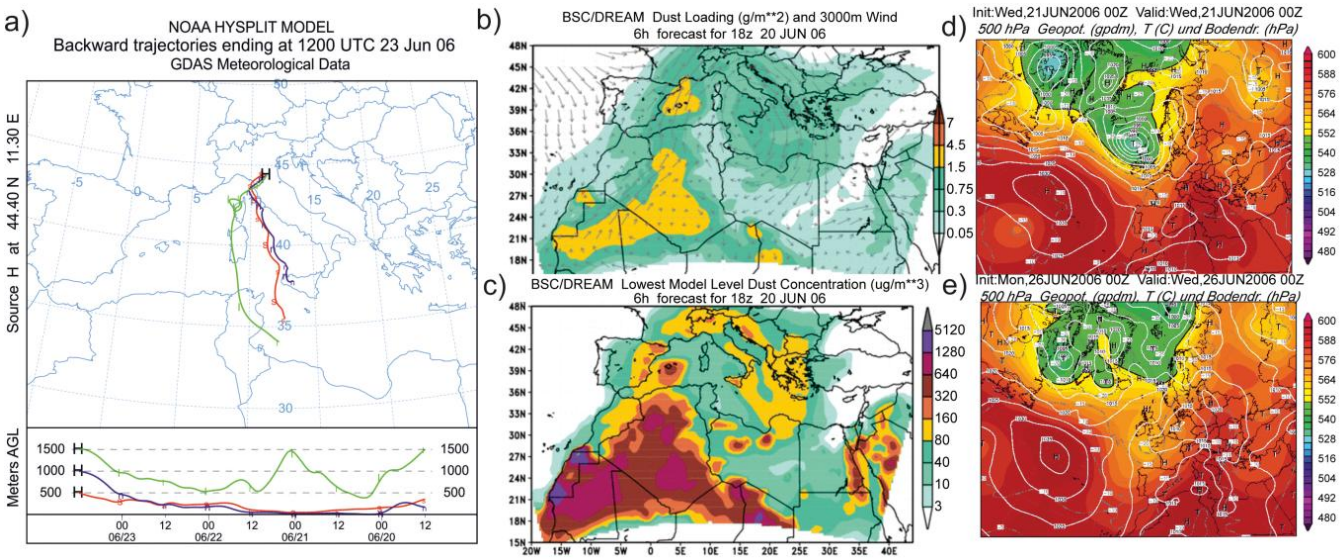

Figure 7.13(a,b,c,d,e) *a) Back trajectories calculated for the day 23/06/06, 12:00 UTC, by the HYSPLIT-4 model, for the city of Bologna (lat 44.40, lon 11.30) at three arrival heights: 100, 500, 1000 m AGL; b) dust loading from the dust regional model DREAM for the day 20th June 2006, 18 UTC; c) lowest model level dust concentration resulting from the dust regional model DREAM (images from the BSC-DREAM8b (Dust REgional Atmospheric Model) model, operated by the Barcelona Supercomputing Center, http://www.bsc.es/projects/earthscience/DREAM/) for the day 20th June 2006, 18 UTC; d,e) Synoptic situation (500 hPa geopotential and ground level pressure in hPa) for the days 21st (d) and 26th June 2006 (e) (http://www.wetterzentrale.de)*

7.4 Conclusions

This Chapter reports the results of an intensive particulate matter sampling campaign in Bologna, a large city in the Po Valley. This region is recognized to have high levels for many atmospheric pollutants in Europe and, then, is of primary importance for the related human health concerns. Major inorganic ions and elements were analyzed on $PM_{2.5}$ and PM_{10}, respectively, and two receptor modeling techniques have been successfully used to identify and characterize the most influencing PM sources. Firstly, the application of a principal component analysis followed by a multilinear regression on chemical data allowed to quantitatively identify 4 main sources: crustal dust, traffic and ammonium nitrate, mixed combustions and "pseudo-marine" aerosol. The mixed combustion was the source mainly contributing to the PM mass (36%), followed by traffic and ammonium nitrate (32%), crustal dust (21%) and "pseudo-marine" aerosol (10%). The multilinear regression analysis also provided the percentage of each element in the sources composition. In a second step, the positive matrix factorization model was also applied on the same dataset. The second model is able to yield a more detailed source profile, splitting the crustal source between the mineral and the road dust component. Moreover, in the PMF model the secondary aerosol source represented by ammonium sulfate is identified separately by the generic traffic source. The main source contributing to the PM levels is found to be the traffic (35%), followed by the secondary aerosol (26%), mineral dust (15%), road dust (11%), "pseudo-marine" (8%) and biomass burning (8%). Summing up the contribution of fine and coarse particles source, however, both the models indicate that about 70% (66% in the PMF and 68% in the PCA/MLRA) of the PM is due to fine particulate (secondary aerosol, traffic, and biomass burning), while the remaining 30% is instead due to coarse particulate source (dust and sea salt).

Even in the absence of significant industrial and energy production point sources, it is worth noting that all the receptor models employed in this study confirm the importance of anthropogenic sources associated mainly to traffic and to regional scale processes affecting secondary aerosol formation especially during the cold season, in agreement with other authors (Marcazzan *et al*., 2003; Lonati *et al*., 2005; Putaud *et al*., 2004, 2010). Given the emissive pattern of the area and the relevant PM levels mainly affected by secondary fractions, it appears that main improvements in air quality standards are likely to succeed only if "tyre" transports are more strictly regulated/substituted by less impacting technologies or policies, and if overall policies are set up and shared over the whole Po Valley district.

Finally, an episode leading to excess PM_{10} in June 2006 was investigated by means of meteorological analysis, back trajectories and aerosol chemistry pointing out a strong influence of long-range transports of Saharan dust. The episode was characterized by elevated PM_{10} mass load not only in the urban sampling site in Bologna, but also at the high elevation WMO-GAW station of

Mt. Cimone. A characteristic value of the ratio of some crustal elements (mean ± standard deviation: Ca/Si = 1.1 ± 0.2, Fe/Si = 0.68 ± 0.05, Mn/Si = 0.015 ± 0.002, Zn/Si = 0.020 ± 0.008) was observed during this event, in agreement with, for example, Kong *et al.* (2011). The synoptic situation was characterized by an extended African high pressure, a situation that has been often observed to be responsible of elevated dust transport to Italy and to Central Europe.

Acknowledgements

The authors wish to thank Fondazione CARISBO for the financial support enabling to acquire the Ion Chromatograph used in this investigation. We acknowledge NOAA for providing the HYSPLIT trajectory model used in this study (available at http://ready.arl.noaa.gov/HYSPLIT.php);Wetterzentrale for providing the synoptic maps from the NOAA-CR20 and NCEP Reanalysis used for the study of the Saharan Dust episode during summer 2006 (available at http://www.wetterzentrale.de/topkarten/fsreaeur.html); PLANIGLOBE BETA (http://omc.planiglobe.com/omc_set.html) for providing the map of Italy with the position of the city of Bologna where PM was sampled for this study; The Barcelona Supercomputing Center for the images from the BSC-DREAM8b (Dust REgional Atmospheric Model) model (http://www.bsc.es/projects/earthscience/BSC-DREAM/).

References

Alastuey A., Querol X., Rodríguez S., Plana F., Lopez-Soler A., Mantilla E., 2004. Monitoring of atmospheric particulate matter around sources of secondary inorganic aerosol. *Atmospheric Environment* 38(30), 4979-4992.

Alastuey A., Moreno N., Querol X., Viana M., Artiñano B., Luaces J.A., Basora J., Guerra A., 2007. Contribution of harbour activities to levels of particulate matter in a harbour area: Hada Project-Tarragona Spain. *Atmospheric Environment* 41, 6366-6378. doi:10.1016/j.atmosenv.2007.03.015.

Almeida S.M., Pio C.A., Freitas M.C., Reis M.A., Trancoso M.A., 2006. Approaching PM2.5 and PM2.5-10 source apportionment by mass balance analysis, principal component analysis and particle size distribution. *Science of the Total Environment* 368, 663-674.

Amodio M., Bruno P., Caselli M., de Gennaro G., Ielpo P., Daresta E., Dambruoso P.R., Placentino C.M., Tutino M., 2007. Fine Particulate Matter in Apulia (South Italy): Chemical Characterization. In: O' Dowd C, Wagner PE (Ed) *Nucleation and Atmospheric Aerosols*. Galway, Ireland. 17th International Conference; Part XI, pp 1235-238, doi:10.1007/978-1-4020-6475-3_245.

ARPA-EMR, 2005. Caratterizzazione chimico-fisica del particolato atmosferico nelle classi dimensionali tra 10 e 0.4 μm. Progetto PolveRe 2ª fase http://www.arpa.emr.it/cms3/documenti/_cerca_doc/aria/aria_re/polvere.pdf Accessed 16 January 2013 (in Italian)

ARPA-EMR, 2013. Calmet meteorological pre-processor. http://www.arpa.emr.it/sim/?qualita_aria/turbolenza Accessed 03 April 2013 (in Italian)

Barkan J., Alpert P., Kutiel H., Kishcha P., 2005. Synoptics of dust transportation days from Africa toward Italy and central Europe. *Journal of Geophysical Research* 110, D07208. doi:10.1029/2004JD005222.

Begum B.A., Kim E., Biswas S.K., Hopke P.K., 2004. Investigation of sources of atmospheric aerosol at urban and semi-urban areas in Bangladesh. *Atmospheric Environment* ***38***(19), 3025-3038.

Belis C.A., Karagulian F., Larsen B.R., Hopke P.K., 2013. Critical review and meta-analysis of ambient particulate matter source apportionment using receptor models in Europe. *Atmospheric Environment* 69, 94-108.

Bonasoni P., Stohl A., Cristofanelli P., Calzolari F., Colombo T., Evangelisti F., 2000. Background ozone variations at Mt. Cimone Station. *Atmospheric Environment* 34, 5183-5189.

Bowen H.J.M., 1979. Environmental Chemistry of the Elements. Academic Press Inc, Oxford.

Bukowiecki N., Lienemann P., Hill M., Figi R., Richard A., Furger M., Rickers K., Falkenberg G., Zhao Y., Cliff S.S,. Prevot A.S., Baltensperger U., Buchmann B., Gehrig R., 2009. Real-world emission factors for antimony and other brake wear related trace elements: Size-segregated values for light and heavy duty vehicles. *Environmental Science and Technology* 43(21), 8072-8078. doi:10.1021/es9006096

Callén M.S., de la Cruz M.T., López J.M., Navarro M.V., Mastral A.M., 2009. Comparison of receptor models for source apportionment of the PM_{10} in Zaragoza (Spain) *Chemosphere* 76(8), 1120–1129.

Camuffo D., Van Grieken R., Busse H.J., Sturaro G., Valentino A., Bernardi A., Blades N., Shooter D., Gysels C., Deutsch F., Wieser M., Kim O., Ulrych U., 2001. Environmental monitoring in four European museums. *Atmospheric Environment* 35: S127-S140.

Carslaw K.S., Boucher O., Spracklen D.V., Mann G.W., Rae J.G.L., Woodward S., Kulmala M., 2010. A review of natural aerosol interactions and feedbacks within the Earth system. *Atmospheric Chemistry and Physics* 10: 1701-1737.

CEN (Comité Européen de Normalisation), 2005. Ambient air quality—Standard gravimetric measurement method for the determination of the $PM_{2.5}$ mass fraction of suspended particulate matter, Ref. No. EN14907:2005.

Chan Y.C., Simpson R.W., McTainsh G.H., Vowles P.D., Cohen D.D., Bailey G.M., 1997. Characterisation of chemical species in PM2.5 and PM10 aerosols in Brisbane, Australia. *Atmospheric Environment* 31, 3773-3785.

Charlson R.J., Schwartz S.E., Hales J.M., Cess R.D., Coakley J.A., Hansen J.E., Hofmann D.J., 1992. Climate forcing by anthropogenic aerosols. *Science* 255, 423-430.

Colb C.E., Worsnop D.R., 2012. Chemistry and composition of atmospheric aerosol particles. *Annual Review of Physical Chemistry* 63, 471-491.

Dan M., Zhuang G., Li X., Tao H., Zhuang Y., 2004. The characteristics of carbonaceous species and their sources in PM2.5 in Beijing. *Atmospheric Environment* 38, 3443-3452.

Davidson C.I., Phalen R.F., Solomon P.A., 2005. Airborne particulate matter and human health: A Review. *Aerosol Science and Technology* 39(8), 737-749.

D'Alessio A., D'Anna A., Ciajolo A., Faravelli T., Ranzi E., 2005. Particolato fine e ultrafine. Emissione da processi di combustione". *La chimica e l'Industria* Anno 87 n.1, 16-24 (in Italian)

Draxler R.R., 1999. HYSPLIT4 user's guide. NOAA Tech. Memo. ERL ARL-230. NOAA Air Resources Laboratory, Silver Spring MD.

Draxler R.R., Rolph G.D., 2011. HYSPLIT (HYbrid Single-Particle Lagrangian Integrated Trajectory) Model access via NOAA ARL READY Website (http://ready.arl.noaa.gov/HYSPLIT.php). NOAA Air Resources Laboratory, Silver Spring MD

EC (European Commission), 1999. Council Directive 1999/30/EC of 22 April 1999 relating to limit values for sulphur dioxide, nitrogen dioxide and oxides of nitrogen, particulate matter and lead in ambient air. http://eur-lex.europa.eu/smartapi/cgi/sga_doc?smartapi!celexplus!prod!CELEXnumdoc&lg=EN&numdoc=31999L0030 Accessed 16 January 2013.

EC (European Commission), 2004. Second Position Paper on Particulate Matter. CAFE Working Group on Particulate Matter (Ed). 231 pp. Available at http://ec.europa.eu/environment/archives/cafe/pdf/working_groups/2nd_position_paper_pm.pdf Accessed 14 October 2013

EC (European Commission), 2008. DIRECTIVE 2008/50/EC OF THE EUROPEAN PARLIAMENT AND OF THE COUNCIL of 21 May 2008 on ambient air quality and cleaner air for Europe http://eurlex.europa.eu/LexUriServ/LexUriServ.do?uri=OJ:L:2008:152:0001:0044:EN:PDF Accessed 16 January 2013.

EEA (European Environment Agency), 2011. Laying the foundations for greener transport. TERM 2011: transport indicators tracking progress towards environmental targets in Europe. European Environment Agency, Report N°7, Copenhagen, Denmark, http://www.eea.europa.eu/publications/foundations-for-greener-transport Accessed 16 January 2013.

EPA (Environmental Protection Agency), 2008. Positive Matrix Factorization (PMF) 3.0 Fundamentals & User Guide. U.S. Environmental Protection Agency Office of Research and Development, Washington, DC 20460 http://www.epa.gov/heasd/products/pmf/EPA%20PMF%203.0%20User%20Guide%20v16_092208_final.pdfAccessed 16 January 2013.

Escudero S., Castillo S., Querol X., Avila A., Alarcón M., Viana M.M., Alastuey A., Cuevas E., Rodríguez S., 2005. Wet and dry African dust episodes over Eastern Spain. *Journal of Geophysical Research* 110 (D18S08). doi:10.1029/2004JD004731.

Finlayson-Pitts B.J., Pitts J.N., 1999. Chemistry of the upper and lower atmosphere. Theory, experiments

and applications. Academic Press, 969 pp.

Fischer H., Kormann R., Klüpfel T., Gurk C., Königstedt R., Parchatka U., Mühle J., Rhee T.S., Brenninkmeijer C.A.M., Bonasoni P., Stohl A., 2000. Ozone production and trace gas correlations during the June 2000 MINATROC intensive measurement campaign at Mt. Cimone. *Atmospheric Chemistry and Physics* 3: 725-738. doi:10.5194/acp-3-725-2003.

Forster P., Ramaswamy V., Artaxo P., Berntsen T., Betts R., Fahey D.W., Haywood J., Lean J., Lowe D.C., Myhre G., Nganga J., Prinn R., Raga G., Schulz M., Van Dorland R., 2007. Changes in atmospheric constituents and in radiative forcing. In: Solomon S, Qin D, Manning M, Chen Z, Marquis M, et al (Ed) Climate Change 2007: The Physical Science Basis, Contribution of Working Group I to the Fourth Assessment Report of the Intergovernmental Panel on Climate Change. Cambridge University Press, Cambridge, UK, and New York, USA.

Frati L., Caprasecca E., Santoni S., Gaggi C., Guttova A., Gaudino S., Pati A., Rosamilia S., Pirintsos S.A., Loppi S., 2006. Effects of NO_2 and NH_3 from road traffic on epiphytic lichens. *Environmental Pollution* 142, 58-64.

Furusjö E., Sternbeck J., Cousins A.P., 2007. PM_{10} source characterization at urban and highway roadside locations. *Science of the Total Environment* 387, 206-219. doi:10.1016/j.scitotenv.2007.07.021.

Garg B.D., Cadle S.H., Mulawa P., Groblicki P.J., Laroo C., Parr G.A., 2000. Brake wear particulate matter emissions. *Environmental Science and Technology* 34(21), 4463-4469. doi:10.1021/es001108h.

Gietl J.K., Lawrence R., Thorpe A.J., Harrison R.M., 2010. Identification of brake wear particles and derivation of a quantitative tracer for brake dust at a major road. *Atmospheric Environment* 44(2), 141-146. doi:10.1016/j.atmosenv.2009.10.016.

Gilbert N.L., Woodhouse S., Stieb D.M., Brook J.R., 2003. Ambient nitrogen dioxide and distance from a major highway. *Science of the Total Environment* 312: 43-46.

Gilli G., Pignata C., Schilirò T., Bono R., La Rosa A., Traversi D., 2007. The mutagenic hazards of environmental $PM_{2.5}$ in Turin. *Environmental Research* 103: 168–175. doi:10.1016/j.envres.2006.08.006.

Godoi R.H.M. Kontozova V., Van Grieken R., 2006. The shielding effect of the protective glazing of historical stained glass windows from an atmospheric chemistry perspective: case study Saint Chapelle, Paris. *Atmospheric Environment* 40, 1255-1265.

Guarnieri F., Calastrini F., Busillo C., Pasqui M., Becagli S., Lucarelli F., Calzolai G., Nava S., Udisti R., 2011. Mineral dust aerosol from Saharan desert by means of atmospheric, emission, dispersion modeling. *Biogeosciences Discussion* 8: 7313-7338. doi:10.5194/bgd-8-7313-2011.

Harrison R.M., Smith D.J.T., Pio C.A., Castro L.M., 1997. Comparative receptor modelling study of airborne particulate pollutants in Birmingham (United Kingdom), Coimbra (Portugal) and Lahore (Pakistan). *Atmospheric Environment* 31(20), 3309-3321.

Hewitt C.N., 2001. The atmospheric chemistry of sulphur and nitrogen in power station plumes. *Atmospheric Environment* 35, 1155-1170.

Iijima A., Sato K., Yano K., Kato M., Kozawa K., Furuta N., 2008. Emission factor for antimony in brake abrasion dusts as one of the major atmospheric antimony sources. *Environmental Science and Technology* 42(8), 2937-2942. doi:10.1021/es702137g.

Kim E., Hopke P.K., Edgerton E.S., 2003a. Source identification of Atlanta aerosol by positive matrix factorization. *Journal of Air & Waste Management Association* 53:6, 731-739.

Kim E., Larson T.V., Hopke P.K., Slaughter C., Sheppard L.E., Claiborn C., 2003b. Source identification of PM2.5 in an arid Northwest U.S. city by positive matrix factorization. *Atmospheric Research* 66, 291-305.

Koçak M., Theodosi C., Zarmpas P., Im U., Bougiatoti A., Yenigun O., Mihapoulos N., 2011. Particulate matter (PM10) in Istanbul: Origin, Source areas and potential impact on surrounding regions. *Atmospheric Environment* 45: 6891-6900. doi:10.1016/j.atmosenv.2010.10.007.

Kong S., Ji Y., Lu B., Chen L., Han B., Li, Z., Bai Z., 2011. Characterization of PM_{10} source profiles for fugitive dust in Fushun - a city famous for coal. *Atmospheric Environment* 45(30), 5351-5365. doi:10.1016/j.atmosenv.2011.06.050

Lantzy R.J., McKenzie F.T., 1979. Atmospheric trace metals: Global cycles and assessment of man's impact. *Geochimica et Cosmochimica Acta* 43, 511-525.

Lee E., Chan C.K., Paatero P., 1999. Application of positive matrix factorization in source apportionment of particulate pollutants in Hong Kong. *Atmospheric Environment* 33, 3201–3212.

Lee S., Liu W., Wang Y., Russell A.G., Edgerton E.S., 2008. Source apportionment of PM2.5: Comparing PMF and CMB results for four ambient monitoring sites in the southeastern United States. *Atmospheric Environment* 42, 4126-4237. doi:10.1016/j.atmosenv.2008.01.025.

Lin C.-C., Huang K.-L., Chen S.-J., Liu S.-C., Tsai J.-H., Lin Y.-C., Lin W.-Y., 2008. NH_4^+, NO_3^-, and SO_4^{2-} in roadside and rural size-resolved particles and transformation of NO_2/SO_2 to nanoparticle-bound NO_3^-/SO_4^{2-}. *Atmospheric Environment* 43(17): 2731-2736. doi:10.1016/j.atmosenv.2009.02.058.

Lonati G., Giugliano M., Butelli P., Romele L., Tardivo R., 2005. Major chemical components of $PM_{2.5}$ in Milan (Italy). *Atmospheric Environment* 39: 1925–1934. doi:10.1016/j.atmosenv.2004.12.012.

Lonati G., Giugliano M., Ozgen S., 2008. Primary and secondary components of $PM_{2.5}$ in Milan (Italy). *Environment International* 34, 665–670. doi:10.1016/j.envint.2007.12.009.

Lucarelli F., Mandò P.A., Nava S., Valerio M, Prati P., Zucchiatti A., 2000. Elemental composition of urban aerosol collected in Florence, Italy. *Environmental Monitoring and Assessment* 65, 165-173. doi:10.1023/A:1006486208406.

Mahowald N.M., Artaxo P., Baker A.R., Jickells T.D., Okin G.S., Randerson J.T., Townsend A.R., 2005. Impacts of biomass burning emissions and land use change on Amazonian atmospheric phosphorus cycling and deposition. *Global Biogeochemical Cycles* 19, GB4030. doi:10.1029/2005GB002541.

Marcazzan G.M,. Ceriani M., Valli G,. Vecchi R., 2003. Source apportionment of PM_{10} and $PM_{2.5}$ in Milan (Italy) using receptor modelling. *Science of the Total Environment* 317, 137–147. doi:10.1016/S0048-9697(03)00368-1.

Marenco F., Bonasoni P., Calzolari F., Ceriani M., Chiari M., Cristofanelli P., D'Alessandro A., Fermo P., Lucarelli F., Mazzei F., Nava S., Piazzalunga A., Prati P., Valli G., Vecchi R., 2006. Characterization of atmospheric aerosols at Monte Cimone, Italy, during summer 2004: Source apportionment and transport mechanisms. *Journal of Geophysical Research* 111, D24202. doi:10.1029/2006JD007145.

Masiol M., Squizzato S., Ceccato D., Rampazzo G., Pavoni B., 2012a. A chemometric approach to determine local and regional sources of PM10 and its geochemical composition in a coastal area. *Atmospheric Environment* 54: 127-133.

Masiol M., Squizzato S., Ceccato D., Rampazzo G., Pavoni B., 2012b. Determining the influence of different atmospheric circulation patterns on PM_{10} chemical composition in a source apportionment study. *Atmospheric Environment* 63: 117-124.

Matassoni L., Pratesi G., Centioli D., Cadoni F., Malesani P., Caricchia A.M., di Bucchianico A.D., 2009. Saharan dust episodes in Italy: influence on PM10 daily limit value (DLV) exceedances and the related synoptic. *Journal of Environmental Monitoring* 11, 1586-1594.

Matta E., Facchini M.C., Decesari S., Mircea M., Cavalli F., Fuzzi S., Putaud J.-P., Dell'Acqua A., 2002. Chemical mass balance of size-segregated atmospheric aerosol in an urban area of the Po Valley, Italy. *Atmospheric Chemistry and Physics Discussion* 2, 2167-2208. doi:10.5194/acpd-2-2167-2002

Matta E., Facchini M.C., Decesari S., Mircea M., Cavalli F., Fuzzi S., Putaud J.-P., Dell'Acqua A., 2003. Mass closure on the chemical species in size-segregated atmospheric aerosol collected in an urban area of the Po Valley, Italy. *Atmospheric Chemistry and Physics* 3: 623-637. doi:10.5194/acp-3-623-2003.

Maxwell J.A., Teesdale W.J., Campbell J.L., 1995. The Guelph PIXE package II. *Nuclear Instruments and Methods B* 95: 407–421.

Mazzei F., D'Alessandro A., Lucarelli F., Marenco F., Nava S., Prati P., Valli G., Vecchi R., 2006. Elemental composition and source apportionment of particulate matter near a large steel plant in Genoa (Italy). *Nuclear Instruments and Methods B* 249 (1-2), 548-551.

Meloni D., di Sarra A., Monteleone F., Pace G., Piacentino S., Sferlazzo D.M., 2008. Seasonal transport patterns of intense Saharan dust events at the Mediterranean island of Lampedusa. *Atmospheric Research* 88, 134-148. doi:10.1016/j.atmosres.2007.10.007.

Miller J.C., Miller J.N., 1993. Statistics for analytical chemistry. 3rd Ed. Ellis Horwood PTR Prentice Hall, Harlow.

Mitra A.P., Morawska L., Sharma C., Zhang J., 2002. Chapter two: methodologies for characterisation of combustion sources end for quantification of their emissions. *Chemosphere* 49(9), 903-922.

Mittner P., Ceccato D., Del Maschio S, Schiavuta E., Chiminello F., Buso P., Agostini S., Prodi V., Mazza M., Belardinelli F., 1996. A multiannual experiment on tropospheric aerosols at Terranova Bay (Antarctica): role of PIXE analysis and related techniques. *Nuclear Instruments and Methods B* 109 (110), 375–380.

Morawska L., Zhang J., 2002. Combustion sources of particles. 1. Health relevance and source signatures. *Chemosphere* 49, 1045-1058

Nava S., Becherini F., Bernardi A., Bonazza A., Chiari M., García-Orellana I., Lucarelli F., Ludwig F., Migliori A., Sabbioni C., Udisti R., Valli G., Vecchi R., 2010. An integrated approach to assess air pollution threats to cultural heritage in a semi-confined environment: The case study of Michelozzo's Courtyard in Florence (Italy). *Science of the Total Environment* 408, 1403-13.

Nava S., Becagli S., Calzolai G., Chiari M., Lucarelli F., Prati P., Traversi R., Udisti R., Valli G., Vecchi R., 2012. Saharan dust impact in central Italy: An overview on three years elemental data records. *Atmospheric Environment* 60, 444-462.

Paatero P., Tapper U., 1994. Positive matrix factorization: a non-negative factor model with optimal utilization of error estimates of data values. *Environmetrics* 5, 111–126. doi:10.1002/env.3170050203.

Paatero P., 1997. Least squares formulation of robust non-negative factor analysis. *Chemometrics and Intelligent Laboratory Systems* 37(1), 23-35. doi:10.1016/S0169-7439(96)00044-5.

Paatero P., 1999. The multilinear engine – A table-driven, least squares program for solving multilinear problems, including the n-way parallel factor analysis model. *Journal of Computational and Graphical Statistics* 8(4), 854-888. doi:10.2307/1390831.

Pachon J.E., Weber R.J., Zhang X., Mulholland J.A., Russell A.G., 2013. Revising the use of potassium (K) in the source apportionment of $PM_{2.5}$. *Atmospheric Pollution Research* 4, 14-21. doi: 10.5094/APR.2013.002

Pant P., Harrison R.M., 2012. Critical review of receptor modelling for particulate matter: A case study in India. *Atmospheric Environment* 49, 1-12. doi:10.1016/j.atmosenv.2011.11.060.

Pathak R.K., Louie P.K.K., Chan C.K., 2004. Characteristics of aerosol acidity in Hong Kong. *Atmospheric Environment* 38(19), 2965-2974.

Pathak R.K., Wu W.S., Wang T., 2009. Summertime PM2.5 ionic species in four major cities of China: nitrate formation in an ammonia-deficient atmosphere. *Atmospheric Chemistry and Physics* 9, 1711-1722. doi:10.5194/acp-9-1711-2009.

Polissar A.V., Hopke P.K., Poirot R.L., 2001. Atmospheric Aerosol over Vermont: Chemical Composition and Sources. *Environmental Science and Technology* 35, 4604-4621.

Ponce N.A., Hoggatt K.J., Wilhelm M., Ritz B., 2005. Preterm birth: The interaction of traffic-related air pollution with economic hardship in Los Angeles neighborhood. *American Journal of Epidemiology* 162(2), 140-148. doi:10.1093/aje/kwi173

Pope C.A., Dockery D.W., 2006. Health effects of fine particulate air pollution: lines that connect. *Journal of Air & Waste Management Association* 56, 709–742.

Pope C.A. III, Ezzati M., Dockery D.W., 2009. Fine-particulate air pollution and life expectancy in the United States. *The New England Journal of Medicine* 360, 376-386.

Prather K.A., Hatch C.D., Grassian V.H., 2008. Analysis of atmospheric aerosols. *Annual Review of Analytical Chemistry* 1, 485-514.

Putaud J.-P., Raes F., Van Dingenen R., Brüggemann E., Facchini M.-C., Decesari S., et al., 2004. A European aerosol Phenomenology-2: chemical characteristics of particulate matter at kerbside, urban, rural and background sites in Europe. *Atmospheric Environment* 38, 2579-2595. doi:10.1016/j.atmosenv.2004.01.041.

Putaud J.-P., Van Dingenen R., Alastuey A., Bauer H., Birmili W., Cyris J., et al. 2010. A European aerosol phenomenology — 3: Physical and chemical characteristics of particulate matter from 60 rural, urban, and kerbside sites across Europe. *Atmospheric Environment* 44, 1308–1320. doi:10.1016/j.atmosenv.2009.12.011

Qin Y., Oduyemi K., 2003. Atmospheric aerosol source identification and estimates of source contributions to air pollution in Dundee, UK. *Atmospheric Environment* 37, 1799-1809. doi:10.1016/S1352-2310(03)00078-5.

Qin Y., Kim E., Hopke P.K., 2006. The concentrations and sources of PM2.5 in metropolitan New York City. *Atmospheric Environment* 40, S312-S332. doi:10.1016/j.atmosenv.2006.02.025.

Querol X., Alastuey A., Puicercus J.A., Mantilla E., Miró J.V., López-Soler A., Plana F., Artiñano B., 1998. Seasonal evolution of suspended particles around a large coal-fired power station particle levels and sources. *Atmospheric Environment* 32(11), 1963-1978.

Querol X., Alastuey A., Rodríguez S., Plana F., Ruiz C.R., Cots N., Massagué G., Puig O., 2001. PM10 and PM2.5 source apportionment in the Barcelona Metropolitan area, Catalonia, Spain. *Atmospheric Environment* 35(36), 6407-6419.

Querol X., Pey J., Pandolfi M., Alastuey A., Cusack M., Pèrez N., et al., 2009. African dust contributions to mean ambient PM10 mass-levels across the Mediterranean basin. *Atmospheric Environment* 43, 4266-4277. doi:10.1016/j.atmosenv.2009.06.013.

Ramadan Z., Song X.H., Hopke P.K., 2000. Identification of sources of Phoenix aerosol by positive matrix factorization. *Journal of Air & Waste Management Association* 50(8), 1308-1320.

Rampazzo G., Masiol M., Visin F., Pavoni B., 2008. Gaseous and PM_{10}-bound pollutants monitored in three sites with differing environmental conditions in the Venice area (Italy). *Water, Air & Soil Pollution* 195 Numbers 1-4, 161–176. doi:10.1007/s11270-008-9735-7.

Reff A., Eberly S.I., Bhave P.V., 2007. Receptor modeling of ambient particulate matter data using Positive Matrix Factorization: Review of existing methods. *Journal of Air &Waste Management Association* 57, 146-154.

Riley J.P., Chester R., 1971. Introduction to marine chemistry, 1st Ed, Academic Press, London and New York.

Rodríguez S., Querol X., Alastuey A., Viana M., Alarcón M., Mantilla E., Ruiz C.R., 2004. Comparative PM10-PM2,5 source contribution study at rural urban and industrial cities during PM episodes in Eastern Spain. *Science of the Total Environment* 328, 95-113. doi:10.1016/S0048-9697(03)00411-X.

Rodríguez S., Van Dingenen R., Putaud J.P., Martins-Dos Santos S., Roselli D., 2005. Nucleation and growth of new particles in the rural atmosphere of Northern Italy-relationship to air quality monitoring. *Atmospheric Environment* 39(36), 6734-6746.

Rolph G.D., 2003. Real-Time Environmental Applications and Display System (READY). Silver Spring MD: NOAA Air Resources Laboratory. http://www.arl.noaa.gov/ready/hysplit4.html Accessed 17 January 2013

Salma I., Maenhaut W., Zemplén-Papp E., Záray G., 2001. Comprehensive characterization of atmospheric aerosols in Budapest, Hungary: physicochemical properties of inorganic species. *Atmospheric Environment* 35(25), 4367-4378.

Schaap M., Mueller K., ten Brink H.M., 2002. Constructing the European aerosol nitrate concentration field from quality analyzed data. *Atmospheric Environment* 36(8), 1323-1335.

Schaap M., van Loon M., ten Brink H.M., Dentener F.J., Builtjes P.J.H., 2004a. Secondary inorganic aerosol simulations for Europe with special attention to nitrate. *Atmospheric Chemistry and Physics* 4, 857-874. doi:10.5194/acp-4-857-2004.

Schaap M., Spindler G., Schulz M., Acker K., Maenhaut W., Berner A., Wieprecht W., Streit N., Müller K., Brüggeman E., Chi X., Putaud J.P., Hitzenberger R., Puxbaum H., Baltensperger U., ten Brink H., 2004b. Artefacts in the sampling of nitrate studied in the "INTERCOMP" campaigns of EUROTRAC-AEROSOL. *Atmospheric Environment* 38, 6487-6496.

Seinfeld J.H., Pandis S.N., 2006. Atmospheric Chemistry and Physics. From Air Pollution to Climate Change. 2nd Ed, John Wiley & Sons Inc, New York

Squizzato S., Masiol M., Brunelli A., Pistollato S., Tarabotti E., Rampazzo G., Pavoni B., 2013. Factors determining the formation of secondary inorganic aerosol: a case study in the Po Valley (Italy). *Atmospheric Chemistry and Physics* 13, 1927-1939. doi:10.5194/acp-13-1927-2013.

Sutton M.A., Dragosits U., Tang Y.S., Fowler D., 2000. Ammonia emissions from non-agricultural sources in the UK. *Atmospheric Environment* 34, 855-869.

Thorpe A., Harrison R.M., 2008. Sources and properties of non-exhaust particulate matter from road traffic: A review. *Science of the Total Environment* 400, 270-282. doi:10.1016/j.scitotenv.2008.06.007.

Thurston G.D., Spengler J.D., 1985. A quantitative assessment of source contribution to inhalable particulate matter pollution in Metropolitan Boston. *Atmospheric Environment* 19, 9–25.

Thurston G.D., Ito .K, Lall R., 2011. A source apportionmnent of U.S. fine particulate matter air pollution. *Atmospheric Environment* 45, 3924-3936. doi:10.1016/j.atmosenv.2011.04.070.

Tositti L., Riccio A., Sandrini S., Brattich E., Baldacci D., Parmeggiani S., Cristofanelli P., Bonasoni P., 2013. Short-term climatology of PM10 at a high altitude background station in southern Europe. *Atmospheric Environment* 65, 145-152. doi: 10.1016/j.atmosenv.2012.10.051

Usher C.R., Michel A.E., Grassian V.H., 2003. Reactions on mineral dust. *Chemical Reviews* 103, 4883-4939.

Vallius M., Janssen N.A.H., Heinrich J., Ruuskanen G.H., Cyrys J., Griekene R.V., de Hartog J.J., Kreyling W.G., Pekkanen J., 2005. Sources and elemental composition of ambient $PM_{2.5}$ in three European cities. *Science of the Total Environment* 337, 147–162. doi:10.1016/j.scitotenv.2004.06.018

Van Dingenen R., Putaud J. –P., Raes F., Brüggemann E., Facchini M. –C., Decesari S., et al., 2004. A European aerosol Phenomenology-2: chemical characteristics of particulate matter at kerbsite, urban, rural and background sites in Europe. *Atmospheric Environment* 38, 2579-2595. doi:10.1016/j.atmosenv.2004.01.041

Vecchi R., Marcazzan G., Valli G., Cerini M., Antoniazzi C., 2004. The role of atmospheric dispersion in the seasonal variation of PM1 and PM2,5 concentration and composition in the urban area of Milan (Italy). *Atmospheric Environment* 38, 4437-4446. doi:10.1016/j.atmosenv.2004.05.029

Vecchi R., Chiari M., D'Alessandro A., Fermo P., Lucarelli F., Mazzei F., Nava S., Piazzalunga A., Prati P., Silvani F., Valli G., 2008. A mass closure and PMF source apportionment study on the sub-micron sized aerosol fraction at urban sites in Italy. *Atmospheric Environment* 42(9), 2240-2253. doi:10.1016/j.atmosenv.2007.11.039

Vecchi R., Valli G., Fermo P., D'Alessandro A., Piazzalunga A., Bernardoni V., 2009. Organic and inorganic sampling artefact assessment. *Atmospheric Environment* 43, 1713-1720.

Viana M., Querol X., Alastuey A., Gil J.I., Menéndez M., 2006. Identification of PM sources by principal component analysis (PCA) coupled with wind direction data. *Chemosphere* 65(11), 2411-2418.

Viana M., Querol X., Götschi T., Alastuey A., Sunyer J., Forsberg B., et al., 2007. Source apportionment of ambient $PM_{2.5}$ at five Spanish centres of the European Community Respiratory Health Survey (ECRHS II). *Atmospheric Environment* 41, 1395–406, doi:10.1016/j.atmosenv.2006.10.016

Viana M., Kuhlbusch T.A.J., Querol X., Alastuey A., Harrison R.M., Hopke P.K., Winiwarter W., Vallius M., Szidat S., Prévot A.S.H., Hueglin C., Bloemen H., Wahlin P., Vecchi R., Miranda A.I., Kasper-

Giebl A., Maenhaut W., Hitzenberger R., 2008a. Source apportionment of particulate matter in Europe: A review of methods and results. *Journal of Aerosol Science* 39(10), 827-849.

Viana M., Pandolfi M., Minguillon M.C., Querol X., Alastuey A., Monfort E., Celades I., 2008b. Inter-comparison of receptor models for PM source apportionment: Case study in an industrial area. *Atmospheric Environment* 42, 3820–3832. doi:10.1016/j.atmosenv.2007.12.056.

Voutsa D., Samara C., Kouimtzis T., Ochsenkuhn K., 2002. Elemental composition of airborne particulate matter in the multi-impacted area of Thessaloniki, Greece. *Atmospheric Environment* 36(28), 4453-4462.

Wahlin P., Berkowicz R., Palmgren F., 2006. Characterisation of traffic-generated particulate matter in Copenhagen. *Atmospheric Environment* 40, 2151-2159, doi:10.1016/j.atmosenv.2005.11.049.

Winkler R., Dietl F., Frank G., Thiersch J., 1998. Temporal variation of ^{7}Be and ^{210}Pb size distributions in ambient aerosols. *Atmospheric Environment* 32, 983-991.

Yatkin S., Bayram A., 2007. Source apportionment of PM_{10} and $PM_{2.5}$ using positive matrix factorization and chemical mass balance in Izmir, Turkey. *Science of the Total Environment* 390(1), 109-123. doi:10.1016/j.scitotenv.2007.08.059

Yin J., Harrison R.M., Chen Q, Rutter A., Schauer J.J., 2010. Source apportionment of fine particles at urban background and rural sites in the UK atmosphere. *Atmospheric Environment* 44, 841-851.

GENERAL CONCLUSIONS

The primary aims of this thesis were to characterize the origin and sources of variability of particulate matter and atmospheric radiotracers ^{7}Be and ^{210}Pb at the WMO-GAW station of Mt. Cimone (44°12' N, 10° 42' E, 2165 m asl). In this work, it was remarked the importance of this high-altitude station in the study of regional and long-range transports of polluted air masses on the background South-European free troposphere. Moreover, because of their contrasting natural origin, the usefulness of the pair ^{7}Be and ^{210}Pb as tracers of vertical transports and scavenging of aerosols was also highlighted. In particular, the ratio $^{7}Be/^{210}Pb$ can be used to determine the sources of chemical species in the lower free troposphere, such as ozone, which together with particulate matter is one of the main secondary atmospheric pollutants. Different methods were applied to fully characterize the physical processes at the basis of variations of PM_{10}, ^{7}Be and ^{210}Pb and their source regions. Receptor modeling based on calculations of back trajectories is one of the tools widely applied in the thesis to this scope: in particular the PSCF receptor model and the cluster analysis of back trajectories have been used.

Firstly, the PM_{10} data time series sampled at the station in the period 1998-2011 was fully analyzed. The PM_{10} series is characterized by marked intra-annual variations as well as by a seasonal cycle described by winter minima and summer maxima. The seasonal effect is connected to a combination of mixed layer expansion, thermal convection and mountain/valley breeze regimes, altogether resulting into the uplift of particulate matter from the lower troposphere and the substantial increase of mass load observed during the warm season. In this framework it was observed that on the regional scale the PM_{10} increase at Mt. Cimone during the warm season is in-phase opposition with stations at ground level, experiencing maxima during the cold period due to stable conditions which inhibit the uplift of PM emitted at ground level. The simultaneous observations of PM_{10} and number densities of fine and coarse particles, as well as the PSCF receptor model were used to provide further insights into the origin of particulate matter at the site. The highest PM_{10} concentrations were found to be connected to three different kinds of events: 1) Saharan dust transports from the Northern African deserts, usually connected to a contemporary decrease of O_3, linked to both reduced sources of pollution in Northern Africa as well as to O_3-destroying reactions happening on the surface of mineral particles; 2) uplift of polluted air masses from the Italian areas north of the Apennines range (Po Valley); 3) advection of PM_{10} enriched air masses from the European continent, and mostly from eastern European countries, where PM emissions are not declining as quickly as in western Europe. While during Saharan dust events increases of both fine and coarse fraction are usually observed, during uplift or advection of polluted air masses it is only the fine fraction that rise up.

Secondly, the seasonal and interannual variations, frequency distributions and correlation patterns of atmospheric radiotracers were examined. While ^{210}Pb seasonal fluctuation is very similar to that of PM_{10}, characterized by a summer maximum, the seasonality of ^{7}Be is more complex, being characterized by two relative maxima. The ^{7}Be maximum during the cold period is associated to Stratosphere-to-Troposphere transport, while the more pronounced maximum during the warm season is connected to tropospheric subsidence balancing low tropospheric air masses ascent occasionally accompanied by Stratosphere-to-Troposphere Exchange. The presence of two different physical mechanisms leading to the two ^{7}Be maxima was confirmed by the analysis of the frequency distributions and of correlation patterns, markedly dissimilar during the cold and warm period. The seasonality of ^{7}Be and ^{210}Pb was also studied by means of the simulations conducted through the global 3D model GMI CTM: in particular, the use of a model enabled a thoroughly knowledge of the roles of transport and precipitation scavenging processes in controlling the seasonal variations of ^{7}Be and ^{210}Pb at Mt. Cimone. The model was able to capture the main circulation patterns observed in the Northern Hemisphere. A general good agreement in the simulations of ^{210}Pb seasonal pattern was observed, and it was confirmed that the summer ^{210}Pb maximum is due to the stronger thermal convection and consequent increased uplift from the boundary layer. The seasonal pattern of ^{7}Be was instead worse represented, especially during the warm season. The results of the simulations showed that the large stratospheric influence is the cause of ^{7}Be increases during the cold period. A general better agreement between the model and observations was observed if the model is sampled at the some adjacent gridboxes. The analysis of simulated wind fields and horizontal distribution of radiotracers suggested that the site is located in a region where there is a large gradient especially in the North-South direction. A series of sensitivity experiments were further conducted to examine and quantify the roles of wet scavenging, dry deposition, and convective transport/scavenging in controlling the seasonality of ^{210}Pb and ^{7}Be at Mt. Cimone. Wet scavenging resulted to be the most important process controlling the seasonal variations of ^{210}Pb and ^{7}Be at Mt. Cimone.

Advection patterns at Mt. Cimone were characterized by means of a back trajectories cluster analysis, and the role of transport in the observed changes in the atmospheric composition has been studied. The clustering algorithm found 8 main flow types arriving at the height of 2200 m asl, roughly corresponding to the height of the measurement site. Most of the trajectories corresponded to westerly flows, as typical of mid-latitude Northern Hemisphere sites. A name was assigned to each flow pattern, identifying its region of provenance: Arctic, Eastern, Mediterranean-Africa, Western, Atlantic, North Atlantic, and North America. The results indicate that flows from North America are related to low pressures and tropopause heights, low temperatures and they are dry air masses. These flows are almost non-existent during summertime and generally linked to low values of atmospheric pollutants such as ozone, PM_{10}, black carbon, carbon monoxide but also of atmospheric radiotracers

^{7}Be and ^{210}Pb. Flows from the Arctic region are also dry, associated to low tropopause height and cold, even if a bit warmer than those from North America. These flows are associated with generally low values of atmospheric compounds such as PM_{10}, O_3, black carbon and carbon monoxide. They are also linked to high ^{7}Be and low ^{210}Pb values. Continental flows from North Western-Europe, Eastern Europe, Western and Mediterranean-Africa are generally associated to higher values of atmospheric components; in particular, North Western-Europe, Western and Eastern flows are associated to high levels of CO, BC, O_3 and fine particles number densities, causing also increases in PM_{10}. Because of their continental origin, these flows are also linked to high ^{210}Pb levels. Mediterranean-Africa flows being related to Saharan Dust events are associated to high PM_{10} values, and increases in both the fine and coarse fraction of particles. Interestingly, this flow type was not only associated to high ^{210}Pb values, but also to high ^{7}Be: this phenomenology might be connected to the combination of African dust uplifting and downward movement from the upper troposphere, which was further studied in the thesis.

This study highlighted also that the seasonality of air mass transports can have a deep influence on variations in atmospheric composition. In fact while ^{7}Be winter maximum can be linked to the seasonal behaviour of Arctic and North-Atlantic air masses, ^{7}Be summer maximum can be associated to Mediterranean-Africa, Western and North Atlantic air masses seasonal pattern. ^{210}Pb summer maximum seems to be well related with the seasonality of Western and North Western-Europe flows, whereas the seasonal pattern of PM_{10} might be influenced by the seasonal pattern of advection patterns bringing about elevated mass loads of particles, such as Mediterranean-Africa, Western, North Atlantic and North Western-Europe air masses. Moreover, it was also found that rare events can contribute a lot to increases of some species during some seasons. In particular, it was observed that even if flows from the Arctic/polar regions are more frequent during the cold period, they can have a large contribution to ^{7}Be summertime increases. Trends were also studied for the time series of advection patterns and of measured variables at Mt. Cimone. Downward trends were detected for Atlantic and North-American flows, and for the monthly medians of ^{210}Pb and PM_{10} measured at the station. An upward trend was instead found for CO_2 and precipitation time series. The contemporary decreasing trend of PM_{10} and ^{210}Pb, which cannot be ascribed to a decrease in anthropogenic emissions, highlights the potential role of meteorology as one of the main causes of these downward trends. The analysis of the magnitude of the seasonal and trend components of the time series revealed that the largest variabilities of the time series are associated to the seasonal components, with a reduced weight of the trend component for all the series.

The association of NAO with flows and atmospheric variables was examined. A positive correlation of NAO with North-American flows and an anti-correlation with Western flows were observed. This is

explained by the fact that the subtropical high at lower latitudes during the negative phase of the NAO facilitates the entrance of westerlies/south-westerlies to the Mediterranean. As for the atmospheric composition, the most important associations of NAO are with carbon monoxide and coarse particles, connected also to the modifications of the flows induced by the shift of the NAO phase.

The PSCF method was again applied to study the source regions of ^{7}Be, ^{210}Pb and O_3 and the influence of stratospheric air masses at Mt. Cimone (also with the help of potential vorticity). ^{210}Pb sources are similar to those of PM10: in fact ^{210}Pb originates mainly in Eastern Europe and Northern Africa, with a more limited, still notable, contribution from the surrounding Italian and French regions. The main source areas of ^{7}Be are located in the Arctic/polar region, Finland and North America, but importantly the region of Northern Africa was observed as a potential source originating high values of ^{7}Be. This led to the important conclusion that two different independent mechanisms may mix and act together during single Saharan dust incursions events: the dust uplift causing increases of crustal particles, PM_{10} and ^{210}Pb, but also a strong downdraft from the upper troposphere causing increases of ^{7}Be, scavenged by African dust and transported with it. The source regions of O_3 are similar to those of ^{210}Pb, even if the surrounding region, such as the Po Basin, France and southern Germany seem to give important contributions to its increase. A separate analysis for the cold and warm periods highlighted that the contributions of the surrounding regions is higher during the warm season, while stratospheric influence can have a more limited, but not negligible, effect during the cold period. Importantly, the PSCF applied separately during the warm and cold period highlighted that long-range transports are more active during winter while during summer regional and short-range transports are more important. This result was similar to the one of the simulations of the GMI CTM: long-range transport dominates the winter/spring season because of higher horizontal winds, while regional effects are more important during the warm season when convection gets stronger.

Generally, high trajectories originate in the Arctic and North America/Atlantic regions, whereas low trajectories are coming from the lowest latitudes. The same areas were associated to high $^{7}Be/^{210}Pb$, pointing out once more the importance of this tracer in the understanding of vertical motions and in connection with STE events. The areas observed in this analysis correspond to preferred regions for cyclone formation (Atlantic region), as well as areas where the polar jet stream is generally stronger (North America/Atlantic). A link to the tropopause discontinuity region at mid-latitudes was also observed. The observation of areas source of high potential vorticity values highlighted the importance of lee cyclogenesis as a mechanism promoting vertical exchanges between stratosphere and troposphere; North Atlantic and North Africa region were again observed as areas source of particles from the upper troposphere/lower stratosphere.

Finally, a source apportionment study was conducted in Bologna, a midsize city located in the centre of the Po Valley, which is recognized as one of the most polluted regions of the whole Europe, and which is located North of Mt. Cimone. The application of receptor modelling identified six sources of particulate matter in the city: traffic, secondary aerosol, biomass burning, mineral dust, road dust, and a "pseudo-marine" factor linked to the use of salt as a de-icing agent on roads during winter. The result of the source apportionment highlighted an important contribution of fine particulate sources (about 70%), while the remaining part (about 30%) is connected to coarse particles.

Overall, the main feature of this study is the use of a multi-tracer and multi-model approach to understand the processes at the basis of observed variations in the measurements. The use of receptor models is extremely important especially at a station such as Mt. Cimone, which is an ideal platform for observing the "crossroads" of pollution transports and where acquired data time series are long enough to provide a short-term climatology of the site. The exploited approach successfully characterized the processes/sources affecting atmospheric composition at the site.

ACKNOWLEDGEMENTS

First of all, my biggest thanks to my supervisor Prof. Laura Tositti: without you I would neither have started this big adventure. Thanks for all the support (also, but not only, financial!), the suggestions, the help you gave me. Thanks for being a mentor, a teacher, but also a bit like a friend to me.

I would like to especially thank Prof. Orza: working with you was a big privilege and a big honor to me, and I feel very lucky I met such an incredible scientist, and more, such an incredible person along my path. Thanks for your help, your hard work and your precious suggestions. The experience in Spain taught me really a lot and I am very grateful for it.

Dr. Hongyu Liu, thank you for teaching me so much, for your help and support: you have been more than a teacher to me, I feel very grateful I had the possibility to work with you and I hope we can keep working on together. Thanks to the National Institute of Aerospace (NIA) for financial support during my one month's visit to Dr. Hongyu Liu: it was one of the most incredible experiences I had during my PhD.

Special thanks also to Prof. Teodoro Georgiadis for reading the first version of my PhD thesis (it's so long that acknowledgements have to be enormous!): thanks for the suggestions and for the help in improving it.

Prof. Esperanza Liger Pérez, Prof. Vladimir Spiridonov and Prof. Prodromos Zanis, thanks for your precious work of reading and evaluating my thesis for the Doctor Europaeus title. Prof. Alexandra Ioannidou, thanks for coming to Italy for the defence of my thesis and for evaluating it.

Italian Air Force Meteorological Office (IAFMS) and ISAC-CNR are gratefully acknowledged for their precious technical support at the Mt. Cimone station and for the help in the collection of compositional datasets. In particular, special thanks to Dr. Paolo Cristofanelli and Dr. Paolo Bonasoni for their help in the sampling campaign at Mt. Cimone.

I acknowledge NOAA (http://www.esrl.noaa.gov/) for providing the HYSPLIT trajectory model and the NCEP/NCAR reanalysis data used in this study.

Thanks to all the people of the Department of Biological, Geological and Environmental Sciences of Bologna, and most of all to Dr. Giorgia Cinelli (now at JRC: you deserved it!! Thanks for teaching me γ-spectrometry!), Deborah Lo Po, Dr. Roberto Braga, and Gianfranco Ulian: we shared offices, thoughts, impressions, feelings, but also courses, meals, coffees... Thanks also to Alberto Previti and Daniele Rossi with whom I did not share the working environment but with whom I centainly shared many moments of this 3-years path.

To all my family, many many thanks, you always supported me in this choice: it was tough, but it was worthwhile! Thanks for always listening to me even if sometimes you don't either know what I am speaking about! Special thanks to my sister and to Mum and Paolo for sharing with me all the bad, but also the pleasant moments during these three years.

Thanks also to all my familiars: even if you are far away, my thoughts are always with you. A special thought to all my grandparents, to those that are still there and with whom I hope to share many other special moments of my life, but also to those I missed along this path. You all always felt very proud of me, but I have to say I am very proud of my big enlarged family!

To all my friends, the old ones and the new ones: thanks for having always encouraged and supported me, but also for the leisure time we shared, without which now I would be crazy for sure (but, are we sure that I am not crazy, though?)!

To Luigi, last but not least, a big thank you, for all the time you listened to me speaking about particulate matter, and models, and problems: thanks for the patience and the love you had with me, most of all in these last months. I am sure it was not easy to bear with me, but finally it seems that you made it!!

RINGRAZIAMENTI

Prima di tutto, i miei più sinceri ringraziamenti alla mia relatrice Prof.ssa Laura Tositti: senza di lei non avrei nemmeno iniziato questa grande avventura. Grazie di tutto il supporto (anche economico, ma non solo!), i suggerimenti, l'aiuto che mi ha dato. Grazie di essere stata un mentore, un'insegnante, ma anche un po' come un'amica per me.

Vorrei ringraziare particolarmente il Prof. Orza: lavorare con lei è stato un grande privilegio ed un grande onore per me, e mi sento molto fortunata di aver incontrato uno scienziato così incredibile, e ancora di più, una così incredibile persona, lungo il mio cammino. Grazie per l'aiuto, il duro lavoro ed i suggerimenti preziosi. L'esperienza in Spagna mi ha insegnato davvero tanto e ne sono molto riconoscente.

Dr. Hongyu Liu, grazie di avermi insegnato così tanto, dell'aiuto e del supporto: è stato più che un insegnante per me, e sono molto riconoscente per aver avuto la possibilità di lavorare con lei e spero potremo continuare a collaborare. Grazie alla NIA (National Institute of Aerospace) per il supporto finanziario durante la mia visita di un mese al Dr. Hongyu Liu: è stata una delle esperienze più incredibili che ho avuto durante il dottorato.

Ringrazio il Servizio Meteorologico dell'Aeronautica Militare (IAFMS) e l'Istituto di Scienze dell'Atmosfera e del Clima del Consiglio Nazionale delle Ricerche (ISAC-CNR) per il loro prezioso supporto tecnico alla stazione di Mt. Cimone e per l'aiuto nella raccolta dei datasets composizionali. In particolare, un sentito ringraziamento speciale al Dr. Paolo Cristofanelli ed al Dr. Paolo Bonasoni per il loro aiuto nella campagna di campionamento a Mt. Cimone.

Grazie al Prof. Teodoro Georgiadis per aver letto la prima bozza della mia tesi di dottorato (è così lunga che i ringraziamenti devono essere enormi!): grazie per i suggerimenti e per l'aiuto per migliorarla.

Grazie ai Proff. Esperanza Liger Pérez, Vladimir Spiridonov e Prodromos Zanis per aver letto e giudicato la mia tesi per il titolo di Doctor Europaeus. Grazie anche alla

Prof. Ioannidou per essere venuta in Italia per la discussione finale della tesi e per averla valutata.

Ringrazio la NOAA (http://www.esrl.noaa.gov/) per aver fornito il modello HYSPLIT ed i dati della rianalisi NCEP/NCAR usati in questo studio.

Grazie a tutte le persone del Dipartimento di Scienze Biologiche, Geologiche ed Ambientali di Bologna, e soprattutto al Dr. Giorgia Cinelli (ora a JRC: te lo meritavi!! Grazie di avermi insegnato la spettrometria-γ!), Dr. Roberto Braga, Deborah Lo Po, e Gianfranco Ulian: abbiamo condiviso uffici, pensieri, impressioni, sentimenti, ma anche corsi, pasti, caffè, …Grazie anche a Daniele Rossi ed Alberto Previti con cui non ho condiviso il luogo di lavoro ma coi quali abbiamo certamente condiviso molti momenti di questo cammino.

A tutta la mia famiglia, molte molte grazie, mi avete sempre supportato in questa scelta: è stata dura, ma ne valeva la pena! Grazie di avermi sempre ascoltato anche se a volte non sapevate nemmeno di cosa stessi parlando! Un grazie speciale a mia sorella e a mamma e Paolo per aver condiviso con me tutti i brutti momenti, ma anche quelli piacevoli durante questi tre anni.

Grazie a tutti i miei parenti: anche se siete lontani, i miei pensieri sono sempre con voi. Un pensiero speciale a tutti i miei nonni, a quelli che ci sono ancora e con cui spero di condividere ancora tanti momenti speciali della mia vita, ma anche a quelli che ho perso lungo questo cammino. Tutti voi vi siete sempre sentiti orgogliosi di me, ma devo dire che io mi sento molto orgogliosa della mia grande famiglia allargata!

A tutti i miei amici, i vecchi ed i nuovi:grazie di avermi sempre incoraggiato e supportato, ma specialmente grazie per il tempo libero che abbiamo condiviso e senza il quale sarei diventata pazza (ma siamo sicuri che non lo sia?)!!

A Luigi, ultimo ma non ultimo, un grande grazie, per tutto il tempo in cui mi hai ascoltato parlare di particolato, e modelli, e problemi: grazie della pazienza e dell'amore che hai avuto con me, soprattutto durante questi ultimi mesi. Sono certa che non è stato facile sopportarmi, ma alla fine sembra proprio che tu ce l'abbia fatta!!

APPENDIX I – Aerosol Characterization at the WMO-GAW Station of Mt. Cimone (2165 m asl) by ^{7}Be, ^{210}Pb and PM_{10}

1. Introduction[1]

The importance of environmental radionuclides in the study of atmosphere and climate dynamics has been often emphasized in the course of the last decades as well documented in the GAW 155 report (WMO, 2004). Though nowadays the radiotracer method constitutes a niche approach to the comprehension of the planetary complexities, it still deserves attention as it provides a powerful tool for the basic characterization of transfer and transformation mechanisms occurring both at local and large scale. For this reason several radionuclides, namely ^{7}Be, ^{210}Pb, ^{222}Rn and others are included among the key atmospheric components that are routinely monitored within the WMO-GAW network (WMO, 2004).

Though an historical reconstruction of radiotracer literature in many geophysical as well as radioprotection studies was partly given in this thesis in Chapters 1, 3 and 4, it is worth noting the steady production of papers where the environmental radiotracers have been used with the role of quantitative descriptors. Examples can be found in Paatero and Hatakka (2000), Liu *et al.* (2004), Lee *et al*. (2007).

In this Appendix a brief compendium of the research activity carried out by the University of Bologna in this field since the 90's is presented. In particular we will introduce the long term monitoring activity of ^{7}Be, ^{210}Pb in the PM_{10} fraction at Mt. Cimone station, a WMO-GAW station in the Northern Italian Apennines hosting a complex activity of atmospheric research.

[1] This chapter consists in parts of a paper by Tositti L. (Dept. of Chemistry, Università di Bologna), Brattich E. (Dept. of Biological, Geological and Environmental Sciences-Section of Geology, Università di Bologna), Cinelli G. (Dept. of Biological, Geological and Environmental Sciences-Section of Geology, Università di Bologna; now at European Commission, DG JRC, Institute for Transuranium Elements, Via E Fermi 2749, I-21027 Ispra (VA), Italy), 2013. Aerosol characterization at the WMO-GAW station of Mt. Cimone (2165 m a.s.l.) by ^{7}Be, ^{210}Pb and PM10. In: Isotopes in Hydrology, Marine Ecosystems and Climate Change Studies. Proceedings of an International Symposium Monaco, 27 March-1 April 2011, Vol.1, 387-393, International Atomic Energy Agency, Vienna. ISBN 978–92–0–135610–9

2. Material and Methods

2.1 Experimental

The experimental activity carried out since the early 90's for the determination of ^{7}Be, ^{210}Pb and aerosol mass loading in the form of PM_{10} at Mt. Cimone station has been described in Chapters 2 and 3 of this thesis.

2.2 Measurement Site

The measurement site of Mt. Cimone (44°12' N, 10°42' E), the highest peak of the Northern Apennines (2165 m asl), has been described in Chapters 2 and 3 of this thesis.

3. Results

In Figure 1, time series of ^{7}Be, ^{210}Pb and PM_{10} are shown. We can notice a distinct seasonal cycle for ^{7}Be, ^{210}Pb and PM_{10}, with maxima in the summer and minima in the winter.

Peaks of Beryllium-7 are often associated with downward transport from the upper troposphere or from the stratosphere. This phenomenology, now defined as Stratosphere-to-Troposphere-Exchange (STE), able to affect ozone budget in the troposphere, is still matter of investigation since its mechanism has not been thoroughly elucidated. Nevertheless research activities carried out at Mt. Cimone within EU projects VOTALP and STACCATO (Bonasoni *et al.*, 1999, 2000; Cristofanelli *et al.*, 2006, 2007, 2009) allowed discovering that STE events are not limited to spring-summer period as previously believed, but they are scattered all the year round, at least in the area investigated. In addition a Stratospheric index based on the use of ^{7}Be, relative humidity and ozone was introduced in order to quickly identify stratospheric air masses through simultaneous data collected on-site (Cristofanelli *et al.*, 2009).

Vertical motion is characterized by both downward and uplift motion, in order to fulfill hydrostatic condition in the troposphere. The concurrence of both transports seems to be very well captured by the use of $^{7}Be/^{210}Pb$ ratio (Lee *et al.*, 2007).

Other studies in progress concern the identification of transport from Saharan deserts and from contaminated areas such as the Po valley and the eastern European areas. In both cases there is a remarkable influence on ozone budget, but in opposite directions: a decrease in the former case and an increase in the latter. We will take advantage of radionuclides such as ^{210}Pb to discriminate these phenomenologies which are both characterized by a mass loading increase, but in order to have a more quantitative point of view, massive use of back-trajectories will be carried out together with multivariate models. In the meantime collection

of samples and their analysis by HPGe will be continued in order to enlarge the time series and the database available.

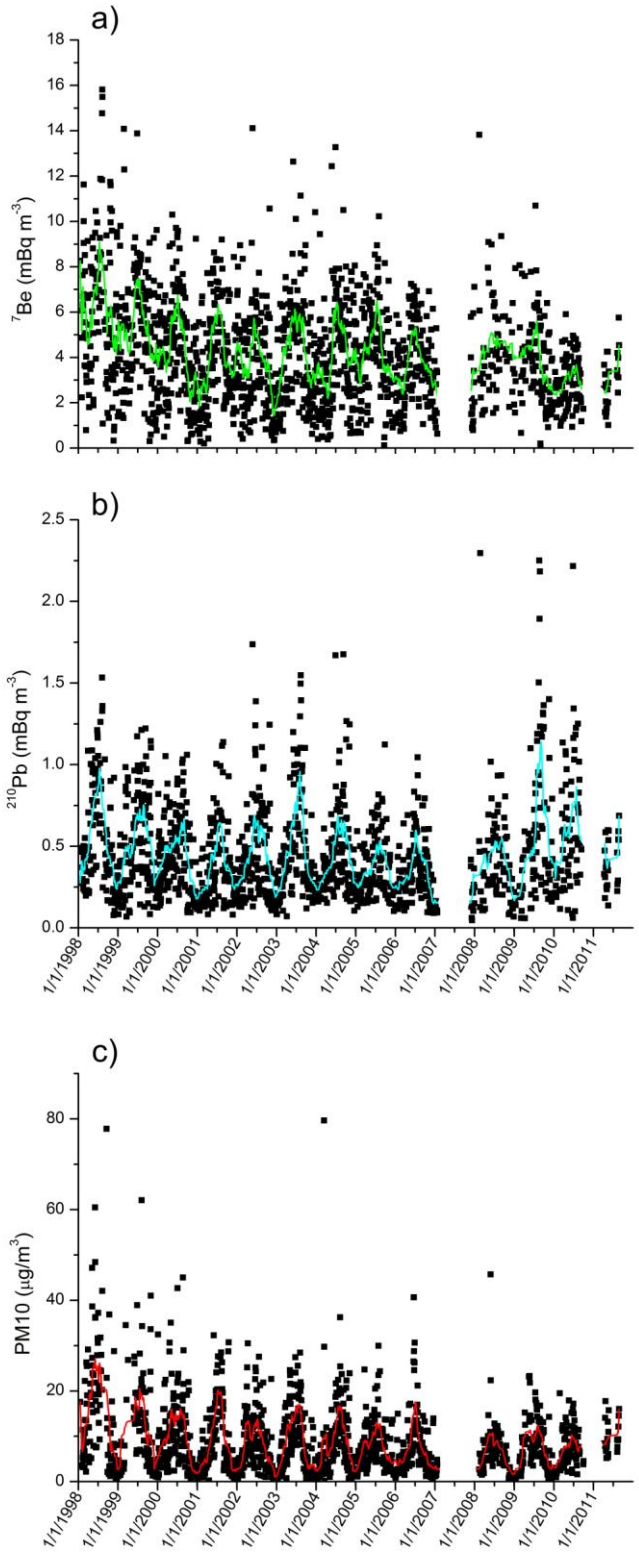

Figure 1 *Time series of a) ^{7}Be (mBq/m^3); b) ^{210}Pb(mBq/m^3) and c) PM_{10}(μg/m^3). Solid line represents the moving average of period 21.*

References

Bonasoni P., Evangelisti, F., Bonafè, U., Feldmann, H., Memmesheimer, M., Stohl, A., Tositti, L., Kromp-Kolb, L.H., and Colombo, T., 1999. Stratosphere-troposphere exchanges: case studies recorded at Mt. Cimone during VOTALP project. *Physics and Chemistry of the Earth, Part C: Solar, Terrestrial & Planetary Science* 24(5), 443-446.

Bonasoni P., Stohl A., Cristofanelli P., Calzolari F., Colombo T., and Evangelisti F., 2000. Background ozone variations at Mt. Cimone Station. *Atmospheric Environment* 34, 5183-5189.

Cristofanelli P., Bonasoni P., Tositti L., Bonafè U., Calzolari F., Evangelisti F., Sandrini S., and Stohl A., 2006. A 6-year analysis of stratospheric intrusions and their influence on ozone at Mt. Cimone (2165 m above sea level). *Journal of Geophysical Research* Vol. 111, D03306, doi:10.1029/2005JD006553

Cristofanelli, P., Bonasoni P., Carboni G., Calzolari F., Casarola L., Zauli Sajani S., and Santaguida R., 2007. Anomalous high ozone concentrations recorded at a high mountain station in Italy in summer 2003. *Atmospheric Environment* 41, 1383-1394.

Cristofanelli P., Calzolari F., Bonafè U., Duchi R., Marinoni A., Roccato F., Tositti L., Bonasoni P., 2009. Stratospheric Intrusion Index (SI^2) from baseline measurement data. *Theoretical and Applied Climatology* 97, 317-325.

Lee H. N., Tositti L., Zheng X., Bonasoni P., 2007. Analyses and comparison of variations of ^{7}Be, ^{210}Pb and $^{7}Be/^{210}Pb$ with ozone observations at two Global Atmosphere Watch stations from high mountains. *Journal of Geophysical Research* 112, D05303, doi:10.1029/2006JD007421.

Liu H., Jacob D.J., Dibb J.E., Fiore A.M., Yantosca R.M., 2004 Constraints on the sources of tropospheric ozone from ^{210}Pb-^{7}Be-O_3 correlations. *Journal of Geophysical Research*, 109, D07306, doi:10.1029/2003JD003988.

Paatero J., and Hatakka J., 2000. Source areas of airborne ^{7}Be and ^{210}Pb measured in Northern Finland. *Health Physics* 79, 6, 691-696.

World Meteorological Organization (WMO), 2004. 1st International Expert Meeting on Sources and Measurements of Natural Radionuclides Applied to Climate and Air Quality Studies. WMO TD 1201, Global Atmosphere Watch, Geneva, Switzerland. Available at ftp://ftp.wmo.int/Documents/PublicWeb/arep/gaw/gaw155.pdf, last accessed 13 September 2013

Appendix II – Comparison of Radioactivity Data Measured in PM_{10} Aerosol Samples at Two Elevated Stations in Northern Italy during the Fukushima Event

1. Introduction[1]

Airborne radioactivity is a powerful tool in the investigation of environmental dynamics. The monitoring of airborne radionuclides has afforded a convenient and efficient approach in investigating both the problems associated to sanitary risks and the efficiency of atmospheric transport processes, including redistribution and removal of pollutants. In this context it is worth referring to some basic works summarizing details on this topic such as Junge (1963), Reiter (1978), Garland *et al.* (1991), Eisenbud and Gesell (1997), Turekian and Graustein (2003), and the recent review by Papastefanou (2008).

As widely recognized, the release of artificial radionuclides into the atmosphere started in 1945 at Alamogordo, New Mexico, within the Manhattan Project, it developed through the tragic war events of Hiroshima and Nagasaki, and continued with nuclear weapon testing which finished only in 1980 when the last Chinese nuclear experiments in air took place. Besides warfare sources, accidental release of radioactivity through the terrestrial airshed has been ascribed to several occurrences such as the fall of nuclear fuelled satellites, accidents in nuclear power plants i.e., Kyshtym, Windscale, Three Mile Island, Chernobyl, to mention the most relevant (see for example Eisenbud and Gesell, 1997; UNSCEAR, 2008; Sykora and Froehlich, 2010). In the recent past, the Algeciras release was observed when radiocontaminated metal scraps were accidentally loaded and melt in a steel mill, leading to the spread of a weak, though well detectable, ^{137}Cs plume over the Mediterranean basin (Papastefanou *et al.*, 2005; Quélo, 2007; Pham *et al.*, 2011).

[1] This chapter consists in parts of a paper by Tositti L. (Dept. of Chemistry, Università di Bologna), Brattich E. (Dept. of Biological, Geological and Environmental Sciences-Section of Geology, Università di Bologna), Cinelli G. (Dept. of Biological, Geological and Environmental Sciences-Section of Geology, Università di Bologna; now at European Commission, DG JRC, Institute for Transuranium Elements, Via E Fermi 2749, I-21027 Ispra (VA), Italy), Previti A. (Laboratory of Nuclear Engineering, Università di Bologna), Mostacci D. (Laboratory of Nuclear Engineering, Università di Bologna), 2012. Comparison of radioactivity data measured in PM10 aerosol samples at two elevated stations in northern Italy during the Fukushima event. *Journal of Environmental Radioactivity* 114, 105-112. This work was also presented as a poster presentation at the Conference "Chernobyl 25 anni dopo: studi, riflessioni e attualità", held in Udine (Italy) 21-22-23 June 2011. Proceedings (in Italian) are available online at http://www.arpa.fvg.it/export/sites/default/tema/radiazioni/radiazioni-artificiali/allegati/Atti_Convegno_STAMPA.pdf, and published by Regione Autonoma Friuli Venezia Giulia, ISBN 978-88735-16-0

The details of the Fukushima accident are described in the abundant data available (IAEA, 2011a,b,c; NISA, 2011a,b,c; MEXT, 2011a,b). The atmospheric release started on 12 March 2011 and proceeded for several weeks following the occurrence of a number of hydrogen driven explosions, which created a variable source term (Stohl *et al.,* 2011). Monitoring activities were promptly organized worldwide. In this framework not only the agencies in charge of radioactivity monitoring networks were active, but many other research units were interested to observe the inception and evolution of Fukushima plume dispersal over the Northern hemispheric troposphere (Bolsunovsky and Dementyev, 2011; Diaz Leon *et al.*, 2011; Lozano *et al.*, 2011; Manolopoulou *et al.,* 2011; Pittauerová *et al.,* 2011). Results from the European Community countries have been already subject of national reports as well as collectively described by Masson *et al.* (2011), showing a large degree of homogeneity in data and time evolution in spite of well recognized inhomogeneity in weather patterns over such a large and complex territory.

The data discussed in the present contribution includes the observations of both Fukushima related radionuclides and the natural components sampled at Mt. Cimone (http://www.isac.cnr.it/cimone/) and Montecuccolino, two stations located in the Northern Italian Apennines. Data description and interpretation is given with the objective of evaluating activity trends at two different altitudes in order to:

a) characterize the transport of artificial radioactivity in airborne particulate matter from a long distant source;
b) point out the effect of altitude on the vertical distribution of radionuclides during atmospheric transport; and
c) determine the extra dose from the Fukushima release as compared to background components present in airborne particulate matter.

1.1 Measurement sites

Air sampling was carried out at two locations (see Figure 1): Montecuccolino, starting 1st April 2011, and Mt. Cimone, starting 8th April 2011.

1.1.1 Montecuccolino

Montecuccolino is a nuclear sciences laboratory of the University of Bologna, founded in the 1960's and still active in the field of nuclear reactor, plasma physics and radiation protection. The Montecuccolino laboratory (44° 27' N, 11° 19' E) is located on the foothills of Bologna, 3.5 km away from downtown, at an altitude of 273 m above sea level. It hosts also the Institute for Radiation Protection of ENEA (Italian National agency for new technologies, Energy and

sustainable economic development). Due to the presence of the research nuclear reactors in the past there has always been an intense activity in radiation measurements, and this was utilized following the Fukushima Dai-ichi accident.

1.1.2 Mt. Cimone

The Mt. Cimone Station is a research platform for the observation of meteorological and climatologic parameters of international relevance with an active role within the WMO-GAW network, recently upgraded to "global station" ranking. The features of this measurement site have been described in Chapters 2 and 3 of this thesis work.

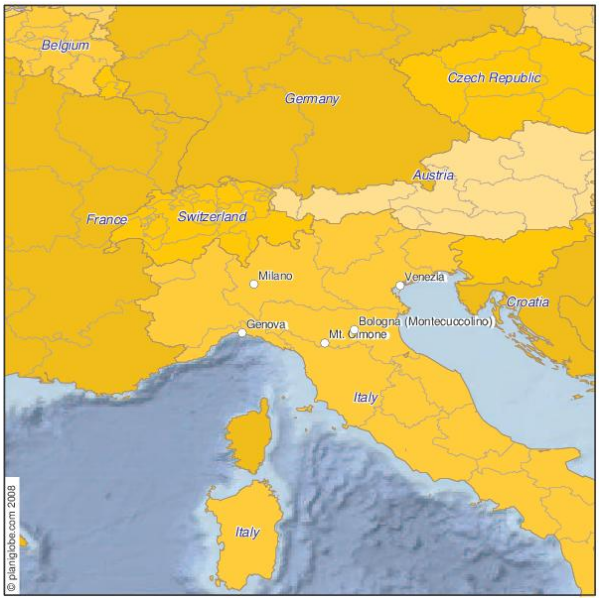

Figure 1 *Locations of Mt. Cimone and Montecuccolino (Bologna) stations in the northern Italian Apennines (Planiglobe, kk&w - digital cartography).*

2. Material and methods

2.1 Experimental activity

The ^{7}Be, ^{210}Pb and aerosol mass loading in the form of PM_{10} have been measured at Mt. Cimone since the early 1990's; however, a steady measurement activity began in 1998 following acquisition of a PM_{10} high volume sampler. The preference for PM_{10} sampling rests on the well-known size distribution of the radionuclides considered, which tend to populate the fine fraction (< 1.0 µm) (Winkler *et al.*, 1998) as a consequence of their physical origin, to wit nuclear spallation reaction in free gas molecule/atoms in the atmosphere for ^{7}Be and decay of gaseous ^{222}Rn to ^{210}Pb. Once formed, both radionuclides become rapidly associated to the finest aerosol particles, becoming

prone to long-range transport. The same fate is shared by those components of radioactive plumes whose radioisotopes are released through high temperature processes and accidents, so that they are first vaporized and thereafter attach onto fine particles, as observed for weapon test fallout and the Chernobyl accident. Still, the 10 μm cut-off allows the substantially quantitative collection of the coarser fraction of aerosols of mineral origin following soil resuspension processes. The supermicron fraction typically of crustal origin (and locally including sea salt contribution) may contain K, U and Th radioisotopes associated to the mineral phases detectable in γ-spectra as a function of meteorological conditions.

At Mt. Cimone, aerosol sampling was carried out with a time resolution of about 48 hours by means of a PM_{10} high-volume sampler (Thermo Environmental Instruments Inc. – Flow rate = 1.13 m^3 min^{-1}) using a rectangular glass fiber filter (20.3 cm x 25.4 cm, exposed area: 407 cm^2). The volume sampled in a period amounted to approximately 3250 m^3. Once collected, samples were transferred to the Laboratory of Environmental Chemistry and Radiochemistry of Bologna University where they were conditioned at a constant temperature (20° C) and relative humidity (30%) prior to weighing for the determination of net mass loads of ambient aerosol. Since high altitude stations such as Mt. Cimone (2165 m a.s.l.) are representative of large regions, but may only partially catch the situation in the lower troposphere, a second sampling point was set at Montecuccolino at the end of March 2011, using analogous sampling conditions and extending the comparison from the activity concentrations of artificial radionuclides to the other γ-emitters detectable in aerosol samples such as ^{7}Be and ^{210}Pb tracing respectively downward and upward transports.

The γ-emitters in aerosol samples were analyzed on a planar Hyper Pure Germanium crystal detector (HPGe) with a 1500 mm^2 active surface, FWHM 0.73 keV at 122 keV, and energy range 0-900 keV. Spectra were accumulated for 1 day, to optimize peak analysis. Spectra were processed with the software package GammaVision-32, version 6.07, ORTEC.

Efficiency calibration is determined with a blank glass fiber filter traced with accurately weighted aliquots of a standard solution of mixed radionuclides (QCY48, Amersham) supplemented with ^{210}Pb, homogeneously dispersed in drops over the filter surface. Once dried under a hood in ambient conditions, the calibration filter was folded into a polystyrene container in the same geometry as the unknown samples. Quantitative analysis on samples was carried out by subtracting the spectrum of a blank filter in the same geometry, while uncertainty on peaks (k = 1, 68% level of confidence) was calculated propagating the combined error over the efficiency fit previously determined with the counting error. Minimum detectable activity was calculated making use of the Traditional ORTEC method with a peak cut-off limit of 40%.

Activity data was corrected to the midpoint of the time interval of collection and for the decay during spectrum acquisition. As expected the latter correction was significant only for ^{131}I owing to the short half-life.

Qualitative analysis of the aerosol spectra was carried out using a selected isotope library extracted by the basic ORTEC mask library. As a rule, typical isotopes searched in spectra are ^{7}Be, ^{210}Pb, ^{40}K, γ emitters from the uranium and thorium families, ^{137}Cs and ^{22}Na. This list was supplemented with a further selection of artificial nuclides based on the experience gathered at the time of the Chernobyl accident and above all on the analysis of a couple of fresh Fukushima samples in the month of March 2011. The samples analyzed in our laboratory were obtained by collecting dust from the turbines of an airliner which flew between Tokyo and Milan during the period of maximum airborne radioactivity in Japan. Both samples were very active compared to typical ambient samples and led to identification of the following artificial radionuclides attributed to the release from Fukushima: ^{132}Te, ^{131}I, ^{132}I, ^{133}I, ^{134}Cs, ^{136}Cs and ^{137}Cs. As a result the isotope library was supplemented, for the present study, with all the "exotic" species detected due to the decay of the less abundant, short-lived Fukushima radionuclides. In the present work, results of gamma spectrometry are reported, using the emission at 661.62 keV for ^{137}Cs, 604.66 and 795.76 keV for ^{134}Cs, 364.48 keV for ^{131}I and 185.99 keV for ^{226}Ra. The ^{226}Ra activity was corrected taking into account the contribution of the ^{235}U peak at 185.71 keV, considering the natural isotopic composition of uranium (Gilmore, 2008).

Fallout was also sampled in the city of Bologna collecting bulk (wet+dry) deposition on the roof of the Department of Chemistry during the periods: 18/03-05/04/2011, 01-11/04/2011, 11-27/04/2011, 27/04-18/05/2011. Fallout samples were collected in a barrel with an open surface of 471 cm^2. The samples were recovered by acidification and analyzed in 1 dm^3 Marinelli beakers by low-level low-background gamma spectroscopy.

To integrate the experimental data apparently deriving from an exotic source, back-trajectories analysis was applied. The use of back-trajectories in atmospheric research is presently widespread. In fact they allow both to characterize typical circulation patterns in a given location and to provide a diagnostic tool (either in retrospective or in forecast mode) useful to associate atmospheric composition variation to circulation. In the present work, 3D-kinematic back-trajectories were calculated using the NOAA - ARL (National Oceanic and Atmospheric Administration – Air Resources Laboratory) Hybrid Single Particle Lagrangian Integrated Trajectory model (HYSPLIT – 4) (Draxler and Rolph, 2003; http://www.arl.noaa.gov/ready/hysplit4.htm; Draxler and Rolph, 2004), employing archived GDAS1 (Global Data Assimilation System) global analysis

meteorological data provided by NCEP (National Weather Service's National Center for Environmental Prediction).

2.2 Dose Estimation

Effective doses and their contribution to the total annual dose to individuals in Italy were estimated, to evaluate the potential radiological impact to the Italian population due to the arrival of the radionuclides from the Fukushima Dai-ichi damaged reactors. Estimates refer only to the measuring site of Montecuccolino, in view of its proximity to a densely populated area, whereas Mt. Cimone is a research station located in a remote, unpopulated environment.

The effective doses due to inhalation of artificial radionuclides (^{137}Cs, ^{134}Cs and ^{131}I) and natural radionuclides (^{226}Ra, ^{7}Be and ^{210}Pb) were estimated following specifications in the Italian Law (Legislative Decree 230/1995, implementing the Council Directive 96/29/EURATOM, based on the recommendations of the ICRP60). To produce an upper bound estimation of the dose, an inhalation rate of 1.2 m^3/h, i.e., that of a working adult, and inhalation dose coefficients for children under 1 year of age, the highest activity-to-dose conversion factors, were considered. Iodine is present both within particulate and in gaseous form, but in the present work only the particulate form was measured: a particulate-to-total ratio of 0.3 was assumed in dose calculation. This value was chosen on the basis of Japanese and European experimental data collected during the Fukushima accident (Masson *et al.*, 2011) and on the basis of Chernobyl data (Battiston *et al.*, 1988). The activity concentrations of the radionuclides measured in Montecuccolino during the days of 4th and 5th April 2011, the days when the highest concentration of artificial radionuclides was measured, were used.

3. Results and discussion

The occurrence of the Fukushima accident suggested inclusion in the monitoring activity of a number of artificial radionuclides usually neglected, with the exception of ^{137}Cs which occasionally has been detected in the high volume samples collected in this framework. In particular, because of the favourable position of Mt. Cimone, samples from May-June 1998 showed the transit of the ^{137}Cs plume released from Algeciras steel plant due to melting of radio-contaminated metal (Papastefanou *et al.*, 2005; Quélo *et al.*, 2007; Pham *et al.*, 2011). The ^{137}Cs concentration reported on that occasion was of the order of a few mBq m^{-3} against the usual absence of this nuclide from γ-spectra due to the absence of soil resuspension on the mountain top. As for the other artificial radionuclides, the choice was made in keeping with what was discussed in the experimental section.

The results of γ-spectrometry for each sample collected are reported in Figure 2 for Mt. Cimone and Figure 3 for Montecuccolino. Artificial radionuclide activities are presented in Figure 2a and Figure 3a, whereas natural radionuclides activities are reported in Figure 3a and Figure 3b.

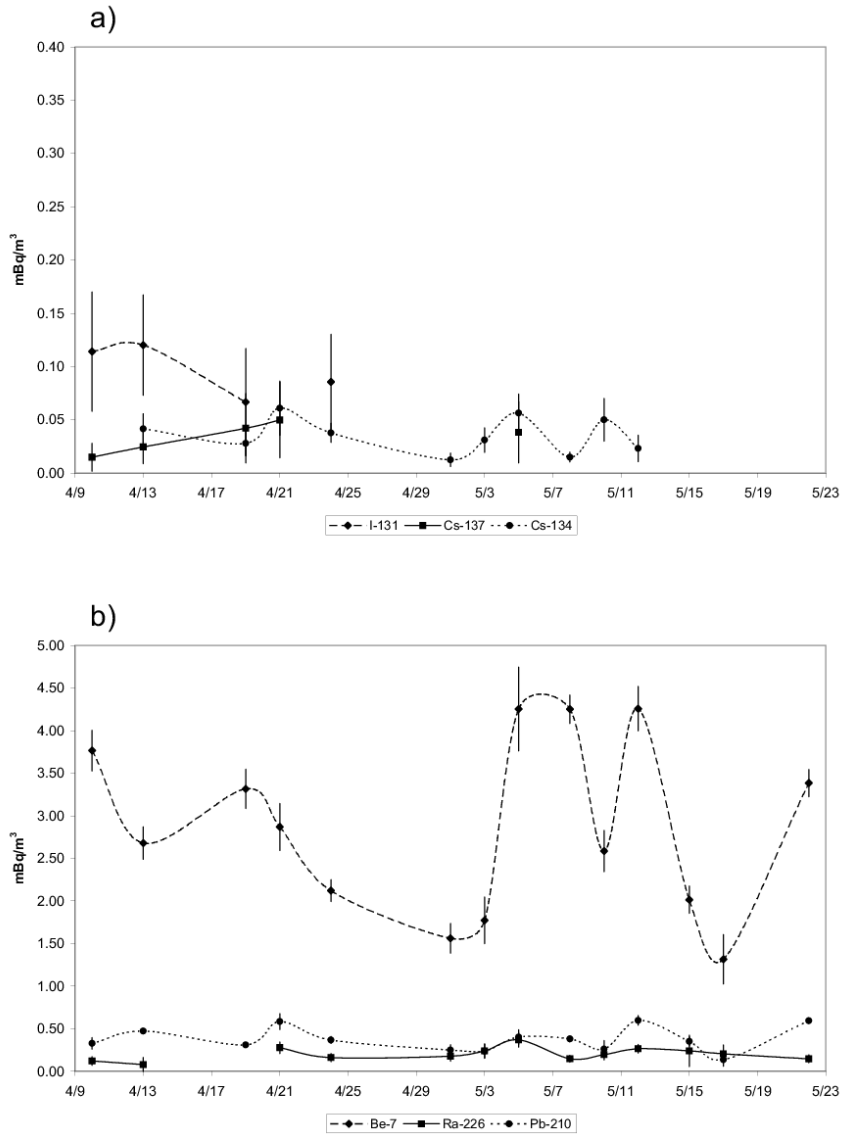

Figure 2 *Activities measured in mBq/m^3 (corrected for standard conditions) with N-type planar detector at Mt. Cimone site: (a) artificial emitters ^{131}I, ^{137}Cs and ^{134}Cs, (b) natural emitters ^{7}Be, ^{226}Ra and ^{210}Pb.*

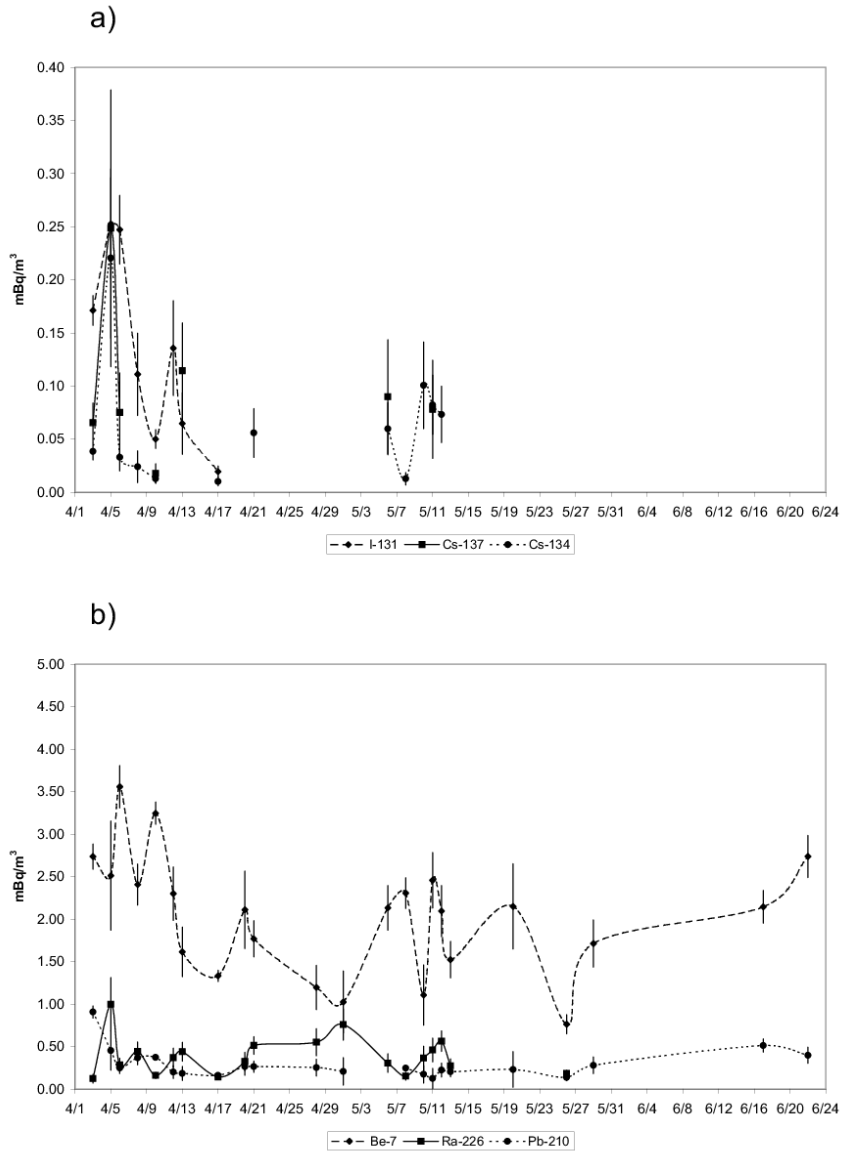

Figure 3 *Activities measured in mBq/m^3 (corrected for standard conditions) with N-type planar detector at Montecuccolino site: (a) artificial emitters ^{131}I, ^{137}Cs ^{134}Cs, (b) natural emitters ^{7}Be ^{226}Ra ^{210}Pb.*

The values for ^{131}I ranged from 0.020 to 0.250 mBq/m^3, those for ^{137}Cs from 0.015 to 0.250 mBq/m^3 and finally those for ^{134}Cs from 0.010 to 0.220 mBq/m^3. The average recorded values of Fukushima radionuclides are in good agreement with data collected over the Italian peninsula, generally from ground level stations as reported from the Institute for Environmental Protection and Research (ISPRA, 2011). Our data are consistent with those observed over the European continent, as discussed in Masson *et al.* (2011), which show a rather large degree of homogeneity of the plume following redistribution processes in the troposphere.

Comparing the maximum activity concentration observed in our time series and that one recorded at Fukushima and Sugitsuma (available at MEXT

http://radioactivity.mext.go.jp/en/monitoring_around_FukushimaNPP_dust_sampling/2011/05/1306621_053110.pdf), the mean transit time between Japan and Northern Italy was roughly estimated as eleven days. As a result, the approximate dilution factor of the plume radioactivity based on ^{137}Cs (the longest lived of the detected γ-emitters) was estimated of about 5 orders of magnitude.

Good agreement was found between the activities (either natural or artificial) measured at both stations, as per Table 1, upon comparing average values at the two sites with a Student's t-test. The t-test value indicated that for all the radionuclides reported, with the sole exception of ^{7}Be and ^{226}Ra, the means of the observed values at the two sites were not statistically different at the 0.05 confidence level. The values for ^{7}Be are slightly higher at Mt. Cimone because of the greater altitude of the location and the negative gradient of this radionuclide due to its cosmogenic origin. On the contrary, the values for ^{226}Ra were slightly lower because of the crustal origin of this radionuclide. Concerning ^{210}Pb, values would be expected higher close to the ground, but data at the two sites were comparable. Such comparable values for ^{210}Pb are expected during the warm season when, as a result of active turbulent motions which stir the innermost tropospheric layer above the Mt. Cimone top, this site lies within the planetary boundary layer (PBL); during the cold season, instead, the PBL and free troposphere are decoupled largely preventing upward transport of ^{210}Pb.

	Mt Cimone		Montecuccolino				
	mean (mBq/m^3)	std dev (mBq/m^3)	mean (mBq/m^3)	std dev (mBq/m^3)	t value	df	p
^{7}Be	2.9	1.0	2.1	0.7	2.66	36	0.012
^{210}Pb	0.38	0.14	0.3	0.2	1.58	34	0.123
^{226}Ra	0.20	0.08	0.4	0.2	-2.92	31	0.007
^{131}I	0.10	0.02	0.13	0.09	-0.76	10	0.462
^{137}Cs	0.03	0.01	0.07	0.07	-1.31	14	0.212
^{134}Cs	0.04	0.02	0.06	0.05	-1.36	26	0.186

Table 1 *Mean, standard deviation and differences between the means (evaluated through the Student's t-test) of the airborne detected radionuclides activity concentration at the two sites, in* mBq/m^3.

Comparison of activity data on Fukushima radionuclides with those on the natural components clearly shows that the background aerosol radioactivity (namely ^{7}Be and ^{210}Pb) was on the average one order of magnitude higher than the artificial component. In all the samples in which the Fukushima radionuclides were detected, associated experimental uncertainty was very high due to low concentrations, as a result of both dispersal-dilution and wet removal, frequent in the region (especially at Mt. Cimone) during spring time. As for ^{7}Be and ^{210}Pb, the values were also typical for

the season, that is at an average concentration between the winter minimum and the summer maximum.

The average $^{134}Cs/^{137}Cs$ ratio at the two sites was found to be 0.9, in good agreement with the 0.95 average European value recorded during the period March 20th – April 4th (Masson *et al.*, 2011), and very different from the 0.5-0.6 value reported after the Chernobyl accident (Arvela *et al.*, 1990; De Cort *et al.*, 1998).

In Figure 4, 3D kinematic fifteen days back-trajectories calculated using the HYSPLIT-4 model for the site of Mt. Cimone on the 4th April 2011, i.e., the day with the maximum observed ^{137}Cs value, are shown. Only Mt. Cimone back trajectories are reported due to the coincidence of the output for Montecuccolino. The analysis of back trajectories of the period end of March – beginning of April confirmed the westerly Japanese origin of the considered air masses, which is very well captured and described by the one shown in Figure 4.

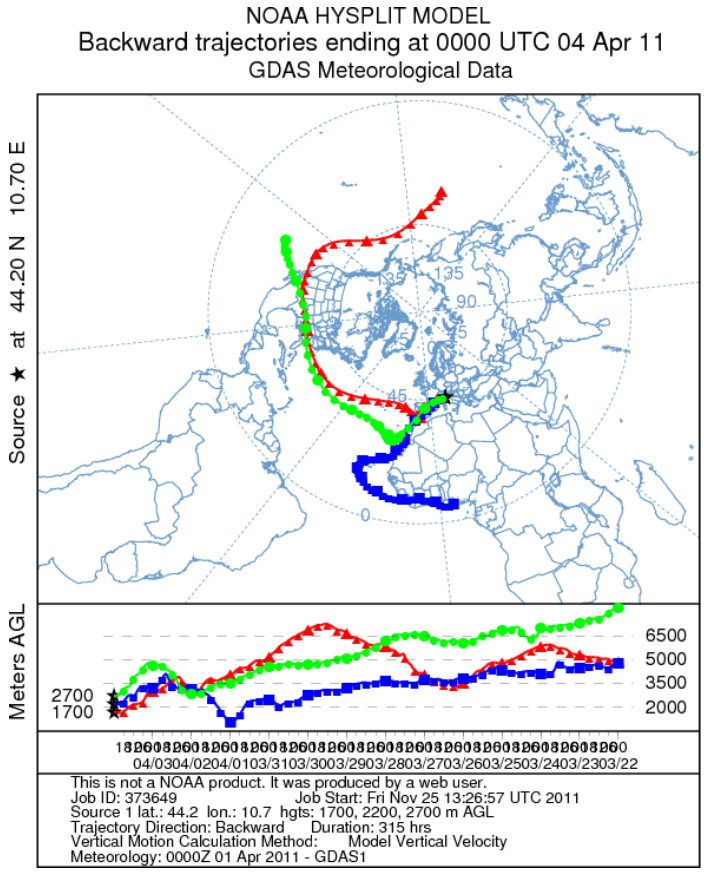

Figure 4 *15 days back-trajectories for 4th April 2011 (00:00 UTC), day of maximum detected ^{137}Cs value, for Mt. Cimone (44°12' N, 10°42' E), calculated by the HYSPLIT-4 model (http://www.arl.noaa.gov/ready/hysplit4.htm) for three arrival heights (1700, 2200 and 2700 m asl)*

From the time series of the artificial radionuclides the influence of emissions from Fukushima appears to have ceased in Italy in the first half of May 2011 (Torri, 2011). For the sake of completeness the data of fallout sampled in the same period is reported: total ^{137}Cs deposition analyzed between March 18th and May 18th 2011 resulted to be 27.1 ± 5.9 Bq/m^2.

The increase in radiological risk due to the Fukushima plume in Italy can be evaluated against the doses due to the natural radionuclides that are always present. Dose calculations were conducted under the worst case hypotheses discussed in section 2.2. The doses calculated for all the radionuclides considered are reported in Table 2. The dose contribution of the nuclides deriving from the Fukushima accident, calculated for a hypothetical one year constant exposure, was assessed at 1.1 μSv/year, to be compared to the 50 μSv/year due to the natural components, including ^{7}Be, ^{210}Pb, ^{226}Ra. This latter in turn amounts to only a minor fraction of the annual dose to members of the public from all sources (natural, medical, etc.), which in Italy averages approximately 4500 μSv/year (Dionisi *et al.*, 2005).

	Hourly dose (μSv/h)	**Annual dose (μSv/y)**
^{7}Be	7.53E-07	6.60E-03
^{210}Pb	2.55E-03	2.24E+01
^{226}Ra	3.11E-03	2.72E+01
^{131}I	7.28E-05	6.38E-01
^{134}Cs	1.85E-05	2.87E-01
^{137}Cs	3.28E-05	1.62E-01

Table 2 *Hourly (μSv/h) and annual (μSv/year) dose deriving from the detected natural (^{7}Be, ^{210}Pb and ^{226} Ra) and artificial radionuclides (^{131}I, ^{134}Cs, ^{137}Cs).*

4. Conclusions

In this work the data of airborne radioactivity in ambient aerosol at two elevated sites in northern Italy under the influence of the Fukushima plume transit are reported. The main artificial radionuclides detected were ^{131}I (0.020-0.250 mBq/m^3), ^{137}Cs (0.012- 0.250 mBq/m^3) and ^{134}Cs (0.010-0.220 mBq/m^3). The activities of the gamma emitters from the Fukushima accident detected at both stations were consistent with those collected at other locations both in the Italian peninsula and elsewhere in Europe, and approximately one order of magnitude lower than those of natural background radionuclides. The Japanese origin of the artificial radionuclides was confirmed by back-trajectories models applied to the locations investigated.

Considering a one-year constant exposure the peak inhalation dose from Fukushima nuclides was estimated at 1.1 μSv/year, whereas the dose from natural gamma emitters yielded a total of 50 μSv/year. These figures can be compared to the dose limit to the general population of 1000 μSv/year. It can be concluded that at the location considered the dose increase due to the Fukushima accident is entirely negligible.

Acknowledgements

NOAA is acknowledged for providing the HYSPLIT trajectories (http://ready.arl.noaa.gov/HYSPLIT.php) used in this study.

PLANIGLOBE (http://www.planiglobe.com/) is acknowledged for providing the map of Italy with the position of the two sampling sites of Mt. Cimone and Montecuccolino.

References

Abstracts of the Workshop "Twenty-five years after the Chernobyl accident: studies, remarks and recent findings", 2011. ISBN 978-88-88735-16-0. Available also online at http://www.arpa.fvg.it/export/sites/default/tema/radiazioni/radiazioni-artificiali/allegati/Atti_Convegno_STAMPA.pdf

Arvela H., Markannen M., Lemmeli H., 1990. Mobile survey of Environmental Gamma Radiation and Fallout Level in Finland after Chernobyl accident. *Radiation Protection Dosimetry* 32, 177-184.

Battiston G.A., Degetto S., Gerbasi R., Sbrignadello G., Tositti L., 1988. Fallout Distribution in Padua and Northeast Italy after the Chernobyl Nuclear Reactor Accident. *Journal of Environmental Radioactivity* 8, 183-191.

Bolsunovsky A., and Dementyev D., 2011. Evidence of the radioactive fallout in the center of Asia (Russia) following the Fukushima Nuclear Accident. *Journal of Environmental Radioactivity*, doi:10.1016/j.jenvrad.2011.06.007

Council Directive 96/29/EURATOM laying down basic safety standards for the protection of the health of workers and the general public against the dangers arising from ionizing radiation. Available at http://ec.europa.eu/energy/nuclear/radioprotection/doc/legislation/9629_en.pdf, pp. 29

De Cort M., et al., 1998. Atlas of Cesium Deposition on Europe after the Chernobyl accident. Office for Official Publications of the European Communities. ECSC-EEC-EAEC: Brussels-Luxemburg.

Diaz Leon J., Jaffe D.A., Kaspar J., Knecht A., Miller M.L., Robertson R.G.H., Schubert A.G., 2011. Arrival time and magnitude of airborne fission products from the Fukushima, Japan, reactor incident as

measured in Seattle, WA, USA. *Journal of Environmental Radioactivity* 102(11), 1032-1038. doi:10.1016/j.envrad.2011.06.005

Dionisi, Fontani, Innocenzi, Menna, Parisi, Salierno, Torri, Zeppa, Wells, 2005. APAT. Environmental Data Yearbook.

Draxler R.R., and Rolph G.D., 2003. HYSPLIT Model access via NOAA ARL READY Website (available at http://www.arl.noaa.gov/ready/hysplit4.htm), NOAA Air Resources Laboratory.

Draxler R.R., and Hess G.D., 2004. Description of the HYSPLIT4 Modeling System, NOAA Technical Memorandum ERL ARL-224.

Eisenbud M., Gesell T.F., 1997. Environmental Radioactivity: from natural, industrial and military sources. Academic Press, 656 pp.

Garland J.A., Cambray R.S., and Johnson C.E., 1991. Atmospheric Radioactivity and Its Variations. In: Chamberlain A.C. (Ed.), Radioactive Aerosols, Chapter 9. Cambridge University Press.

Gilmore G., 2008, Practical Gamma-Ray Spectrometry, John Wiley & Sons.

IAEA (International Atomic Energy Agency), 2011a. Fukushima Nuclear Accident Update, available at http://www.iaea.org/newscenter/news/2011/fukushima110311.html

IAEA (International Atomic Energy Agency), 2011b. IAEA International Fact finding Expert Mission of the Nuclear Accident following the Great East Japan Earthquake and Tsunami. Tokyo, Tokyo, Fukushima Dai-ichi NPP, Fukushima Dai-ni NPP and Tokai NPP, Japan, available at http://www.iaea.org/newscenter/focus/fukushima/missionsummary010611.pdf

IAEA (International Atomic Energy Agency), 2011c. Report of Japanese Government to IAEA Ministerial Conference on Nuclear Safety - Accident at TEPCO's Fukushima Nuclear Power Stations. Available at http://www.iaea.org/newscenter/focus/fukushima/japan-report/

ICRP (International Commission on Radiological Protection) Publication 60, 1990. Recommendations of the International Commission on Radiological Protection. Annals of the ICRP Volume 21/1-3, Elsevier. ISBN 13**:** 978-0-08-041144-6.

ISPRA (Institute for Environmental Protection and Research), 2011. Emergenza nucleare in Giappone, available at http://www.isprambiente.gov.it/site/it-IT/Documenti_emergenza_nucleare_Giappone/

Junge C.E., 1963. Air Chemistry and Radioactivity. International Geophysics Series; vol. 4. New York: Academic Press, pp. 382.

Legislative Decree 230, 1995. "Attuazione delle direttive 89/618/Euratom, 90/641/Euratom, 92/3/Euratom e 96/29/Euratom in materia di radiazioni ionizzanti." available at http://www.aimn.it/lex/DLgs_230_modificato.pdf

Lozano R.L., Hernández-Ceballos M.A., Adame J.A., Casas-Ruíz M., Sorribas M., San Miguel E.G., Bolívar J.P., 2011. Radioactive impact of Fukushima accident on the Iberian Peninsula: Evolution and plume previous pathway. *Environment International* 37, 1259-64.

Manolopoulou M., Vagena E., Stoulos S., Ioannidou A., Papastefanou C., 2011. Radioiodine and radiocesium in Thessaloniki, Northern Greece due to Fukushima nuclear accident. *Journal of Environmental Radioactivity* 102, 796-797.

Masson O., et al., 2011. Tracking of airborne radionuclides from the damaged Fukushima Dai-Ichi nuclear reactors by European Networks. *Environmental Science and Technology* 45, 7670–7677, doi:10.1021/es2017158. 28323, 28332.

MEXT (Ministry of Education, Culture, Sports, Science and Technology Japan), 2011a. http://www.mext.go.jp/english/incident/1304796.htm

MEXT (Ministry of Education, Culture, Sports, Science and Technology Japan), 2011b. Readings of dust sampling http://radioactivity.mext.go.jp/en/monitoring_around_FukushimaNPP_dust_sampling/2011/05/1306621_053110.pdf

NISA (Nuclear and Industrial Safety Agency), 2011a. INES (the International Nuclear and Radiological Event Scale) Rating on the Events in Fukushima Dai-ichi Nuclear Power Station by the Tohoku District - off the Pacific Ocean Earthquake, 3 pp. [available at http://www.nisa.meti.go.jp/english/files/en20110412-4.pdf]

NISA (Nuclear and Industrial Safety Agency), 2011b. Regarding the Evaluation of the Conditions on Reactor Cores of Unit 1, 2 and 3 related to the Accident at Fukushima Dai-ichi Nuclear Power Station, Tokyo Electric Power Co. Inc. 64 pp., [available at http://www.nisa.meti.go.jp/english/files/en20110615-5.pdf]

NISA (Nuclear and Industrial Safety Agency), 2011c. Conditions of Fukushima Dai-ichi Nuclear Power Station Unit 1（As of 6:00 July 14, 2011）[available at http://www.nisa.meti.go.jp/english/press/2011/07/en20110715-1-2.pdf

Papastefanou C., Manolopoulou M., Stoulos S., Ioannidou A., Gerasopoulos E., 2005. Cesium-137 in air late after the Chernobyl reactor accident. *Journal of Radioanalytical and Nuclear Chemistry* 264(3), 699-700.

Papastefanou C., 2008. Radioactive Aerosols. In: Radioactivity in the Environment, Volume 12. Elsevier New York, pp. 178.

Pham M.K., Betti M., Nies H., Povinec P.P., 2011. Temporal changes of ^{7}Be, ^{137}Cs and ^{210}Pb activity concentrations in surface air at Monaco and their correlation with meteorological parameters. *Journal of Environmental Radioactivity* 102(11), 1045-1054.

Pittauerová D., Hettwig B., Fischer H.W., 2011. Fukushima fallout in Northwest German environmental media. *Journal of Environmental Radioactivity* 102, 877-880.

Quélo D., Krysta M., Bocquet M., Isnard O., Minier Y., Sportisse B., 2007. Validation of the POLYPHEMUS platform on the ETEX, Chernobyl and Algeciras cases. *Atmospheric Environment* 41(26), 5300-5315.

Reiter E.R., 1978. Atmospheric transport processes: Radioactive tracers, Part 4. U.S. Atomic Energy Commission, p. 605.

Stohl A., Seibert P.,Wotawa G., Arnold D., Burkhardt J.F., Eckhardt S., Tapia C., Vargas A., and Yasunari T.J., 2011. Xenon-133 and caesium-137 releases into the atmosphere from the Fukushima Dai-ichi nuclear power plant: determination of the source term, atmospheric dispersion, and deposition. *Atmospheric Chemistry and Physics Discussion*, 11, 28319–28394.

Sykora I, Froehlich K., 2010. Radionuclides as Tracers of Atmospheric Processes. In: Froehlich, Klaus (Ed.), Environmental Radionuclides: Tracers and Timers of Terrestrial Processes. Edited by ISBN: 978-0-08-043873-3, Chapter 3.

Torri G., 2011. La rete di monitoraggio RESORAD e la sua risposta all'incidente di Fukushima. Twenty-five years after the Chernobyl accident: studies, remarks and recent findings, 21-22-23 June 2011, Udine, Italy [available at: http://www.arpa.fvg.it/export/sites/default/tema/radiazioni/radiazioni-artificiali/allegati/Atti_Convegno_STAMPA.pdf].

Turekian K.K., and Graustein W.C., 2003. Natural Radionuclides in the Atmosphere. Treatise on Geochemistry, Volume 4. In: Ralph Keeling F. (Ed.). Executive Editors: Heinrich D. Holland and Karl K. Turekian. pp. 347. ISBN 0-08-043751-6. Elsevier, p.261-279.

UNSCEAR (United Nations Scientific Committee on the Effects of Atomic Radiation), 2008. UNSCEAR 2008 Report to the General Assembly, with scientific annexes**.** Volume I: Report to the General Assembly, Scientific Annexes A and B. available at http://www.unscear.org/unscear/en/publications/2008_1.html

Winkler R., Dietl F., Frank G., and Thiersch J., 1998. Temporal variation of ^{7}Be and ^{210}Pb size distributions in ambient aerosols. *Atmospheric Environment* 32, 983-991.